Council for Geoscience

Enhanced SSHAC Level 2 Probabilistic Seismic Hazard Analysis for the Duynefontyn nuclear site, Western Cape Province, South Africa.

by

J.A. Stamatakos, J. Watson-Lamprey, H.C. Cawthra, D. Claassen, R.T. Coppersmith, C.B. Johnson, V. Midzi, V. Montaldo Falero, T.F. Mulabisana, E.M. Rathje, P.J. Stafford, K. Ulmer, M. Largent, T. Williams and K.A. Shaw.

Caption: ***Duynefontyn site***

Photo/figure by: *Vincent Jele*

Report number: *2024-0001*

Project number: *CO-2018-5813*

Publication date: *2024-03-11*

UNIT NAME		
REPORT NUMBER 2024-0001	Council for Geoscience	**LEVEL OF CLASSIFICATION** Confidential
REVISION 0		**PROJECT NUMBER** CO-2018-5813

ENHANCED SSHAC LEVEL 2 PROBABILISTIC SEISMIC HAZARD ANALYSIS FOR THE DUYNEFONTYN NUCLEAR SITE, WESTERN CAPE PROVINCE, SOUTH AFRICA

DOCUMENT APPROVAL		
SUBMITTED BY (PRINCIPAL AUTHOR): John Stamatakos Digitally signed by John Stamatakos Date: 2024.03.12 07:54:33 -05'00'	**SUBMITTED BY (PRINCIPAL AUTHOR):**	**PPRP CHAIR:**
NAME: Dr John Stamatakos	NAME: Dr Jennie Watson-Lamprey	NAME: Dr Julian J. Bommer
DATE: 12/03/2024	DATE: 12/03/2024	DATE: 12/03/2024
ACCEPTED BY (PROJECT MANAGER): Duynefontyn Proj - 2024 - 03	**ACCEPTED BY (MANAGEMENT REPRESENTATIVE):** for	**ACCEPTED BY (UNIT MANAGER)** for
Name: Dr Johann Neveling	**Name:** Ms Nomvelo Mkhize	**Name:** Ms Nomvelo Mkhize
Date: 12/03/2024	**Date:** 12/03/2024	**Date:** 12/03/2024
APPROVED BY (EXECUTIVE MANAGER):	**AUTHORISED BY (CHIEF EXECUTIVE MANAGER):**	
Name: Mr Willem Meintjes	**Name:** Mr Mosa Mabuza	
Date: 12-03-2024	**Date:** 14 March 2023	

PROJECT LEADER	Dr Johann Neveling	
TECHNICAL LEADER	Dr John Stamatakos	
AUTHOR(S)	Dr John Stamatakos	
	Dr Jennie Watson-Lamprey	
	Dr Hayley Cawthra	
	Ms Debbie Claassen	
	Mr Ryan Coppersmith	
	Ms Courtney Johnson	
	Dr Vunganai Midzi	
	Dr Valentina Montaldo Falero	
	Dr Thifhelimbilu Mulabisana	
	Prof. Ellen Rathje	
	Prof. Peter Stafford	
	Dr Kristin Ulmer	
	Ms Micaela Largent	
	Ms Kelley Shaw	
	Ms Tessa Williams	

EXECUTIVE SUMMARY

This report documents a probabilistic seismic hazard analysis (PSHA) executed by the Council for Geoscience (CGS) as a Senior Seismic Hazard Analysis Committee Enhanced Level 2 (SSHAC EL-2) process for the Duynefontyn nuclear site, situated to the north of Cape Town, South Africa (Figure ES-1). This work was done under contract (Contract Number 4600062664) for Eskom Holdings SOC Ltd. (Eskom), which operates the Koeberg Nuclear Power Station (KNPS) hosted on the site. This PSHA superseded a preliminary Baseline PSHA for the site that was completed in 2022.

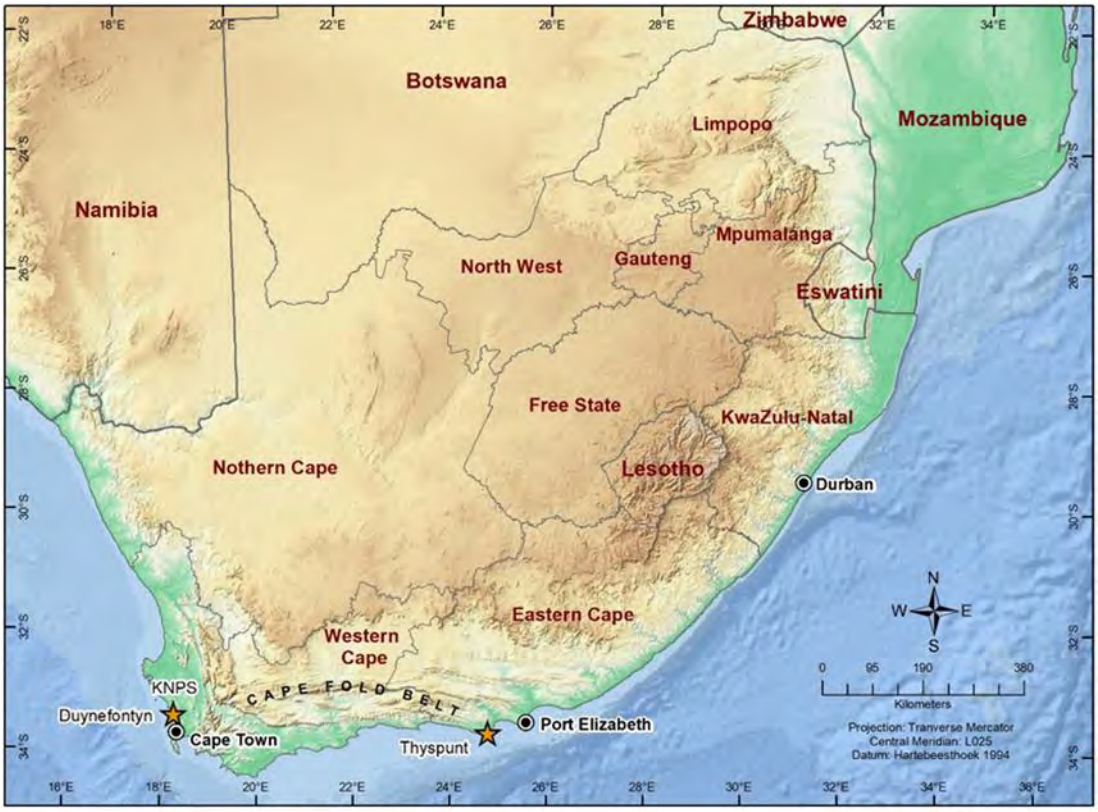

Figure ES-1. Location of the Duynefontyn site, including the Koeberg Nuclear Power Station (KNPS). The Thyspunt site, where a prior SSHAC Level 3 was completed in 2013, is also shown.

The focus of the PSHA is exclusively on vibratory ground motions due to natural earthquakes and its purpose is to quantify the earthquake ground-shaking hazard at the Duynefontyn site. The PSHA will provide input to the Duynefontyn Site Safety Report (SSR), which, in turn, will provide input to the Safety Assessment Report (SAR) that Eskom will submit to the National Nuclear Regulator (NNR) in support of their application to extend the Long-Term Operation (LTO) licence for the KNPS. It will also serve as input to the design of a possible new nuclear power plant (NPP), situated to the north of the KNPS, at the Duynefontyn site.

The final product of the Duynefontyn PSHA is this report, summarising the entire study. It is supported by reports produced on individual components of the study and associated documents and data files. The final PSHA is a detailed characterisation of the ground shaking at the Duynefontyn site from potential future earthquakes. The basic parameter is spectral ordinates of pseudo-acceleration response at 5% of critical damping, using the geometric mean definition of the horizontal component of motion. The target sites are:

- Duynefontyn site, top of bedrock (interface between Tygerberg Formation and overlying strata): S 33° 39' 39.99" E 18° 25' 41.95"
- KNPS, top of bedrock (interface between Tygerberg Formation and overlying strata): S 33° 40' 36.82" E18° 25' 53.03"

The basic outputs are seismic hazard curves and uniform hazard response spectra (UHRS) for the site, as well as the design basis response spectra in accordance with RG 1.208, *A Performance-Based Approach to Define the Site-Specific Earthquake Ground Motion,* and the American Society of Civil Engineers document ASCE/SEI 43-18, *Seismic Design Criteria for Structures, Systems, and Components in Nuclear Facilities*. Satisfying these stringent guidelines means that the study will also satisfy the requirements and standards of the International Atomic Energy Agency (IAEA), including Specific Safety Guide SSG-9, *Seismic Hazards in Site Evaluation for Nuclear Installations*. The specific outputs are:

- Seismic hazard curves for spectral ordinates at 10 target oscillator frequencies; the hazard curves are expressed in terms of the mean hazard and the associated fractiles from 5% to 95%, including the median. These are calculated for annual exceedance frequencies down to 10^{-8}.
- UHRS of horizontal motion at annual frequencies of exceedance (AFEs) (10^{-2}, 10^{-3}, 10^{-4}, 10^{-5}, 10^{-6}, 10^{-7} and 10^{-8}).

Disaggregation plots are also produced for specific combinations of response period and AFE, to show how different combinations of earthquake magnitude, source-to-site distance and ground-motion level (within the probabilistic distribution of accelerations predicted by ground-motion equations for a specific magnitude and distance).

Duynefontyn PSHA

The Duynefontyn PSHA comprises three main components (1) the seismic source model (SSM), (2) the ground motion model (GGM) and (3) the PSHA calculations. The SSM defines the occurrence of possible future earthquakes in terms of location, frequency of occurrence, type of faulting and size up to the maximum considered physically possible. The GMM defines the expected distribution (defined by a logarithmic mean value and an associated logarithmic standard deviation) of spectral accelerations at the sites accounting for the effects of the source, path and the site on the earthquake energy and given the earthquake scenarios provided in the SSM. The PSHA calculates the resulting ground motions from all possible earthquake scenarios and samples the full distribution of ground motion amplitudes, to obtain estimates of the total rate at which each level of acceleration is expected to be exceeded at the site. This rate and the associated uncertainties are quantified in terms of the AFE for various ground-motion levels at the site.

A key objective of the study was to ensure regulatory assurance, by demonstrating that the PSHA considered all uncertainties. Uncertainties are classified into two categories: aleatory variability and epistemic uncertainty. Aleatory variability is the inherent randomness in earthquake and ground-motion processes and the components of ground-motion that are not explicitly modelled within the mean ground-motion of the GMM. For example, in the Duynefontyn study this included the style-of-faulting and orientations of future fault ruptures, and the inherent randomness of ground motions. The probabilistic approach to seismic hazard

analysis is specifically formulated to integrate all sources of variability into the estimation of the annual exceedance frequency of different levels of each ground-motion parameter.

Epistemic uncertainty refers to the lack of knowledge regarding earthquake processes. Regardless of the amount of data available for the construction of the SSM and the GMM, these will never be defined unambiguously. One challenge is that the models are used to develop scenarios which are not represented in the available data, because the PSHA has to consider all possible earthquakes. Another challenge is that the nature of the available data is such that it is always plausible to identify multiple, alternative technically justifiable interpretations. Both challenges impede the definition of unique models. These challenges are especially acute in regions of relatively low levels of seismicity, such as South Africa, because the less frequent occurrence of significant earthquakes leads to data that are inevitably sparse. In the GMM, an example of epistemic uncertainty includes the analysis of the shear-wave velocity (V_S) at the site from either borehole data or from the dispersion of surface waves based on surface wave analysis, specifically multichannel analysis of surface waves (MASW) and microtremor array measurement (MAM). There is epistemic uncertainty associated with nearly every element of the SSM and GMM.

Epistemic uncertainty in the Duynefontyn PSHA is captured in logic trees that organise each model element or parameter as nodes, with the branches of each node for alternative models or alternative parameter values. Weights are then assigned to each branch, reflecting the relative confidence the Technical Integration (TI) Teams have in that branch as an appropriate model or parameter value. The branch weights, which are subsequently treated as probabilities, sum to unity at each node. The PSHA calculations are then performed for all possible combinations of branches, with each hazard run yielding a separate hazard curve. The total weight associated with each hazard curve is obtained from the product of the weights associated with the branches selected for its calculation. The hazard output is expressed in terms of the statistics of the resulting suite of hazard curves, calculating the weighted AFE associated with each ground-motion level. In this way, the mean hazard curve, and the hazard curves for different fractiles, or confidence levels, are calculated. The spread of the fractiles, and the separation of the mean and median hazard curves, reflect the total epistemic uncertainty in the hazard estimates. These naturally increase with the return period, which is simply the reciprocal of the AFE.

To accurately account for the influence of the near-surface soil and bedrock materials on the design ground motions at the two sites, the hazard was computed directly at the top of the interface between the bedrock formed by the late-Precambrian to early Cambrian Tygerberg Formation and overlying semi-consolidated sediments of the Cenozoic Sandveld Group. The approach used to compute the frequency-dependent site adjustment factors (SAF) is shown in Figure ES-2. It is referred to as the one-step approach and is the SAF are the ratio of the surface response spectra from two separate site response analyses: one for the site condition associated with the reference Ground Motion Prediction Equations (GMPE) and one for the site-specific reference condition plus the near-surface condition. The SAF were included within the PSHA calculations following Approach 4 (as defined in USNRC NUREG/CR-6728, *Technical Basis for Revision of Regulatory Guidance on Design Ground Motions: Hazard- and Risk-Consistent Ground Motion Spectra Guidelines)*.

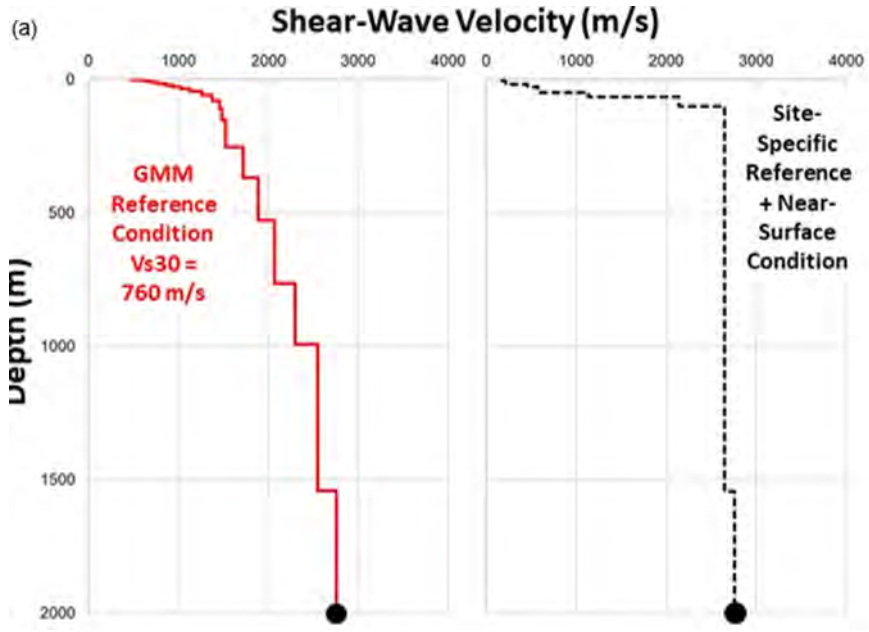

Figure ES-2. The one-step approach to develop site adjustment factors.

The SSHAC Process

A detailed, formal process for conducting PSHA was developed by the Senior Seismic Hazard Analysis Committee (SSHAC) which was convened by the United States Nuclear Regulatory Commission (USNRC), the Electric Power Research Institute (EPRI), and the United States Department of Energy (USDOE) following two landmark PSHAs conducted in the 1980s for nuclear facilities in the Central and Eastern United States (CEUS). The Commission report was issued as NUREG/CR-6372, *Recommendations for Probabilistic Seismic Hazard Analysis: Guidance on Uncertainty and the Use of Experts Experts*—known informally as the SSHAC Guidelines. This guidance recommended methods for conducting a structured and objective multiple-expert hazard assessment. The guidance also focussed on addressing uncertainties in PSHAs using expert judgement. NUREG/CR-6372, and subsequent SSHAC guidelines, defined the ultimate goal of any SSHAC study is to capture the centre, body and range of technically defensible interpretations, known as the CBR of TDI.

NUREG/CR-6372 defined four study levels, increasing in complexity from Level 1 to Level 4, with Levels 3 and 4 intended for application in safety-critical facilities such as nuclear power plants. These higher study levels involve a greater number of participants and a longer duration to assess available data, models, and methods more fully. Another motivation for adopting higher study levels was that the highest levels increase regulatory assurance because of the more comprehensive treatment of epistemic uncertainty. Following NUREG/CR-6372, the USNRC originally considered only Level 4 as being suitable for nuclear installations.

Since NUREG/CR-6372 was first published in 1997, the SSHAC process has been applied to many hazard studies and the lessons learned from these SSHAC studies provided the basis for two updates to the SSHAC guidelines. The first update was published in 2012 as NUREG-2117, *Practical Implementation Guidelines for SSHAC Level 3 and 4 Hazard Studies* and the second and latest update to the SSHAC guidelines was published in 2018 as NUREG-2213, *Updated Implementation Guidelines for SSHAC Hazard Studies*. The intent of NUREG-2213

was to provide the most current and standalone guidance for SSHAC studies, based on a systematic review of all the projects that have successfully applied the SSHAC guidelines since 1997. Following NUREG-2117, the NRC no longer made a distinction between Level 4 and Level 3 studies in terms of regulatory assurance for nuclear installations. Level 3 studies have been found to be a more efficient approach and Level 3 studies have been routinely applied to most recent PSHA studies for nuclear power plant sites. It also introduced the concept of an augmented (or enhanced) Level 2 study, in which options for augmenting a Level 2 study were introduced to increase the degree of regulatory assurance without necessarily adopting all the requirements of a Level 3 study. In 2019 Eskom recommended that the Duynefontyn PSHA be executed as an Enhanced Level 2 study (EL-2), since this was considered much more agile than a Level 3 study. In practice, however, the Duynefontyn PSHA meets all the requirements of an SSHAC Level 3 study (see Chapter 3). The terminology of “SSHAC EL-2” is retained to maintain clear communication.

The SSHAC EL-2 PSHA for the Duynefontyn site and the KNPS was conducted in accordance with the guidelines provided by USNRC in NUREG-2213. By closely adhering to the SSHAC process the TI Teams ensured that epistemic uncertainty and aleatory variability was properly accounted for in the SSM and GMM, and thus properly captured in the resulting uncertainty in the hazard results. These PSHA results therefore provide Eskom with an up-to-date and defensible seismic hazard characterisation that meets the regulatory requirements for nuclear facilities at the Duynefontyn site.

Like all SSHAC studies, the Duynefontyn PSHA has clearly defined roles for all participants. The Project Manager, Dr Johann Neveling of the CGS, had overall responsibility for the coordination of the project in terms of contractual issues, schedule, budget and logistics, with support from several colleagues at CGS. Dr John Stamatakos was appointed as Project Technical Integrator (PTI), with overall technical responsibility for the project. Dr Stamatakos was also assigned the role of Technical Integrator (TI) Lead for the SSM TI Team. Dr Jennie Watson-Lamprey was appointed as TI Lead for the GMM TI Team. It falls to the TI Lead to ensure that the TI Team, collectively and individually, assumes full intellectual ownership of the final model. The SSM TI Team included South African seismologists and geologists with extensive local knowledge, joined by international experts with experience in the development of SSM for PSHA, particularly in regions of low-to-moderate seismicity. The GMM TI Team was assembled with experts in the development of ground-motion prediction models and site response analysis. The Hazard Analysis Team (HAT) was led by Ms Micaela Largent and supported by a team of hazard experts.

The responsibility for the process and technical review of the entire project, commensurate with the requirements, for a SSHAC Level 3 process, was assigned to a Participatory Peer Review Panel (PPRP). According to these requirements the PPRP had ultimate responsibility for confirming that the study has captured, and adequately documented, the CBR of the TDI of the available data, models and methods. A highly qualified and experienced PPRP was selected and appointed, according to regulatory requirements, in liaison with the project sponsor (Eskom). The PPRP was chaired by Dr Julian Bommer, formerly Professor of Earthquake Risk Assessment at Imperial College London, who has more than 30 years of consultant experience in seismic hazard analysis projects around the world, much of it for critical facilities. Dr Bommer was joined on the Panel by five other distinguished experts specialising in disciplines relevant to seismic hazard analysis, and they included: Prof. Jon

Stewart (University of California, Los Angeles) specialising in geotechnical earthquake engineering, seismologists Prof. Raymond Durrheim (University of the Witwatersrand) and Dr Jon Ake (retired from the USNRC) and geologists Prof. Thomas Rockwell (San Diego State University) and Dr Marc Goedhart (Kainos South Africa).

The Duynefontyn SSHAC EL-2 process was structured around a series of in-person working meetings, near-weekly TI Team virtual meetings, three formal workshops, and a PPRP briefing. The three formal workshops were the cornerstones of a SSHAC EL-2 process and were attended by the PTI, TI Leads and Teams, PPRP, HAT, Database Developers, Project Management Team, and observers, including both the sponsor (Eskom) and the regulator (NNR). Due to various Covid-related travel restrictions, all workshops included a virtual element. Workshop 1 was combined with a Kick-Off meeting and was held at the Blaauwberg Beach Hotel in Bloubergstrand, Cape Town, South Africa, from 23–25 February 2022. Presentations of the Baseline PSHA results and hazard sensitivity calculations helped the TI Teams to identify the key issues that would warrant the major focus of their efforts, and several presentations on relevant databases were made by Resource Experts, who joined the workshop.

Workshop 2 was held at the Protea Hotel outside Stellenbosch, South Africa, from 20–24 June 2022. This workshop focussed on alternative models and methods as they pertain to key technical issues and the seismic hazard at the Duynefontyn site. The primary objective of the workshop was to enable members of the broader technical community, represented by 17 Proponent Experts, to present on topics relevant to the development of the SSM and GMM. Ample opportunity was provided for discussion, and this helped the TI Teams to assess the strengths and weaknesses of the proposed models and any assumptions implicit in their derivation. The aim was not primarily to assess the innate merits of each model, but rather to determine the degree to which they are applicable to the Duynefontyn PSHA.

Workshop 3 was held from 19–22 June 2023 at the Devon Valley Hotel located outside Stellenbosch, South Africa. At this Workshop, the TI Teams presented the bases for the preliminary SSM and GMM and were questioned and challenged on these by the members of the PPRP. Hazard sensitivity results were also shown that enabled the TI Teams to identify how different elements of the preliminary models were influencing the hazard, and in particular the sources of the largest contributions to the overall uncertainty.

Geology and Tectonics

The evaluation of the SSM data, models and methods was informed by an understanding of the tectonic setting of the Western Cape. The Duynefontyn site region lies within a stable continental region (SCR) well removed from active tectonic plate boundaries and, like other SCRs, is characterised by low rates of tectonic deformation and low rates of seismicity. The Western Cape is geomorphically stable and characterised by very low rates of erosion and isostatic uplift.

The exposed geological landscape is largely the product of several periods of active contraction and transpressional tectonism over the last 600 Ma or more. Near the Duynefontyn site, bedrock is formed by sedimentary rocks (rhythmic alternations of greywacke, phyllitic shale, siltstone, immature quartzite, and a few thin impure limestone and conglomerate beds) of the Malmesbury Group that were folded and subject to low-grade metamorphic processes

during a Neoproterozoic (1000–541 Ma) mountain building event referred to as the Pan-African orogeny. This produced the tight upright folds with axial planes striking northwest to north-northwest near the site, as well as the predominantly northwest-southeast orientated strike-slip faults in the region (e.g., Colenso and Piketberg faults). These rocks are intruded by areally extensive syn-, late- and post-tectonic granites of the 550–510 Ma Cape Granite Suite, emplaced during late-stage deformation, although some may be post-tectonic. The granites buttressed the site and area to the south against the last major compressional event to impact the Western Cape. The Permo-Triassic Cape Orogeny deformed the overlying sedimentary rocks of the Cape Supergroup strata, to form the mountains of the Cape Fold Belt to the east and the north.

The third major tectonic event in the region was characterised by extension which commenced in the Early Jurassic (~180 Ma) when Gondwana began to break up through a series of rifting events, concluded by the mid-Cretaceous (~90 Ma). Rifting reactivated the Cape Fold Belt contractional fault system as extensional and transtensional faults, which was associated with the right-lateral rifting of the Agulhas-Falkland Fracture Zone, located offshore along the southeastern margin of South Africa. Regionally extensive, predominantly northwest-southeast trending dykes assigned to the False Bay Dolerite Suite intruded rocks of the Malmesbury Group and Cape Granite Suite rocks during the Early Cretaceous.

Since the end of rifting along the western margin of South Africa in the late Mesozoic, the region has been passive and remarkably stable. Along the coastline, the folded and faulted bedrock is overlain by unconsolidated to semi-consolidated sequences of marine, estuarine, and aeolian deposits that reach thicknesses of generally less than 20 m.

Duynefontyn PSHA Database

A key activity from the start of the project was to assemble SSM and GMM databases of information relevant to the characterisation of seismic hazard at the Duynefontyn site. The databases were created through compilation of all available data identified by the TI Teams, assisted by suggestions from the PPRP, and included published papers, unpublished reports, maps, recordings, catalogues, and other quantitative data.

Additionally, activities were conducted for the collection of new data where key information could be gathered within the schedule of the project and contribute to better constraint of the SSM and GMM, thereby reducing the overall epistemic uncertainty. These data collection activities focussed on those elements of the SSM and GMM which, based on Thyspunt PSHA and the Baseline Study, were considered to have the greatest impact on the hazard, including those with large epistemic uncertainty. Most of these elements were part of an established research programme conducted by the CGS and described in the Duynefontyn Data Collection (DDC) project execution plan. The data collection activities involved CGS staff members (some of whom were also members of the TI Teams) and external specialist contractors engaged specifically for these tasks. The work also included the services of others, such as geochronology specialists. In addition to the above studies, several Specialty Contractors were identified by the TI Teams to assist in their evaluations and appointed by CGS to undertake additional investigations.

Staff from the CGS reanalysed the recordings of seismicity from the Cape Syntaxis area for the period between 1971 to 2020, to improve the quality of the earthquake record from this

region. The improvements to the earthquake catalogue from this study included more accurate location data, homogenised magnitudes, the identification of additional earthquakes and new hypocentral depth calculations.

Extensive and detailed research was undertaken of the pre-instrumental seismic record to identify and characterise all earthquakes that occurred within a 350 km radius of the Duynefontyn site during the period from 1620 to 29 September 1969. Historical documents consulted included, but were not limited to, published and unpublished archival sources (e.g., documents pertaining to the Dutch and British colonial administration), contemporaneous narrative sources by residents, travellers and missionaries and periodical sources (e.g., newspapers and reports from meteorological stations). The study evaluated 74 possible historical events, of which 23 were defined by more than one historical record of earthquake shaking. From these 23 events, ten yielded sufficient data to be added to the project earthquake catalogue.

A regional marine terrace investigation was conducted along the southwest coastline of South Africa to document the altimetry and chronology of marine terraces in the region. The objective was to evaluate the regional and local rates of tectonic uplift that can then be used to identify and characterise potential seismic sources such as large faults, including potential deformation at the Duynefontyn site. The palaeoshoreline records showed no obvious evidence of neotectonic deformation or large-scale vertical warping of the coastal margin. The collated estimates of regional isostatic rock uplift rates for the southwest Cape coast of South Africa all revealed slow uplift rates, on the order of only a few metres per million years (generally between <1 to 6.6 m/My) that is consistent with a stable continental margin.

The lack of active deformation at the Duynefontyn site is also evident in a supporting study commissioned by the SSM TI Team to document a first-hand account of the exposed bedrock geology of the Koeberg footprint site that was documented during construction. Fossil evidence from the sediments overlying mapped fractured/faulted zones in the bedrock imply that there have been no large-scale displacements of these structures since at least the Pliocene (~5 Ma).

Investigations of onshore faults in the Western Cape was undertaken to reduce the uncertainties regarding important fault parameters such as geometry, recency of slip and slip rate, for input to the fault source characterisation of the Duynefontyn PSHA. This investigation was supported by two additional supporting studies, an offshore hydroacoustic study and a microseismicity monitoring effort along the Colenso Fault. In addition, a structural analysis of bedrock faulting in the Western Cape was performed by the CGS in parallel to the onshore mapping effort.

The objectives of the onshore fault mapping investigation were to compile existing publications and CGS reports detailing past fault investigations, understand the structural complexity, sense of slip, and other features associated with faulting in the syntaxis, and conduct field reconnaissance along regional bedrock faults looking for evidence of recent (Quaternary) fault activity. Field mapping did not uncover any geologic evidence of active faulting on the large, mapped faults in the Western Cape, nor was there any evidence of geomorphic features commonly associated with active deformation such as pressure ridges, pull-apart grabens, linear scarps, or range-front facets. The lack of observed deformation becomes even more evident when the very slow erosion rates for the Western Cape are factored in, meaning that

if these features were formed in the recent geologic past, they would be well preserved in the present-day landscape.

Offshore, multibeam echosounder mapping in the large marine embayments of Table Bay and False Bay illuminated numerous structural features of the bedrock and the superficial sediment cover. Both bays are relatively sediment-starved, and the bedrock is well exposed on the seafloor. The bathymetric images reveal the detailed structural and sedimentary fabric of the Malmesbury Group strata, which is characterised by a strong northwest-southeast structural grain (including large isoclinal folds) dissected by small faults and fractures, palaeo-drainages, and several cross-cutting dolerite dykes. The SSM TI Team systematically evaluated geological features revealed by the detailed multibeam bathymetry imagery, especially along the trend of the Table Bay and postulated Milnerton Fault Zones but did not observe any fault offsets (at least within the 1-5 m resolution of the imagery). Based on the lack of observed fault offsets, the SSM TI Team concluded that bedrock faults in Table Bay and False Bay have not been active since the dolerite dykes intruded in the early Cretaceous and perhaps not since contractional deformation of the margin ended in the Palaeozoic.

An assessment of the potential for fault slip based on neotectonic stress data was provided to the SSM TI Team in an independent specialty contractor study. This stress analysis was used by the SSM TI Team to inform their assessment of the seismogenic probability of fault sources and to assign the range of fault orientations generated by the virtual fault rupture generator. The stress state solutions were derived from inversions of earthquake hypocentres (strike, dip, seismic moment) that occurred within ~200 km of the Duynefontyn site. The results of the stress analysis indicate a predominantly strike-slip stress regime.

As part of the overall stress analysis, three offshore seismic profiles of the Petroleum Agency of South Africa (PASA) were examined to provide a regional tectonic context for the present-day stress state assessment, and to identify any faults in the seismic profiles that show evidence for relatively recent activity. Interpreted structures from these profiles include faults in the continental basement that likely developed during Mesozoic rifting and the opening of the South Atlantic Ocean, but these faults do not appear to cut the younger post-rifting strata. Fault-like structures observed within the shallower post-rift layers appear to be related to soft sediment deformation (slumping, flexure, and compaction) rather than crustal scale tectonic faulting.

Ground-motion recordings are essential for estimating various components of a GMM and the GMM TI Team used three such databases during the project. The GMM TI Team compiled the first database for use by the GMM TI Team and engaged a specialty contractor to invert for seismic properties of South Africa that could be used for GMPE adjustments. This database, the inversion ground-motion database (GMDB), was composed of earthquake locations and event times from the project earthquake catalogue compiled by the SSM TI Team and waveforms from the South African National Seismograph Network provided to the GMM TI Team by the CGS. From the 2,100 earthquakes within the declustered SSM earthquake catalogue, 1,313 events produced at least one waveform recording captured by the network of available stations.

Datasets compiled for South Africa inversions ideally have significant overlap with the rupture scenarios of interest for the hazard calculations. In areas of low seismicity like this project, the empirical data is heavily dominated by recordings of relatively small-magnitude events, many

of which occur at significant distances from the target site. As a result, the seismic parameters obtained from inverting the empirical data, regardless of the approach adopted, may not be directly comparable with those from the inversions of the backbone GMPE given that the latter parameters are obtained for a very different range of rupture scenarios. This introduces epistemic uncertainty into the process.

Another key challenge when performing inversions of the available empirical data is to understand the extent to which the dataset meets the ideal requirements for the project and how seismic parameter estimates from the rupture scenarios represented in the dataset can be mapped to the rupture scenarios of interest. Many of the records in the Inversion GMDB are from earthquakes hundreds of kilometres from the target site, and very few events are located within the host seismic zone that dominates the PSHA calculations. This also introduces epistemic uncertainty into the process.

At the behest of the GMM TI Team, the CGS installed two vertical arrays at the Duynefontyn site between February and April of 2023, with data collection starting in April 2023. From April to June 2023 the stations recorded 12 earthquakes, one of which had a sufficiently high signal-to-noise ratio to be used for evaluation. The Duynefontyn GMDB therefore included a single earthquake record from the Duynefontyn stations, which was used to obtain site-specific estimates of κ_0[1].

The GMM TI Team requested Drs Quiros and Sloane of University of Cape Town to estimate κ using data they collected from a temporary array they deployed prior to the start of the SSHAC EL-2 PSHA to monitor microseismicity in the area north of Cape Town. The Temporary Array GMDB that they developed as a result was used by the GMM TI Team in their evaluation of κ_0 at the Duynefontyn site.

The site-specific V_S characteristics are a fundamental input to the site response analysis. Measurements of V_S can come from a variety of sources, each with advantages and limitations. Several phases of geotechnical and geophysical tests were performed across the proposed Duynefontyn site (i.e., northwest of the existing KNPS). Prior to the SSHAC project, site investigations at the Duynefontyn site were performed by SRK Consulting using downhole (DH) seismic testing in eight boreholes. Site investigations commissioned for this project included combined MASW and microtremor array measurements (MAM) performed at two locations (centred over two boreholes, DA and SA) by the CGS and interpreted by Prof. Brady Cox. Wireline Workshop performed PS-suspension logging in six boreholes (DA, SA2, and ST1–ST4) drilled by the CGS; these data were ultimately re-interpreted by Dr Cox and CGS personnel.

Three different seismic techniques, complementary in terms of depth of profiling, ability to resolve thin layers and wavelength of seismic waves, were used to measure V_S. Additionally, the different techniques provided confirmation of the general velocity structure and quantification of epistemic uncertainty across different test methods. The MASW/MAM method provided the deepest profiling of V_S and represents wavelengths more similar to earthquake waves but had difficulty resolving thin layers at depth. Additionally, the presence of the semi-consolidated sand above the bedrock at the site introduced uncertainty in the inverted V_S

[1] κ_0 is the site decay parameter.

profiles. The DH method employed by SRK utilises the same type of waves associated with the site response analyses and can resolve relatively thin layers, but it is difficult to measure V_S in deep layers. The PS logging method is able to record data from deeper layers in the wells and potentially resolve very thin layers, but the wavelengths of the seismic waves are so small that the measurements show significant variability over small lateral distances.

Seismic Source Model

The SSM is a conceptual and mathematical representation of the physical characteristics of earthquake sources that are deemed capable of producing hazard-significant ground motions at the Duynefontyn site. There are two types of sources in the SSM. Fault sources are planar fractures or fracture zones in the Earth's crust that localise seismicity. Seismic source zones are regions of the Earth's crust with diffuse seismicity in which future earthquakes are not assigned to specific known faults.

Some geological publications have considered the Colenso Fault and Milnerton Fault Zone as active faults due to a simple spatial correlation with a past earthquakes. However, the SSM TI Team found no data to justify their inclusion as fault sources in the SSM for the purpose of a PSHA. For a similar lack of data, the SSM TI Team excluded most of the major faults of the Western Cape in their PSHA model.

The only exception was the Groenhof Fault, for which there is a record of aftershocks that clearly defined the fault plane of the 1969 Ceres earthquake. An analysis of the focal mechanism for the Ceres mainshock in the published literature indicated a steeply dipping, left-lateral rupture aligned with microseismicity observed along a northwest-striking plane. The aftershock data were evaluated by the SSM TI Team to understand the spatial association of the focal plane relative to the mapped fault trace of the Groenhof Fault Zone and several topographic lineaments seen in satellite imagery. While field mapping did not find direct evidence of the surface rupture associated with the 1969 Ceres earthquake, the fault is spatially associated with a bedrock fault at the surface that includes fault gouge. Mapping of this bedrock fault shows that it deflects steeply dipping bedrock strata atop a ridge at the Wakkerstroom site. The amount of bedding rotation measured at this site (including uncertainty) was used by the SSM TI Team to develop estimates of fault offset and slip rate.

In contrast to fault sources, seismic source zones are used to model the temporal and spatial distribution of seismicity in the crust where there is insufficient geologic or geophysical evidence to allow the SSM TI Team to assign past recorded earthquakes to a mapped fault. These recorded earthquakes could have been produced by a fault that did not rupture the ground surface, and thus did not leave geological evidence for the earthquake. Alternatively, the fault could have produced surface rupture, but this surface rupture remains obscure and unidentified in the landscape. The lack of geological evidence for significant repeated events on a single fault surface suggest to the SSM TI Team that future seismicity will most likely continue to occur on a distributed network of faults in the crust. Even on the Groenhof Fault, where the SSM TI Team reported evidence for repeated deformation with up to 50 m of fault offset, our assessment is that offset likely occurred over millions or even tens of millions of years, since the Mesozoic or even earlier. This observation leads to very low slip rates assessed for the Groenhof Fault (mean of 0.01 mm/yr). This low slip rate translates to one 0.5 m slip event (~**M** 6.3 earthquake) on the Groenhof Fault every 10,000 – 50,000 years.

The SSM TI Team identified and characterised five seismic source zones (Figure ES-3), with the Saldania Zone (SDZ) being the host zone for the Duynefontyn site. The source zone boundaries were based on changes in the type of crust, composition of the crust, structural fabric and style-of-faulting. Modelling possible future earthquakes in the source zones requires a set of source zone and rupture characteristics. These include the thickness of the seismogenic crust, spatial location of future earthquakes (correlation of the spatial distribution of past earthquakes with the spatial distribution of future earthquake), rupture style (normal, reverse, strike-slip), hypocentre depth distributions, maximum magnitude and rates. The record of past earthquakes in South Africa is sparse, thus the SSM TI Team relied on appropriate analogues to similar crustal settings where the database of past earthquakes is sufficient to develop these source zone characteristics. Seismogenic thickness, focal and hypocentre depth distributions and maximum magnitude were derived from the CEUS SSHAC Level 3 study. The analysis of the spatial distribution of past earthquakes and magnitude-frequency distribution of possible future earthquakes were developed based on the record of past earthquakes in South Africa.

Possible future earthquakes within the SDZ could occur relatively close to the site, thus the GMM required future earthquakes within the zone to be modelled as fault ruptures rather than point sources. These virtual fault ruptures were developed to capture the relevant seismicity parameters consistent with the seismotectonic setting of the SDZ.

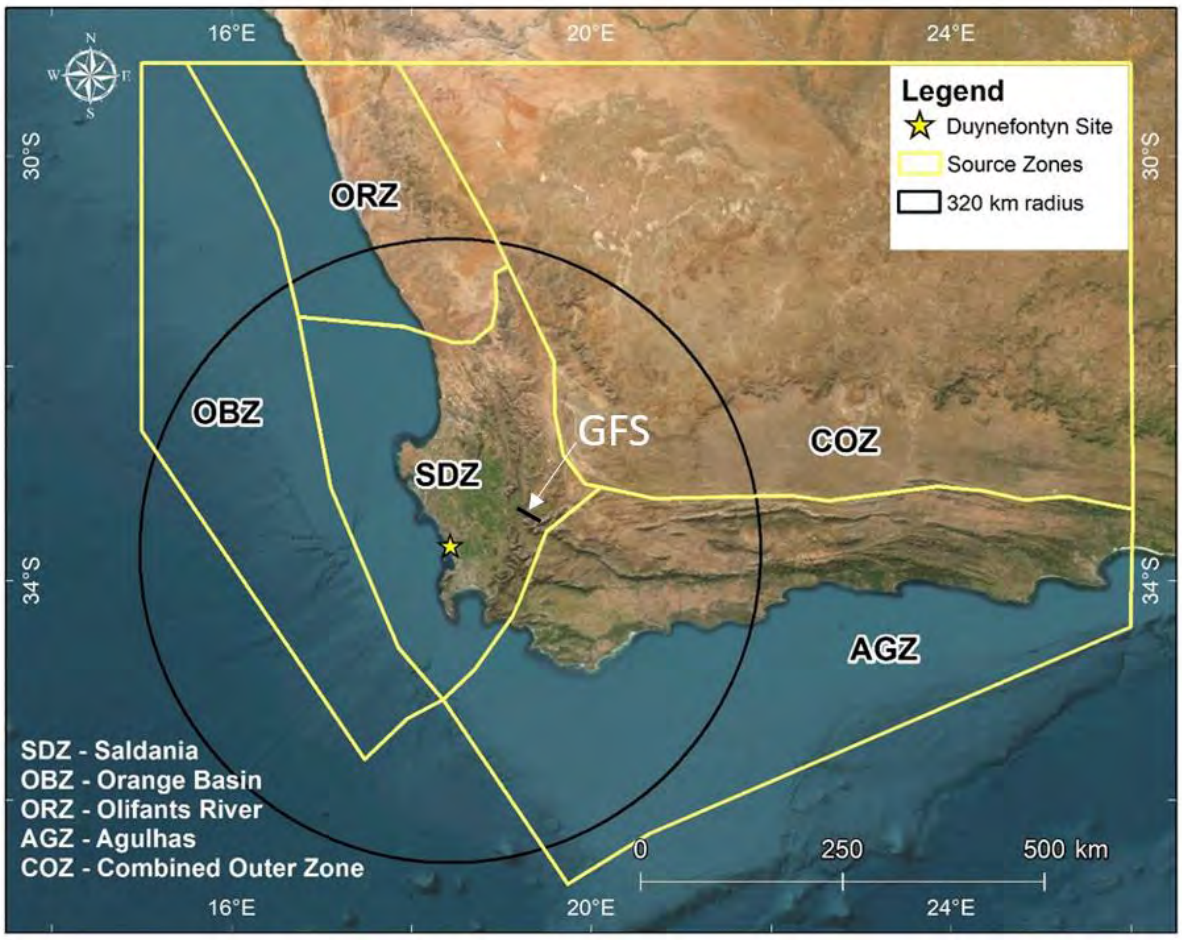

Figure ES-3. Seismic source zones defined in the SSM for the Duynefontyn PSHA.

The best estimate for the recurrence rates of future earthquakes is obtained from the average rates of earthquakes in the project earthquake catalogue. The project earthquake catalogue was constructed by combining earthquake records from national, regional and global seismograph networks and reporting sources. This data was supplemented with the historical earthquakes from the study mentioned above. The resulting database was then processed in a stepwise fashion to produce a final project catalogue (Figure ES-4). These steps included removing duplicates and non-tectonic events, homogenising the recorded magnitudes to a single moment magnitude scale (**M**), and declustering the records to remove aftershocks and foreshocks so that each entry is an independent event (including the identification of earthquake clusters and swarms). To capture the epistemic uncertainty in the completeness analysis, the catalogue was evaluated for completeness based on two alternative analyses, the Stepp plot analysis method and the probability of detection method. The result was to generate two versions of the catalogue, one for each completeness method.

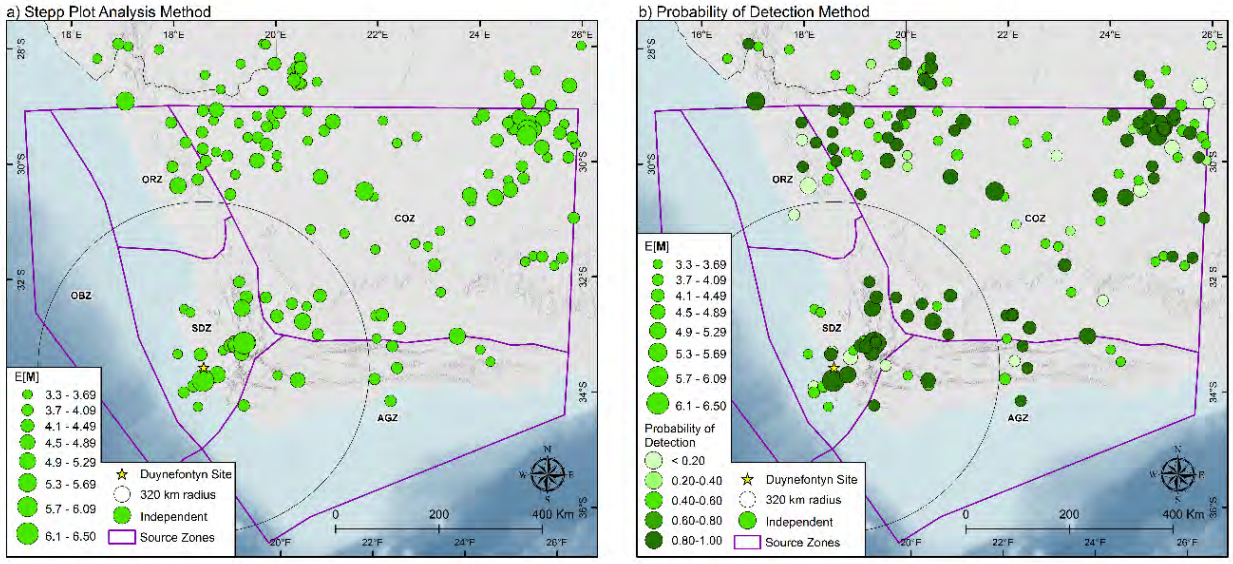

Figure ES-4. Map showing the location and magnitudes of the earthquakes in the final project catalogue used for smoothing analysis. Map (a) for the Stepp plot analysis completeness method catalogue and (b) for the probability of detection completeness method catalogue.

Based on these two versions of the catalogue, the SSM TI Team parameterised the rate of future earthquakes within all source zones combined based on the slope or *b*-value and the activity rate or *a*-value (y-intercept or y-value of the recurrence curve at a defined magnitude). Two alternative methods were used to determine the *b*-values, the log-likelihood and *b*-positive approaches, in order to capture the epistemic uncertainty in the *a*-value and *b*-value estimates. The *b*-values calculated for all source zones combined were used as *b*-prior values to develop *b*-values and *a*-values for each zone. The doubly truncated exponential distribution was used to model magnitude-frequency distributions (MFDs) for each zone. Each MFD was parameterised using correlated sets of *a*-value, *b*-value, and maximum magnitude distributions. These analyses resulted in four sets of *a*-value and *b*-value estimates for each source zone based on combining the two completeness approaches with the two recurrence methods (see Table ES-1 for the SDZ results). These epistemic uncertainties were then carried through to the final hazard calculation, ensuring that the SSM provides an accurate and objective representation of the seismic sources at the Duynefontyn site that fully captures the CBR of TDI.

Table ES-1. SDZ rate parameters for recurrence.

Recurrence Method	Completeness Method	Mean		Upper		Lower	
		b-value	Activity at E[M] 5.0	*b*-value	Activity at E[M] 5.0	*b*-value	Activity at E[M] 5.0
***b*-positive**	**Stepp Completeness**	0.81	1.48E-02	0.72	2.87E-02	0.97	5.32E-03
	PoD	0.81	2.38E-02	0.72	4.52E-02	0.97	8.88E-03
Log-likelihood	**Stepp Completeness**	0.85	1.30E-02	0.67	3.51E-02	1.03	4.31E-03
	PoD	0.87	1.98E-02	0.68	5.31E-02	1.05	6.68E-03

Based on the results of the source zone analyses, the mean annual rate for earthquakes with **M**≥5 across the Western Cape is approximately 0.02 and the mean annual rate for earthquakes with **M**≥6 across the Western Cape is approximately 0.002-0.003. These rates are consistent with the rates modelled by the SSHAC Level 3 PSHA for the Thyspunt site in the Eastern Cape Province (South Africa) which incorporated a source zone similar to the SDZ and are also generally consistent with the rates modelled for the most stable parts of Central and Eastern United States.

The spatial distribution of earthquakes was also an important characteristic to capture in the SSM, as it defines where future events are more likely to occur. A uniform spatial distribution (normally applied in regions with sparse data) means that future earthquakes are equally likely to occur anywhere in a seismic source zone; it maximises the uncertainty in location of future earthquakes within each zone. The assumption of spatial stationarity posits that the location of past earthquakes provides a reliable basis for predicting where future earthquakes are likely to occur, at least over the lifetime of the proposed facility (i.e., the next 50 years). If spatial stationarity is assumed, then spatial smoothing algorithms may be implemented to model the signature of seismicity rate concentrations. Since the SSM TI Team could neither verify nor refute the assumption of stationarity for the source zones in the SSM, they developed two alternative branches (assigned equal weight) in the logic tree to capture this epistemic uncertainty. One branch developed spatial density maps of past earthquakes for predicting the location of future events assuming stationarity, and a second branch applied uniform smoothing if stationarity does not apply.

For the stationarity branch, the SSM TI Team concluded that the application of an adaptive smoothing technique or a fixed kernel with bandwidth of 100 km implies different levels of confidence in the accuracy of earthquake locations in the project catalogue, particularly for the pre-instrumental and early instrumental records. A 100-km fixed bandwidth implies less confidence in the accuracy of earthquake locations in the catalogue compared to the adaptive smoothing technique. The SSM TI Team evaluated these two models (Figure ES-5) as equally possible and thus assigned them equal weights.

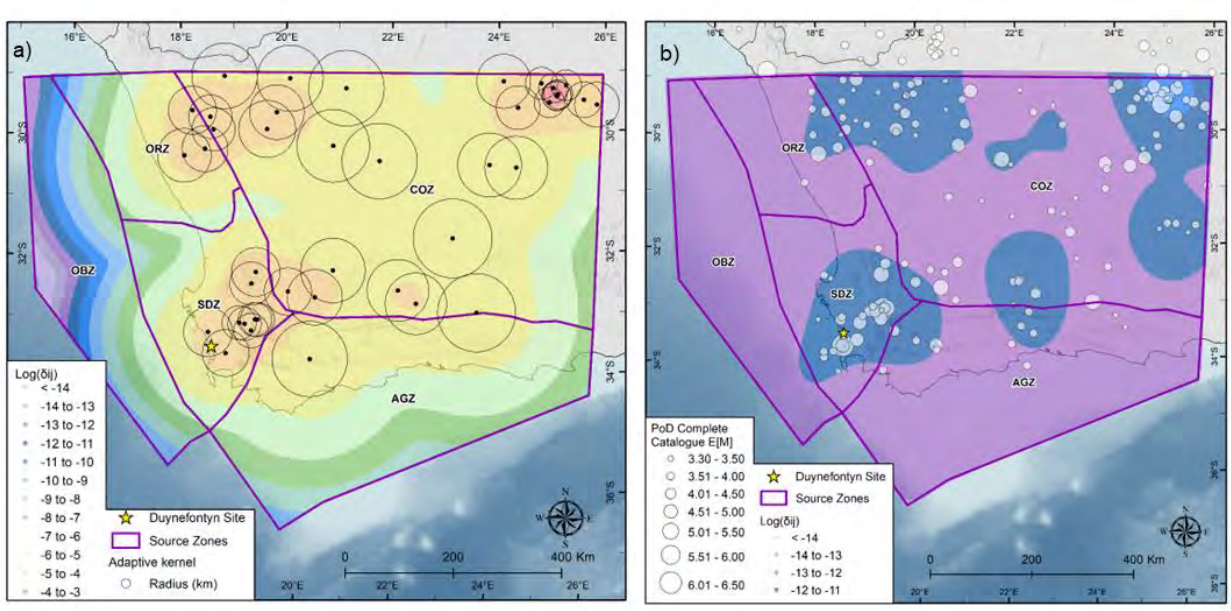

Figure ES-5. Spatial smoothing using (a) the adaptive kernel method and (b) smoothing using fixed kernel bandwidth of 100 km.

Ground Motion Model

The GMM describes the distribution of ground-motion at the Duynefontyn site for the earthquake scenarios contained in the SSM. The distribution of ground-motion for these scenarios was defined using a mean and the deviation from this mean (the aleatory variability) as well as the epistemic uncertainty. In practice, the distribution of ground-motion amplitudes is estimated in two parts: the reference rock ground-motion amplitudes and the site adjustment factors. For this project, and as described above, the GMM TI Team adopted the one-step approach for estimating site response, thus what was termed the reference rock ground-motion was consistent with source and path characteristics of South Africa with site characteristics consistent with the backbone GMPE, which in this case represents a generic site from regions of shallow crustal earthquakes. The site adjustment factors convert the rock ground-motion from the generic site to the Duynefontyn site.

The GMM TI Team adopted a ‘backbone’ approach for the development of the median reference rock model. This approach creates a logic-tree where each branch is occupied by a modified version of a single GMPE. The GMM TI Team selected the Chiou and Youngs (2014) GMPE, referred to as CY14, as the backbone GMPE. The GMM TI Team adopted a host-to-target adjustment approach that required seismic parameter sets to be available for both the ‘host’ and ‘target’ regions, where these parameters were those defined as part of the point-source stochastic model. The alternative branches were then obtained by applying scale factors to the backbone GMPE, where the scale factors account for differences in host-to-target seismic parameter adjustments.

For the target region, seismic parameters were required that were consistent with the point-source stochastic model that describes the source and path characteristics of the rupture scenarios relevant for the Duynefontyn site. Two approaches were integrated by the GMM TI Team for estimating the target parameters, one based on Fourier amplitude spectra, the other based on elastic response spectra. Following these approaches, the GMM TI Team and a

specialty contractor developed seven suites of target-region parameters that each predict the ground-motion in South Africa while making different assumptions about data, the treatment of the site decay parameter (κ_0), regression process, and additional issues outlined in the report.

Host-to-target source and path adjustments were developed for each of the seven suites of target parameters and applied to the CY14 GMPE. To capture the CBR of TDI with mutually exclusive branches, the GMM TI Team developed a meta-model that is a combination of the seven adjusted GMPEs. The epistemic uncertainty of the meta-model is a combination of the model-to-model variability, near-source saturation uncertainty, and additional epistemic uncertainty.

Aleatory variability describes the expected deviation from the mean ground-motion that can occur at a given site. The GMM TI Team decided to use single-station sigma because a site-specific amplification model was developed for this project, thus the site-to-site aleatory variability was not needed. The epistemic uncertainty of the site-specific amplification model was considered using a logic-tree approach.

To evaluate the use of global single-station-sigma models, the GMM TI Team examined the residuals from the inversions performed to estimate target seismic parameters to determine whether there was sufficient data to deviate from global models. The GMM TI Team decided the data was insufficient for this purpose and therefore opted to use the single-station sigma model developed by Al Atik (2015) to represent aleatory variability at the Duynefontyn site. The mixture model was also applied to capture the widening of the tails of the aleatory variability that is observed in large ground-motion datasets.

The GMM TI Team adopted the “one-step approach” recommended by Rodriguez-Marek et al. (2021) and Williams and Abrahamson (2021) to develop site adjustment factors. The one-step approach computes the frequency-dependent site adjustment factors (SAF) as the ratio of the surface response spectra from two separate site response analyses: one for the site condition associated with the reference GMPE and one for the site-specific reference condition plus the near-surface condition.

The GMM TI Team quantified the CBR of TDI for the site adjustment factors using a site response logic-tree that defined alternative site properties (e.g., V_S profiles, κ_0) with associated weights and performed site response analyses for each combination of site properties in the logic-tree. The site response analyses used to develop the SAF required the following, each of which was considered in the logic-tree:

- Selection of the numerical approach utilised to compute site amplification.
- Site-specific shear-wave velocity profiles that extend to a depth that merges with the V_S profile of the reference condition associated with the host backbone model of CY14.
- Site-specific κ_0 values to constrain the small-strain damping profile.
- Nonlinear modulus reduction and damping (MRD) curves for the site-specific subsurface conditions.

Preliminary evaluations of the geologic conditions and associated V_S profiles at the Duynefontyn site indicated that the site response should not be significantly nonlinear. This

assessment was based on the fact that the overlying sediment layers were excavated prior to the construction of the existing KNPS (and the assumption that a similar course of action will be followed for any future new build at the Duynefontyn site) and the large shear-wave velocities measured for the rock materials at the site. Thus, the GMM TI Team decided to perform the site response analyses using the equivalent-linear approach which can account for modest levels of nonlinearity in material properties.

Several phases of geotechnical and geophysical site investigations were performed across the Duynefontyn site to measure V_S, including multichannel analysis of surface waves and microtremor array measurements (MASW/MAM), DH and PS logging. The MASW/MAM and DH methods of V_S measurement are considered complementary techniques, with MASW/MAM providing a more global measurement and DH providing a more local, point measurement. A comparison of the V_S profiles from the MASW/MAM methods and the DH methods at two sites are shown in Figure ES-6.

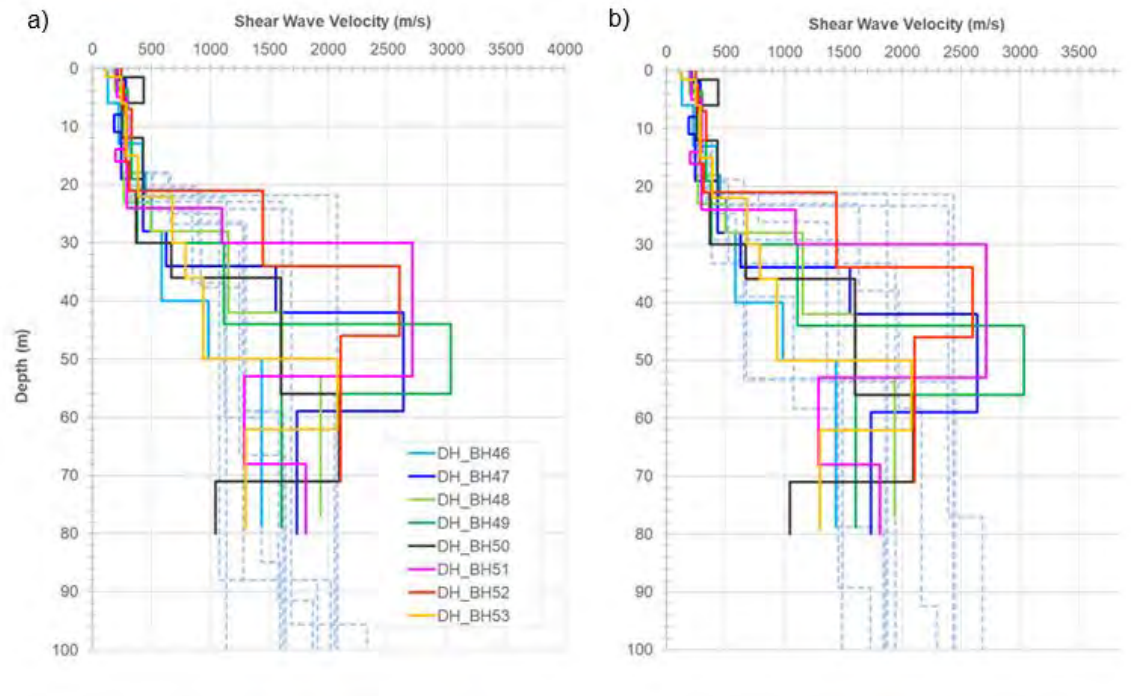

Figure ES-6. Comparison of SRK downhole shear-wave velocities and MASW/MAM profiles in dashed lines as (a) DA site and (b) SA2 site.

The GMM TI Team considered both the MASW/MAM and the DH methodologies to be equally viable approaches and assigned them equal weights of 0.5. The PS logging results were not used to develop V_S base case profiles for the site response analyses because of the difficulty in identifying shear-wave arrivals in the waveforms, and thus were given a weight of zero.

The high-frequency decay parameter at the site (κ_0) controls the roll-off of the Fourier amplitude spectra (FAS) at high frequencies. An important part of the site response is defining κ_0 at the site, as it has been interpreted to represent the small-strain damping at the site and it controls the high-frequency components of motion, which are generally significant for response of sensitive components at nuclear power plants. Higher κ_0 values correspond to

higher small-strain damping, which in turn corresponds with lower values of FAS at high frequencies.

Two datasets were available to the GMM TI Team for the evaluation of κ_0 that included nearby recordings on the same geologic unit as the site: the Temporary Array GMDB from Quiros and Sloane (2023), and the Duynefontyn GMDB. The GMM TI Team created a logic-tree for the κ_0 values from the Temporary Array GMDB, and the Duynefontyn GMDB to display the mean and epistemic uncertainty on κ_0. The GMM TI Team had a strong preference for the Duynefontyn station data over the Temporary Array data because it reflects measurements at the project site with multiple depths and two locations, robust site-specific site corrections, plus multiple frequency bands and smoothing approaches. Within the Duynefontyn GMDB the GMM TI Team had a strong preference for the κ_0 values obtained from smoothed Fourier spectra as the value is impartial to the choice of frequency band. From the κ_0 logic-tree a mean and sigma can be derived by examining the cumulative density function. This distribution is incorporated into the site response logic-tree by using the mean and sigma to develop three equivalent branches.

Nonlinear properties of rock materials are difficult to measure directly in the laboratory due to fractures from the coring process and the large shear stresses required to induced nonlinearity. Given the absence (as far as the GMM TI Team could determine) of an available laboratory in South Africa with the appropriate resonant column, torsional shear, or cyclic triaxial equipment to measure these properties, the difficulty with transporting samples internationally, and the small impact on the site response calculations, the GMM TI Team instead relied on a range of existing modulus reduction and damping (MRD) curves for bedrock instead of developing site-specific curves.

The materials at the site can be characterised as soft to very hard rock. Due to the stiffness of the site, strains induced in the subsurface will be limited and the impact of nonlinear soil properties should be minimal. The logic-tree for MRD curves included two branches that represent two different sets of MRD curves, assigned based on the V_S of the material. The GMM TI Team assigned equal weights to these branches in the logic-tree.

Two approaches, presented at Workshop 2, are available to incorporate model error in the SAFs . Alternative 1 is to add model error as an additional uncertainty component such that it is combined with the epistemic uncertainty associated with the material characterisation. This alternative assumes that the model error is uncorrelated from all other sources of epistemic uncertainty, and thus the variances are summed to represent the total epistemic uncertainty in the SAF. Alternative 2 is to use model error as the minimum epistemic uncertainty in the SAF. This assumes that the model error cannot be separated from the parametric uncertainties in site response and is only considered when the parametric uncertainty falls below the model error. Alternative 2 has been applied in several recent projects (including the SSHAC Level 3 PSHAs for Thyspunt, Hanford, Spain, and Idaho National Laboratory). The TI Team assigned equal weights of 0.5 to Alternative 1 and Alternative 2 for incorporating the model error, because both alternatives were considered equally valid and represent reasonable methods to incorporate model error.

The GMM TI Team performed site response analyses for 60 randomised profiles for each of the end-branches of the site response logic-tree using a site response analysis. Input motions were developed using Random Vibration Theory (RVT) and scaled to match seven intensity

levels for the reference rock condition (PGA = 0.05, 0.1, 0.2, 0.4, 0.8, 1.6, and 3.2 g) at three magnitudes (**M** 5.5, **M** 6.5, **M** 7.5). Thus, 60 randomisations for 408 terminal branches, three magnitudes, and seven intensity levels yields 514,080 site response analyses. The results for one terminal branch for a **M** 6.5 and PGA of 0.4 g are shown in Figure ES-7.

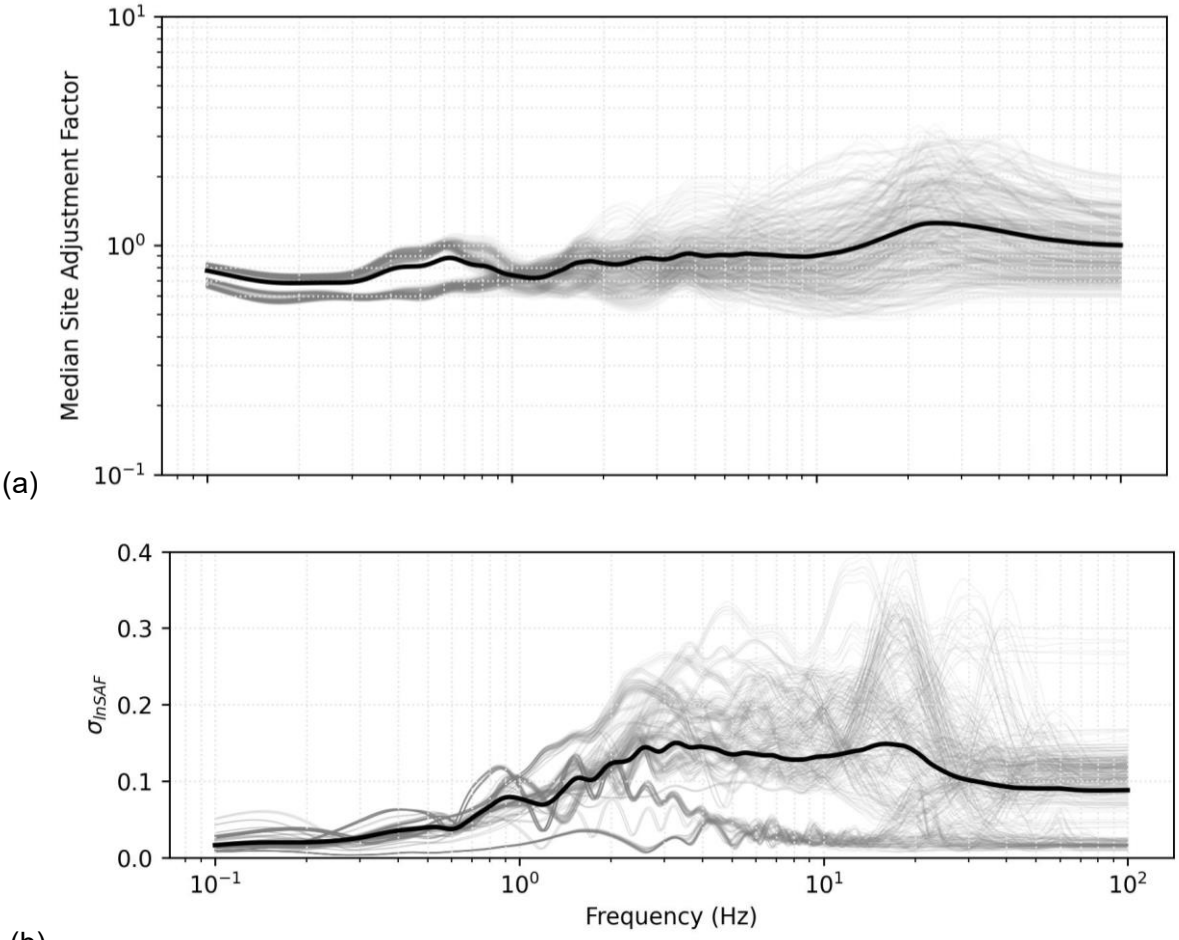

Figure ES-7. A) SAF and b) $\sigma_{\ln SAF}$ Vs frequency for M 6.5 and PGA = 0.4 g intensity input motion. Thin grey lines represent median SAFs for each of the 408 terminal branches of the logic-tree, bold lines represent weighted average SAFs and $\sigma_{\ln SAF}$.

Figure ES-8 shows the median SAF values across terminal branches for a given κ_0 value. For frequencies below 1 Hz, the median SAF for the three κ_0 values are indistinguishable because κ_0 predominantly affects high oscillator frequencies. Thus, the difference between these κ_0 values is more apparent for frequencies above 1 Hz, where the SAF values increase as κ_0 decreases.

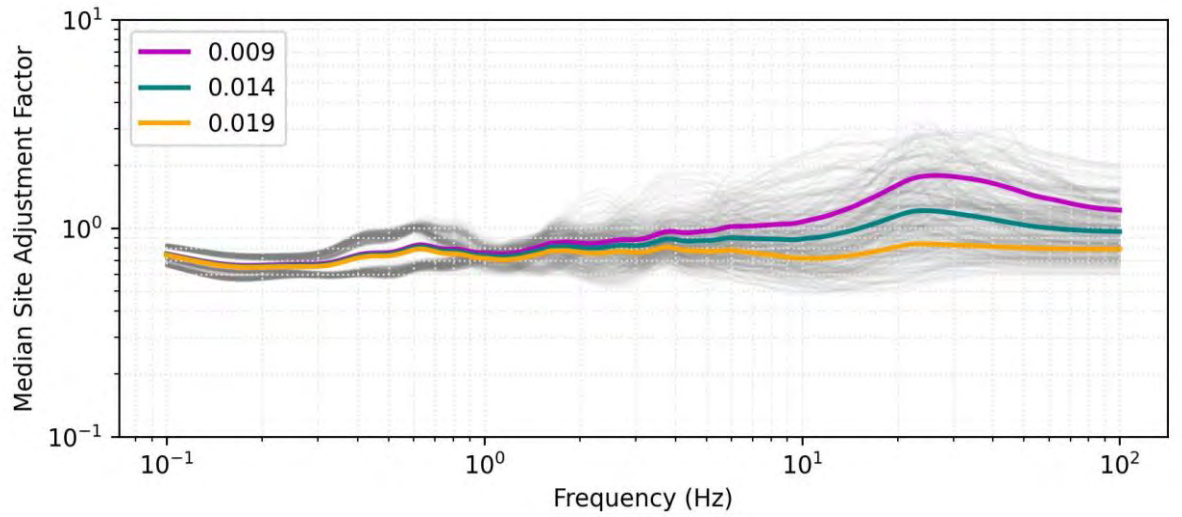

Figure ES-8 . SAF vs frequency for M 6.5 and PGA = 0.4 g intensity input motion. Thin grey lines represent median SAF for each of the 408 terminal branches of the logic-tree, bold coloured lines represent median SAF for all terminal branches corresponding to nodes of the κ_0 level of the logic-tree.

Typical logic-trees contain many branches, thus fully sampling the logic-tree potentially requires performing several thousand site response analyses. Incorporating this many results into the hazard calculation is computationally difficult, so Rodriguez-Marek et al. (2021) proposed an approach to re-sample the weighted distribution of computed SAF into a manageable number of SAFs (usually between five and seven) that together capture the distribution associated with the full logic-tree. The standard deviation of the SAF, representing the epistemic uncertainty associated with the logic-tree (σ_{ep}), is also computed and quantifies the epistemic uncertainty associated with the site response logic-tree. The GMM TI Team decided that the bi-modal distribution of SAFs at frequencies less than 1 Hz would not be well represented using an odd-numbered discrete distribution in which the branch with the highest weight would fall between the two groups of SAF values where there are no data. Thus, the GMM TI Team decided to use a 6-point distribution. The site amplification model considers the influence of the intensity of the reference motion, as quantified by Sa_{ref}, and the earthquake magnitude on the SAF, as well as the epistemic uncertainty.

Hazard Results

All components of both the SSM and the GMM were summarised in a Hazard Input Document (HID). In this way, the TI Teams ensured that the transmittal of the logic-trees representing the SSM and GMM to the HAT was proper, complete and accurate. PSHA calculations were performed using the computer program HAZ45.3. This program was validated as part of the Pacific Earthquake Engineering Research (PEER) centre PSHA Code Verification Project (*Probabilistic Seismic Hazard Analysis Code Verification. Report No. 2018/03. Pacific Earthquake Engineering Research Center*). Custom modules added to the code during the PSHA study underwent additional verification and validation as described in the project Verification and Validation Plan (VVP). The hazard calculations were run for the 10 target oscillator frequencies identified previously. Disaggregation was then performed at selected oscillator frequencies and AFEs.

Each hazard analysis was performed for 16 targeted ground-motion levels, which are consistent for all periods: 0.00001, 0.0025, 0.005, 0.01, 0.025, 0.05, 0.1, 0.2, 0.3, 0.35, 0.45, 0.7, 1, 2, 3, and 12g, with the exception of frequencies of 5, 10, 20, and 25 Hz where an additional analysis at 18g was performed in order to determine the 10^{-8} uniform hazard response spectra (UHRS). Linear interpolation in log-space was used to obtain the acceleration values at required AFEs. The hazard calculations were then repeated to compute the total mean hazard value at each of the target oscillator periods for AFEs of 10^{-4}, 10^{-5}, and 10^{-6} to obtain the disaggregation at each AFE. To capture the three epistemic branches for the GMM developed for reference rock conditions, the nine aleatory variability models implemented, and the 12 SAFs, a total of 324 input models were used in the hazard analysis.

Figure ES-9 depicts the total mean hazard curves for each of the ten oscillator frequencies for the KNPS, although the results are nearly identical for new-build site at Duynefontyn. The dashed lines show the three AFE values used in the disaggregation. Figure ES-10 shows the fractile results for KNPS for 100 Hz.

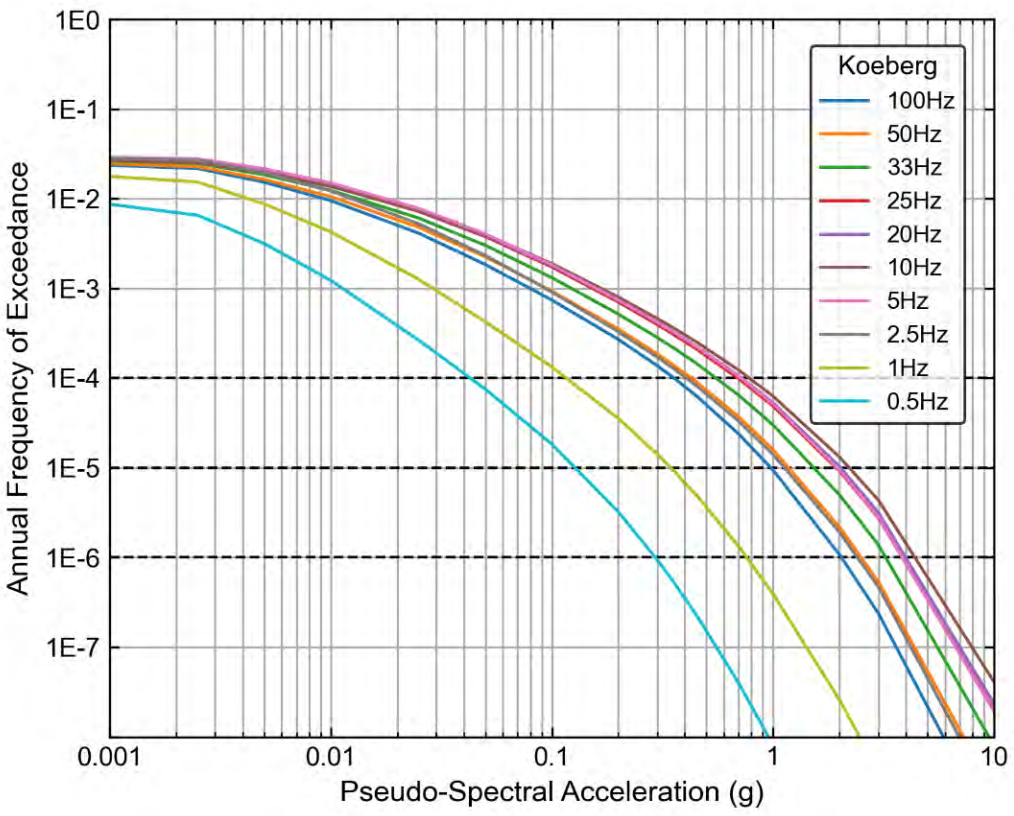

Figure ES-9. Hazard results for the KNPS.

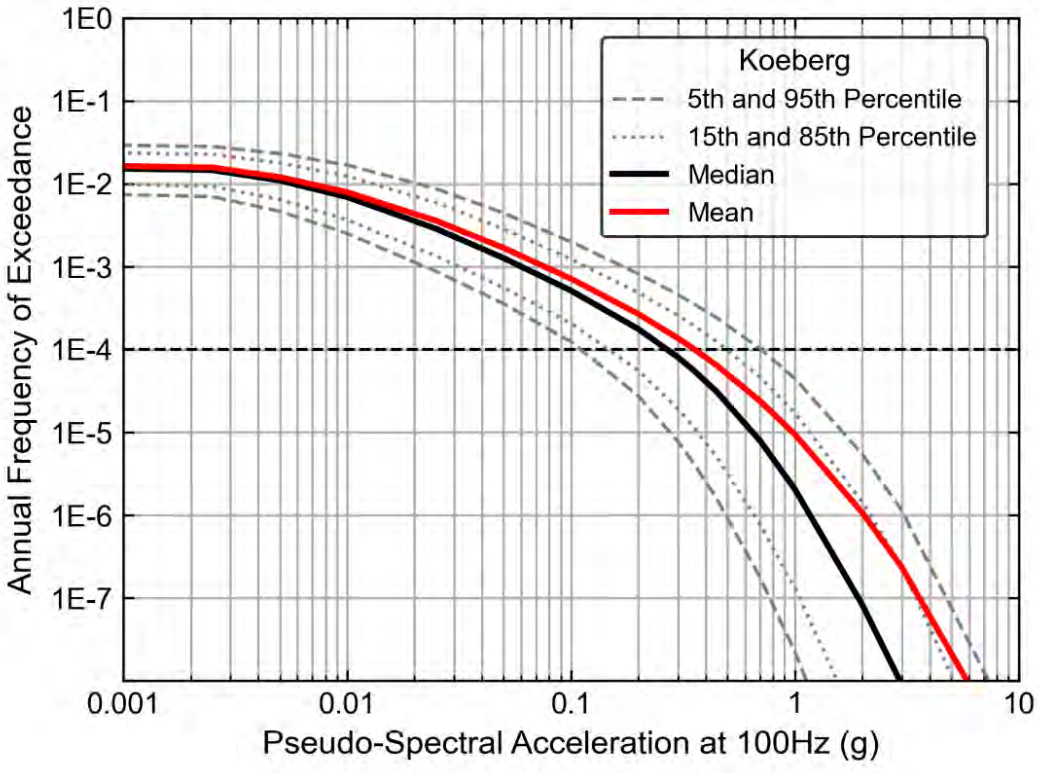

Figure ES-10. Fractile hazard curves for the host zone at 100 Hz at the KNPS.

As evident in Figure ES-11, the total hazard is dominated by the contribution from the SDZ at AFEs less than 10^{-2}. Figure ES-11 shows the results for the 10 Hz, but the results for the other oscillator frequencies are similar, except at 0.5 Hz, where the contribution from the Groenhof Fault contributes slightly more to the total hazard. This is not surprising because the activity rate in the SDZ is higher than the other source zones and the earthquakes in this zone are closest to the site.

Disaggregation of the hazard (Figure ES-12) shows that earthquakes with approximately **M** 6 located close to the site are the dominant contributors to the hazard.

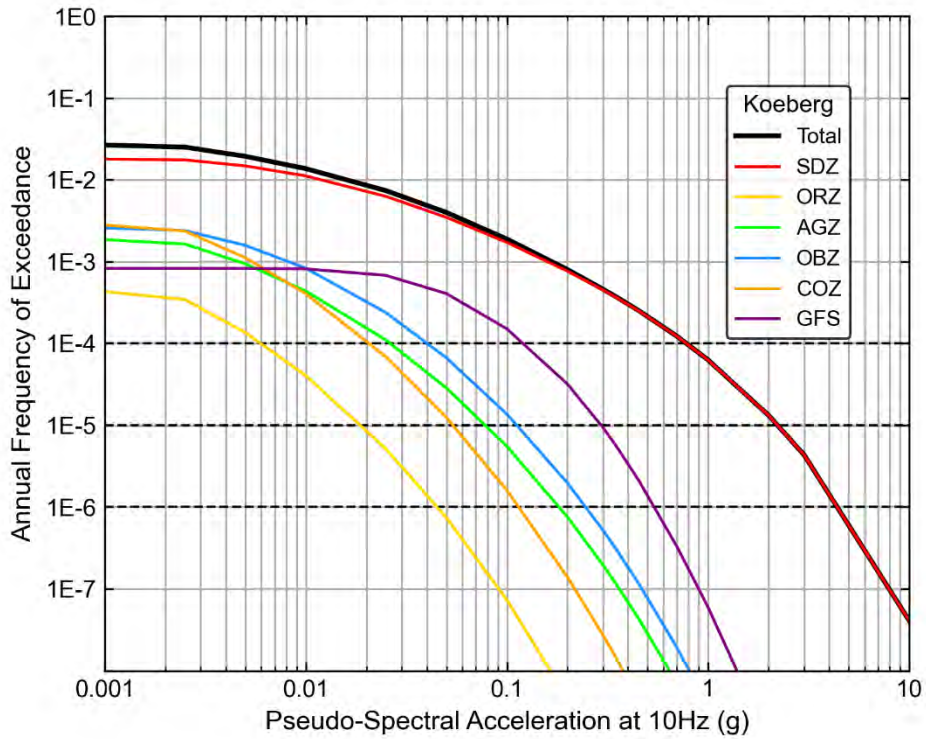

Figure ES-11. Source contribution hazard curves for 10 Hz at the new build site at Duynefontyn.

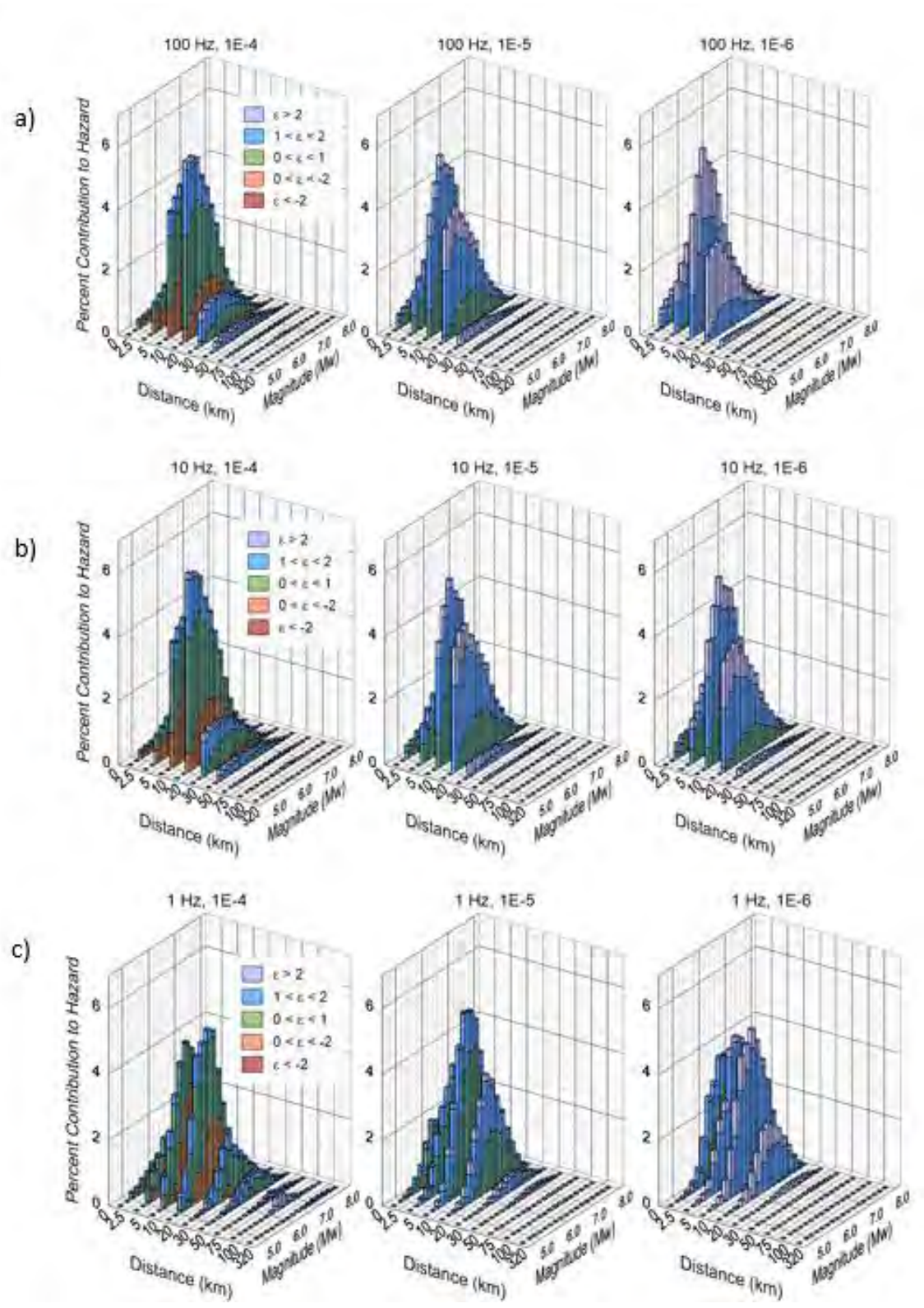

Figure ES-12**. Disaggregation for three AFEs at (a) 100 Hz, (b) 10 Hz, and (c) 1 Hz at the KNPS.**

These hazard curves were then used to generate UHRS at selected AFEs. The ground-motion response spectrum (GMRS) was calculated in accordance with ASCE/SEI 43-19. A

comparison of the GMRS with the UHRS for AFEs of 10^{-4} through 10^{-5} is presented in Figure ES-13.

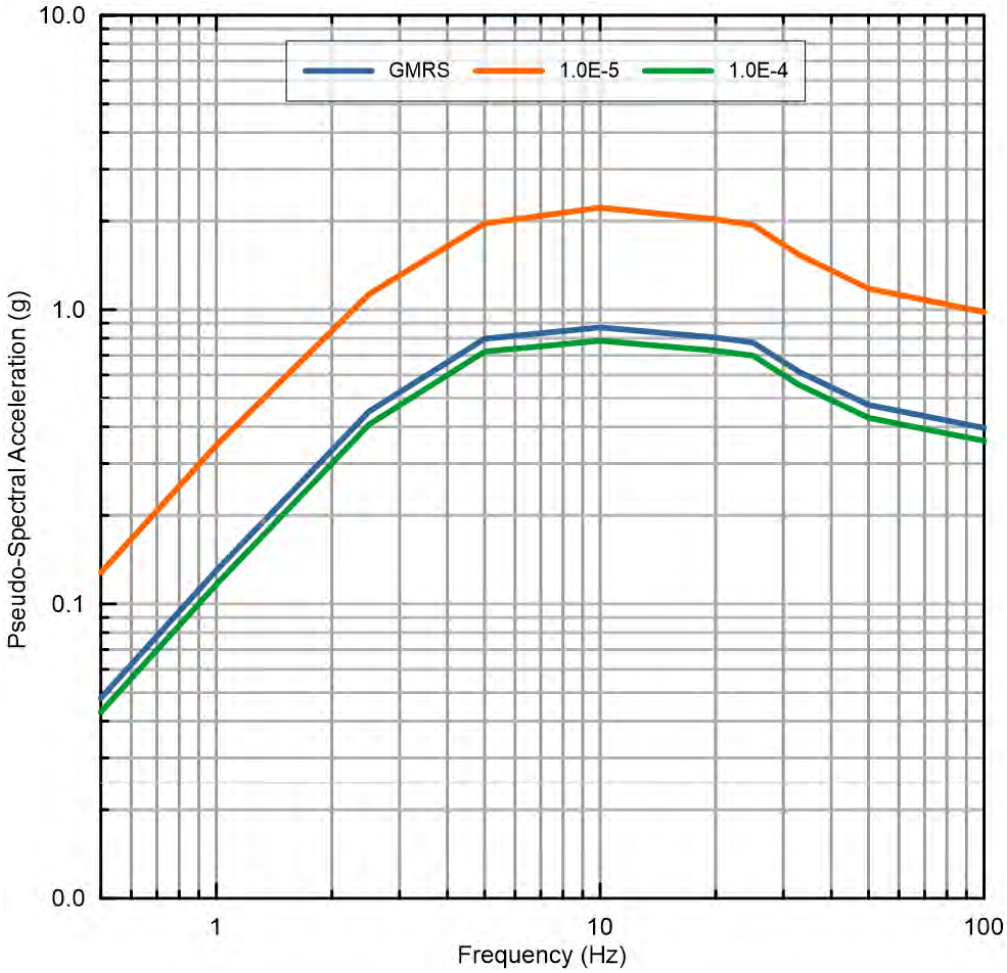

Figure ES-13. Design response spectrum for the KNPS compared to the UHRS at 10^{-4} and 10^{-5}.

To provide some contextual comparisons for the horizontal GMRS at the new build site at Duynefontyn and the KNPS, the design basis response spectra are compared with the GMRS from three nuclear power plant (NPP) sites in the Eastern United States. The GMRS are compared in Figure ES-14, which also shows the USNRC RG 1.60 design response spectrum anchored at 0.30g. These GMRS were developed by the USNRC staff as part of the review of all updated seismic hazard curves for all US commercial NPPs following the accident at the Fukushima Dai-ichi NPP, and in response to USNRC direction.

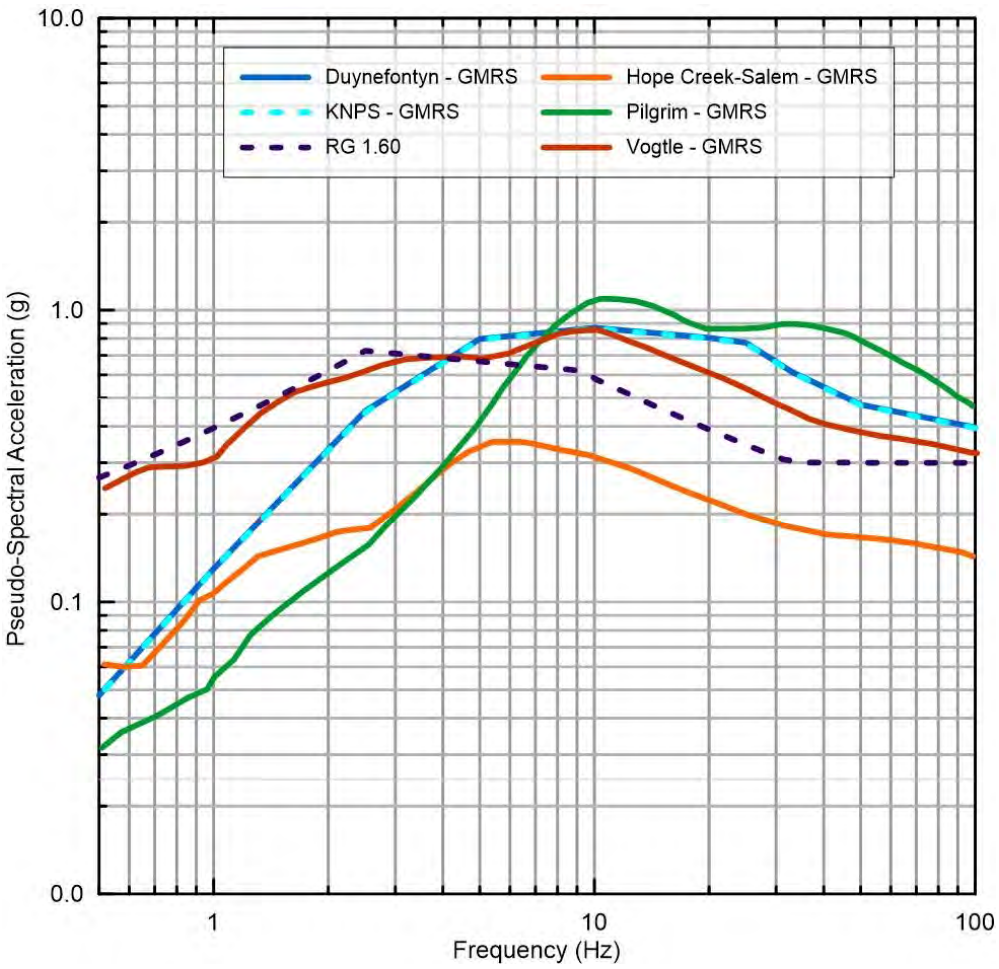

Figure ES-14. Comparison of the GMRS for the new-build at Duynefontyn and the GMRS for the KNPS with the GMRS for three NPP sites in the Eastern United States. A USNRC RG 1.60 design response spectrum anchored at 0.30 g is also shown.

Conclusion

In the evaluation phase of the project, the TI Teams assessed a wide range of available geological, geophysical, seismological, and geotechnical information. During the integration phase, the TI Teams constructed the SSM and GMM that captured the CBR of TDI. All the decisions used to construct the logic trees in the SSM and GMM and the associated weights for alternatives were supported by defensible technical bases that are fully documented in this report. The SSHAC process, including evaluation, integration, and documentation were thoroughly reviewed and accepted by the PPRP. By closely adhering to the SSHAC process, the TI Teams accounted for epistemic uncertainty and aleatory variability in the SSM and GMM. These uncertainties and variabilities are also properly accounted for in the hazard results. Therefore, the Duynefontyn PSHA provides Eskom with an up-to-date and defensible seismic hazard characterisation that meets the regulatory requirements for the LTO license of the KNPS and the license application for a potential new-build at the Duynefontyn site.

ACKNOWLEDGEMENTS

The authors of this report are the 13 members of the Technical Integration (TI) Teams and Hazard Analysis Team, who, in accordance with the requirements for a SSHAC process, assume exclusive intellectual ownership of the Seismic Source Model (SSM), Ground Motion Model (GMM) and hazard results presented herein. This does not imply that the TI Team members can claim the sole credit for the tremendous body of work which contributed to, and are reported in, this report. It was only made possible through the stellar contributions made by many individuals.

Credit must first be given to Eskom for embracing the SSHAC process and setting out to achieve the highest possible levels of regulatory assurance with regards to assessment of the seismic hazard at the Duynefontyn site. The TI Teams are grateful for the trust that was placed in us to undertake this study. Particular thanks are due to Israel Sekoko and Frans van Mosseveld (Eskom) for their support of the project effort and numerous efforts to ensure the project remains on track. Many other people at Eskom (past and present) also contributed greatly to the development and success of the project in a variety of ways. The list (which is unlikely to be comprehensive enough) includes Sadika Touffie, Neil Foster, Anita Kilian, Babalwa Lebaya, Kashif Marcus, Maria Modise, Melvin van Zyl, Emuel Venter, Geneen Williams, Andre Nel, Irené Saayman and Suzette Laas.

The project was coordinated by the Council for Geoscience (CGS) in South Africa. The executive management of the CGS is thanked for their support of this project, especially the CEO Mr Mosa Mabuza and Executive Managers Dr David Khoza and Mr Willem Meintjes. We also extend our thanks to the following managers for their support; Taufeeq Dhansay, Willem Meintjes (in his capacity as manager), Nomvelo Mkhize, Thabo Molikoe, Magda Roos and Supi Tlowana.

Practical project execution depended on the contributions of several CGS staff members. Johann Neveling, Project Manager for the study, guided us through numerous contractual, logistical, administrative, and bureaucratic obstacles. He was supported by the Emmanuel Chirenje as Assistant Project Manager, who also actively participated in or supported several field investigations. Chameney Engelbrecht and Gosia Paweska were alternately responsible for all administrative duties without which this project would not have been possible. Annabel Percy-Lancaster, Kwena Komape and Christo Craill also made numerous contributions to ensure the success of all project activities. This included the three formal Workshops, which also benefited from the graphic design by Jane Abraham.

The Duynefontyn PSHA was executed in accordance with nuclear guides and standards, which necessitated the establishment and implementation of an Integrated Management System (IMS) to guide all work. The CGS's IMS for nuclear project was developed, improved, and maintained by many people over several years. Chief amongst these is Annabel Percy-Lancaster, who assumed overall responsibility for ensuring the IMS achieved ISO 9001:2015 certification, was maintained and appropriately implemented during the project. Important contributions to the development of the IMS were made by Jannie van der Merwe, Michelle Gouverneur, Johann Neveling, Kwena Komape and Emmanuel Chirenje. Contributions to the development of guides and procedures under the IMS were also made in particular by Paula Albini, Dawn Black, Hayley Cawthra, Emmanuel Chirenje, Debbie Claassen, Christo Craill, Taufeeq Dhansay, Nicky Flint, Neo Moabi, Ponani Mthembi, Khuliso Nedzingahe and Johann

Neveling. The ground geophysics, offshore mapping and seismic network technical teams, listed further below also made valuable contributions to CGS procedures. Sharon Nkoana and Kgaogelo Kekana provided invaluable assistance in the collation of quality and safety records for the project quality assurance data pack (QADP).

The Duynefontyn Data Collection investigations benefitted tremendously from contributions made by a large number of people. In addition to Hayley Cawthra, Thifelimbilu Mulabisana, Debbie Claassen and Ryan Coppersmith (co-authors of this report), important contributions to studies relevant to the SSM were made in the field by Dawn Black, Taufeeq Dhansay, Neo Moabi, Ponani Mthembi, Emmanuel Chirenje, Vindina Mitha, Portia Munyangane, Andisani Makhado, Zusakhe Nxantsiya, Simon Sebothoma, Matome Sekiba, Melvin Sethobya, (all of the CGS), and Christopher Slack (GEI Consultants) and Martitia Tuttle (M. Tuttle and Associates). Michael MacHutchon, Wilhelm van Zyl, Willem Kupido, Uzair Adam and Norman Krantz are thanked for their contributions to various offshore data collection activities. A special thanks is extended to Dawn Black and Ponani Mthembi who managed the drilling programme at the Duynefontyn site, supported by Mzoli Breakfast, Zusakhe Nxantsiya and Tshiamo Moleele. We are grateful to the drilling teams of Geomech Africa and EDRS and especially Brett Mannix (Geomech Africa) for their efforts to satisfy the sometimes-unusual requirements of the project geologists. Muneiwa Mukwevho and Clement Ndou (CGS) assisted with the hyperspectral scanning and storage of the core.

For the development of the GMM the measurement of shear-wave velocity profiles was indispensable. In this regard Brassnavy Manzunzu, Thifelimbilu Mulabisana, Vincent Jele, Reuben Mantsha, Zusakhe Nxantsiya, Simon Sebothoma, Melvin Sethobya and Leonard Tabane all contributed to the surface measurement of velocity profiles at the Duynefontyn site and selected seismic stations. The data was analysed and interpreted by Brady Cox and Aser Abbas (Utah State University). Borehole PS logging at Duynefontyn was undertaken by Wireline Workshop under the supervision of Joseph Matamela (CGS). We are grateful for the stellar efforts by Joseph Matamela and Simon Sebothoma (CGS) to undertake the wave picking of PS logging data. Brady Cox is thanked for his patient guidance and oversight of almost all work related to surface (MASW and MAM) and borehole (PS Logging) shear-wave measurements as well as analyses of generated data; his contribution has been immense. The team is also grateful for the fruitful interactions with Bruce Engelsman (SRK) and Alten du Plessis (Open Ground Resources) on the site response work they performed at the Duynefontyn site. Vincent Jele, Reuben Mantsha, Zusakhe Nxantsiya, Matome Sekiba, Melvin Sethobya and Leonard Tabane are commended for the installation of borehole seismograph stations at the Duynefontyn site.

The support of Jurina le Roux, Eskom Environmental Officer at Duynefontyn, is gladly acknowledged. We also extend our gratitude to all landowners for granting the field teams access to their property. We thank Paul Bierman of the University of Vermont for many discussions on dating results which greatly aided the technical team.

Frederick Stapelberg and Kefyalew Tegegn (CGS) made important contributions to the source data on geological stress in the Western Cape Province, while the stress analysis was undertaken by Kevin Smart, David Ferril and Adam Cawood (Southwest Research Institute). The compilation of the historical earthquake catalogue was led and coordinated by Paola Albini who, together with Nicky Flint (CGS) went to great effort to source historical accounts of earthquake effects for the historical seismology study. Ian Saunders re-assessed the

available records of seismicity in the region of Duynefontyn and is thanked for his input into the project catalogue. We are especially grateful for the work and professional interactions of Dr Laura Gulia (University of Bologna), who was a proponent expert at Workshop 2 and was then invited to participate in the work of the SSM TI Team in a supporting capacity, culminating in a key presentation at Workshop 3.

Several other Specialty Contractors and scientists at the CGS undertook additional investigations at the behest of the TI Teams. For this we extend our gratitude to Diego Quiros and Alastair Sloan (both University of Cape Town), Ben Edwards (Intraseis), Christopher de la Torre and Brendon Bradley (Bradley Seismic), Andrzej Kijko (University of Pretoria), Leonie Maré, Janine Cole, Brassnavy Manzunzu, Minenhle Buthelezi, Emmanuel Chirenje, Vincent Jele, Reuben Mantsha, Zusakhe Nxantsiya, Simon Sebothoma, Matome Sekiba and Leonard Tabane (all CGS). Oliver Barker (Banzi Geotechnics) is thanked for his interactions with the SSM TI Team and sharing of information on the bedrock mapping of the Koeberg footprint.

Both the SSM and the GMM TI Teams are indebted to the numerous Proponent Experts (listed by name in Section 2.6) who participated in Workshop 2 and made an enormous contribution to the development of the SSM and GMM models. We are grateful for their willingness to attend the Workshop, with many travelling very large distances to participate in discussions with the TI Team members. The openness and good will of all the Proponent Experts as they engaged in this process was very much appreciated.

The work presented in this report would not have been possible without the technical and editorial support of many people who are not listed as authors. We would like to thank the following for their invaluable contributions from Slate Geotechnical Consultants: Charlie Carasis, Tom Clifford, Kathryn Francis, Paige Hval, Sarah Smith and Michael Yust.

At CGS, Melissa Cawthra and Zusakhe Nxantsiya provided invaluable support in the editing of the report and made many improvements to the draft and final versions of this report. Khuliso Nedzingahe is thanked for his curation of spatial data.

Last, we thank the members of the Participatory Peer Review Panel (PPRP) – Julian Bommer, Jon Ake, Raymond Durrheim (University of the Witwatersrand), Marc Goedhart (Kainos South Africa), Tom Rockwell (San Diego State University) and Jon Stewart (University of California) for their willingness to participate in this project, providing their time and expertise and thereby linking their reputations to the Duynefontyn PSHA. Their diligent work and continuous constructive feedback benefitted the project immensely. The commitment they displayed at the Workshops, which included a full day of extra work after the Workshop to ensure their report was finalised before their departure, is greatly appreciated. We are also grateful that the PPRP made several members available to attend Working Meetings, as well as several virtual meetings of the TI Teams. We extend our thanks for the additional work done by Julian Bommer who, as chairman of the PPRP, kept the review on course and aligned with the project objectives.

TABLE OF CONTENTS

LIST OF FIGURES

LIST OF TABLES

LIST OF ABBREVIATIONS

Abbreviation	Explanation
$\|A(f)\|$	Fourier acceleration spectra
$\|A(f)\|$	Fourier amplitude spectrum
$\|H(f;T,\zeta)\|$	frequency response function
1D	depth
2D	depth and surface location
3D	three-dimensional
a	acceleration
A_0	offset
$a_{17}R_{RUP}$	magnitude-independent anelastic attenuation
ACR	active crustal regions
AF	amplification factor
AFE	annual frequency of exceedance
AGZ	Agulhas Zone
amsl	above mean sea level
ANS	American Nuclear Society
ANSI	American National Standards Institute
ANSS	Advanced National Seismic System
A_R	slope factor, defined in ASCE/SEI 43-19
AR	aspect ratio
AS	acceleration spectrum
ASCE	American Society of Civil Engineers
ASCE/SEI	American Society of Civil, Engineers Structural Engineering Institute
asl	above sea level
ASPASA	Aggregate and Sand Producers Association of Southern Africa
BE	backedge of terrace
BH	borehole
BOXER	the Centroid method of Gasperini et al (1999)
bsl	below sea level
b-value	slope
cat	catalogue
CBR	centre, body, and range
CBR of TDI	centre, body and range of technically defensible interpretations
CC	Stepp plot completeness cutoff
CDF	cumulative density function
CENIEH	Centro Nacional de Investigación sobre la Evolución Humana [English: National Center for Research on Human Evolution]
CER	Ceres

CERES	task-specific catalogue, using data primarily from the South African National Seismological Database
CEUS	Central and Eastern United States
CF	Coega fault
CFR	Cofe of Federal Regulations
CGS	Council for Geoscience
CKBC	Ceres-Kango-Baviaanskloof-Coega
C-Kk	Kirkwood Formation Mudstone
CN	cosmogenic nuclides
COL	Colenso Fault
COZ	Combined Outer Zone
c_Q	velocity used to estimate *Q(f)*
CY	CY14 predictions
D	material damping
D/N	day-to-night ratio
$D_{20\text{-}80\%}$	signifigant duration for the accumulation of 20-80% of the final Arias intensity
D85	depth above which 85% of earthquakes occur
D90	90% probability value
D90	depth above which 90% of earthquakes occur
D95	depth above which 95% of earthquakes occur
Davg	average displacement
DDC	Duynfontyn Data Collection (PSHA support studies)
DDC2	Catalogue for area in and around Ceres as determined by Ian Saunders (CGS)
DE	damage earthquake
DEM	digital elevation model
DEM	digital elevation model
DFT	Discrete Fourier Transform
DH	downhole
D_{hys}	nonlinear hysteretic damping
DM	standard deviation
Dmax	maximum displacement
D_{min}	small-strain damping
DMRE	Department of Mineral Resources and Energy
d_{res}	resolution depth
$D_{rms}(T,\zeta_n)$	root-mean-square duration
DRS	design response spectrum
DS	displacement spectrum
DS	dip slip (combined normal and reverse)
DSHA	deterministic seismic hazard analysis

E[**M**]	expected value of the true moment magnitude
E_i	given earthquake from source *i*
ELIM	Elim
EPRI	Electric Power Research Institute
EPRI-SOG	Electric Power Research Institute Seismicity Owners Group
EQCLUSTER	Computer code for earthquake analysis (EPRI-SOG, 1988, volumes 1-3)
EQL	equivalent-linear
ETAS	Epidemic-type aftershock sequence
FAS	Fourier amplitude spectra
FAS	Fourier amplitude spectrum
f_c	source corner frequency
FDD	focal depth distribution
f_{hi}	upper frequency
f_{lo}	lower frequency
FM	fundamental mode
FOCMEC	focal mechanism determinations
G	secant shear modulus
g(R)	geometric spreading function
Ga	billion years ago
GCMT	Global Centroid-Moment-Tensor
GF	Gamtoos fault
GFS	Groenhof fault source
GHF	Groenhof Fault
GIS	Geographic Information System
G_{max}	small strain shear modulus
GMC	ground-motion characteristics
GMDB	ground-motion databases
GMICE	ground-motion intensity correlation equation
GMM	ground motion model
GMM TI	Ground Motion Model Technical Integration
GMPE	ground-motion prediction equation
GMRS	ground-motion response spectra
GNSS	Global Navigation Satellite System
GPS	Global Positioning System
GR	Gutenberg-Richter
G-R	Gutengerg-Richter (equation)
GRHM	Grahamstown
h	kernal bandwidth
h(**M**)	saturation length
h[**M**]	near-source saturation distance

HAT	Hazard Analysis Team
HDR	hypocentral depth ratio
HEM	hybrid empirical method
HID	hazard input document
H_P	P_F (selected from ASCE/SEI 43-19 Table1-1)
H_{seismo}	seismogenic thickness
HVSR	horizontal-to-vertical spectral ratio
i	source
IAEA	International Atomic Energy Agency
iasp91	velocity model
IDP	intensity data points
IDP	intensity data point
IGS	International Global Navigation Satellite System (GNSS) Service
im	Inensity Measure
IMS	Integrated Management System
INL	Idaho National Laboratory
INPO	Institute if Nuclear Power Operations
INSAG	International Nuclear Safety Advisory Group
IRIS	Incorporated Research Institutions for Seismology
ISC	International Seismological Centre
ISO	International Standards Organization
J	the entire length of the catalogue is subdivided into J time periods
j	individual time periods
ka	thousand years ago
KAF	Kango fault
KF	Kouga fault
KKF	Kalbaskraal-Klipheuwel Fault
KNPS	Koeberg Nuclear Power Station
K-S	Kolmogorov-Smirnov
K-S	Kijko-Sellevol
K-S-B	Kijko-Sellevol-Bayes
ky	thousand years
kya	thousand years ago
L	magnitudes obtained as part of DDC2
L	subsurface horizontal rupture length
LANDSAT	land remote sensing satellite
LEPH	Lephepe
LGM	Last Glacial Maximum
LiDAR	light detection and ranging
LL	maximum likelihood method

ll	log likelihood
LLNL	Lawrence Livermore National Laboratory
lnSA	natural log of spectral acceleration for a given period
LR	layering ratio
LR	layering ratio
LTO	long-term operation
M	*moment magnitude*
M	magnitude
M_L	local magnitude
M_w	moment magnitude
M	moment magnitude
M*	approach that adjusts magnitudes to correct bias
M|X	vector of magnitudes converted from other magnitude types
M_0	seismic moment
$m_0(T,\zeta_n)$	zeroth spectral moment
Ma	million years ago
MAM	microtremor array measurements
MASW	multi-channel analysis of surface waves
MATJ	Matjiesfontein
m_b	body wave magnitude
m_{b1}	a short period body wave magnitude
m_{bLg}	Lg-wave magnitude
MBMmax	maximum magnitude of potential mining events
m_{btmp}	short-period body wave magnitude, with a depth fixed at the surface
M_{BUL}	magnitudes reported by Goetz Observatory
M_C	completeness magnitude
MCE	maximum credible earthquake
Mchar	charectoristic magnitude
Mchar	characteristic rupture length
M_D	duration magnitude
MEEP	Computer Code, Macroseismic Estimation of Earthquake Parameters
MEEP2	Computer Code, Macroseismic Estimation of Earthquake Parameters (version 2.0)
MESE	Mesozoic extended crust
MFD	magnitude-frequency distribution
m_{i-1} to m_i	magnitude interval
MIL	Milnerton Lineament
MIS	Marine Isotope Stage
M_L	local magnitude
MM	multi-mode

Mmax	maximum magnitude
MMI	modified Mercalli intensity
Mmin	minimum magnitude
MRD	modulus reduction and damping
M_W	moment magnitude
$M_{W,crit}$	critical moment magnitude
My	million years
n	number
N*	corrected count
NGG	Nuclear Geo-Hazards Group
$N_i(E_i)$	annual rate of the given earthquake per year from source *i*
n_{ij}	probability of observing the recorded number of earthquakes
NM	normal
NMESE	non-Mesozoic extended crust
NNR	National Nuclear Regulator
NPP	nuclear power plant
NR	Newly Retr.
n_{rup}	total number of ruptures
n_{Ti}	number of response spectral ordinates for rupture scenario rup_i
NUREG	U.S. Nuclear Regulatory Commission technical report designation.
OBZ	Orange Basin Zone
ORZ	Olifants River Zone
OSL	optically simulated luminescence
P	likely explosion
P	probability
p[S]	seismogenic probability
P_2O_5	phosphorus pentoxide
PASA	Petroleum Agency of South Africa
PBMR	Pebble Bed Modular Reactor
P^D	probability of detection
PD	probability of detection method
pd	probability of detection completeness
PDF	probability density function
PE	Port Elizabeth
PEER	Pacific Earthquake Engineering Research
PEGASOS	English translation from German: Probabilistic Seismic Hazard Analysis for Swiss Nuclear Power Plant Sites
PEP	Project Execution Plan
PFS LLC	Private Fuel Storage Limited Liability Company

PGA	peak ground acceleration
$P_i^D(t)$	the P^D of earthquakes in that magnitude bin as a function of time
$P_i^{D_j}$	the P^D of earthquakes in the *i-th* magnitude interval in the time-period *j*
PMT	Project Management Team
PNNL	Pacific Northwest National Laboratory
PPE	personal protective equipment
PPRP	Participatory Peer Review Panel
PS	psuedo-spectral
PS	point source
PSA	psuedo-spectral acceleration
pSA1D	psuedo-spectral acceleration at the ground surface from 1D analyses
pSA2D	psuedo-spectral acceleration at the ground surface from 2D analyses
PSHA	Probabilistic Seismic Hazard Analysis
PTI	Project Technical Integrator
PVHA	probabilistic volcanic hazard analysis
PWF	Piketberg-Willington Fault
PyGMI	Python geoscience modelling and interpretation
Q(f)	anelastic attenuation filter
Q(f)	quality factor
q(r,f)	anelastic filter
Q_0	quality factor
QA	quality assurance
QADP	quality assurance data pack
QCP	Quality Control Plan
r	source-to-site distance
R	fault ruptures
R	Riedel
R	number of observed size measures
R	distance
R	reverse
R'	anti-Riedel
RA	rupture area
RC	radiocarbon
RD	requirement document
R_{epi}	epicentral distance
R_{hypo}	distance to the hypocenter
r_{jb}	surface projection of rupture
R_{jp}	Joyner-Boore distance
RL	rupture length
RLD	rupture length at depth

RLME	Repeated Large Magnitude Earthquake
RMS	root mean square
ROI	region of interest
R_{PS}	equivalent point source distance
R_{RUP}	rupture distance
RSA	Republic of South Africa
r_{up}	closest distance between a site and the three-dimensional rupture plane
rup	vector/list of all rupture scenarios within the database
rup_i	rupture scenario
RVT	Random Vibration Thoery
RW	rupture downdip width
RW_{max}	maximum width of the rupture
RW_{max}	maximum rupture width obtained dividing the seismogenic thickness by sin(dip)
S(f)	site impedance relative to source properties
S[f]	site parameter
SA	Inversion GMDB empirical data
SA	spectral accelerations
Sa(t)	individual spectral ordinate
sa^*_{ref}	surface response spectrum for the host reference condition
SA_{avg}	geometric mean of spectral ordinates over a range of periods
Sa_{avg}	average spectral acceleration
SAC	Seismic Analysis Code
SACS	South African Committee for Stratigraphy
SAF	site adjustment factors
SA_{HP}	spectral acceleration value at the AFE H_P
SAMINDABA	South African Mineral Deposits database
SANRAL	South African National Roads Agency Limited
SANSD	South African National Seismological Database
SANSN	South African National Seismograph Network
SAR	Safety Assessment Report
Sa_{ref}	infleuence of the intensity of the reference motion
SA^{RVT}	predicted spectral ordinate obtained via RVT
SA^{SA}	South African computed spectral ordinate
SAST	South Africa standard time
s_c	aleatory availability in Mchar
SC	sea cliff
SCEP	Safety Culture Enhancement Programme
SCR	stable continental region
SD	standard deviation

SDZ	Saldania Zone
SEI	Structural Engineering Institute
SF	scale factor
SH	seismic housing
SHA	seismic hazard analysis
SLA	shoreline angle
SM	safety management
SNR	signal-to-noise ratio
SRA	site response analysis
SRL	surface rupture length
SS	strike-slip
SSC	seismic source characterisation
SSE	safe shutdown event
SSHAC	Senior Seismic Hazard Analysis Committee
SSHAC EL-2	Senior Seismic Hazard Analysis Committee Enhanced Level-2
SSM	seismic source model
SSM TI	Seismic Source Model Technical Integration
SSR	site safety report
Subd	subdution
SwRI	Southwest Research Institute
t	time
T	period
T	spectral periods
TauP	seismic time calculator
TBF	Table Bay Fault
TDI	technically defensible interpretations
TE	effective time of completeness
TE_{ij}	equivalent time of completeness
Tg	Grahamstown Formation
TI	technical integration
T_{ij}	duration of the completeness time period
TNSP	Thyspunt catalogue
T_S	slip tendency
UCERF	Uniform California Earthquake Rupture Forecast
UHRS	uniform hazard response spectra
$UHRS_{HP}$	uniform hazard response spectrum for AFE of H_P
UHS	uniform hazard spectra (spectrum)
USA	United States Atomic Energy Commission
USAEC	United States of America
USDOE	United States Department of Energy
USNRC	United Stated Nuclear Regulatory Commission

UTC	Universal Time Coordinated
v	events per year, "annual frequency of exceedence"
V&V	verification and validation
$var_{\mathbf{M}}$	average variance of the **M** data used
var_{regr}	regression variance
v_i	rate of observed earthquakes
VR	virtual rupture
VSZ	Vredenburg Shear Zone
VRG	virtual rupture generator
V_S	shearwave velocity
$V_{s,30}$	shear-wave velocity over the top 30 m
V_{S30}	shear-wave velocity over the top 30 m
VSZ	Vrendenburg Shear Zone
VVP	Validation and Verification Plan
W	M_W from Ian Saunders, reported in DDC2
WAACY	Wooddell, Abrahamson, Acevedo-Cabrera and Youngs
WANO	World Association of Nuclear Operators
W-C/B	Worcester and Cango-Baviaanskloof (faults)
WCP	wave-cut platforms
WM	working meetings
WOR	Worcester Fault
WWSSN	World-Wide Standardized Seismograph Network
Z	ground-motion parameter
z	specified ground motion to exceed
z	depth below the top of the subsurface model
$Z_{1.0}$	the depth to material with a shear-wave velocity of 1.0 km/s
$Z_{2.5}$	the depth to material with a shear-wave velocity of 2.5 km/s
Z_{TOR}	distance to top of rupture
β	b value in natural log units
β_0 and β_1	fixed effects regression coefficients
γ	geometric attenuation rate
γ_j	geometric spreading rates
$\gamma\zeta_{NGA}$	epistemic correlations computed using the scenario-to-scenario covariances of the NGA West2 GMPEs
$\gamma\zeta_{RSA}$	epistemic correlations computed using the seven GMPEs developed for this project
δ_{ADD}	deviation linked to additional epistemic uncertainty
δ_{M2M}	deviation linked to model-to-model variability
δ_{SAT}	deviation linked to the choice of saturation model
δx	

ΔZ_{TOR}	relative depth to the top of rupture
$\Delta\sigma$	stress parameter
ε	the number of standard deviations
ε	error term
ε_i	random variable
ε_{ij}	event-and station-corrected residual
ζ	epistemic reduction factor
ζ_{COR}	reduction factor for correlation of epistemic uncertainty
ζ_n and ζ	damping ratio
$\zeta_{\sigma bb,i}$	where ζ is computed on a site-specific basis
$\eta(\boldsymbol{M})$	magnitude-dependent quality exponent
η_i and η_j	random effects that reflect event and station effects respectively
η_j and η	quality exponent
$\boldsymbol{\theta}$	vector of seismic parameters
κ	Spectra decay parameter
κ_0	small strain damping
κ_0	site kappa
κ_0	high-frequency decay parameter at the site
κ_{AS}	κ_0 from the acceleration spectrum
κ_{DS}	κ_0 from the displacement spectrum
$\lambda_{3.0}$	the annual mean activity rate for events of local $M_L \geq 3.0$
λ_i	true rate of earthquakes
λ_{res}	resolution wavelength
μ^*_{lnSA}	possible level of the mean logarithmic amplitude
$\mu_{bb,i}$	overall mean logarithmic prediction relating to rupture scenario rup_i
μ_{lnSA}	global mean amplitude
$\mu_{lnSa,}$	overall mean logarithmic prediction
$\rho^2_{M2M,SAT}$	assumed correlation between the saturation and model-to-model deviations
ρ_{IL}	interlayer correlation
$\rho_{\mu i,\mu j}$	correlation of epistemic deviations away from the mean model between rupture scenario rup_i and rup_j
σ	standard deviation
σ	total ergodic variability
$\sigma[\mathbf{M}]$	Stress as a function of magnitude
$\sigma 1$	maximum principal stress
$\sigma 2$	intermediate principal stress
σ^2_{ADD}	additional epistemic uncertainty
σ^2_{CSAT}	conditional parametric variance associated with near-source saturation
σ^2_{M2M}	model-to-model variability
$\sigma 3$	minimum principal stress

σ_{CSAT}	near-source saturation effects
σ_{ep}	epistemic uncertainty associated with the logic-tree
$\sigma_{ep,LT}$	epistemic uncertainty associated with the logic-tree
$\sigma_{ep,total}$	total epistemic uncertainty in the SAF
σ_{lnSAF}	total aleatory variability
$\sigma_{lnSAF,lin}$	total aleatory variability linear component
$\sigma_{lnSAF,NL}$	total aleatory variability nonlinear component
σ_{lnVs}	standard deviation of Vs
σ_{ME}	model error
σ_{mix1}	standard deviations obtained by using $0.8\varphi_{SS}$
σ_{mix2}	standard deviations obtained by using $1.2\varphi_{SS}$
σ_{MW}	estimate of the error
σ_n	normal stress
σ_{ss}	single-station sigma
τ	ratio of shear stress
τ	interevent standard deviation
τ	between-event ergodic variability
φ	stress ratio
φ	within-event ergodic variability
Φ	the cummulative distribution function of the standard normal distribution
φ_{S2S}	within-event site-to-site variability
φ_{SS}	within-event single-station variability
$\psi(T,\zeta_n)$	peak factor
Ω_0	signal moments

ω^2	Corner Frequency
$\mathbf{M}$	observed moment magnitude
$\hat{X}_i$	single member of $\hat{\mathbf{X}}$
$E[\mathbf{M}\|\hat{X}_i]$	vectors of the expected moment magnitude given another magnitude estimate
$\sigma^2[\mathbf{M}\|\hat{X}_i]$	corresponding varience for each earthquake
$\sigma[\mathbf{M}\|\hat{\mathbf{M}}]$	moment magnitude uncertainty

CHAPTER 1: INTRODUCTION

1. INTRODUCTION

1.1 SCOPE AND PURPOSE OF THE PROJECT

This report documents a probabilistic seismic hazard analysis (PSHA) executed by the Council for Geoscience (CGS) as a Senior Seismic Hazard Analysis Committee Enhanced Level 2 (SSHAC EL-2) process for the Duynefontyn nuclear site, situated to the north of Cape Town, South Africa (Figure 1-1). This work was done under contract (Contract Number 4600062664) for Eskom Holdings SOC Ltd. (Eskom), which operates the Koeberg Nuclear Power Station (KNPS) hosted on the site.

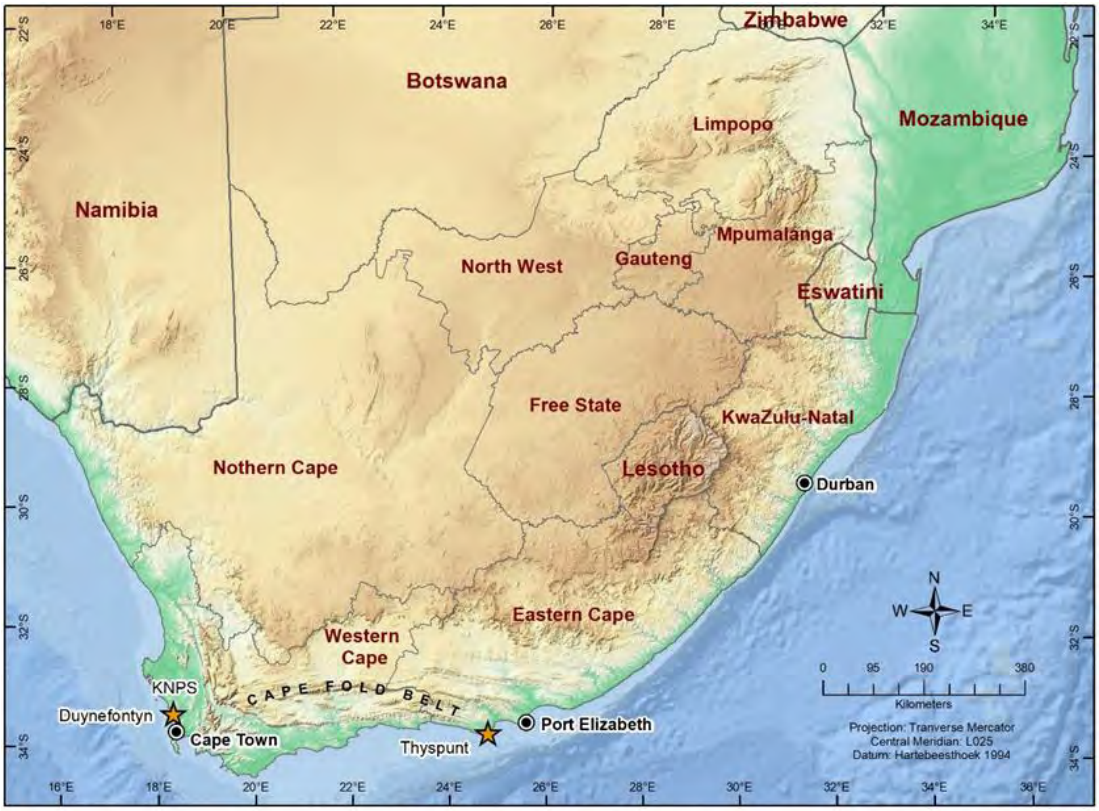

Figure 1-1. Location of the Duynefontyn site, including the Koeberg Nuclear Power Station (KNPS). The Thyspunt site, where a prior SSHAC Level-3 Study (Bommer et al., 2013) was completed in 2013, is also shown.

The focus of the PSHA is exclusively on vibratory ground motions due to natural earthquakes. The purpose of the PSHA is to quantify the earthquake ground-shaking hazard at the KNPS, as well as to inform a nuclear new-build licence application at the Duynefontyn site. The footprint for the new-build installation is defined to the northwest of the KNPS (Figure 1-2). The PSHA will provide input to the Duynefontyn Site Safety Report (SSR), which, in turn, will provide input to the Safety Assessment Report (SAR) that Eskom will submit to the National Nuclear Regulator (NNR) in support of their application to extend the Long-Term Operation (LTO) licence for the KNPS. It will also serve as input to the design of a possible new nuclear power plant (NPP) at the Duynefontyn site.

Figure 1-2. Overhead view of the KNPS and the proposed location for a possible nuclear new build, just to the north of the KNPS, at the Duynefontyn site.

The PSHA study was executed in two phases (Eskom, 2019; Stamatakos and Watson-Lamprey, 2023), with a Baseline PSHA (Stamatakos et al., 2022) succeeded by a PSHA that followed the SSHAC process as specified in NUREG-2213 (regulatory guidance document published by the U.S. Nuclear Regulatory Commission [USNRC], 2018). The Baseline PSHA is supplanted by the Enhanced SSHAC Level 2 PSHA and in this document the term "Duynefontyn PSHA" exclusively refers to the latter.

This chapter describes the scope and objectives of the study, presents an overview of seismic hazard assessments (SHA), and summarises and compares the basic components of deterministic and probabilistic analyses[1]. A summary of prior seismic hazard analyses conducted for the KNPS or locations near the Duynefontyn site are provided to establish the context of the current PSHA. The final section of the chapter identifies the deliverables in terms of the specific seismic hazard and seismic engineering outputs from the Duynefontyn PSHA.

[1] The important components of a generic PSHA are summarised here. A detailed explanation and specific description of the Duynefontyn PSHA is provided in the remaining chapters of this report.

1.2 SEISMIC HAZARD ANALYSIS

As illustrated diagrammatically in Figure 1-3, the ground shaking at a nuclear power plant site depends on several geological, geotechnical, and seismological factors. These include the location, depth, rupture type, aspect ratio, magnitude, and stress drop at the earthquake's source. It also includes the geometric spreading and attenuation of earthquake energy along the path away from the fault rupture toward the site. Finally, it includes the effects of impedance contrasts and damping due to the near-surface rock and soil strata as the earthquake energy reaches the ground surface.

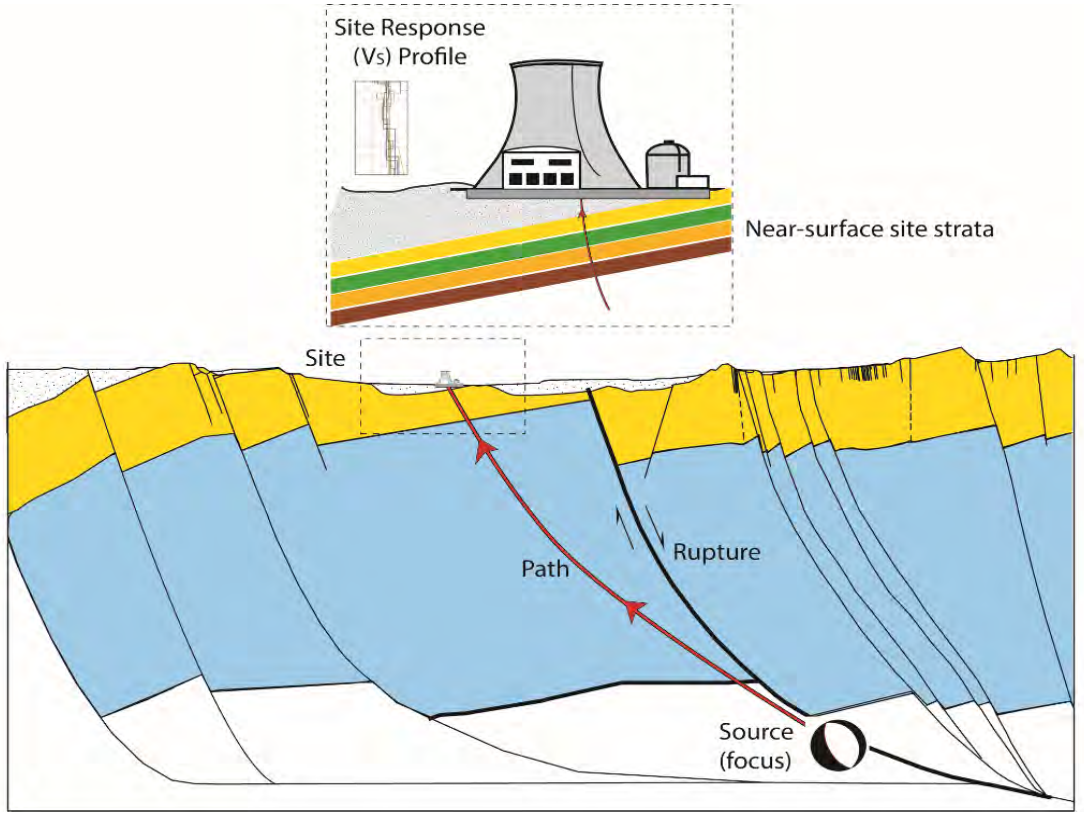

Figure 1-3. Diagrammatic cross-section showing the components that comprise a SHA, namely, the earthquake source, path from source to the site, and site response due to the strata directly beneath the site.

Seismic hazards can be quantified either through deterministic or probabilistic analyses. The deterministic analysis is described in Section 1.2.1 because this was the methodology used previously to define the design basis ground motion for the KNPS, described in Sections 1.3.1 and 1.3.2.

1.2.1 Deterministic seismic hazard analysis

In a deterministic seismic hazard analysis (DSHA), individual earthquake scenarios (magnitude and distance to site) are developed for each identified seismic source. For example, at the proposed Private Fuel Storage Facility site in Utah (Figure 1-4), several faults and fault segments were identified as potential fault sources based on geological and geophysical data (PFS LLC, 2000) and reviewed for the USNRC (2000) by Stamatakos et al. (2000).

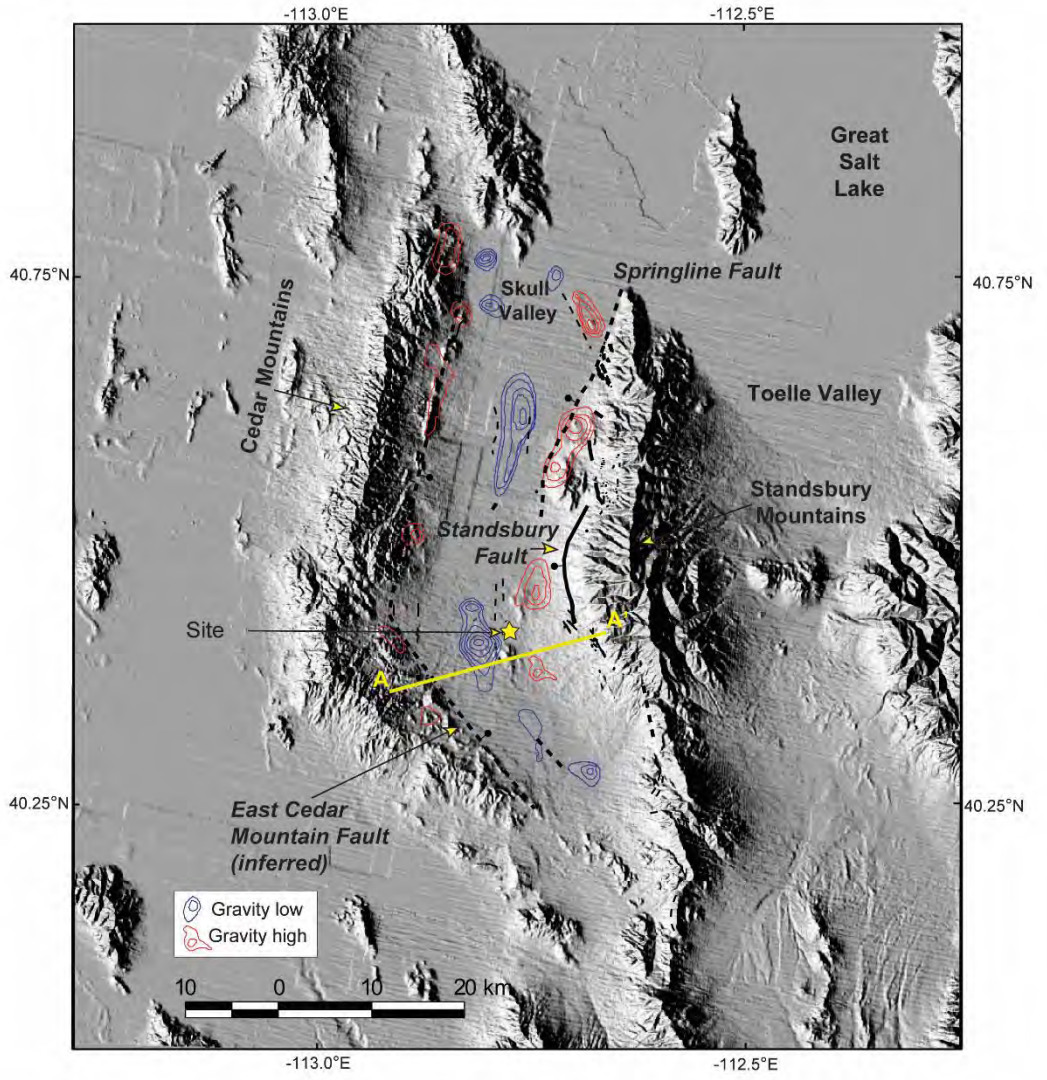

Figure 1-4. Digital elevation model (DEM) showing the location of the proposed Private Fuel Storage Facility site in Skull Valley, Utah, US, adapted from Stamatakos et al. (2000). The site is located between two mountain ranges with active range-front faults. Two fault segments of the East Cedar Mountain Fault and one segment from the Stansbury Fault were selected to illustrate the steps in a DSHA.

These fault sources can be used here to illustrate the steps in developing a DSHA. For this illustration, two fault segments of the East Cedar Mountain Fault and one segment of the Stansbury Fault were selected to demonstrate the DSHA process, although more seismic sources were evaluated in the original SHA for the site. Seismic sources are selected for a DSHA based on an analyst's assessment that they can contribute to the ground shaking hazard.

The first step in the DSHA is to develop a set of credible earthquake scenarios. The complexities of the fault patterns evident in Figure 1-4 for the three fault segments are simplified, such that the surface expression of each fault source is represented in the DSHA by a line or curvilinear segment (Figure 1-5 a). The source-to-site distance (r) is then computed for each fault source based on the closest approach of the fault trace to the site. The maximum magnitude earthquake (Mmax) for each fault source is then estimated based either on evidence from past earthquakes derived from geological or palaeoseismic data, or from an

empirical fault scaling relationship based on a compilation of worldwide earthquake and fault rupture data (e.g. Wells and Coppersmith, 1994). In these fault scaling relationships, Mmax, or more generally moment magnitude (**M**), is correlated with fault rupture length or fault rupture area. The result of the first step is a set of three **M**–*r* pairs that comprise the three earthquake scenarios.

Next, the ground shaking at the site is computed for each **M**–*r* earthquake scenario using a specified ground-motion prediction equation (GMPE)[2]. The GMPE calculates the seismic ground-motion intensity at the site as a response spectrum and accounts for the characteristics of the source, path, and perhaps site response effects. GMPEs are usually constructed by statistical regression analysis of many strong motion records and corrected for site conditions, although theoretical considerations may also be included. The ground-motion associated with each **M**–*r* earthquake scenario is based on the median GMPE, or the 84th percentile ground-motion (Figure 1-5 b).

Finally, the largest ground motion predicted by the GMPE from among the three **M**–*r* earthquake scenarios, often called the maximum credible earthquake (MCE) or the design earthquake, is then used to define the seismic design ground motion (Figure 1-5 c). This is either a site-specific response spectrum or a design response spectrum, such as the one defined in USNRC Regulatory Guide 1.60 (USAEC, 1973), anchored to the peak ground acceleration (PGA) that corresponds to the MCE.

[2] GMPE is used here in reference to a single regression model, in comparison to a ground-motion model (GMM), which is herein defined as two or more GMPEs combined within a logic tree, or a backbone approach that populates the ground motion characterisation logic tree with scaled or adjusted versions of the backbone model to capture the epistemic uncertainty in median ground motions.

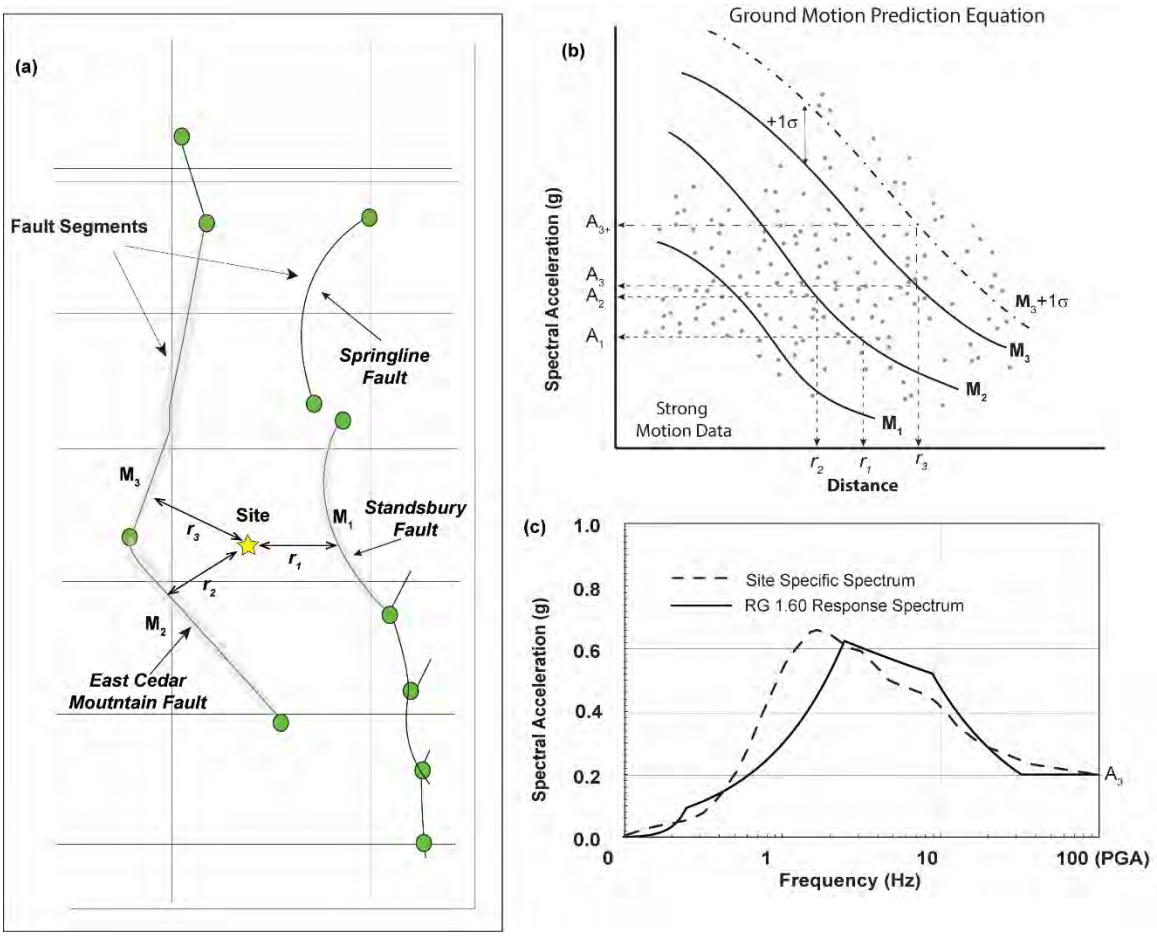

Figure 1-5. (a) The faults shown in Figure 1-4 are abstracted as fault sources in the DSHA. Three earthquake rupture scenarios are developed, one on the Stansbury Fault and two on the two segments of the East Cedar Mountain Fault. For each scenario, a magnitude (M) and distance (*r*) pair is obtained. (b) The ground-motion amplitude at the site then is estimated for each M–*r* pair, based on a ground motion prediction equation (GMPE). (c) The scenario with the largest ground motion is used to define the site-specific response spectrum, or a standard-shaped spectrum that is anchored to the largest PGA of the three scenarios.

An added complexity to the DSHA is the way in which *r* is measured. Not all GMPEs use the same measure of source-to-site distance. Each GMPE defines the appropriate distance metric that is needed to calculate ground motion. In the example shown in Figure 1-4, cross-section A-A' shows that Skull Valley is a basin bounded by normal faults that dip beneath the site (Figure 1-6 a). Thus, it is important to specify *r* to be consistent with the GMPE, either as measured to the surface projection of the rupture (r_{jb}), or the distance to the hypocentre (r_{hypo}), or the closest distance between a site and the three-dimensional rupture plane (r_{rup}), among other options (Figure 1-6 b).

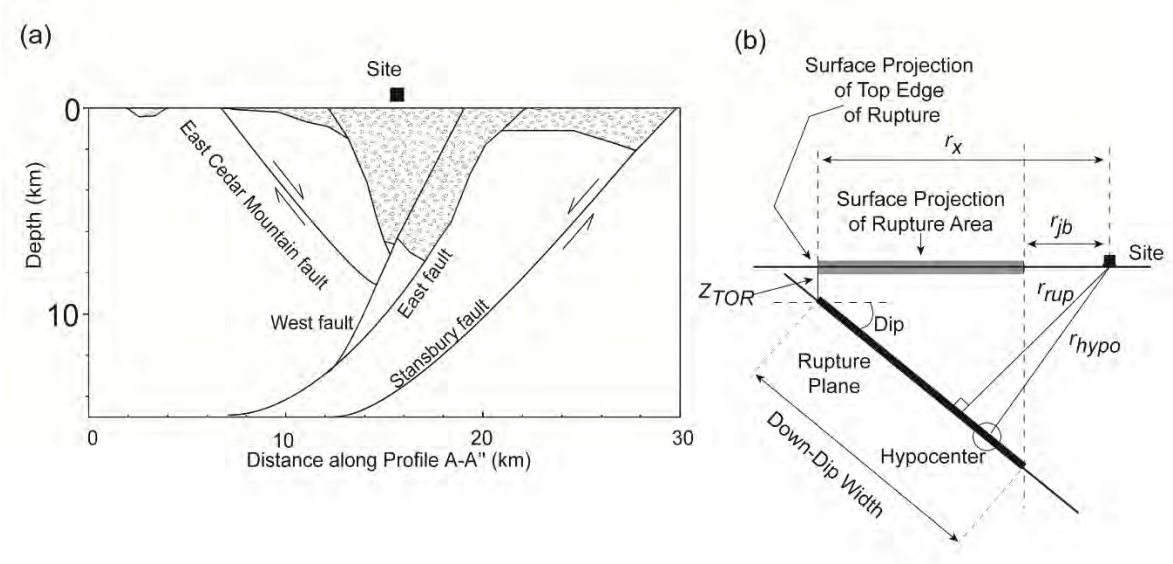

Figure 1-6. (a) Cross section A-A' from Figure 1-4, showing that the site in Skull Valley is bound by normal faults (Stamatakos et al., 2000). In (b), the commonly used GMPE-specific distance measures are defined: Z_{TOR} is the distance to the top of rupture, r_{jb} is the Joyner-Boore distance and is defined as the shortest distance from a site to the surface projection of the rupture plane, r_{hypo} is the distance from the site to the hypocentre, and r_{up} is the closest distance between a site and the three-dimensional rupture plane. The figure is adapted from figure 1 of Kaklamanos et al. (2011). The length of the fault rupture plane is measured along the strike of the fault and perpendicular to the plane of the page.

1.2.2 Probabilistic seismic hazard analysis

In contrast to the small number of earthquake scenarios examined in a DSHA, in a probabilistic seismic hazard analysis (PSHA), many earthquake scenarios are generated for a range of magnitudes and all potential fault sources that contribute to the shaking hazard, including uncertainty and variability. The rates of these scenarios are combined with the probability of exceeding a specific ground-shaking level and summed to produce hazard curves. A PSHA also uses a ground-motion model (GMM) that captures the full range of uncertainty in ground-motion prediction from the source, path, and site effects. However, it is important to note that some SHA studies may be a more complex DSHA, in which a PSHA-level GMM is used in conjunction with the maximum credible earthquake (MCE) to define the design response spectra (e.g. McGuire, 2001; Bommer, 2002; Bommer and Scherbaum, 2008).

The basic outline for a PSHA was first proposed by Cornell (1968) and refined in subsequent publications (e.g. Bommer and Abrahamson, 2006; McGuire, 2008). In a PSHA, all earthquake scenarios that contribute to the hazard are included in the analysis (magnitudes, locations, probability of occurrence) along with the rate at which they occur. This is the most important factor distinguishing a probabilistic analysis from a deterministic analysis. This is because the goal of a PSHA is not to determine the MCE but to quantify the frequency of exceeding various ground-motion levels at a site given all possible earthquake scenarios.

1.2.2.1 PSHA seismic source characterisation

There are several important differences between a PSHA and a DSHA. First, because fault ruptures (*R*) that generate earthquakes can occur anywhere along the fault or consume the entire fault area, there are many possible source-to-site distances (Figure 1-7a), which are captured in the PSHA as a probability distribution function for all distances r_1 to r_n (Figure 1-

7b). As in the DSHA, *r* must be measured to be consistent with the needs of the GMM (e.g. r_{rup} or r_{jb} in Figure 1-5 b). The distribution of source-to-site distance (*r*) is treated as a random variable in the PSHA calculation.

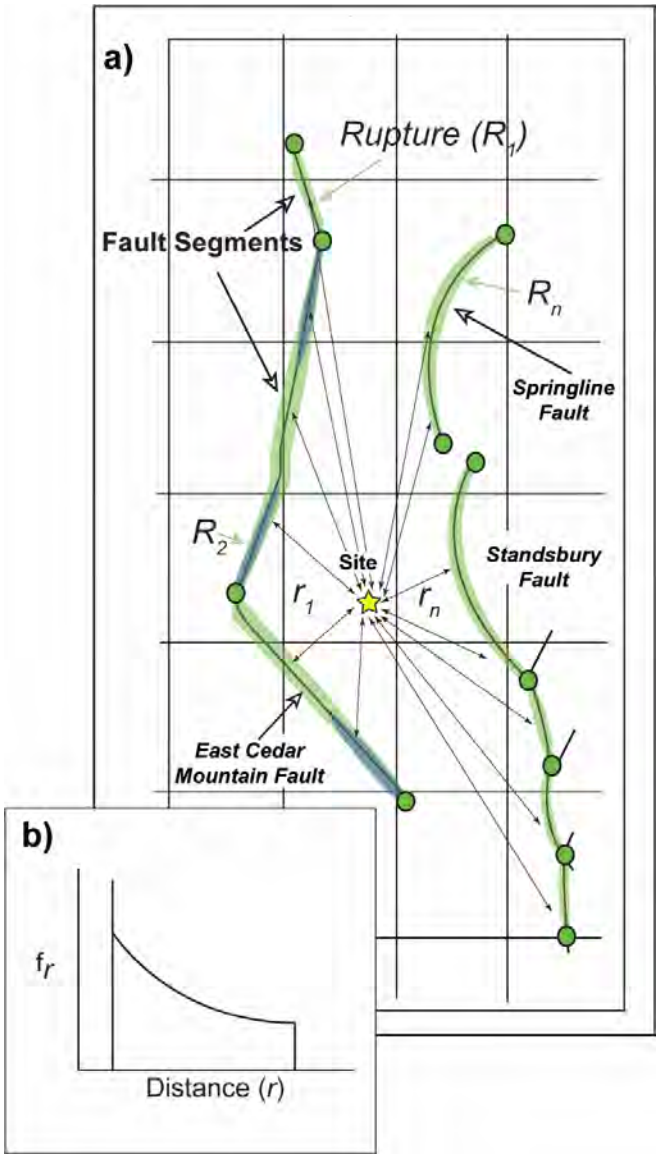

Figure 1-7. In (a), the same fault sources that are shown in Figure 1-5 illustrate how a probability distribution of source-to-site distances (b) is compiled for the PSHA. The colour shading illustrates a range in ruptures, from ruptures limited to a portion of the fault segment (blue) to full-segment and multi-segment ruptures (green).

Second, because the contributions from all earthquake scenarios that contribute to hazard are accounted for in the PSHA, the contribution from possible future earthquakes that are not associated with known faults must also be included. Source zones (also referred to as areal source zones or background zones) are defined as regions or volumes of the Earth's crust wherein future seismicity that cannot be attributed to a known fault source occur. These are used to model the temporal and spatial distribution of seismicity in a volume of the earth's crust for cases where there is limited geological or geophysical evidence to allow all past earthquakes to be associated with known faults and there is uncertainty in hypocentral locations. Source zones are defined in terms of their crustal properties such as seismogenic

thickness, crustal thickness, crustal type (i.e. continental, oceanic, transitional), topography, structural grain of mapped faults and folds, and heat flow. Figure 1-8 shows an example of source zones defined in the Hanford PSHA study (PNNL, 2014).

The source-to-site distance for future earthquakes in the source zone has to be modelled in the PSHA (also see Sections 8.2.5, 8.2.6 and 10.2.2). There are two main alternatives. In the first alternative, the occurrence of future earthquakes could be treated as random and occurring anywhere in the zone. In this case the probability distribution function of *r* can be developed from a uniform or random distribution of grid points in the source zone. However, If the past locations of earthquakes is used to predict where future earthquakes are likely to occur, then a spatial distribution density map derived from a statistical analysis of the locations of past earthquakes is used to develop the probability distribution function of *r.* These two alternatives are illustrated in Figure 1-9. In Figure 1-9a, an example seismic source zone (not based on an actual hazard study) is shown with a site location surrounded by a distribution of past earthquakes. Figure 1-9b shows a 3D Gaussian distribution of the locations of these earthquakes. If the location of future earthquakes is considered to be random in the zone, then the past location of earthquakes is ignored, and the probability distribution function of *r* is based on a uniform grid (Figure 1-9c). However, if the location of future earthquakes is considered to depend on the location of past events, then the probability distribution function of *r* depends on the 3D Gaussian distribution (Figure 1-9d).

Third, in a PSHA, the rate at which earthquakes are predicted to occur is determined based on a detailed characterisation of each seismic source. For each seismic source, earthquakes of all possible magnitudes above a minimum magnitude (Mmin) threshold, up to a maximum magnitude (Mmax) threshold, are considered. For each source, a magnitude-frequency distribution (MFD) is developed that defines the expected rate of future earthquakes between Mmin and Mmax. Two of the more commonly used MFDs are shown in Figure 1-10. These are the classic Gutenberg-Richter form (Gutenburg and Richter, 1956) or, for fault sources, the characteristic model (Schwartz and Coppersmith, 1984; Youngs and Coppersmith, 1985). Mmax is based on an assessment of the physically largest possible earthquake that could occur in each source or along each fault, whereas Mmin is the smallest magnitude earthquake that could generate motions of engineering significance (Bommer and Crowley, 2017), assumes a common value in the PSHA calculations. The distribution of **M** is also treated as a random variable in the PSHA.

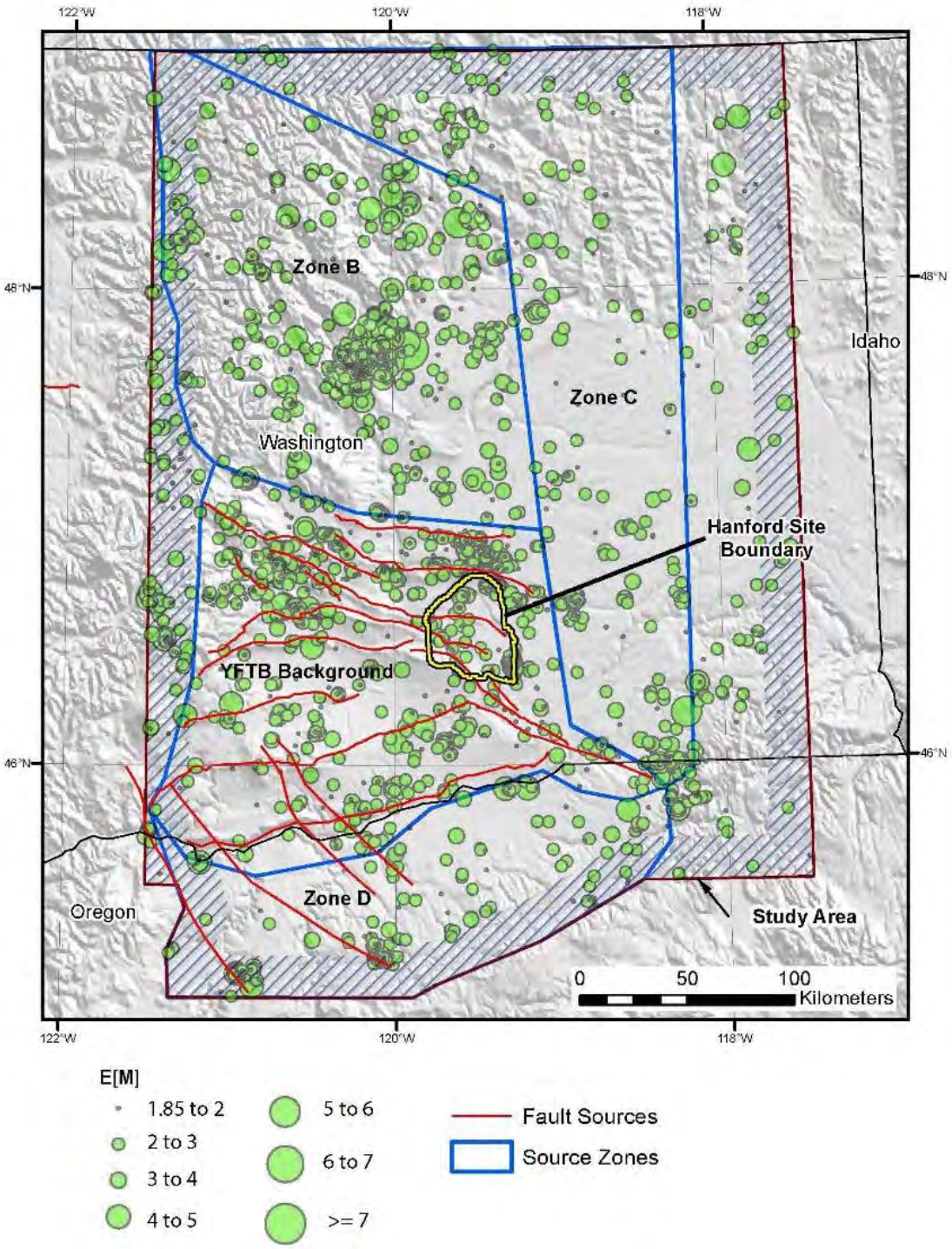

Figure 1-8. Seismic source zones in the Hanford PSHA. The epicentres are depicted by the green circles, with M≥1.85. The red lines indicate fault sources. This figure was adapted from Figure 8.1 of PNNL (2014). E[M] is the expected moment magnitude as defined in NUREG-2115 (EPRI/DOE/USNRC, 2012).

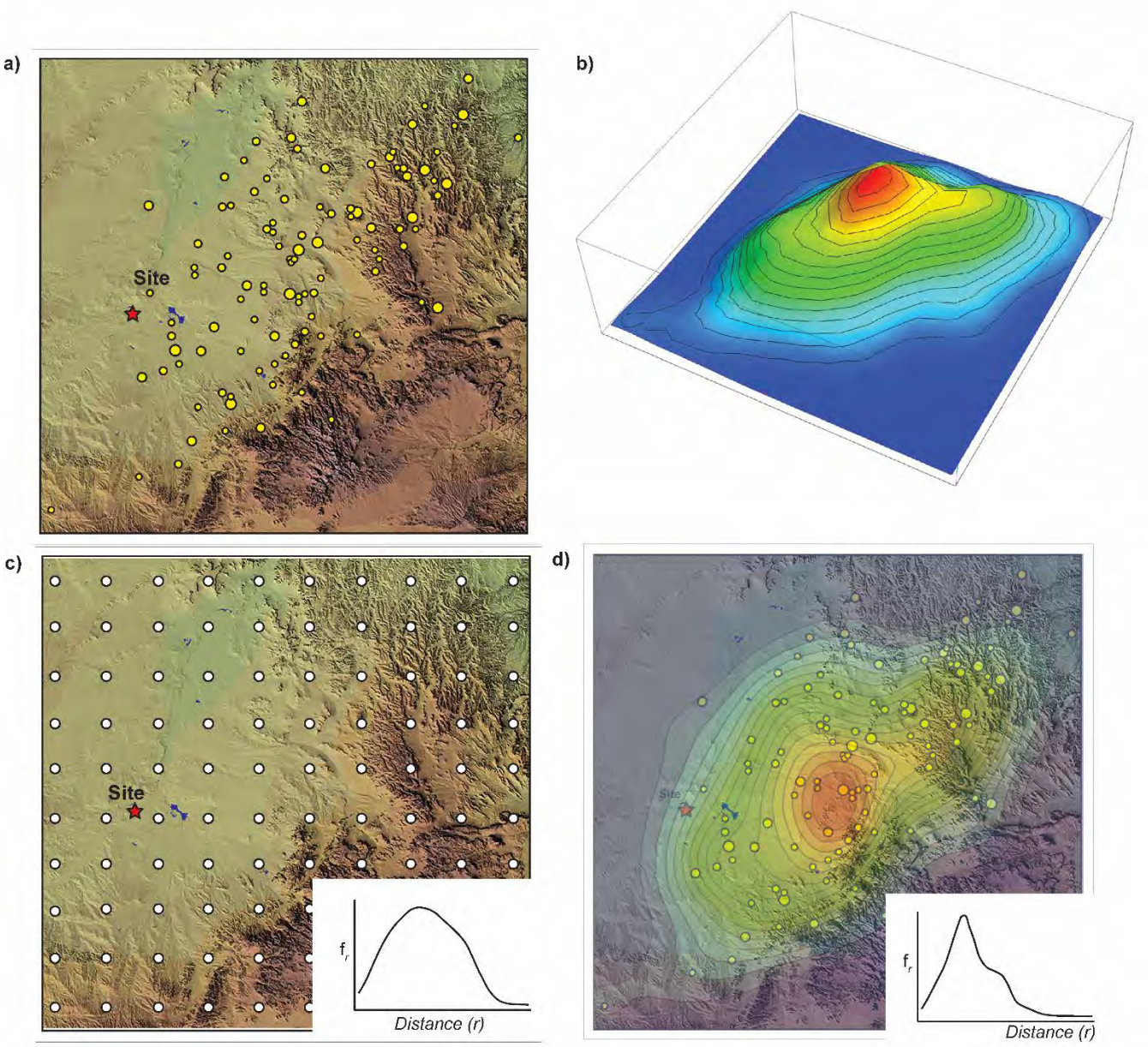

Figure 1-9. (a) Stylized example seismic source zone (not based on an actual hazard study) showing a distribution of past earthquakes relative to a site. (b) Spatially smoothed earthquake density plot using a fixed kernel bandwidth. (c) Uniform grid with the source-to-site distance probability function. (d) Spatially smoothed plot showing the effects of using the past pattern of earthquake locations to develop the source-to-site distance probability function.

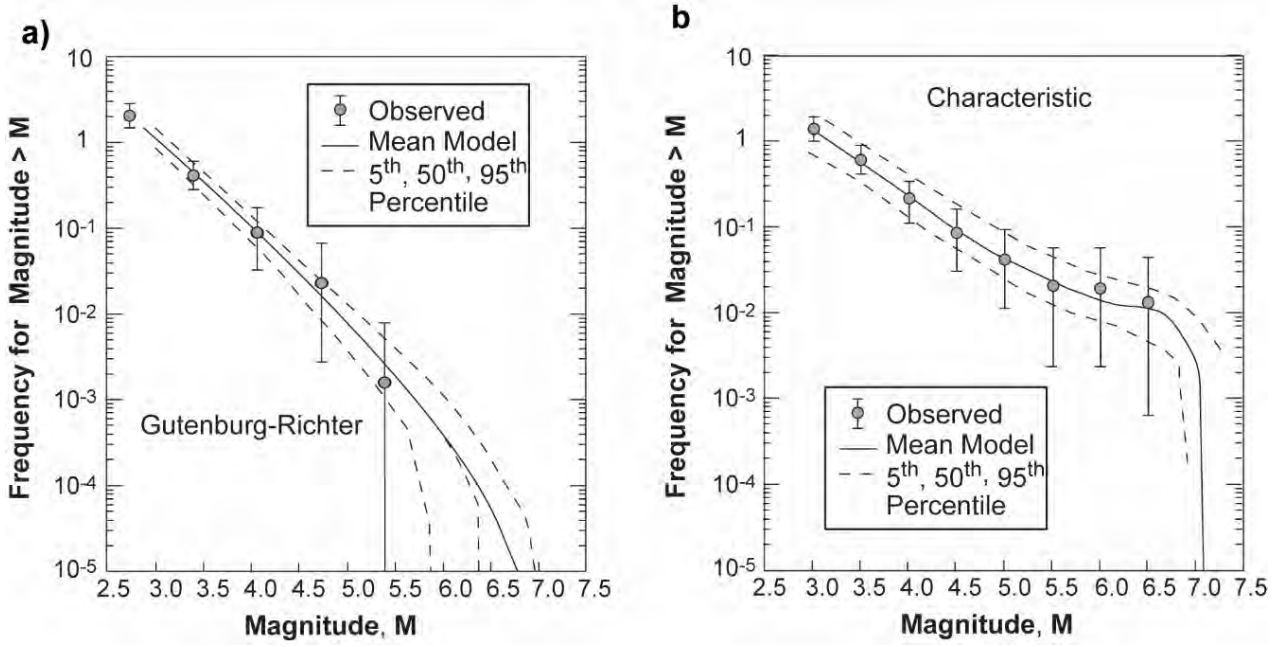

Figure 1-10. Magnitude-frequency distributions that define the relative frequency of earthquakes of different magnitudes.

1.2.2.2 Ground-motion characterisation

The fourth step in a PSHA is the ground-motion characterisation, which is generally more sophisticated than that applied to a DSHA. For each **M**–*r* pair, the resulting amplitude of ground motion at the site is calculated using a GMM that does not predict unique values of the selected ground-motion parameters. Rather, a log-normal distribution of values is calculated that is fully characterised by the logarithmic mean value predicted by the GMM and the standard deviation of the ground-motion residuals (Figure 1-11), often represented by sigma (σ). The number of standard deviations sampled from this distribution is usually represented by epsilon (**ε**), which is the third random variable considered in the PSHA calculations.

Other features of the seismic sources—such as focal depths and style of faulting—may be treated as additional distributions of random variables, but the essence of PSHA calculations is an integration over the distributions of **M**, *r*, and ***ε***. Therefore, each **M**–*r*–***ε*** triplet defines a ground-motion amplitude (entering these values into the GMM) as well as an associated annual frequency of exceedance (AFE). The latter is obtained as the product of the average annual frequency of earthquakes of that **M**–*r* pair and the probability of exceeding the ***ε*** value (i.e. 50% for ***ε*** = 0, 16% for ***ε*** =1, etc.). Plotting these total exceedance frequencies against the corresponding levels of acceleration creates a seismic hazard curve, as illustrated in Figure 1-12.

By assuming that all earthquakes are independent—an assumption that requires the removal of foreshocks and aftershocks from the earthquake catalogue prior to calculation of the recurrence parameters—the frequencies of all **M**–*r*–***ε*** combinations causing a particular ground-motion level at the site can be summed to obtain the total AFE for that level of motion. In this way, a hazard curve can be constructed depicting AFEs as a function of the amplitude of the specified ground-motion parameter.

The ground-motion characterisation may be as simple as a GMPE, but for site-specific studies for critical facilities such as nuclear power plants, this is generally not considered sufficient. The reason for this is that site effects, related to the influence of near-surface materials on the ground motion, are represented in GMPEs by generic models conditioned on simple parameters such as V_{S30} (the time-averaged shear-wave velocity over the uppermost 30 m at the site) and possibly also $Z_{1.0}$ or $Z_{2.5}$ (the depth to material with a shear-wave velocity of 1.0 or 2.5 km/s). When these parameters are applied in global models, the resulting site response carries a high level of uncertainty that is generally considered unacceptable for such projects.

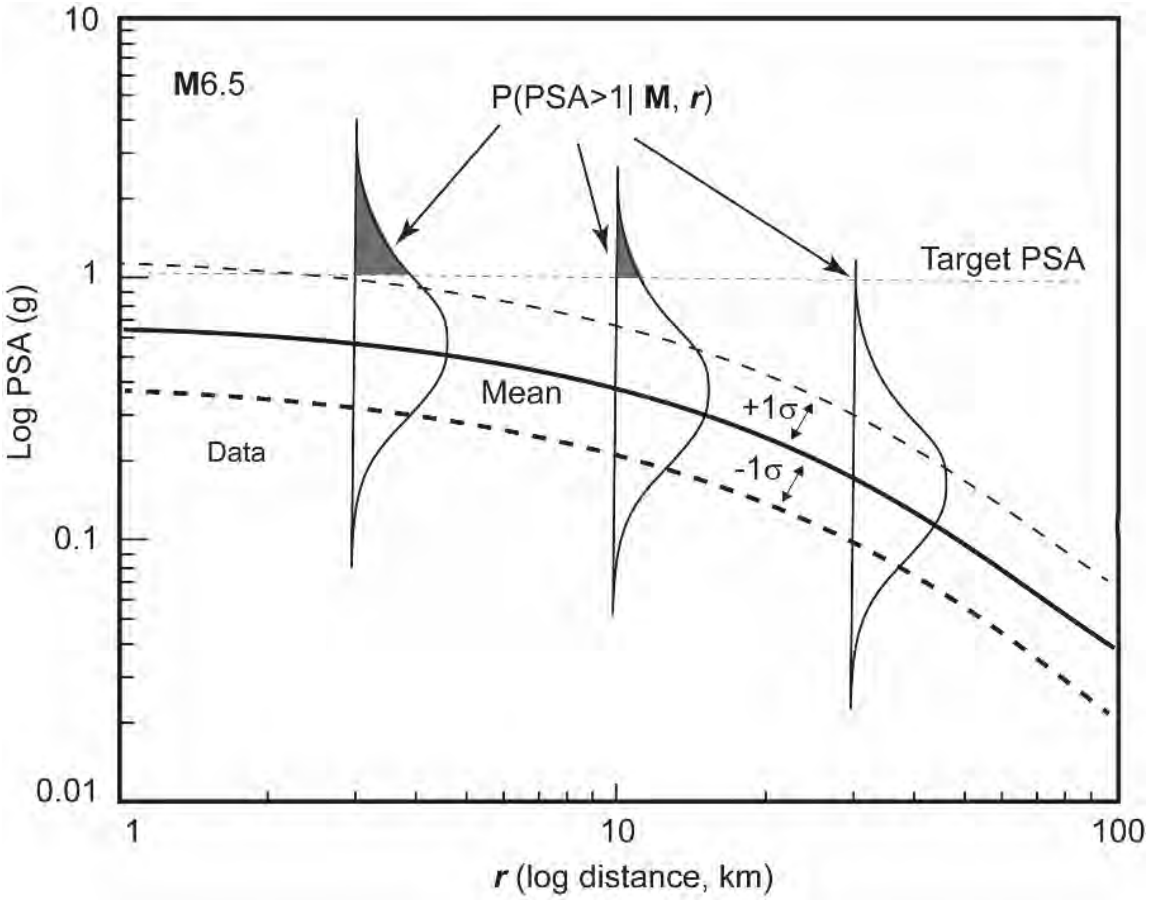

Figure 1-11. GMPE for PSHA depicting the example ground-motion model for a magnitude 6.5 earthquake, and the probability of PSA >1 g at three source-to-site distances, modified from Figure 2.1.1 of Baker et al. (2021).

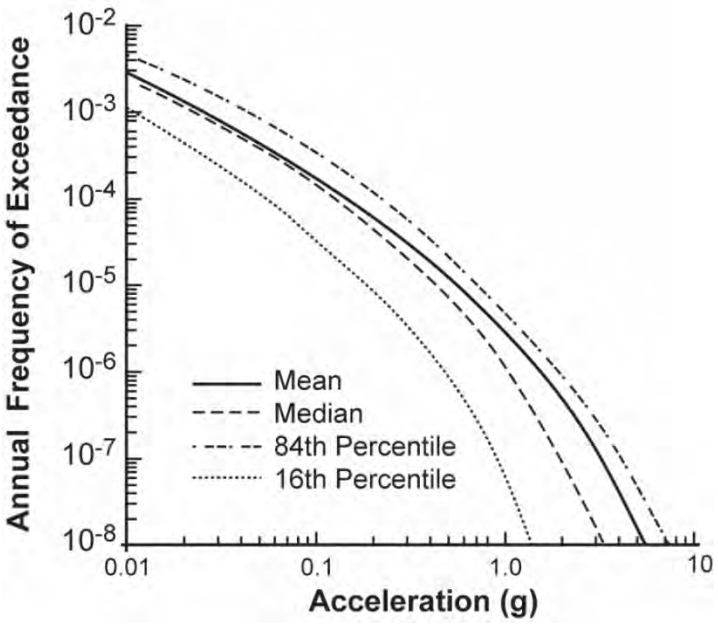

Figure 1-12. PSHA hazard curves showing the level of ground acceleration plotted as a function of the AFE. The fractiles represented in this figure are explained in Section 1.2.3.

To capture local site effects, it is standard practice to define a reference rock horizon at some depth and treat this as the top of an elastic half-space to perform site response analyses to calculate the dynamic response characteristics of the overlying layers. Ground-motion estimates are developed for the reference rock horizon, following which the rock hazard can be convolved with the probabilistic site amplification factors obtained from the site response analyses (Bazzurro and Cornell, 2004; McGuire et al., 2001; Rodriguez-Marek et al., 2014). Recent developments have prompted a move away from the convolution approach to incorporate site amplification factors into the estimate of hazard at the target horizon (e.g. Rodriguez-Marek et al., 2021). First, hazard fractiles (see Section 1.2.3) are more accurately obtained by embedding the amplification factors (AFs) directly into the hazard integral rather than applying the convolution with PSHA, results at the rock horizon, especially if there is significant non-linearity in the soil response. Second, if the linear part of the AFs for high-frequency spectral accelerations is found to depend on magnitude and/or distance (Stafford et al., 2017), then it becomes advantageous to embed the AF within the PSHA integral. In view of these developments, for the Duynefontyn PSHA, the approach was adopted to include the AFs directly within the hazard integral (see Chapter 9).

1.2.2.3 PSHA process

The PSHA process is therefore essentially an integration of individual contributions from combinations of **M**, ***r***, and ground-motion exceedance levels. The process can subsequently be reversed to determine the relative contributions to the hazard—for a specified combination of response frequency, *f*, and AFE—from different bins of **M**, ***r*** and $\boldsymbol{\varepsilon}$. This process is known as de-aggregation (or disaggregation) (Bazzurro and Cornell, 1999) and it can be used to identify the dominant scenarios contributing to the hazard, which may be the modal or mean values (Harmsen et al., 1999). These scenarios can provide the starting point for defining other representations of the hazard that are useful for engineering analysis such as acceleration time-histories.

Thus, a PSHA comprises three main components: (1) the seismic source model (SSM)[3], which predicts the occurrence of possible future earthquakes in terms of location, size, type of faulting, (2) the GMM, which predicts the ground shaking at the site given the source model and the effects of the path and the site on the earthquake energy, and (3) the hazard calculation, which quantifies the seismic hazard and associated uncertainty (See Section 1.2.3) in terms of the annual frequency of exceeding various ground-motion levels at the site. Hazard calculations may also include the associated seismic engineering inputs needed for seismic design, performance analyses, and risk assessments (e.g. de-aggregation or ground-motion response spectra). As described in the Project Execution Plan (Stamatakos and Watson-Lamprey, 2023), the Duynefontyn PSHA includes: (1) the completed SSM, (2) the completed GMM, (3) a family of seismic hazard curves at the two designated facility sites that express the annual frequency of exceeding different levels of ground motion, and (4) various seismic hazard products derived from the seismic hazard curves that are needed for seismic design and review, and seismic safety analyses.

In the Duynefontyn PSHA, each of these components falls under the remit of three teams of subject matter experts. As described in Section 4 of the Project Execution Plan (Stamatakos and Watson-Lamprey, 2023), the project organisation included an SSM Technical Integration (TI) Team, a GMM TI Team, and a Hazard Analysis Team (HAT). In addition, other designated project teams were critical to the success of SSHAC study, including the Participatory Peer Review Panel (PPRP), the project management team, resource and proponent experts, and specialty contractors. Finally, a number of data collection activities and specialty contractor studies supported the TI Team's evaluation and integration.

The SSM TI Team assesses the potential for all possible future earthquakes that could impact the hazard at the site based on the geological and seismological characteristics of the site and region. The SSM is a prediction of the locations, magnitudes, rupture types (normal, reverse, and strike-slip), and recurrence rates of possible future earthquakes that contribute to the seismic hazard at the site, along with associated aleatory variability and epistemic uncertainty of the SSM attributes.

The GMM TI Team characterises the earthquake ground motion at the site based on the seismological and geotechnical properties of the source, path, and site in terms of attenuation, the effects of impedance contrasts in the site strata, damping, stress drop, and the associated variabilities and uncertainties[4] associated with each of these parameters. The goal of both the SSM and GMM TI Teams is to capture the centre, body, and range (CBR) of technically defensible interpretations (TDI).

The HAT, under the leadership of the Hazard Analyst, performs all the required hazard calculations using the project-approved set of computer codes and software based on inputs from the SSM and GMM TI Teams. Specifically, the SSM and GMM TI Teams produce the Hazard Input Document (HID), which provides the HAT with a full set of instructions and input parameters used to construct the full PSHA logic tree. The HID also includes the weights that the TI Teams assign to all the alternative logic tree branches. The HID does not contain

[3] In most prior SSHAC studies, the components of the PSHA were referred to as the seismic source characterisation (SSC) and ground motion characterisation (GMC) models. In ANS 2.29 (ANS, 2020) the terminology changed to seismic source model (SSM) and ground motion model (GMM).
[4] Variability refers to aleatory and uncertainty refers to epistemic. See Section 1.2.3.

technical justifications for the models or weights, only elements for implementation; the technical justifications are provided in this PSHA report.

The PPRP provides technical review and process review. The technical review by the PPRP ensures that the full range of data, models, and methods have been duly considered; that the SSM and GMM represent CBR of TDI; that all technical decisions are adequately justified and documented; and that the TI Teams followed throughout the SSHAC process as described in NUREG-2213.

Although the SSHAC EL-2 PSHA study focusses on the ground shaking at the Duyenfontyn site, comprising both KNPS and the new build location, that could be generated by future earthquakes, the study supports the evaluation of other geo-hazards at the site, even where the quantitative assessment of these other hazards falls outside the scope of this project. For example, the characterisation of seismic sources that contribute to site hazard will inform the assessment of both the surface fault rupture hazard and the tsunami hazard associated with local sources. The vibratory ground motions would also provide inputs to the assessment of secondary geotechnical hazards such as liquefaction and slope instability.

1.2.3 Uncertainties

The PSHA presented in this report has been carried out explicitly to support an application for licence renewal and a new nuclear facility in a regulated environment. A key objective of the study was therefore to develop a seismic hazard assessment to ensure regulatory assurance, by demonstrating that the PSHA considered all uncertainties. Uncertainties are classified into two categories: aleatory variability and epistemic uncertainty.

1.2.3.1 Aleatory variability

The first category, aleatory variability, reflects the inherent randomness in earthquake and ground-motion processes, including the location, number, and magnitude of future earthquakes that could occur during the useful life of the facility being designed. This was expressed by Cornell (1968) in a landmark paper that introduced the basis for PSHA: "*In the determination of the distribution of maximum annual earthquake intensity at a site, one must consider not only the distribution of the size (magnitude) of an event, but also its uncertain distance from the site and the uncertain number of events in any time period.*" Shortly afterwards, a missing element of aleatory variability, namely, the resulting level of ground motion at a particular site with respect to median prediction for each earthquake scenario (i.e. integration over $\boldsymbol{\varepsilon}$ as well as over **M** and *r*), was included in standard formulations of PSHA (Bommer and Abrahamson, 2006; McGuire, 2008).

The probabilistic approach to seismic hazard analysis is specifically formulated to integrate all these sources of variability into the estimation of the annual exceedance frequency of different levels of each ground-motion parameter. Therefore, adoption of a PSHA as the basis for determining the seismic design loads and executing the PSHA in terms of characterising design ground motions according to the specification of Regulatory Guide 1.208 (USNRC, 2007) ensures adequate consideration of aleatory variability.

1.2.3.2 Epistemic uncertainty

The second category, epistemic uncertainty, recognises that the calculation is based on incomplete knowledge. The TI Teams responsible for the development of the SSM and GMM made full use of all available data to calibrate the models to the characteristics of the region and the site. All available data of potential relevance was compiled and analysed as part of the SSM and GMM development, including new data specifically collected for the project to better constrain the models to local conditions. These data included historical and instrumental earthquake catalogues, geological data for the region in general and specifically for all identified faults, site characterisation data, characterisation of the site, and instrumental recordings of seismic motions.

Regardless of how much data was available for the construction of the SSM and the GMM, these will never be defined uniquely and unambiguously. One challenge is that the models are applicable to scenarios not represented in the available data because the PSHA calculations considered all possible earthquakes. Another challenge is that the nature of the available data is such that there are always technically justifiable interpretations resulting in alternatives. Both challenges impede the definition of unique models. These challenges are especially acute in regions of relatively low levels of seismicity, such as South Africa, because the less frequent occurrence of significant earthquakes leads to data that are inevitably sparse.

The ambiguity in defining models and selecting model parameters for a PSHA is the result of epistemic uncertainty. New data collection helped to reduce epistemic uncertainty in elements of the SSM and GMM, but the remaining uncertainty was still quantified and incorporated in the PSHA calculations. In fact, there will always be epistemic uncertainty associated with nearly every element of PSHA.

A key challenge in any PSHA study is therefore to identify and quantify the important sources of epistemic uncertainty, and to incorporate these in the hazard calculations. The tool most widely used to organise and incorporate epistemic uncertainty, and employed in this study, is the logic tree (e.g. Kulkarni et al., 1984). The basic concept of the logic tree is simple: a node is established for each model, model element or parameter value defining the SSM and GMM, and branches for alternative models or alternative parameter values defined at each node. Weights are then assigned to each branch, reflecting the relative confidence in that branch representing the most appropriate model or parameter value. The branch weights, which are subsequently treated as probabilities, sum to unity at each node (Figure 1-13). The PSHA calculations are then performed for all possible combinations of branches, with each hazard run yielding a separate hazard curve. The total weight associated with each hazard curve is obtained from the product of the weights associated with the branches selected for its calculation. The hazard output is expressed in terms of the statistics of the resulting suite of hazard curves, calculating the weighted AFE associated with each ground-motion level. In this way, the mean hazard curve and the hazard curves for different fractiles, or confidence levels, can be calculated (Figure 1-12). The spread of the fractiles, and the separation of the mean and median hazard curves, reflect the total epistemic uncertainty in the hazard estimates. These naturally increase with the return period, which is simply the reciprocal of the AFE.

There are a few important points to stress regarding the construction of logic trees for a PSHA. The first is that the branches and their associated weights together define the distribution of epistemic uncertainty for a feature or output of the SSM and GMM, such as Mmax, the

recurrence rate of earthquakes of a particular magnitude, or the median ground-motion amplitudes for a particular **M**–*r* combination. Second, the branches at each node should theoretically be mutually exclusive and collectively exhaustive. Third, there is not necessarily a correlation between the complexity of a logic-tree structure and its effectiveness in capturing epistemic uncertainty. For example, logic-trees that include many branches with low weights may predict a distribution that is more mean-centred than logic-trees with few branches, each with higher weight, leading to a broader distribution about the mean.

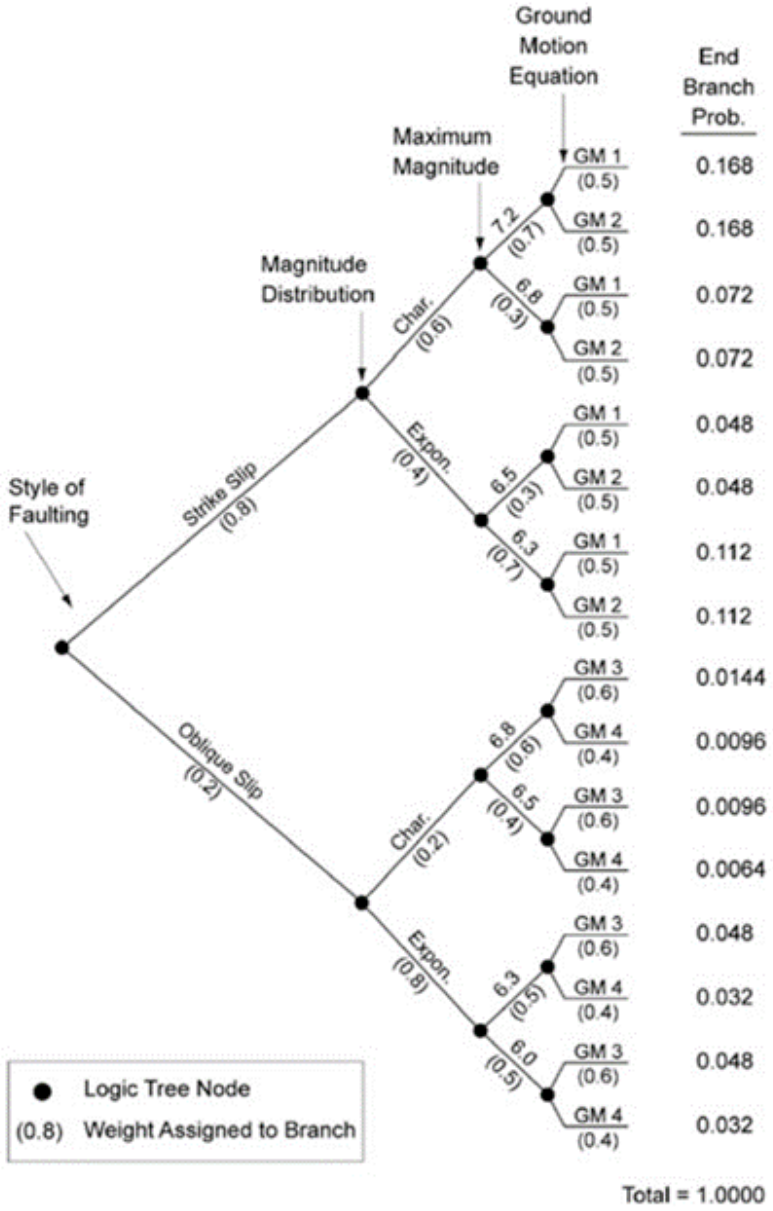

Figure 1-13. Example of a logic tree for a PSHA, with three nodes related to the SSM and one for the GMM, from Figure 50 of McGuire (2004).

1.3 PREVIOUS SEISMIC HAZARD STUDIES

For completeness, this section provides a brief overview of previous seismic hazard studies that have provided estimates of ground-shaking hazard at the KNPS site. The methods and reference parameters (such as site conditions and return periods, etc.) used in these earlier studies are inconsistent with the results of this study as they were generally limited in their approach (e.g., some were deterministic) and in their limited accounting for uncertainty, thus direct comparisons of the ground-motion amplitudes are questionable. The studies are briefly summarised here because they provide some context for this study.

These studies included:

- Studies by Dames and Moore in the period from 1973 to 1981.
- Studies by the Council for Geoscience in 1999 and 2005.
- A study by Rizzo (2008).

The main aim in reviewing these past studies was to obtain information on the input models used in calculating the seismic hazard at the study site at Koeberg. Information on the seismic source and ground-motion models used to develop these studies is relevant to the current study because it is within the realm of existing data, models, and methods, and is thus within the CBR of TDI.

1.3.1 Dames and Moore studies

Following the intention by Eskom to build a nuclear power station at Koeberg, the U.S. consulting company Dames and Moore conducted a series of seismic studies for the KNPS site (Table 1-1). Their aim was to develop a design earthquake based on geological and seismological data compiled in their investigations.

Dames and Moore selected an approach that included analyses of regional and site geology conditions, regional seismotectonics, and an evaluation of regional seismic history. This included efforts to identify the sources of major earthquakes, such as the 1809 Cape Town and 1969 Ceres earthquakes. Dames and Moore identified major fault zones located just east of Koeberg, which parallel the northwest extension of the Worcester Fault. In addition, they identified a major fault system extending northwest from the area near Stellenbosch. The fault system was projected to pass within 18 km of the KNPS site. A smaller structure was observed to pass within 11 km of the KNPS site. Dames and Moore also recognised the existence of the syntaxis area where the regional structural grain changes from an east–west strike to a northwest–southeast strike. A few faults were identified north of the site, near Darling, trending predominantly northwest, with a major subsidiary striking west (Figure 1-14).

Table 1-1. List of reports prepared and presented by Dames and Moore as part of their study to determine the seismic suitability of the site selected for the KNPS.

Reports	Date
Geotechnical Studies: Koeberg Nuclear Power Station (Dames and Moore, 1973)	July 1973
Report: Koeberg Nuclear Power Station Seismic Risk Analysis (Dames and Moore, 1974)	January 1974
Foundation Report: Koeberg Nuclear Power Station (Dames and Moore, 1975)	December 1975
Geologic Report: Risk of Surface Faulting to the Koeberg Nuclear Power Station site (Dames and Moore, 1976)	May 1976
Supplementary Geologic Report (Dames and Moore, 1977)	July 1977
Final Report: Boring Programme and Groundwater Simulation (Dames and Moore, 1980)	November 1980
Revised Draft Report: Seismic Design Requirements Koeberg Nuclear Power Station for the Electricity Supply Commission (Dames and Moore, 1981)	October 1981

The source of the 1969 Ceres earthquake was investigated, and it was determined that it occurred in the general area of the towns of Tulbagh, Ceres, Worcester, and Wolseley, a junction of regional structural grain with different trends. No surface expression of faulting was detected to help in the identification of an active structure along which the event occurred. Some surface deformations were located along a line connecting two ancient faults that are parallel to the Worcester Fault. The fault plane solution calculated for this event indicated a strike that is parallel to many faults in the region, especially the Groenhof Fault.

According to Dames and Moore (1976), the possibility of a destructive earthquake occurring close to Koeberg was credible. The occurrence of the 1809 Cape Town earthquake and the 1969 Ceres earthquake provided the justification for this conclusion. They also concluded that the seismic sources of the study area were not understood well enough to align seismic activity with any specific active fault source. Based on the work by Hartnady (1969) and Hartnady et al. (1974), Dames and Moore (1976) identified two major NNW-striking Precambrian fault zones, the Saldanha–Darling–Franschhoek and the Piketberg–Wellington fault zones (Figure 1-15). The zones were said to divide the southwestern Cape Province into three tectonic domains of different lithologic and tectonic style. They also concluded that there was evidence that suggests the presence of a third similar fault zone between Milnerton and Cape Hangklip (Figure 1-15).

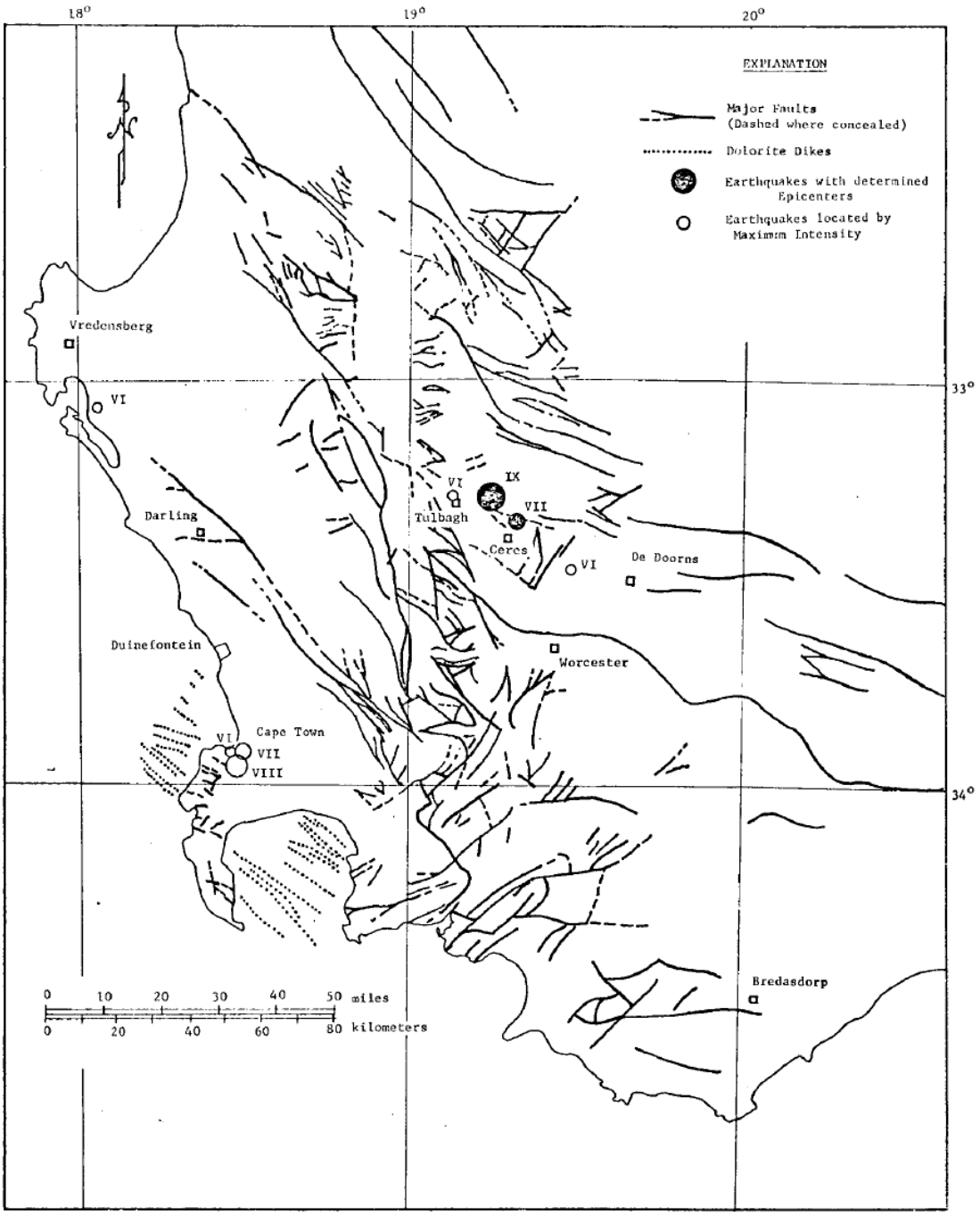

Figure 1-14. Map of the southwestern Cape showing the major faults and earthquake epicentres with Intensity VI (Modified Mercalli) or greater (Dames and Moore, 1973).

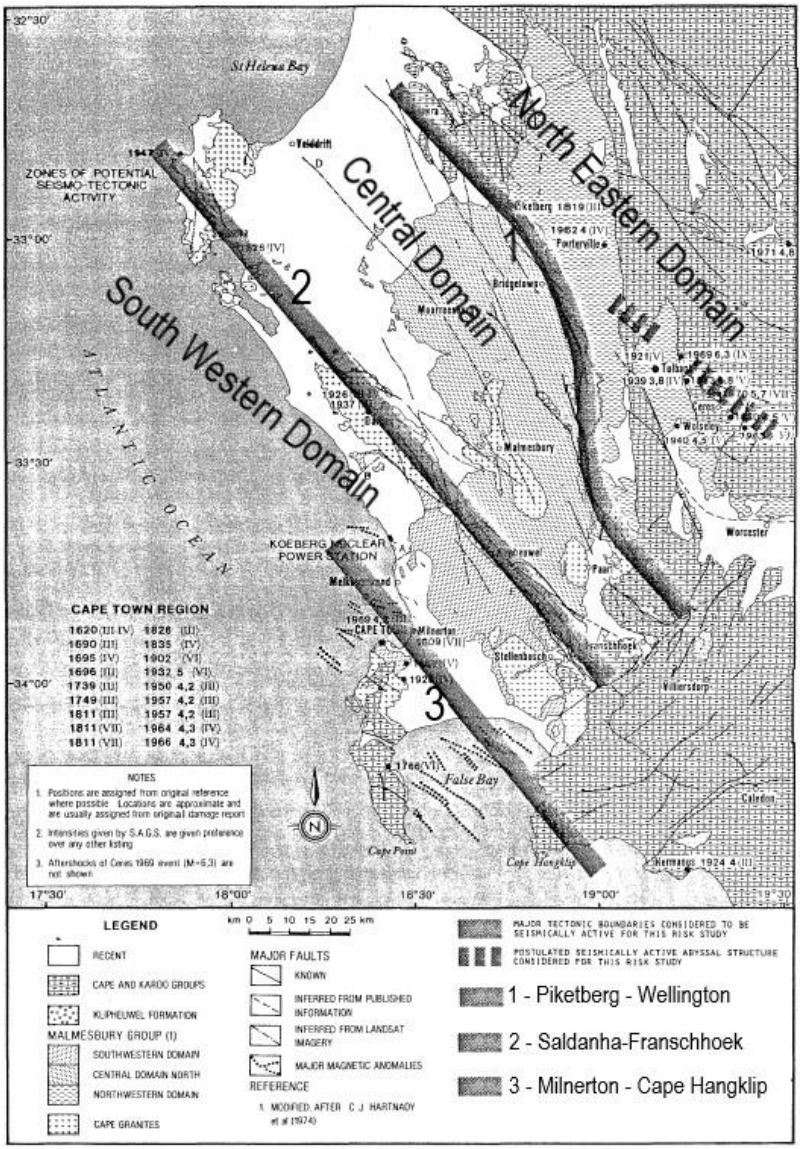

Figure 1-15. Location of the three postulated major fault zones in the southwestern Cape Province, copied from Plate 2 of Dames and Moore (1981).

The 1809 and 1969 events could not be clearly associated with any faults as they did not produce any surface rupture, nor was any major earthquake identified within 20 km of the KNPS site. Based on the International Atomic Energy Agency (IAEA) draft guidelines, "*Safety guide on Earthquakes and Associated Topics for Nuclear Power Station Siting*" (1976), Dames and Moore (1976) concluded that the three major fault zones identified could be classified as potentially seismically active.

1.3.1.1 Seismotectonic model

In preparing their seismotectonic model, Dames and Moore (1976) took into account the subdivision of the southwestern Cape into the three tectonostratigraphic units based on the division of the Western Cape by the three major fault zones shown in Figure 1-15. The KNPS site lies within the Southwestern Domain, which was characterised by a simple style of deformation of the Tygerberg Formation. In contrast, the Central Domain is a significantly more complex geological unit. The North Eastern Domain is made up of the Piketberg and Porterville

Formations and is separated from the Central Domain by the Piketberg–Wellington Fault Zone.

Dames and Moore did not find clear geological evidence for the existence of the postulated Milnerton–Cape Hangklip fault zone. They attributed this to urbanisation of the area through which the fault was presumed to occur, preventing further exploration by geological, geophysical, or even remote sensing techniques. From the results of an offshore geophysical survey that they conducted in 1975, Dames and Moore (1976) identified an NNW-trending anomaly about 8 km west of Koeberg, which they assumed could represent a fault zone. Dames and Moore (1976) suggested that the observed seismicity can mostly be associated with the postulated Milnerton–Cape Hangklip, Saldanha–Darling–Franschhoek, and Piketberg–Wellington fault zones. Thus, they considered these three fault zones could be potentially seismically active. The location of the fault zones relative to Koeberg (Table 1-2) implied that large events along the faults would result in shaking that could damage the KNPS.

Table 1-2. Location of the major three fault zones relative to the KNPS site, as identified by past Dames and Moore studies.

Fault Zone	Distance from the Site (km)
Piketberg–Wellington	Over 70 km northeast of site
Saldanha–Darling–Franschhoek	18 km from site at its closest point
Postulated Milnerton–Cape Hangklip	8 km from site at its closest point

Dames and Moore (1976) also evaluated the risk of surface faulting at the KNPS site. From the geological and remote sensing evidence they collected, they could not find any evidence of surface fault rupture at the site, nor anywhere in the study region, leading them to conclude that surface faulting was not a risk at the site.

1.3.1.2 Ground motion

Given the lack of strong motion data in South Africa, there were no ground-motion prediction equations in 1976 specifically derived for the Western Cape or South Africa. In their studies, Dames and Moore considered whether attenuation of ground motion in South Africa can be classified as similar to that in other continents. Specifically, they considered whether South African attenuation was similar to that recorded in California or to the slow anelastic attenuation with distance recorded in eastern North America. Measurements of non-seismic attenuation (i.e. from explosions in Cape Town) suggested that the rate of attenuation was similar to that recorded in western North America. However, this suggestion may not be reliable because shallow events generally attenuate rapidly.

Other South African data used for attenuation evaluation came from isoseismal data published for earthquakes from Southern Africa. Using intensity data obtained from the isoseismal maps, a dataset of magnitude, distance, and intensity was prepared. These data were used in the Dames and Moore studies because at that time there were no strong motion data recorded in South Africa. The ground-motion levels (e.g., PGA) associated with the collected intensity

levels were estimated based on data and ground-motion intensity correlation equations (GMICEs) from other countries (Figure 1-16).

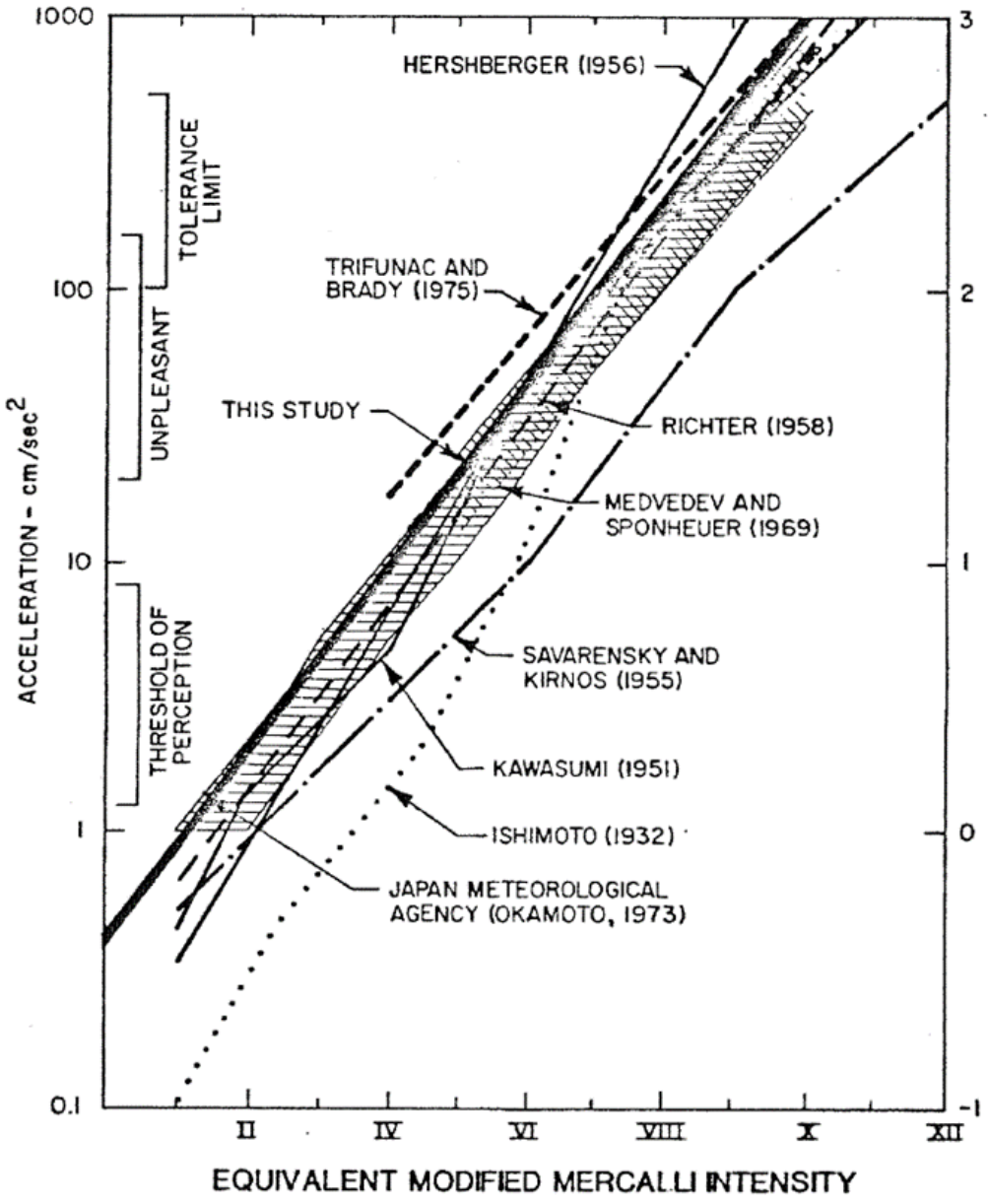

Figure 1-16. Relationships between PGA and modified Mercalli intensity (MMI), or equivalent intensity when applicable. This figure is copied from Figure 1 of Dames and Moore (1981).

For each intensity level, internationally available GMICEs were used to estimate acceleration values, which were then averaged to obtain one acceleration value for each intensity level. The estimated acceleration values are given in Table 1 of Dames and Moore (1981). These individual intensity measurements were then fit with a least-squares regression to produce the relationship in Equation 1-1.

1-1

$$\log_{10}(a) = -0.415 + 0.343I$$

where *a* is the acceleration in cm/sec^2 and *I* is the modified Mercalli intensity (MMI).

Equation 1-1 was then used together with existing intensity data to calculate PGA for earthquakes of predetermined magnitude values, shown as the heavy black line in Figure 1-16. Equation 1-1 was also used to convert intensity data to acceleration values for many earthquakes of varying magnitudes and to determine the coefficients of an attenuation relationship (Equation 1-2), which was subsequently used in the Dames and Moore (1981) Koeberg seismic hazard assessment.

1-2

$$a = 71.5e^{0.76M}(R + 25)^{-1.1}$$

where ***a*** is the acceleration in cm/sec^2, *M* is the magnitude (defined as local magnitude M_L[5]) and *R* is the epicentral distance in kilometres.

1.3.1.3 Maximum expected magnitude

In preparing the input parameters for the seismic hazard assessment, Dames and Moore (1981) estimated Mmax for each potential seismic hazard source. They implemented two techniques, namely, use of seismic histories and the use of geological and tectonic data.

In the seismic history assessment, Dames and Moore (1981) used two seismic data sets in implementing the cumulative magnitude-frequency distribution (MFD) of Gutenberg and Richter (1944), as shown in Figure 1-17. The first dataset was made up of all earthquakes recorded within 400 km of Koeberg (from 1695 to 1971), whilst the second dataset had earthquakes located within a 180 km radius of Koeberg. The second dataset included events from 1900 but excluded the 1969 Ceres event and its aftershocks.

Using the methodology previously developed by Nuttli (1981) and the GMICEs in Figure 1-16, Dames and Moore (1981) estimated Mmax of M_L 6.5 for the area of radius of 180 km around Koeberg. Using geological and tectonic data, Dames and Moore (1981) concluded that the large earthquakes with intensity values of MMI > VII, which occurred in the Western Cape, could be associated with the major shear zones. Based on an analysis of earthquakes in stable continental regions, Dames and Moore (1981) concluded that earthquake with $M_L \leq 6.5$ could occur in continental settings without producing surface fault rupture. They also concluded that an earthquake of M_L 6.5 is the most likely maximum magnitude earthquake for the region.

[5] *M* in this case is Richter magnitude (Richter, 1935) and is equivalent to local magnitude M_L.

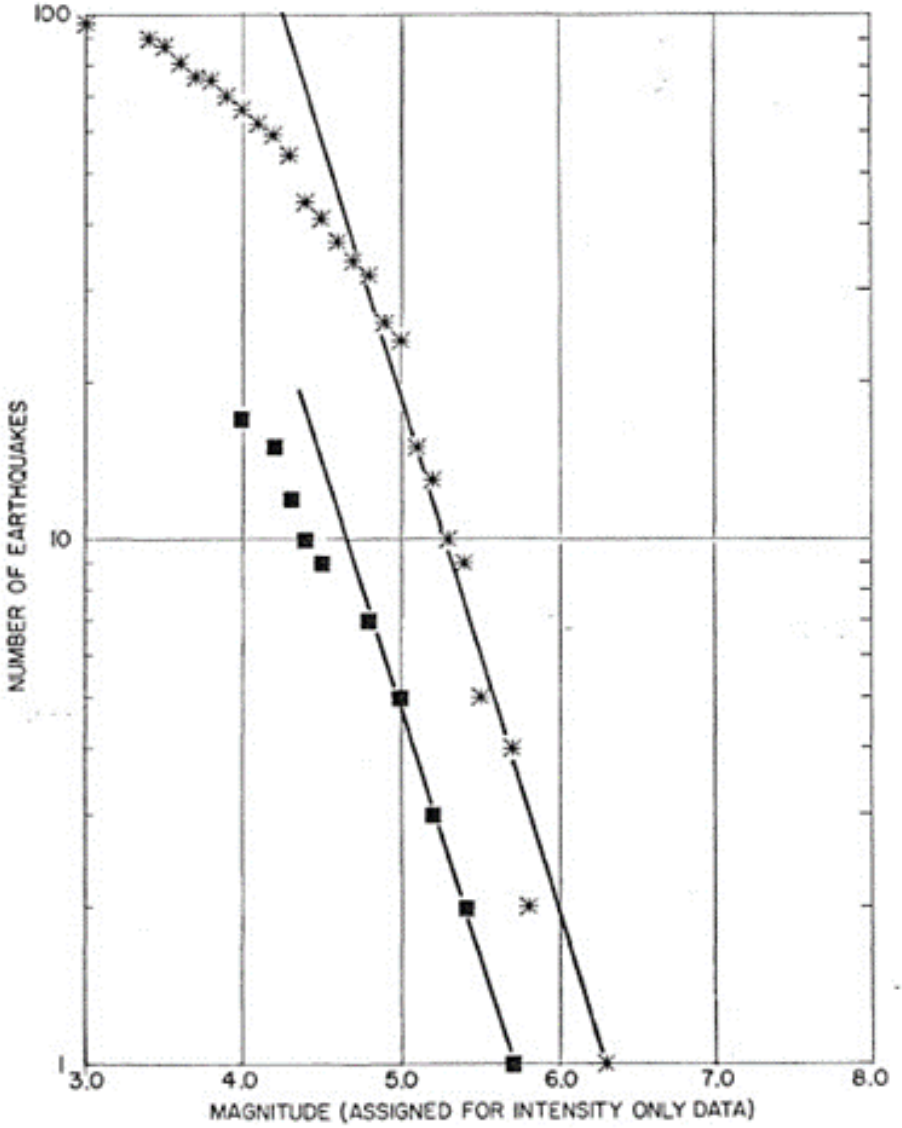

Figure 1-17. Recurrence curves for seismicity of the region (Dames and Moore, 1981). The uppermost curve (stars) considers all events within a radius of 400 km from Koeberg. The lower curve (squares) is based on those events occurring since 1900 in a radius of 180 km from Koeberg, with the main 1969 Ceres event and its aftershocks removed.

Based on their observations and studies, Dames and Moore (1981) concluded that the Saldanha–Darling–Franschhoek, Piketberg–Wellington, and postulated Milnerton–Cape Hangklip fault zones were the most likely fault sources capable of producing earthquakes sufficiently large to affect the KNPS site. The conservative estimate for the seismic zoning model is the occurrence of earthquakes with a magnitude up to M_L 6.5 occurring anywhere along the three fault zones. The location of these sources implied that the closest event to Koeberg would occur along the postulated Milnerton–Cape Hangklip fault zone. The Dames and Moore (1981) analysis followed the DHSA procedure described in Section 1.2.1.

1.3.1.4 Design basis ground motion

Following the seismic source and ground motion characterisation, the design basis ground motion was calculated using deterministic procedures. Although assessments carried out by

Dames and Moore (1981) strongly point towards an M_L 6.5 event for the southwestern Cape region, a conservative decision was made to use an M_L 7.0 event. It was also decided that an earthquake with this magnitude can equally occur along any of the three fault zones in the source model including the Milnerton–Cape Hangklip fault zone.

As a result, Dames and Moore determined the Safe Shutdown Earthquake (SSE) to be an earthquake of local magnitude, M_L 7.0, at 8 km from the KNPS site. Using this information and the GMPE shown in Equation 1-2, a PGA of 0.3g was obtained. A slightly higher damage earthquake (DE) acceleration was obtained for M_L 6.5, occurring at the same distance of 8 km, but assuming the attenuation equation fixed at one standard deviation above the median value. The PGA obtained then was 0.36g. In addition, a "distant" event on the Saldanha–Darling–Franschhoek Fault Zone was specified as an M_L 7 event occurring at 17 km from the site. For this event, the PGA value was calculated as 0.24g. The response spectra for 5% damping were based on a PGA of 0.3g, representing the SSE level for the “distant” earthquake of PGA of 0.24g (Figure 1-18). These two spectra are compared in Figure 1-18, with the USNRC Regulatory Guide 1.60 (USAEC, 1973) response spectrum anchored at 0.3g.

Interestingly, Dames and Moore (1974) also assigned an AFE to their event. Based on Bayesian probabilities described by Benjamin (1968) and applied to a limiting magnitude of M_L 6.5 for zones similar to the Western Cape, they determined that there was less than a 2% chance that one or more earthquakes producing greater than 0.15g PGA would occur in the next 100 years. This is approximately equal to a 10,000-year return period earthquake, or 1×10^{-4} AFE. According to Dames and Moore (1974), a 10,000-year return period earthquake was considered acceptable for other nuclear power plants and thus, the 0.15g PGA was initially recommended as the design basis.

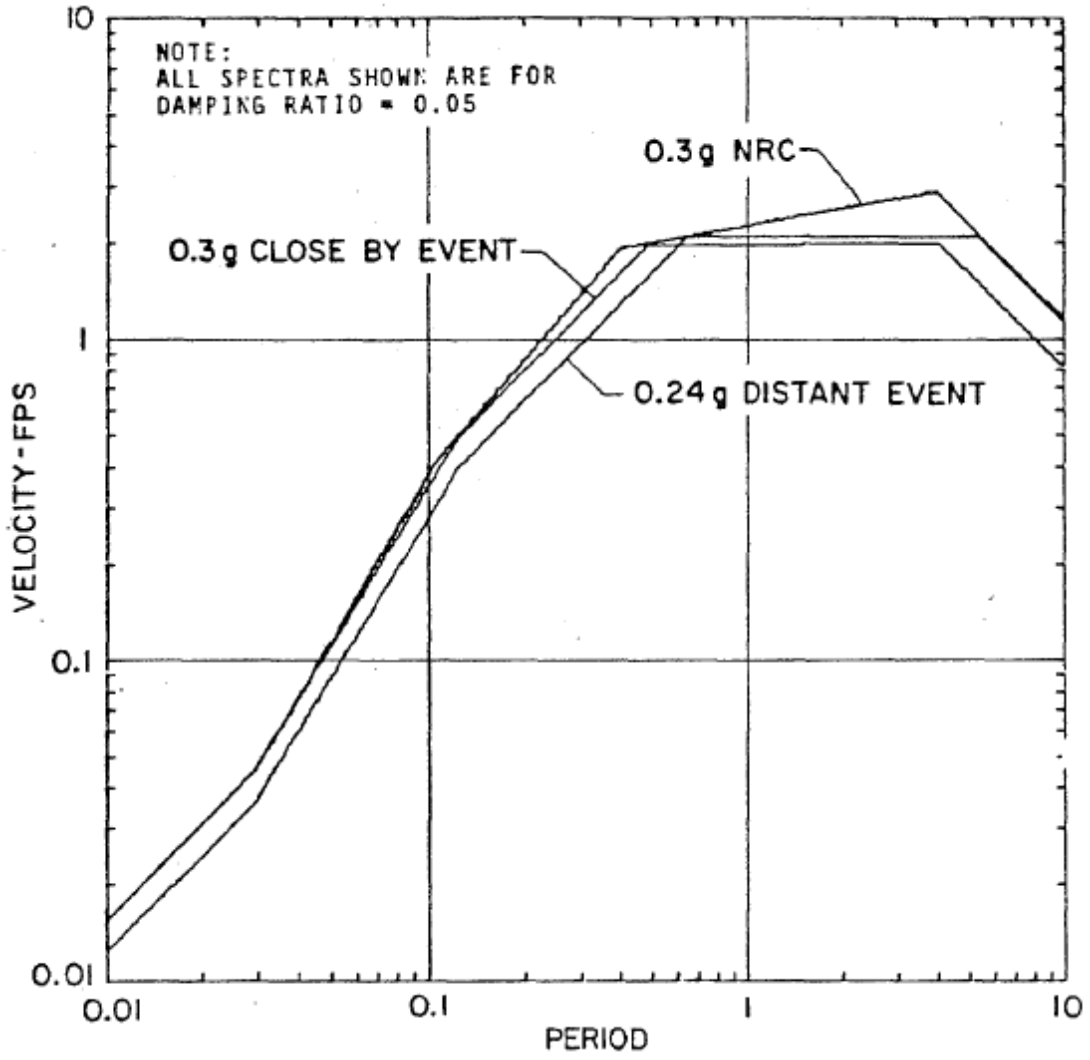

Figure 1-18. Recommended horizontal motion design spectra for the SSE compared to that for the distant earthquake as well as Regulatory Guide 1.60 (USAEC, 1973) design spectra anchored at 0.30g.

1.3.2 1999 Council for Geoscience SHA

In 1999, the CGS re-evaluated the design basis ground motion developed by Dames and Moore (1981). By considering the various strengths and weaknesses of the then current techniques and methodologies for calculating site-specific seismic hazard, Kijko et al. (1999) used a technique that does not require specifying seismic source zones and accounts for the varying quality of different parts of the earthquake catalogue. The selected approach was referred to as a parametric-historic approach. Kijko et al. (1999) used a statistical technique to evaluate a regional maximum magnitude earthquake. As outlined in IAEA (1991), which was followed in the CGS study by Kijko et al. (1999), this is the first step in generating a data-driven seismotectonic model. Kijko et al. (1999) made use of available information on the seismotectonics of South Africa as compiled by Du Plessis (1996a), Partridge (1995), and Hartnady (1996). Kijko et al. (1999) primarily used the model by Du Plessis (1996b), which provides detail on seismic clusters in the region. The model recognises four major regions of diffuse and enhanced seismicity (Figure 1-19).

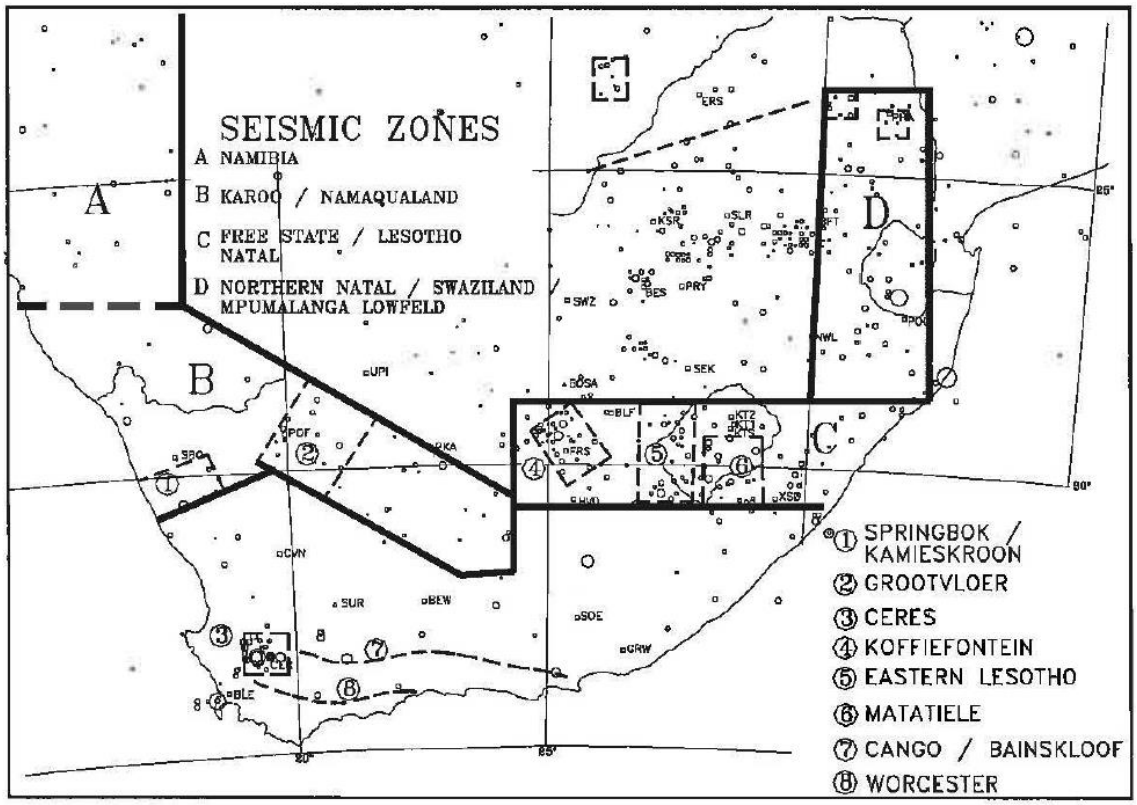

Figure 1-19. Seismotectonic provinces by Du Plessis (1996).

Du Plessis (1996) identified three clusters of seismicity, which were eventually selected by Kijko et al. (1999) as possible locations of sources of earthquakes that can affect the seismic hazard at Koeberg. The three clusters are as follows:

1. The Ceres seismicity cluster: the epicentres in the Ceres–Tulbagh area appear to be located in a region with a dominant NW–SE fault orientation, at the point where the Worcester and Cango–Baviaanskloof Fault Systems converge and terminate.
2. The Worcester and Cango–Baviaanskloof Fault Systems: a few earthquakes appear to have been located on these faults or their extensions, implying that the faults are seismogenic structures.
3. The Cape Town seismicity cluster (Figure 1-20): this cluster was mainly made up of historical events whose occurrence was obtained from reports in newspapers (Fernandez and Guzman, 1979).

Kijko et al. (1999) concluded that their model was a vast improvement on that prepared by Dames and Moore (1981), mainly because theirs was based on reports created using “better” geophysical and seismological data and information. Kijko et al. (1999) then went on to prepare a seismic source model made up of four seismic sources: (1) the Worcester and Cango–Baviaanskloof (W-C/B) faults, (2) the Ceres cluster, (3) the Cape Town cluster, (4) and background seismicity. For each of these sources, Kijko et al. (1999) used associated seismicity to determine recurrence parameters (Table 1-3).

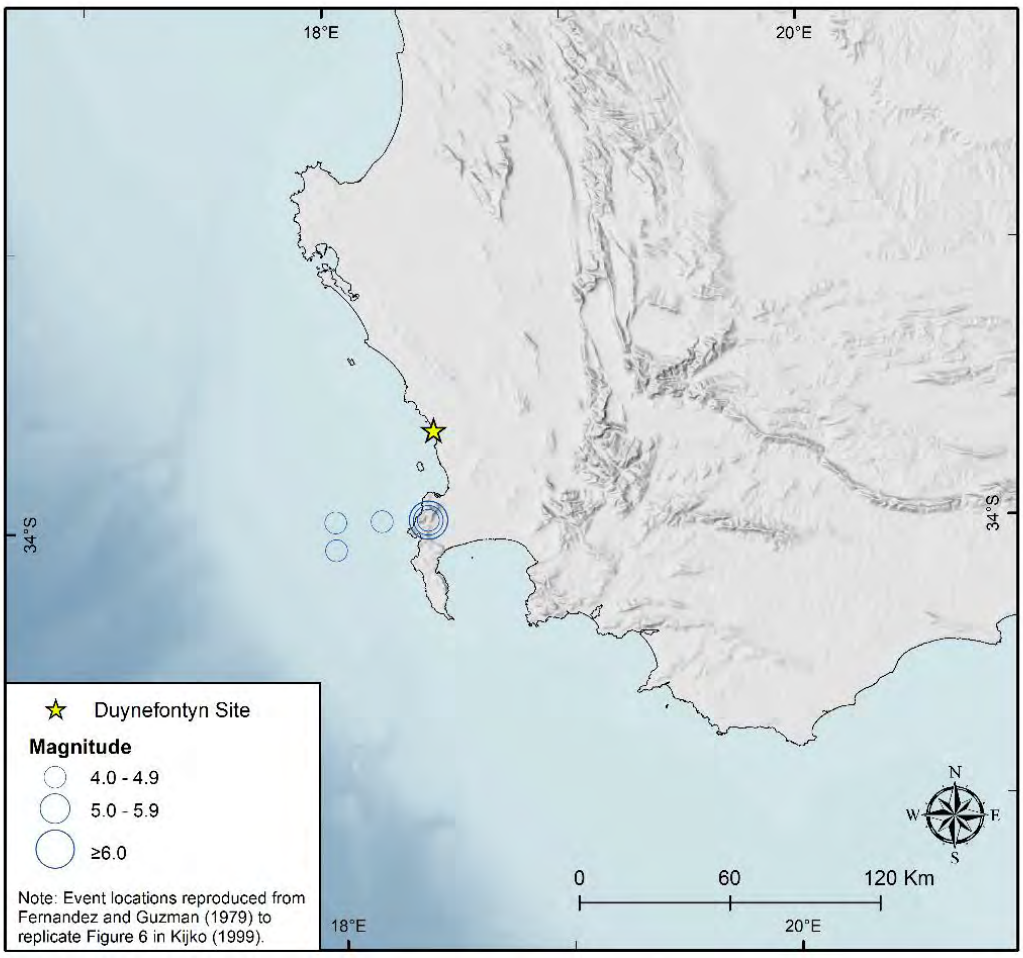

Figure 1-20. Map of the Western Cape showing the Cape Town seismicity cluster. The image was reproduced from Figure 6 of Kijko et al. (1999) because the original optical scan of that report was of poor visual quality.

Table 1-3. Evaluated earthquake hazard parameters, from Kijko et al. (1999).

Source zones	*b*-value (± SD)	$\lambda_{3.0}$ (± SD)	Mmax (± SD)	Max Observed
W-C/B	0.47 ± 0.43	3.22 ± 6.89	5.79	5.4
Ceres	0.69 ± 0.16	0.25 ± 0.18	6.73 ± 0.50	6.3
Cape Town	1.06 ± 0.24	0.63 ± 0.63	6.51 ± 0.48	6.1
Background	0.95 ± 0.24	0.38 ± 0.21	5.79 ± 0.38	5.5

SD is standard deviation.
$\lambda_{3.0}$ is the annual mean activity rate for events of local $M_L \geq 3.0$.
Mmax is the maximum expected earthquake magnitude.
Max Observed is the maximum observed earthquake magnitude.

1.3.2.1 Ground-motion prediction

Kijko et al. (1999) used the ground-motion prediction equations (GMPEs) developed by Atkinson and Boore (1995, 1997) for the PGA and 5% damped acceleration response spectra. Kijko et al. (1999) were of the opinion that these equations did not adequately match the spectral shape of the attenuation curve for small to moderate earthquakes, thus they recalculated the coefficients of the attenuation equations by applying an alternative model, which did not include the quadratic element of the magnitude (Equation 1-3).

1-3

$$\ln(a) = c_1 + c_2\mathbf{M} + c_3 R + c_4 \ln(r) + \varepsilon$$

where **M** is moment magnitude, *r* is distance in km, c_1 = -2.682 ± 0.501, c_2 = 0.980 ± 0.06, c_3 = 0.00058 ± 0.0014, and c_4 = -1.522 ± 0.117, *a* is acceleration in g, and ε is the error term.

Kijko et al. (1999) used a different value for the c_4 coefficient, which they felt resulted in an equation that better fits the tabulated values of the PGA and response spectra. This was obtained from PGA values recorded from earthquakes of magnitude values 4.0 ≤ **M** ≤ 7.25, at distances of 10 ≤ *r* ≤ 500 km (Atkinson and Boore, 1995, 1997). The PGA values refer to sites that would be categorised as firm rock.

1.3.2.2 Koeberg site characteristic ground motion

Following a deterministic-based approach, Kijko et al. (1999) calculated ground-motion intensity values for the site. They first calculated PGA values at the KNPS site inferred from the four seismic sources (Table 1-4).

Table 1-4. Contribution from the W-C/B, Cape Town, Ceres, and background source zones to the seismic hazard at the KNPS site, from Kijko et al. (1999).

Source Zone	MCE	Average Hypocentral Distance (km)[1]	Peak Ground Acceleration (g)
W-C/B	5.79	206.5	0.02
Background	5.79	19.7	0.22
Cape Town cluster	6.51	26.9	0.27
Ceres cluster	6.73	66.0	0.12

[1]In their report Kijko et al. (1999) used the term average hypocentral distance. It's unclear what Kijko et al. (1999) used to determine average.

The largest contributor of hazard to the KNPS site was from an MCE value of 6.51 ± 0.48 from the earthquakes that made up the Cape Town cluster, located at a hypocentral distance of 26.9 km from Koeberg. Kijko et al. (1999) also considered the MCE for all four sources (as in Table 1-4) to determine the horizontal component of the ground acceleration response spectra. In the hazard calculations, they determined ground motions over a spectral frequency range of 0.5–50 Hz (Figure 1-21).

The response spectra obtained for the KNPS site using data for the W-C/B faults and the Ceres seismicity cluster are shown in Figure 1-22 and Figure 1-23, respectively. An Mmax value of 5.79 was determined for the background seismicity and the worst-case scenario was considered for an hypocentral distance of 17 km. In considering the worst-case scenarios for all seismic sources, the seismic hazard for the KNPS site contributed by the W-C/B faults, the Ceres seismicity cluster, and the background seismicity, are very low compared to that contributed by the Cape Town cluster. The acceleration response spectrum of Kijko et al. (1999) for the Cape Town cluster was compared to that obtained by Dames and Moore (1981) to demonstrate that the design of the plant met the requirements proposed by the CGS re-evaluation (Figure 1-24).

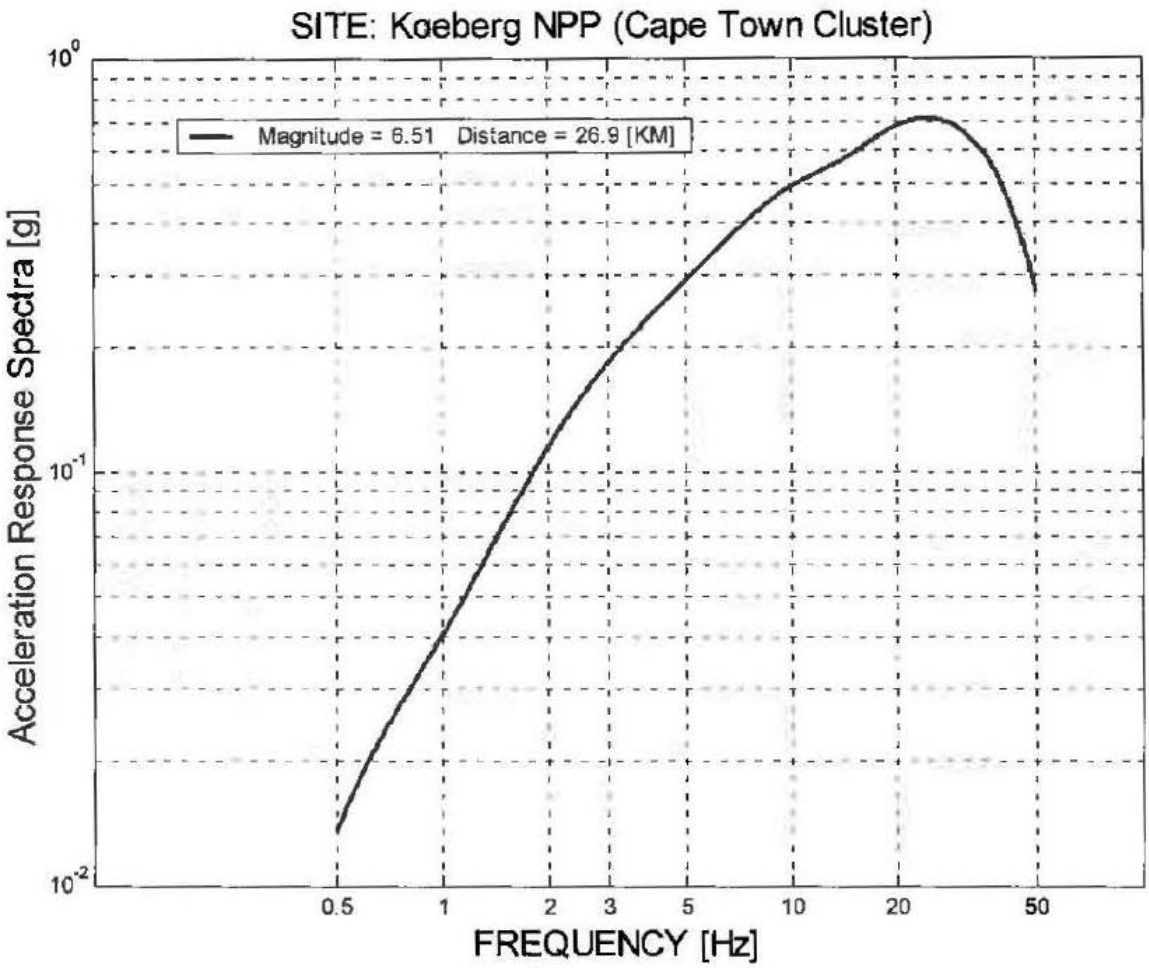

Figure 1-21. Median value of the horizontal acceleration response spectra (5% damping, hard rock site) predicted at the KNPS site for Mmax = 6.51 at a hypocentral distance of 26.9 km, from Kijko et al. (1999).

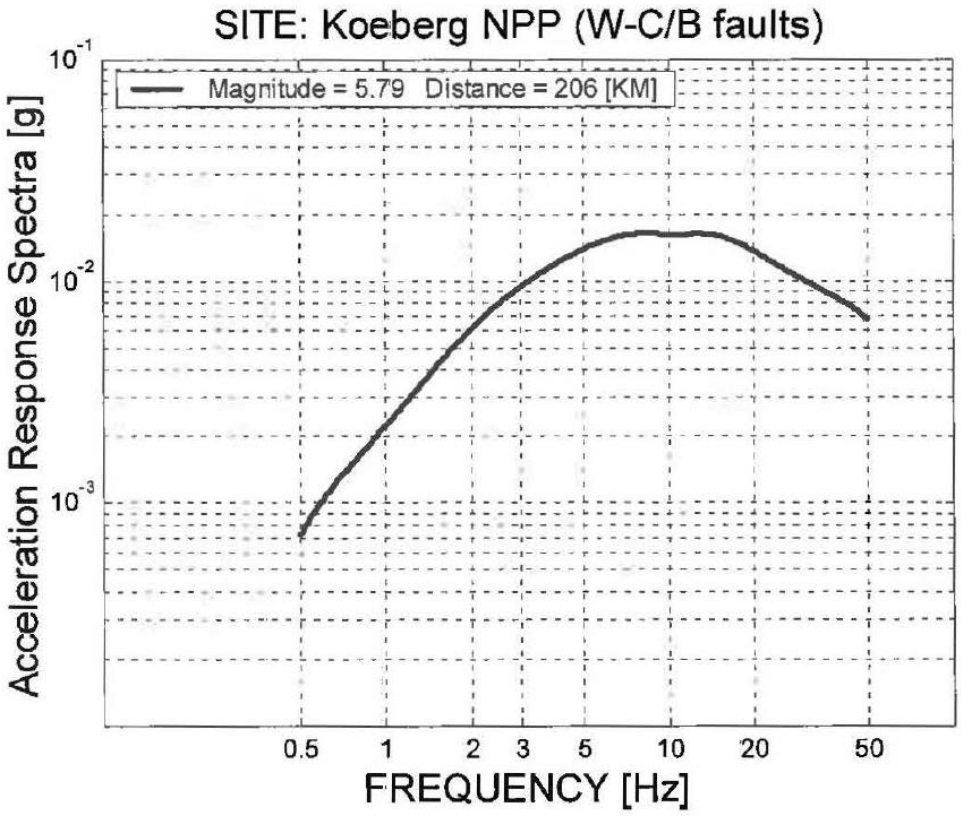

Figure 1-22. Median value of the horizontal acceleration response spectra (5% damping, hard rock site), predicted at the KNPS site for Mmax = 5. 79 at a hypocentral distance of 206 km, from Kijko et al. (1999).

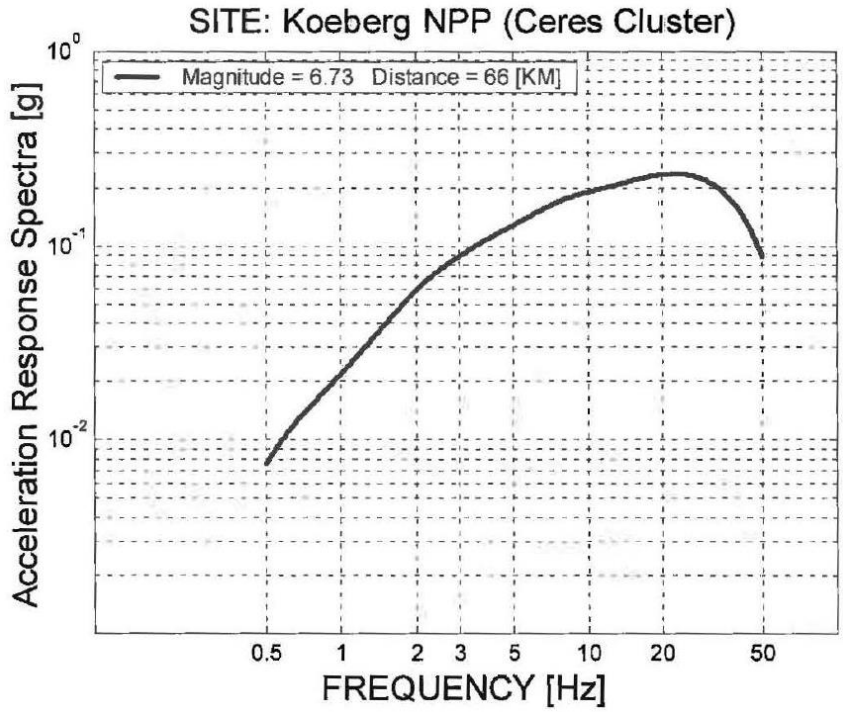

Figure 1-23. Median value of the horizontal acceleration response spectra (5% damping, for sites of hard rock) predicted at the KNPS site for Mmax = 6. 73 at a hypocentral distance of 66 km, from Kijko et al. (1999).

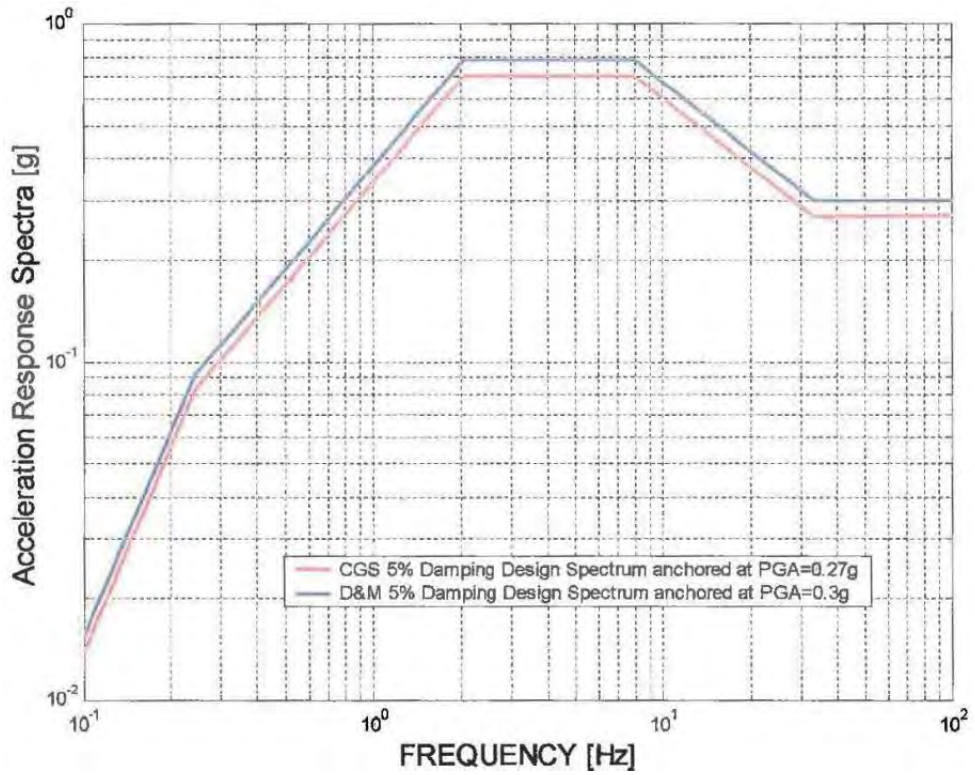

Figure 1-24. A comparison of the 5% damped acceleration response spectrum predicted for the KNPS site for Mmax= 6.51 at a hypocentral distance of 26.9 km (red), and the adopted SSE response spectrum for 5% damping (blue) as given by Dames and Moore (1981) and as shown by Kijko et al. (1999).

1.3.3 Updated 2006 CGS Koeberg SHA

The SHA for three nuclear sites—KNPS, Bantamsklip, and Thyspunt—was reassessed in 2006 (Bejaichund et al., 2006 a,b). The main objective for the study was to update the SHAs as a long time had elapsed since the previous seismic hazard studies (1999 for the KNPS site and 2002 for Bantamsklip and Thyspunt). In addition, the seismic catalogue had been significantly updated and improved, with the catalogue extending to 30 April 2005. Palaeoseismic and neotectonic studies (De Beer, 2006a,b; Goedhart, 2006; Roberts, 2006), which formed part of a nuclear siting investigation programme, yielded data to be considered in the SHAs (Bejaichund et al., 2006b).

Only the assessment carried out for the KNPS site is summarised here. Bejaichund et al. (2006a) followed a similar methodology for the assessment to that employed by Kijko et al. (1999). Significantly, the palaeoseismic and neotectonic studies did not yield any data, apart from the new, updated earthquake catalogue, that could be used to update the existing seismotectonic model (Bejaichund et al., 2006b). Rather, they incorporated the tectonic model of Du Plessis (1996) and used the SSM developed by Kijko et al. (1999). The difference between the source models of the 1999 and 2006 studies was that the seismicity was more populated in the 2006 study (Figure 1-25).

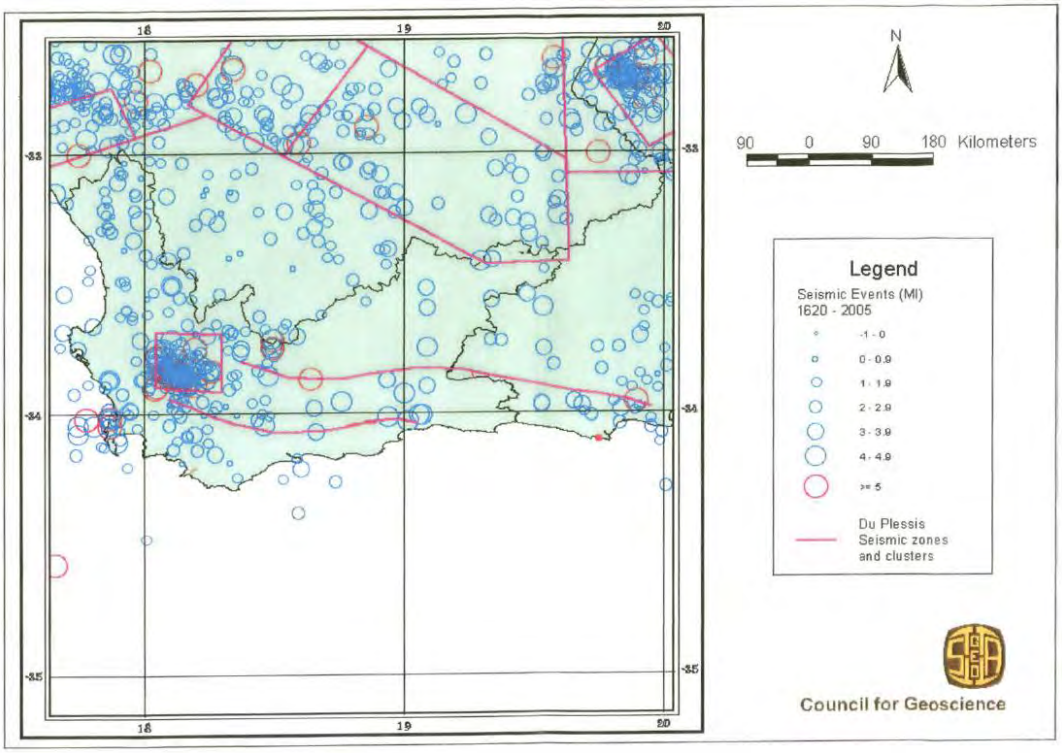

Figure 1-25. Seismicity in the southwestern Western Cape Province as provided by Du Plessis (1996), with updated earthquake catalogue up to 2005 (Bejaichund et al., 2006a).

Using the updated earthquake catalogue, Bejaichund et al. (2006a) recalculated the recurrence parameters (activity rate and *b*-value) and Mmax values for the four seismic source zones, W-C/B faults, Ceres seismicity cluster, Cape Town cluster, and background seismicity. Apart from the updated earthquake catalogue, the authors also used an updated version of the technique used to estimate Mmax, namely the K-S-B estimator as described by Kijko and Graham (1998) and Kijko (2004). A comparison of the parameters obtained in the 2006 study to those obtained in the 1999 study shows a modest to significant changes in the values (Table 1-5), which can be attributed primarily to the updated earthquake catalogue.

Table 1-5. Re-evaluated earthquake hazard parameters for the four source zones of Kijko et al. (1999).

Source Zone	*b*-value ± SD	$\lambda_{3.0}$ ± SD[1]	Mmax[2] ± SD
W-C/B faults	0.94 ± 0.10 (0.47)	1.26 ± 0.74 (3.22)	5.83 ± 0.44 (5.79) [3]
Ceres cluster	0.90 ± 0.09 (0.69)	0.65 ± 0.27 (0.25)	6.73 ± 0.50 (6.73)
Cape Town cluster	1.01 ± 0.10 (1.06)	0.37 ± 0.27 (0.63)	6.60 ± 0.32 (6.51)
Background seismicity	1.05 ± 0.09 (0.95)	1.29 ± 0.37 (0.38)	5.81 ± 0.33 (5.79)

1 - SD is standard deviation. $\lambda_{3.0}$ is the annual mean activity rate for events of local $M_L \geq 3.0$.
2 - Mmax is the maximum expected earthquake magnitude.
3 - The values in parentheses are values of the same parameters obtained in the Kijko et al. (1999) study.

1.3.3.1 Site-characteristic maximum PGA for Koeberg

The resulting PGA values at the KNPS site for the MCEs in Table 1-5 are provided in Table 1-6. A deterministic approach was implemented, making use of the Atkinson and Boore (1995, 1997) GMPEs (as was done by Kijko et al., 1999). The site-specific deterministic response spectrum for the horizontal component of the ground acceleration was also calculated (Figure 1-26).

The contributions to the hazard by source zones around the KNPS site are shown in Table 1-6. The envelope of these curves is the spectrum derived for the Cape Town cluster. As seen earlier in the 1999 study (Kijko et al., 1999), the contribution by the W-C/B fault, Ceres clusters and background seismicity to the seismic hazard (in terms of the amplitude of spectral acceleration at Koeberg) is very low in comparison to the contribution by the maximum possible earthquake (Mmax = 6.6) from the Cape Town cluster. Based on these results, the CGS (Bejaichund et al., 2006a) recommended that the value of 0.27 ± 0.13g, as obtained by Kijko et al. (1999), remain as the design event for the KNPS site until further information became available, especially for the postulated Milnerton seismic source.

Table 1-6. Contribution of the four seismic source zones to the seismic hazard at the KNPS site (Bejaichund et al., 2006a).

Source Zone	Mmax or MCE (M_L)	Average Hypocentral Distance (km)	PGA (g)
W-C/B faults	5.83	206.8	0.007
Ceres cluster	6.73	66.7	0.087
Cape Town cluster	6.60	29.2	0.27
Background seismicity	5.81	22.7	0.18

Figure 1-26. Plot of scenario horizontal acceleration response spectra for different earthquakes (from different source zones) used in the analysis of Bejaichund et al. (2006a).

1.3.4 2008 Design ground motion at Koeberg by Rizzo

The fourth study was conducted by Rizzo (2008) to define the ground motion for a Pebble Bed Modular Reactor (PBMR) demonstration power plant at the Duynefontyn site. This study was carried out to update the SHA for the KNPS site to conform to a probabilistic approach. This followed an international, instructed by the NNR in December 2006, on the seismic hazard studies performed up to that point. The subsequent review found the parametric-historic approach to be inconsistent with global best practice at the time, necessitating a more standard PSHA methodology for nuclear licensing submittals. Rizzo (2008) used data and information from the CGS, supplemented by available published literature, to develop the PSHA. No new field investigations were carried out.

The PSHA followed the following steps:

1. Identification of seismic source zones that can produce earthquakes likely to affect the seismic hazard of the KNPS site, including a definition of their respective geometries.
2. Determination of recurrence parameters defining the magnitude distribution associated with each seismic source and the respective Mmax.
3. Preparation or selection of ground-motion models that relate intensity values such as PGA and spectral acceleration with magnitude and distance of the seismic event from the study site of interest.
4. Combining information from Steps 1 to 3, to compute the annual rate of exceedance of a given ground motion intensity.

1.3.4.1 Seismic sources in the Rizzo (2008) model

The seismic source characterization was developed using available geological, tectonic setting, structural geology, and seismic data. Given the uncertainties associated with the models and data used, an effort was made to model these uncertainties and incorporate them in the assessment utilising the logic-tree formalism. In assessing the available geology and seismology data, Rizzo (2008) considered and presented information from the site region (area of radius between 40 km and 300 km from KNPS site) and the site area (area of radius

less than 40 km from Koeberg site) to aid in the identification of seismogenic and capable tectonic sources.

In a discussion of the regional tectonic structures in the southwestern part of the Western Cape, Rizzo (2008) summarised the description in a similar way to that in Dames and Moore (1981). They recognised the three tectonic domains that are separated by the Saldanha–Darling–Franschhoek and Piketberg–Wellington Fault Zones and referred to the possible presence of a fault zone between Milnerton and Cape Hangklip. Rizzo (2008) also recognised clusters of seismicity previously described by Du Plessis (1996) as potential locations of future earthquakes capable of affecting the seismic hazard of Koeberg. These clusters include the Ceres seismicity cluster and the Worcester and Cango–Baviaanskloof Fault (Figure 1-27). Although the Cape Town seismicity was also recognised as a cluster, it mostly comprises historic earthquakes. A fourth seismogenic source zone, referred to as "Diffuse Seismic", was essentially the same as Kijko et al.'s (1999) background seismicity source or the Cape Low Province of Du Plessis (1996).

1.3.4.2 Earthquake catalogue

Rizzo (2008) adopted the catalogue of earthquakes previously prepared by the CGS and used by Bejaichund et al. (2006a), which includes events with a minimum M_L = 3.0. In preparing the catalogue for the seismic hazard assessment, Rizzo (2008) removed mining events and dependent events (foreshocks and aftershocks). The magnitude values in the CGS catalogue were quoted as M_L. These were converted to body-wave magnitude (m_b) and subsequently to moment magnitude (M_W)[6]. The conversion to m_b was carried out using Equation 1-4, which was developed by the Electric Power Research Institute (EPRI) (1986).

1-4

$$m_b = 0.655 + 0.812\mathrm{M_L}$$

To be consistent with the definition of magnitude in GMPEs, the m_b values were further converted to M_W using the following relationships (Equations 1-5,1-6 and 1-7), each of which was given a weight of 1/3.

Atkinson and Boore (1987):

1-5

$$M_W = 2.715 - 0.277m_b + 0.127m_b^2$$

EPRI (1993):

1-6

$$M_W = 0.3281 + 1.9437m_b - 0.4302m_b^2 + 0.0419m_b^3$$

Johnston et al. (1994):

[6] In current seismic hazard studies, moment magnitude is now designated as **M**.

$$M_W = 1.14 + 0.24m_b + 0.0933m_b^2$$

However, in the assessment, m_b was used for calculating seismicity parameters and M_W in attenuation equations. The spatial distribution of the epicentres from the declustered catalogue is shown in Figure 1-27.

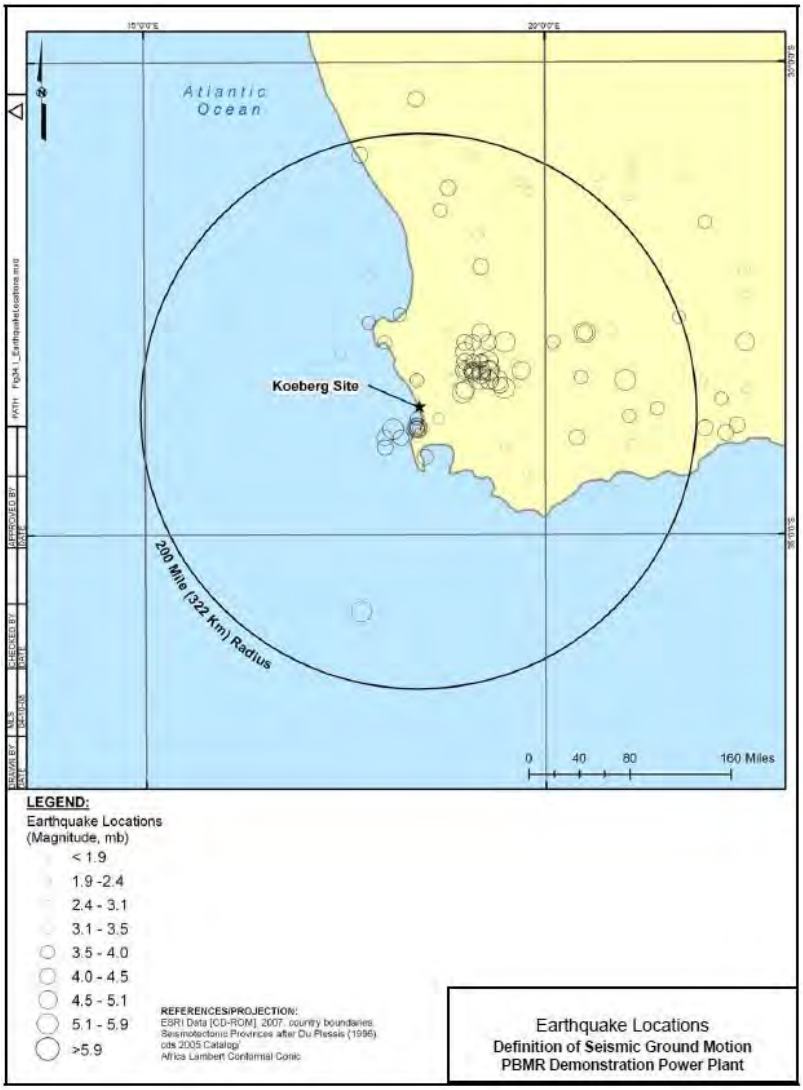

Figure 1-27. Earthquake locations of events in the catalogue prepared by Rizzo (2008).

1.3.4.3 Seismotectonics in Rizzo (2008) model

Using available information on the geology and activity in the region, Rizzo (2008) developed a model of seismic sources with the potential to produce earthquakes capable of inducing vibratory ground motions at the Koeberg site. As with the earlier studies by Dames and Moore (1981), Kijko et al. (1999) and Bejaichund et al. (2006a), Rizzo (2008) also considered four seismic sources (Figure 1-28 a).

Rizzo (2008) decided to modify the earlier sources. The major changes included removing the Cape Town cluster as a separate source zone and incorporating its seismicity as part of the diffuse (background) seismicity. This decision was informed by the large uncertainties

associated with the Cape Town earthquakes, with the authors considering it almost impossible to confidently demarcate a small source zone around the events. Another change was to reduce size of the source zone around the Ceres cluster. In addition, the separate W-C/B source was also removed, and the associated events included in the background seismicity. These changes resulted in a source model consisting only of the Ceres seismicity cluster and background seismicity (Figure 1-28 b).

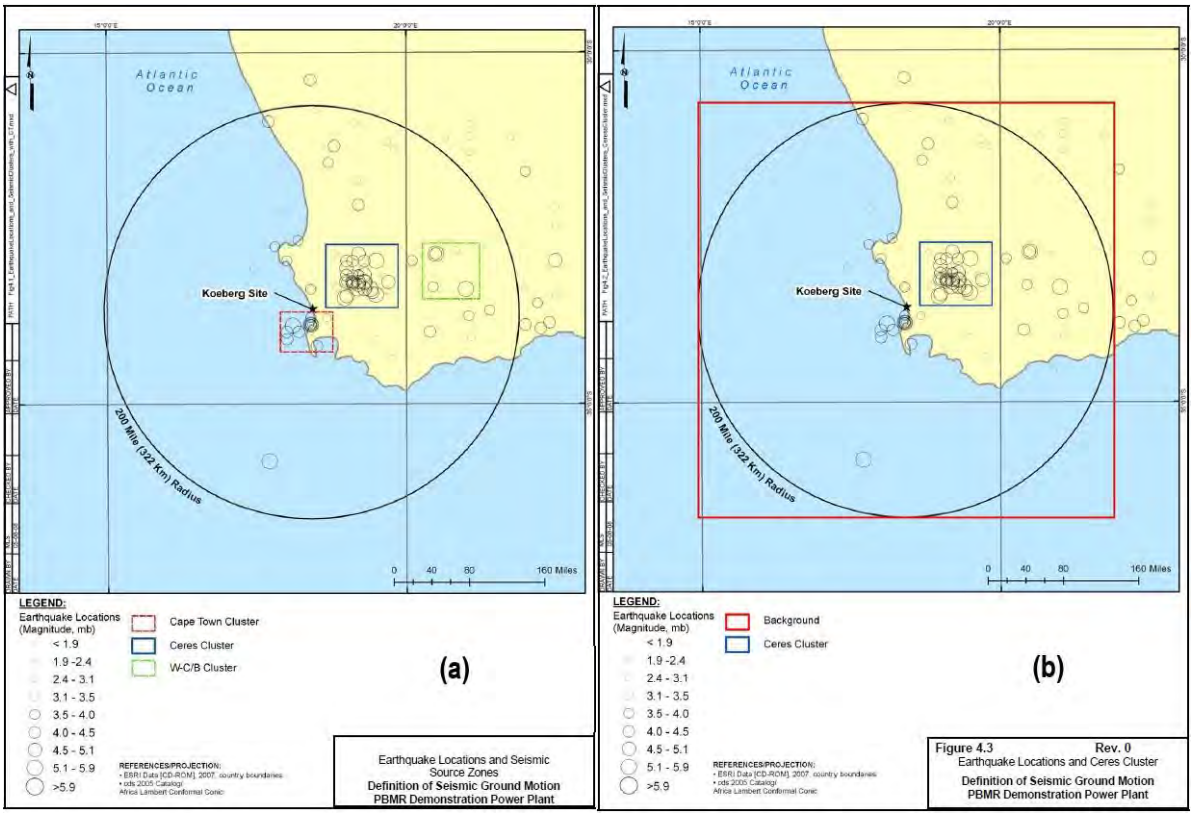

Figure 1-28. (a) Preliminary seismic sources outlined by Rizzo (2008) from previous studies by Kijko et al. (1999). (b) Final seismic source model used by Rizzo (2008) in his seismic hazard assessment.

The recurrence parameters for the defined area source zones were described using the Gutenberg-Richter (G-R) equation. Thus, the activity rate (*a*) and *b*-value were determined for each source using the updated earthquake catalogue and the smoothing approach for activity rate (Frankel et al., 2002). The approach used considers only the variation of *a*, for prescribed constant values of the *b*-value. The obtained *b*–values are shown in Table 1-7.

Table 1-7. Seismic parameters for the two seismic source zones identified in Rizzo (2008).

Source Zone	*b*-value	*b*–value weight	Mmax (m_b)	Mmax weight	Moment Magnitude, M_W			Mmax (M_W)
					AB87[1]	EPRI93[2]	Johnston94[3]	
Ceres	0.90	1	6.12	0.60	5.78	5.72	6.10	5.86
			6.53	0.20	6.32	6.34	6.69	6.45
			5.71	0.20	5.27	5.20	5.55	5.34
Background	1.10	1	6.01	0.60	5.64	5.57	5.95	5.72
			6.28	0.20	5.98	5.95	6.33	6.09
			5.75	0.20	5.32	5.25	5.60	5.39

1 - AB87 is the Atkinson and Boore (1987) relation.

2 - EPRI93 is the EPRI (1993) relation.

3 - Johnston94 is the Johnston et al. (1994) relation.

The upper magnitude, or Mmax, was also determined as part of the characteristics of the seismic source zones. However, Rizzo (2008) decided to adopt the statistically determined Mmax values previously developed by Bejaichund et al. (2006a). The only difference is that Rizzo converted the CGS M_L values to M_W values by using Equations 1-5, 1-6 and 1-7 as described earlier to obtain the values in Table 1-7.

1.3.4.4 Ground-motion model

In selecting GMPEs for use in the seismic hazard for Koeberg, Rizzo (2008) assumed that tectonically, South Africa is a stable continental region (SCR) similar to eastern North America. Three models previously developed for SCRs in North America were selected and used in the PSHA. The first model selected was that developed for eastern North America by Atkinson and Boore (2006) for spectral values of hard rock with shear-wave velocity of 2,000 m/s. The second model was a hybrid model, also for eastern North America, developed by Campbell (2003), applicable to hard rock with shear-wave velocity of 2,000 m/s. Each of these two models was given a weight of 0.4 in the ground-motion model logic tree. The third model selected was the EPRI (2004,2006) model, which was slightly modified in 2006 to correct the aleatory variabilities previously obtained in the 2004 study (EPRI, 2004, 2006). This third model, developed for the central–eastern United States, was used to introduce additional epistemic uncertainty. A lower weight of 0.2 was assigned for this model, mainly because Rizzo (2008) decided that the EPRI model reflects mid-1990s data and an outdated understanding of the subject matter based on that data.

Using the models and parameters described above, Rizzo (2008) calculated the seismic hazard at seven frequencies: 100 Hz (assumed equivalent to PGA), 25, 10, 5, 2.5, 1 and 0.5 Hz (see an example of overlapping hazard curves in Figure 1-29). The mean uniform hazard spectra (UHS) for 10^{-4} and 10^{-5} annual frequencies of exceedance were also calculated (Figure 1-30).

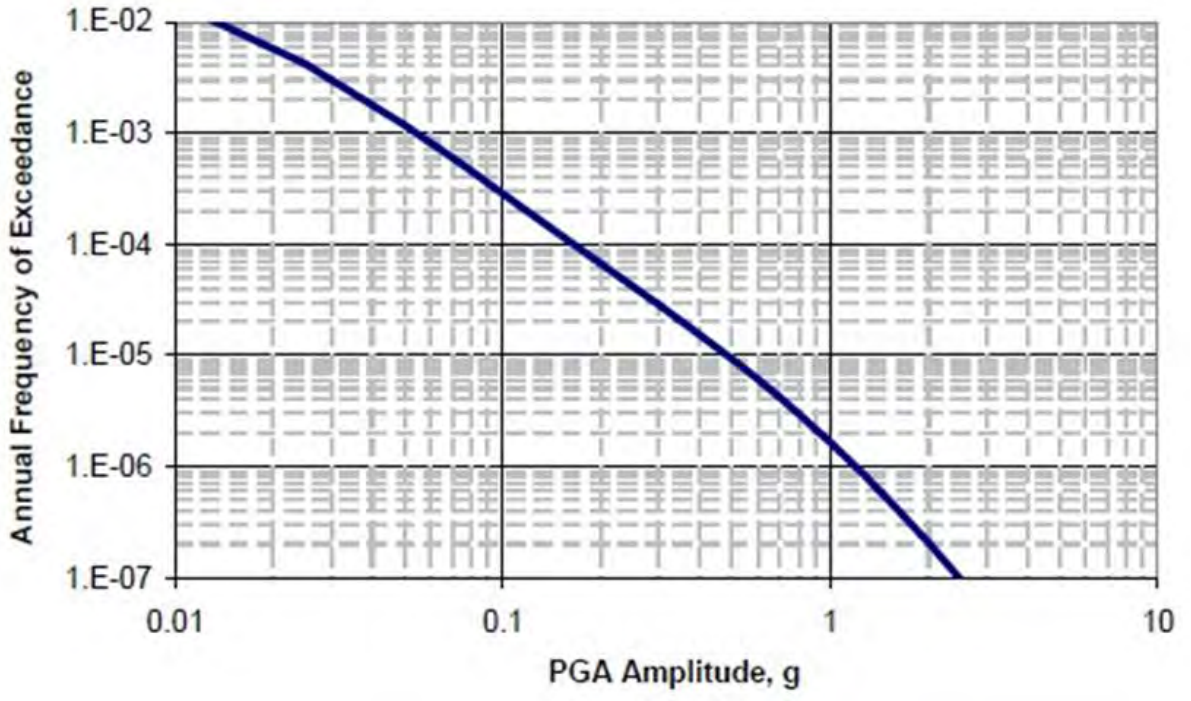

Figure 1-29. Mean PGA hazard of hard rock calculated for the KNPS site by Rizzo (2008).

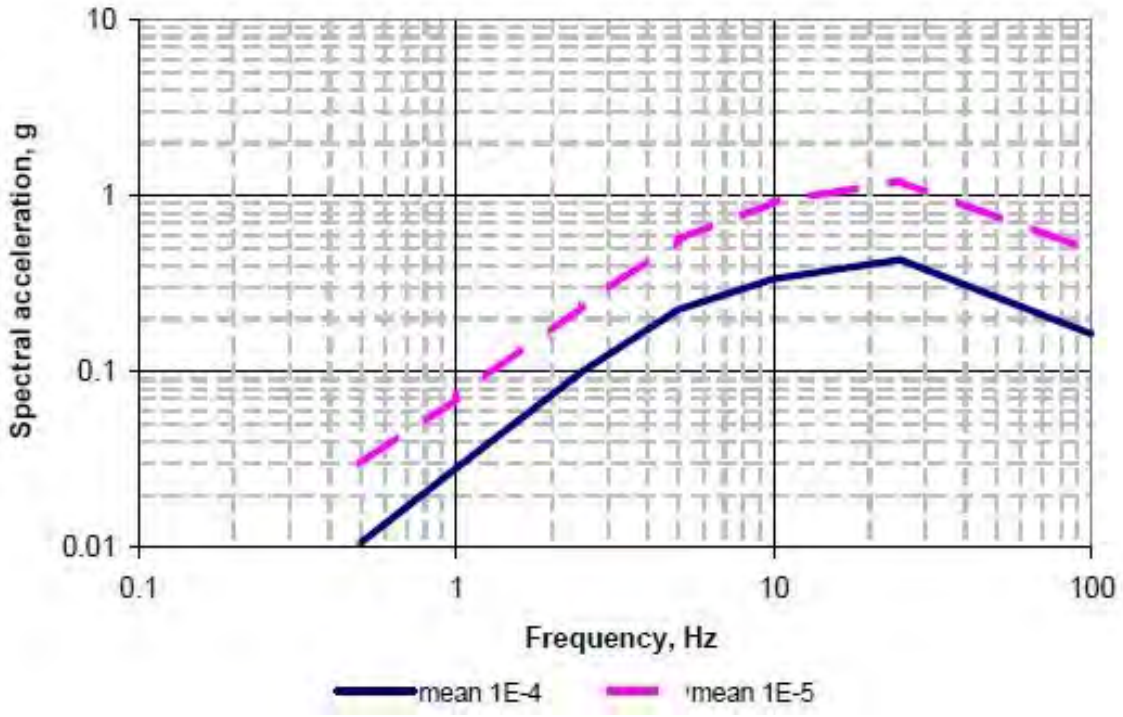

Figure 1-30. Mean hard rock uniform hazard response spectra (UHRS) for the KNPS site by Rizzo (2008).

Unlike in previous studies (e.g. Dames and Moore, 1981; Kijko et al., 1999), where ground motion was determined only at bedrock, Rizzo (2008) conducted a site response analysis (SRA) to determine the ground-motion response spectra (GMRS) at the free-field surface. The free-field surface GMRSs are based on the seismic hazard of hard rock and reflect the wave transmission characteristics of the site represented by horizontal frequency-dependent scaling factors or scaling functions.

The following steps, as described in detail by Rizzo (2008), were taken in the SRA:

1. De-aggregation and identification of the dominant events. The results of the de-aggregation were used to obtain the size and location of the dominant events.
2. Hard rock ground-motion response spectra: uniform hazard response spectra (UHRS) were determined for 10^{-4} and 10^{-5} annual frequencies of exceedance as shown in Figure 1-30. These were determined for hard rock conditions.
3. The next step was the selection of time histories, which in this case were obtained from the NUREG/CR-6728 (USNRC, 2001) database, consistent with the corresponding de-aggregated magnitudes and distances at both 10^{-4} and 10^{-5} annual frequencies of exceedance.
4. Wave transmission characteristics (site conditions): geological investigations as well as a review of existing literature were carried out to determine the characteristics of the soil profile at the Koeberg site. From this process, the shear-wave velocity profiles down to hard rock of velocity 2,000 m/s, strain-dependent shear modulus and viscous damping for each soil/rock material layer, were obtained. Uncertainties associated with these parameters were also assessed and incorporated in the SRA.
5. Development of site amplification functions/factors: Using the results from the first four steps, the ground motion amplification caused by the materials overlying hard rock were calculated for the range of frequencies of interest (Figure 1-31).

The UHRS at the free-field ground surface (Figure 1-32) is based on the hard rock PSHA results and the mean frequency-dependent site amplification functions. By applying a cumulative absolute velocity filter on the free-field UHRS (Figure 1-32), a horizontal SSE spectrum was obtained (Figure 1-33).

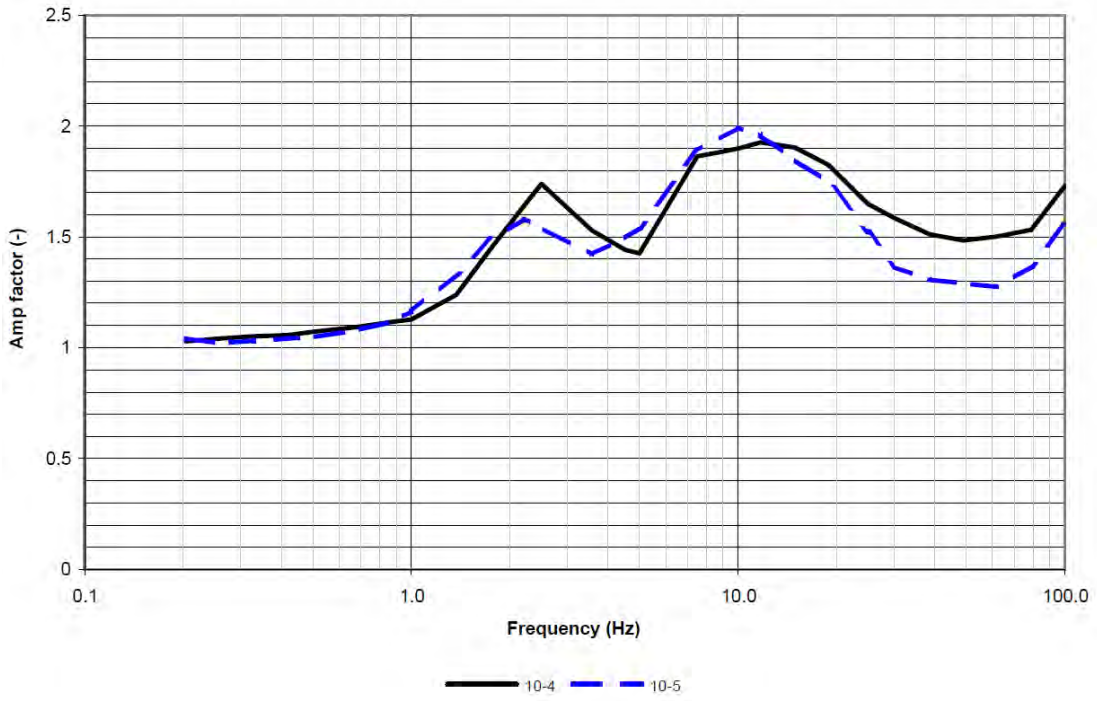

Figure 1-31. Average amplification factors for the KNPS site as obtained by Rizzo (2008).

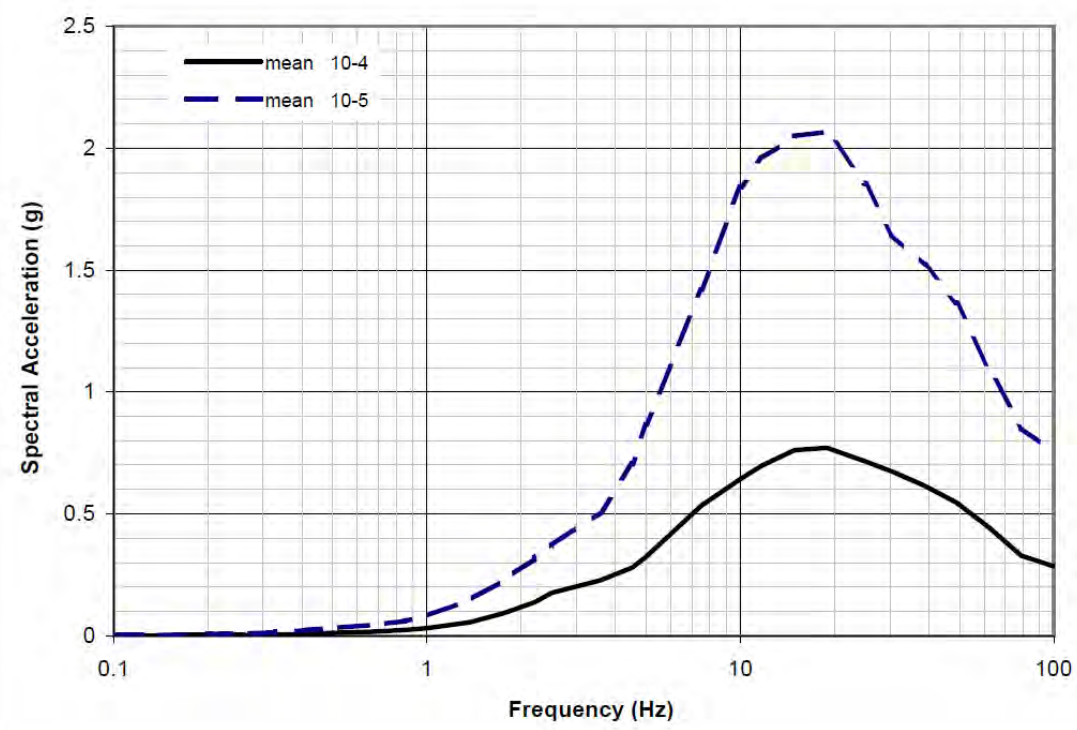

Figure 1-32. Updated soil UHRS at the KNPS site as obtained by Rizzo (2008).

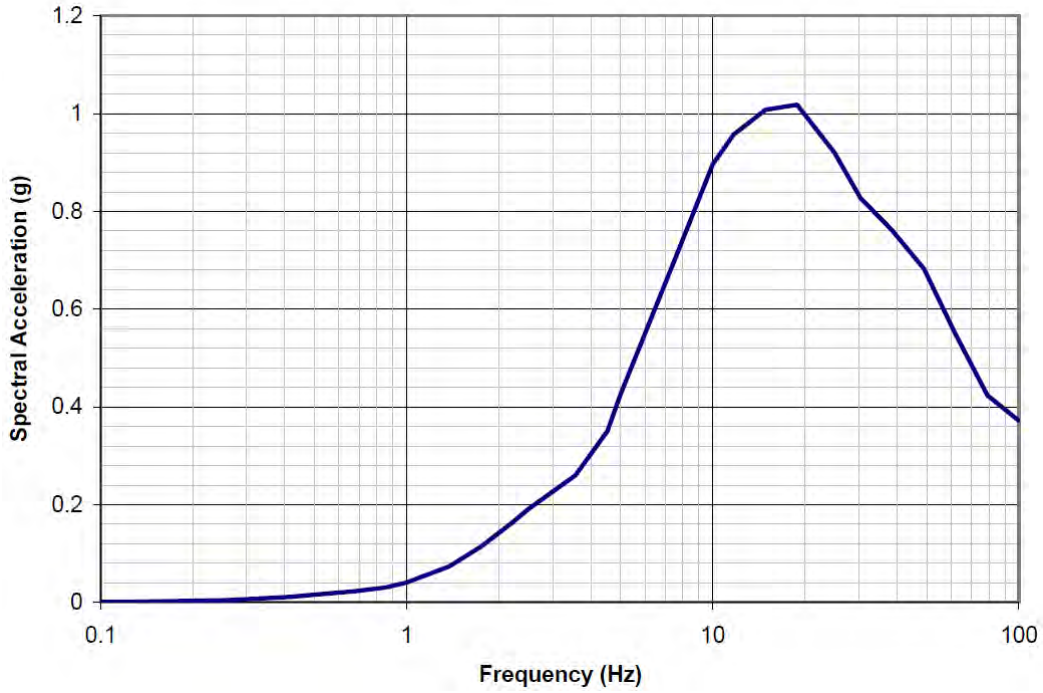

Figure 1-33. Updated SSE horizontal spectra (GMRS) at the KNPS site as obtained by Rizzo (2008).

1.3.5 Summary Assessment and Conclusions

A comprehensive critique of all three previous SHA studies is not provided in this report. Rather, the reason for summarising them is to document that the TI Teams considered their data, model, and methods as part of the SSHAC evaluation process. Nevertheless, some commentary on these prior studies is provided to highlight their deficiencies and to support

the conclusion that this Duynefontyn PSHA study was needed as a replacement. While each prior study was constrained by the accepted methodologies and limited available data, models, methods, and budgets at the time they were developed, all three studies contain technical and procedural shortcomings.

Without exception, the previous SHAs were built on comparatively simplistic seismic source and ground motion analyses that are no longer used in modern seismic hazard studies. For example, in the 1981 Dames and Moore study, the magnitude assigned to each of the three faults was arbitrary, without significant consideration of geological or seismological information. In addition, the GMPE that was created from the 20 isoseismal maps used global equations to convert the isoseismal intensities to PGA. These conversions correlated magnitude to epicentral distance (using linear scaling), without accounting for the seismological properties of the Western Cape or the geotechnical properties of the site. The 1999 and 2006 CGS studies provided additional geological and seismological information about potential faults sources, but the recurrence parameters for these sources were based on indiscriminately associating historical and instrumental seismicity to each fault source. The detailed analysis of the location of historical earthquakes provided in Chapter 3 of this report shows that some of these associations are not valid. In addition, the 1999 and 2006 CGS studies used the GMPEs developed by Atkinson and Boore (1995, 1997), but recalculated the coefficients of the attenuation equations by applying an alternative attenuation model that was not reviewed and omitted the quadradic quadratic element of the magnitude term. In the Rizzo (2008) study, some of the Mmax values assigned to the Ceres source zone (Table 1-7), which is the magnitude of the largest possible future earthquake, were smaller than the 1969 Ceres **M** 6.3 earthquake.

In addition, there appear to be some inconsistencies and errors in the actual reports. In the Dames and Moore analysis, some magnitude values were obtained from intensity data (historical earthquakes) while others were from recorded earthquakes (instrumental), though that was not stated clearly in the Dame and Moore (1981) report. In Rizzo (2008), equation 1-5 was attributed to Atkinson and Boore (1987) but appears to instead be equation 11 from Atkinson and Boore (1995). Moreover, the variables should instead be m_N (Nuttli magnitude), not m_b (body wave magnitude). These errors and inconsistencies make it difficult to verify the accuracy of the resulting ground motions produced by Rizzo (2008).

More significantly, none of the three studies included an evaluation of parameter variability and uncertainty in the inputs, nor did they include any reliable estimates of the uncertainty in the results. There is also no evidence that any of these studies included rigorous peer review. Hence, when measured against modern standards, none of the prior seismic hazard characterisations for the KNPS and the Duynefontyn site meet current regulatory requirements for seismic design, seismic safety, and seismic risk assessments of commercial nuclear power reactors. They are therefore considered indefensible and obsolete and need to be replaced.

The Duynefontyn PSHA documented in this report provides this needed replacement. In contrast to the prior SHA studies, the Duynefontyn PSHA is based on a comprehensive evaluation of all available data, models, and methods and produced hazard results that capture the CBR of TDI, following a tested and internationally accepted methodology. As described in Chapters 2 and 3, the Duynefontyn PSHA meets all the requirements for a full SSHAC Level 3 study per NUREG-2213 (USNRC, 2018), including a comprehensive participatory peer review.

During the evaluation phase of the project, the TI Teams assessed available tectonic, seismological, geological, and geophysical data and models including new data generated by a series of supporting studies and additional site characterisation. For the SSM, these new studies included a comprehensive field investigation in the Western Cape looking for any evidence of geologically recent fault activity, new hydroacoustic offshore data to evaluate potential active faulting in Table Bay and False Bay, a thorough and methodical analysis of the coastal marine terrace data, and a detailed compilation of historical and instrumental seismicity to produce a defensible project earthquake catalogue. For the GMM, these new studies included installation of two vertical microseismicity borehole arrays, new site shear-wave velocity (V_S) data from down-hole measurements and Multichannel Analysis of Surface Waves (MASW) surveys, and two detailed studies that inverted South African earthquake waveform data collected after 2007 to develop a GMM that accounts for the crustal properties of the Western Cape. The evaluations by the SSM and GMM TI Teams are documented in Chapters 3 through 7 of this report.

Chapters 8 and 9 of this report document the integration of the data, models, and methods evaluated by the TI Teams. In these chapters, the SSM and GMM TI Teams describe each branch and node of the logic tree, including the technical bases for the logic tree components and the weights assigned to each branch. These logic tree components of the SSM and GMM are also summarized in the Hazard Input Document (HID), which is the vehicle for transmitting the quantitative model to the hazard analysts for preliminary and final PSHA calculations. A key component of the integration was a thorough consideration by the TI Teams of the aleatory variability and epistemic uncertainties in all the model inputs.

Chapter 10 of this report provides the hazard results, including selected sensitivity analyses to evaluate the hazard inputs and to identify those components of the model that are most important to the hazard results. These sensitivity analyses also highlight those components that contribute most to hazard uncertainty. By closely adhering to the SSHAC process the TI Teams ensured that epistemic uncertainty and aleatory variability was properly accounted for in the SSM and GMM, and thus properly captured in the resulting uncertainty in the hazard results. These PSHA results therefore provide Eskom with an up to date and defensible seismic hazard characterisation that meets the regulatory requirements for the LTO license of the KNPS and the license application for a potential new-build at the Duynefontyn site.

1.4 DELIVERABLES

The final product of the Duynefontyn PSHA is this report, summarising the entire study. Together with the various reports produced on individual components of the study and associated documents and data files, all of which are provided as electronic supplements to the report (for listing, see Appendix E). The key technical product of the Duynefontyn PSHA Project is a probabilistic assessment of the hazard at the KNPS and Duynefontyn sites in terms of vibratory ground motion, which will be used as the basis for Eskom's application to extend the Long-Term Operation (LTO) licence for the KNPS and for a licence application, engineering design of the plant and auxiliary structures, input to other hazard analyses, and risk analyses for the new build at the Duynefontyn site. To cover all the requirements, the hazard output is expressed in several different forms. The basic definition of the vibratory ground motion is the acceleration response spectrum, satisfying the following requirements:

- The basic parameter is spectral ordinates of pseudo-acceleration response at 5% of critical damping, using the geometric mean definition of the horizontal component of motion.
- The hazard results are provided at two locations:
  - Duynefontyn site, top of bedrock (interface between Tygerberg Formation and overlying strata): S 33° 39' 39.99" E18° 25' 41.95"
  - Koeberg, top of bedrock (interface between Tygerberg Formation and overlying strata): S 33° 40' 36.82"S E 18° 25' 53.03"
- The basic outputs are seismic hazard curves and uniform hazard response spectra (UHRS) for the site, as well as the design basis response spectra in accordance with RG 1.208 (USNRC, 2007):
  - Seismic hazard curves for spectral ordinates at the 10 target oscillator periods listed above; the hazard curves are expressed in terms of the mean hazard and the fractiles from 5% to 95%, including the median, calculated for annual exceedance frequencies as low as 10^{-8}.
  - UHRS of horizontal motion at annual exceedance frequencies (10^{-2}, 10^{-3}, 10^{-4}, 10^{-5}, 10^{-6}, 10^{-7} and 10^{-8}).

After delivery of this report, additional products will be developed for Eskom to meet additional engineering analysis and design requirements. These will include scenario response spectra and associated suites of acceleration time-histories. These will be generated in a manner that is entirely consistent with the output from the PSHA but is outside the scope of the PSHA study itself. Another deliverable that is outside the scope of this report is the relevant chapters of the SSR. Chapter 5.14 of the SSR on Seismic Hazard will be based entirely on the contents of this report, and other SSR chapters (particularly Chapter 5.13 Geology) will incorporate relevant material from this report as needed.

1.5 REFERENCES

American Nuclear Society (ANS) (2020). Probabilistic Seismic Hazard Analysis. American National Standard ANSI/ANS-2.29-2020. American Nuclear Society, La Grange Park, Illinois, USA.

Atkinson, G.M. and Boore, D.M. (1987). On the mN, M Relation for Eastern North American Earthquakes. Seismological Research Letters 58(4). 119-124.

Atkinson, G.M. and Boore, D.M. (1995). Ground-Motion Relations for Eastern North America. Bulletin of the Seismological Society of America 85. 17-30.

Atkinson, G.M. and Boore, D.M. (1997). Some Comparisons Between Recent Ground Motion Relations. Seismological Research Letters 68. 24-40.

Atkinson, G.M. and Boore, D.M. (2006). Ground Motion Prediction Equations for Earthquakes in Eastern North America. Bulletin of the Seismological Society of America 96. 2181-2205.

Baker, J.; Bradley, B. and Stafford, P. (2021). Seismic Hazard and Risk Analysis. Cambridge University Press, Cambridge, England.

Bazzurro, P. and Cornell, C.A. (1999). Disaggregation of Seismic Hazard. Bulletin of the Seismological Society of America 89 (2). 501-220.

Bazzurro, P. and Cornell, C.A. (2004). Nonlinear Soil-Site Effects in Probabilistic Seismic Hazard Analysis. Bulletin of the Seismological Society of America 94. 2110-2123.

Bejaichund M.; Kijko, A. and Hattingh, E. (2006a). Re-Assessment of the Seismic Hazard Parameters for the Site of Koeberg NPP and the NSIP of Bantamsklip and Thyspunt, Volume I: Updating of the SHA with Recent Seismic Event Catalogues. NSIP-SHA-017222#P1-180. CGS Report 2005-0274. Council for Geoscience, Pretoria, South Africa.

Bejaichund M.; Kijko, A. and Hattingh, E. (2006b). Re-Assessment of the Seismic Hazard Parameters for the Site of Koeberg NPP and the NSIP of Bantamsklip and Thyspunt, Volume II: Integration of Palaeoseismic and Neotectonic Information into the SHA. NSIP-SHA-017269#P1-121. CGS Report 2005-0274. Council for Geoscience, Pretoria, South Africa.

Benjamin, J. R. (1968). Probabilistic Models for Seismic Force Design. Journal of the Structural Division, ASCE 94 ST5. 1175-1196.

Bommer, J.J. (2002). Deterministic vs. Probabilistic Seismic Hazard Assessment: An Exaggerated and Obstructive Dichotomy. Journal of Earthquake Engineering 6 Spec01 43-73.

Bommer, J.J. and Abrahamson, N.A. (2006). Why Do Modern Probabilistic Seismic Hazard Analyses Lead to Increased Hazard Estimates?. Bulletin of Seismological Society of America 96(6). 1967-1977.

Bommer, J.J. and Crowley, H. (2017). The Purpose and Definition of the Minimum Magnitude Limit in PSHA Calculations. Seismological Research Letters 88(4). 1097-1106.

Bommer J.J and Scherbaum, F. (2008). The Use and Misuse of Logic Trees in Probabilistic Seismic Hazard Analysis. Earthquake Spectra 24(4). 997-1009.

Bommer, J.J.; Coppersmith, K.J.; Coppersmith, R.; Hanson, K.; Mangongolo, A.; Neveling, J.; Rathje, E.; Rodriguez-Marek, A.; Scherbaum, F.; Shelembe, R.; Stafford, P. and Strasser, F. (2013). Probabilistic Seismic Hazard Analysis for the Thyspunt Nuclear Site, South Africa. CGS Report 2013-0190 (Rev. 0). Council for Geoscience, Pretoria, South Africa.

Campbell, K.W. (2003). Prediction of Strong Ground Motion Using the Hybrid Empirical Method and Its Use in the Development of Ground-Motion (Attenuation) Relations in Eastern North America. Bulletin of the Seismological Society of America 93. 1012-1033.

Cornell, C.A. (1968). Engineering Seismic Risk Analysis. Bulletin of the Seismological Society of America 58. 1583-1606.

Dames and Moore (1973). Interim Report on Geotechnical Studies at Koeberg Nuclear Power Station. NSIP-WC-006723#P1-85.

Dames and Moore (1974). Report on Koeberg Nuclear Power Station Risk Analysis, Cape Province, RSA.

Dames and Moore (1975). Foundation Report for the Koeberg Power Station, Cape Province, RSA. For the Electricity Supply Commission. NSIP-KBG-007669#P1-6.

Dames and Moore (1976). Geologic Report. Koeberg Power Station, Cape Province, South Africa. For The Electricity Supply Commission. Job 9629-014-45.

Dames and Moore (1977). Supplementary Geologic Report for the Koeberg Power Station, Cape Province RSA. For the Electricity Supply Commission. Job 9629-026-45.

Dames and Moore (1980). Final Report on the Boring Programme and Groundwater Simulation at Koeberg Power Station, Cape Province RSA. For the Electricity Supply Commission. Job 9629/039/45.

Dames and Moore (1981). Revised Draft Report, Seismic Design Requirements, Koeberg Nuclear Power Station, Johannesburg, South Africa. For the Electricity Supply Commission. Job 9629-041-45.

De Beer, C.H. (2006a). Investigation into Evidence for Neotectonic Deformation Within Onland Neogene to Quaternary Deposits Between Alexander Bay and Port Elizabeth — Executive Summary Report. CGS Report 2006-0065 (Rev. 0). Council for Geoscience, Pretoria, South Africa.

De Beer, C.H. (2006b). Investigation into Evidence for Neotectonic Deformation Within Onland Neogene to Quaternary Deposits Between Alexander Bay and Port Elizabeth-West Coast Report. CGS Report 2005-0287 (Rev. 0). Council for Geoscience, Pretoria, South Africa.

Du Plessis, A. (1996a). Seismicity in South Africa and Its Relationship to the Geology of the Region. Report 1996-0019.

Du Plessis, A. (1996b). A Seismotectonic Map for South Africa - the First Step in Determining Seismic Hazard at Prospective Nuclear Power Sites. Summary Statement of Reports by Hartnady, Du Plessis, and Partridge. Report (Unpublished), Council for Geoscience, 6 pp & 3 Maps. CGS PNI&I Reference Archive as Report G192.

Electrical Power Research Institute (EPRI). (1986). Seismic Hazard Methodology for the Central and Eastern United States, Electric Power Research Institute. Report NP-4726 1-10. July 1986.

Electrical Power Research Institute (EPRI) (1993). Guidelines for Determining Design Basis Ground Motions, Early Site Permit Demonstration Program. Vol. I RP3302. Electric Power Research Institute, Palo Alto, California, USA.

Electrical Power Research Institute (EPRI). (2004, 2006). Ground-Motion Model Review Project: Project Plan. Electric Power Research Institute, Palo Alto, California, USA: 2012. 1025770.

Electric Power Research Institute/ Department of Energy/United States Nuclear Regulatory Commission (EPRI/DOE/USNRC) (2012). Central and Eastern United States Seismic Source Characterization for Nuclear Facilities. NUREG-2115. US Nuclear Regulatory Commission, Washington DC, USA.

Eskom. (2019). Justification of the Approach for the Duynefontyn Probabilistic Seismic Hazard Analysis Study. NSIP03836.

Frankel A.D.; Petersen, M.D.; Mueller, C.S.; Haller, K.M.; Wheeler, R.L.; Leyendecker, E.V.; Wesson, R.L.; Harmsen, S.C.; Cramer, C.H.; Perkins, D.M. and Rukstales, K.S. (2002). Documentation for the 2002 Update of the National Seismic Hazard Maps. US Geological Survey Open-File Report 02-4202.

Fernandez, L.M. and Guzman, J.A. (1979). Seismic History of Southern Africa. Seismological Series 9. Geological Survey of South Africa, Pretoria.

Goedhart, M.L. (2006). A Geological Investigation of Neotectonic Reactivation Along the Ceres-Kango-Baviaanskloof-Coega Fault System in the Southern and Eastern Cape, South Africa. Trench Report. CGS Report 2006-0085 (Rev. 0). Eskom NSIP-SHA-018229#P1-286. Council for Geoscience, Pretoria, South Africa.

Gutenberg, B. and Richter, C.F. (1944). Frequency of Earthquakes in California, Bulletin of the Seismological Society of America 34(4). 185-188.

Gutenberg, B. and Richter, C.F. (1956). Seismicity of the Earth and Associated Phenomena. Princeton University Press.

Harmsen, S., Perkins, D. and Frankel, A. (1999). De-aggregation of Probabilistic Ground Motions in the Central and Eastern United States. Bulletin of the Seismological Society of America 89(1). 1-13.

Hartnady, C.J.H. (1969). Structural Analysis of Some Pre-Cape Formations in the Western Province. MSc Thesis (Unpublished), University of Cape Town.

Hartnady, C.J.H. (1996). Seismotectonic Provinces of Southern Africa: Critical Review and New Proposals CGS Report 1996-0029. Council for Geoscience, Pretoria, South Africa.

Hartnady, C.J.H.; Newton, A.R. and Theron, J.N. (1974). The Stratigraphy and Structure of the Malmesbury Group in the South-Western Cape. Bulletin Chamber of Mines Precambrian Research Unit 15, University of Cape Town. 193-213.

International Atomic Energy Agency (IAEA). (1976). Earthquakes and Associated Topics in Relation to Nuclear Power Plant Siting, A Safety Guide. Safety Series NO.50-SG-S1(Rev. 0). International Atomic Energy Agency, Vienna, Austria.

International Atomic Energy Agency (IAEA). (1991). Earthquakes and Associated Topics in Relation to Nuclear Power Plant Siting. A Safety Guide. Safety Series 50-SG-SI (Rev. 1). International Atomic Energy Agency, Vienna, Austria.

Johnston, A.C.; Coppersmith, K.J.; Kanter, L.R. and Cornell, C.A. (1994). The Earthquakes of Stable Continental Regions: Final Report Submitted to Electric Power Research Institute (EPRI). TR-102261. 5-Volume Proprietary Report Prepared for Electric Power Research Institute, Palo Alto, California, USA.

Kaklamanos, J.; Baise, L.G. and Boore, D.M. (2011). Estimating Unknown Input Parameters When Implementing the NGA Ground-Motion Prediction Equations in Engineering Practice. Earthquake Spectra 27(4). 1219-1235.

Kijko, A. (2004). Estimation of the Maximum Earthquake Magnitude, Mmax. Pure and Applied Geophysics 161. 1655-1681.

Kijko, A. and Graham, G. (1998). "Parametric-Historic" Procedure for Probabilistic Seismic Hazard Analysis. Part 1: Assessment of Maximum Regional Magnitude Mmax. Pure and Applied Geophysics 152. 413-442.

Kijko, A.; Graham, G. and Retief, S.J.P. (1999). Seismic Hazard Assessment of the Koeberg Nuclear Power Plant as a Re-evaluation of the Seismic Design Level. CGS Report 1999-0158. Council for Geoscience, Pretoria, South Africa.

Kulkarni, R.B.; Youngs, R.R. and Coppersmith, K.J. (1984). Assessment of Confidence Intervals for Results of Seismic Hazard Analysis. Proceedings of the Eighth World Conference on Earthquake Engineering 1, San Francisco, California, USA. 263-270.

McGuire, R.K. (2001). Deterministic vs. Probabilistic Earthquake Hazards and Risks. Soil Dynamics and Earthquake Engineering 21(5). 377-384.

McGuire, R.K. (2004). Seismic Hazard and Risk Analysis. EERI Monograph MNO-10. Earthquake Engineering Research Institute, Oakland, California, USA.

McGuire, R.K. (2008). Probabilistic Seismic Hazard Analysis: Early History. Earthquake Engineering & Structural Dynamics 37. 329-338.

McGuire, R.K.; Silva, W.J. and Costantino, C.J. (2001). Technical Basis for Revision of Regulatory Guidance on Design Ground Motions: Hazard- and Risk-Consistent Ground Motion Spectra Guidelines. NUREG/CR-6728. US Nuclear Regulatory Commission, Washington, DC, USA. ML013100232.

Nuttli, O.W. (1981). On the Problem of the Maximum Magnitude of Earthquakes. US Geological Survey Open-File Report.

Partridge, T.C. (1995). A Review of Existing Data on Neotectonics and Palaeoseismicity to Assist in the Assessment of Seismic Hazard at Possible Nuclear Power Station Sites in South Africa. Confidential Report to the Council for Geoscience. Report 1-7/95 (Unpublished).

Private Fuel Storage Limited Liability Company (PFS LLC). (2000). Safety Analysis Report for Private Fuel Storage Facility, Revision 18, Docket 72-22. La Crosse, Wisconsin, USA.

Pacific Northwest National Laboratory (PNNL). (2014). Hanford Sitewide Probabilistic Seismic Hazard Analysis. PNNL-23361. Pacific Northwest National Laboratory, Richland, Washington, USA.

Richter, C.F. (1935). An Instrumental Earthquake Scale. Bulletin of the Seismological Society of America 25. 1-32.

Rizzo Associates Inc. (Rizzo) (2008). Definition of Design Ground Motions for the PBMR Demonstration Power Plant, Plant PBMR Project PBMR003224 Koeberg, South Africa. Prepared for PBMR, Centurion, South Africa. Project 07-3835.

Roberts, D.L. (2006). Dating and Preliminary Correlation of Raised Marine and Estuarine Terraces on the Western and Southern Coasts of South Africa: Final Report. CGS Report 2006-0186 (Rev. 0). Eskom NSIP-SHA-018230#P1-206.

Rodriguez-Marek, A.; Rathje, E.; Ake, J.; Munson, C.; Stovall, S.; Weaver, T.; Ulmer, K. and Juckett, M. (2021). Documentation Report for SSHAC Level 2: Site Response. RIL 2021-15. US Nuclear Regulatory Commission.

Rodriguez-Marek, A.; Rathje, E.M.; Bommer, J.J.; Stafford, P.J. and Scherbaum, F. (2014). Application of Single-Station Sigma and Site Response Characterization in a Probabilistic Seismic Hazard Analysis for a New Nuclear Site. Bulletin of the Seismological Society of America 104 (4). 1601-1619.

Schwartz, D.P. and Coppersmith, K.J. (1984). Fault Behavior and Characteristic Earthquakes: Examples from the Wasatch and San Andreas Fault Zones. Journal of Geophysical Research 89. 5681-5698.

Stafford, P.J.; Rodriguez-Marek, A.; Edwards, B.; Kruiver, P.P. and Bommer, J.J. (2017). Scenario Dependence of Linear Site Effect Factors for Short-Period Response Spectral Ordinates. Bulletin of the Seismological Society of America 107(6). 2859-2872.

Stamatakos, J.A.; Chen, R.; McCann, Jr.; M.W. and Chowdhury, A.H. (2000). Seismic Ground Motion and Faulting Hazard at the Private Fuel Storage Facility in The Skull Valley Indian Reservation, Tooele County, Utah. Final Report, Prepared for the Nuclear Regulatory Commission. Contract NRC-02-97-009. Center for Nuclear Waste Regulatory Analysis, San Antonio, Texas, USA.

Stamatakos, J.; Watson-Lamprey, J.; Cawthra, H.C.; Claassen, D.; Coppersmith, R.; Johnson, C.; Largent, M.; Manzunzu, B.; Midzi, V.; Mulabisana, T.; Murphy, D.; Rathje, E. and Wooddell, K. (2022). Baseline PSHA for the Duynefontyn Site and the Koeberg Nuclear Power Station. CGS Report 2022-0009 (Rev. 1). Council for Geoscience, Pretoria, South Africa.

Stamatakos, J. and Watson-Lamprey, J. (2023). Project Execution Plan for the Senior Seismic Hazard Analysis Committee Enhanced Level-2 Probabilistic Seismic Hazard Analysis at the Duynefontyn Nuclear Site. NGG-PLN-003 (Rev 1).

United States Atomic Energy Agency (USAEC) (1973). Design Response Spectra for Seismic Design of Nuclear Power Plants. Regulatory Guide 1.60 (Rev 1.0).

United States Nuclear Regulatory Commission (USNRC) (2000). Safety Evaluation Report of the Site-Related Aspects of the Private Fuel Storage Facility Independent Spent Fuel Storage Installation. December 15, 1999 (Revised and Reissued January 4, 2000). Docket 72-22.

United States Nuclear Regulatory Commission (USNRC). (2001). Technical Basis for Revision of Regulatory Guidance on Design Ground Motions, Hazard- and Risk-Consistent Ground Motion Spectra Guidelines. NUREG/CR-6728. US Nuclear Regulatory Commission.

United States Nuclear Regulatory Commission (USNRC) (2007). A Performance-Based Approach to Define the Site-Specific Earthquake Ground Motion. Regulatory Guide 1.208. US Nuclear Regulatory Commission.

United States Nuclear Regulatory Commission (USNRC) (2018). Updated Implementation Guidelines for SSHAC Hazard Studies. NUREG-2213. US Nuclear Regulatory Commission, Office of Nuclear Regulatory Research, Washington, DC, USA.

Wells, D.L. and Coppersmith, K.J. (1994). New Empirical Relationships Among Magnitude, Rupture Length, Rupture Width, Rupture Area, and Surface Displacement. Bulletin of the Seismological Society of America 84(4). 974-1002.

Youngs, R.R. and Coppersmith, K.J. (1985). Implications of Fault Slip Rates and Earthquake Recurrence Models to Probabilistic Hazard Estimates. Bulletin of the Seismological Society of America 75. 939-964.

CHAPTER 2: PROJECT ORGANISATION

2. PROJECT ORGANISATION

This chapter presents an overview of the planning and organisation of the Duynefontyn probabilistic seismic hazard analysis (PSHA) project. The first section outlines the Senior Seismic Hazard Analysis Committee (SSHAC) framework and the selection of the appropriate SSHAC level for the study. The second section of the chapter provides an overview of the project management structure, the technical and review teams, and their interactions. This section also details the contribution of each group of participants to the project, including their roles, requirements, and responsibilities. All the key individuals involved in the study are listed in these sections, and the curricula of all technical participants are provided in Appendix A. The closing section of the chapter provides an overview of the Integrated Management System (IMS) developed by the Council for Geoscience (CGS) for the project.

2.1 THE ORIGIN OF SSHAC

Two landmark probabilistic seismic hazard studies were conducted in the 1980s to evaluate the probabilistic seismic hazard at nuclear facilities in the Central and Eastern United States (CEUS). Studies by the Electric Power Research Institute Seismicity Owners Group (EPRI-SOG, 1988; and EPRI 1989) and Lawrence Livermore National Laboratory (LLNL) (Bernreuter et al., 1989) were both conducted for the same sites, using multiple experts, and both studies were conducted with an explicit recognition of the importance of uncertainty. These studies relied on assessments by experts (either individually or as members of teams) to address specific seismic source or ground motion characterisation issues. The goal of the studies was to quantify the annual frequency of exceeding (AFE) and the safe shutdown earthquake (SSE) for all U.S. commercial nuclear power plant sites. The SSEs for these sites were established prior to the application of probabilistic methods and were instead based on deterministic methods.

However, the processes used to conduct the two studies were quite different. These process differences led to significantly dissimilar results between the two studies, including the assessments made by individual experts participating in each study as well as in the mean hazards and associated uncertainties. These differences between the LLNL and EPRI-SOG hazard estimates were observed in spectral accelerations important to nuclear power plant design (1 to 10 Hz and peak ground acceleration) and were pronounced in the range of AFE (10^{-4} to 10^{-6}) that is most relevant for seismic risk assessments for nuclear power plants (United Stated Nuclear Regulatory Commission [USNRC, 2010]). In addition, the relatively large uncertainties in the LLNL study, and difference between the LLNL and EPRI-SOG studies led to a range of distributions of SSE AFEs, as seen in the cumulative plot of the probability of exceeding the SSE for all nuclear plants in the CEUS (Figure 2-1).

The SSHAC was convened by the USNRC, the EPRI, and the United States Department of Energy (USDOE) to reconcile these differences. The Commission report was issued as NUREG/CR-6372 (Budnitz et al., 1997). The Committee concluded that the differences between the LLNL and EPRI-SOG studies could largely be attributed to procedural, not technical, differences. The main issues were the organisation of the studies and the interactions among experts. Guidance in the report went on to recommend methods for conducting a structured and objective multiple-expert hazard assessment. The guidance also focussed on addressing uncertainties in PSHAs using expert judgement. This formal process for structuring and conducting expert assessments has come to be known as a “SSHAC

process," and the recommendations made in the report are known as "SSHAC guidelines." NUREG/CR-6372 defined the core value of an SSHAC study as capturing "*the center, the body, and the range that the larger informed technical community would have if they were to conduct the study*."

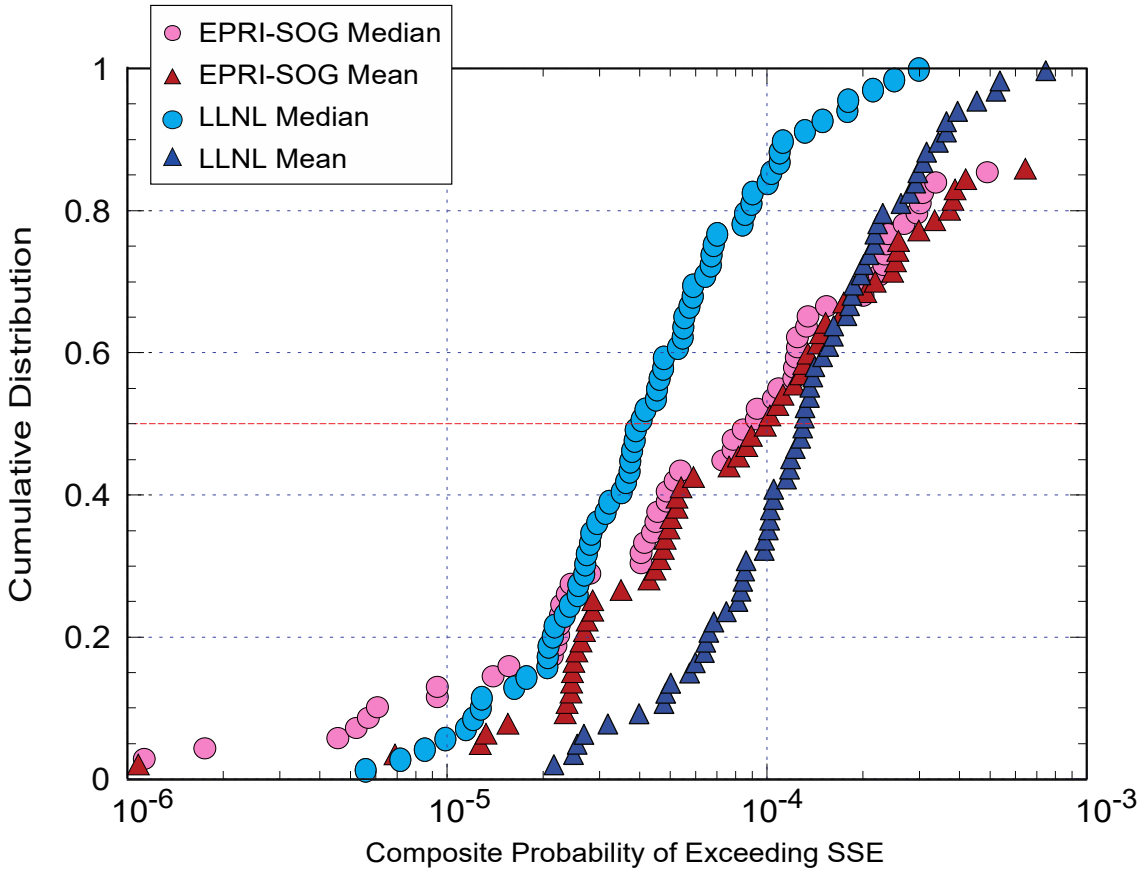

Figure 2-1. Median and mean annual frequency of exceeding the SSE for all U.S. nuclear power plants. The EPRI data come from Figure 4-1 of McGuire et al. (1989). The LLNL data was derived from the data provided in NUREG-1488 (Sobel, 1994)

NUREG/CR-6372 defined four study levels, increasing in complexity from Level 1 to Level 4, with Levels 3 and 4 intended for application in safety-critical facilities such as nuclear power plants. These higher study levels involve a greater number of participants and a longer duration to assess available data, models, and methods more fully. The SSHAC guidelines also recognised that the four levels were needed to allow epistemic uncertainty to be effectively captured, depending on the project needs. Another motivation for adopting higher study levels was that the highest levels increase regulatory assurance because of the more comprehensive treatment of epistemic uncertainty.

2.1.1 SSHAC guidance updates

Since NUREG/CR-6372 was first published in 1997, the SSHAC process has been applied to many hazard studies. Most of these studies were conducted to develop a PSHA for nuclear power plant applications. However, there were also SSHAC studies for a probabilistic volcanic hazard analysis (PVHA) and two groundwater flow studies, which were conducted by the

USDOE for the Yucca Mountain high-level waste repository program. The lessons learned from all these SSHAC studies provided the basis for two updates to the SSHAC guidelines.

The first update was published as NUREG-2117 (USNRC, 2012a) and provided additional, focussed implementation guidance for the conduct of Level 3 studies. In NUREG-2117, the SSHAC process centred around two critical activities: evaluation and integration. In this context, evaluation is defined as an assessment of the complete set of data, models, and methods that are relevant to the hazard analysis and are proposed by the larger technical community. Evaluation entails identifying important technical issues and the applicable data to address those issues, assessing the data in terms of their quality and relevance regarding the assessments being made, and facilitating interaction with the experts and members of the larger technical community to exchange viewpoints and to challenge proponents. Integration is defined as the development of seismic source and ground motion models that capture all technically defensible interpretations, as informed by the evaluation of existing data, models, and methods. Integration is model building used to arrive at a defensible expression of knowledge and uncertainty in inputs to the hazard model, giving due consideration to the available data and the views of members of the technical community who are not necessarily directly participating in the project. This includes the full expression of the model elements (logic-tree nodes and branches), their relative weights, and the range of credible uncertainties. To better align with the evaluation and integration activities as defined in NUREG-2117, the expression from "*center, body, and range of the informed technical community"* was rephrased as the "*center, body, and range of technically defensible interpretations*," which is now often referred to by its acronym: CBR of TDI.

In NUREG-2117, the USNRC explicitly stated that all new nuclear site licence applications must include a seismic hazard assessment conducted as an SSHAC Level 3 or 4 process. In addition, following the 2011 Great East Japan Earthquake and tsunami and resulting accident at the Fukushima Dai-ichi nuclear power plant, the USNRC issued an information request to all licensees under Title 10 of the Code of Federal Regulations (10 CFR 50.54(f); see USNRC 2012b). In the information request (USNRC, 2012b), the USNRC asked all nuclear power plant licence holders in the United States to re-evaluate the seismic hazard at their sites. For sites in the CEUS, licensees were permitted to use the existing SSHAC Level 3 source characterisation in NUREG-2115 (EPRI/DOE/USNRC, 2012) and the updated regional EPRI ground-motion characterisation (EPRI, 2013). Through the issuance of the 50.54(f) letter, the USNRC stated that an SSHAC Level 3 provides an appropriate basis for the seismic design review of existing nuclear power plants. For sites in the western United States, the USNRC requested that each licensee develop a site-specific SSHAC Level 3 PSHA.

The second and latest update to the SSHAC guidelines was published as NUREG-2213 (USNRC, 2018). This update complemented and augmented guidance contained in NUREG/CR-6372 and NUREG-2117, and incorporated lessons learned from the SSHAC studies completed between 2012 and 2018. These included the 50.54(f) Level 3 studies for the nuclear power plants in the western United States, which were later summarised in NUREG/KM 0017 (USNRC, 2021). The intent of NUREG-2213 was to provide the most current and standalone guidance for SSHAC studies, based on a systematic review of all the projects that have successfully applied the SSHAC guidelines since 1997. NUREG-2213 also incorporated extensive inputs from the many seismic hazard practitioners who participated in previous SSHAC studies as a way to develop practical insights. In addition, lessons learned

from the Thyspunt PSHA project (Bommer and Coppersmith, 2013; Bommer et al., 2013a) were used to inform this SSHAC update[1].

Based on this feedback, the updated guidance in NUREG-2213:

1. Described, in detail, the key features that are essential for all SSHAC studies.
2. Strengthened the implementation framework for Level 3 studies based on extensive recent experiences.
3. Provided guidance on the essential attributes of Level 1 and 2 studies (missing from the earlier SSHAC documents).
4. Introduced options to augment Level 2 studies.
5. Developed a revised and more rigorous framework for decision-making regarding when and how to update existing SSHAC studies.

In NUREG-2213, the concept of the centre, body, and range of technically defensible interpretations (CBR of TDI) was explained within the context of the PSHA results and uncertainty. Specifically, NUREG-2213 clarified that the SSHAC process will yield the CBR of estimates of the AFE of different levels of each ground-motion parameter given all TDI, which is required information for undertaking a risk-informed design and evaluations for seismic safety of critical facilities. Once the geological, seismological, and geotechnical experts have completed the evaluation and integration of available data, models, and methods, the centre of their interpretations can be thought of as the best estimate or central value (median) of the distribution. The body can be thought of as the shape of distribution of interpretations that lie around this best estimate and capture the major portion of the mass of the distribution. The range refers to the tails of this distribution and the limiting credible values (Figure 2-2).

[1] For context, the Thyspunt SSHAC Level 3 study was conducted in strict accordance with the guidance of NUREG-2117 (USNRC, 2012a), now superseded by NUREG-2213 (USNRC, 2018).

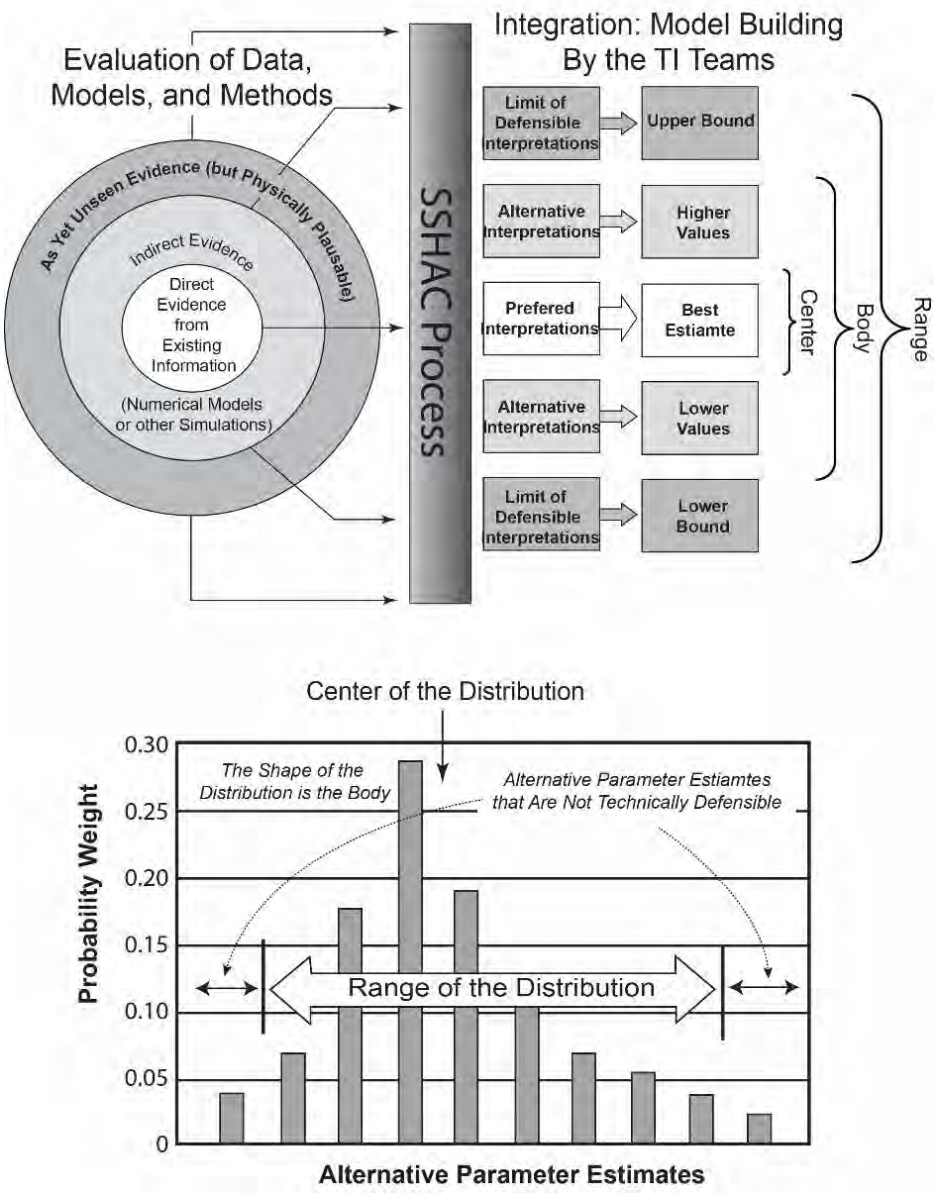

Figure 2-2. Diagrammatic representation of the centre, body, and range of technically defensible interpretations (CBR of TDI), adapted from Figure 2-1 of NUREG-2213 (USNRC, 2018).

2.1.2 The five essential features of an SSHAC study

Fundamentally, there are five essential features required for any study to be considered an SSHAC study. These are:

1. **Clearly defined roles** for all participants, including the responsibilities and attributes associated with each role.
2. **Objective evaluation** of all available data, models, and methods that are relevant to the characterisation of the hazard at the site. This process includes identifying the limits of the existing data, gaps in the existing data, and the resolution and uncertainties of the available data. It may include the collection of new data that are needed for the hazard assessment.

3. **Integration** of the outcome of the evaluation process into models that reflect both the best estimate of each element of the hazard input with the current state of knowledge and the associated aleatory variability and epistemic uncertainty. This distribution is referred to as the centre, body, and range of technically defensible interpretations (CBR of TDI) and involves the construction of a seismic source model (SSM) and a ground motion model (GMM), including site response, that address both aleatory variability and epistemic uncertainties.
4. **Documentation** of the study with sufficient detail to allow reproduction of the hazard analyses. Documentation includes evidence of the participatory review having taken place. The documentation must identify all the data, models, and methods considered in the evaluation, and justify in detail the technical interpretations that support the hazard input models.
5. **Independent participatory peer review** to confirm that the evaluation considered relevant data, models, and methods, and that it was conducted objectively and without bias. The peer review is conducted following a participatory or continual process throughout the entire project. The peer review is also required to confirm that the SSM and GMM captured the CBR of TDI and that the technical bases for all elements of the models are adequately documented. The peer review process is considered to be complete once the peer review panel has submitted a Closure Letter (Appendix B) to the Project Sponsor.

In addition to these five essential features of an SSHAC study, a sixth essential feature (one that was not formally included in the listing in NUREG-2213) is the recognition of cognitive bias. Because the SSHAC process relies on expert judgement, it is important to be aware of cognitive bias in the evaluation and integration (whether intentional or unintentional). Section 2.4 of NUREG-2213 provides a detailed summary of the specific types of cognitive bias that can permeate an SSHAC study. To capture the CBR of TDI, the Technical Integration (TI) Team members must act as impartial and objective assessors of all available data, models, and methods. This involves avoiding cognitive bias in their assessments. Toward that end, it is important that the TI Leads discuss cognitive bias with the experts and make them aware that efforts will be devoted throughout the project to counter bias, particularly in working meetings where the experts are offering their judgements. Likewise, the Participatory Peer Review Panel (PPRP) Chair should remind the PPRP of the importance of being attentive to cognitive bias, both in terms of the potential for it to be present among the TI Teams and within the PPRP itself. Expert interactions that specifically include a technical challenge intended to reveal the genuine biases of experts' assessments are key components of countering cognitive bias.

2.1.3 SSHAC levels

The four SSHAC levels described in section 2.1.1 were intended to bring ever-increasing regulatory assurance to the results, with Level 4 studies culminating in the most complete and most rigorous outcomes. However, based on the lessons learned during the many applications of the SSHAC process to nuclear projects around the world, the authors of NUREG-2117 concluded that the Level 4 process was cumbersome. In NUREG-2117, the USNRC clarified that Level 3 and Level 4 studies should be viewed as equally rigorous alternative approaches without making any distinction in terms of regulatory assurance. With the exception of the USDOE Yucca Mountain SSHAC studies (PSHA, PVHA, and groundwater studies) and the PEGASOS (Abrahamson et al., 2002) and PEGASOS Refinement (Renault et al., 2010) PSHA

projects in Switzerland, all SSHAC studies for nuclear power plant applications have been conducted as Level 3 studies.

It is important to note that the basic attributes of SSHAC studies (e.g. clearly identified roles, evaluation, integration, documentation, and participatory review) apply to all SSHAC levels. However, there are important differences in implementation across the four levels. These differences are summarised in Table 2-1. Central to the successful implementation of the SSHAC process (irrespective of level) is the clear definition of the different roles within a project and of the responsibilities assigned to each role.

Table 2-1. Attributes of SSHAC level studies from Level 1 to Level 3 (adapted from Table 3-1 in NUREG-2213 [USNRC, 2018]).

	Level 1	**Level 2**	**Level 2 Enhanced (Augmentation Options)**	**Level 3**
Participatory Peer Review Panel (PPRP)	At least two reviewers; communication with the PPRP during evaluation and integration	Two or more reviewers; feedback on preliminary models	One or more PPRP representative(s) observe(s) working meetings; TI Team interactions with external experts, and/or workshops	Ideally five reviewers; engagement during evaluation and integration process; PPRP briefing on final model
Technical Integration (TI) Team	Small TI Team (depending on nature and complexity of issues)	Small TI Team; possibly multiple teams (e.g. SSM and GMM)	Larger TI Team	Five or more TI Team members
Evaluation	Sensitivity analysis to identify significant issues; systematic review of literature	Outreach to proponents and resource experts (e.g. phone interviews)	Add Workshop 1, 2, or hybrid that includes resource experts and/or proponents	Two workshops with resource expert and proponents; data summary tables
Integration	Develop models that capture the centre, body, and range of technically defensible interpretations (CBR of TDI)	TI Team interaction and hazard feedback during model-building	Add Workshop 3 with feedback from PPRP	One workshop to discuss preliminary models plus the PPRP briefing

[1] All attributes are additive, moving from left to right on the table; Level 4 is essentially the same as Level 3 with respect to these attributes.

2.1.4 Selection of SSHAC level for Duynefontyn PSHA

Based on the justification provided in Eskom (2019), the Duynefontyn project was planned to be conducted as an SSHAC Enhanced Level 2 study (SSHAC EL-2). Eskom's decision to select the SSHAC process for the Duynefontyn PSHA was motivated by the complexity of the tectonic environment of the Western Cape and the relatively limited amount of data available

for seismic source and ground motion characterisation, which necessitated the use of significant expert judgement in developing the PSHA. The SSHAC approach was selected because it is a multilevel and structured assessment process that is well suited to the use of expert judgement. This decision was supported by the NNR's acceptance of the PSHA for the Thyspunt nuclear site (Bommer et al., 2013b), which employed a SSHAC Level 3 methodology. The SSHAC process has been demonstrated to satisfy the regulatory goals of a carefully structured, transparent, and thoroughly documented approach to assessing hazards that fully considers available information, quantifies uncertainties, and fully documents the analysis (e.g. NNR, 2008a, 2008b, 2012, 2015).

Eskom (2019) recommended that the Duynefontyn PSHA study be executed as a highly enhanced SSHAC Level 2 PSHA, since this was considered much more agile than a Level 3 study. The concept was to conduct an SSHAC Level 2 study for the GMM, given the perceived continued relevance of the GMM from the Thyspunt PSHA (Bommer et al., 2013b), supplemented with the insights gained from international PSHA studies conducted over the intervening period. A slightly different approach was proposed for the SSM since the seismic sources in the Western Cape would be different from those that drove the hazard in the Thyspunt PSHA. Eskom (2019) deduced that their characterisation warranted an approach more aligned with an SSHAC Level 3 process, and possibly exceeding the minimum requirements for a Level 3 process when it comes to the most critical elements of the SSM. This would mean that, on balance, the Duynefontyn SSHAC would be an SSHAC EL-2 made up of an SSHAC Level 2 GMM and elements of an SSHAC Level 3 SSM. Given the lower uncertainty then assumed for the GMM, relative to the Duynefontyn SSM (due to the perceived applicability of the Thyspunt GMM to the Duynefontyn site), the proposed SSHAC EL-2 study would conserve resources (manpower and funds) that would best be directed towards reducing the uncertainty in the SSM. Eskom (2019) concluded that the application of an SSHAC EL-2 would ensure the delivery of a defensible and robust PSHA study that would be available in time to also support the application for the long-term operation (LTO) license of the Koeberg Nuclear Power Station (KNPS).

The objective of the SSHAC EL-2 PSHA is to produce seismic hazard curves defining the annual probability (or rate) of exceeding increasing levels of earthquake ground shaking at the Duynefontyn site over a range of decreasing AFE. The PSHA results quantifiy a suite of hazard curves (mean hazard and fractiles for spectral accelerations between 0.5 and 100 Hz) and their associated uniform hazard response spectrum. This PSHA forms the technical basis for Eskom to characterise the site and the regional geology, seismology, seismic sources, and ground-shaking hazards at Duynefontyn. In addition, the PSHA will be incorporated into Eskom's Site Safety Report (SSR), which seeks to characterise the ground-motion hazard in a way that satisfies the regulatory requirements as defined by the National Nuclear Regulator (NNR, 2008a, 2008b, 2012, 2015). In particular, the SSHAC EL-2 PSHA study satisfies the regulatory goals of a carefully structured, transparent, and thoroughly documented approach to assessing hazards that fully considers available information, quantifies uncertainties, and transparently documents the analysis and peer review.

In practice, however, the Duynefontyn PSHA has essentially met all the requirements of an SSHAC Level 3 study as described in Table 2-1. The only exception was the conduct of Workshop 1, which was combined with the project Kick-off Meeting following the end of the Baseline study (Stamatakos et al., 2022). There were six PPRP members. Following the

restructuring of the TI Teams to align with NUREG-2213 (USNRC, 2018) after Workshop 1 (see Sections 2.2.3 and 3.4), the SSM and GMM TI Teams each comprised six experts (although this changed when one member of the GMM TI Team emigrated to take up new employment immediately before Working Meeting 3). Three formal workshops were held. At Workshop 1, the resource experts presented on available data, models, and methods and included a detailed description of the data, models, and methods evaluated in the Baseline PSHA study. At Workshop 2, proponent experts presented and defended their models. At Workshop 3, the TI Teams presented their preliminary models and preliminary hazard sensitivity result to the PPRP. The PPRP engaged directly with the TI Teams by challenging and querying the preliminary SSM and GMM, then providing written feedback after each workshop.

The overall workflow of the Duynefontyn PSHA is illustrated in Figure 2-3, which was adapted from Figure 3-4 of NUREG-2213. The Duynefontyn PSHA constituted three main phases. The first phase was an **evaluation** of all available data, methods and models that are potentially relevant to the seismic hazard characterisation of the site. The second phase was an **integration** of the evaluation assessment into a model that reflected the TI Team's knowledge about the seismic characterisation of the region and site. A vital part of the integration process was to identify, quantify and incorporate all major sources of epistemic uncertainty in order to capture the CBR of TDI. The third phase, **documentation** of the evaluation and integration, included a detailed narration of the decision-making process and the technical justifications underpinning the TI Teams' integration.

The SSHAC process represents international best practice and is specifically identified as an acceptable and appropriate framework for conducting a PSHA in several important regulatory guidance documents. Specifically, the Duynefontyn PSHA study was conducted in accordance with the following regulatory guidance and industry standards:

- Regulatory Guide 1.208: A Performance-Based Approach to Define the Site-Specific Earthquake Ground Motion (USNRC, 2007).
- ASCE/SEI 43-19: Seismic Design Criteria for Structures, Systems, and Components in Nuclear Facilities (American Society of Civil Engineers (ASCE)/Structural Engineering Institute (SEI), 2019).
- ANSI/ANS 2.29-2020: Probabilistic Seismic Hazard Analysis (American National Standards Institute (ANSI)/American Nuclear Society (ANS), 2020).

These documents are widely regarded as representing international best practice and provide the most reliable procedures for conducting analyses of the seismic loading to be considered in the design and operation of nuclear power plants. Satisfying the requirements of these stringent guidelines means that the study also satisfied the requirements and standards specified by the International Atomic Energy Agency (IAEA), including Safety Guide SSG-9 (IAEA, 2022) and Specific Safety Requirements SSR-1 (IAEA, 2019).

At the outset of the project, a Project Execution Plan (PEP) was developed and distributed to all project participants as the guiding document for the organisation and conduct of the Duynefontyn PSHA. As the project progressed and some changes were made to both schedule and personnel, the PEP (Stamatakos and Watson-Lamprey, 2023) was modified and distributed to project participants.

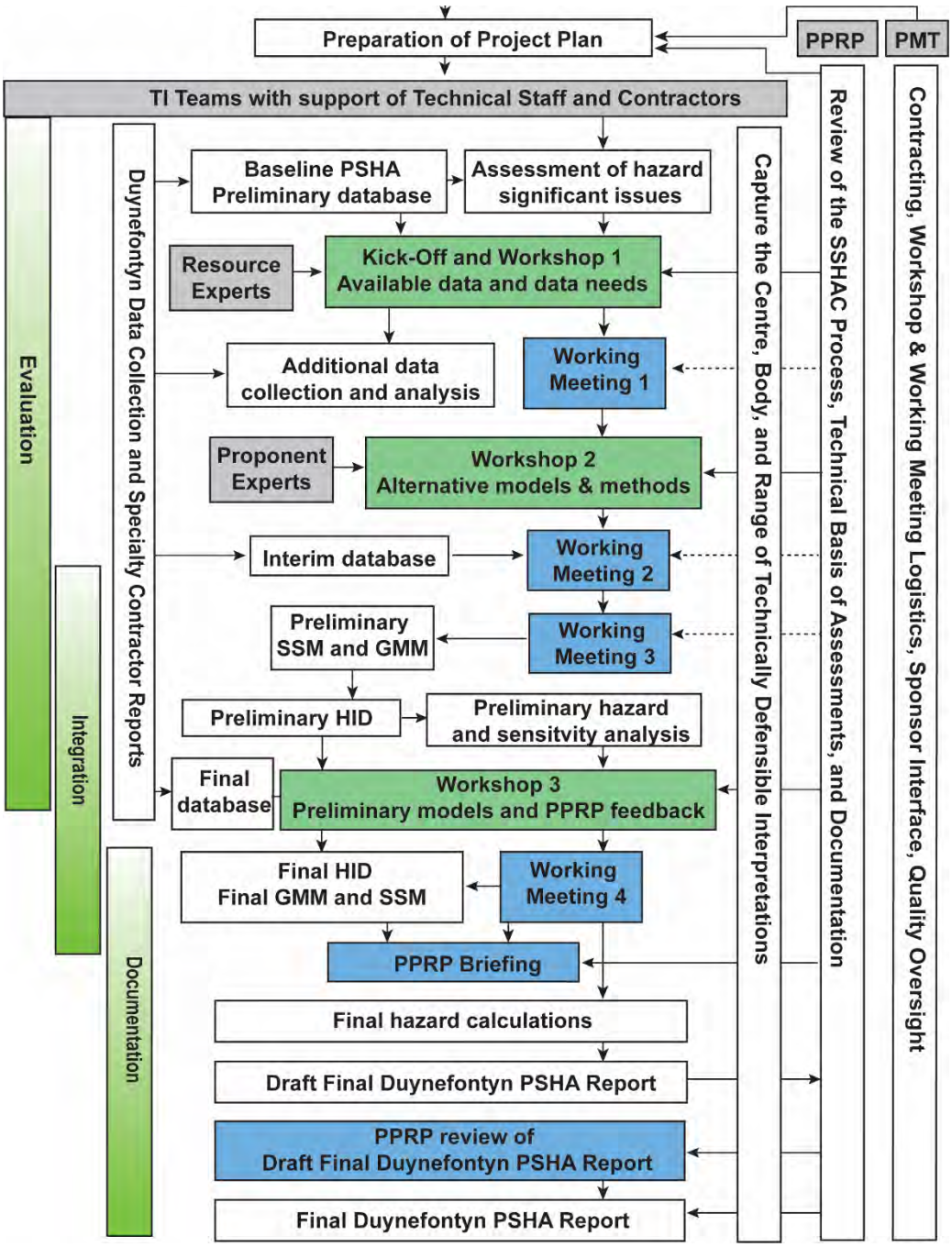

Figure 2-3. Flowchart illustrating the key features in the SSHAC EL-2 process for the Duynefontyn PSHA. The order of activities runs from top to bottom of the diagram. The dashed arrows indicate activities where one (or more) member of the PPRP observes and represents the larger panel.

2.2 ORGANISATION MANAGEMENT STRUCTURE

Central to the success of the process, therefore, is a clear definition of the different roles within a project and of the responsibilities that each role entails. The organisational structure of the Duynefontyn PSHA is illustrated in Figure 2-4. Details about each of the roles and responsibilities in the project are described in the following sections, which were adapted for this report from NUREG-2213.

Eskom appointed the Council for Geoscience (CGS) as the entity responsible for the execution and management of the project. The CGS, in consultation with Eskom, appointed the key technical personnel, including the Project Technical Integrator (PTI), SSM and GMM TI Team Leads, TI Teams, Hazard Analyst, Database Manager, Project Quality Officer, and Project Quality Controller. Given the prominent role the PPRP plays in quality assurance, the panel was selected and appointed through an intensive consultative process with Eskom. The Specialty Contractors, Resource Experts, and Proponent Experts were identified by the TI Teams, Hazard Analysis Team (HAT), and the PTI. The specific attributes and responsibilities associated with these roles are described in NUREG-2213. Working meetings and workshops were observed by individuals representing the CGS, Eskom and (for the formal workshops) also the NNR, which was invited by Eskom.

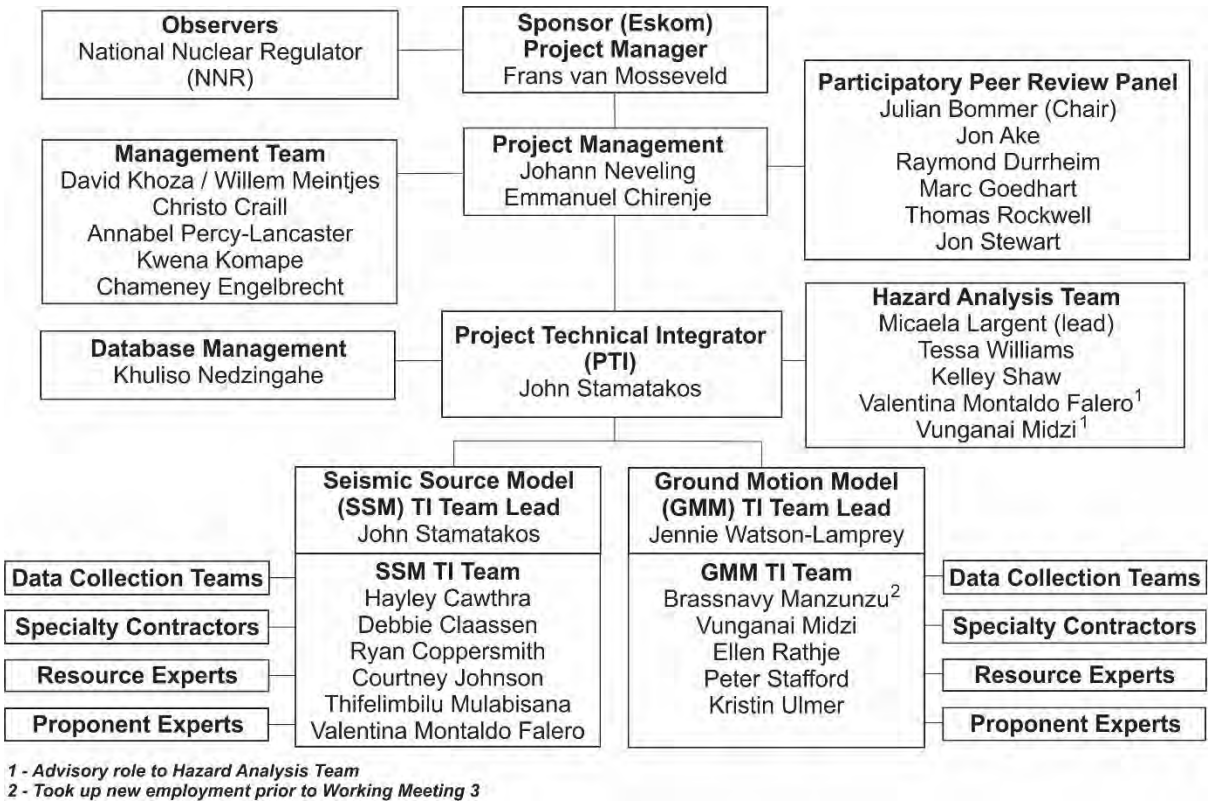

Figure 2-4. Organisational structure of the Duynefontyn PSHA. Details about the Specialty Contractors, Resource Experts, and Proponent Experts are provided in the following sections.

2.2.1 Sponsor and Project Manager

The Sponsor (Eskom) was represented by Mr Frans Van Mosseveld, who was the Eskom Project Manager for the Duynefontyn PSHA. He was supported by a small team of administrative and technical Eskom staff members, and enabled direct interaction between the PTI, the TI Leads, and Eskom's engineering staff members who would be the end-users of the PSHA results.

The Project Manager for the Duynefontyn PSHA project, Dr Johann Neveling of the CGS, played a central role in project implementation. The Project Manager had overall responsibility for running the project, including ensuring adherence to schedule, budget, and scope, and compliance with quality and safety requirements. At the outset of the project, the Project Manager was involved in the appointment of the PTI and the TI Leads. He was also responsible for contracting all participants shown Figure 2-4, as well as making logistical arrangements for the project meetings. Dr Neveling was also the primary point of contact for Eskom, the PPRP Chair and the PTI. He reported to the relevant CGS Executive Manager, a role filled at the project conclusion by Mr Willem Meintjes.

In addition to ensuring adherence to scope, schedule, and budget, the Project Manager was ultimately responsible for delivery of all products within the framework of the applicable quality assurance requirements. In executing this wide range of tasks, the Project Manager was supported by a project management team including individuals responsible for quality, safety, technical editing, and logistical support. Mr Emmanuel Chirenje, a Senior Geophysicist with extensive project management experience, was the Assistant Project Manager; a role that provides support to the Project Manager and coordinates specific tasks and processes. Mr Chirenje was intimately involved in the early data collection activities and the planning and execution of the Duynefontyn PSHA. He also filled the role of Project Planner.

Ms Annabel Percy-Lancaster was the Project Quality Officer, responsible for the establishment and implementation of an integrated management system (IMS) that addressed quality, safety, and nuclear safety. Ms Kwena Komape, the Project Safety Coordinator, was responsible for implementing a conventional safety system and a nuclear safety culture. General support and oversight on the implementation of the IMS was provided by the management representative (an NNR RD-0034 requirement), Mr Christo Craill. Administrative and logistical support was provided by the Project Administrator, Ms Chameney Engelbrecht. The project management team also included the services of a Technical Editor, a role that was at various times filled by Ms Melissa Cawthra, Mr Zusakhe Nxantsiya, and Ms Nicky Flint. All members of the project management team (listed in Figure 2-4) were permanent staff members at CGS.

2.2.2 Project Technical Integrator

The PTI for the Duynefontyn PSHA project was Dr John Stamatakos, who provided overall technical coordination and was the technical lead and spokesperson for the technical products of the project. The PTI worked closely with the Project Manager and the TI Leads to ensure that adequate time was available for the preparation, execution, checking, and reporting of the hazard calculations. The PTI accompanied the Project Manager to Eskom briefings to address all technical issues outside the remit of the Project Manager. In liaison with Eskom, the PTI

ensured that the project deliverables satisfied the requirements of Eskom and the NNR. In this regard, the PTI and Project Manager also worked closely with the Project Quality Officer.

The PTI participated in the selection of suitable candidates for key roles in the project, including TI Leads, TI Team members identified in conjunction with the TI Leads, and the HAT. The PTI also worked closely with the TI Leads. This collaboration was aided by the fact that the PTI, Dr Stamatakos, also served as the TI Lead for the SSM. The PTI attended all the formal working meetings of the SSM TI Teams and many of the GMM TI Team meetings. The PTI also coordinated the work of the Database Manager to ensure the timely and convenient provision of all relevant data, models, and methods to the TI Teams and the HAT, including quality aspects. The PTI maintained overall technical responsibility for the project, in particular, coordinating the production of the final Duynefontyn PSHA report. The PTI was also responsible for presenting the technical products to Eskom and the NNR.

2.2.3 Technical Integration Teams

As explained in Section 2.1.3, the core components of the SSHAC process are the evaluation and integration of data, models, and methods. The roles of evaluator and integrator are combined in the individuals who comprise the TI Teams. There were two TI Teams, one for the SSM and one for the GMM. The composition of the teams, which combine international experts in developing SSMs and GMM, with the local knowledge possessed by key CGS staff members, is shown in Figure 2-4. There were a few changes to the TI Teams over the course of the project. The TI Teams were restructured and strengthened following Workshop 1 (Section 3.4). Later Dr Valentina Montaldo Falero joined the SSM TI Team after Working Meeting 3 and Dr Brassnavy Manzunzu resigned from the CGS immediately prior to Working Meeting 3.

The role of each TI Team member, as an expert evaluator, was to objectively identify existing data, models, and methods and to evaluate them in terms of their general quality and reliability, as well as their specific applicability to the assessments. The TI Team members evaluated data and diverse models, challenged their technical bases and underlying assumptions, and, where possible, tested the models against observations. During the Integration phase of the project, the TI Teams constructed the SSM and GMM and developed technical justifications and rationales for their choices, both in terms of the selected models and the weights assigned to them.

Individual TI Team members executed this responsibility as part of an integrated team, accomplished by open and constructive interaction. All TI Team members contributed to the production of the final project documentation and worked together to develop the consensus needed to ensure that all TI Team members assume intellectual ownership of the final SSM and GMM, individually and collectively.

Each TI Team was coordinated by a TI Lead, with Dr John Stamatakos assuming this role for the SSM TI Team and Dr Jennie Watson-Lamprey for the GMM TI Team. The TI Leads communicated closely with each other throughout the project to ensure that all technical issues were dealt with appropriately. The ultimate responsibility of the TI Lead was to ensure timely delivery of an SSM or GMM that captured the CBR of TDI. The TI Leads also ensured that the TI Teams, collectively and individually, assumed full intellectual ownership of the final model. The TI Leads had the responsibility to ensure the TI Team members remained aware of the

potential for cognitive bias. This was especially relevant where TI Team members participated in data collection efforts, effectively taking on a Resource Expert role. When necessary the TI Leads had to alert TI Team members when cognitive biases may be influencing their assessments. When required, the TI Leads were also responsible for instructing TI Team members in the concepts of aleatory variability and epistemic uncertainty and their application in the Duynefontyn PSHA.

The TI Leads served as the technical leaders of their respective teams. They were responsible for working with their teams to identify suitable Resource Experts and Proponent Experts and providing them with clear instructions regarding the issues to be addressed by their presentations. The TI Leads ran the workshops and ensured that all participants clearly understood the workshop objectives, their individual roles, the required output from the workshops, and the implications of the issues under discussion for the seismic hazard analysis. The TI Leads convened and organised working meetings of the TI Teams and ensured that all members had full access to the available data and information. The TI Leads also assumed the key responsibility of ensuring that the project documentation was complete and comprehensive.

2.2.4 Participatory Peer Review Panel

The PPRP is an indispensable element of the Duynefontyn PSHA. The PPRP fulfilled two parallel roles, conducting both a technical and a process review. In the technical review, the PPRP ensured that the full range of data, models, and methods was duly considered in the evaluation phase and that the CBR of TDI was captured in the integrated SSM and GMM. Importantly, the PPRP also ensured that all technical decisions were adequately justified and documented. As part of the process review, the panel ensured that the process followed by the project conformed to the requirements of SSHAC EL-2, which meant ensuring project compliance with the requirements of the selected SSHAC process level. The PPRP members are listed in Figure 2-4.

The PPRP for the Duynefontyn PSHA was selected based on the selection criteria identified in NUREG-2213. As outlined in the SSHAC regulatory guidance, the PPRP played a fundamental role in ensuring the quality of the project activities and the associated documentation.

Throughout the Duynefontyn PSHA, the PPRP members provided clear and timely feedback to the PTI and TI Leads, through the PPRP Chair to the Project Manager. This feedback included technical and process reviews of key activities and milestones. The PPRP attended all three workshops and submitted a consensus report at the conclusion of each workshop, containing comments and suggestions to improve the project. Consistent with current regulatory guidance, the PPRP members attended Workshop 1 and Workshop 2 as observers and then participated more actively in Workshop 3 by challenging and querying the TI Teams about their preliminary SSM and GMM. In addition, representatives from the PPRP attended the working meetings, except for SSM Working Meeting 4. The PPRP did not attend the final SSM Working Meeting as the objective of this meeting changed to become largely a writing session for the SSM TI Team. After Workshop 3, the final integration activities of the SSM were completed via weekly videoconferences, and the PPRP attended all those video-conference sessions.

It was paramount that each member of the PPRP preserve their independent status throughout the project. This meant that each PPRP member had to maintain objectivity and not be drawn into the technical assessments. It also involved resisting any temptation to represent the views of the organisation to which they were affiliated. The members of the PPRP also remained cognisant that their duty was not to determine whether they agreed with the SSM and GMM being developed, but, rather, whether they were satisfied that the technical bases of those models were adequately justified.

The PPRP completed the following specific duties:

1. Reviewed workshop agendas and the lists of invited resource experts and proponent experts and made proposals regarding these as required.
2. Attended all three workshops and submitted written reports in a timely fashion.
3. Reviewed the preliminary SSM and GMM and participated actively in Workshop 3 to provide feedback to the TI Teams.
4. Reviewed two sets of white papers, the first of which was written by the TI Teams ahead of Workshop 3 to document the data, models, and methods used to develop the preliminary models. The second set of white papers was written to document the data, models, and methods used to develop the final models. This second set served to inform the PPRP of the final models prior to the PPRP briefing, as a way to improve the effectiveness of the briefing given the scheduling and travel constraints for all project participants.
5. Reviewed the final Hazard Input Document (HID).
6. Participated in a PPRP Briefing with the PTI, TI Leads and TI Teams, during which the final SSM and GMM were discussed.

After receiving the Draft Report, the PPRP:

1. Reviewed the Draft Project Report and submitted written review comments for consideration in the finalisation of the report.
2. Upon review and acceptance of the Final Report, issued a PPRP Closure Letter.

The role of the Chair, fulfilled by Dr Julian Bommer, was vital to the effective functioning of the PPRP. Dr Bommer's first duty as Chair was to liaise with the CGS and Eskom regarding the technical needs of the PPRP, and to coordinate the development of appropriate selection criteria to support the appointment of the other PPRP members. Throughout the course of the project, the PPRP Chair was the point of contact with the Project Manager and the spokesperson for the PPRP in all situations. The PPRP Chair was also tasked with coordinating the work to ensure that the PPRP remained independent and impartial and adhered to the SSHAC principles during its assessment of the technical evaluation and integration process.

The specific duties of the PPRP Chair included organising pre- and post-workshop meetings of the PPRP and drafting written assessments of the workshops and other PPRP communications on the technical work of the TI Teams. The Chair selected appropriate observers from the PPRP to attend the formal and informal working meetings of the TI Teams. He also made sure that the PPRP arrived at a consensus view, and that concerns were communicated clearly and in a timely fashion to the Project Manager. The Chair compiled the views and comments from the PPRP members into a single cohesive document and ensured

that the comments and feedback from the PPRP were clear, objective, and relevant to the goals and objectives of the Duynefontyn PSHA.

2.2.5 Hazard Analysis Team

The execution of the PSHA calculations was clearly of central importance to the project. The hazard calculations were coordinated by the PTI and undertaken by the appointed HAT, with technical support provided by CGS staff and Slate Geotechnical Consultants. Ms Micaela Largent served as the HAT Lead, supported by Ms Tessa Williams and Ms Kelley Shaw from Slate Geotechnical Consultants.

The role of the HAT was to perform all the PSHA calculations the TI Teams required. These included initial sensitivity analysis runs, hazard calculations based on the preliminary SSM and GMM, and the final PSHA calculations that are documented in Chapter 10 of the Final Project Report. The HAT Lead worked closely with the PTI to ensure that the TI Teams were aware of any limitations or input requirements specific to the hazard calculation code employed, and to understand the way in which the SSM and GMM were specified. The Primary Hazard Analyst also coordinated with the PTI and the Project Manager to ensure that there was sufficient time allocated in the schedule for the hazard calculations to be executed and checked. The Primary Hazard Analyst worked with the PTI and the Project Quality Officer to ensure that appropriate quality assurance (QA) checks were applied to the hazard calculations. The Primary Hazard Analyst completed the necessary Verification and Validation (V&V) exercise applied to the PSHA calculations.

In addition to the HAT, Dr Vunganai Midzi and Dr Valentina Montaldo Falero were assigned as advisors to the Primary Hazard Analyst to provide technical support in the implementation of the SSM and GMM HID in the hazard code. Both have extensive experience in hazard code applications. Dr Montaldo Falero has served as a Hazard Analyst on several SSHAC studies, including recently completed SSHAC Level 3 studies at the Idaho National Laboratory (INL), Hanford, and Spain. Dr Midzi supported the hazard calculations for the Thyspunt PSHA (Bommer et al., 2013b), was the lead author of the 1999 GSHAP paper for Eastern and Southern Africa (Midzi et al., 1999) and the technical lead of the CGS team responsible for developing national hazard maps for South Africa (Midzi et al., 2020).

The final SSM and GMM HID was used by the HAT to produce the final hazard calculations presented in Chapter 10. Final hazard calculations were completed by the HAT consistent with the hazard targets and under the direction of the PTI. The final hazard calculations were performed to produce the technical products required for the study as described in Section 1.4.

2.2.6 Resource and Proponent Experts

Resource Experts have specific knowledge of data and information, which they provided to the TI Teams either through presentations at Workshop 1 and Workshop 2, outside of the workshop process via presentations during weekly team video conferences, or in writing. Resource Experts were asked to provide their data in an impartial manner to the TI Teams and to avoid interpretations that could bias the TI Teams' evaluation of the data. The Resource Experts who participated in the Duynefontyn PSHA are listed in Table 2-2.

Unlike most SSHAC Level 3 studies, the Duynefontyn PSHA commenced just after a Baseline PSHA study was completed for the KNPS site (Stamatakos et. al., 2022). Much of the data

used in the Duynefontyn PSHA was assembled in the Baseline study. In addition, several scientific investigations were included in the contract scope (Eskom, 2020a), designed to specifically provide information to reduce the uncertainties in the key inputs to the PSHA (Neveling and Chirenje, 2022). Most of these investigations, also referred to as the Duynefontyn Data Collection (DDC) activities, were ongoing at the time of Workshop 1. As a result, three sources of data were available to the TI Teams at Workshop 1, as listed in Table 2-2:

(1) Summaries of the Baseline PSHA study.
(2) Summaries of the DDC activities (as fully described in Chapters 4, 5, 6 and 7 of this report).
(3) Invited resource experts discussing additional available data.

The presentation materials from Workshop 1 are in the project management system and listed in Appendix E. Much of the project-specific data relied on by the TI Teams were acquired through the DDC activities.

Another approach to engage with Resource Experts was exemplified by the interactions between the TI Team and Mr Oliver Barker. Mr Barker was one of the field geologists who mapped the bedrock of the KNPS footprint just after the cover strata was stripped off during construction of the plant in the 1970s. He provided the SSM TI Team with his recollections of the bedrock exposures, first as a presentation during an SSM weekly video conference, and then in a written report (Barker, 2023).

In contrast with Resource Experts, Proponent Experts are advocates of scientific models and methods, and were asked to present their proponent viewpoints at Workshop 2. Provision was also made for other Proponent Experts to provide their views outside of the workshop process, principally during weekly TI Team video conferences. All the presentations made during weekly meetings, working meetings, or workshops are captured in the project management system and listed in Appendix E. In other cases, proponent viewpoints were solicited by the TI Teams through publications or other written pre-publication materials. The Proponent Experts who participated in Workshop 2 or outside of the workshop process are listed in Table 2-3.

Table 2-2. Resource experts at Workshop 1.

Resource Experts	Topic
Dr Vunganai Midzi	Prior seismic hazard analysis (SHA) results for Duynefontyn
Dr John Stamatakos Dr Jennie Watson Lamprey	Overview of the Baseline PSHA
Mr Ryan Coppersmith Ms Debbie Claassen	Summary of Fault Sources in the Baseline PSHA
Dr Vunganai Midzi Ms Courtney Johnson	Summary of the Earthquake Catalogue in the Baseline PSHA
Ms Courtney Johnson	Summary of the Seismic Source Zones in the Baseline PSHA
Dr John Stamatakos Dr Thifhelimbilu Mulabisana	Western Cape, South Africa Crustal Structure
Mr Ian Saunders	Syntaxis Studies (DDC 2)
Ms Paola Albini Ms Nicky Flint	Historical Seismicity Investigation (DDC4)
Ms Debbie Claassen Ms Dawn Black Ms Ponani Mthembi	Marine Terrace Mapping Fieldwork (DDC5)
Mr Neo Moabi Dr Taufeeq Dhansay	Fault Studies (DDC6 and DDC7)
Dr Hayley Cawthra Ms Debbie Claassen Mr Michael MacHutchon Mr Wilhelm van Zyl Mr Norman Krahtz Mr Uzair Adam	How to find a fault on the seafloor – Looking for the Milnerton "Fault"
Dr Brassnavy Manzunzu	Multichannel Analysis of Surface Waves (MASW) Survey Conducted at Ceres Seismic Station
Ms Debra Murphy	Site Profile in the Baseline PSHA
Ms Katie Wooddell	Ground Motion Database in the Baseline PSHA
Dr Jennie Watson-Lamprey	Additional Ground Motion Datasets Used in the Baseline PSHA
Dr Brassnavy Manzunzu	MASW for Elim and Matjiesfontein stations
Prof. Brady Cox Prof. Ellen Rathje	Seismic Site Characterisation and Downhole Array Plan

Table 2-3. Proponent experts at Workshop 2.

Proponent Experts	Topic
Prof. Alex Kisters	Capacity of structures in the Cape Fold Belt, especially in the Western Cape and constraints on activity rates and Western Cape fault studies
Dr Janine Cole	Western Cape structures from potential field data and constraints on activity rates and Western Cape fault studies
Dr Alastair Sloan	Neotectonics of South Africa (onshore and offshore)
Dr Marco Andreoli	Neotectonics of South Africa (onshore and offshore)
Dr Tony Tankard	Western Cape crustal thickness and composition
Dr Douglas Paton	Western Cape crustal thickness and composition
Dr Laura Gulia	*b*-values and source zone recurrence rates
	Host zone earthquake clusters
Mr Ian Saunders	Host zone earthquake clusters
Dr Martin Brandt	Host zone earthquake clusters
	The Western Cape as a stable continental region?
Dr Thomas Weaver	Areal source zone spatial smoothing
Dr Gabriel Toro	Areal source zone spatial smoothing
Dr Olga Ktenidou	Kappa estimates
Prof. Ben Edwards	Kappa estimates using noise
	Ground Motion data inversion methodology
Prof. Peter Stafford	Ground Motion Prediction Equations inversions
Dr Linda Al Atik	Sigma model
	Ground Motion Prediction Equations, shear wave velocity (V_S) Inversions
Prof. Ellen Rathje	Host to Target Site Response Methodologies
Prof. Brady Cox	Epistemic Uncertainty for V_S Profiles
Dr. Vunganai Midzi	South African intensity data
Prof. Norm Abrahamson	Use of intensity data
	Ground Motion Prediction Equation (GMPE) residuals and kappa
Prof. Andreas Rietbrock	Ground Motion data inversion methods and stress drop estimates in SA
Prof. Peter Stafford	Ground Motion data inversion methodology

2.2.7 Database management

The data used by the TI Team in the execution of their tasks, such as literature, meeting logs, working meeting and weekly meeting presentations, reference material, draft and final milestones, the HID, and routine Microsoft Excel spreadsheet calculations, were stored in a SharePoint Folder maintained by Slate Geotechnical Consultants. Ms Courtney Johnson and Ms Kelley Shaw were responsible for maintaining the Slate server and organising access and permission for the TI Team, the TI Team support staff, and the PPRP. The components of this data that supported technical conclusions (e.g. references) and recorded project activities (e.g. presentations and minutes) and other QA requirements, were downloaded by, or submitted to, the Project Quality Officer at intervals during project execution for incorporation in the project Quality Assurance Data Pack (QADP). Also included in the QADP were records such as workshop presentations and other records. Spatial and Geographic Information System (GIS) data was maintained by Mr Khuliso Nedzingahe of the CGS.

2.2.8 Project schedule and workshops

The three formal workshops, as suggested for an enhanced (or augmented) SSHAC Level 2 and prescribed for an SSHAC Level 3 process, formed the core of the Duynefontyn PSHA, around which all project activities were organised. Each of the three workshops had a specific theme and focus. These, together with other milestones such as working meetings and deadlines for the submission of the report, formed the basis for the development of the project schedule. A high-level schedule was provided in the PEP (Stamatakos and Watson-Lamprey, 2023), with a much more detailed schedule developed by Mr Emmanuel Chirenje for project management purposes. The latter schedule was reviewed monthly, updated as circumstances dictated and incorporated into monthly reports to the Project Sponsor. The most significant change was a delay in Workshop 3, which was originally scheduled for 13-17 March 2023, but was postponed because of internal bureaucratic delays (non-technical) at the CGS. This change necessitated changing the dates for Working Meeting 4, the PPRP briefing, and schedule milestones for the draft and final reports.

The three formal workshops provided the TI Team with an opportunity to interact with invited experts in the presence of the PPRP (in addition to the Sponsor and other observers) and to solicit feedback from the PPRP on the preliminary models. However, most of the actual evaluation and integration processes took place outside these workshops, with four formal working meetings representing key milestones in the development of the preliminary and final SSM and GMM. The dates of key events and milestones in the project are summarised in Table 2.4.

Table 2-4. Key milestones of the Duynefontyn PSHA.

Milestone	Dates
Duynefontyn PSHA Kick-off (Hybrid meeting, Cape Town, RSA)	23 February 2022
Workshop 1 (Hybrid meeting, Cape Town, RSA)	23–24 February 2022
Working Meeting 1 (In-person meeting, Walnut Creek, USA)	2–5 May 2022
Workshop 2 (Hybrid meeting, Stellenbosch, RSA)	20–24 June 2022
Working Meeting 2 (In-person meeting, Pretoria, RSA)	10–14 October 2022
Working Meeting 3 (In-person meeting, San Antonio, USA)	23–27 January 2023
Workshop 3 (In-person meeting, Stellenbosch, RSA)	19–23 June 2023
GMM Working Meeting 4 (Virtual meeting)	10–14 July 2023
SSM Working Meeting 4 (In-person meeting, South Lake Tahoe, USA)	28 August–1 September 2023
PPRP Briefing (Virtual meeting)	21–22 September 2023
Submission of Draft Report to the PPRP	6 November 2023
PPRP Writing Meeting (In-person meeting, San Diego, USA)	11–15 December 2023
PPRP Comments on Draft Report	15 December 2023
Submission of Final Report and TI Team responses to PPRP	15 February 2024
PPRP Closure Letter	7 March 2024
Submission of Final Report	12 March 2024

2.3 INTEGRATED MANAGEMENT SYSTEM

The CGS established an integrated management system (IMS) to manage the quality, safety, and environmental requirements for scientific projects for the nuclear industry. The IMS met the ISO 9001 quality requirements: it is ISO 9001:2015 certified (ISO, 2015; see Certificate # 20258) and satisfies the quality and safety requirements of the NNR, in particular, Regulatory Document RD-0034. The IMS supported all activities executed as part of Contract Number 4600062664 for Eskom, which include, but are not limited to, the DDC activities, the Baseline PSHA for Duynefontyn, and the Duynefontyn PSHA (i.e. the Enhanced SSHAC Level 2 study). The principles of quality management, which included the methodology of "Plan-Do-Check-Act", were applied to these activities, as required in ISO 9001 (ISO, 2015) and the RD-0034 (NNR, 2008b).

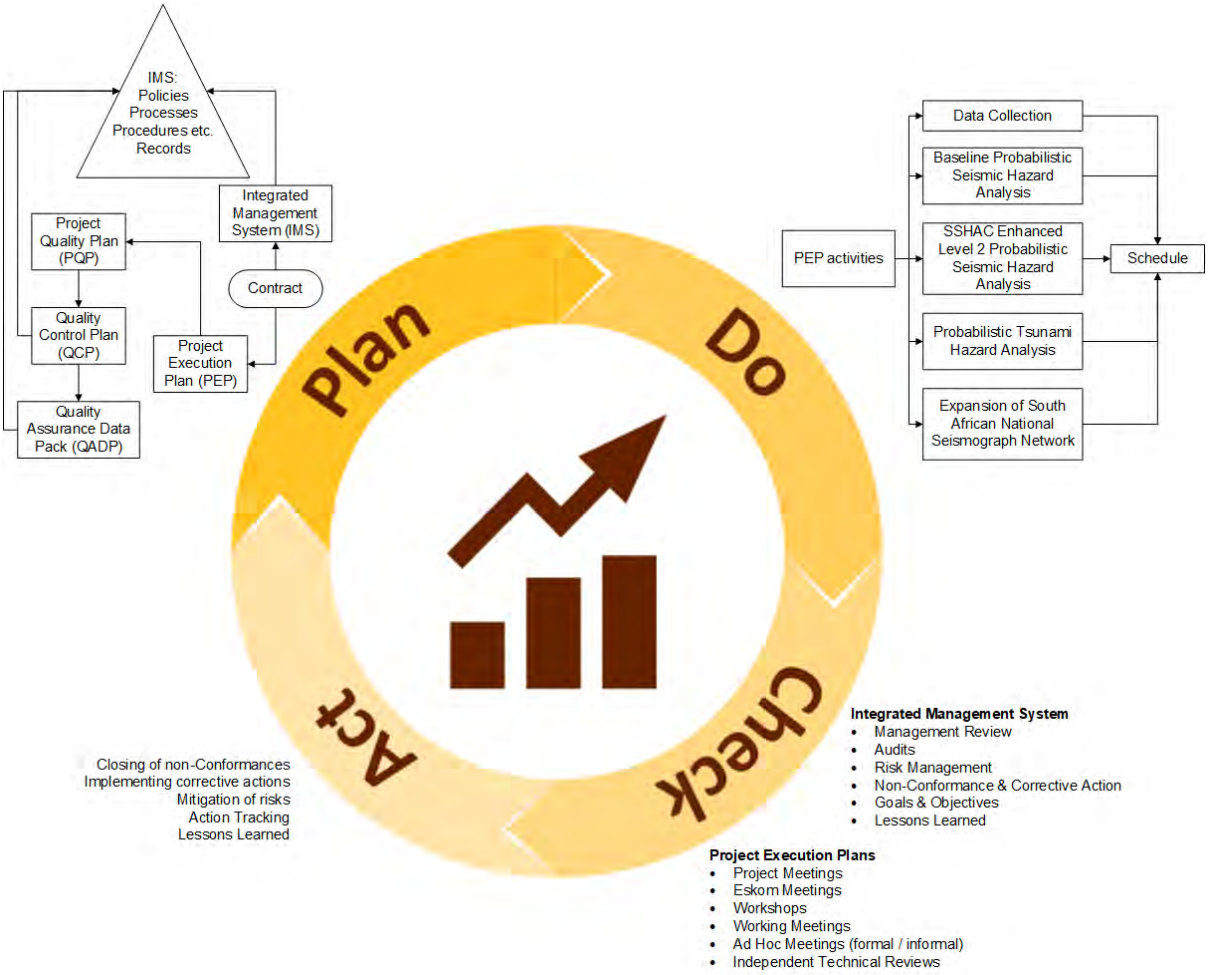

Figure 2-5: The Plan-Do-Check-Act approach used in the Duynefontyn PSHA project to support quality assurance (QA).

The contract deliverables consisted of numerous technical reports, a QADP, and records demonstrating the achievement of project management and compliance requirements.

The NNR's RD-0034 (NNR, 2008b) required that the scope of the IMS be appropriate to the safety importance of the project's products. To comply with this multilevel safety and quality classification system, the DDC activities were classified as either NNR Level 2 or 3, while the

Baseline PSHA and Duynefontyn PSHA were classified as NNR Level 1; the highest safety level with most stringent quality and safety requirements (Eskom, 2021).

To ensure the achievement of these deliverables, separate PEPs were developed for the DDC activities (Neveling and Chirenje, 2023), the Baseline PSHA (Stamatakos and Watson-Lamprey, 2021) and the Duynefontyn PSHA (Stamatakos and Watson-Lamprey, 2023) as well as, where appropriate, other activities stipulated by the contract. These PEPs were supported by Project Quality Plans (Percy-Lancaster, 2021; 2022b; 2022c) to ensure the technical output satisfied contractual requirements (Eskom, 2014, 2017, 2018a).

In addition to quality and safety management system requirements (Eskom, 2017; 2018a; 2018b), safety management and a Safety Culture Enhancement Programme (SCEP) (Eskom 2014) were required by the NNR (2008b) for Level 1 and Level 2 activities.

As part of this IMS, the project management team managed its quality and safety through a risk-based approach (ISO, 2018b) and improved its performance to:

- Foster and support a strong safety culture.
- Eliminate or minimise risk to employees and other parties who may be exposed to risks associated with the project.
- Actively manage safety.
- Monitor the effectiveness of performance measures.
- Ensure conformance with the stated policies, objectives and requirements.

2.3.1 Quality management

The guideline for quality management in projects, ISO 10006 (ISO, 2017), was followed. The project also followed the process approach as required by ISO 9001 (ISO, 2015) and NNR RD-0034 (NNR, 2008b). This approach is described fully in the IMS Manual (Percy-Lancaster, 2022a). Quality assurance (QA) is described in the Project Quality Plans (Percy-Lancaster, 2021; 2022b; 2022c), which followed the guidelines of ISO 10005 (ISO, 2018a). To control the delivery of a conforming product, processes, procedures, and Quality Control Plans (QCPs) were developed. QCPs are practical tools to ensure project activities meet the necessary quality and safety requirements and deliver the records that should be captured in the QADP. Thus, the QADP formed the foundation for ensuring quality for all the project deliverables and was systematically developed and compiled as the project progressed (Percy-Lancaster, 2022d; Percy-Lancaster and Nkoana, In Prep.a; In Prep.b; In Prep.c). The CGS has a comprehensive master list of relevant quality management documented information.

Self-assessment and audits (quality and safety) were performed on the IMS and PEPs. These were monitored by the Management Review Committee through Management Review Meetings to ensure the quality and safety of the various key deliverables and the development of the final product. Where observations, review comments, non-conformities and opportunities for improvement became apparent, corrective actions were implemented. This ensured the effective closure of any of the above to produce a quality product.

As the project progressed, lessons learned were identified by the different team members. The Project Management Team (PMT) and TI Leads will draw on these experiences and compile a lessons learned report to be used for future projects.

The Management Review Meeting was an opportunity for the project management team to review the progress, effectiveness, and efficiency of the IMS, and to identify improvement opportunities.

The PTI, SSM TI Lead, GMM TI Lead, and HAT were jointly responsible for the key steps in delivering the Baseline and Duynefontyn PSHA studies. Contributions and presentations were made at working meetings and workshops. The V&V actions included, but were not limited to, evaluations, questions, and peer reviews by the SSM and GMM TI Team members and the PPRP. V&V reports were compiled by the HAT for the Baseline and SSHAC EL-2 PSHAs (Wooddell and Watson-Lamprey, 2022; Largent et al., In Prep.) to provide objective evidence for the formulation, development, and implementation of the SSM and GMM as well as the PSHA. V&V on computer software, per the NNR's RG-0016 (NNR, 2016) and Eskom's NSIP02761 (Eskom, 2020b), are also addressed in these reports and summarised in Section 10.2.6.

V&V focussed on high-level activities forming part of the SSHAC EL-2 process, and the data used in the models. It can be described as:

- Process V&V: process verification was done through reviews described in the SSHAC EL-2 process. Process validation occurred via the input of the PPRP during the SSHAC EL-2 process, where the process was validated on behalf of Eskom.
- Model V&V: the SSM and GMM were developed by the TI Teams. Internal review and interrogation of the models by the TI Teams were considered as the first stage of model verification. The input, questions and feedback provided by the PPRP represent validation of the SSM and GGM, especially the reasoning supporting the development of these models.
- Data V&V: data gathering for the project took place as prescribed by the different procedures or processes. The acquisition of data was dependent on the type of analysis and the interpretation thereof. Verification and validation of data collection products were undertaken by independent technical reviewers for the specific task. Where external review was not possible, verification of the gathered data took place during working meetings and workshops, where data was reviewed by the TI Teams for completeness, accuracy, relevance, accessibility, and location. The PPRP validated that the models reflect the use of the site-specific dataset.

2.3.2 Safety management

The requirements of the Occupational Health and Safety Act (Act 85 of 1993) were incorporated into the IMS to enable the project team to control its occupational, health and safety risks and improve its performance. Compliance with the NNR (NNR, 2008b) and Eskom's requirements for safety management (SM) and SCEP were graded as Level 1 and 2 activities (Eskom, 2021), while SM formed part of Level 3 activities.

Safety activities were implemented for all project activities, regardless of the grading, and included:

- Monthly quality and safety themes.
- Safety and quality inductions.
- Safety and quality presentations at workshops (including Eskom SC presentations).

- Safe work method statements (incorporating method statements, risk assessments and safety plans).
- Safety Culture Committee meetings.
- Provision of personal protective equipment (PPE).
- Provision of emergency equipment (e.g. first aid kits, fire extinguisher, vehicle recovery kits [if applicable]).
- Project team member routine medical examinations.
- Training (i.e. first aid, firefighting, snake awareness, 4x4, ISO 9001, ISO 14001, ISO 45001, risk management).
- Activity safety files.
- Safe vehicles.
- Toolbox talks (covering relevant topics).
- Implementation of SCEP activities (e.g. rewards and recognition).
- Where applicable, demarcated sites (e.g. drilling).
- Where applicable, field amenities (e.g. drilling).
- Self-assessments.
- Oversight by CGS, Eskom and the NNR.

Figure 2-6: The project team's commitment to safety in the field: (a) usage of PPE on site; (b) visibility in remote areas; (c) calibration of equipment; (d) daily toolbox talks; (e) promoting teamwork; (f) adherence to Eskom's environmental requirements.

2.3.3 Safety culture

Nuclear safety encompasses the safety of all processes, including the reliability of the products with respect to their nuclear safety functions. The RD-0034 (NNR, 2008b) requirement document prompted the incorporation of IAEA safety reports INSAG 4 (IAEA, 1991) and INSAG 15 (IAEA, 2002), with the specific aim to establish and enhance a safety culture. Reliability was achieved through adequate management of the procedures (a deliverable of this contract) as a supporting attribute for safety.

As part of the CGS's commitment to the SCEP, safety culture surveys were undertaken during the project. The survey results indicate that the CGS has successfully introduced the applicable concepts of nuclear safety for the Level 1 and Level 2 activities. Additionally, the survey results indicated that the CGS's project leadership and the project team placed nuclear safety as a priority within the project. The project team also demonstrated an understanding of the CGS's safety culture awareness interventions and familiarised themselves with the principles and traits of the Nuclear Safety Culture, as laid out by the Institute of Nuclear Power Operations (INPO) and the World Association of Nuclear Operators (WANO) (INPO, 2004; WANO, 2013; Komape et al. 2022; Komape and Percy-Lancaster, 2023; Komape and Kekana, 2023).

2.3.4 Environmental management

For all work on the Duynefontyn site, Eskom took a leading role, with the development of an approved specification (Eskom, 2016) followed by a site-specific Environmental Management Plan (Eskom, 2012). The CGS implemented an Environmental Management Plan (Komape and Percy-Lancaster, 2021), which the project team followed. Eskom's environmental officer inducted all visitors to the Duynefontyn site and delivered environmental and safety impact awareness training sessions during the DDC activities. During the DDC activities, project team members adhered to the environmental requirements. In addition, as part of awareness, a Safe Work Method Statement was developed to address environmental aspects. It was essential to limit the impact on the environment so the drilling and shear-wave velocity measurements were, as far as possible, restricted to access roads for this purpose. Where additional paths had to be cleared, this was done under supervision of Eskom's environmental officer, and special care was taken not to damage sensitive vegetation.

2.4 REFERENCES

Abrahamson, N.A.; Birkhauser, P.; Koller, M.; Mayer-Rosa, D.; Smit, P.; Sprecher, C.; Tinic, S. and Graf, R. (2002). PEGASOS - A Comprehensive Probabilistic Seismic Hazard Assessment for Nuclear Power Plants in Switzerland. Proceedings of the Twelfth European Conference on Earthquake Engineering, London, UK. Paper 633.

American Nuclear Society (ANS) (2020). Probabilistic Seismic Hazard Analysis. American National Standard ANSI/ANS-2.29-2020. American Nuclear Society. La Grange Park, Illinois, USA.

American Society of Civil Engineers/Structural Engineering Institute (ASCE/SEI) (2019). Seismic Design Criteria for Structures, Systems, and Components in Nuclear Facilities. ASCE/SEI 43-19. American Society of Civil Engineers, Reston, Virginia, USA.

Barker, O. (2023). Koeberg - 1976 to 1978 - Memories Observations and Ideas (2023). Prepared for the Council for Geoscience Enhanced SSHAC Level 2 PSHA, Koeberg Nuclear Power Station.

Bernreuter, D.L.; Savy, J.B.; Mensing, R.W.; Chen, J.C. and Davis, B.C. (1989). Seismic Hazard Characterization of 69 Nuclear Plant Sites East of the Rocky Mountains. NUREG/CR-5250 1-8. US Nuclear Regulatory Commission, Washington DC, USA.

Bommer, J.J. and Coppersmith, K.J. (2013). Lessons Learned from Application of the NUREG-2117 Guidelines for SSHAC Level 3 Probabilistic Seismic Hazard Studies for Nuclear Sites. Proceedings of 22nd International Conference on Structural Mechanics in Reactor Technology (SMiRT22), San Francisco, California, USA.

Bommer, J.J.; Coppersmith, K.J. and Hattingh, E. (2013a). Lessons Learned from SSHAC Level 3 Site-Specific PSHA for Thyspunt. CGS Report 2013-0247 (Rev. 0). Council for Geoscience, Pretoria, South Africa.

Bommer, J.J.; Coppersmith, K.J.; Coppersmith, R.; Hanson, K.; Mangongolo, A.; Neveling, J.; Rathje, E.; Rodriguez-Marek, A.; Scherbaum, F.; Shelembe, R.; Stafford, P. and Strasser, F. (2013b). Probabilistic Seismic Hazard Analysis for the Thyspunt Nuclear Site, South Africa. CGS Report 2013-0190 (Rev. 0). Council for Geoscience, Pretoria, South Africa.

Budnitz, R.J.; Apostolakis, G.; Boore, D.M.; Cluff, L.S.; Coppersmith, K.J.; Cornell, C.A. and Morris, P.A. (1997). Recommendations for Probabilistic Seismic Hazard Analysis: Guidance on Uncertainty and the Use of Experts. NUREG/CR-6372 1-2. US Nuclear Regulatory Commission, Washington DC, USA.

Electric Power Research Institute Seismic Owners Group (EPRI-SOG) (1988). Seismic Hazard Methodology for the Central and Eastern United States. PRI NP-4726A (Rev. 1) 1-11. Electric Power Research Institute, Palo Alto, California, USA.

Electric Power Research Institute (EPRI) (1989). Probabilistic Seismic Hazard Evaluations at Nuclear Plant Sites in the Central and Eastern United States: Resolution of the Charleston Earthquake Issue. EPRI NP-6395-D. Electric Power Research Institute, Palo Alto, California, USA.

Electric Power Research Institute (EPRI) (2013). EPRI Ground Motion Model Review Final Report. ADAMS Accession ML13155A553. Palo Alto, California, USA.

Electric Power Research Institute/ Department of Energy/United States Nuclear Regulatory Commission (EPRI/DOE/USNRC) (2012). Central and Eastern United States Seismic Source Characterization for Nuclear Facilities. NUREG-2115. US Nuclear Regulatory Commission, Washington DC, USA.

Eskom (2012). Environmental Management Plan (Nuclear Sites). NSIP01014 (Rev. 1).

Eskom (2014). Level-1 Supplier Safety Culture Enhancement Programme (SCEP) Requirements (Rev. 0). 238-219.

Eskom (2016). Generic Environmental Requirements. NSIP03281 (Rev. 1).

Eskom (2017). Quality and Safety Management Requirements for Nuclear Suppliers (Rev. 1). 238-101.

Eskom (2018a). Quality Management Requirements for Nuclear Suppliers Level 2 (Rev. 1). 238-102.

Eskom (2018b). Supplier Quality General Requirements (Rev. 1). 238-103.

Eskom (2019). Justification of the Approach for the Duynefontyn Probabilistic Seismic Hazard Analysis Study. NSIP03836 (Rev. 0). Eskom, South Africa.

Eskom (2020a). Duynefontyn Geological Investigations, Micro-Seismic Monitoring, Probabilistic Seismic Hazard Analysis and National Nuclear Regulator Licensing Support. NSIP03280 (Rev. 2). Eskom, South Africa.

Eskom (2020b). Specifications for Verification and Validation Tasks for Simulation Models Used in Nuclear Siting. NSIP02761 (Rev. 1).

Eskom (2021). Safety Classifications of SSR Production Processes. NSIP02189 (Rev. 2).

Institute of Nuclear Power Operations (INPO) (2004). Principles for a Strong Nuclear Safety Culture. Institute of Nuclear Power Operations, Atlanta, Georgia, USA.

International Atomic Energy Agency (IAEA) (1991). Safety Culture. Safety Series 75. INSAG 4.

International Atomic Energy Agency (IAEA) (2002). Key Practical Issues in Strengthening Safety Culture. INSAG 15.

International Atomic Energy Agency (IAEA) (2019). Site Evaluation for Nuclear Installations. IAEA Safety Standards Series SSR-1. International Atomic Energy Agency, Vienna, Austria.

International Atomic Energy Agency (IAEA) (2022). Seismic Hazards in Site Evaluation for Nuclear Installations. Specific Safety Guide SSG-9 (Rev. 1). International Atomic Energy Agency, Vienna, Austria.

International Standards Organisation (ISO) (2015). Quality Management System - Requirements. ISO 9001. Edition 5.

International Standards Organisation (ISO) (2017). Quality Management - Guidelines for Quality Management in Projects. ISO 10006. Edition 3.

International Standards Organisation (ISO) (2018a). Quality Management - Guidelines for Quality Plans. ISO 10005. Edition 3.

International Standards Organisation (ISO) (2018b). Risk Management - Guidelines. ISO 31000. Edition 2.

Komape, K. and Kekana, K. (2023). Nuclear Safety Culture Survey Report (Duynefontyn SSHAC EL-2 Workshop 3). CGS Report 2023-0146.

Komape, K. and Percy-Lancaster, A. (2021). Environmental Management Plan. NGG-PLN-007 (Rev. 2).

Komape, K. and Percy-Lancaster, A. (2023). Nuclear Safety Culture Survey Report. Duynefontyn SSHAC EL-2 Workshop 2. CGS Report 2022-0128. Council for Geoscience, Pretoria, South Africa.

Komape, K.; Percy-Lancaster, A. and Mathebula, R. (2022). Nuclear Safety Culture Survey Report. Duynefontyn SSHAC EL-2 Kick-Off Meeting & Workshop 1. CGS Report 2022-0063. Council for Geoscience, Pretoria, South Africa.

Largent, M.; Williams, T.; Yust, M. and Shaw, K. (In Prep.). Verification and Validation for SSHAC-EL2 PSHA Inputs for the Duynefontyn Site and Koeberg Nuclear Power Station. CGS Report 2023-0196. Council for Geoscience, Pretoria, South Africa.

McGuire, R.K.; Sewell R.T.; Toro, G.R. and Cornell, C.A. (1989). Approaches to Evaluate the Influence of Possible Large Earthquakes in the Eastern United States on Seismic Safety of Nuclear Power Plants. Research Project 2356-50. Electric Power Research Institute, Palo Alto, CA, USA.

Midzi, V.; Hlatywayo, D.J.; Chapola, L.; Kebede, F.; Atakan, K.; Lombe, D.K.; Turyomurugyendo, G. and Tugume. F. (1999). Seismic Hazard Assessment in Eastern and Southern Africa. Annali di Geofisica [English: Annals of Geophysics] 42(6). 1067-1083.

Midzi, V.; Manzunzu, B.; Mulabisana, T.; Zulu, B.S.; Pule, T. and Myendeki, S. (2020). Probabilistic Seismic Hazard Maps for South Africa. Journal of African Earth Sciences 162. 103689.

National Nuclear Regulator (NNR) (2008a). Requirements on Risk Assessment and Compliance with Principal Safety Criteria for Nuclear Installations. Requirements Document RD-0024. National Nuclear Regulator, South Africa.

National Nuclear Regulator (NNR) (2008b). Quality and Safety Management Requirements for Nuclear Installations. Requirements Document RD-0034 (Rev. 0). National Nuclear Regulator, South Africa.

National Nuclear Regulator (NNR) (2012). Consideration of External Events for New Nuclear Installations. Position Paper PP-0014 (Rev. 0). National Nuclear Regulator, South Africa.

National Nuclear Regulator (NNR) (2015). Interim Guidance for the Siting of Nuclear Facilities. Regulatory Guide RG-0011. National Nuclear Regulator, South Africa.

National Nuclear Regulator (NNR) (2016). Guidance on the Verification and Validation of Evaluation and Calculation Models Used in Safety and Design Analyses. Regulatory Guide RG-0016 (Rev. 0).

Neveling, J. and Chirenje, E. (2023). Project Execution Plan: The Investigation of the Site Geology and Micro-Seismic Monitoring in Support of the Probabilistic Seismic Hazard Analyses for the Duynefontyn Site. NGG-PLN-001 (Rev. 2).

Percy-Lancaster, A. (2021). Project Quality Plan: Baseline Probabilistic Seismic Hazard Analysis at the Duynefontyn Nuclear Site. NGG-PLN-020 (Rev. 1).

Percy-Lancaster, A. (2022a). Nuclear Geo-Hazards Group Integrated Management System Manual. NGG-MN-001 (Rev. 4).

Percy-Lancaster, A. (2022b). Project Quality Plan: The Investigation of the Site Geology and Micro-Seismic Monitoring in Support of the Probabilistic Seismic Hazard Analyses for the Duynefontyn Site. NGG-PLN-004 (Rev. 4).

Percy-Lancaster, A. (2022c). Project Quality Plan for the Senior Seismic Hazard Analysis Committee Enhanced Level-2 Probabilistic Seismic Hazard Analysis at the Duynefontyn Nuclear Site. NGG-PLN-014 (Rev. 0).

Percy-Lancaster, A. (2022d). Duynefontyn Baseline Probabilistic Seismic Hazard Analysis Quality Assurance Data Pack Road Map. CGS Report 2022-0045. Council for Geoscience, Pretoria, South Africa.

Percy-Lancaster, A. and Nkoana, K.S. (In Prep.a). Duynefontyn Data Collection Quality Assurance Data Pack Road Map. CGS Report 2023-0003. Council for Geoscience, Pretoria, South Africa.

Percy-Lancaster, A. and Nkoana, K.S. (In Prep.b). Duynefontyn Senior Seismic Hazard Analysis Committee Enhanced Level-2 Probabilistic Seismic Hazard Analysis Quality Assurance Data Pack Road Map. CGS Report 2023-0188. Council for Geoscience, Pretoria, South Africa.

Percy-Lancaster, A. and Nkoana, K.S. (In Prep.c). Duynefontyn Project Management and Compliance Quality Assurance Data Pack Road Map. CGS Report 2023-0191. Council for Geoscience, Pretoria, South Africa.

Renault, P.; Heuberger, S. and Abrahamson, N.A. (2010). PEGASOS Refinement Project: An Improved PSHA for Swiss Nuclear Power Plants. Proceedings of the 14th European Conference of Earthquake Engineering, Ohrid, Republic of Macedonia. Paper ID 991.

Sobel, P. (1994). Revised Livermore Seismic Hazard Estimates for Sixty-Nine Nuclear Power Plant Sites East of the Rocky Mountains. NUREG-1488. US Nuclear Regulatory Commission, Office of Nuclear Regulatory Regulation, Washington DC, USA.

Stamatakos, J. and Watson-Lamprey, J. (2021). Project Execution Plan for the Baseline PSHA for the Duynefontyn Nuclear Site. NGG-PLN-015 (Rev. 2).

Stamatakos, J. and Watson-Lamprey, J. (2023). Project Execution Plan for the Senior Seismic Hazard Analysis Committee Enhanced Level-2 Probabilistic Seismic Hazard Analysis at the Duynefontyn Nuclear Site. NGG-PLN-003 (Rev. 1).

Stamatakos, J.; Watson-Lamprey, J.; Cawthra, H.; Claassen, D.; Coppersmith, R.; Johnson, C.; Largent, M.; Manzunzu, B.; Midzi, V.; Mulabisana, T.; Murphy, D.; Rathje, E. and Wooddell, K. (2022). Baseline PSHA for the Duynefontyn Site and the Koeberg Nuclear Power Station. CGS Report 2022-0009 (Rev. 0). Council for Geoscience, Pretoria, South Africa.

United States Nuclear Regulatory Commission (USNRC) (2007). A Performance-Based Approach to Define the Site-Specific Earthquake Ground Motion. Regulatory Guide 1.208. US Nuclear Regulatory Commission, Washington DC, USA

United States Nuclear Regulatory Commission (USNRC) (2010). Resolution of Generic Safety Issues: Issue 194: Implications of Updated Probabilistic Seismic Hazard Estimates (NUREG-0933, Main Report with Supplements 1-32). US Nuclear Regulatory Commission, Washington DC, USA.

United States Nuclear Regulatory Commission (USNRC) (2012a). Practical Implementation Guidelines for SSHAC Level 3 and 4 Hazard Studies. NUREG-2117 Revision 1. US Nuclear Regulatory Commission, Office of Nuclear Regulatory Research, Washington, DC, USA.

United States Nuclear Regulatory Commission (USNRC) (2012b). Letter from Eric J. Leeds, Director, Office of Nuclear Reactor Regulation and Michael R. Johnson, Director, Office of New Reactors, to All Power Reactor Licensees and Holders of Construction Permits in Active or Deferred Status. Washington DC. March 12. ADAMS Accession ML12053A340.

United States Nuclear Regulatory Commission (USNRC) (2018). Updated Implementation Guidelines for SSHAC Hazard Studies. NUREG-2213. US Nuclear Regulatory Commission, Office of Nuclear Regulatory Research, Washington DC, USA.

United States Nuclear Regulatory Commission (USNRC) (2021). Seismic Hazard Evaluations for US Nuclear Power Plants: Near-Term Task Force Recommendation 2.1 Results. NUREG/KM-0017. US Nuclear Regulatory Commission, Office of Nuclear Regulatory Research, Washington DC, USA.

World Association of Nuclear Operators (WANO) (2013). Traits of a Healthy Nuclear Safety Culture. PL 2013-1. World Association of Nuclear Operators.

Wooddell, K. and Watson-Lamprey, J. (2022). Validation and Verification for Baseline PSHA Inputs for the Duynefontyn Site and Koeberg Nuclear Power Station. CGS Report 2022-0074 (Rev. 0).

CHAPTER 3: KEY TASKS AND ACTIVITIES

3. KEY TASKS AND ACTIVITIES

This chapter concludes the overview of the Duynefontyn Probabilistic Seismic Hazard Analysis (PSHA) project. The context, purpose, and objectives of the Duynefontyn PSHA were introduced in Chapter 1. Chapter 2 outlined the way in which the project was organised, including the identification of key participants and the roles that they played in the project. This chapter provides brief information on key tasks and activities that made up the Senior Seismic Hazard Analysis Committee (SSHAC) Enhanced Level 2 PSHA for the Duynefontyn site (referred to as the Duynefontyn PSHA). This overview provides the basis to demonstrate that the Duynefontyn PSHA process followed the guidance provided in the regulatory guidance of the United States Nuclear Regulatory Commission (NUREG-2213, USNRC, 2018). More detailed information on the project activities and results are provided in Chapters 4 through 10 of this report.

3.1 PROJECT EXECUTION PLAN

The Technical Integration (TI) Leads developed a Project Execution Plan (PEP) (Stamatakos and Watson-Lamprey, 2023) that described the plan to carry out the Duynefontyn PSHA project as well as each participant's role and associated responsibilities. The purpose of the PEP was to provide a succinct overview of the complete project for all participants, observers, reviewers, and the sponsors. The key tasks described in the PEP are summarised in Table 3-1.

Modifications to project execution were made over the course of the project and are captured in Revision 1 of the PEP (Stamatakos and Watson-Lamprey, 2023). These changes included changes to the project execution based on the TI Teams' evaluations and data needs identified during the evaluation phase of the project; personnel changes (see Sections 2.2 and 3.4); changes to the schedule, especially those brought about because of the change to the Workshop 3 dates; a change in the delivery date of this report to the Participatory Peer Review Panel (PPRP) and Eskom; and minor editorial corrections. All these modifications are recorded at the beginning of the final version of the PEP.

3.2 DATABASE DEVELOPMENT

Gathering data is an important part of the evaluation phase of the PSHA. A fundamental principle of SSHAC projects is that a comprehensive database of all available data, methods, and models must be assembled and made fully accessible to all members of the TI Teams, as well as to the PPRP. To provide a repository for the information gathered for use by the TI Team, a SharePoint folder for all project data were established and maintained by Slate Geotechnical Consultants for the duration of the project. All scientific or technical data used by the TI Teams were downloaded by, or submitted to, the Project Quality Officer at intervals during project execution for incorporation into the project Quality Assurance Data Pack (QADP).

In establishing the project databases, two distinct activities were followed: compiling existing data and collecting new data. The compilation of existing information utilised the following available data sources:

- Published scientific papers from journals and conferences.
- Published and unpublished scientific reports.
- Geological maps, borehole logs, and trench logs.
- Geophysical data sets and maps.
- Instrumentally-derived information on earthquakes.
- Historical accounts of earthquake effects in South Africa.
- National seismological database curated by the Council for Geoscience (CGS).
- Data from the Intensity questionnaires and newspaper reports for observed effects of earthquakes in South Africa.
- Geological and geotechnical profiles at the Duynefontyn site.

Several parties contributed to the development of the project database from available information. The CGS made its existing database of scientific reports, papers, and other publications available to the TI Teams. Technical reports of all seismic hazard, geological and geotechnical studies performed at, or for the Duynefontyn site, were made available by the project sponsor, Eskom. Proponent Experts provided copies of the scientific publications cited in their presentations to the TI Teams. The TI Teams, supported by staff members from Slate Geotechnical Consultants and the CGS, explored the scientific and engineering literature for relevant papers and reports and uploaded those publications onto the database. The TI Teams were aided in their evaluation of existing information by suggestions made by the PPRP, based on their extensive background and experience in the seismology and geology of the Western Cape and seismic source and ground motion characterisation information that was adopted in other SSHAC PSHA studies conducted across the world over the past 20 years.

Table 3-1. Summary of tasks for the Duynefontyn PSHA.

No	Technical Task	Task Details
DS1	Prepare PEP	Establish the project teams, develop the draft and final version of the PEP and respond to review comments from the PPRP and Eskom
DS2	Kick-Off Meeting/ Workshop 1	Develop a meeting programme, conduct SSHAC training, and prepare slides for technical discussions, respond to PPRP comments.
DS3	Seismic Source and Ground Motion Model Database	Organise a database to capture all information evaluated by the TI Teams in the construction of the SSM and GMM.
DS4	Workshop 2	Develop a meeting programme and agenda, invite Proponent Experts, develop sets of questions for the Proponent Experts, prepare slides for technical discussions, respond to PPRP comments.
DS5	Earthquake Catalogue	Construct a uniform and up-to-date catalogue of historical and instrumental seismic events in the region of interest (ROI) that is used for seismic source characterisation at the Duynefontyn site. This catalogue is an updated version of the one developed for the Baseline PSHA study.
DS6	Preliminary Seismic Source Model (SSM), Ground Motion Model (GMM) and Hazard Input Document (HID)	Construct the preliminary SSM and GMM. This marks the start of the integration phase of activities and consists of constructing logic-trees to represent the centre, body, and range (CBR) of technically defensible interpretations (TDI) for all key elements of the SSM and GMM, defining future earthquake occurrence in the region and ground-motion predictions at the site resulting from each earthquake scenario. The HID defined all the inputs required to perform the PSHA calculations. The purpose of the HID is to provide the Hazard Analysis Team (HAT) with all information required to conduct the hazard calculations.
DS7	Preliminary and Final Hazard Calculations	The full set of preliminary hazard results are computed by the HAT, including a set of sensitivity analyses, as recommended by the SSM and GMM TI Teams. After completion of the final HAT a full set of hazard results are computed by the HAT, as recommended by the SSM and GMM TI Teams.
DS8	Workshop 3	The TI Teams present the preliminary SSM and GMM to the PPRP, justifying the technical basis for all decisions underlying the models and explaining how they capture the CBR of TDI. In WS3, the role of the PPRP is expanded to include questioning and challenging the TI Team members directly regarding the models and their bases. In addition, the TI Teams receive and discuss model sensitivity results based on the preliminary hazard results.
DS9	Final SSM, GMM, and HID	The Preliminary SSM and GMM are revised to capture adjustments needed to resolve PPRP review comments, any changes to the SSM and GMM based on the sensitivity analyses, and any new information acquired after the development of the preliminary HID. The final HID defines all the inputs required to perform the PSHA calculations. The purpose of the HID is to provide the HAT with all the information required to conduct the hazard calculations.
DS10	PPRP Briefing	The briefing provided an opportunity for the PPRP to question (and provide comment to) the TI Teams on relevant elements of SSM and GMM, before the finalisation of the Draft Duynefontyn PSHA Report
DS11	Final Duynefontyn PSHA Report and Site Safety Report (SSR) Chapters	Write the final project report, obtain PPRP review comments and develop the inputs to the SSR Chapters.
DS12	PPRP Closure Letter	The PPRP writes a letter documenting the PPRP's final review and its endorsement or rejection of the final PSHA.

The availability of a comprehensive database of existing information relating to earthquake processes and ground motions in South Africa in general, and at the Duynefontyn site specifically, enabled the TI Teams to consider such data in their evaluations and, if they were found to be applicable, to use this data in their assessments. It also ensured that due consideration was given to the range of interpretations of the available data by the broader technical community. This broad evaluation of data, models, and methods ensured that the CBR of TDI was captured by the TI Teams in the SSM and GMM. Evaluating the limitations of the data and the different interpretations and hypotheses that have been put forward contributed to the TI Teams' assessment of epistemic uncertainty in the various elements of the SSM and GMM. Epistemic uncertainty reflects incomplete knowledge of the factors influencing earthquake occurrence and ground-motion generation in a region and may be reduced with additional data. Therefore, in order to reduce the epistemic uncertainty in the SSM and GMM, and by extension the final hazard estimates, the project included activities to gather additional data.

These data collection activities focussed on those elements of the SSM and GMM that have the greatest impact on the final hazard estimates, including those with large epistemic uncertainty. Most of these elements were part of an established research programme conducted by the CGS. This research is described in the Duynefontyn Data Collection (DDC) PEP (Neveling and Chirenje, 2023), which is part of the Integrated Management System (IMS) for the Nuclear Geo-Hazards Group (NGG) within the CGS. Examples of new data collection activities, most of which are presented in detail in Chapters 4, 5, 6, and 7 of this report, include the following:

- Shear-wave velocity measurements at the Duynefontyn site and surrounding area to support accurate modelling of the dynamic response of the near-surface materials (Chapter 4).
- Geological investigation of marine terraces to constrain regional uplift rates and local deformation (Chapter 5).
- Onshore and offshore geological investigation to characterise regional faults (Chapter 5).
- Investigation of geological stress data to provide an indication of the type of seismogenic faulting mechanism that may be expected to dominate in the study region (Chapter 5).
- Investigation of instrumental earthquake recordings of the Cape Syntaxis region from the South Africa National Seismograph Network and older networks (Chapter 6).
- Historical accounts of pre-instrumental earthquake effects in South Africa from newspaper reports and archival sources in South Africa and Europe used to extend the earthquake record back in time (Chapter 6).
- Installation of vertical seismic arrays at the Duynefontyn site to constrain uncertainty on high-frequency attenuation at the site (Chapter 7).

The data collection activities involved CGS staff members (some of whom were also members of the TI Teams) and external specialist contractors engaged specifically for these tasks. The work also included the services of others not listed, such as geochronology analyses conducted at the Community Cosmogenic Laboratory (University of Vermont), and the OSL

Laboratory at the Centro Nacional de Investigación sobre la Evolución Humana (CENIEH) in Burgos, Spain.

In addition to the above studies, several Specialty Contractors were identified by the TI Teams to assist in their evaluations and appointed by CGS to undertake additional investigations. These investigations included:

- Estimation of kappa values in the coastal plain between Cape Town and Saldanha Bay by the University of Cape Town (Chapter 7).
- Assessment of earthquake recurrence parameters for the Duynefontyn area by The University of Pretoria Natural Hazard Centre (Chapter 8).
- Inversion of ground-motion data to determine target source and path parameters for the development of the Ground Motion Model for Duynefontyn by Intraseis Ltd. (Chapter 9).
- 2D site response analysis to determine the influence of steeply inclined interbedded rock layers at the Duynefontyn site by Bradley Seismics Ltd. (Chapter 9).

3.3 IDENTIFICATION OF HAZARD-SIGNIFICANT ISSUES

A key task at the outset of the PSHA was to identify those elements of the SSM and GMM with the largest influence on the hazard results. This enabled the TI Teams to focus their work on the input elements of the SSM or GMM that had the greatest impact on the hazard results. It also allowed data collection studies to focus on activities with the greatest likelihood of reducing uncertainty in the SSM and GMM.

One of the objectives of Workshop 1 in an SSHAC Enhanced Level 2 (SSHAC EL-2) study (USNRC, 2018) is to present the SSM and GMM TI Teams with issues that are of the greatest significance to the PSHA. The Duynefontyn PSHA benefited from the fact that it was preceded by a Baseline PSHA that included a sensitivity analysis highlighting the greatest contributors to epistemic uncertainty.

3.4 WORKSHOP 1: KEY ISSUES AND AVAILABLE DATA

Workshop 1 was combined with a Kick-Off meeting for the Duynefontyn PSHA and was held at the Blaauwberg Beach Hotel in Bloubergstrand, Cape Town, South Africa, from 23–25 February 2022. The first two days were devoted to meetings held at the venue, while the TI Teams and the PPRP undertook a site visit to the Duynefontyn site on the third day. The workshop assembled the PTI, TI Leads and Teams, PPRP, Resource Experts, Database Developers, Project Management Team, and observers. International Covid-related travel restrictions were still in force at the time of the workshop, which meant that not all members of the TI Teams were able to travel to Cape Town, so the workshop was conducted as a hybrid (i.e. combined in-person and virtual) meeting.

At the time of the workshop, the TI Teams were already familiar with a significant amount of data through their participation in the Baseline PSHA, which was completed by early 2022. The database established for the Baseline PSHA formed the foundation of the database for the Duynefontyn PSHA. The sensitivity analysis contained in the Baseline report (Stamatakos et al., 2022) clearly identified the most significant hazard issues on which the TI Teams and project needed to focus. Given these circumstances, the following objectives were established for Workshop 1:

- To provide an overview of the Duynefontyn PSHA to participants, including the structure and tasks of the seismic source and ground motion sub-projects, so that each active participant understands their own role and contribution to the project and its objectives.
- To review and introduce the SSHAC EL-2 methodology that would be employed to execute the Duynefontyn PSHA, including a description of the various roles required in the project.
- To review all previous seismic hazard analysis studies performed for the Duynefontyn site, including the Baseline PSHA, in order to discuss hazard sensitivities. The purpose was to identify the elements of the SSM and GMM exerting the greatest influence on the hazard estimates for the site and to focus attention and efforts on these components of the hazard input model.
- To review available data for constructing the SSM and GMM, including the data gathered and compiled during the initial phase of the project, and to identify additional data requirements to constrain these models, including the identification of how, when and by whom such data would be collected.
- To identify all interface issues within and between the seismic source and ground motion models.

The first day of the workshop was devoted to a PSHA overview, an introduction to the SSHAC methodology, and a review of previous seismic hazard analyses, including the Baseline PSHA. The second day of the workshop focussed on available data. Resource Experts were asked to provide summaries of various types of existing data that are available and may be useful to the development of the SSM and GMM. Members of the project team (including database developers and members of the TI Teams) were asked to provide overviews of the ongoing data collection activities and the associated issues they encountered. Ample time was included in the workshop schedule to allow for discussions of the relevant issues among the TI Team members and the database developers. All presentations were retained by the project management team and captured in the project database and incorporated into the QADP.

At the end of each day of the workshop, the TI Leads and the Project Manager met for an informal debriefing with the PPRP. These meetings allowed issues and concerns to be raised so that they could be clarified within the meeting or addressed in the following days of the workshop. Following the completion of Workshop 1, the PPRP remained at the hotel for another full day to draft its consensus report. This was transferred to the TI Leads via the Project Manager. The TI Leads composed a written response to every point raised in the PPRP's report.

Based on suggestions made by the PPRP, the Project Manager, PTI and TI Leads decided to strengthen the TI Teams with additional personnel, including Prof. P. Stafford, Dr V. Montaldo-Falero, and Dr K. Ulmer. Dr V. Midzi was moved from the SSM to the GMM to offer better support to the GMM regarding the earthquake record in South Africa. Summaries of key decisions were recorded in the open sessions, and these defined the plan of action for each TI Team going forward. The full proceedings from the workshop, including the agenda, all presentations, the summary report, the PPRP report, and the TI Leads' responses, are included in the project QADP.

3.5 WORKSHOP 2: ALTERNATIVE MODELS AND METHODS

Workshop 2 of the Duynefontyn PSHA was held at the Protea Hotel outside Stellenbosch, South Africa, from 20–24 June 2022. This workshop focussed on the merit of alternative models and methods as they pertain to key technical issues and the seismic hazard at the Duynefontyn site. The workshop was attended by the PTI, TI Leads and Teams, TI Team support staff, Proponent Experts, PPRP, HAT, Speciality Contractors, Database Developers, the Project Management Team, and observers. A list of the Proponent Experts invited to Workshop 2 and of their presentation topics is provided in Table 2-3. Most delegates attended in person, but the meeting was conducted as a hybrid meeting to enable several Proponent Experts and TI Team members not able to travel to Stellenbosch to participate remotely.

The primary objective of the workshop was to enable members of the broader technical community, acting as Proponent Experts, to present on topics relevant to the development of the SSM and GMM. These presentations allowed the TI Teams to obtain greater insight into these models. Specifically, the workshop allowed the Proponent Experts and TI Teams to:

- Present, discuss, and debate alternative models and methods pertaining to key technical issues.
- Identify and debate the technical bases for the alternatives and to discuss the associated potential hazard significance and uncertainties.
- Develop a basis for the subsequent development of the preliminary hazard models that consider these alternative models and methods.

The first two days of the workshop were devoted to SSM issues and the last two days to GMM issues, with the middle day being devoted to overlapping issues common to both TI Teams. The Proponent Experts were given an opportunity to present their models, and technical support for these, to the TI Teams. Ample time was allowed in the agenda for the members of the TI Teams to question the Proponent Experts on their presentations and models. Other Proponent Experts were also given an opportunity to pose questions to one another since such interactions were likely to provide additional insights that could prove useful to the TI Teams in their evaluations. This helped the TI Teams to assess the strengths and weaknesses of the proposed models and any assumptions implicit in their derivation. The aim was not primarily to assess the innate merits of each model, but rather to determine the degree to which they are applicable to the Duynefontyn PSHA. At the end of each day of the workshop, the TI Leads, the Project Manager and the PPRP met for a closed debriefing meeting, as had been done at Workshop 1. Similarly, the PPRP remained at the hotel for an additional day after the workshop to draft its consensus report. This was transferred to the TI Leads by the Project Manager, and the TI Leads responded in writing to every point raised in that report.

As at Workshop 1, at the end of the SSM and GMM sessions, summaries of key decisions were recorded in the open sessions, and these defined the plan of action for each TI Team going forward. The full proceedings from Workshop 2, including the agenda, all presentations, the summary report, the PPRP report, and the TI Leads' responses, were incorporated into the project QADP.

3.6 WORKING MEETINGS

The formal workshops provided an opportunity for the TI Teams to interact with external experts, the PPRP, and the Project Sponsor. The bulk of the work to develop the SSM and GMM took place outside the workshops and required interactions among the members of the TI Teams. This included emails, telephone calls, and regular virtual meetings using video conferencing technology. Formal working meetings, as outlined in NUREG-2213 (USNRC, 2018), were held in which all TI Team members participated. These working meetings served as opportunities for individual team members to present work and for the TI Teams to discuss data, models, methods, and the technical decisions that needed to be made to develop the SSM and GMM. The members of the TI Teams were distributed over three continents and multiple time zones; thus, these meetings were viewed as an indispensable element in ensuring that the work was fully integrated. Compared to the workshops, the setting for the working meetings was less rigid, and included prepared presentations as well as informal discussions, thereby providing a more conducive opportunity for the free-flowing discussions that characterise the process of technical challenge and defence. This process of challenge and defence is vital to building consensus within the TI Teams because the TI Teams are expected to assume full intellectual ownership of the final SSM and GMM.

Each TI Team held four working meetings (see Table 3-2), with the first three meetings being held jointly at the same venue, breaking out into different rooms as required. The first Working Meeting was scheduled between Workshops 1 and Workshop 2, while Working Meetings 2 and 3 were held prior to Workshop 3. The main purpose of the first Working Meeting was to plan for Workshop 2, whereas the second and third Working Meetings marked the transition from the evaluation phase to the integration phase (Figure 2-3), with the latter primarily focussed on the development of the preliminary SSM and GMM (Section 3.7). The SSM and GMM TI Teams conducted separate fourth Working Meetings after Workshop 3. The GMM TI Team held their fourth working meeting as a virtual meeting due to the limited schedule availability of the TI Team members. Their objective was to modify the preliminary GMM considering the feedback from Workshop 3, and to develop the final GMM. This was attended by the PPRP. In contrast, the SSM TI Team completed the final integration activities of the SSM after Workshop 3 via weekly videoconferences, which the PPRP attended. The final working meeting of the SSM TI Team was therefore primarily treated as an in-person writing session.

To provide the PPRP an opportunity to observe the evaluation and integration processes, they were invited to send a representative to each of the working meetings as observers. Since the PPRP report to the Project Manager (see Figure 2-4), the Project Manager or the Assistant Project Manager attended all working meetings. One or more representatives from Eskom also attended Working Meetings 2–3 as observers. For Working Meetings 1, 2 and 3, other project participants (database developers, specialty contractors) were also present, or linked in by videoconference during short sessions to clarify previously provided information or to provide additional information to the TI Teams.

Table 3-2. List of Working Meetings (WM) for the Duynefontyn PSHA with dates, venues, and PPRP representatives.

Working Meeting (WM)	Date	Venue	PPRP representatives
WM 1	2–4 May 2022	Walnut Creek, California, USA	J. Bommer J. Ake R. Durrheim T. Rockwell J. Stewart
WM 2	10–13 Oct. 2022	Protea Hotel Fire and Ice, Pretoria, RSA	J. Bommer R. Durrheim M. Goedhart
WM 3	23–27 Jan. 2023	SwRI offices, San Antonio, Texas, USA	J. Bommer J. Ake T. Rockwell
WM 4 (GMM)	10–14 Jul. 2023	Virtual	J. Bommer J. Ake J. Stewart
WM 4 (SSM)	28 Aug–1 Sep. 2023	South Lake Tahoe, California, USA	N/A

3.7 PRELIMINARY SSM AND GMM DEVELOPMENT

Following Workshop 2, the project transitioned from the evaluation phase to the integration phase of the PSHA. The TI Teams developed the SSM and GMM during the integration process based on the data, models, and methods that were considered during evaluation. The TI Teams implemented the two rounds of model building as described in NUREG-2213 for Enhanced Level 2 to Level 4 SSHAC studies (USNRC, 2018). The first round is represented by the development of the preliminary SSM and GMM, with hazard calculations and sensitivity analyses presented at Workshop 3. That was followed by the development of the final SSM and GMM, and the final hazard calculations documented in this report.

The preliminary SSM and GMM models typically represent the first attempt by the TI Teams to capture the CBR of TDI, although for the Duynefontyn PSHA this was preceded and informed by the models developed for the Baseline PSHA. The preliminary models provided the basis for further hazard sensitivity analyses and therefore had to be complete, both in terms of representing the elements that were most supported by the data, and in their expressions of uncertainty. As a result, the effort devoted to the development of the preliminary models was significant. This was the focus of Working Meetings 2 and 3.

The Duynefontyn PSHA made extensive use of informal White Papers to guide and document the progress of the TI Teams' work and to keep the PPRP informed of their progress and plans. The first set of White Papers (one each for the SSM and GMM), a mechanism first proposed by the PPRP, was finalised between Working Meeting 2 and Working Meeting 3, a period that marked the transition from the evaluation phase to the integration phase. These documents described the TI Teams' evaluation of existing data, models, and methods, and the approaches and methods the TI Teams were planning to adopt for integration. For each topical area, the White Paper summarised the current information, described the TI Team's evaluation of that information, and discussed the technical challenges that the TI Teams needed to overcome to begin integration. This first set of White Papers were submitted to the PPRP who provided informal feedback on the TI Teams' proposed approaches to integration. This version of the White Papers established a structure for the TI Teams to start integrating the data, models, and methods into the initial framework of the logic trees that constitute the preliminary SSM and GMM. This approach assisted the TI Teams in capturing the CBR of the TDI, because it required them to organise and document all the information gleaned from the evaluation phase of the project. The White Papers also focussed the TI Teams on establishing the technical basis for the logic-tree nodes and assigning weights to the logic-tree branches.

3.7.1 Preliminary SSM and GMM

Shortly after Workshop 2, the SSM TI Team began the process of constructing the preliminary SSM, taking into consideration all available data, models, and methods. At the same time, work on the project earthquake catalogue continued, and the results of ongoing work of the DDC activities were provided to the SSM TI Team to assist in the model-building exercise. During the course of Working Meetings 2 and 3, the SSM TI Team defined the criteria that would be used to identify the seismic source zones and considered a range of alternative source boundaries. Decisions were made regarding the approaches that the SSM TI Team used to assess maximum magnitude, magnitude scaling, and earthquake recurrence, given the tectonic environment and available earthquake data. In addition, criteria for assessing the seismogenic potential of fault sources were established. Decisions were also made on

methods to determine seismogenic thickness and to test the assumption of earthquake stationarity based on the earthquake record and heat flow data.

The preliminary SSM included seven seismic source zones and the Groenhof Fault Corridor, which was modelled to be similar to a Repeated Large Magnitude Earthquake (RLME) source in the Central and Eastern United States (CEUS) PSHA (EPRI/DOE/USNRC, 2012). Of the seven source zones, future earthquakes in the three nearest the site were modelled as virtual ruptures. Because most modern GMPEs rely on source-to-site distance metrics that are defined relative to extended fault ruptures rather than to the epicentre or hypocentre, virtual fault ruptures are needed within the source zones closest to the site in order to correct calculation of distance of each earthquake scenario from the site. For more distant source zones, the difference between the source-to-site distance from point sources or virtual ruptures is too small to impact the hazard results. Thus, in the remaining four source zones, future earthquakes were modelled as point sources. Despite the model being “preliminary” in the sense that it would be updated later, it included all the elements needed for the hazard analysis, including the parameter distributions and the weights associated with the logic-tree branches.

With the completion of the preliminary SSM, the SSM TI Team developed a Hazard Input Document (HID) for the model. The SSM TI Team also identified the hazard sensitivity analyses for Workshop 3 that were needed to give them additional insights into the relative importance of various elements of their preliminary model.

The development of the GMM for this project faced the challenge of working in a region with little relevant ground-motion data and no locally derived Ground-Motion Prediction Equations (GMPEs) for response spectral ordinates. The evaluation phase of the GMM was therefore focussed on selecting the approach to developing the ground-motion model, one that would be conducive to providing an appropriate solution within the timescale of the project. At Working Meeting 1 the GMM TI Team established a basic framework that included the development of a GMM logic tree for host-to-target adjustments to an existing GMPE. This framework also supported the subsequent integration of the adjusted GMPE with calculated site amplification factors to model the difference in the dynamic response between the profile for the original GMPE (host) and the site (target).

At Working Meetings 2 and 3, the GMM TI Team developed the preliminary model within this general framework. The GMM TI Team also accounted for information provided by the Proponent Expert presentations at Workshop 2. The key elements of the model-building process at these working meetings were the integration of inversions performed to develop target parameters for the host-to-target adjustments and the development of site-specific profiles to use in the site amplification calculations. The target seismic properties fill the logic-tree branches to define the “rock” ground motion. A methodology for developing a site response model was developed with the available shear-wave velocity (V_s) profiles that had been measured at the site as inputs. Additional V_s profiles were developed as part of the project and were constructed in parallel with the model-building process (see Section 4.6).

In addition to the logic-tree branches for the prediction of median spectral ordinates, branches for the sigma model were developed, taking account of the uncertainty in site response factors. The preliminary GMM HID was then drafted by the TI Lead and reviewed by all members of

the TI Team, before being handed over to the Hazard Analysis Team (HAT) for implementation.

3.7.2 Preliminary hazard calculations

Based on the preliminary SSM and GMM HID, the HAT developed a set of preliminary hazard results. These results were normalised by scaling the spectral acceleration such that the hazard for PGA (100 Hz) was set to 0.1g at the 10^{-4} annual frequency of exceedance (AFE). They were normalised because the TI Teams wanted to focus on hazard sensitivities as opposed to absolute hazard results. Normalisation of the hazard results at this juncture of the project was also important to avoid potential cognitive bias, in which TI Team member's judgements regarding updates to the preliminary model could be influenced by or anchored to the preliminary results.

A critical application of the preliminary SSM and GMM was to explore the relative hazard significance of various elements of the models and the relative contributions of the uncertainties in the elements to the total uncertainty in hazard. The preliminary models included the full range of assessments necessary to explore these hazard sensitivities. The results of the specified hazard sensitivity analyses were presented by the Lead Hazard Analyst at Workshop 3.

3.8 WORKSHOP 3: PRELIMINARY SSM AND GMM, HAZARD FEEDBACK, PPRP COMMENTS

Workshop 3 was initially scheduled to take place in Cape Town from 20–24 March 2023, but had to be postponed due to internal bureaucratic delays at the CGS (non-technical in nature). The Workshop was eventually held from 19–22 June 2023 at the Devon Valley Hotel located outside Stellenbosch, South Africa. This delay also necessitated changes to the post-workshop schedule, including the dates for Working Meeting 4, PPRP Briefing, and the submission of draft and final PSHA reports.

The main purpose of Workshop 3 was to present the preliminary SSM and GMM to the PPRP, and to elicit their comments, challenges, and feedback. Participants included the PTI, the TI Teams, the HAT and the PPRP. Other attendees included the project management team and observers from the CGS, Eskom and the National Nuclear Regulator (NNR). The first two days of the workshop were devoted to the SSM. Topics relevant to both the SSM and GMM TI Teams were discussed on the morning of the third day, before transitioning to GMM issues for the remainder of the workshop.

The second purpose of Workshop 3 was to present preliminary hazard results and hazard sensitivity analyses to the SSM and GMM TI Teams. These hazard results and sensitivity analyses were needed to shed light on the most hazard significant issues and important technical findings. The feedback gained at this workshop ensured that no significant issues had been overlooked. This allowed the TI Teams to understand the hazard implications of their models, including the contributions from the associated epistemic uncertainties and aleatory variabilities. It also allowed the TI Teams to understand the hazard significance of their assessment of weights to their logic tree branches. This information provided a basis for focussing subsequent project efforts on the most hazard significant issues as the TI Teams finalise the SSM and GMM.

The discussions at the workshop provided the TI Teams with additional insight into the range of information and level of detail that the PPRP expects in the final PSHA report. To this end, the PPRP Chair reminded all participants that documentation was one of the five essential elements of a successful SSHAC project, which includes a complete and comprehensive report with sufficient detail to allow the PSHA to be understood and replicated. He stressed that the final report must identify all the data, models, and methods considered in the evaluation, and justify, in detail, the technical interpretations that support the hazard input models.

At the end of the workshop, the PPRP remained at the hotel for an additional day to draft its consensus report. Their findings were also discussed in a closed debriefing with the PTI, the TI Leads, and the Project Manager. The PPRP submitted its consensus report and formal workshop comments to the Project Manager the following day. The PTI and TI Leads, supported by the TI Teams, responded in writing to each comment in the PPRP report. This written response was submitted to the PPRP along with the second set of White Papers on 7 September 2023. The proceedings from Workshop 3, including the agenda, all presentations, the summary report, the PPRP report, and the TI Leads' responses were incorporated into the QADP.

3.9 FINALISATION OF SSM AND GMM

The interactions at Workshop 3, feedback received from the PPRP during the workshop sessions, and the PPRP's consensus report provided extremely valuable feedback to the TI Teams for the finalisation of the SSM and GMM. The SSM TI Team addressed the questions raised by the PPRP in a series of weekly videoconferences before finalising their model. The GMM TI Team held a virtual Working Meeting 4 to facilitate the finalisation of their model.

At GMM Working Meeting 4, the GMM TI Team integrated the final host-to-target adjustments and V_S profiles based on the recently completed ground-motion inversions and site investigations. The TI Team decided to develop a single backbone GMPE with scale factors to represent the host-to-target adjusted GMPEs. The total epistemic uncertainty within the model was compared with other similar projects to ensure that the results were appropriate. Final logic-tree branch weights were developed by the GMM TI Team following these discussions.

The SSM Working Meeting 4 was held in South Lake Tahoe from 28 August to 1 September 2023. At this working meeting, the SSM TI Team collectively wrote significant portions of the text for the Draft PSHA report, and based on the process of writing, the SSM TI Team identified and made minor but necessary adjustments to the SSM. This writing process also enabled the SSM TI Team to ensure that consensus was reached by all team members on all key technical decisions.

The Duynefontyn PSHA project used an innovative two-step process to inform the PPRP about the final SSM and GMM. After their respective fourth Working Meetings, the TI Teams documented the final models in a second set of White Papers. These version 2.0 White Papers summarized available data, models, and methods and described how the TI Teams systematically evaluated and integrated this information to construct the SSM and GMM. They documented the logic tree inputs and the technical bases for all logic tree weights. They were written in sufficient detail to ensure that the supporting text and figures resulted in a coherent, transparent, and comprehensive final PSHA report; one that will meet the documentation requirements of a successful SSHAC project. The White Papers were submitted to the PPRP on 7 September 2023 for review.

A PPRP Briefing Meeting was scheduled for 21–22 September 2023 and attended by the PPRP, PTI, TI Leads, TI Team, and members of the project management team. This meeting differed from the standard format for PPRP briefings, which were designed (USNRC, 2018) to inform the PPRP of the content of the final SSM and GMM prior to receiving the draft PSHA report; the overall objective being to expedite the review process. In a traditional PPRP Briefing Meeting the TI Leads (sometimes supported by TI Team members) present all elements of the final SSM and GMM, as well as the associated technical justifications, to the PPRP. The PPRP is then given the opportunity to question the bases for the branches and weights in the logic trees, as well as the technical assessments that led to the final TI Team decisions.

Given the interactive nature of a PPRP Briefing Meeting, it is best conducted as an in-person meeting. However, the version 2.0 White Papers submitted to the PPRP in early September largely replaced the PPRP Briefing Meeting as primary mechanism to inform the PPRP of the final SSM and GMM (it also afforded the PPRP more time for contemplation). This made it

possible to execute the PPRP Briefing Meeting as a virtual meeting. Since the PPRP preferred that the available time be utilised to discuss the information on the SSM and GMM contained in the White Papers, it was also decided to forego any presentations by the TI Leads. Instead, the PPRP Briefing Meeting was structured as debriefing sessions during which the PPRP asked clarifying questions or provided comment on the final SSM and GMM as presented in the White Papers; and to convey any concerns to the TI Teams before the final report was drafted. It also afforded the TI Team the opportunity to seek clarity from the PPRP on any of their comments.

These additional interactions between the PPRP and TI Teams after Workshop 3 enabled the PPRP to review and understand the final SSM and GMM, including all the changes that were made following Workshop 3, the reasons for those changes, and the TI Teams' response to the PPRP's written comments. The PPRP briefing provided the PPRP members with an opportunity to convey their questions and concerns to the TI Teams before the final report was drafted. This reduced the risk of serious technical questions being raised at this late stage of the review of the draft version of this report, after the models had been finalised and the final hazard calculations run, which could cause severe delays to the project.

This was the first SSHAC project to take this approach. Documenting the progress of the TI Teams' efforts through the White Papers, which were reviewed by the PPRP prior to the PPRP briefing where the latter provided feedback, yielded valuable feedback to the TI Team to aid in the development of a complete, comprehensive, and technically sound report. As stated by the PPRP Chair in his 25 September 2023 email to the Project Team, PTI, TI leads, and TI Teams,

> '*I suspect that this project may have established a new paradigm for good practice because the White Papers have communicated to us very effectively the essential features of the final SSM and GMM, and the technical bases for these models, and I believe we have been able to provide much more constructive feedback – that is directly related to the documentation rather than just giving general indications of items to which particular attention should be given in the final report."*

3.10 HAZARD INPUT DOCUMENT

The HID provides the essential elements of the SSM and GMM that the HAT needs to calculate the seismic hazard. The HID is owned by the TI Teams and provides instructions to the HAT on how to implement the SSM and GMM, including all logic trees, parameter distributions, and derived parameters, along with any additional information required to execute the PSHA calculations (such as the site coordinates and the minimum magnitude). It does not include any discussion or description of the technical bases for the model elements. Two rounds of HID development occurred during the course of the project, one following the development of the preliminary SSM and GMM and one when the models were finalised. The preliminary HID developed after Working Meeting 3 (Section 3.7.2) was reviewed by the members of both TI Teams to ensure that it contained a complete and accurate set of instructions that fully captured the SSM and GMM. This preliminary HID formed the basis for the hazard calculations that were performed to provide sensitivity feedback at Workshop 3.

Following the finalisation of the SSM and GMM after Workshop 3, the TI Teams updated the HID for the final hazard calculations. The TI Leads worked closely with Ms Largent in her role as Lead Hazard Analyst during the development of the final HID. The draft final HID was submitted to the PPRP ahead of the PPRP Briefing for review. Additional minor modifications (mainly clarifications and corrections) were made as the logic trees were implemented and an updated version submitted to the PPRP. These changes are documented in the communication records contained within the QADP.

3.11 SUMMARY OF VERIFICATION AND VALIDATION EXERCISES

The purpose of verification and validation (V&V) is to ensure that the SSM and GMM are correctly implemented, and the seismic hazard is accurately calculated. The quality assurance (QA) process of checking the calculations was a vital part of the PSHA. It ensures that the hazard results, which will be used as inputs to structural and risk analyses for the KNPS license extension and as inputs to the design of safety-related components of the new build power plant, are correct. In this context, validation means ensuring that programs and computer codes are performing the calculations correctly and that the algorithms are valid and have been implemented without errors or inconsistencies. Verification means that the model parameters are correctly entered into the software, and that the results obtained from the calculations accurately reflect the instructions in the HID. Chapter 10 provides information regarding the measures taken to ensure that the hazard calculations were performed without error. These measures also ensured that the requirements of RD-0016 (NNR, 2016) were met. A summary list of all V&V activities is provided in the V&V Report (Largent et al., 2024).

3.12 DRAFT REPORT DEVELOPMENT

The development of the draft PSHA report constituted the main documentation phase of the Duynefontyn PSHA project. The draft report recorded the TI Teams' evaluation and integration of available data, models, and methods, including the technical bases for all critical decisions made by the TI Teams in developing their models. It documented the entire SSHAC EL-2 process, including database development, the conduct of workshops and working meetings, important PPRP interactions, data collection activities, supporting studies, and the integrated management system. It provided the final hazard results and identified the main contributions to hazard and their associated sensitivities and uncertainties. It described how the SSHAC objectives of the project were met, per the guidance in NUREG-2213, and it provided the evidence that the resulting hazard reflected the CBR of TDI that were captured in the SSM and GMM.

This documentation phase started in earnest after Workshop 3 and intensified after Working Meeting 4. The TI Leads drafted a Table of Contents, which was submitted to the PPRP for their comment, to guide the development of the draft report. Additional modifications to the Table of Contents were implemented during the writing process as practical problems were encountered and resolved. The project management team, in conjunction with the PTI, also drafted formatting guidelines to ensure consistency in layout and presentation and circulated these to the TI Teams.

The PTI and Project Manager decided to develop and submit the PSHA report to the PPRP in the form of individual, standalone chapters; each with their own Table of Contents and reference list. The PTI and Project Manager made this decision to improve the efficiency and effectiveness of the TI Teams' writing and the way in which the text was reviewed by PTI, TI Leads, and PPRP. In addition, the chapters were edited by a CGS technical editor and other members of the Project Management team. Once each individual draft chapter was completed and internally reviewed, it was transferred to the PTI, who maintained it as the master copy and assumed final responsibility for submission to the Project Manager. The PTI also made sure that each chapter conformed with CGS formatting guidelines, contained consistent and correct cross-referencing, and was otherwise complete. After the TI Team responded to the PPRP's comments and updated the chapters of the final report, the PTI undertook a review of all chapters to ensure that report is coherent and complete, with consistent and correct cross-referencing.

3.13 DRAFT REPORT PPRP REVIEW

Chapters 1 to 9 of the draft PSHA report was transmitted to the PPRP by the Project Manager between 31 October 2023 and 7 November 2023, with the final chapter submitted on 20 November 2023. In order to provide the TI Leads with a single, unified set of comments and feedback, the members of the PPRP held a meeting in San Diego from 11–14 December 2023 to discuss the draft PSHA report and provided a single set of documents that formed their consensus review.

3.14 FINAL REPORT DEVELOPMENT

After receipt of the PPRP review comments, the TI Teams revised the draft PSHA report, considering all the comments from the PPRP. The TI Teams produced a draft final PSHA report which was submitted, along with written responses to the PPRP comments, to the PPRP for final review and concurrence. The PPRP drafted its closure letter which indicated whether the PSHA conformed to the SSHAC requirements and whether all technical assessments were adequately supported and documented. It is only after the PPRP letter was issued that the final PSHA report was published. The final PSHA report includes an Executive Summary, List of Acronyms, Abbreviations and merged Table of Contents. The PPRP closure letter is included as Appendix B.

3.15 REFERENCES

Electric Power Research Institute/ Department of Energy/United States Nuclear Regulatory Commission (EPRI/DOE/USNRC) (2012). Central and Eastern United States Seismic Source Characterization for Nuclear Facilities. NUREG-2115. US Nuclear Regulatory Commission, Washington DC, USA.

Largent, M.; Williams, T.; Yust, M. and Shaw, K. (2024). Verification and Validation for SSHAC-EL2 PSHA Inputs for the Duynefontyn Site and Koeberg Nuclear Power Station. CGS Report 2023-0196.

National Nuclear Regulator (NNR). (2016). Guidance on the Verification and Validation of Evaluation and Calculation Models Used in Safety and Design Analyses. Regulatory Guide RG-001 (Rev. 0).

Neveling, J. and Chirenje, E. (2023). Project Execution Plan: The Investigation of the Site Geology and Micro-Seismic Monitoring in Support of the Probabilistic Seismic Hazard Analyses for the Duynefontyn Site. NGG-PLN-001 (Rev. 2). Council for Geoscience, Pretoria, South Africa.

Stamatakos, J. and Watson-Lamprey, J. (2023). Project Execution Plan for the Senior Seismic Hazard Analysis Committee Enhanced Level-2 Probabilistic Seismic Hazard Analysis at the Duynefontyn Nuclear Site. NGG-PLN-003 (Rev 1). Council for Geoscience, Pretoria, South Africa.

Stamatakos, J.; Watson-Lamprey, J.; Cawthra, H.; Claassen, D.; Coppersmith, R.; Johnson, C.; Largent, M.; Manzunzu, B.; Midzi, V.; Mulabisana, T.; Murphy, D.; Rathje, E. and Wooddell, K. (2022). Baseline PSHA for the Duynefontyn Site and the Koeberg Nuclear Power Station. CGS Report 2022-0009 (Rev. 0). Council for Geoscience, Pretoria, South Africa.

United States Nuclear Regulatory Commission (USNRC) (2018). Updated Implementation Guidelines for SSHAC Hazard Studies. NUREG-2213. U.S. Nuclear Regulatory Commission, Office of Nuclear Regulatory Research, Washington DC, USA.

CHAPTER 4: GEOLOGIC SETTING

4. GEOLOGIC SETTING

This chapter provides the detailed assessment of the geologic setting of the KNPS and Duynefontyn sites (hosting the KNPS and a new build site) and surrounding region. It begins with a review of the tectonic history of Africa and the Western Cape, which is summarized in Section 4.1. The regional geologic and seismotectonic setting is described in Section 4.2, including the alternative tectonic interpretations for the Western Cape and their implications for the SSM TI Team's evaluation and integration of seismic source data, models, and methods that is described in Chapter 8. Information about available geodetic measurements and crustal stress for the Western Cape are also discussed in Section 4.2. Section 4.3 summarises the historical seismicity analysis from Albini and Flint (2023) and provides the SSM TI Team's evaluation and assessment of their analysis. This evaluation and assessment informs the SSM TI Team's project earthquake catalogue that is described in Chapter 6. The geology of bedrock and surficial deposits at the KNPS and new build sites is described in Section 4.4. The details of the geotechnical and geophysical tests that were performed to develop the shear-wave velocity (V_S) profiles of the Duynefontyn site are described in Section 4.5. Information from sections 4.4 and 4.5 support the GMM TI Team's site response modeling that is described in Section 9.4.

4.1 TECTONIC HISTORY OF THE WESTERN CAPE

The tectonic history recorded in the geology of Africa spans nearly 4 billion years of Earth history (e.g., Tankard et al., 1982). The African continent comprises several Precambrian cratons that formed between about 3.6 and 2 billion years ago. The cratons are bounded by younger mobile belts that formed between 2 billion and 300 million years ago. These mobile belts are narrow zones of sedimentary and volcanic strata that were deposited between the cratons. They were subsequently deformed during the convergent plate tectonic processes that stitched the cratons together to make the African plate (Figure 4-1). The active tectonism recorded in the mobile belts range from Archean-age orogenesis (2 billion years ago) to Proterozoic orogenesis such as the Kibaran Orogeny (1.2 billion to 950 million years ago) which occurred in eastern and southern Africa (e.g., Tack et al., 2010, Thomas et al. 1994). All these orogenic events reflect an active period of tectonism in the Proterozic and earliest Palaeozoic involving the assembly and breakup of several supercontinents (including Rodinia and Pannotia) that culminated with the formation of Gondwana (e.g., Hartnady et al., 1985; Meert and Van der Voo, 1997; Meert and Lieberman, 2008; Gaucher et al., 2009). Gondwana later collided with Laurasia in the Carboniferous (359 to 299 Ma) to form a single supercontinent called Pangea.

Collectively, the series of major Neoproterozoic orogenic events which related to the formation of the supercontinents Gondwana is referred to as the Pan-African orogeny (e.g., van Hinsbergen et al., 2011). This orogeny is also known as the Pan-Gondwanan or Saldanian Orogeny (Rozendaal et al., 1999). The Saldania belt (Figure 4-1) is an arcuate fold belt along the southern tip of Africa that is part of the larger system of Pan-African orogenic belts (e.g., Hartnady et al., 1985; Gaucher et al., 2009). Poor exposures and uniformly low grades of metamorphism make correlating the Saldania belt with similar Pan-African belts to the north difficult, and there are several contrasting views about the tectonostratigraphic make-up and overall geodynamic setting of the Saldanian belt (Hartnady et al., 1974; Von Veh 1983; Rozendaal et al., 1999; Belcher and Kisters 2003; Gresse et al. 2006; Frimmel, 2009; Frimmel

et al., 2011, 2013; Buggisch et al., 2010; Rowe et al., 2010). Nearest the Duynefontyn site, the Saldania belt comprises a low-grade metamorphic and folded supracrustal strata collectively referred to as the Malmesbury Group. Areally extensive syn-, late- and post-tectonic granites of the 550–510 Ma Cape Granite Suite intrude the Malmesbury Group. Structural relationships indicate that the granites were emplaced during late-stage deformation, although some may be post-tectonic (e.g., Scheepers 1995; Scheepers et al., Schoch 2006). Synmagmatic deformation of the granite is evident in the Darling batholith that has intruded the central Colenso fault zone over a strike length of more than 40 km (Kisters and Belcher, 2018).

The last major compressional event to impact the Western Cape was the Permo-Triassic (~245 and ~278 Ma) Cape Orogeny (Söhnge and Hälbich, 1983; De Beer, 1990; Hansma et al., 2015). The Cape Orogeny formed the Cape Fold Belt by deforming the Early Palaeozoic Cape Supergroup strata (e.g., Thamm and Johnson, 2006). The orogeny is responsible for the dominant structural characteristics seen along the southern coast of Africa today (Hälbich, 1983). Karoo Supergroup sedimentation within the Karoo basin located north of the Cape Fold Belt, farther inland, continued from ~350 to ~180 Ma (Tankard et al., 2012).

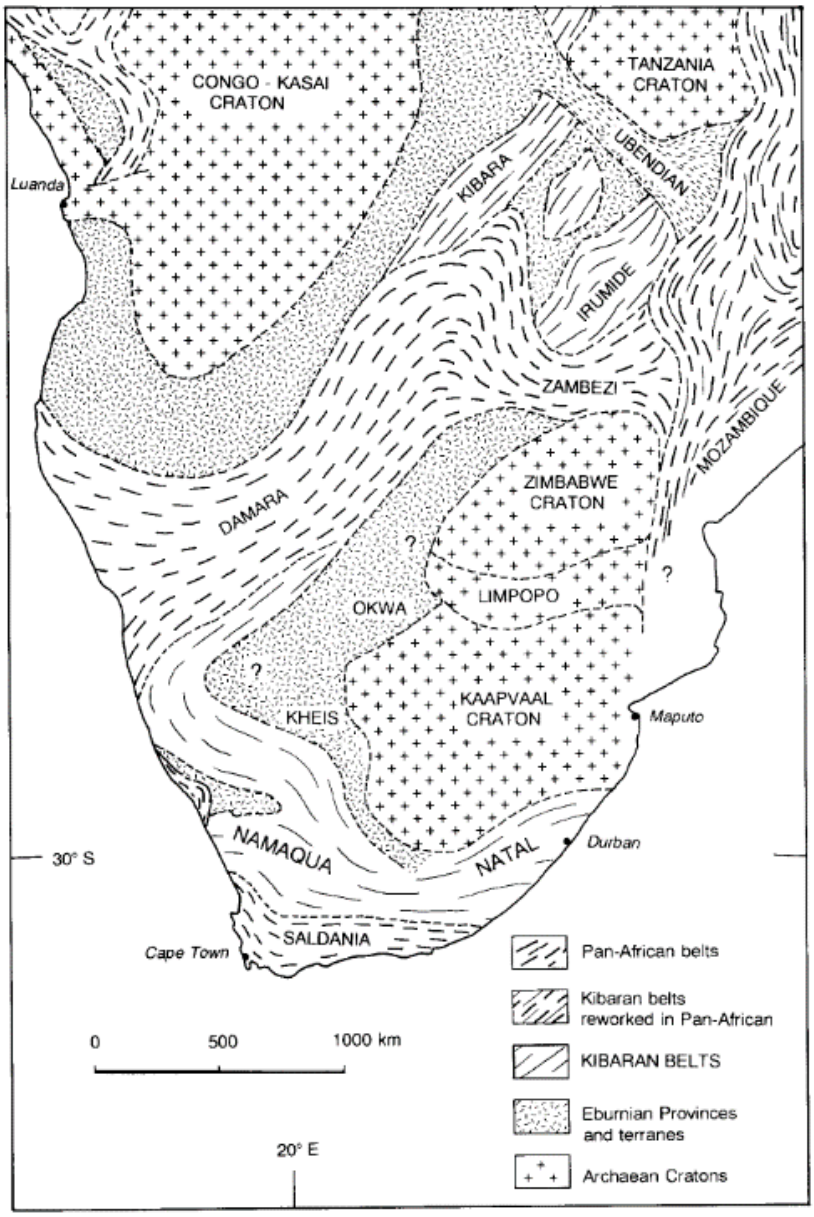

Figure 4-1. Sketch map of the tectonic framework of central and southern Africa, showing the distribution of Archaean cratons and Proterozoic mobile belt, copied from Figure 1 of Thomas et al, (1994).

Contraction was followed by extension in what can be described as the third major tectonic event in the region. In the Early Jurassic (~180 Ma), Gondwana began to breakup though a series of rifting events (Conrad and Gurnis, 2003; Watkeys, 2006; Broad et al., 2006). Rifting reactivated the Cape Fold Belt contractional fault system as extensional and transtensional faults, which was associated with the right-lateral rifting of the Agulhas-Falkland Fracture Zone, located offshore along the southeastern margin of South Africa (Broad et al., 2012). Unfortunately, the absence of Table Mountain Group strata across most of the site vicinity greatly hinders discernment of possible Mesozoic reactivation along the older basement faults in the Western Cape (De Beer et al., 2008). During Late Jurassic to Early Cretaceous extension, rifting initiated a series of grabens and half-grabens along the southern margin of Africa, including the Orange Basin (McMillan et al., 1997; Broad et al., 2006, 2012; Paton et al., 2006).

The last major events that shaped the region's geology were the Late Neogene to Recent sea-level fluctuations (Roberts et al., 2006). Along the coastline, bedrock is overlain by unconsolidated to semi-consolidated sequences of marine, estuarine, and aeolian deposits of the Sandveld Group that reach thicknesses of generally <20 m at Koeberg (Figure 4-2). Pedogenic silcretes and ferricretes, developed on weathered basement, are sporadically preserved inland beyond the reach of the Middle Miocene to Pliocene marine transgressions (De Beer et al., 2008). Section 4.4 provides a detailed description of the Sandveld Group sediments at the Duynefontyn site.

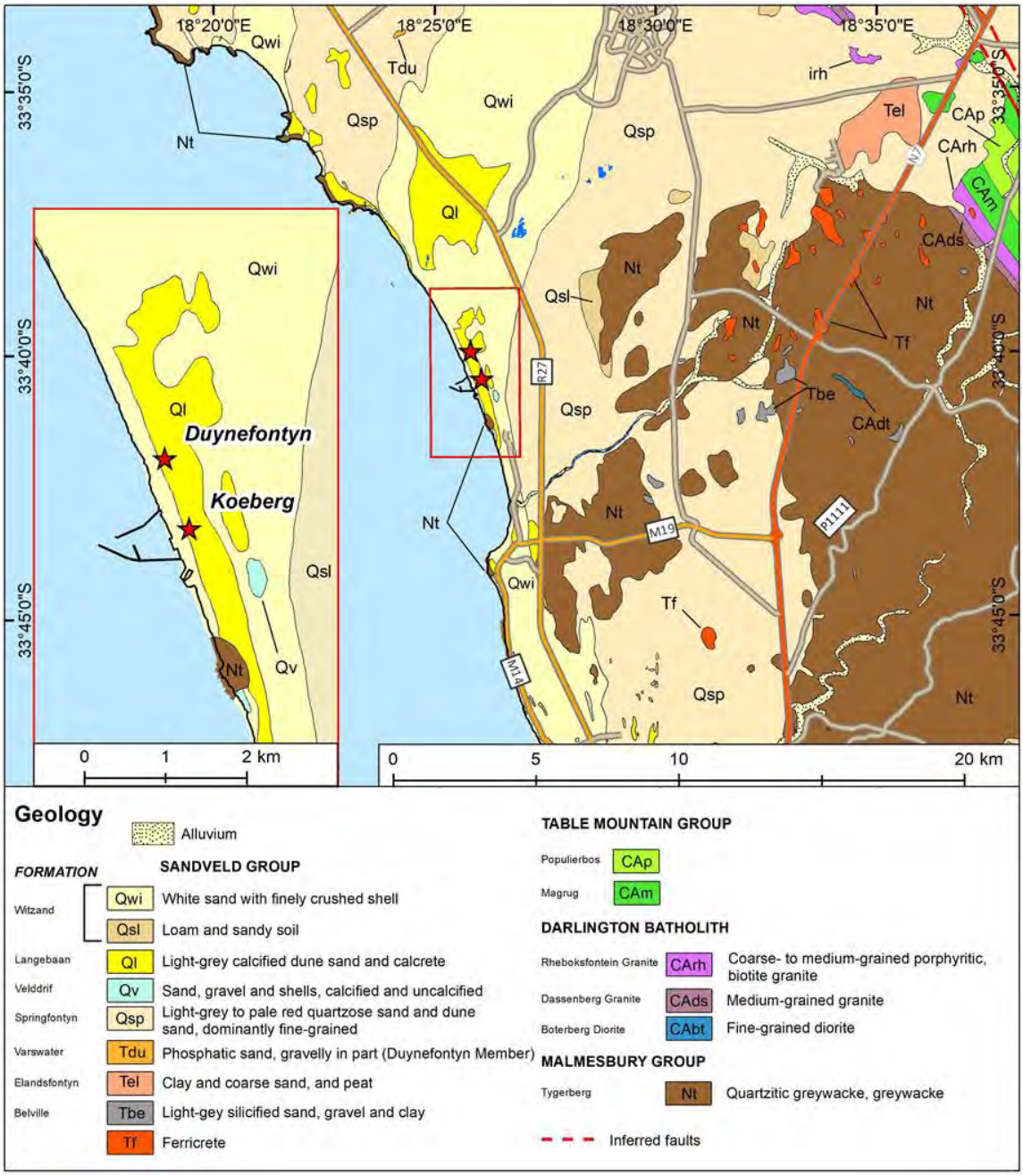

Figure 4-2. Lithostratigraphy in proximity of the KNPS. Duynefontyn and KNPS locations indicated by red stars on map and inset, reproduced from De Beer et al., 2008).

4.2 REGIONAL GEOLOGIC SETTING

The regional geology of the southwest coast of South Africa has been investigated by numerous authors (e.g., Van der Merwe, 1963; Visser and Schoch, 1973; Hartnady et al., 1974; Dames and Moore, 1975, 1976, 1977; Rogers, 1980; Von Veh, 1982; Theron, 1984, 1992; Day and Ridgway, 2000, 2006; Roberts, 2001; Kisters et al., 2002; Gresse et al., 2006; De Beer et al., 2008; Roberts et al., 2011, 2013; Roberts and Siegfried, 2014). This section provides a condensed summary of relevant findings from these and other studies with additional results derived from this PSHA (e.g., Claassen et al., 2024; Coppersmith et al., 2024) that highlight the lithostratigraphy and structural characteristics of the region surrounding the Duynefontyn site.

4.2.1 Lithostratigraphy

The geology of the region around Koeberg and Duynefontyn is mapped in detail at various published and unpublished scales ranging from 1:5000 to 1:250,000 (Beeson, 1973; Theron, 1975, 1984, 1990; Gresse, 1980; Roberts, 2001, 2002; Viljoen, 2008; Siegfried, 2008a,b; De Beer et al., 2008). Maps depict rocks ranging from the oldest Neoproterozoic basement of the Malmesbury Group to the youngest sediments of thick and extensive Late Holocene alluvium and soil cover (Figure 4-3). The low-grade metasediments and subordinate metavolcanic rocks of the Malmesbury Group (Tygerberg, Moorreesburg and Franschhoek Formations) include rhythmic alternations of greywacke, phyllitic shale, siltstone, immature quartzite, and a few thin impure limestone and conglomerate beds. These basement rocks are intruded by the Cambrian (550 and 510 Ma) Cape Granite Suite (e.g., Scheepers, 1995; Kisters et al., 2002; Scheepers et al., 2006), spatially subdivided into five batholiths, each with its own of assemblage of granites, granodiorite, diorite, and gabbro with a broad compositional range. The batholiths are cut by thin dykes of aplite, quartz porphyry, pegmatite, and microcrystalline aphanitic rocks of basaltic composition (Kisters et al., 2002; De Beer et al., 2008; Gresse et al., 2006). At ~515 to 520 Ma the coarse-clastic Klipheuwel Group, composed of an assemblage of immature shales, mudstones, sandstones, and conglomerate, was deposited in fault-bounded rift basins.

Late Proterozoic to early Palaeozoic extension formed an Atlantic-type passive margin along the southern edge of Gondwana, which allowed deposition of the Mid-Cambrian to Ordovician fluvial to shallow-marine and glacial sequences of the Cape Supergroup within the area. The Graafwater, Peninsula, and Pakhuis Formations of the Table Mountain Group comprise quartz arenite, siltstone, shale and diamictite (Theron et al., 1992; Thamm and Johnson, 2006). Within the 40 km radius around the Duynefontyn site, these rocks crop out southwest of Cape Town. Regionally extensive, predominantly NW-SE trending dykes assigned to the False Bay Dolerite Suite intruded rocks of the Malmesbury Group and Cape Granite Suite rocks along the SW Cape during the Early Cretaceous. A swarm of these dykes traverse the coastline between Milnerton and Bloubergstrand (e.g., Day, 1986; Reid et al., 1991; Theron et al.,1992).

(a)

Age	Group	Subgroup	Formation	Lithology	Origin
Holocene				Alluvium	Fluvial
				Scree	Hill-wash
			Witzand	Calcareous quartzose sand	Aeolian
Pleistocene	SANDVELD GROUP		Langebaan	Calcarenite Calcrete	Aeolian
			Velddrif	Calcarenite	Marine
			Springfontyn	Aeolian quartz sand, peaty	Aeolian and estuarine
Pliocene			Varswater	Gravelly, phosphatic sand	Marine, fluvial
Neogene			Elandsfontyn	Clay and coarse sand, peat	Fluvial
			Bellville	Silcrete	Pedogenic
				Ferricrete	Pedogenic
Palaeocene to Neogene	*Continued uplift and erosion of the Cape Fold Belt and Cretaceous Basins, deposition in offshore basins*				
Cretaceous			False Bay Dolerite Dyke Swarm	Dolerite	Syn-rift
Jurassic-Cretaceous	*Uplift and erosion of the Cape Fold Belt, Gondwana breakup, pull-apart rift basins, marine syn-drift sedimentation in offshore basins*				
Permian-Triassic	*Cape Orogeny: Non-coaxial folding, thrusting and cleavage formation (in the study area)*				
Ordovician	TABLE MOUNTAIN GROUP		Pakhuis	Diamictite	Glacial
			Peninsula	Quartz arenite	Fluvial marine
			Graafwater	Sandstone Shale	
Cambrian	KLIPHEUWEL GROUP		Populierbos	Red mudrock	Fluvial
			Magrug	Conglomerate, sandstone	Alluvial fan
	Aborted rifting, sedimentation in Klipheuwel Group rift basins, volcanism				
	CAPE GRANITE SUITE (550-515 Ma)		*Batholiths*	Granite	Syn-to post collisional and A-type granites
			Cape Peninsula Kuils River Stellenbosch Darling Paardeberg	Alkali-feldspar granite Quartz syenite Gabbro Granodiorite Diorite	
	Pan-African Event: Non-coaxial folding, thrusting, cleavage formation, intrusion of Cape Granite and Yzerfontein Suites				
Pre-Cambrian		Tygerberg Terrain	Tygerberg	Greywacke Phyllite, volcanic rocks	Turbidites Volcanic
	MALMESBURY GROUP	Moorrees-burg Terrain	Franschhoek	Conglomerate Quartzite Volcanic rocks	Fluvial Volcanic
			Moorreesburg	Greywacke Phyllite	Turbidites

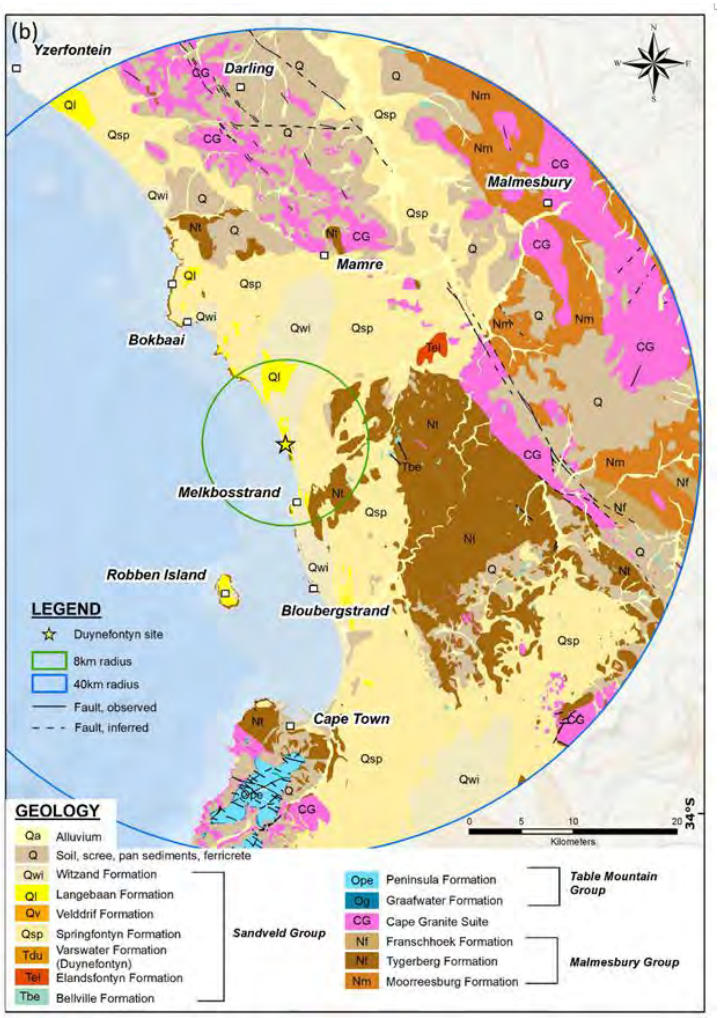

Figure 4-3. (a) Lithostratigraphy of the area within a 40 km radius of the Duynefontyn site (copied from De Beer et al., 2008). Lithological units highlighted in red are known to occur at both sites. (b) Geological map depicting the location of lithostratigraphic units within a 40 km radius around the Duynefontyn site (copied from De Beer et al., 2008).

The large majority of all these rocks are overlain by well-developed soil cover and Cenozoic sediments of the Neogene to Holocene Sandveld Group, composed of unconsolidated to semi-consolidated sequences of marine, estuarine, and aeolian deposits that attain thicknesses of more than 60 m in places (Rogers, 1980, 1982, 1983; Roberts, 2001; Roberts et al., 2006). Occurrences of silcretes (Belville Formation) and ferricretes are also developed on weathered basement and are sporadically preserved inland beyond the reach of the Middle Miocene to Pliocene marine transgressions (De Beer et al., 2008) (Figure 4-3)

4.2.2 Regional structural geology

Along the southwestern margin of South Africa and within the site vicinity, the structural geology is largely dominated by NW-SE striking, NE or SW steeply dipping (frequently >60°) Malmesbury Group rocks which are deformed in a succession of tight upright folds with axial planes trending NW to NNW. The SE-NW trending fold axes gently plunge NW with a weakly-developed axial plane cleavage (Dames and Moore, 1976; Theron et al., 1992; De Beer at al., 2008). NW-SE orientated, SW and NE steeply dipping strike-slip faults dominate (e.g., Colenso and Piketberg faults) (Figure 4-4). Generally shorter normal faults (e.g., the Mamre Fault) and localised reverse and thrust faults are also present. These fault and fold styles, as well as their orientation, change across this region towards the south coast across the Cape Fold Belt syntaxis where faults take on a mainly E-W and NE-SW orientation with a predominantly normal sense of fault displacement (e.g., Worcester Fault) and E-W trending folds. Detailed descriptions of the dominant structural geologic features are provided in Section 8.3 and 8.5. Figure 4-4b shows the regional and local stress data. The three main sources of stress data shown in the figure are structural geological mapping, borehole breakouts, and focal mechanism. The SSM TI Teams assessment of the regional stress is provided in Section 4.2.11 and Section 5.2.5.

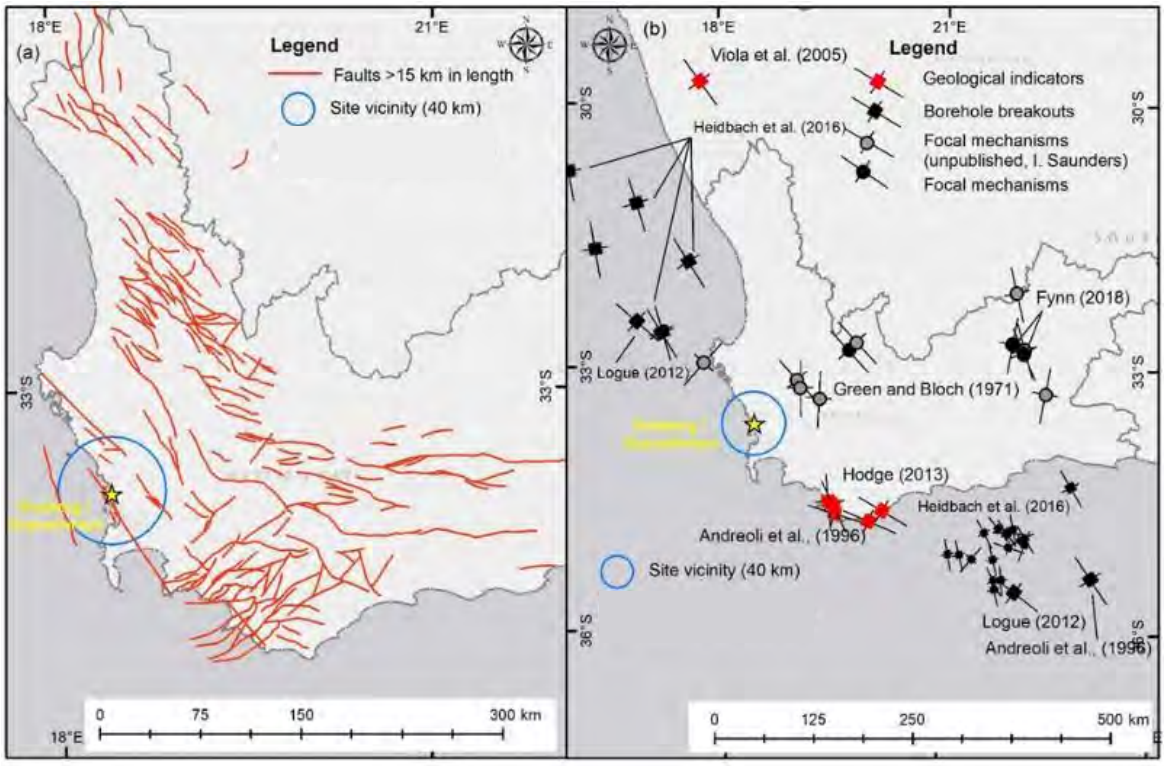

Figure 4-4. Map of (a) identified tectonic structures and (b) indicators of stress across the region.

4.2.3 Seismotectonic setting

In the Baseline PSHA report (Stamatakos et al., 2022), the SSM TI Team summarised the tectonic history based on the original three-terrane interpretation of Hartnady et al. (1974). This interpretation, which we have named the Proterozoic terrane model, was the accepted interpretation of Western Cape tectonic history for several decades (Kent, 1980) and was revisited by Gresse et al. (2006) in the most recent version of the Geology of South Africa book (Johnson et al., 2006). At Workshop 2, however, three alternative tectonic models were proposed by the proponent experts (Kisters, 2022; Tankard, 2022; Paton, 2022). The SSM TI Team has named these three models the 'accretionary prisms and fore-arc basin model', the 'Vredenburg Shear Zone Duplex model', and the 'lateral ramp on an inclined plate-margin detachment model', respectively. Table 4-1 summarises these three alternative tectonic models, in addition to the model relied on for the Baseline PSHA report. Table 4-1 also describes the tectonic models and identifies the key features of each interpretation, the technical bases, technical challenges, and the implications for the site hazard results.

However, it is important to recognise that the tectonic models are not used as direct inputs to the SSM. Rather, the tectonic models provide the SSM TI Team with base knowledge and a common understanding of the tectonic and geological framework of the Western Cape (and the uncertainties of that framework). This base knowledge and common understanding of the tectonic framework underlie and connect the more hazard-specific assessments needed to build and populate the SSM. For example, the SSM TI Team's assessment of seismogenic thickness or fault activity is based on earthquake data in the project catalogue or detailed geologic mapping of fault traces. However, the SSM TI Team's certainty (or uncertainty) in these specific assessments comes in part from how well (or how poorly) these assessments fit within the SSM TI Team's overall understanding of the tectonic and geological framework. Earthquake data or field observations that are compatible with the SSM TI Team's understanding of the tectonic framework may be judged by the SSM TI Team as reliable and credible. Data and field observations that conflict with the tectonic framework suggest that the given interpretation of the tectonic framework needs to be challenged by the SSM TI Team and may require additional study and verification.

The SSM TI Team's assessment of uncertainty in the SSM logic tree and HID inputs is also informed by an understanding of the range of possible tectonic interpretations. Because the four alternative tectonic models included in the current SSM TI Team's evaluation span a relatively broad range of tectonic interpretations, the SSM TI team will need to include sufficient uncertainty in many of the model inputs that are rooted in an understanding of the tectonic and geological framework. The alternative tectonic models used to form the base knowledge and common understanding of the tectonic and geologic framework of the Western Cape are summarised below and in Table 4-1. Discussions of the SSM implications and methods for model assessment are provided, followed by descriptions of geodetic and tectonic stress analyses that are considered within the tectonic and geological framework of the Western Cape.

4.2.4 Proterozoic terrane model

In this model, the Western Cape is underlain by the Saldania Belt, one of the Pan-African orogenic belts that mark the suture zones along which continental fragments were amalgamated during the Late Neoproterozoic to Early Palaeozoic construction of Gondwana

(Miller, 1983; Hartnady et al., 1985; Gresse and Scheepers, 1993; Frimmel et al., 1996; Frimmel and Frank, 1998; Rozendaal et al., 1999). The terranes include the Damara, Kaoko, Gariep and Saldania Belts, and record the main phase of collisional tectonism at ~550 to ~530 Ma (Frimmel and Frank, 1998; Fitzsimmons, 2000) (Figure 4-5).

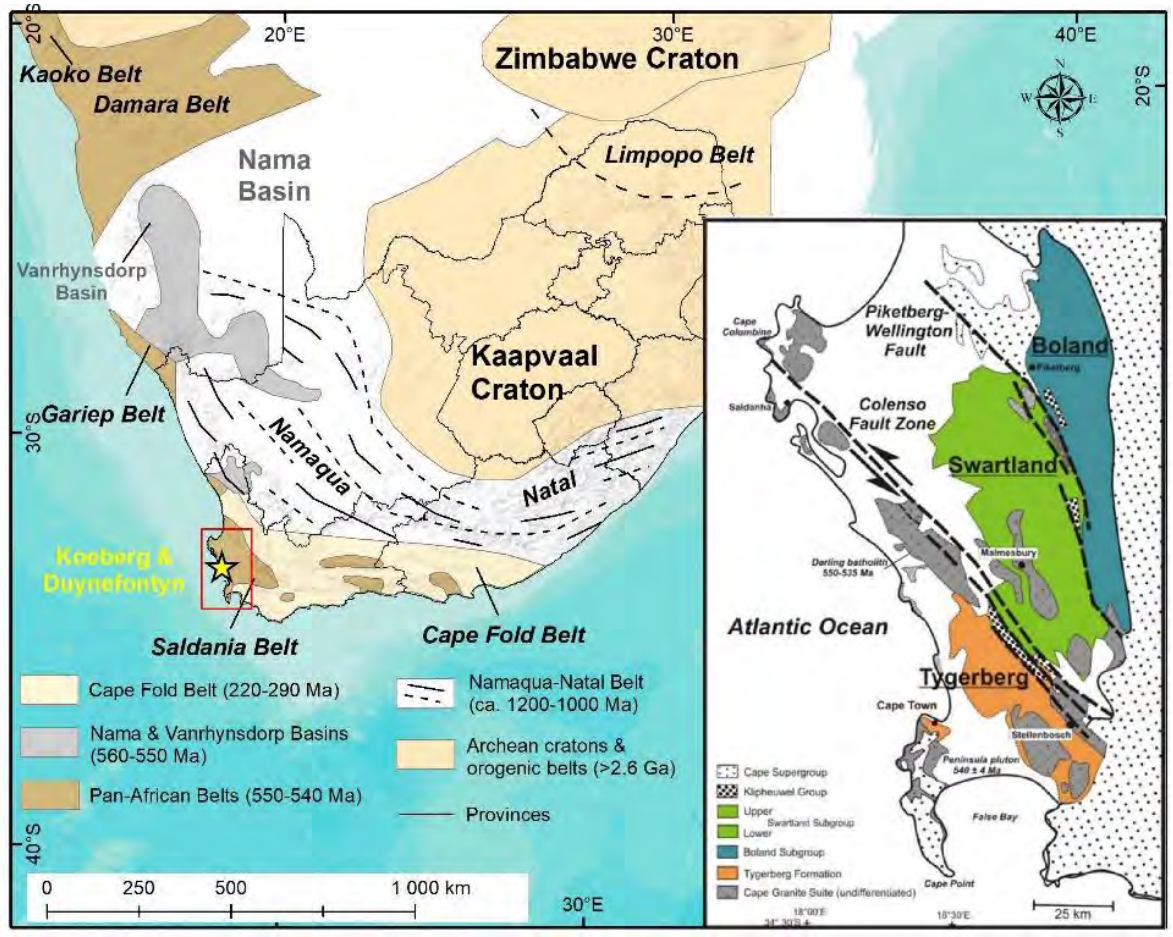

Figure 4-5. Map showing the large-scale seismotectonic features for the Proterozic terrane model, including cratons and orogenic belts in Southern Africa. Inset map shows the northern branch of the Saldania Belt and its simplified geology (after Scheepers, 1995; modified by Kisters et al., 2002).

The Proterozoic terrane model was first proposed by Hartnady et al. (1974), who suggested that the southwestern branch of the Saldania Belt comprises three allochthonous and para-allochthonous terranes (Tygerberg, Swartland, and Boland) that were amalgamated against the Kaapvaal Craton by a series of terrane-bounding transpressional strike-slip faults, including the Colenso and Piketberg–Wellington faults. These terranes are underlain by Meso- to Paleoproterozoic crystalline basement.

The terranes comprise low-grade metamorphic Neoproterozoic metasediments and subordinate metavolcanic rocks assigned to the Malmesbury Group that include rhythmic alternations of greywacke, phyllitic shale, siltstone, immature quartzite, and a few thin impure limestone and conglomerate beds. The Proterozoic terrane model separates the three sub-sections according to how they are dissected by the two regional fault systems, the distribution of deposits on geological maps, as well as some noted changes in the structural style among the three terranes.

4.2.5 Accretionary prisms and fore-arc basin

At Workshop 2, Professor Alex Kisters proposed a tectonic model in which the Western Cape originated as an accretionary prism akin to the present-day subduction tectonics along the Indonesian archipelago (Figure 4-6). The details of this interpretation are laid out in Kisters and Belcher (2018). In this tectonic model, the Neoproterozoic tectonic assemblages that were interpreted as allochthonous terranes by Hartnady et al. (1974) are reinterpreted as autochthonous relics of a Late Neoproterozoic convergent margin. Kisters and Belcher (2018) divided the Neoproterozoic stratigraphy into two structural units: a lower domain (Swartland Complex) comprising an imbricate stack of marine sediments and relic ocean crust, overlain by a less deformed domain (Malmesbury Group) comprising shales, phyllites, and metagreywackes, and thin limestones and conglomerates that were folded into tight west-trending upright to southwest-verging folds. Tectonic underplating during subduction in the deeper parts of the prism and deposition of fore-arc sediments at higher structural levels are contemporaneous between >560 Ma and at least 520 Ma.

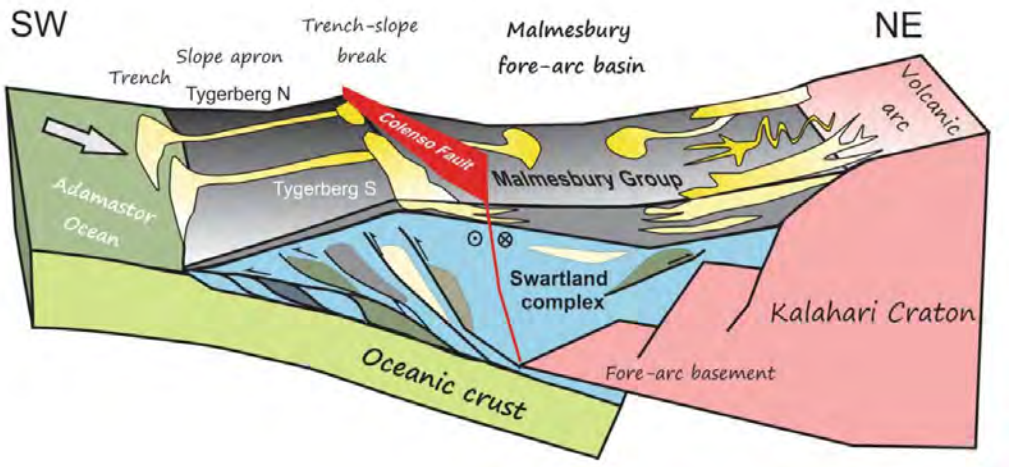

Figure 4-6. Schematic illustration showing the different lithological and structural elements of the Tygerberg prism and Malmesbury fore-arc with respect to the Kalahari Craton[1], from Kisters and Belcher (2018, Figure 14.9). The Swartland Complex corresponds to the Swartland Subgroup in the inset map legend of Figure 4-5.

The key evidence supporting this interpretation comes from a detrital zircon study by Frimmel et al. (2013), which demonstrates within the margin of error that rocks of the two domains are identical in age, and thus simply represent two different structural levels of the same fore-arc complex. The Swartland Complex exposes the upper parts of the accretionary prism while the overlying Malmesbury Group is the remnant (albeit deformed) fore-arc basin resting atop the accretionary prism. In this model, the Colenso Fault is recognised as a regional-scale fault or fault zone that originates within the accretionary prism, but it is not a terrane boundary. The Colenso Fault is the primary fault separating the continental crust (upper domain) from the accretionary prism (lower domain). Frimmel et al. (2013) suggest that the Piketberg Fault represents the major terrane boundary in the western Saldania Belt. Although not

[1] The Kalahari Craton consists of two cratons separated by the Limpopo Belt: the larger Kaapvaal Craton to the south and the smaller Zimbabwe Craton to the north. The Namaqua Belt is the southern margin of the Kaapvaal Craton.

characterised as such in Kisters and Belcher (2018), the Piketberg-Wellington Fault, in this model, could be interpreted as the tectonic backstop of the accretionary wedge against the craton.

4.2.6 Vredenburg shear zone duplex

The Vredenburg Shear Zone Duplex model, developed by Dr Anthony (Tony) Tankard, is not yet published but was presented at Workshop 2. This model proposes a deep pan-African crustal structure, dating back to the Neoproterozoic-Early Cambrian assembly of western Gondwana (Figure 4-7). Dr Tankard proposes that there is a deep primary controlling north–south structure, which he calls the Vredenburg Shear Zone (VSZ).

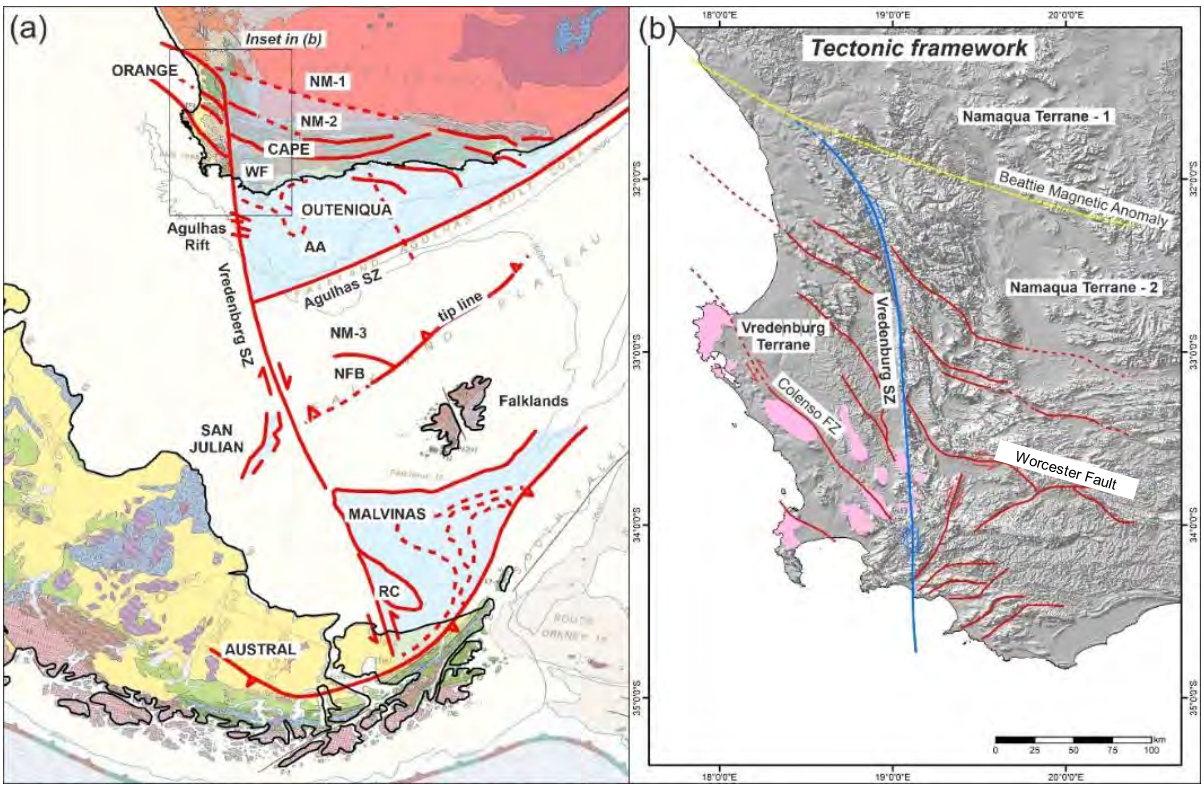

Figure 4-7. The Vredenburg Shear Zone model proposed by Dr Tony Tankard at Workshop #2. (a) The VSZ is a controlling primary tectonic structure (right lateral transform fault) that placed South America against Africa during the assembly of Gondwana. At the regional scale (b), there are no surface manifestations of the VSZ, but Riedel and conjugate Riedel shear structures of the model are manifest as the Colenso and Worcester faults, among other mapped faults.

The VSZ is interpreted as a basement shear zone above which a suite of linked and rotated faults occur in the cover sequence. The width of the shear zone may vary by up to several kilometres, which Dr Tankard attributes to the blank space or corridor on the 1:250,000 geological sheets of the Western Cape in the vicinity of the syntaxis that separates two disconnected sets of structures. There is no surface expression of the VSZ or principal displacement zone, but measurable offsets of associated structures are present, with surface displacement of generally less than one kilometre. The Colenso Fault Zone is one of several associated Riedel shear structures.

The VSZ and the Colenso Fault now occur at the trailing edge of this structural complex, and at the southern part of the onland portion of the structure (Figure 4-7b), and Tankard proposes

that these two structures are the principal focus of recent seismic activity in the southwestern Cape. In his model, Dr Tankard cites the interplay of synthetic shears (Riedel structures) and antithetic shears (conjugate Riedels) on mapped geological structures in the Western Cape.

Dr Tankard cites the following evidence for his model:

- Zircon xenocryst ages of 2.0 Ga in the Vredenburg and Darling granites (dated by Rozendaal et al., 1999) suggest the origin of the Vredenburg basement may have been derived as a fragment of the Rio de la Plata craton of northeast Argentina. Dr Tankard suggests that Rio de la Plata-type basement was accreted during Gondwana assembly and is believed to underlie the Malmesbury platform and western edge of the Cape Fold Belt up to the VSZ.
- There is an intermediate zone where the antithetics are inverted by a suite of reverse faults. This can be observed on the geological map, where the western end of the Worcester fault bends northwards.
- At Caledon, a structural complex that forms a ‘pop-up structure’ was compared with the sandbox modelling of McClay and Bonora (2001). Tankard’s explanation of a pop-up is that the fault system comprises a jog or offset in the trace of the strike-slip fault. In this case, uplift occurred where the dextral fault system met a left-stepping jog.
- Although there is a scarcity of subsurface data, Dr Tankard interprets the vertical shape of the Colenso Fault as a listric, down-to-the-southwest fault, rather than a planar fault. He infers that reflection seismic profiles from comparable areas show that anything other than listric would have created ‘space problems.’
- The Late Cambrian Klipheuwel Basin and its structural architecture provide an important template for basin evolution along the Colenso Fault Zone. At its southeastern end, the Colenso Fault Zone consists of a principal strike-slip fault as well as a secondary synthetic fault to accumulate the strain, thus accommodating the Klipheuwel Basin. It is a useful yardstick to compare with the Langebaanweg and Elandsfontein deposits. This synthetic fault is expressed as a magnetic lineament. The angular deviation of the synthetic fault to the principal fault zone is ~15˚, typical of a synthetic shear. Dr Tankard attributes the magnetic lineament to magmatism, such as a basic dyke, along the synthetic fault plane which occurs because the role of the synthetic and antithetic faults is to conserve strain. Translation along the Colenso Fault Zone included a component of uplift. This is also observed in unroofing of the Darling granite along strike (Figure 4-5 inset).

Dr Tankard interpreted relatively recent geologic deformation in the area he mapped based on a series of Cenozoic deposits along the Colenso Fault Zone, including the Langebaanweg and Elandsfontein phosphate deposits and underlying wetland accumulations. The Elandsfontein phosphate deposits are found in the present at the Kropz phosphate mine. Clay-cake deformation models (Groshong, 1989) together with a display from Mandl (1988) were re-oriented to match the Langebaanweg geology. The inboard peak of the accumulation, isopached based on phosphorous pentoxide (P_2O_5) percent, presently occurs at an elevation of 52 m above present sea level (Tankard, 1974). This elevation has been structurally restored, showing that the pre-deformation height was 21 m asl (above sea level). As a secondary check, chronological equivalents at Sandheuwel (Saldanha Bay) and Koingnaas confirmed this pre-deformation elevation of 21 m. This implies that the Mid-Pliocene sea-level

was at 21 m asl, whereas the world average is 22 m asl. Uplift of the Langebaanweg and Elandsfontein Early Pliocene sediments across the Colenso Fault Zone is therefore believed to have occurred in the Late Pliocene to Early Pleistocene. More importantly, it involved ~30 m of structural uplift along the Colenso Fault in an inferred time span of about 1.5 Ma. There were no geochronological dates on these deposits to verify the proposed uplift rate. Furthermore, the intervening Miocene-Pliocene unconformity is mapped in the offshore Orange Basin, where it is dated at 5.5 Ma.

4.2.7 Lateral ramp on an inclined plate-margin detachment

Based on extensive analysis of mainly offshore seismic images and cross-section restoration across the southern coast of South Africa presented at Workshop 2, Dr Douglas Paton proposed a seaward-dipping regional detachment model that was formed in the Neoproterozoic during the assembly of Gondwana (Figure 4-8). This detachment has continued to play a role in subsequent phases of tectonism, including the break-up of Pangaea and Gondwana and the subsequent transition from rift to drift to passive margin tectonism throughout the Mesozoic and Cenozoic.

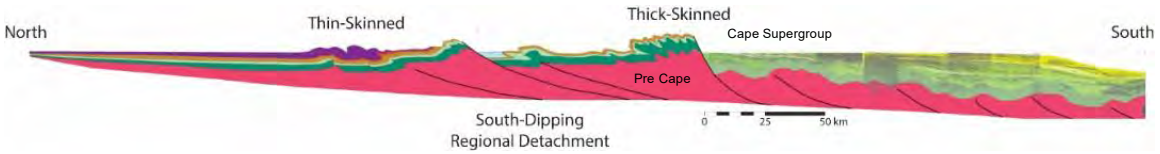

Figure 4-8. Composite cross-section from the southern Karoo Supergroup (left), through the Cape Fold Belt (centre), to the offshore Mesozoic extensional basins (right), redrafted from slide #50 of Dr Paton's Workshop #2 presentation (Paton, 2022).

In these restorations, Dr Paton documents a change in structural style from thin-skinned shortening inboard, where the crustal detachment is shallow, to thick-skinned shortening outboard, where the crustal detachment is deeper. The thin-skinned deformation is characterised by northward-verging thrust sheets on low angle faults, while the thick-skinned shortening is characterised by steep basement-cored faults and large box folds in the cover rocks. Dr Paton also showed similar structural and stratigraphic relationships that appear to be preserved in the Falkland Islands and Patagonia, which were juxtaposed against South Africa as part of Gondwana, and thus share a common tectonic evolution to South Africa. Extension during the breakup of Gondwana was accomplished by reactivation of the contractional faults as transpressive strike-slip faults, and reactivation of the normal faults as transtensional strike-slip faults.

Although a detailed analysis of similar data was not available for the west coast of the Western Cape, Dr Paton extended his interpretation of a seaward-dipping detachment based on his reconstruction of the various tectonic plates and micro-plates prior to the breakup of Gondwana. An important distinction in his model is that the Western Cape is highly oblique to both convergent and divergent plate motions, unlike the southern to south-eastern margin of South Africa. In addition, Dr Paton interprets the SW part of the coastal region of the Western Cape as resting atop a large southwest-dipping lateral ramp (Figure 4-9) within the detachment zone. The region is therefore dominated by margin-parallel strike-slip and oblique strike-slip deformation. In this model, the lateral ramp constitutes a deep-rooted tear fault.

Based on his model, Dr Paton explains the nearly orthogonal sets of mapped faults in the syntaxis as coeval conjugates or orthogonal fault sets that reflect the underlying geometry of a seaward-dipping detachment over its lateral ramp.

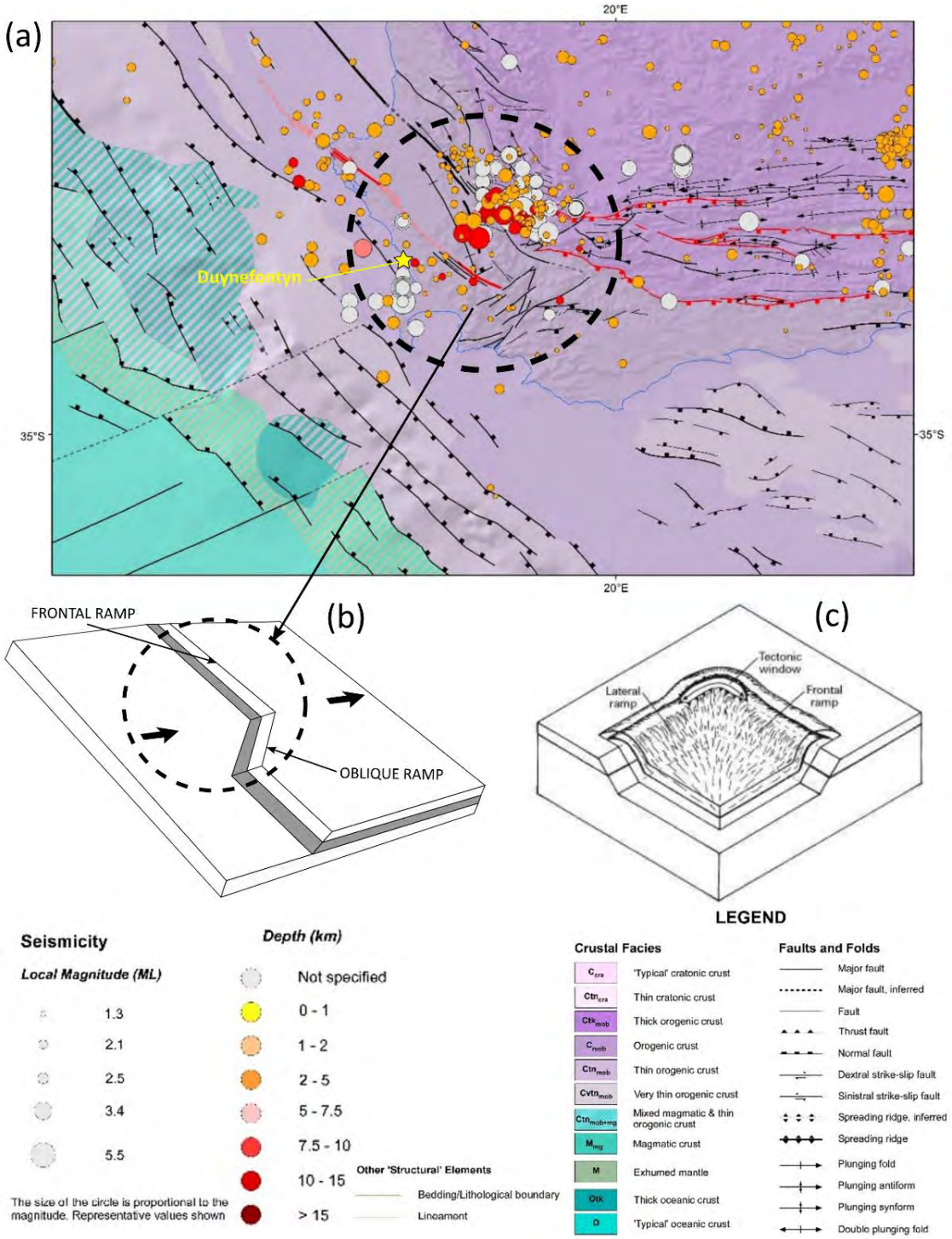

Figure 4-9. Lateral ramp tectonic model presented by Dr Paton at Workshop #2. (a) Geological map of the Western Cape showing the location of earthquakes in the syntaxis, from Markwick et al. (2021). (b) Diagram showing the three-dimensional (3D) footwall ramp structure, after Figure 10 of McClay (1992). (c) Diagram showing how orthogonal fault sets form above a lateral thrust ramp, from https://pubs.usgs.gov/bulletin/b2163/html/fig33.html.

An interesting alternative to the lateral ramp concept proposed by Dr Paton, is a hypothesis of the Syntaxis as an orocline that formed in response to dextral transpression along the continental margin (Johnston, 2000). This interpretation uses a similar tectonic reconstruction as that proposed by Dr Paton. In this interpretation, the east-west Cape Fold Belt, including the Falkland Islands, formed a 300 km left-step within the dextral shear zone (similar to a restraining bend along a strike-slip fault system but much larger). According to this model, dextral margin-parallel translation of the crustal blocks outboard of the orogen was accommodated by strike-slip deformation in South America and Antarctica, and inboard of the margin by convergence along the east-west portion of the Cape Fold Belt and the growth of its foreland-verging fold-thrust structures (Figure 4-8). In this interpretation, the Syntaxis (and its counterpart, the Port Elizabeth Antitaxis) are oroclinal bends in the Cape Fold Belt that developed in response to two large rotations of the Falkland Islands, a 90° clockwise rotation during plate convergence followed by a 60°-70° clockwise rotation from shear along the Agulhas-Falkland Fracture zone during the break-up of Gondwana. This interpretation is however at odds with the conventional interpretation in which the Falkland Island rotations are considered to post-date the Cape Fold Belt. This age constraint on the rotations is based on palaeomagnetic data, which show that these rotations took place sometime after 190 Ma (Mitchell et al. 1986; Taylor and Shaw, 1989).

Table 4-1. Summary of tectonic models following Workshop #2.

Model	Conceptual Image	Key Features	Technical Basis	Technical Challenges	Implications for Hazard
Proterozoic terrane [Hartnady] [Baseline PSHA report]	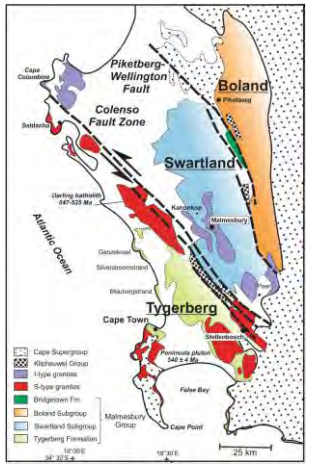	Three terranes amalgamated along transpressive northwest–southeast-trending shear zones. Post-amalgamation intrusion of large granite plutons.	Geological mapping revealed subvertical, northwest-southeast strike-slip (SS) faults with intensely mylonitised and brecciated rocks, that separate terranes. These SS faults have been interpreted as the terrane boundaries.	Gleaning direct evidence of recent (Quaternary) faulting and seismicity along any one of these shear zones from the geological record. Integration of the tectonic model with other data e.g., heat flow, gravity, magnetics.	Active faulting primarily occurs as reactivation on a subset of these early faults, those that are optimally oriented for slip in the current stress regime.
Accretionary prism and fore-arc basin [Kisters]	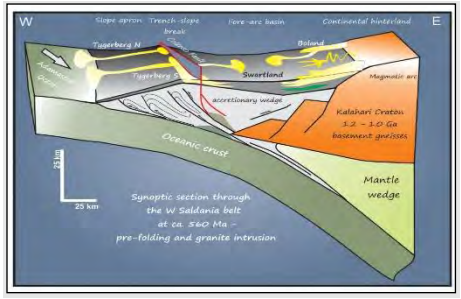	The Western Cape is a relict accretionary prism and fore-arc basin developed by sinistral Gondwana transpression. The Colenso Fault (which dips to the northeast in this model) is the primary fault separating the continental crust (upper domain) from the accretionary prism (lower domain).	Strong differentiation in metamorphic grade within the Malmesbury strata between the accretionary prism and fore-arc. Similar detrital zircon ages for strata across the belt indicating a common depositional setting.	How can this be differentiated from the terrane model? Integration of the tectonic model with other data, e.g., heat flow, gravity, magnetics.	Primarily SS earthquakes on reactivated Colenso Fault or parallel structures. The model divides the Western Cape crust along the Colenso Fault. Clear delineation between deep crust and shallow crust. Deep earthquakes east of the Colenso Fault.

Model	Conceptual Image	Key Features	Technical Basis	Technical Challenges	Implications for Hazard
Vredenburg Shear Zone Duplex [Tankard]	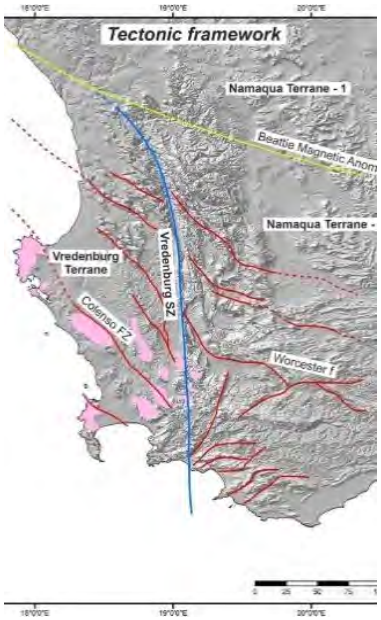	Western Cape faulting is controlled by a cryptic north–-south-oriented shear zone at depth with a detached (partially coupled?) cover of Riedel (R) and anti-Riedel (R’) faults. Depth to detachment is about 6–8 km. In this model the Colenso Fault dips to the southwest.	Geometry of mapped faults and basins along the Vredenburg Shear Zone mimics features produced by clay-cake models. Zircon xenocryst ages of 2.0 Ga in the Vredenburg and Darling granites (dated by Rozendaal et al., 1999) suggest the origin of the Vredenburg basement may have been linked to the Rio de la Plata craton of northeast Argentina.	The shear zone is not visible/ evident in the cover sequence (difficult to verify). Buried shear zone models imagine a wide variety of surficial deformation that, in and of themselves, are non-unique to the shear zone itself. Integration of the tectonic model with other data, e.g., heat flow, gravity, magnetics.	Partitioned (and thus smaller M) seismicity between cover and shear zones. The shear-zone is a 5–10 km wide zone of anastomosing faults. R and R’ structures are active normal and reverse faults in the cover, including the Colenso.

Model	Conceptual Image	Key Features	Technical Basis	Technical Challenges	Implications for Hazard
Lateral ramp on an inclined plate-margin detachment [Paton]	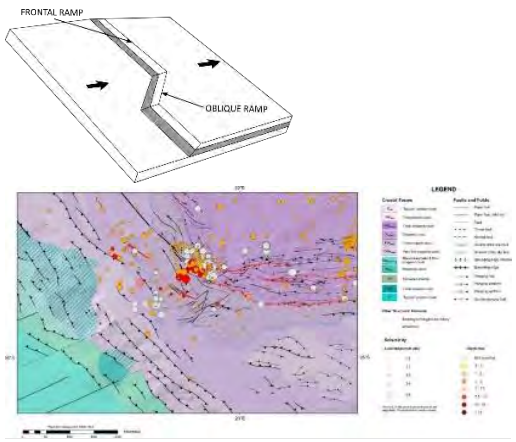	Western Cape is a lateral ramp along a reactivated convergent-divergent plate margin (see Figure 4-8). The lateral ramp leads to SS faulting parallel to the plate margin. Plate margin is inclined seaward. Syntaxis is an overlapping network of orthogonal faults reflecting the later ramp architecture.	Consistent plate-scale deformational history based on detailed cross-sections and linked to tectonic history (e.g., assembly and break-up of Gondwana/Pangaea). Explains the thin and thick-skin crust.	Identifying a similar tectonic history developed for the Southern Cape from offshore 2D seismic profiles. Integration of the tectonic model with other data, e.g., heat flow, gravity, magnetics.	Primarily SS earthquakes on margin-parallel faults. Seismogenic depth shallows to the west, consistent with tapered plate margin. Earthquakes occur on reactivated structures.

4.2.8 Implications for the SSM

Alternative tectonic models are not usually segregated in the SSM logic tree as distinct branches. Rather, the models are used to support the SSM TI Team's assessment of various aspects of the model that are captured as logic-tree inputs, such as seismogenic thickness or Mmax and their uncertainty. Specifically, for the Duynefontyn SSHAC EL-2, the SSM TI Team assessed the following aspects of the SSM based on the four tectonic models.

- Source zone boundaries: Source zone boundaries are often defined by important crustal features. Most important are considerations of differences in crustal properties, crustal thickness, changes in the structural grain or types of faulting, and whether the crust was involved in Mesozoic extension. Identification and characterisation of these kinds of features requires a firm understanding of the tectonic forces that produced these features. A detailed description of the SSM TI Team's approach and criteria for defining source zone boundaries is provided in Sections 8.1 and 8.3.
- Orientation and geometry of ruptures in the virtual fault generator: To generate site-to-event distances appropriate for use with most modern GMPEs, potential future earthquakes generated from zones within 100 km of the site were modelled on virtual faults. To model the virtual faults, the SSM TI Team needed a technical basis to define the location, size, geometry, orientation, and style (normal, reverse, strike-slip) of these virtual ruptures, as described in Section 8.2.5. The approach adopted by the SSM TI Team was to assume that these ruptures would most likely be reactivations of existing bedrock faults. Thus, the mapped surface pattern of existing faults that are optimally oriented in the current stress field (see Section 4.2.11) were used to develop the input distributions of virtual faults. However, the VSZ model, and to some extent the lateral ramp model, predict that a broader distribution of surface faults may be involved. Movement on the VSZ may result in reactivation on the western set of northwest–southeast faults. In this model, the VSZ and perhaps the Colenso Fault are the principal foci of recent seismic activity in the southwestern Cape. The proximal trailing-edge margin or Riedel shear closest to the VSZ may be more susceptible to reactivation, especially faults such as the Colenso and southern trace of the VSZ. Farther away from the trailing edge, towards the distal end of the Riedel or conjugate anti-Riedel shears, the yield strength of the crust and its tectonic fault structures caused by buttressing may dampen the risk of earthquakes. This aspect of the seismotectonic framework informed the SSM TI Team's broader range of fault orientations and styles of faulting used in the virtual fault generator.
- Crustal type: Many of the models relied on to generate inputs to the distributions for Mmax (Section 8.2.9) and the magnitude-frequency distribution for the source zone (Sections 8.2.10 and 8.4.6) depend, in part, on how the crust is classified. Specifically, the SSM TI Team classified the crust as stable continental and determined whether this crust can be considered highly extended by the Mesozoic breakup of Pangaea and Gondwana. The SSM TI Team assessed the crustal properties of the source zones considering the differences among the four tectonic models. The SSM TI Team concluded that the crust of the Western Cape shares properties with Stable Continental Regions (SCRs) around the world (see Section 8.2.2 for more details about SCRs). SCRs are defined as regions of continental crust that have not experienced major tectonism, magmatism, basement metamorphism,

or anorogenic intrusion since the early Cretaceous (~145 Ma), and no rifting or major extension or transtension since the Palaeogene (~60 Ma). In this assessment, the SSM TI Team noted that the Duynefontyn site is approximately 2,000 km from the nearest active plate margin and underlain by Precambrian metasedimentary and crystalline strata with no known major deformation in the Neogene and Quaternary periods (~23 Ma). The SSM TI Team believes that the largest historical earthquakes (i.e., 1809 and 1969) occurred on faults within the crust that didn't rupture the surface or otherwise did not leave evidence of their rupture. For source zones off the west coast of South Africa, and the Orange Basin in particular, the crust is considered by the SSM TI Team to be Mesozoic extended crust. In addition, the SSM TI Team evaluated the information about crustal type provided by Dr Brandt at Workshop 2, and related information, including recent tomographic studies of southern Africa (Fadel et al., 2018; White-Gaynor et al., 2020; White-Gaynor et al., 2021; Afonso et al., 2022), Pn arrivals in southern Africa (Kwadiba et al., 2003), aftershocks (Marimira et al., 2021; Shumba et al., 2020; Yang and Chen, 2008), and the **M** 6.5 Botswana earthquake of April 2017 (Chisenga et al., 2020; Gardonio et al., 2018; Kolawole et al., 2017; Midzi et al., 2018; Moorkamp et al., 2019; Mulabisana et al., 2021).

- Seismogenic thickness: Seismogenic thickness is typically determined from the depth distribution of recorded earthquakes in the project earthquake catalogue (Section 8.2.2). Specifically, the depth distribution of the recorded earthquakes is plotted as a cumulative distribution, and the depth corresponding to the 90% probability value (D90) is then taken as the seismogenic thickness (e.g., Pacific Northwest National Laboratory [PNNL], 2014). However, because the earthquake record in the Western Cape is relatively sparse, a reliable depth distribution cannot be determined. Thus, the SSC TI Team relied on analogue regions where there is sufficient data to develop a reliable estimate of the seismogenic thickness. The technical basis for selecting appropriate analogue settings comes from an understanding of the nature of the crust.

4.2.9 Assessment methods

The complex geological and geophysical character of the Western Cape makes identification of a single seismotectonic model difficult. Many of the geological features observed at the surface, or interpreted from offshore seismic images, could equally be attributed to the tectonic driving forces from several of these tectonic models. For example, normal faults observed in the syntaxis could arise from the complex shear generated at the top of a lateral ramp, or from the flower structures generated above the buried VSZ. Thus, the SSM TI Team needed to maintain a broad perspective of alternative conceptual models to ensure that the full range of uncertainty was included in the hazard calculations to capture the CBR of TDI. Each diagnostic feature of the alternative conceptual models was carefully evaluated against the full range of existing geological, geophysical, and seismological information.

The assessments began with a summary of the existing tectonic model information presented at Working Meeting 2 for the SSM TI Team to discuss and assess. In this presentation and discussion, the SSM TI Team integrated the tectonic models with other data (e.g., geodesy, heat flow, gravity, and magnetics) and identified areas of agreement and incompatibility. Based on this assessment, the SSM TI Team produced a range of fault scenarios at Working

Meeting 3, consistent with each of the tectonic models, and evaluated those against geological, geophysical, and seismological data.

A critical component of the assessment was to evaluate results generated by the PSHA support studies (DDCs). This assessment included:

- Marine multibeam bathymetry data in Table Bay and False Bay;
- Recent field investigations of the Colenso Fault, where Tony Tankard indicated he found evidence for geologically recent deformation when the phosphate mine at Langebaanweg was active (1980s);
- Evaluation of microseismic data recorded by a temporary network, composed of seven stations, installed along the Colenso Fault;
- Results from the marine terrace data;
- Reprocessed seismic images from offshore data obtained from the Petroleum Agency of South Africa (PASA);
- 3DStress™ analysis supported by a database of stress indicators (Green and Bloch, 1971; Stacey and Wesseloo, 1998; Hodge, 2013; Fynn, 2018; Heidbach et al., 2018); and
- Remote sensing mapping with field verification for fault scarps.

Regarding the marine terrace studies, two points that garnered specific attention from the SSM TI Team were: (1) constraints on landscape uplift and (2) a comprehensive review of past sea-level fluctuations in the southwestern Cape, such as the recent work of Hearty et al. (2020). The marine terrace investigation (Claassen et al., 2024) addressed these two points. This study provided a basis for evaluating the stability of coastal geomorphic features and processes.

Regarding the offshore seismic images, the SSM TI Team acquired 48 seismic profiles from Cape Columbine to Cape Agulhas, and from the inner- to mid-continental shelf to the base of the continental slope from PASA. With these data, the SSM TI Team was able to construct regional onshore-offshore geological cross-sections spanning the northern extent of the Cape Fold Belt through the offshore Mesozoic Orange Basin (see Section 5.2.6) to evaluate the potential for recent offshore fault activity and to compare to cross-sections from the Cape South Coast through the Outeniqua Basin by Paton et al. (2006).

Regarding heat flow, the SSM TI Team evaluated the study from Dhansay et al. (2017) where they utilised subsurface temperature and heat flow measurements to determine potentially anomalous geothermal gradients, as described in Section 8.2.2.

4.2.10 Geodetic data

Geodetic measurements, especially Global Positioning System (GPS) data, can also be an important constraint in evaluating the seismotectonic framework in SSHAC PSHA studies (e.g., BC Hydro, 2012). GPS data for South Africa can be obtained from TrigNet, which is a network consisting of approximately 65 (mostly) continuously observing stations across the country with an average distance of 200 km between stations, and locally more dense station configurations of approximately 70 km around Cape Town, Johannesburg, and Durban (Figure 4-10). GPS data is also available from the International Global Navigation Satellite System (GNSS) Service (IGS).

GPS data for South Africa is reported in Malservisi et al. (2013), which shows that the South African region is rigid within the measurement uncertainties, with present strain rates on the order of 1 nanostrain yr^{-1}. The Cape Town region exhibits a slightly higher strain rate, with a north westerly direction relative to the stable Karoo region. However, Malservisi et al. (2013) determined that a significant part of the observed "higher" strain rate may actually be related to human activity such as agriculture and mining or increased noise due to atmospheric water vapour. Based on this analysis, Malservisi et al. (2013) concluded that unless these noise effects can be isolated, they could not definititively estimate small deformations from the GPS data that arise from tectonic processes within the Western Cape.

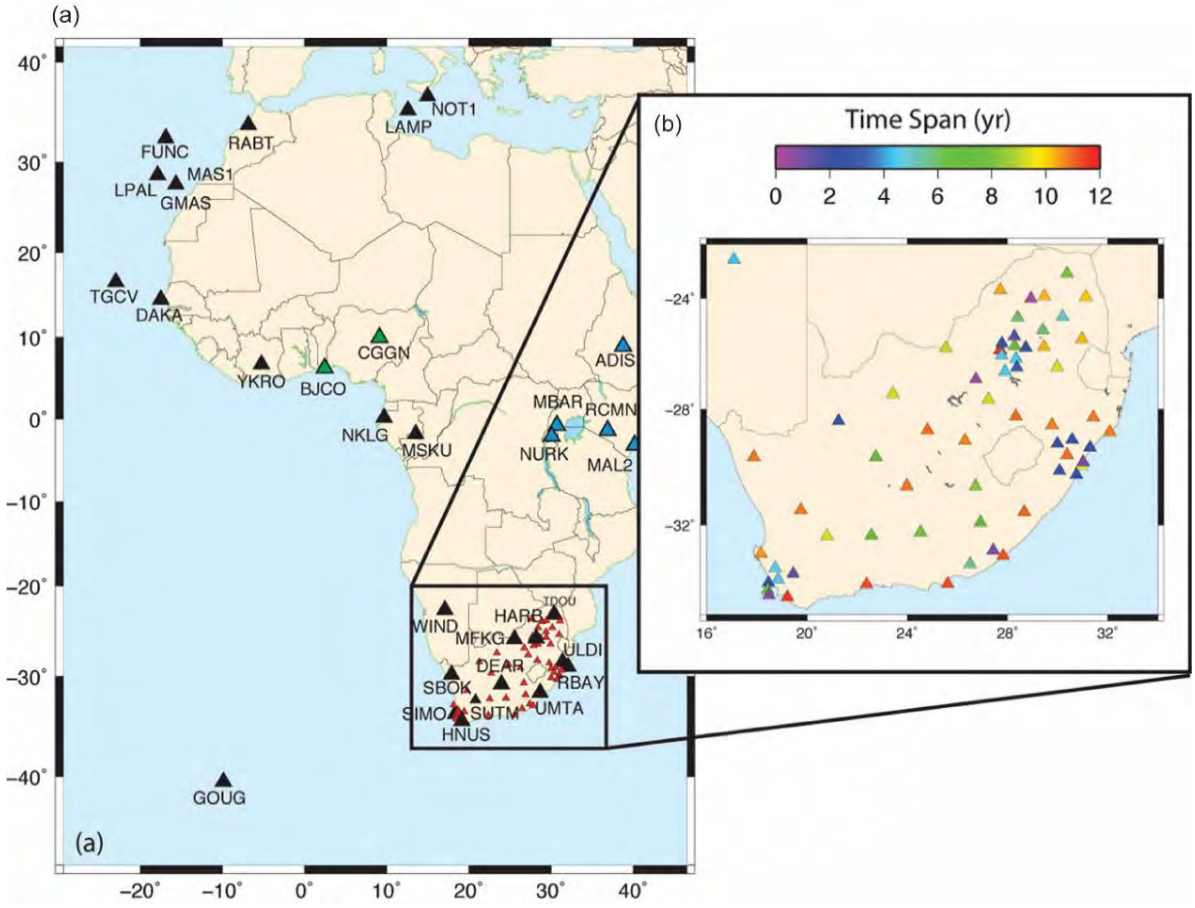

Figure 4-10. IGS and TrigNet stations used in the analysis provided in Malservisi et al. (2013), reprinted from Figure 2 of Malservisi et al. (2013). (a) The black triangles show IGS Nubia Plate sites, green triangles show sites with short time series, blue triangles show Somalia Plate or plate boundary sites, and red triangles show TrigNet sites. (b) Trignet sites colour coded by the time span of the data processed.

In September 2022, researchers from Cape Town and Universität München published a preliminary report (Abolghasem et al., 2022) using data from the GNSS study that intends to update the work from Malservisi et al. (2013). Their preliminary observations are: "*predominantly strike-slip strain rates at the 1-2 ns/yr level, typical of a stable continental region and consistent with the predominantly strike-slip earthquake focal mechanisms observed.*" They show relative velocities of the Western Cape in the 0.1-0.5 mm/yr range (see Figure 6 of their report). However, like Malservisi et al. (2013), these authors caution that a longer time series is needed to characterise the strain rates for the region and reduce noise. Given these conclusions and cautions, the SSM TI Team considered these data in their

development of the SSM, but only to the extent that they confirmed SSM TI Team's assessments of very low slip rates for the Groenhof Fault (Section 8.5.6) and the lack of observed slip and deformation on the regional-scale faults, including the Colenso Fault (Section 8.5.2).

4.2.11 Tectonic stress analysis

The SSM TI Team assessed the potential for fault slip based on an evaluation of tectonic stress data that was conducted within the DDC6 and 7 study on faults (Section 5.2.5) and a separate, independent specialty contractor study conducted by a research team at Southwest Research Institute (SwRI) in San Antonio Texas, in the USA. The goal of both studies was to define the tectonic stress tensor for the Western Cape based on earthquake hypocentre data and borehole breakouts and use that information to identify the most likely style of deformation (horizontal shear, extension, or compression) and the associated faulting regimes (strike-slip, normal, reverse). This leads to the most favourable orientations of fault surfaces that will fail under this tectonic stress.

The SSM TI Team considered several sources of information regarding the stress state of the Western Cape. These included the presentation at WS2 from Dr Andreoli and the references therein as well as published papers suggested to the SSM TI Team by the PPRP. These included Viola et al. (2005, 2012), Bird et al. (2006), White et al. (2009), Logue (2012), Hodge (2013), Paton (2022), Andreoli et al. (1996), and Andreoli (2012). In discussions with our specialty contractors at SwRI, the SSM TI Team decided that the earthquake focal mechanisms from the earthquake catalogue were the most reliable indicators of the stress state because they are the most direct representations of stress and the boreholes that were used by the specialty contractor were all in the Western Cape. The stress analysis performed by SwRI was based on these focal mechanisms. All other information regarding the stress state was considered by the SSM TI Team to be supporting information of the primary stress analysis. In a similar way, the borehole-breakout-based SHmax orientations from the World Stress Map database were not used directly by Smart et al. (2023) in their stress state determination. Rather, the borehole-breakout-based SHmax orientations were qualitatively compared to the 3DStress™-inversion-based maximum principal stress orientation (NW-SE trend) and shown to be generally compatible.

An intricate array of bedrock faults is mapped across the Western Cape. These faults were produced by the long and complex tectonic deformation of South Africa. This is especially evident in the syntaxis, which is characterised by two or three sets of fault orientations (Figure 4-11). However, not all these faults may be favourably oriented for future fault rupture given the present stress conditions. To assess which of the existing faults are most likely to reactivate, the SwRI team conducted a 3DStress analysis (McFarland et al., 2012; Morris et al., 2013) for the Western Cape region. The 3DStress code includes a patented stress inversion technique that can be used to estimate the stress states based on fault orientations and seismic moments, and then assess which faults are most likely to rupture (reactivate) in this stress state using the slip tendency analysis of Morris et al. (1996).

Fault displacement can be defined in terms of net slip measured paralleled to the fault plane, the horizontal component (heave), or as the vertical component of slip (throw). As an alternative, the fault area or earthquake magnitude can be scaled to slip using magnitude area or magnitude-displacements scaling relationship (Morris et al., 2016). The stress state

solutions are derived from inversion of earthquake events (strike, dip, seismic moment) that are within ~200 km of the Duynefontyn site. Slip tendency (T_S) is the ratio of shear stress (τ) to normal stress (σ_n) on a fault surface, as defined in equation 4-1 (Morris et al., 1996).

4-1

$$T_S = \tau / \sigma_n$$

For the 3DStress-based stress inversion analysis, SwRI staff used six earthquake focal mechanism solutions within approximately 200 km of the Duynefontyn site, including the selected nodal plane orientation and magnitude of each earthquake. To provide qualitative verification of the stress inversion results, SwRI staff considered maximum horizontal stress azimuth data from the World Stress Map database release in 2016 (Heidbach et al., 2016, 2018) that included both onshore earthquake-based orientations and offshore borehole-breakout-based orientations. This slip tendency analysis was used by the SSM TI Team to inform their assessment of seismogenic probability (p[S]) of active faults and to assign the range of fault orientations that were replicated in the virtual fault generator used to model faulting in the source zones nearest to the site, as described in Section 8.2.6.

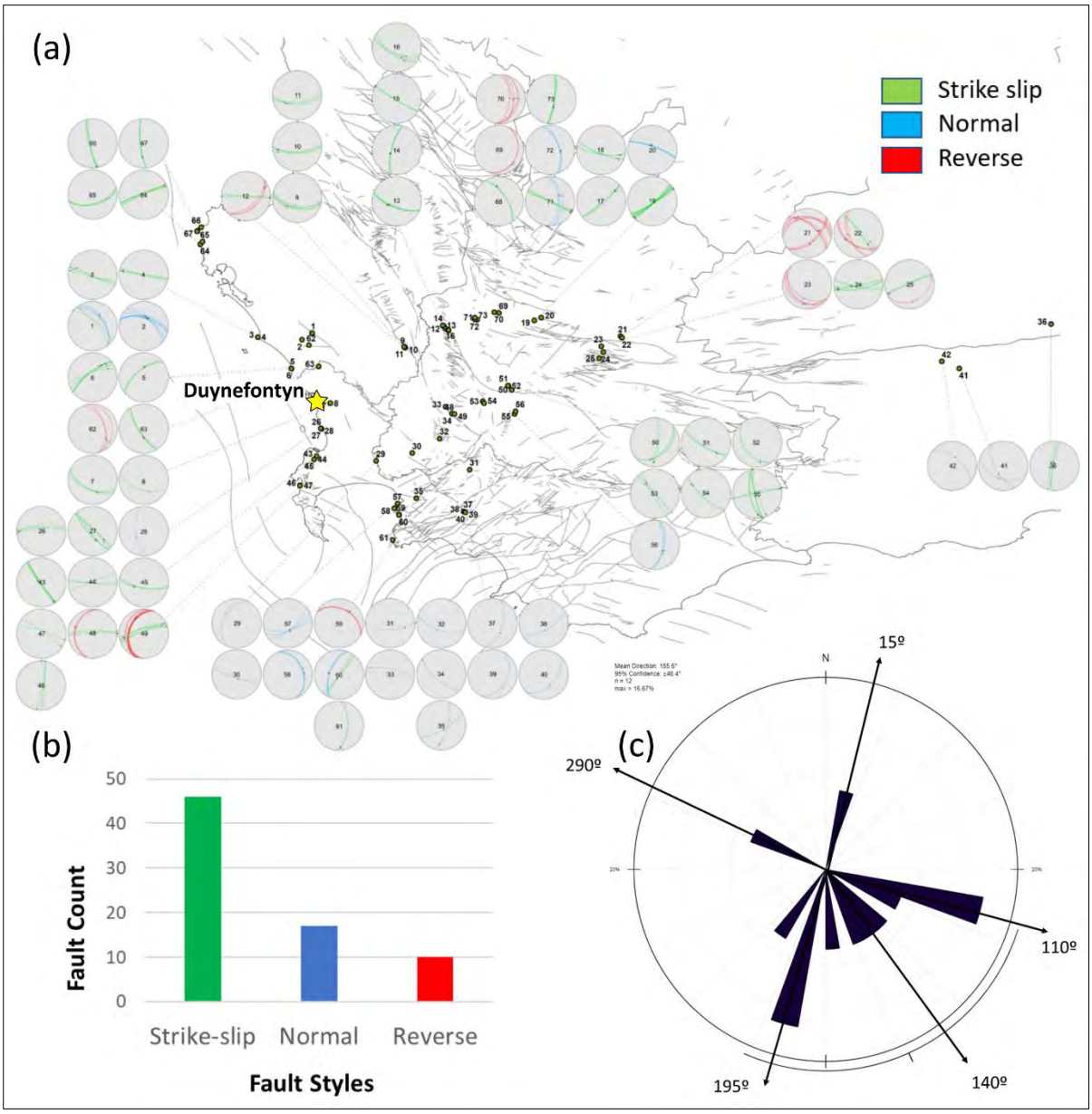

Figure 4-11. Mapped bedrock faults in the Western Cape compiled by CGS geologists and presented to the SSM TI Team at Workshop 1. In (a), stereonet plots show the style and orientation of each measure bedrock fault. The colour coding indicated the style of faulting, strike-slip (green), normal (blue), and reverse (red). (b) A histogram plot shows the number of each style of fault in (a). (c) A rose diagram showing the distribution of fault orientations in (a).

4.3 HISTORICAL SEISMICITY

The DDC4 report by Albini and Flint (2023) examined historical seismicity in the Western Cape region. It included characterisation of identified historical earthquakes and observations of the effects of these earthquakes that were obtained from various historical documents including newspapers and logs. They also went on to determine intensity data points (IDPs) using the compiled observations. There are 74 earthquakes evaluated in the report (Table 4-2), with an emphasis on the three largest earthquakes that occurred on 4 December 1809, 14 August 1857, and 29 September 1969.

Table 4-2. List of 74 reported events analysed and reported on by Albini and Flint (2023).

Year	Month	Day	Time local (SAST)	Area or Place Most Affected	Type	No. IDPs	Imax (MMI-56)	Newly Retr.
1620	Apr	7		Table Bay/ Robben Island	False			
1643	Apr	12		Cape Town, False Bay	False			
1690				Cape Town	Solitary	1	2–3	1 2
1693	Jun	3 to 5		Rockfall, Table Mountain	Confirmed			
1695	July			Rockfall, Table Mountain	False			
1695	Sep	4	18:00 to 19:00	Cape Town and neighbourhood	Solitary	1	4	
1696	Jan	11	14:00	Cape Town	Solitary	1	2–3	
1699	Oct	16		Rockfall, Table Mountain	Confirmed			
1739	Sep	5	2:00	Cape Town	Solitary	1	2–3	
1749	Aug	27	dawn	Cape Town	Solitary	1	2–3	
1760	May	27		Rockfall, Table Valley	Unverified			
1766	Jul	14	2:00	Cape Town	Solitary	1	3	
1801	Dec	8	10:00	Rockfall, Table Mountain	Confirmed			
1806	Jan	25	evening	Griquatown/ Griekwastad or Klaarwater	Solitary	1	3	
1809	Dec	4	22:10	"Cape Colony"	Multiple	13	7	
1810	Jan	23	3:45	Cape Town	Multiple	3	3	NR
1810	Jan	29	7:45	Cape Town	Multiple	3	3	
1810	Feb	5	1:00	Cape Town	Solitary	1	2–3	NR
1810	Apr	11	3:00	Cape Town	Solitary	1	3	
1810	Dec	12		Genadendal	False			
1810	Dec	26		Genadendal	Unverified			
1811	Jan	2		Cape Town	False			
1811	Jan	7	6:00	Cape Town	Solitary	1	3	
1811	Jun	2		Cape Town	False			

Year	Month	Day	Time local (SAST)	Area or Place Most Affected	Type	No. IDPs	Imax (MMI-56)	Newly Retr.
1811	Jun	10		Cape Town	False			
1811	Jun	7	12:00	Rietvlei	Multiple	4	6	
1811	Jun	19	10:00	Rietvlei	Multiple	4	6	
1813	Sep	12	2:00 to 3:00	Genadendal	Solitary	1	3	NR
1814	July	18	22:00	Mamre	Solitary	1	3	NR
1819	April	14	5:00	Leliefontein	False			
1819	Jun	24		Piketberg	Unverified			
1819	Jun/ Jul	30	5:00	Leliefontein	Solitary	1	3 4	
1826				Saldanha Bay	Unverified			
1826	Apr	14	7:00	Cape Town	Solitary	1	3	
1830				Rockfall, Table Mountain	Confirmed			
1835	Nov	11	3:48	Cape Town	Multiple	4	3	
1842	Mar	22	16:00	Cape Town	Solitary	1	3	NR
1844	Jan	23	14:00 to 15:00	Cape Town	Solitary	1	3	NR
1852	Nov	12	9:00 to 10:00	Western Cape	Multiple	8	3	NR
1857	Aug	14	23:30	Western Cape	Multiple	38	5–6	
1862	Jun	23	2:00	Cape Town	Multiple	3	4	
1864	Feb	24	1:20	Knysna	Multiple	4	4	
1868	Oct	8	4:20	George	Multiple	3	4–5	(NR)
1869	Oct	31		Cape Town	False			
1869	Nov	23	19:50	Riethuis, NC	Multiple	3	4	
1874	Feb	26	2:30	Namaqualand, NC	Solitary			NR
1875	Oct	30	23:00 to 24:00	Rondebosch	Solitary	1	3	NR
1880	Jul	16	12:30	Darling	Multiple	6	4–5	NR
1882	Apr	28	1:15	Springbok, NC	Multiple	4	4	
1885	May	10	23:41	South western Cape	Multiple	10	4	
1887	Mar	4	morning	Cape Town	Solitary	1	3	NR
1894	Dec	13	11:00	Darling	Multiple	2	3–4	NR
1899	Aug	9		The Towers, near Darling	Solitary	1	3	NR
1899	Sep	15	12:23	Cape Town	Multiple	19	5	
1901	Mar	24	16:42	Bishop's Court	Solitary	1	3	NR

Year	Month	Day	Time local (SAST)	Area or Place Most Affected	Type	No. IDPs	Imax (MMI-56)	Newly Retr.
1901	Apr	24		The Towers, Darling	Solitary	1	3	NR
1902	May	28		Cape Town	False			
1903	Jan	27	3:30	Tokai	Solitary	1	3	NR
1903	Jul	9		Cape Town	Multiple	7	3	
1903	Jul	10	3:00	Green Point	Solitary	1	3	NR
1909	Dec	9	16:22	Blaauwberg	Solitary	1		NR
1909	Dec	9	19:20	Worcester	Multiple	7	4	NR
1910	Feb	19	7:30	Montagu	Solitary	1	3	NR
1921	Oct	9	15:20	Tulbagh	Solitary	1	4	
1922	Jan	4	1:10	Tulbagh	Solitary	1	3	NR
1932	Nov	28	night	Moorreesburg	Solitary	1	3–4	NR
1940	Oct	11	23:40	Langebaan	Solitary	1	3–4	NR
1941	Oct	24	20:30	Van Rhynsdorp	Solitary	1	3–4	
1952	Feb	26	21:45	Swellendam	Solitary	1	3–4	NR
1960	Aug	29	7:35	Western Cape	Multiple	10	4	
1963	Aug	27	2:45 to 2:50	Western Cape	Multiple	39	4–5	
1963	Sep	17	1:40 to 6:00	Karoopoort	Solitary	1	3	
1969	Sep	11	23:45	Heidelberg	Multiple	19	5	
1969	Sep	29	22:05	Western Cape	Multiple	57	8–9	

Notes: IDP – Intensity Data Point; MMI 56 – Modified Mercalli Intensity scale; Newly Retr. (NR) – Indicates record was retrieved as part of DDC4.

The spatial distribution and quality of IDPs in any region is dependent on the spatial and temporal and spatial evolution of towns, cities, settlements, farms and population (especially for historical IDPs). It must be noted that earthquakes are usually limited in the geographical area over which shaking was experienced. This is clearly seen in the number and distribution of IDPs of events in the SW Cape Province as reported by Albini and Flint (2023). The growth of settlements in the province from Cape Town going inland with time is reflected by earthquakes felt mostly in the Cape Town in the Seventeenth Century with the number of earthquakes felt inland as immigrants moved further inland with time. A more detailed review of the temporal evolution of IDPs in the SW Cape Province was reported by Albini and Flint (2023).

Of the 74 events, Albini and Flint (2023) identified 14 to be false or unverified events. They were identified as fake events because they lacked any verifiable intensity observations. It appears original assessments had misinterpreted the observations as signs of an earthquake. Detailed information explaining how these events came to be reclassified as false events was given by Albini and Flint (2023). They also identified 25 newly recognized events that were not included in any previous catalogue. Thirty-three events had a single observation each resulting

in a single IDP for each event. Twenty-three events were each characterised by at least 2 IDPs. The 29 September 1969 earthquake at Ceres had 57 IDPs, the largest number of IDPs in the list. Albini and Flint (2023) did not extend their analysis to determine the location of the epicentre or estimate the moment magnitude of the events. However, in this study, an effort was made to determine the source parameters for those events with an adequate number of IDPs that also had a good spatial distribution.

The SSM TI Team made use of methods that are based on interpreting the spatial distribution and value of observed intensities to determine the epicentres and magnitudes of the events in Table 4-3. Usually, three levels of methods where macroseismic information is used to estimate earthquake source parameters are used. These methods differ according to the complexity and reliability of their application. They are classified under 1st, 2nd and 3rd generation techniques. Of these, the 3rd generation technique is used where a good spatial distribution and number of IDPs is available (Manzunzu et al., 2023). In this study the historical earthquakes assessment by the SSM TI Team was carried out using the 3rd generation methods that are included in the MEEP2 software (Musson, 2009). In the process, they utilize IDPs that are evenly distributed for location and magnitude determination (Musson, 2009). There are four methods that are implemented in the MEEP2 software (Musson, 2009; Musson and Jiménez, 2008). These methods include the Macroseismic Estimation of Earthquake Parameters (MEEP) by Musson (2009), the Bakun and Wentworth (1997) approach as initially described by Peruzza (1992), the Centroid method (BOXER) of Gasperini et al. (1999) and the Pairwise comparison of IDPs method presented by Vladimir Shumila at the ESC General Assembly in Athens, 1994, but was never published,□□ According to Musson (2009) he was personnally informed by Shumila, that all the files linked to his method were lost. As a result, Musson (2009) reconstructed a simplified version of the method (Musson and Jiménez, 2008, Musson 2009).

The four methods use the individual IDPs to compute the epicentral location of the earthquake without computing the isoseismal lines. This is achieved through either the Centroid method (Gasperini et al., 1999) or the use of an empirical attenuation equation which assumes a function of distance that the IDPs follow and then applies a grid search to an area where each IDP must follow the attenuation equation (Kövesligethy, 1906; Bakun and Wentworth, 1997; Musson and Jiménez, 2008). Moment magnitude is determined according to a procedure prepared by Frankel (1994) and reported by Musson (2009) used for comparison purposes relative to the other historical events. For the project catalogues, the SSM TI team derived independent estimates of magnitude for all catalogue entries. The methodology of those independent estimates is described in Section 6.6.

The major advantage of the four techniques implemented in the MEEP2 software is that they use individual IDPs directly to compute the source parameters instead of converting them into isoseismals first. This has the advantage of removing outliers and wrong IDPs to constrain the final solution. These methods are computationally different, and they generally yield comparable results (e.g., Strasser et al., 2015; Albini et al., 2014) especially with well distributed IDPs. The SSM TI Team analysed the historical earthquakes with sufficient spatial coverage and number of IDPs using the MEEP2 software. Most of the analysis involved carefully summarising the observed IDPs and then using them to determine the earthquake source parameters (e.g., epicentre and magnitude). This was mainly done for those events without instrument solutions.

For each event, the epicentres and magnitudes obtained from each of the different methods were combined by the SSM TI Team to obtain the best estimate values using assigned event specific weights for each method. The weighing scheme that is provided in each of the TI Team's analysis for each earthquake was based on individual epicentre and magnitude error values for each method. The method that produced a solution with the lowest error was given the highest weight by the SSM TI Team. It should be noted that this process results in the weights assigned to each method fluctuating considerably from one earthquake to another.

Linking the assignment of weights to the errors of the locations reduces the subjectivity that is normally associated with such an exercise. The combined solution obtained using this method is selected as the preferred solution for each event except where instrumental solutions are available. Also included in Table 4-5 to Table 4-14 the published solution for each event as reflected in the CGS database (i.e. written as CGS Solution in tables). A bootstrap resampling routine was employed by the SSM TI Team to compute an uncertainty on all parameters. This involved repeating the calculations for source parameters 1,000 times using random resamples. From the 1,000 estimates of each parameter, a standard deviation is calculated from which root-mean-square (RMS) values are determined and are referred to here as the error. The error values vary for each earthquake depending on the number and distribution of the IDPs. The actual values of the weights assigned are different for each event but are consistent in that high values are assigned for solutions with low errors.

Table 4-3. Historical earthquakes assessed by the SSM TI Team using the MEEP2 software.

No.	Earthquake	Number of IDPs
1	04 December 1809	13
2	14 August 1857	38
3	10 May 1885	10
4	15 September 1899	19
5	9 July 1903	7
6	9 December 1909	8
7	29 August 1960	10
8	27 August 1963	39
9	11 September 1969	19
10	29 September 1969	57

Solutions determined using these methods by the SSM TI Team depend on the spatial distribution of IDPs. Generally, IDPs with the highest intensity values are modelled first and the rest are added in descending order. In this regard, the reliability of the final solution depends on the distribution of intensities of different values. For example, an earthquake with 10 IDPs where three have intensity of VI, five intensity values of V, and two with intensity values of IV, will yield reliable estimates of source parameters compared to another event with 10 IDPs all with intensity values of IV. This is because the basic assumption is that the

epicentral location is close to the IDP with the highest intensity (Musson, 2009). Different intensity values will generally show attenuation from high intensities closer to the epicentral areas to low intensities farther away.

4.3.1 The 4 December 1809 earthquake

In their study of this earthquake, Albini and Flint (2023) focused on retrieving as many contemporary and independent first-hand sources as possible to determine the maximum number of IDPs for the event. Thirty-three observations were obtained and used to determine the 12 IDPs shown in Figure 4-12. Albini and Flint (2023) also obtained observations of liquefaction (Table 4-4) that were linked to the earthquake.

There were reliable reports of many aftershocks of this event in the region. However, the SSM TI Team was not able to find any reliable locations of the main event and its aftershocks apart from the general region of the Cape Colony. Albini and Flint (2023) also did not give an estimate for the location of the event.

However, an existing location was given by Brandt et al. (2005). It was relocated to near Cape Town based on reports by Von Buchonroder (1830) of fissures at Jan Biesjes Kraal and sand boils near Blaauwberg's Valley (near present day Milnerton) Using the program MEEP2 (Musson, 2009; Musson and Jimenez, 2008), the SSM TI Team estimated an alternative location using the spatial distribution of the IDP that were estimated for this event. The solutions obtained are shown in Table 4-5 and Figure 4-13. The Bakun and Wentworth solution had a large location error value and thus it was not used in the calculation of the combined solution as shown by the assigned weight of zero (Table 4-5).

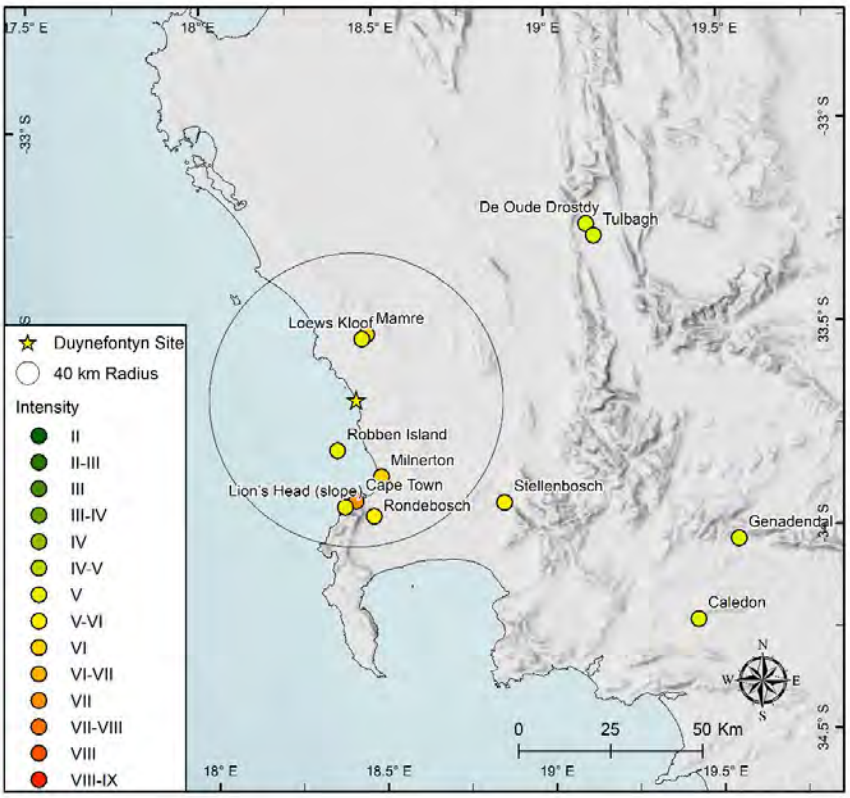

Figure 4-12. Distribution of Intensity Data Points in the Modified Mercalli Intensity (MMI-56) scale (Richter, 1958) for the 4 December 1809 earthquake.

Table 4-4. Liquefaction effects observed during and after the 4 December 1809 earthquake.

Observed at	Kuester, 1809 Dec 5 Kuester and Kuehnel, 1809 Dec 5	von Buchenroder, 1809 Dec 9
On the road between Mamre (Gruenekloof) and Cape Town Blauweberg's Valley Blaauwberg	On the 5th [Dec], we left Gruenekloof [Mamre] for Cape Town. On the road we saw many singular appearances, occasioned by the earthquake. In some places there were chasms in the ground, into which we could put our hands. In others, fountains had burst forth, where formerly no water had been found and they also threw up quantities of white sand.	At Blauweberg's Valley, I found the sandy surface studded with innumerable holes, resembling in shape, but in nothing else, craters in miniature. These holes were from six inches to a foot and a half, and some even three feet in diameter, and from four inches to a foot and a half deep; of a circular form, and the sides sloping to the centre. They were lined with a crust of bluish clay, of about a quarter of an inch in thickness, which had been baked by the sun, and according to its nature had cracked and curled up in fragments, which however adhered still to the sloping sides of the holes. I reckoned seven of these holes, of different dimensions, in an area, contained within a circle, which I drew around me with a walking stick, and which might have been somewhat more than ten feet in diameter. The people at Blauweberg's Valley, stated, that "they saw jets of coloured water spout from these holes to the height of six feet, in the night of the 4th of December, at the time that the shocks were felt"
Jan Biesjes (Beesjes) Kraal Milnerton	On the following day [5 Dec], towards evening, we set off in company with Brother Schmitt and his wife, for Cape Town. On the road we beheld with surprize [*sic*] the effects of the earthquake at a farm, where no less than twelve fountains had burst forth, and brought up water, and a quantity of white sand from a great depth. The nearer we approached to the Cape, the more accounts we heard of the mischief done.	Near the Kraal I found rents and fissures in the ground, one of which I followed for about the extent of a mile. In some places they were more than an inch wide, and in others much less. In many places I was able to push into them, in a perpendicular direction, a switch to its full length, of three or four feet. By the people residing in the vicinity, I was informed, that they had observed these fissures on the morning of 5th December, in some instances three and four inches wide, and that one person had been able to push the whole length of an iron rod used to fix curtains upon into them, and that others had been able to do the same with whip-handles of even ten feet in length.

Table 4-5. The 1809 earthquake locations using the MEEP2 software.

Method	Latitude	Longitude	Location error (± km)	Magnitude, M	Magnitude error, (±)	Depth (km)	Weight of solutions
Centroid	-33.918	18.467	30.9	5.2	0.3	20	0.3
MEEP	-33.899	18.281	26.5	5.5	0.4	20	0.5
Bakun and Wentworth	-35.020	17.586	195.7	6.8	1.1	-	0.0
Pairwise	-33.902	18.641	51.6	5.2	0.3	-	0.2
Combined	**-33.906**	**18.409**	**32.84**	5.3	**0.33**	**20**	**1**
CGS Solution	**-34.0**	**18.400**		6.3			

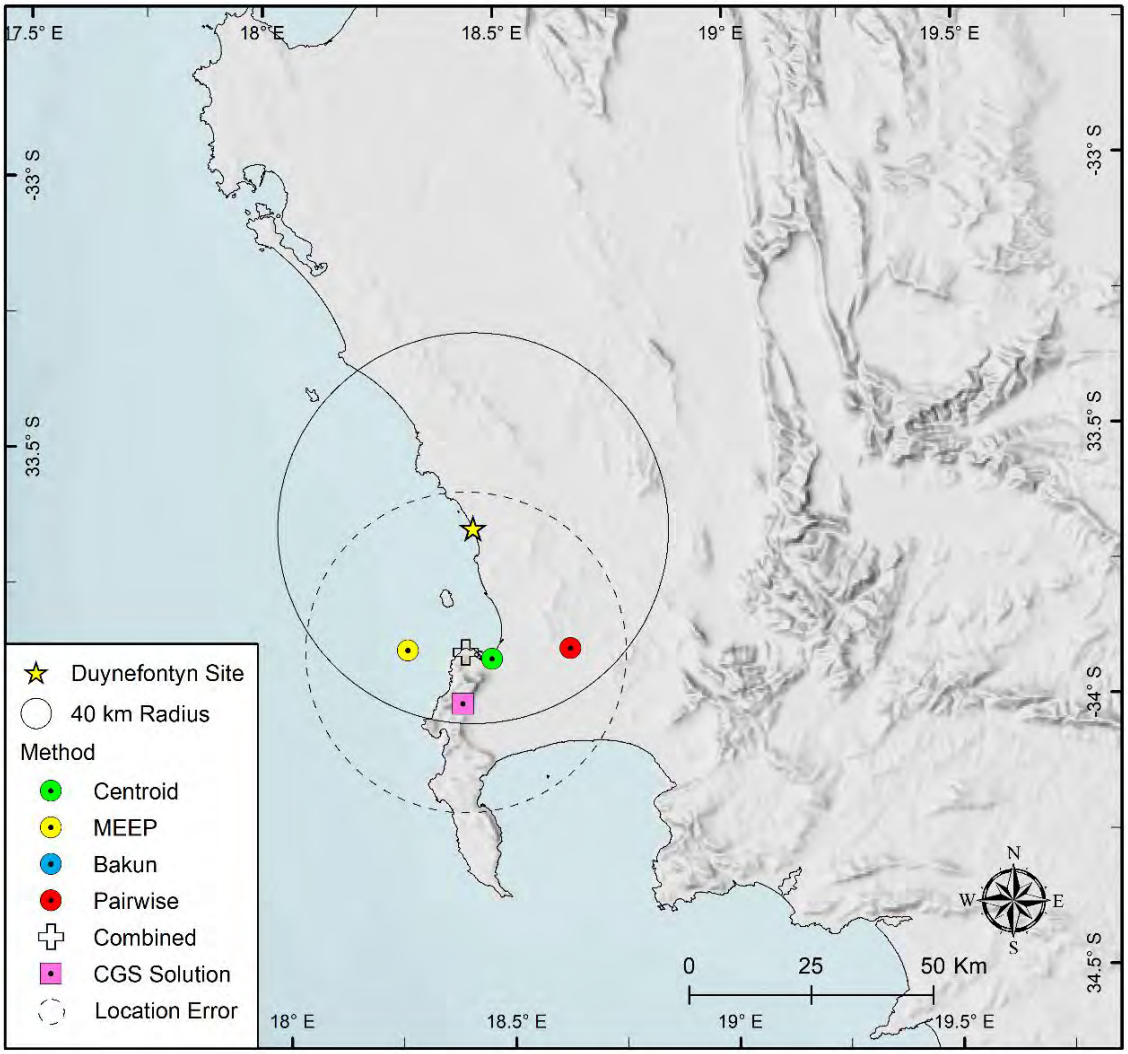

Figure 4-13. Location of epicentral solutions obtained for the 1809 earthquake using intensity data (Figure 4-12) and the MEEP2 software.

4.3.2 The 14 August 1857 earthquake

This event was well recorded with 72 observations used to determine or prepare 38 IDPs (Figure 4-14). However, Albini and Flint (2023) did not give an estimate of the event location and magnitude. The current location of the event is based on intensity data as reported by Brandt et al. (2005) and shown in Table 4-6. Using the program MEEP2 (Musson, 2009; Musson and Jimenez, 2008), the SSM TI Team estimated an alternative location using the spatial distribution of the IDPs that were newly estimated for this event. The obtained solutions are shown in Table 4-6 and Figure 4-15.

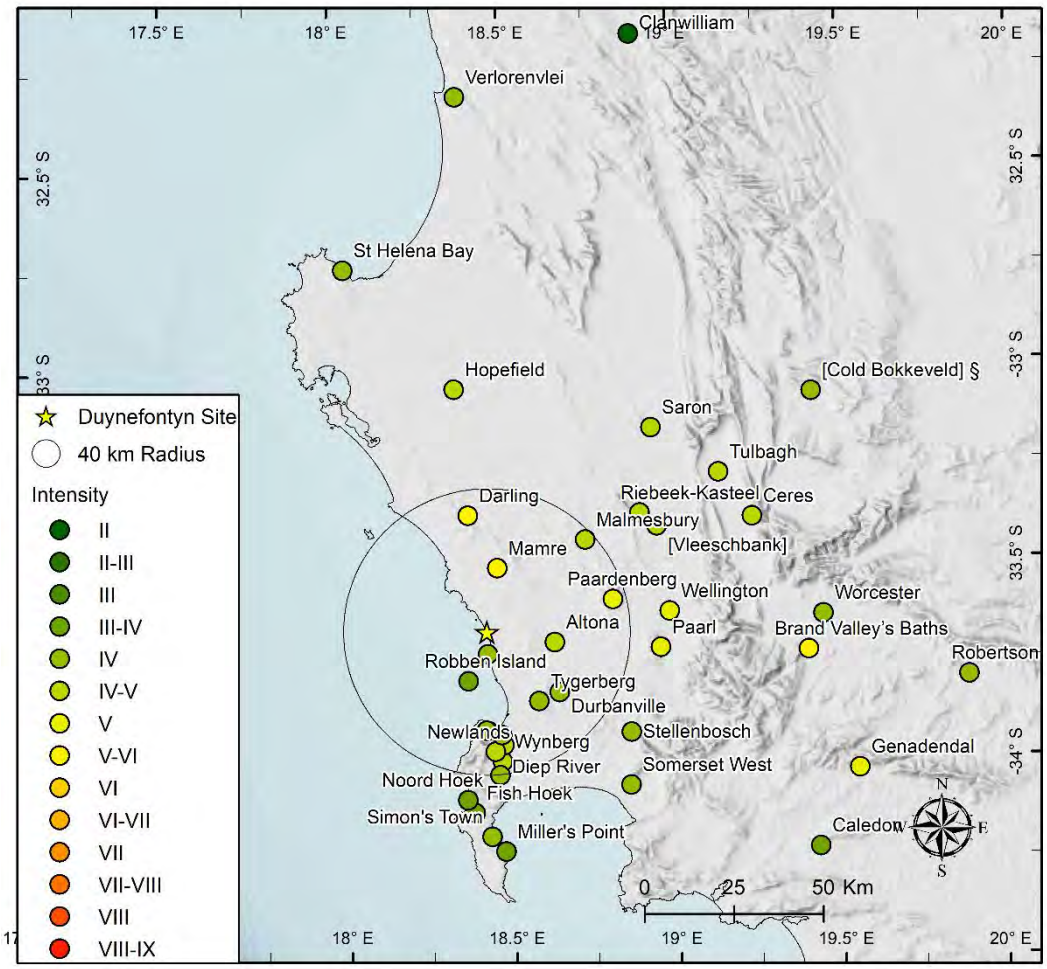

Figure 4-14. Distribution of Intensity Data Points in MMI-56 scale for the earthquake of 14 August 1857.

Table 4-6. The epicentre solutions for the 14 August 1857 earthquake using the MEEP2 software.

Method	Latitude	Longitude	Location error (± km)	Magnitude, M	Magnitude error, (±)	Depth (km)	Weight of solutions
Centroid	-33.643	18.923	22.4	4.1	0.0	20.0	0.4
MEEP	-33.532	18.691	29.5	4.1	0.0	20.0	0.3
Bakun and Wentworth	-33.281	18.534	83.3	4.8	0.3		0.1
Pairwise	-33.316	18.732	55.1	4.1	0.2		0.2
Combined	**-33.508**	**18.776**	**37.2**	4.17	0.1	**20.0**	**1.0**
CGS Solution	-33.500	19.000		5.0			

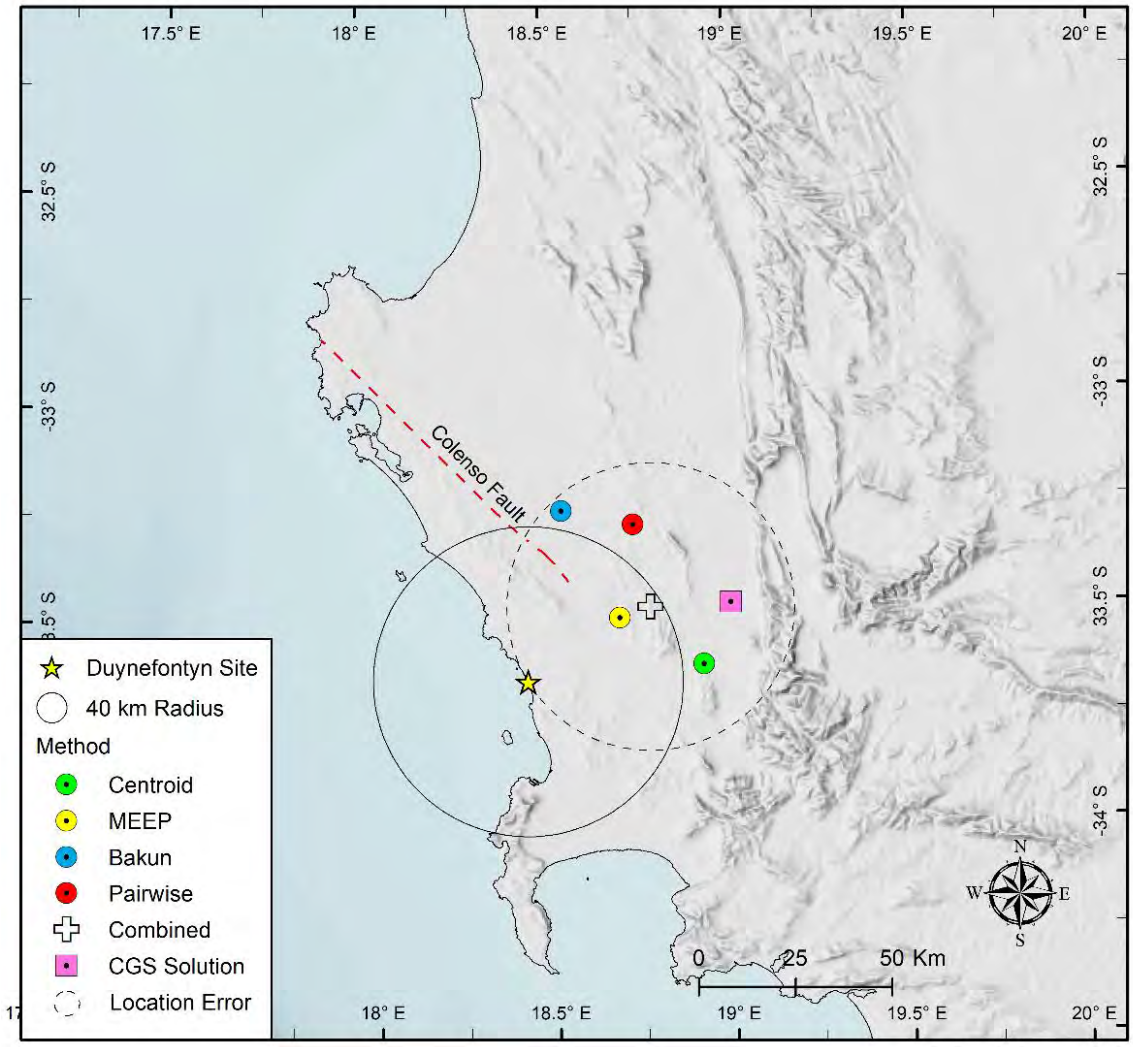

Figure 4-15. Location of epicentral solutions obtained for the 14 August 1857 earthquake using intensity data (Figure 4-14) and the MEEP2 software.

4.3.3 The 10 May 1885 earthquake

Using 14 observations, Albini and Flint (2023) created ten IDPs which showed that the event was mostly felt in the Western Cape Province close to Cape Town (Figure 4-16). The source solutions obtained for this event using the four methods in the MEEP2 software package are all generally in good agreement. To obtain the best and preferred location of the event, the four solutions were combined by the SSM TI Team according to the weight values shown in Table 4-7. The epicentral error of the obtained solution had a radius of 19 km, while the magnitude error was 0.2. The obtained solutions are shown in Table 4-7 and Figure 4-17.

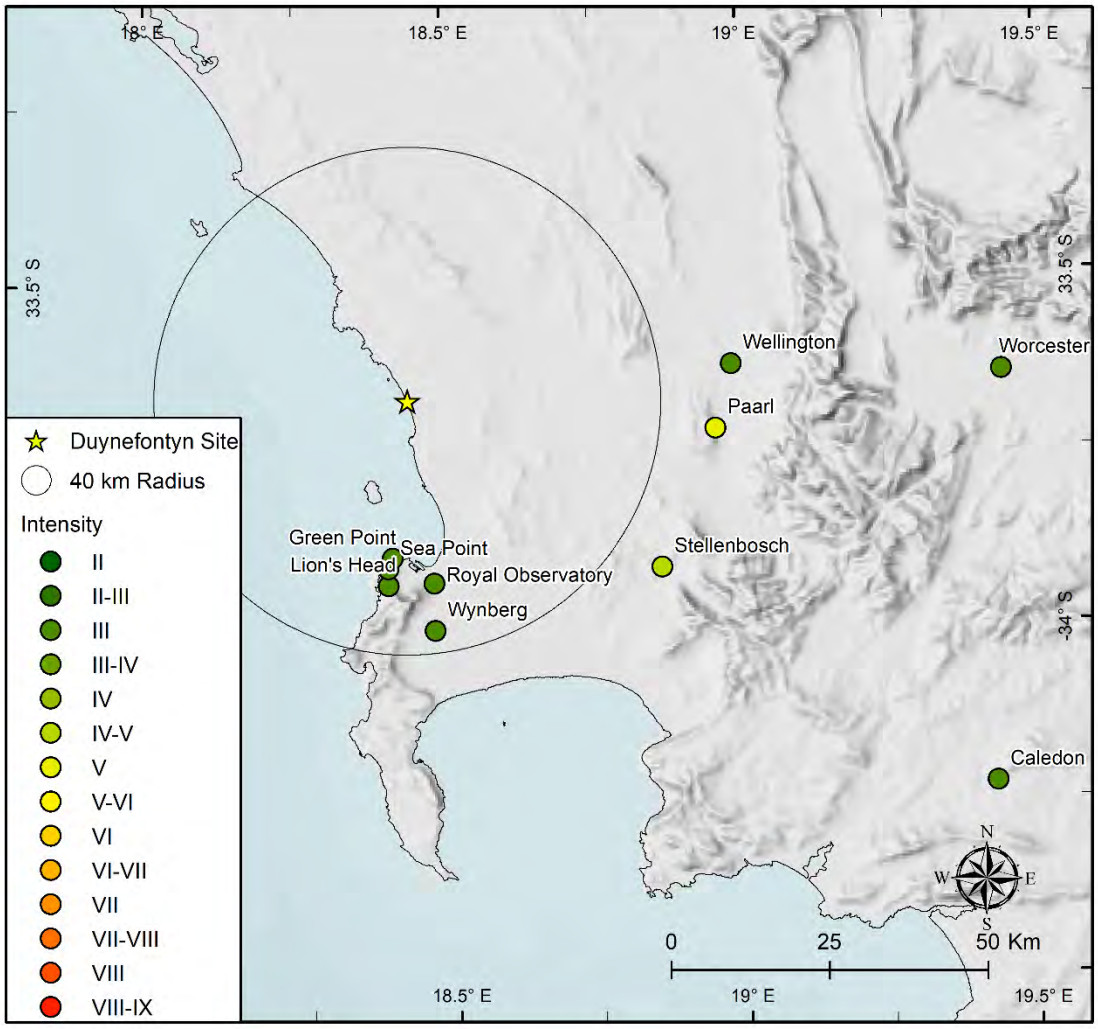

Figure 4-16. Distribution of Intensity Data Points in MMI-56 scale for the 10 May 1885 earthquake.

Table 4-7. The epicentre solutions for the 10 May 1885 earthquake using the MEEP2 software.

Method	Latitude	Long-itude	Location Error (± km)	Magnitude M	Magnitude Error	Depth (km)	Depth Error (± km)	Weight of Solutions
Centroid	-33.872	18.615	14.6	3.7	0.2	20.0	7.0	0.3
MEEP	-33.785	18.941	9.3	3.4	0.1	10.0	4.0	0.3
Bakun and Wentworth	-33.854	18.983	21.8	3.4	0.2			0.2
Pairwise	-33.932	18.74	40.7	3.6	0.2			0.2
Combined	**-33.8543**	**18.811**	**19.7**	**3.5**	0.2	14.0	**5.2**	**1.0**
CGS Solution	-33.900	18.400		3.3				

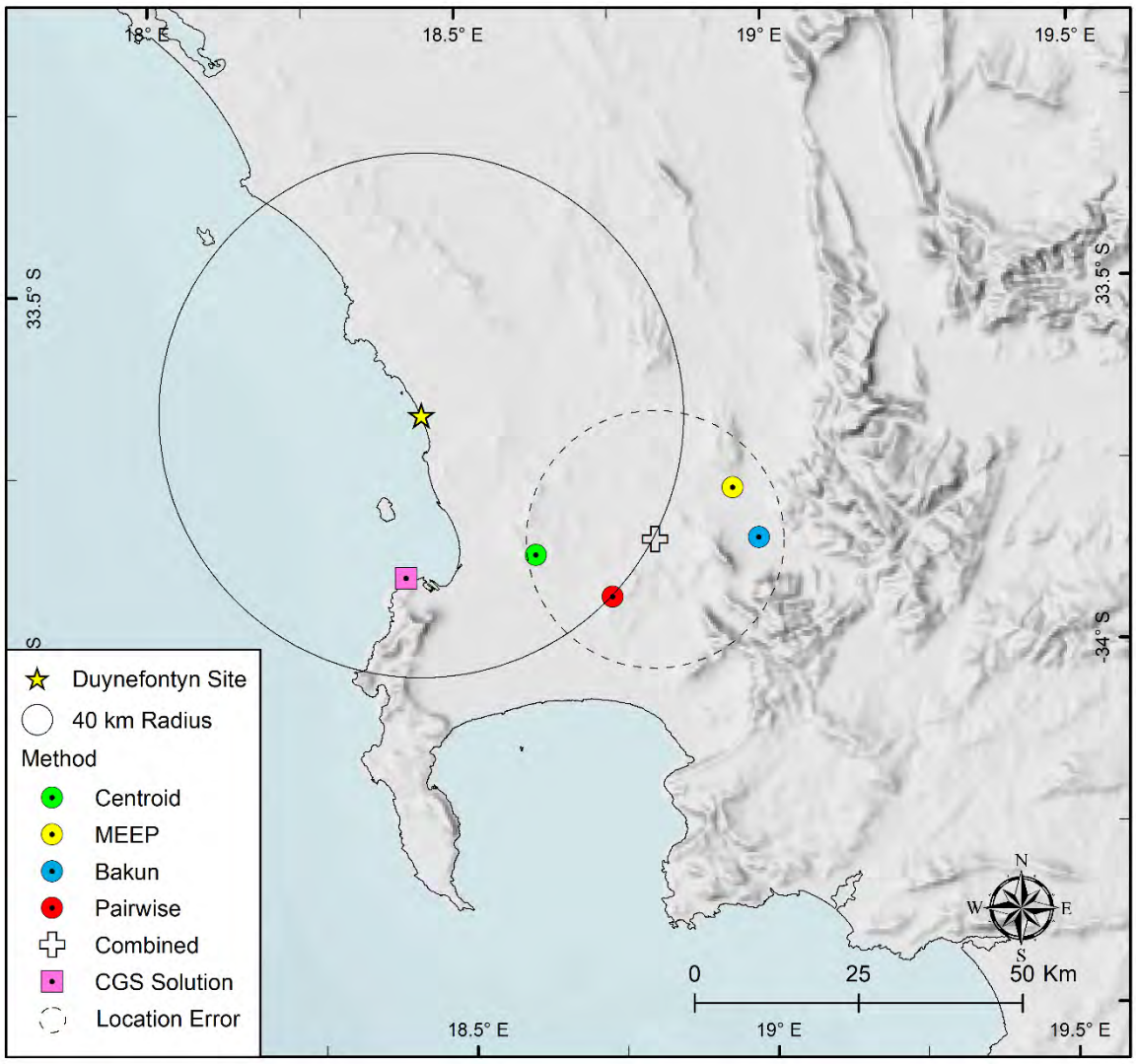

Figure 4-17. Location of epicentral solutions obtained for the 10 May 1885 earthquake using intensity data (Figure 4-16) and the MEEP2 software.

4.3.4 The 15 September 1899 earthquake

Using observation data from newspapers and brief reports from the Meteorological Commission, 19 IDPs were created for this event (Figure 4-18). Using the obtained IDPs and the software MEEP2, the SSM TI Team obtained source parameters for the event (Figure 4-19).

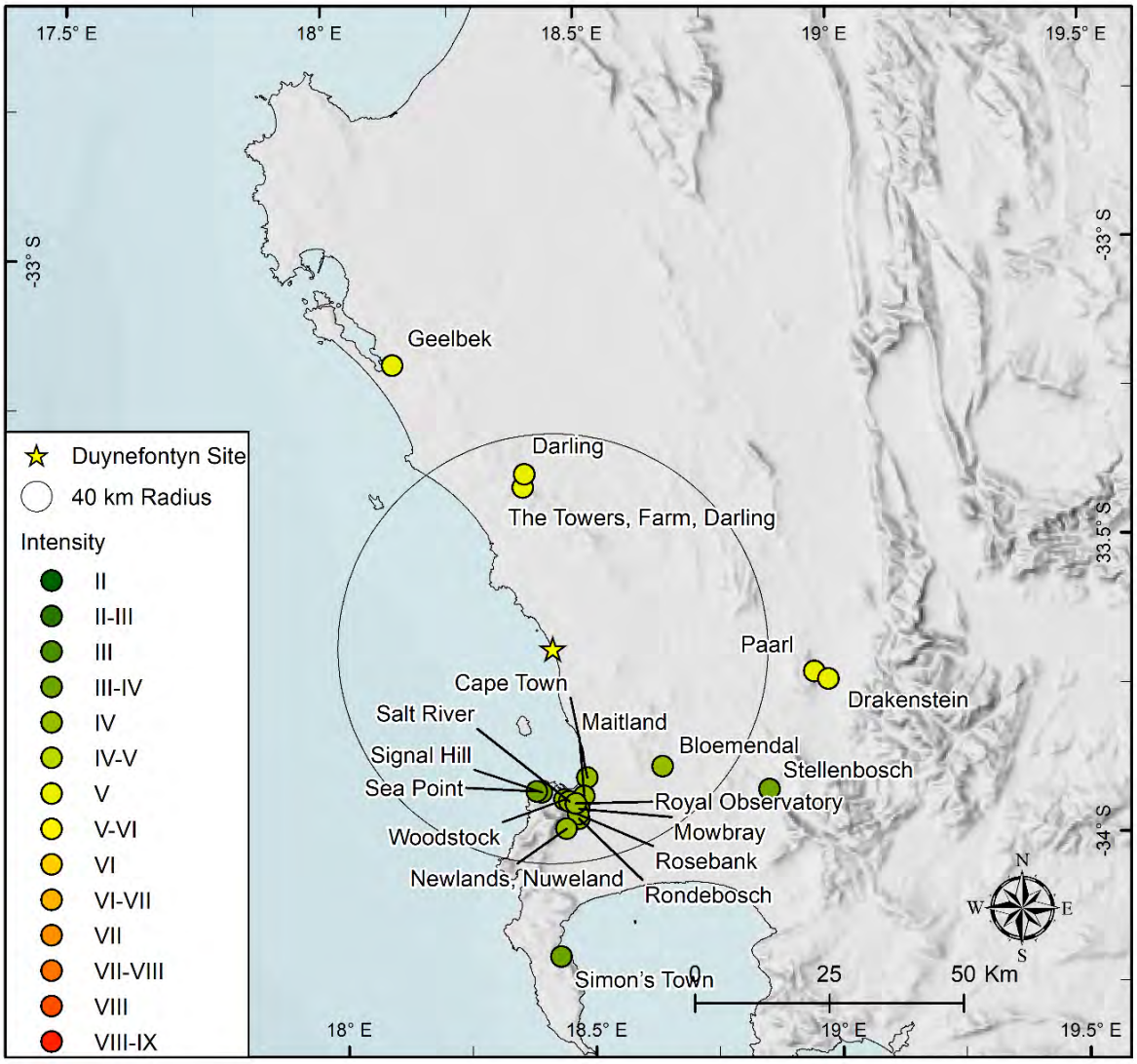

Figure 4-18. Distribution of Intensity Data Points in MMI-56 scale for the 15 September 1899 earthquake.

Though the locations obtained are not too far from each other, the epicentral error for the Bakun and Wentworth solution is quite large at 195 km, especially when compared to values obtained for the other solutions (Table 4-8). Therefore, only the three solutions obtained using the Centroid, MEEP and Pairwise techniques were combined to obtain the combined solution, which was taken as the preferred solution for this event. The SSM TI Team determined a magnitude of **M** = 5.3 with an error of 0.3. The obtained solutions are shown in Table 4-8 and Figure 4-19.

Table 4-8. The epicentre solutions for the 15 September 1899 earthquake using the MEEP2 software.

Method	Latitude	Longitude	Location error (± km)	Magnitude, M	Magnitude error, (±)	Depth (km)	Weight of solutions
Centroid	-33.918	18.467	30.90	5.2	0.3	20.0	0.30
MEEP	-33.899	18.281	26.50	5.5	0.4	20.0	0.50
Bakun and Wentworth	-35.020	17.586	195.70	6.8	1.1		0.00
Pairwise	-33.902	18.641	51.60	5.2	0.3		0.20
Combined	**-33.905**	**18.409**	**32.84**	5.29	0.33	**20.0**	**1**
CGS Solution	-34.000	18.400		6.3			

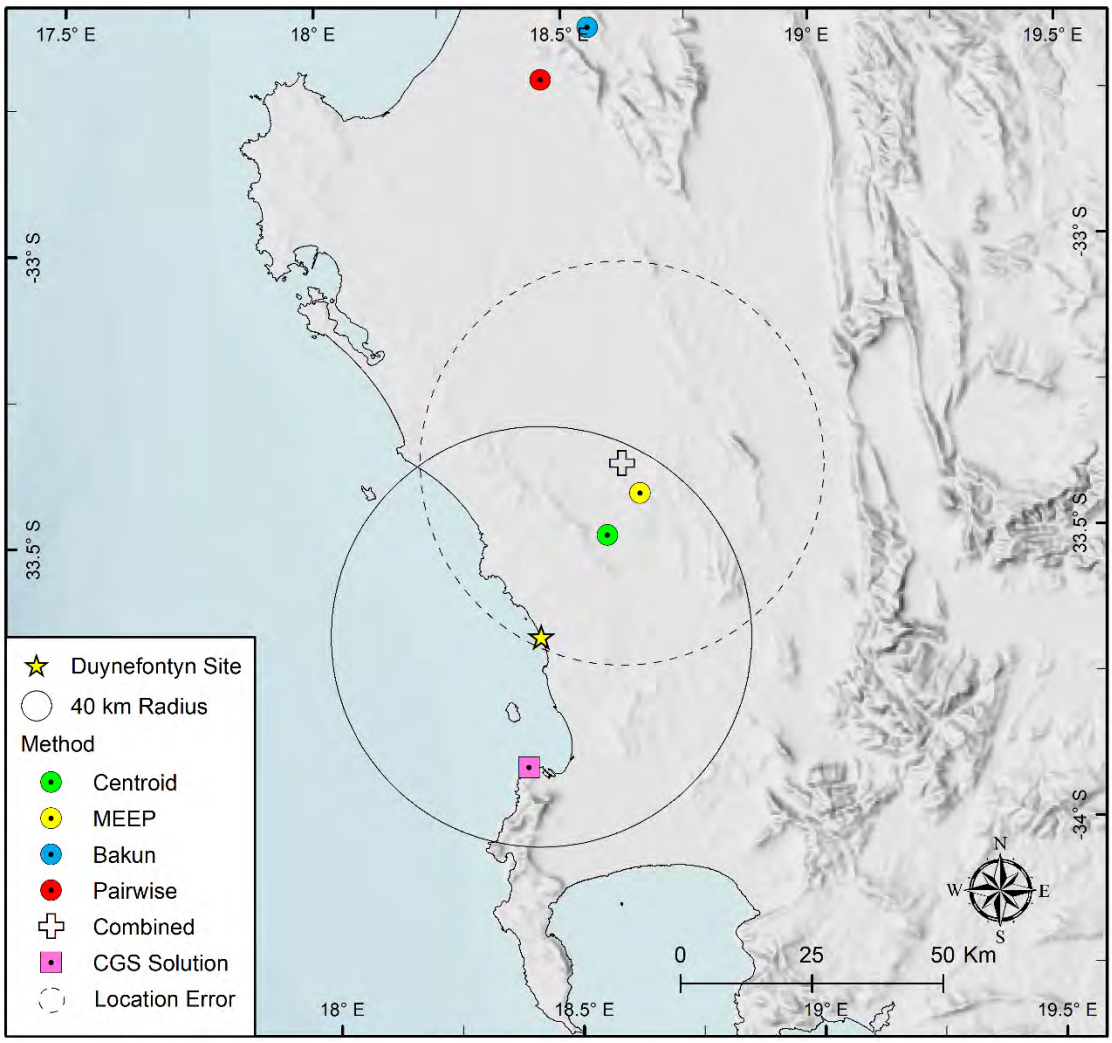

Figure 4-19. Location of epicentral solutions obtained for the 15 September 1899 earthquake using intensity data (Figure 4-18) and the MEEP2 software.

4.3.5 The 9 July 1903 earthquake

Using multiple observations, Albini and Flint (2023) created seven IDPs for the 9 July 1903 earthquake (Figure 4-20). However, all the created IDPs had the same intensity value of III. Normally such a distribution will not yield a reliable estimate of the source parameters (Manzunzu et al., 2023). However, an effort was still made to determine the source parameters (Figure 4-21, Table 4-9) for this event with the compiled IDPs. The preferred solution was obtained by combining the solutions obtained using the Centroid, MEEP and Pairwise methods. The solution obtained using the Bakun method had a large error of 279 km, which was much larger than the other three methods and the Bakun epicentre was located more than 150 km to the east (Figure 4-21). Thus, the SSM TI Team decided not to use the Bakun solution in determining the final solution.

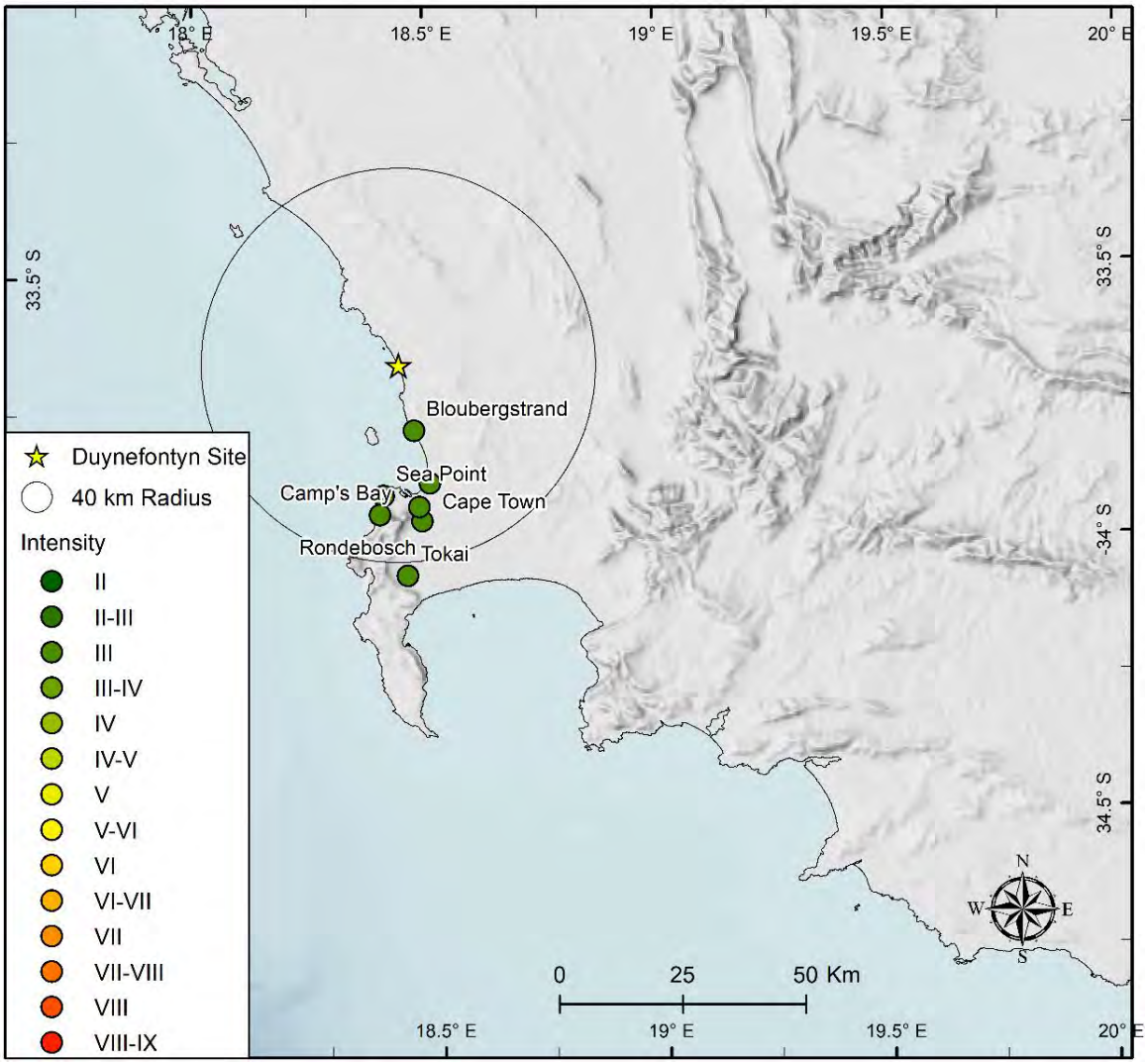

Figure 4-20. Distribution of IDPs in MMI-56 scale for the 9 July 1903 earthquake.

Table 4-9. The epicentre solutions for the 9 July 1903 earthquake using the MEEP2 software.

Method	Latitude	Longitude	Location error (± km)	Magnitude, M	Magnitude error, (±)	Depth (km)	Weight of solutions
Centroid	-33.932	18.443	3.7	3.0	0.0	10.0	0.4
MEEP	-33.923	18.674	26.9	3.0	0.0	10.0	0.2
Bakun and Wentworth	-34.003	19.954	279.4	4.6	0.1		0
Pairwise	-33.932	18.443	3.7	3.0	0.0		0.4
Combined	**-33.9302**	**18.489**	**8.34**	3.2	0.01	**10.0**	**1**
CGS Solution	-33.900	18.400		3.7			

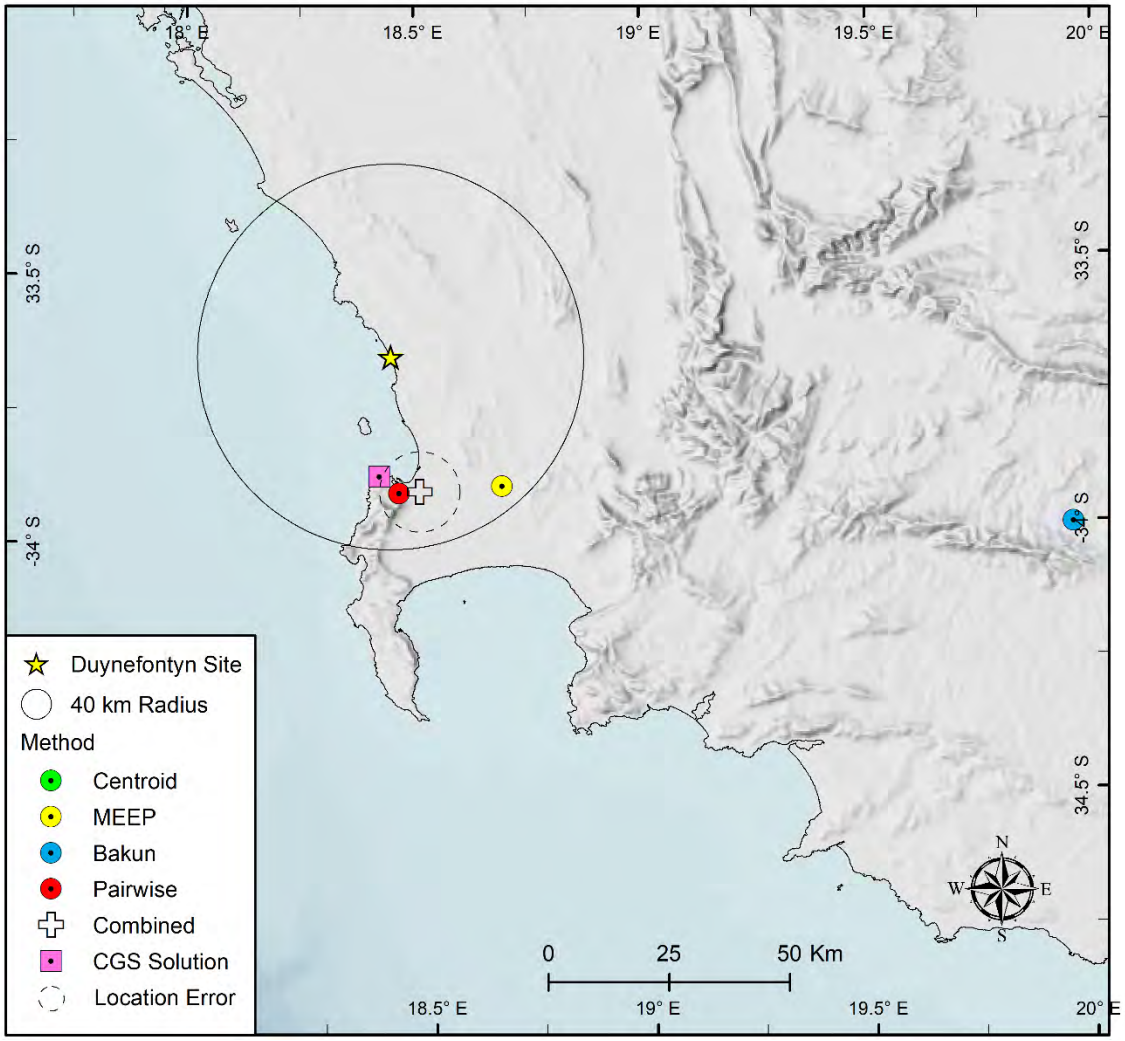

Figure 4-21. Location of epicentral solutions obtained for the 9 July 1903 earthquake using intensity data (Figure 4-20) and the MEEP2 software.

4.3.6 The 9 December 1909 earthquake

Seven IDPs were created by Albini and Flint (2023) using the observations obtained from newspapers and an Agricultural Journal (1909). The IDPs were located in the Western Cape close to Cape Town (Figure 4-22). The epicentre for this event (Figure 4-23) was estimated by the SSM TI Team using the obtained IDPs and the MEEP2 software. As observed with solutions obtained for other events, the Bakun solution had a large epicentral error of about 120 km (Table 4-10) and thus, it was not used by the SSM TI Team in determining the final preferred (combined) solution for this event.

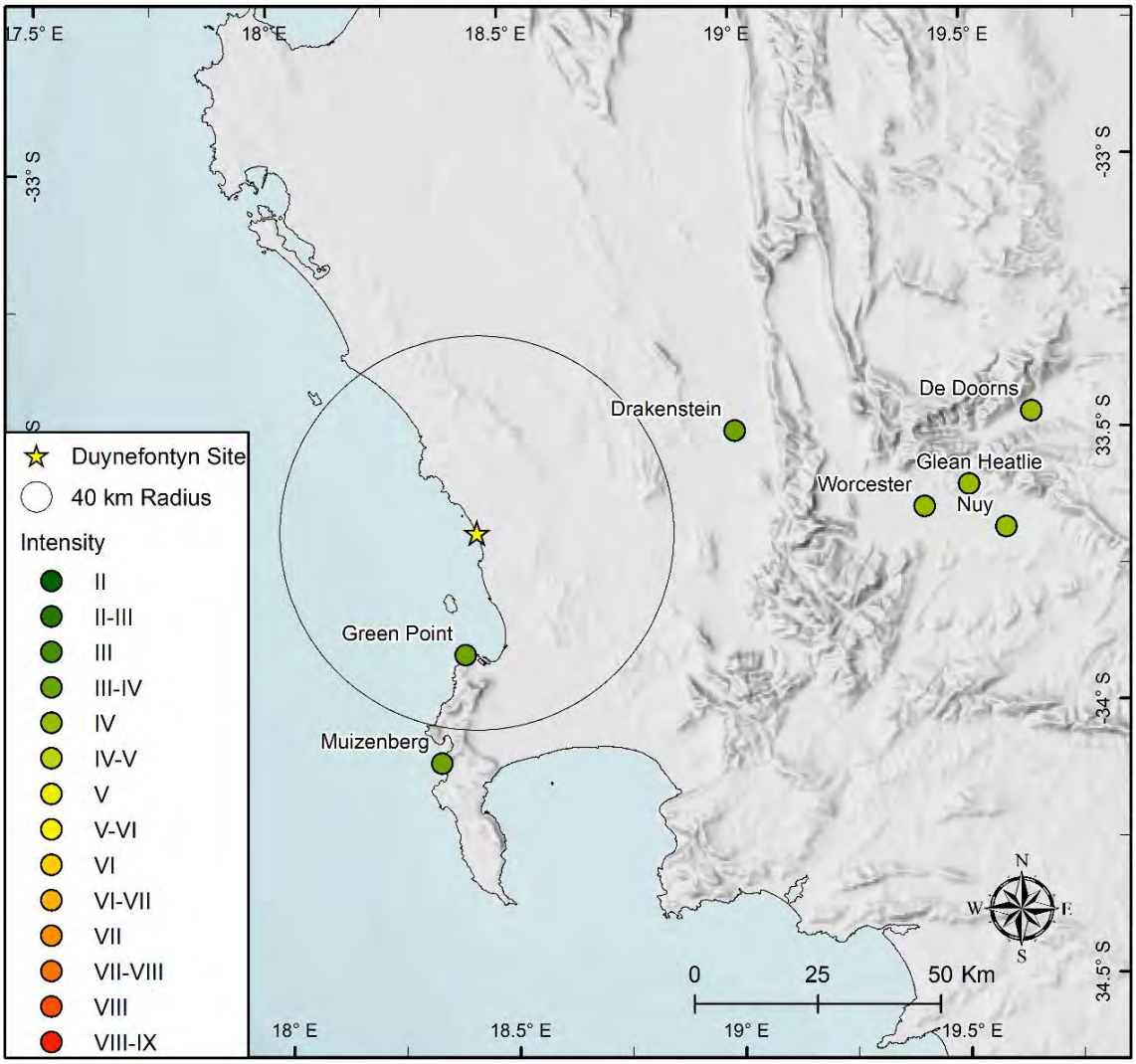

Figure 4-22. Distribution of IDPs in MMI-56 scale for the 9 December 1909 earthquake.

Table 4-10. The epicentre solutions for the 9 December 1909 earthquake using the MEEP2 software.

Method	Latitude	Longitude	Location error (± km)	Magnitude, M	Magnitude error, (±)	Depth (km)	Weight of solutions
Centroid	-33.644	19.551	15.2	3.9	0.2	20.0	0.4
MEEP	-33.713	19.234	16.6	3.8	0.1	20.0	0.4
Bakun and Wentworth	-34.534	20.042	120.5	5.2	0.2		0
Pairwise	-33.593	19.977	38.7	4.2	0.2		0.2
Combined	**-33.6614**	**19.5094**	**20.46**	3.9	0.17	**20.0**	**1**
CGS Solution	-33.900	18.400		3.7			

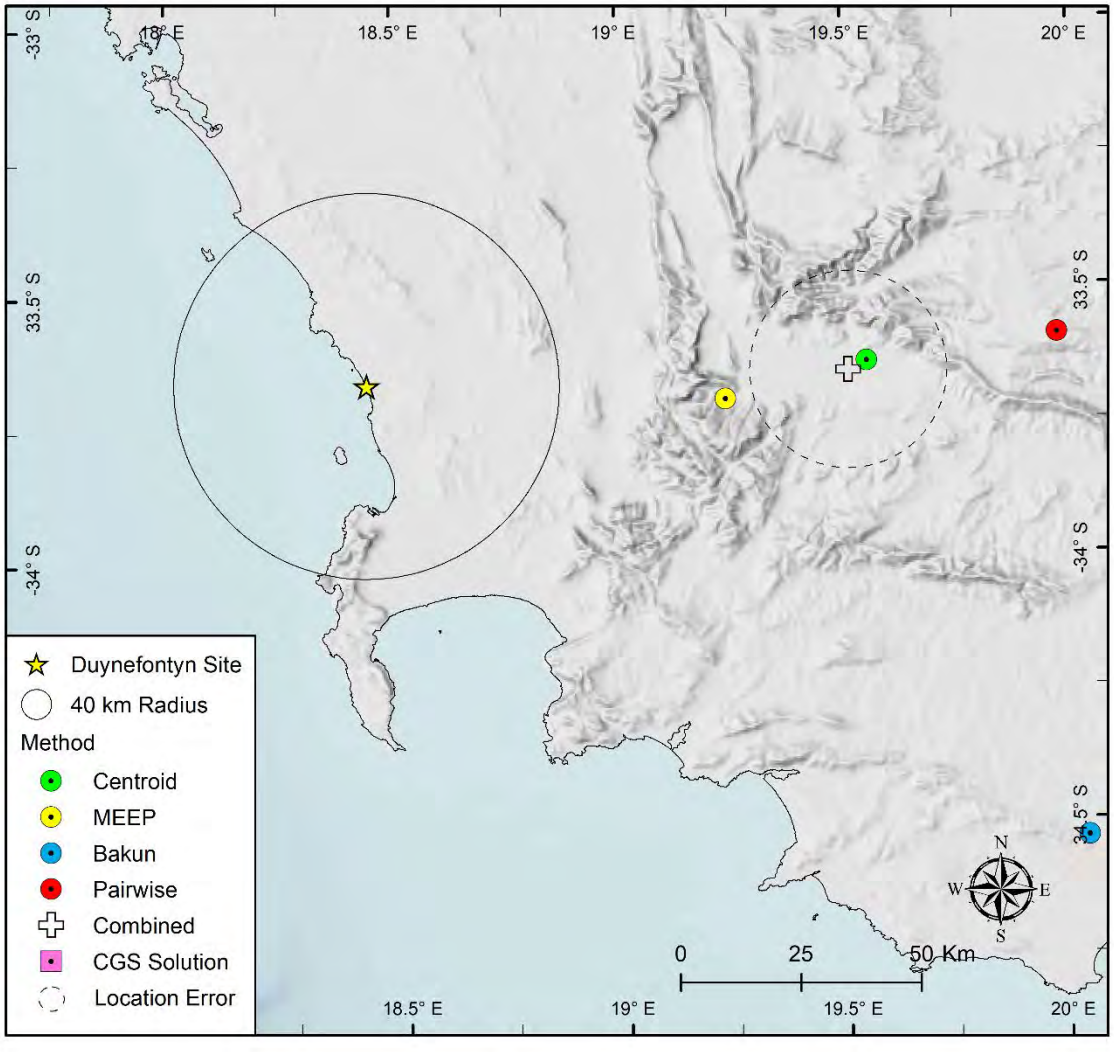

Figure 4-23. Location of epicentral solutions obtained for the 9 December 1909 earthquake using intensity data (Figure 4-22) and the MEEP2 software.

4.3.7 The 29 August 1960 earthquake

The records related to the 29 August 1960 earthquake were obtained by Albini and Flint (2023) from three newspapers that were published in Cape Town at the time. Using these records, Albini and Flint (2023) created ten IDPs located along the south-western coast of the Western Cape Province (Figure 4-24). Using the compiled IDPs and the MEEP2 software, source parameters were obtained by the SSM TI Team for this event using the four techniques that are part of the software. However, only two of the solutions (Centroid and MEEP solutions) were combined to produce the preferred solution (white star in Figure 4-25) because the Bakun and Pairwise solutions had large epicentral error values (Table 4-11) and had suspect locations that were far from the other two (MEEP and Centroid). Thus, these two solutions were not used by the SSM TI Team to determine the combined preferred solution.

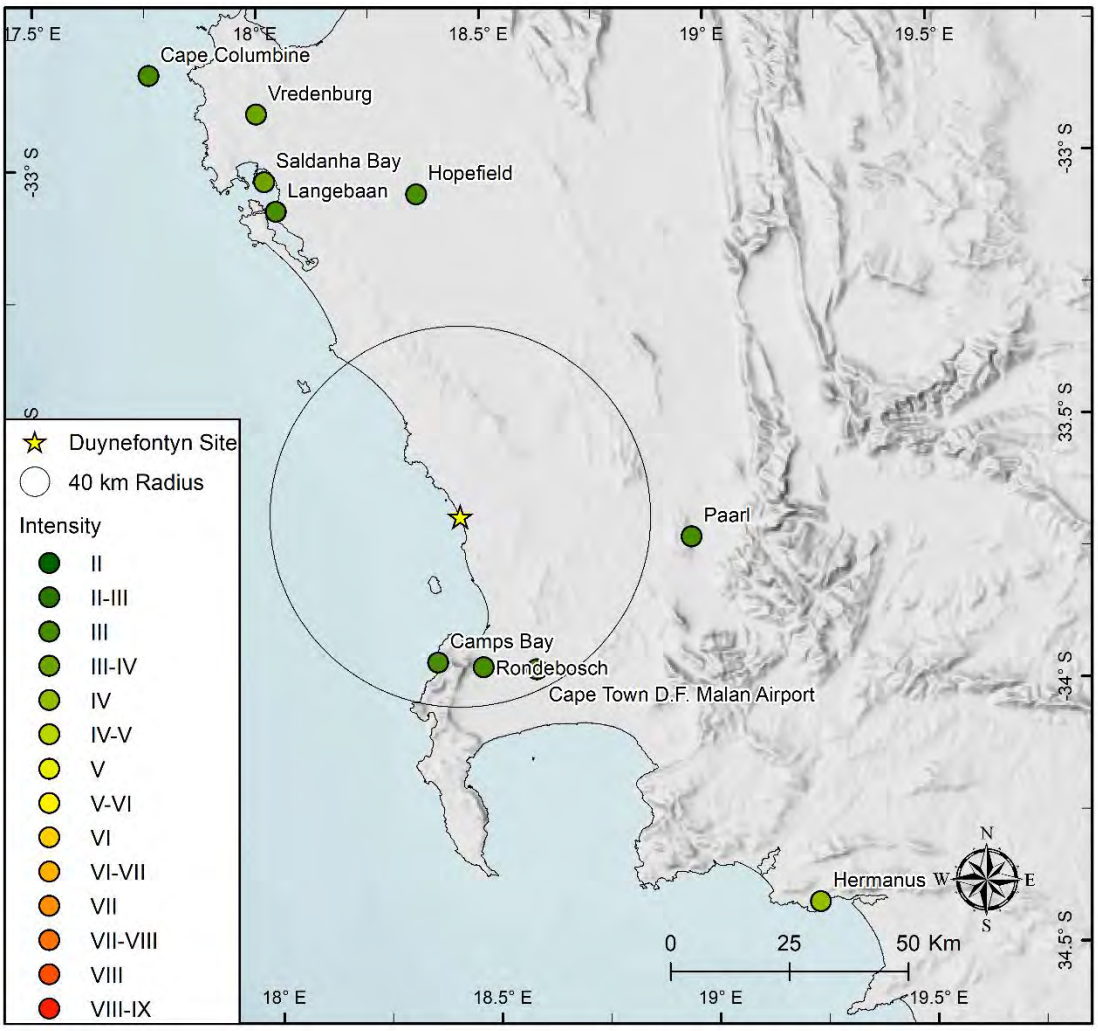

Figure 4-24. Distribution of IDPs in MMI-56 scale for the 29 August 1960 earthquake.

Table 4-11. The epicentre solutions for the 29 August 1960 earthquake using the MEEP2 software.

Method	Latitude	Longitude	Location error (± km)	Magnitude, M	Magnitude error, (±)	Depth (km)	Weight of solutions
Centroid	-33.464	18.346	44.2	4.4	0.4	20.0	0.6
MEEP	-33.424	18.414	76	4.4	0.3	20.0	0.4
Bakun and Wentworth	-33.543	18.018	110.6	4.1	0.6		0
Pairwise	-32.892	18.079	178.6	4.8	0.6		0
Combined	**-33.448**	**18.373**	**56.92**	4.4	0.45	**20.0**	**1**
CGS Solution	-33.400	19.300		4.0			

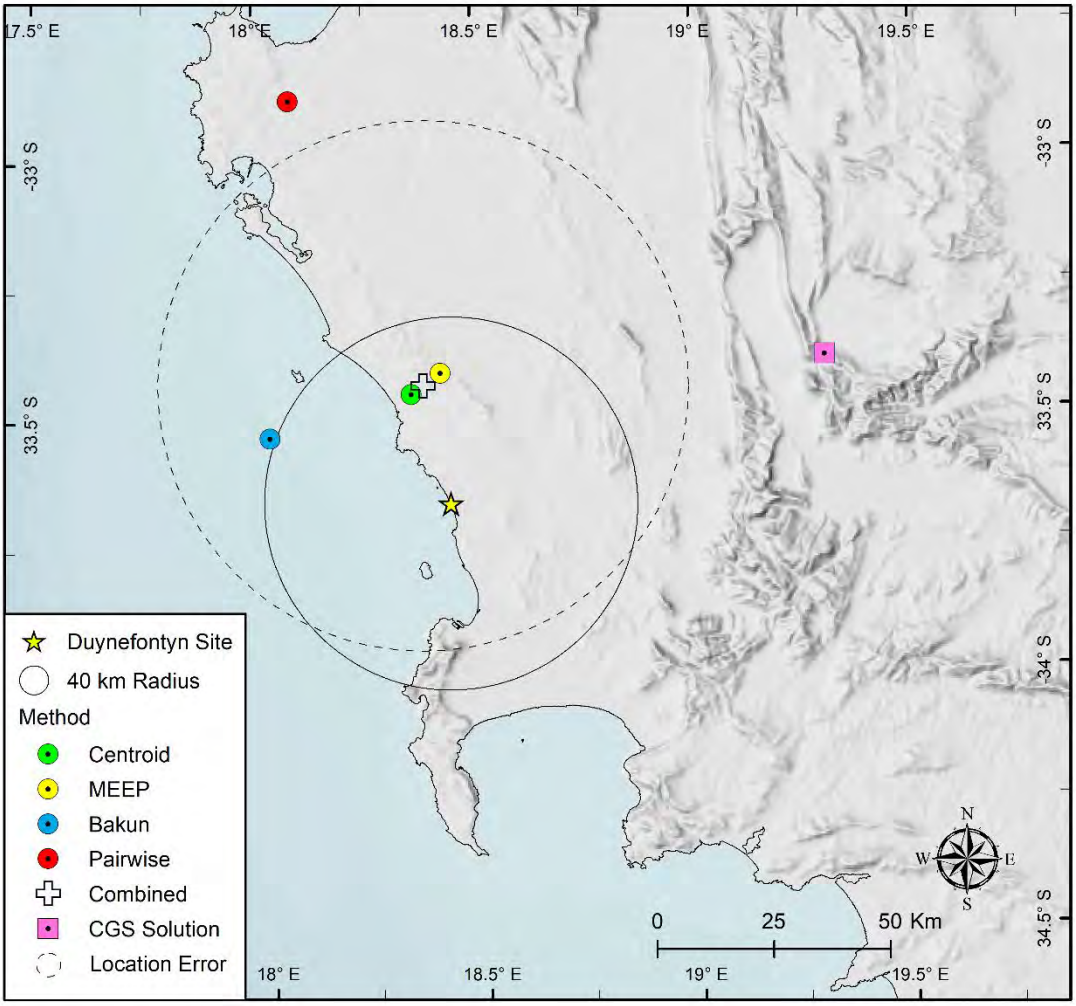

Figure 4-25. Location of epicentral solutions obtained for the 29 August 1960 earthquake using intensity data (Figure 4-24) and the MEEP2 software.

4.3.8 The 27 August 1963 earthquake

The 27 August 1963 earthquake was well recorded with the descriptions of the earthquake effects reported in six issues of four different Cape Town newspapers. Using the observations obtained from the reports, Albini and Flint (2023) created 38 IDPs (Figure 4-26). The distribution of the IDPs imply that the epicentre of the event is located northeast of Cape Town towards the Ceres area. This was confirmed by the source parameters estimated by the SSM TI Team using the intensity data and techniques in the MEEP2 software (Figure 4-27, Table 4-12). Though the Bakun solution had an error value less than 100 km, it was not used by the SSM TI Team in determining the combined solution because its location is far to the northeast compared to the other group of three solutions (i.e., Centroid, MEEP and Pairwise in Table 4-12).

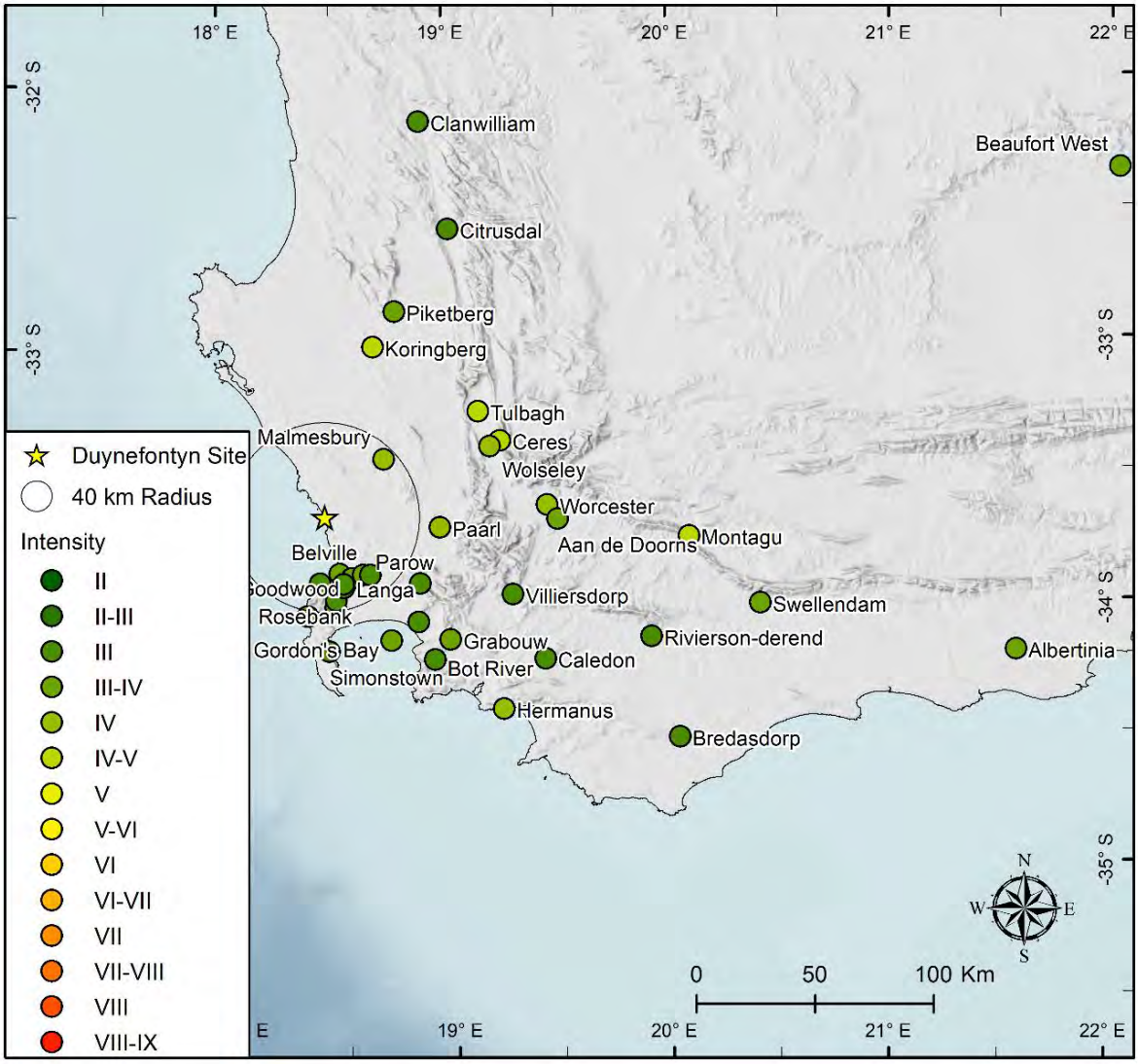

Figure 4-26. Distribution of IDPs in MMI-56 scale for the 27 August 1963 earthquake.

Table 4-12. The epicentre solutions for the 27 August 1963 earthquake using the MEEP2 software.

Method	Latitude	Longitude	Location error (± km)	Magnitude, M	Magnitude error, (±)	Depth (km)	Weight of solutions
Centroid	-33.341	19.186	56.7	4.3	0.2	20.0	0.3
MEEP	-33.557	19.167	50.5	4.2	0.2	20.0	0.4
Bakun and Wentworth	-32.995	20.39	74.8	5.2	0.2		0.0
Pairwise	-33.383	19.356	61.7	4.2	0.3		0.3
Combined	**-33.440**	**19.229**	**55.7**	4.4	0.23	**20.0**	**1**
CGS Solution	-33.100	19.000		4.7			

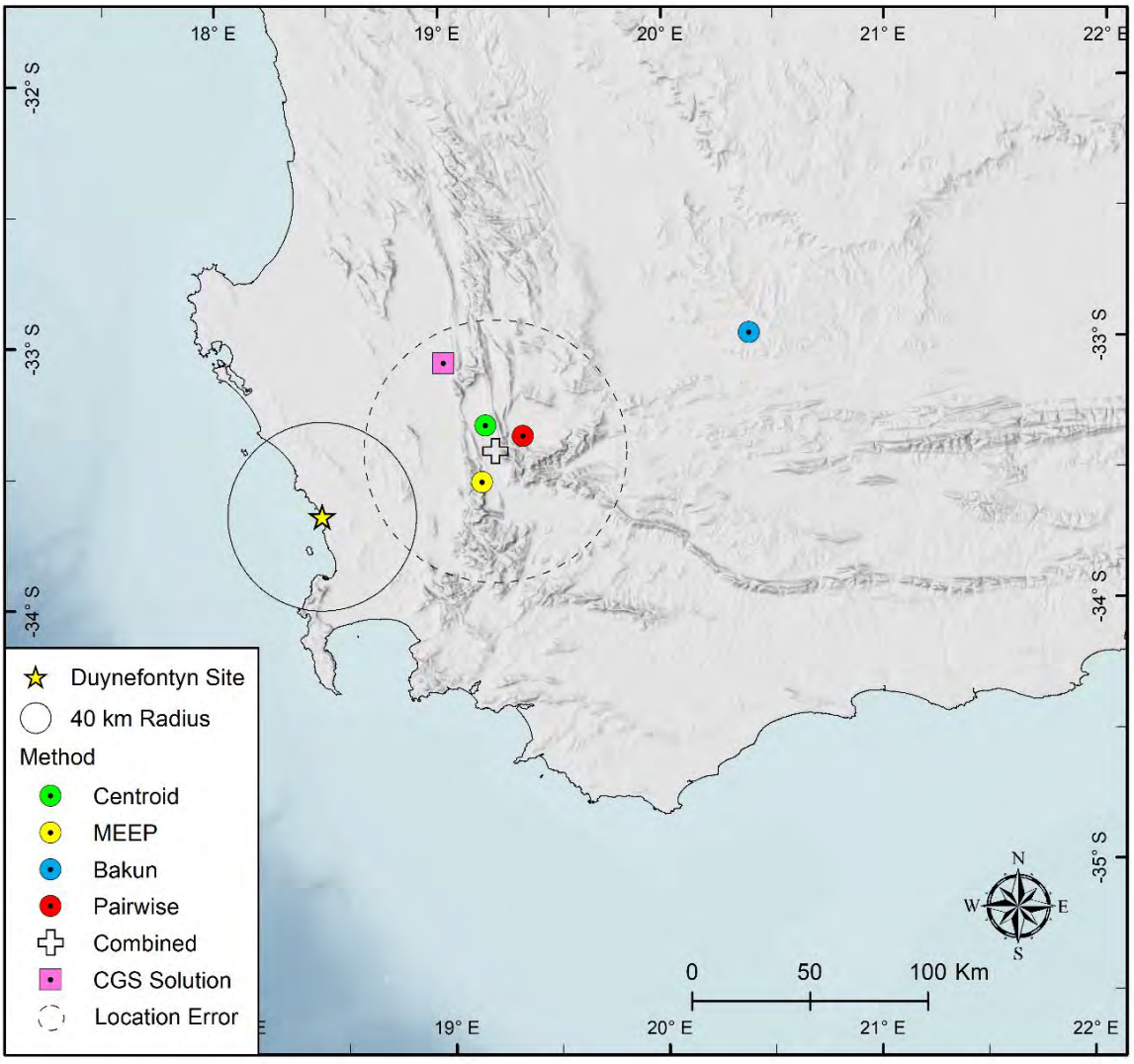

Figure 4-27. Location of epicentral solutions obtained for the 27 August 1963 earthquake using intensity data (Figure 4-26) and the MEEP2 software.

4.3.9 The 11 September 1969 earthquake

According to newspaper reports the 11 September 1969 earthquake was widely felt along the southern coast and immediate interior of the Western Cape Province (Figure 4-28). However, the distribution of the intensity values of the obtained IDPs is suspect given the higher values observed both to the east and the west, with the highest value of intensity V located in the centre of the distribution. Such a distribution made it difficult for the SSM TI Team to identify the epicentral location of the event. It is likely that site effects played a part in the higher intensity values observed both to the east and west. Thus, the epicentral solutions obtained by the SSM TI Team using these data and the software MEEP2, all had quite large errors (Table 4-13). Given the similar and large epicentral error values, the same weight value of 0.25 was applied to each of the solutions to develop the combined solution (Table 4-13, Figure 4-29). The significant location uncertainty was handled in the SSM by consideration of two possible locations for the event: 1) the CGS solution located far east of the site, and 2) the combined location northeast of Cape Town. The SSM TI Team evaluated the impact of these two locations on the catalogue declustering (Section 6.9) and spatial smoothing (Section 8.2.4). Sensitivity of the hazard results to the event location and the final SSM TI Team disposition for dealing with the 11 September 1969 event location are discussed in Section 6.9 and are shown in Figure 6-26. It should be noted that the magnitude value used in sensitivity analysis was the CGS value for both alternative locations.

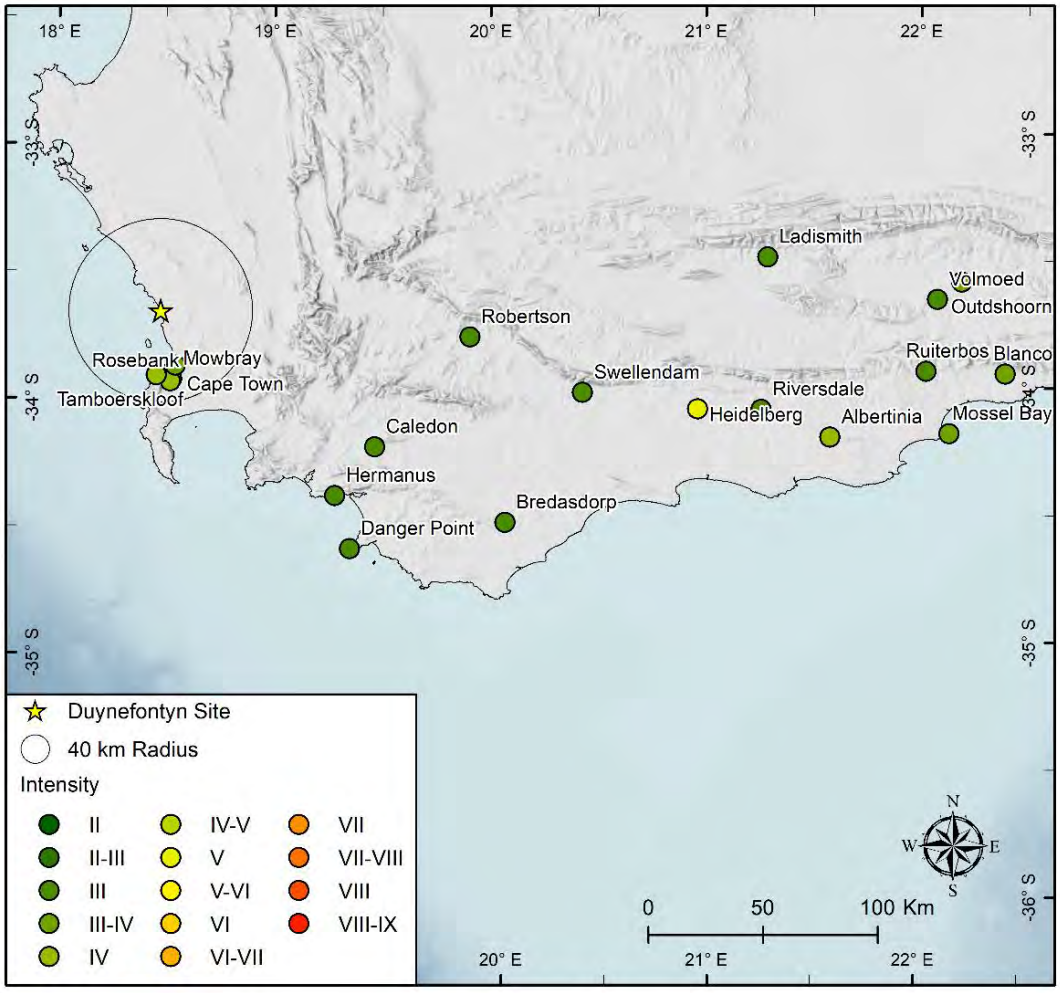

Figure 4-28. Distribution of IDPs in MMI-56 scale for the 11 September 1969 earthquake.

Table 4-13. The epicentre solutions for the 11 September 1969 earthquake using the MEEP2 software.

Method	Latitude	Longitude	Location error (± km)	Magnitude, M	Magnitude error, (±)	Depth (km)	Weight of solutions
Centroid	-33.943	18.45	195.3	5.4	0.5	20.0	0.25
MEEP	-34.044	19.184	148.3	5.0	0.3	20.0	0.25
Bakun and Wentworth	-32.588	19.225	292.0	5.5	0.4		0.25
Pairwise	-34.652	17.996	280.2	5.6	0.5		0.25
Combined	**-33.807**	**18.714**	**229.0**	5.37	0.41	**20.0**	**1**
CGS Solution	-34.000	21.000		4.8			

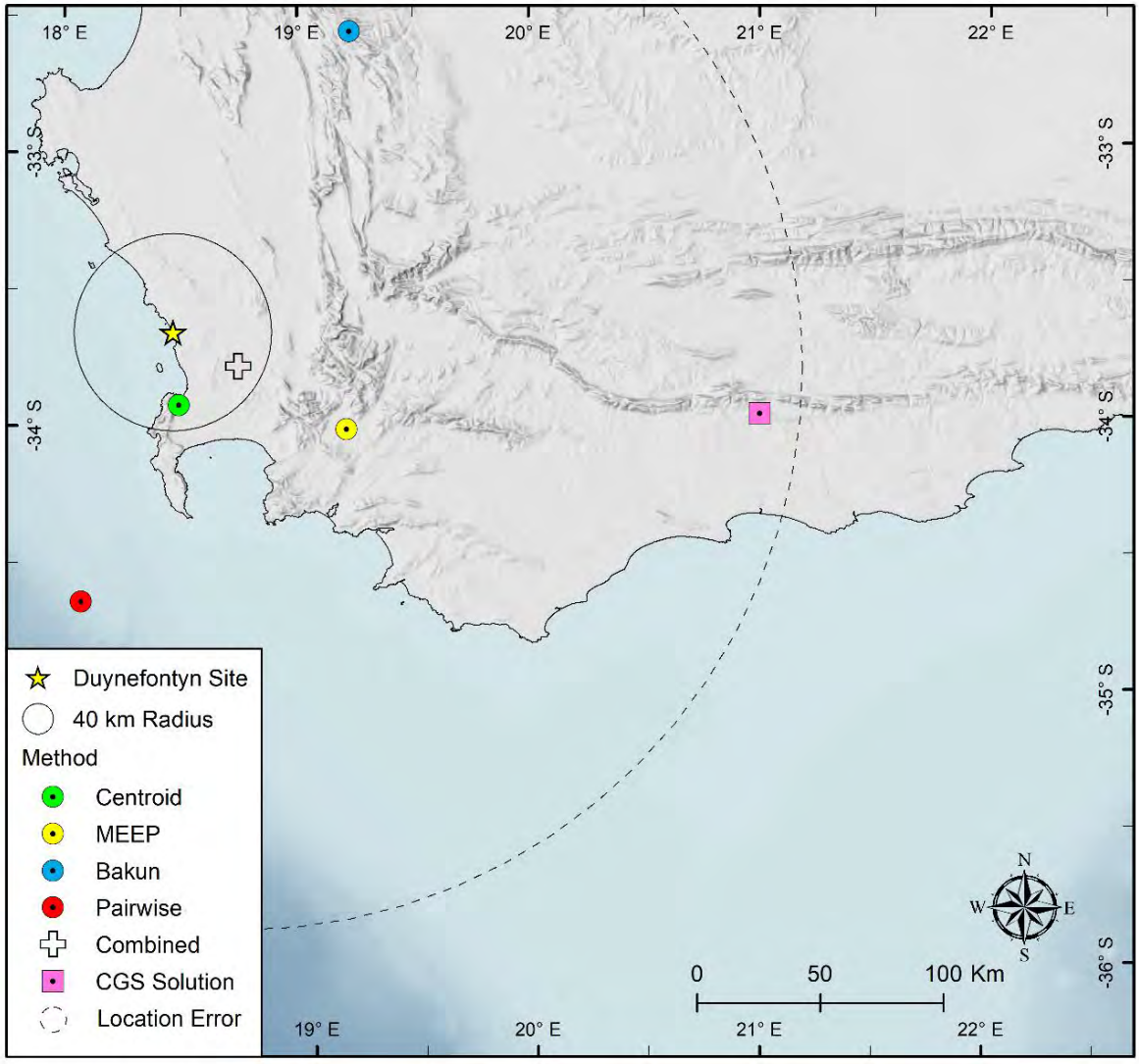

Figure 4-29. Location of epicentral solutions obtained for the 11 September 1969 earthquake using intensity data (Figure 4-28) and the MEEP2 software. Pink square (CGS solution) and cross (Combined solution) show the two alternative locations considered by the SSM TI Team.

4.3.10 The 29 September 1969 earthquake

This earthquake was widely felt throughout the country. The most affected area was near Tulbagh, where there was severe damage to property and 12 fatalities. From newspaper reports, Albini and Flint (2023) created 57 IDPs (Figure 4-30). However, this event has a reliable instrumental location. As a result, the SSM TI Team decided to determine its source parameters (Table 4-14 and Figure 4-31) using the collected IDPs for comparison and estimation of the reliability of the 3rd Generation methods used.

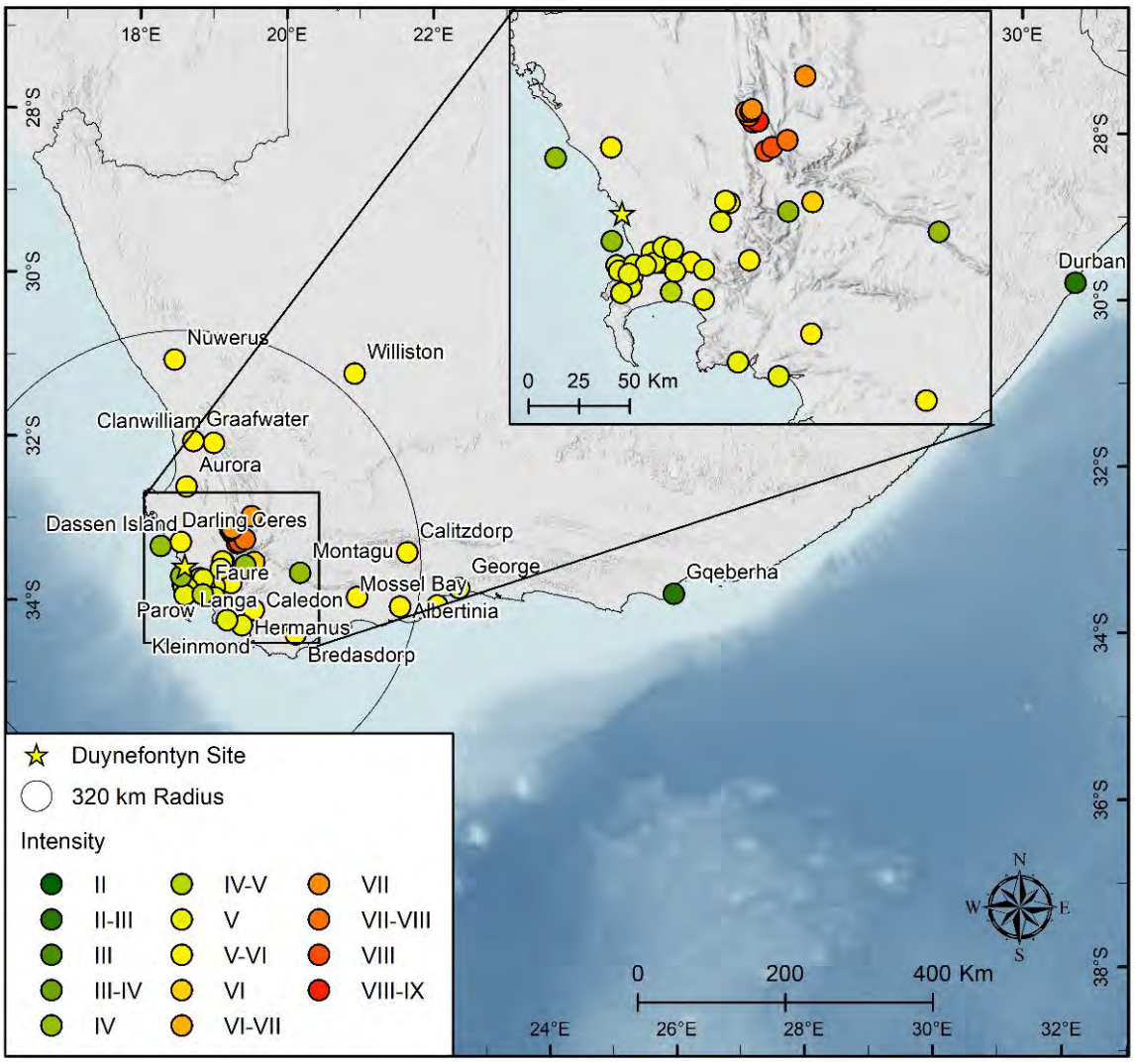

Figure 4-30. Distribution of IDPs obtained for the 29 September 1969 earthquake by Albini and Flint (2023).

Table 4-14. The epicentre solutions as obtained for the 29 September 1969 earthquake using the MEEP2 software.

Method	Latitude	Longitude	Location error (± km)	Magnitude, M	Magnitude error, (±)	Depth (km)	Weight of solutions
Centroid	-33.344	19.184	12.1	6.6	0.6	12.0	0.5
MEEP	-33.225	19.303	14.7	6.6	0.6	14.0	0.5
Bakun and Wentworth	-32.234	20.029	137.1	6.9	0.8		0
Pairwise	-32.772	20.363	116.6	6.6	0.6		0
Combined	**-33.2845**	**19.2435**	**13.4**	6.6	0.62	13.0	**1**
CGS Solution	-33.280	19.240		6.2			

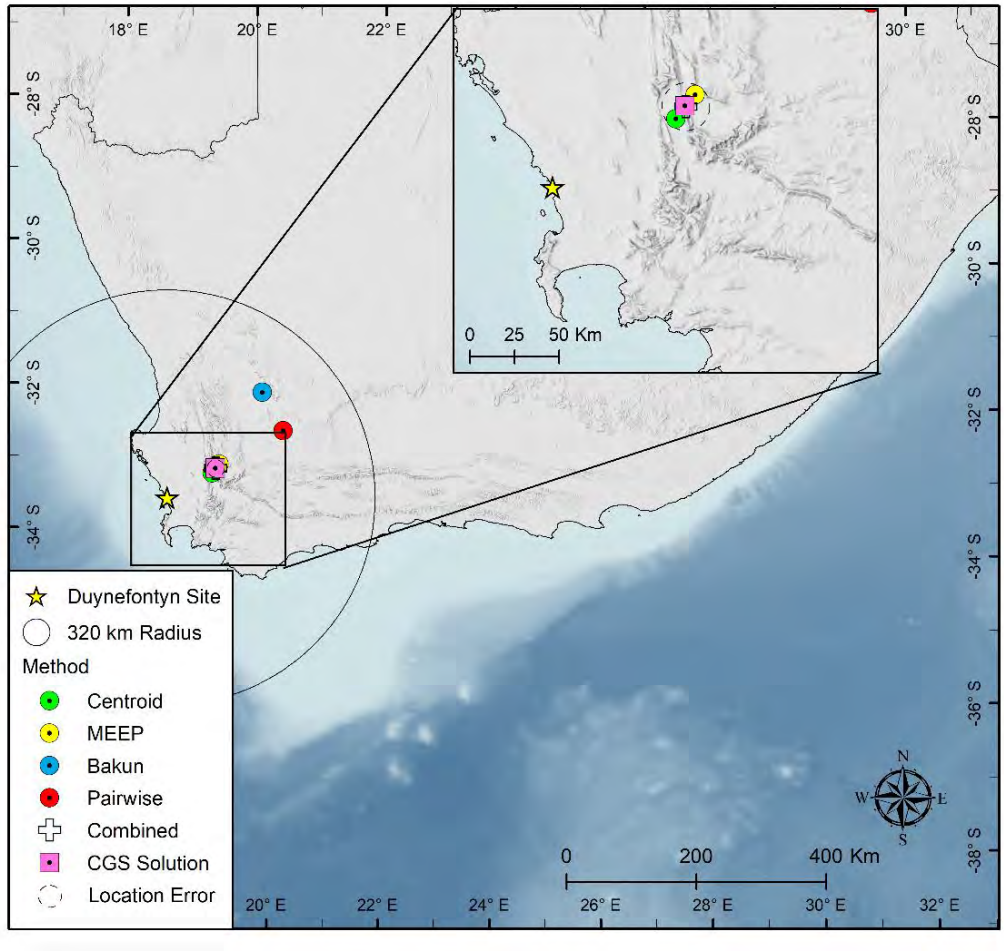

Figure 4-31. Location of epicentral solutions obtained for the 29 September 1969 earthquake using intensity data (Figure 4-30) and the MEEP2 software.

Of the four source parameter solutions obtained, two (Bakun and Pairwise) had epicentral errors greater than 100 km (Table 4-14). Thus, only two solutions (Centroid and MEEP) were used to determine the combined and preferred solution for this event. On comparing, the solution obtained in this study is at the same location as the published CGS instrumental solution (Figure 4-31), giving us confidence in the 3rd Generation techniques used as well as the assumptions made in the process followed in determining the combined solution. In addition, many earthquake-related phenomena were observed and recorded. A summary of the earthquake related phenomena observed during the earthquake are provided on pages 251-253 of Albini and Flint (2023). However, the magnitude value obtained in the MEEP2 analysis is an overestimation of the of the instrumentally determined moment magnitude of 6.2. However, the MEEP 2 analysis does not always overestimate magnitude as half of the MEEP2 estimates were larger than the CGS Solution and half were smaller. The SSM TI Team is uncertain about the reason for this variation in the magnitude values, but it might be caused by the spatial distribution and values of the IDPs. According to Bandt et al. (2005), the CGS local magnitude values for the events analysed in this study were derived from the maximum intensity (I_{max}), using the Richter formula $M_L = 0.66I_{max} + 1.0$ (Gutenberg and Richter, 1954). As described in Section 6.6, the 29 September 1969 instrumental magnitude was used for this study.

Using intensity data and 3rd generation techniques, epicentres are usually estimated according to two basic procedures. The first involves use of an estimate of the centroid of the higher intensities. The second assumes a distance function that the IDPs should follow, and then apply a grid search in which residuals are to be minimised. The second method is applied mainly in the Bakun and Wentworth method, making it susceptible to poor solutions. This happens in cases where the function or attenuation method used is not compatible with local geology. The poor solutions obtained using the Bakun and Wentworth method are illustrated by the large errors (greater than 100km) obtained in the solutions (e.g., Table 4-14 solutions for the 29 September 1969 earthquake).

4.4 DUYNEFONTYN SITE GEOLOGY

The Duynefontyn site sits atop relatively complex geology characteristics that consist of steeply-dipping to nearly vertical bedding of the Malmesbury Group strata uncomfortably overlain by Miocene to Holocene marine, estuarine, and aeolian strata atop a large wave-cut platform. Differential erosion of the Malmesbury Group layers on the wave-cut platform produced a corrugated bedrock surface (Figure 4-32a and b).

The SSM and GMM TI Teams determined that this bedding geometry and erosional fabric could potentially challenge one-dimensional site response analyses, which is traditionally based on an assumption of infinite horizontal layers that are then used to derive one-dimensional vertical V_S profiles. Thus, to characterise the Duynefontyn site, the SSM TI Team evaluated and assessed the site geology in detail. As described below, this evaluation and assessment included borehole data, geologic maps, photographic records, and a first-hand account of the construction of the KNPS (Barker, 2023). During construction of the KNPS, the Cenozoic cover was cleared off to expose the wave-cut platform and the corrugated steeply dipping beds of the underlying Malmsbury strata (Figure 4-32a). The SSM TI Teams assessment was provided to the GMM TI Team who used this information to investigate possible two-dimensional site response effects, as described in Section 9.4.6. The two-dimensional analysis was also the subject of a GMM TI Team supporting study conducted by de la Torre and Bradley (2023). While the GMM TI Team ultimately did not deviate from one-dimensional site response, this evaluation of the geological conditions at the Duynefontyn site may provide a template for studies at other geologically complex sites.

4.4.1 Bedrock geology (Malmesbury Group)

Within 40 km of the Duynefontyn site, comprehensive data collection activities and investigations (e.g., Dames and Moore, 1976; Rogers, 1979; 1980; Visser, 1988; De Beer et al., 2008 Engelsman, 2022; Claassen et al., 2024) reveal that both the Duynefontyn and Koeberg sites are exclusively underlain by bedrock of the Tygerberg Formation that comprises low-grade, immature, deep water, turbiditic metasediments of predominantly fine- to medium-grained, thinly bedded alternating greywackes/metagreywackes, shales, siltstones, and mudstones with occurrences of phyllites that exhibit a fining sequence from east to west (Figure 4-32). Borehole data at Koeberg and Duynefontyn (Dames and Moore, 1976; Day, and Ridgway, 2000; 2006; SRK, 2008b) indicate roughly equal proportions of arenaceous and argillaceous lithological units for the Tygerberg Formation. Lithological units are generally laterally persistent in thickness along strike. The formation consists of gradational sequences with beds grading mainly from coarse to fine in upward-fining successions.

Figure 4-32. (a) Tygerberg Formation exposed in excavations during the construction of the KNPS. (b) Coastal exposures of the alternating metasediments of predominantly fine- to medium-grained, thinly bedded alternating greywackes/metagreywackes, shales, siltstones, and mudstones of the Tygerberg Formation just south of Grotto Bay (S 33°31'35.8"; E 18°19'01.2").

Dames and Moore (1977) identified four different rock sequences at Koeberg that can be extended along strike to the Duynefontyn site (Figure 4-33).

1. Greywacke: Massive, light to dark grey or greenish grey, medium to fine grained poorly graded greywacke with occasional dark grey shale partings and very thin mudstone beds. These units range in thickness from <2-10 m.
2. Predominant greywacke: Greywacke with numerous thin beds and laminae of greenish orange siltstone and grey mudstone. Interbedded mudstone units of up to 40 cm were mapped. Units range in thickness between <2-12 m.
3. Predominant mudstone: Dark grey to dark greenish grey mudstone with abundant siltstone and thin beds of greywacke. Units range in thickness from <2-9 m.
4. Mudstone: Dark grey to dark greenish grey mudstone with minor grey siltstone laminae and occasional thin beds of fine-grained greywacke. Thickness for these units range from <2-5 m.

Quartz dominated (70%) greywackes are fine-to-medium grained and are generally massive or laminated, occasionally containing subrounded to angular clasts. Small-scale cross-stratification, cross-lamination and bedding-parallel lamination are noted in finer-grained greywackes. Siltstone and mudstone are massive or frequently horizontally laminated. Lensoidal bodies exhibit whitish weathering laminae, possibly due to diagenetic silicification. Soft-sediment deformation structures are abundant and include load casts, ball-and-pillow structures, and convolute bedding (Theron, 1984; Roberts, 2001). Similar lithologies to those observed at the KNPS were identified in boreholes at Duynefontyn (Figure 4-34) but given the metre-scale alternating sequence of lithologies, and spacing of boreholes, the construction of a lithostratigraphic section for the site was not possible.

Most boreholes at Koeberg and Duynefontyn do not exceed 30 m depths, with the maximum depth drilled being 120 m in borehole ST1 (Claassen et al., 2023). Although granitic intrusions associated with the Cape Granite Suite were not encountered in any boreholes, given the shallow borehole depths their presence at depth in the area cannot be excluded.

In addition, no boreholes at Duynefontyn intercepted a Mesozoic dyke. However, given their narrow extent (frequently less than 10 m) and wide borehole spacing, their possible presence cannot be excluded, especially considering their occurrence along coastal exposures between Milnerton and Bloubergstrand. A ~7 m thick mafic dyke was encountered near the south-eastern boundary of the KNPS site in inclined borehole 603, some 300 m from the coastline (Dames and Moore, 1976).

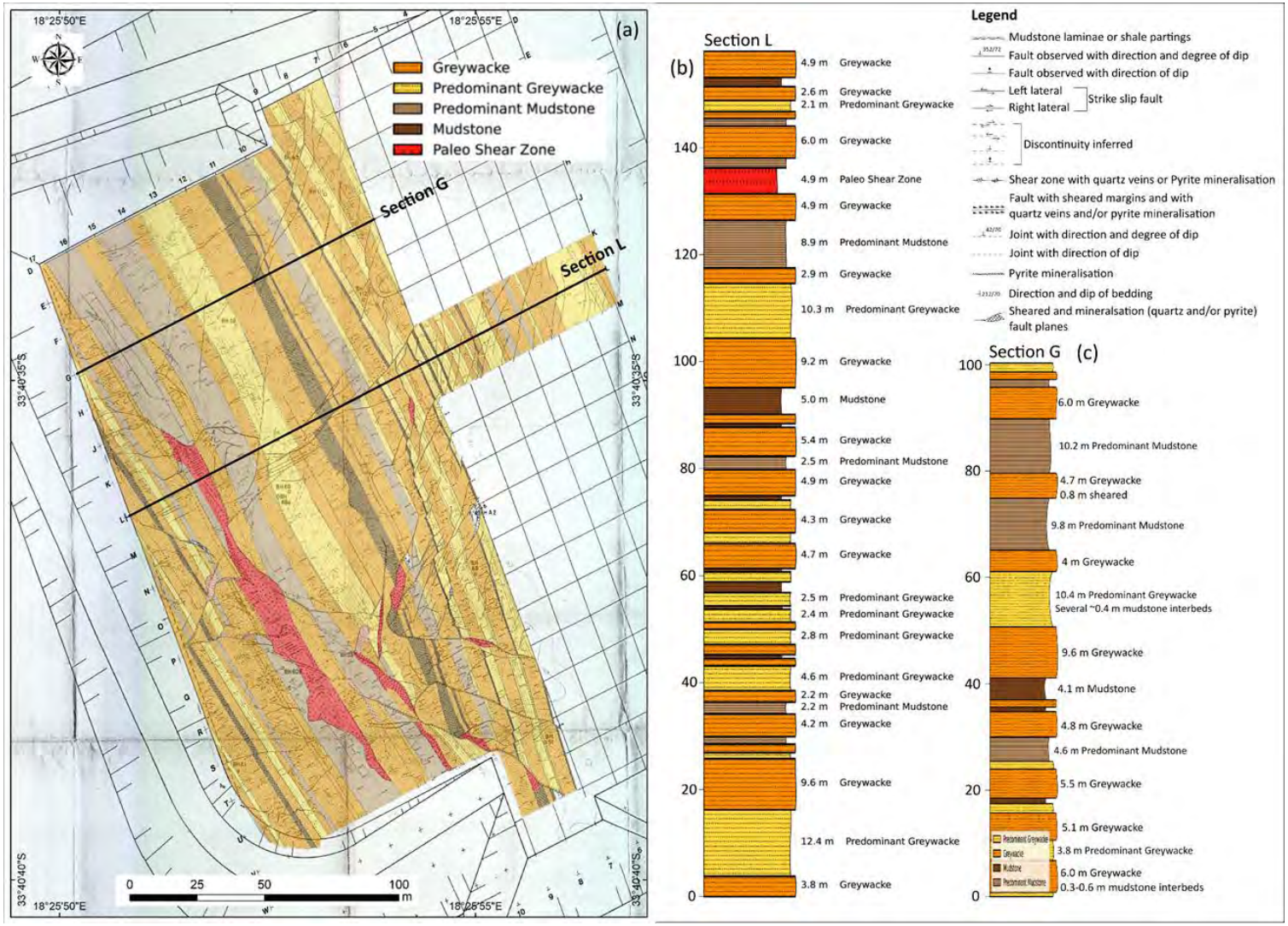

Figure 4-33. (a) Surface lithology and structure of the Tygerberg Formation mapped at excavations during the construction of the KNPS (after Dames and Moore, 1976). (b and c) Lithostratigraphic sections G and L orientated perpendicular to bedding strike. The thicknesses of lithological units were calculated perpendicular to strike (150°) using an average dip of 75°.

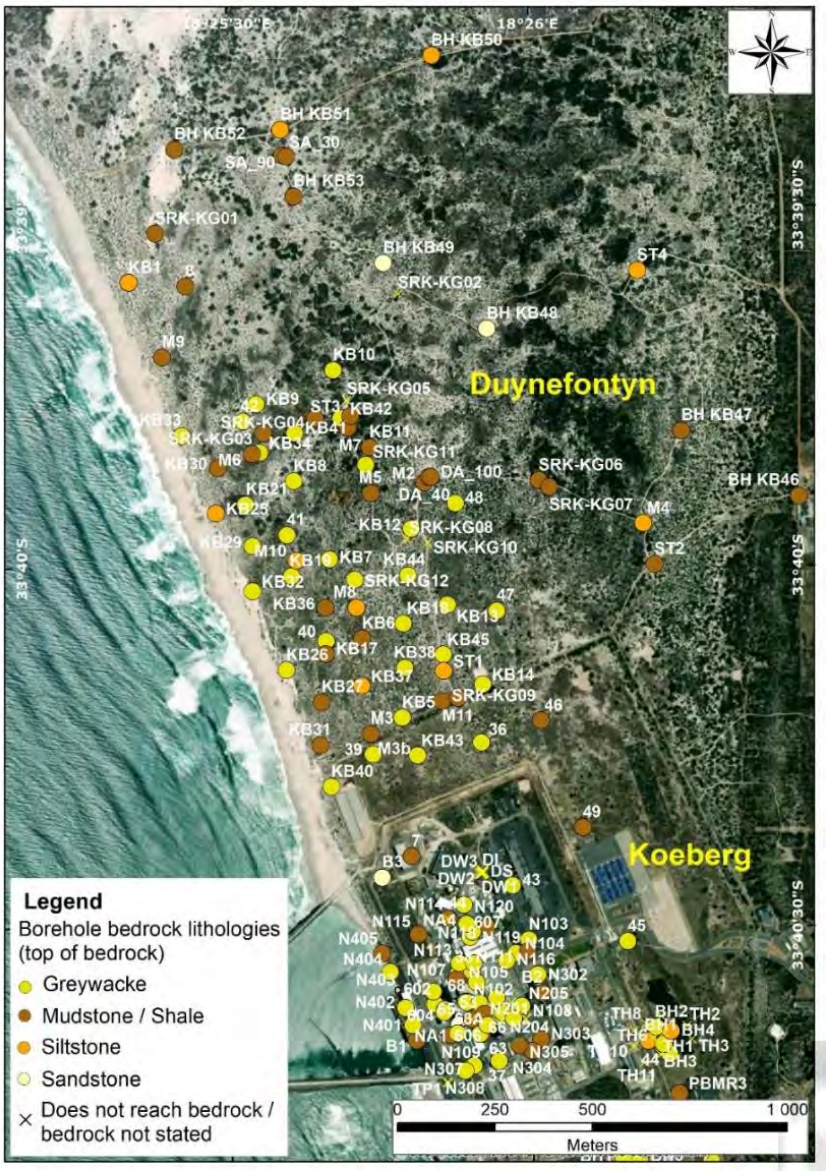

Figure 4-34. Top of bedrock lithology types intercepted in borehole data at Koeberg and Duynefontyn.

Excavations undertaken during the construction of the KNPS revealed that the overburden sediments were deposited on a weathered, uneven, gently seaward sloping bevelled and bioturbated wave-cut bedrock surface with steeply SW or NE dipping (70° – 90°), NNW-SSE striking beds. The broad planation surface at Koeberg is situated at an average elevation of 11 m bmsl. The bedrock surface exhibited thousands of shallow tubular *Pholad* burrows (Piddock bivalve molluscs) that penetrated bedding planes, joints, and faults, especially in more argillaceous lithologies (Figure 4-35a and b). No offset of these trace fossils was observed across mapped fractured/faulted zones (Rogers 1979, 1980; Barker, 2023), suggesting that the mapped bedrock faults must predate the age of the trace fossils. Unfortunately, the age on the terrace is unknown but is assumed to be older than a unit containing shark teeth roughly 2 m above bedrock that forms part of the Duynefontyn Member of the Varswater Formation which has an age range of Early Miocene to Pliocene. The lowermost gravel unit (Silwerstroom Member) of the Varswater Formation above bedrock was most likely laid down as a regressive deposit during the pre-terminal Miocene, before the early Pliocene regression.

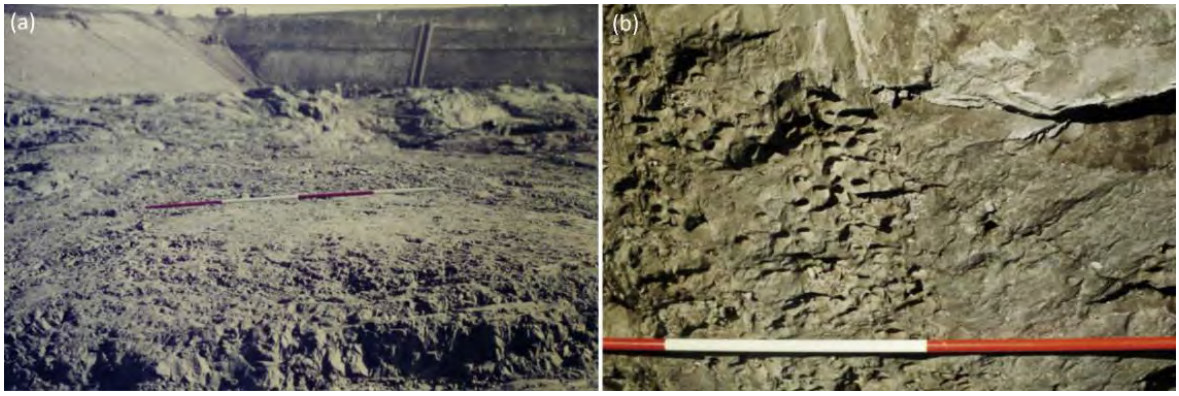

Figure 4-35. (a) Bedrock surface at Koeberg exbibit numerous shallow tubular *Pholad* burrows (Piddock bivalve molluscs). (b) A close-up image of the burrows that penetrated bedding planes, joints, and faults, especially in more argillaceous lithologies.

The Duynefontyn site contains a high density of boreholes (Murray and Saayman, 2000; Day and Ridway, 2006; SRK, 2008 a, b; Flanagan and Rosewarne, 2008; SRK, 2021; Claassen et al., 2024) that enabled the creation of an interpolated 1 m contour interval palaeotopography map of the bedrock surface (Figure 4-36a). Results show all bedrock within the contoured map area occurs below present-day sea level with elevations ranging between 26.6 m bmsl (BH607, just NW of the KNPS) and 1.0 m bmsl (SRK-KG04, at Duynefontyn, -390 m from the coastline) below overburden cover. Both these maximum and minimum elevations are extreme and isolated values, with average values across both sites calculated at 10.1 m bmsl. Topographically, bedrock elevation increases in a NE direction inland away from the coastal margin. At the Duynefontyn site itself, the lowest bedrock elevation of 16.34 m bmsl was encountered in borehole KB31. Towards the northwest extent of the Duynefontyn site, a NE-SW trending topographic low extends inland for at least 1 km. Claassen et al. (2024) identified two coast parallel, NNW-SSE trending wave-cut platforms at Duynefontyn based on the interpolated palaeobedrock topography and presence of overlying marine gravels. The first, lower, near-coastal marine terrace occurs at elevations between 10 to 12 m bmsl. A second, slightly higher probable terrace is located at elevations between 5 to 7 m bmsl (Figure 4-36b to e).

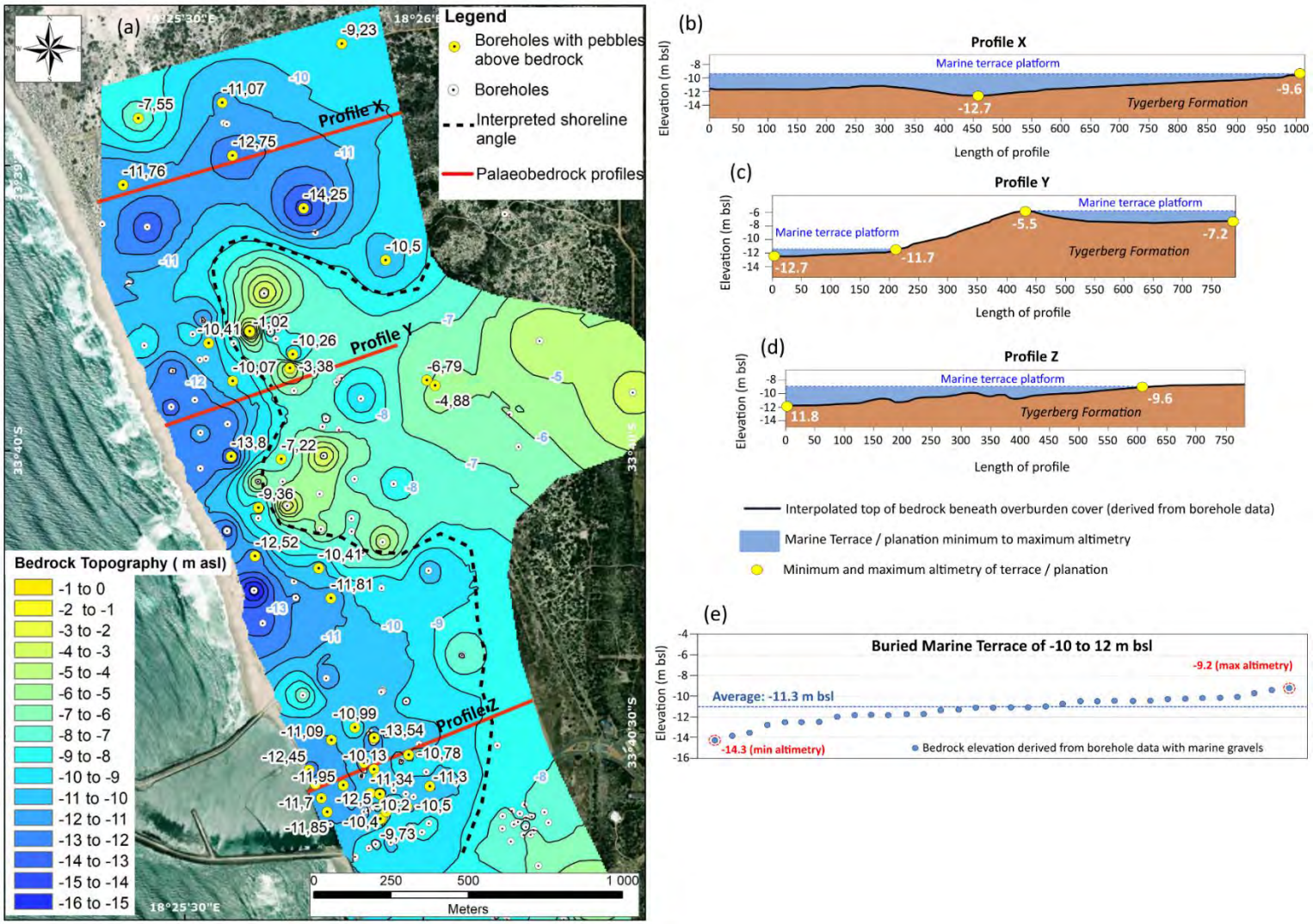

Figure 4-36.(a) Map depicting interpolated 1 m contour interval elevation map of the bedrock below Cenozoic overburden at the Duynefontyn site. (b-d) Cross-sections X, Y and Z perpendicular to the coastline and bedding strike across the interpolated palaeotopography surface. (e) Elevations of bedrock encountered in boreholes across the lower 10 to 12 m bmsl marine terrace platform.

The degree and depth of weathering of the Tygerberg Formation is highly variable across both sites (Figure 4-37). Strata range from unweathered to highly weathered. Unweathered greywacke is found within 6 m of the bedrock surface while weathering in the mudstones and siltstones extends to depths of 26 m in places. Generally, strata are highly weathered at the surface and become moderately to slightly weathered/unweathered with depth. The degree of weathering appears linked to lithology types with localised bedrock lows often forming in less competent strata such as mudstone. Zones of highly to completely weathered, brecciated/crushed rock are associated with the very fine-grained mudstones (Day and Ridgway, 2006). Geotechnical boreholes drilled by SRK (2008, 2021) defined weathered (soft to medium hard rock) and unweathered (hard to very hard rock) at the Duynefontyn site (Figure 4-38).

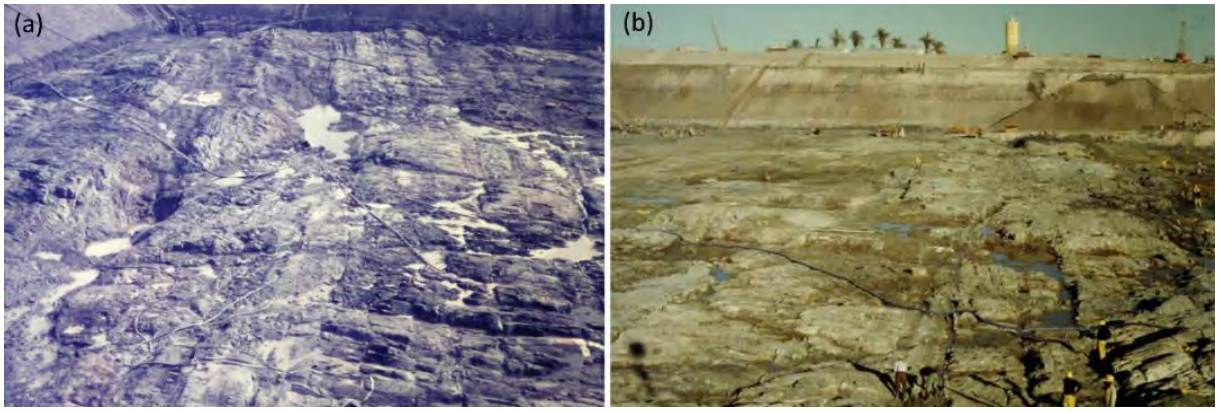

Figure 4-37. (a and b) Undulating, uneven planated bedrock surface exposed during excavations at Koeberg showing the differential weathering associated with the various lithologies (Photos J.Rogers).

4.4.2 Overburden geology (Sandveld Group)

Bedrock at Koeberg and Duynefontyn is overlain by unconsolidated to semi-consolidated, marine and aeolian sediments of the Sandveld Group deposited during a series of marine transgressions and intervening regressions. Borehole data (Murray and Saayman, 2000; Day and Ridgway, 2006; SRK, 2008a, b; Flanagan and Rosewarne, 2008; SRK, 2021, Claassen et al., 2024) enabled the creation of a 1 m interval isopach map across the Koeberg and Duynefontyn sites (Figure 4-39). The thickness of these overburden sediments range between 12.3 m (borehole B3, ~320m NW of Koeberg) to 35.2 m (borehole KB50, northwestern extent of Duynefontyn, ~1040 m from the coastline) with an average thickness of 20.8 m. Thickness increases with increasing distance from the coastline. Delineating the thickness of individual formations within the Sandveld Group across boreholes at Duynefontyn is not possible because borehole log descriptions are often not formation specific, and do not provide adequate lithological descriptions to facilitate accurate differentiation to formation level to facilitate correlation.

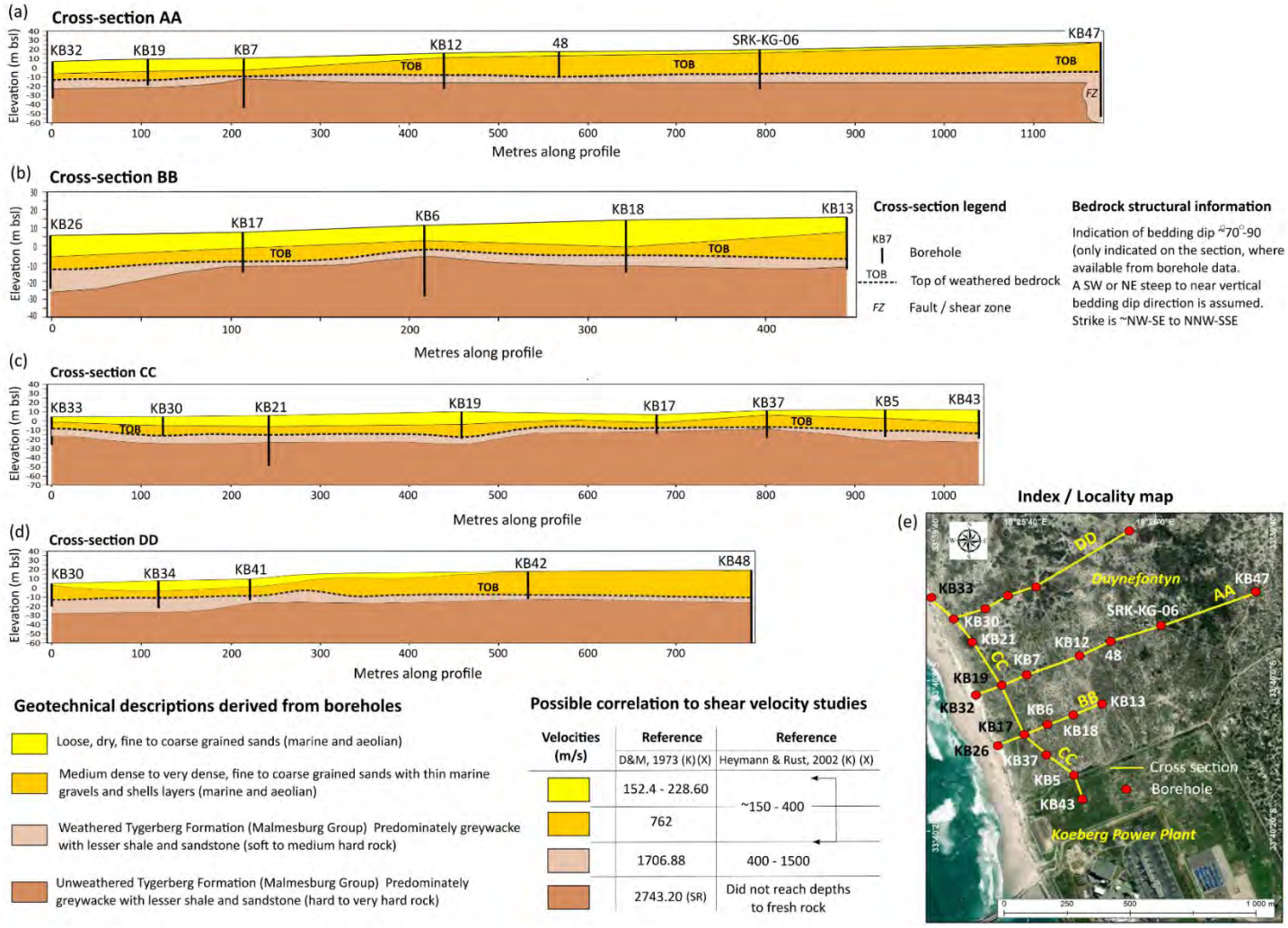

Figure 4-38. (a-d) Cross-sections depicting the geotechnical properties of overburden and bedrock, as defined by the SRK (2008, 2021) drilling programme at Duynefontyn, where differentiation was made between weathered (soft to medium rock) and unweathered (hard to very hard rock). (e) Index map showing locations of cross sections.

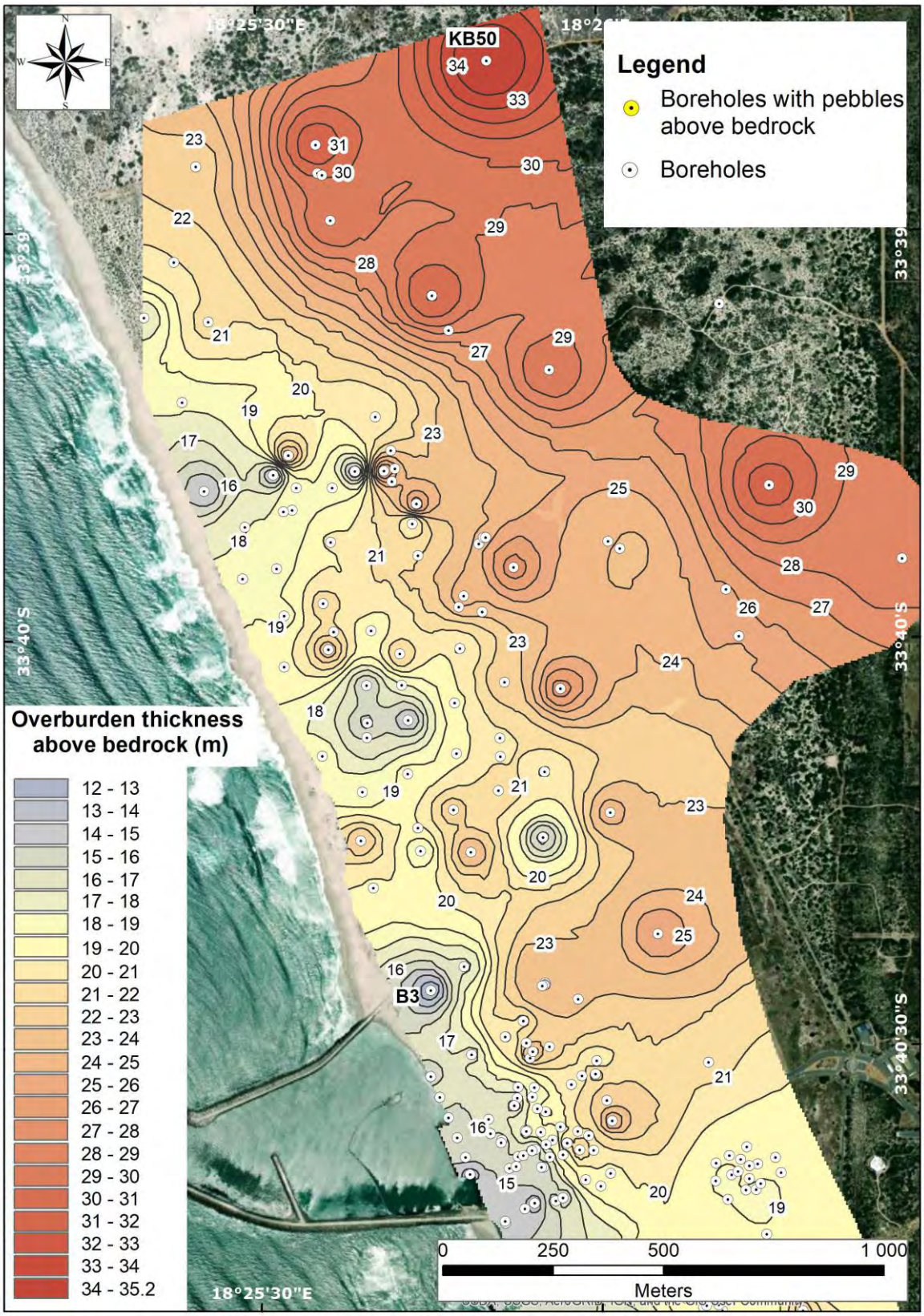

Figure 4-39. Interpolated isopach map (1 m intervals) showing the overburden thickness at the Duynefontyn site.

Figure 4-40 provides a lithostratigraphy for the Sandveld Group along the southwest coast as it is currently accepted by the South African Commitee for Stratigraphy (SACS) and detailed by Roberts et al. (2006). Although the lithostratigraphic subdivisions of the various formations and their members have varied between authors (e.g., Rogers 1979, 1980, Roberts 2001, 2002), the SSM TI Team has chosen to adopt the SACS approved lithostratigraphy and the additional two non-SACS approved members of the Varswater Formation at the Koeberg site as subdivided by (Roberts, 2001) and (De Beer, 2008). The SSM TI Team also notes that overburden lithostratigraphy can be highly variable across both sites as well as the greater southwest coast and that the lithostratigraphy of the Sandveld Group as represented by Roberts et al (2006) is an idealised, composite section. At Koeberg and Duynefontyn the Sandveld Group comprises the Varswater, Velddrif, Langebaan, Springfontyn, and Witzand Formations

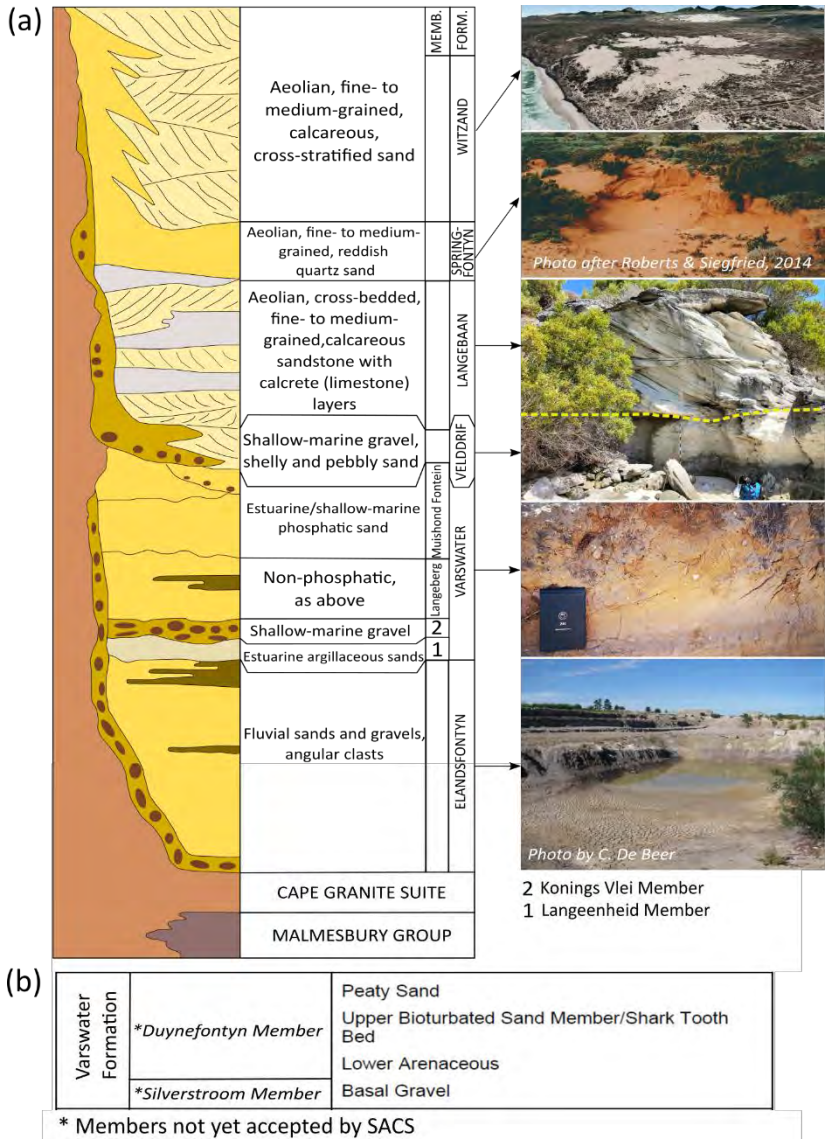

Figure 4-40. (a) Lithostratigraphy of the Sandveld Group (after Roberts et al., 2006). (b) Two additional members (Silwerstroom and Duynefontyn) of the Varswater Formation, identified during excavations at KNPS (Rogers, 1979; 1980). These member subdivisions as outlined by Roberts, (2001) have not yet accepted by the South African Committee for Stratigraphy (SACS).

Varswater Formation

The estuarine to shallow marine phosphatic Varswater Formation is traditionally subdivided into four Members across the southwest coast: Langeenheid Clayey Sand, Konings Vlei Gravel, Langeberg Quartz Sand, and the Muishond Fontein Pelletal Phosphorite Sand (Tankard, 1974; Rogers 1980, 1982; Hendey, 1981; Hendey and Dingle, 1983) (Figure 4-41a). Rich and diverse fauna of the Langeberg Quartz Sand and Muishond Fontein Pelletal Phosphorite Members suggests a Mio-Pliocene age (~5 Ma) (Hendey and Gentry, 1970; Hendey, 1976, 1981) and an inferred Middle Miocene age (~10 Ma) for the Konings Vlei Gravel Member. Two additional units, recognised as the Silverstroom and Duynefontyn Members (Miocene-Pliocene), but not yet accepted by SACS, were identified during excavations at the KNPS (Rogers, 1979, 1980; Rogers et al., 1990; Roberts, 2001) (Figure 4-40b). The various lithological beds and correlation of the lithological facies comprising these two members, as originally subdivided by Rogers (1979, 1980), were questioned by Roberts (2001). Therefore, the description as it follows below, details the more recently published works of Roberts (2001) that described the geology of the Melkbosstrand area as well as from De Beer et al. (2008) who mapped the geology of 40 km radius around Koeberg. The Silwerstroom Member occurs above the Tygerberg Formation and correlates to the marine *'Basal Gravel bed*' first identified by Rogers (1979). The unit is composed of well-rounded to angular pebbles and cobbles of Malmesbury Group and vein quartz clasts set in a matrix of dark grey quartzose sand rich in phosphatised shell fragments (Figure 4-41a and b). Borehole data indicates that this horizon is generally a few centimetres to <2 m thick at average elevations of 10-12 m below sea level. Some boreholes (SRK, 2008a) record thicker gravel accretions up to 14 m in isolated bedrock pockets. The lowermost gravel unit of the Varswater Formation was likely deposited as a regressive deposit during the pre-terminal Miocene, before the Early Pliocene regression.

Figure 4-41. (a) Basal gravels of the Silwerstroom Member (Varswater Formation) that correlates to the '*Basal Gravel bed'* first identified by Rogers (1979) during excavations at Koeberg and (b) at Duynefontyn in borehole M3 at a depth of 19.7-20 m (Claassen et al., 2023).

Overlying the Silwerstroom Member is the Duynefontyn Member which collectively correlates to the '*Lower Arenaceous'*, *'Upper Bioturbated Sand'* and *'Peaty Sand'* beds mapped by Rogers (1979, 1980) at the Duynefontyn site. The member comprises a widespread and persistent basal arenaceous horizon of light grey, very well-sorted fine quartzose sand with minor phosphatised shell fragments that is subhorizontally bedded with signs of bioturbation and generally less than 2 m in thickness. Overlying this unit is a bed composed of a bioturbated, light olive grey to pale yellowish brown, slightly muddy and somewhat gravelly, well sorted, and fine sand (Figure 4-42) that reaches a thickness of 10 m between the elevations of 8.1 m bmsl and 1 m amsl. This bed is of particular importance since it contains a 10 cm thick bed of slightly gravelly to coarse sand containing ample shark's teeth, fish and whale debris referred to by Rogers (1979, 1980) as the '*Shark Tooth Bed'.* The fossil content ranges from sharks' teeth (*Megaselachus megalodon* and *Carcharodon carcharias*) (Figure 4-43) to teleost fish remains (vertebrae, teeth, scales, and spines), marine-mammal fossils (whale vertebrae, earbones and ribs; dolphin teeth; seal teeth) as well as bird bones (heelbones of the penguin *Nucleornis insolatis*). Similar fossils are found throughout the Duynefontyn Member, but they are most abundant in this layer at elevations ~8 m below present sea level. A 10-15 cm thick unit of moderately sorted, gravelly, muddy fine sand, rich in organic matter, sporadically caps the Duynefontyn Member in places.

Figure 4-42. A portion of the Duynefontyn Member exposed in excavations during the construction of the KNPP. The lower portion shows a completely bioturbated bed overlain by a sandy bed containing gastropods and cobble-sized peaty intraclasts (Photo by J.Rogers).

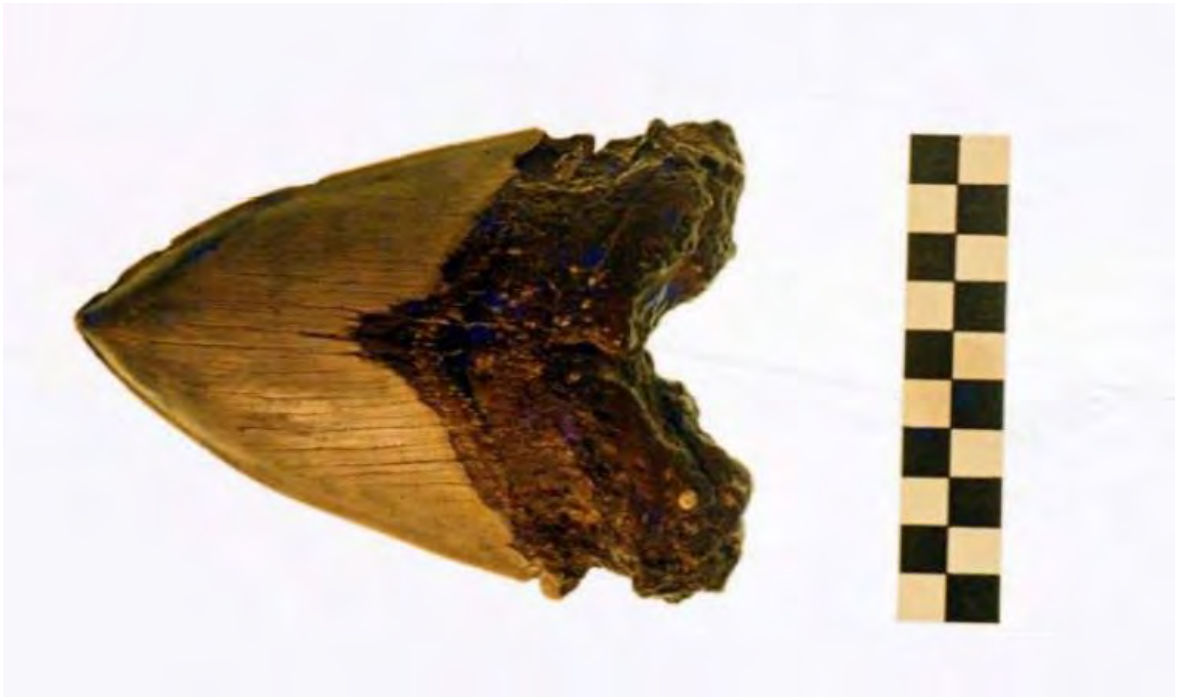

Figure 4-43.Tooth of the Miocene-Pliocene shark *Megaselachus carcharodon* found in excavations at the KNPP in the Duynefontyn Member (Photo taken by J.Rogers). Scale is in centimetres.

Velddrif Formation

The Late Pleistocene ~120 ka (Roberts and Berger, 1997) Velddrif Formation is composed of non-phosphatic gravelly conglomerate, shelly foreshore and coquina deposits with cold water fauna related to Marine Isotope Stage 5e (Tankard, 1976a; Rogers, 1983). The formation reaches a maximum thickness of 17 m and is intermittently exposed along the southwest coast, with most exposures situated outside the site areas near Velddrif, Saldanha Bay, and in the vicinity of Milnerton. The Velddrif Formation deposits are well documented by various authors who also referred to deposits as the outdated and SACS unproved lithostratigraphic names of *'Milnerton Beach Member', 'Milnerton Formation'*, '*Diep River Member'* and *'Killarney Member'* (Kensley, 1972; Rogers, 1980; Theron et al., 1992; Roberts, 2001, 2006; Roberts and Siegfried, 2014). A maximum height of ~7 m asl was initially indicated (Tankard, 1976a, b; Rogers 1980). The formation was encountered by Rogers (1980) at the pumphouse excavations, near the coastal margin at the KNPS site, where the formation attained a 3.5 m thickness.

Langebaan Formation

The sporadically occurring Langebaan Formation represents a multigenerational dune system comprises of the older Diazville Member and younger Kraal Bay Member. Both members comprise cross-bedded biocalc-siliclastic aeolianite, with terrestrial snail fossils and rhizoliths (Rogers et al., 1990; Roberts et al., 2006; Roberts and Siegfried, 2015). The age of the Langebaan Formation ranges from Early Pleistocene Diazville Member to the Late Pleistocene Kraal Bay Member (Roberts and Siegfried, 2015). Archaeological evidence and infrared stimulated luminescence conducted on aeolianites of the Kraal Member known to overly marine-related MIS 5 e deposits of the Velddrift Formation provided dates of 107±7 ka and 103±7 (Roberts and Berger, 1997). Studies undertaken of the Geelbek dunes also supported the existence of at least two chronologically distinct dune formations of ~140 ka and 65 ka North of Duynefontyn. In the Velddrif area, Mammalian fossils in aeolianites of the lower Diazville Member unconformably overlying the marine packages of the Varswater Formation suggest a Late Pliocene age (Hendey 1981a, b). The Langebaan Formation is well exposed only along the Springfontyn Cliffs (Rogers, 1980). Borehole data indicate that the formation probably does not exceed 10 m in thickness in the Duynefontyn site.

Figure 4-44. Langebaan Formation sediments encountered (a) in borehole BH8 (Day and Ridgway, 2000) at the Duynefontyn site between 0-6 m depth, and (b) exposures of cross-bedded aeolianite south of Tieties Baai (S 32°50'30.68"; E 17°51'55.83").

The Springfontyn Formation

The Middle Pleistocene to Holocene aeolian Springfontyn Formation is characterised by unconsolidated, fine- to medium-grained, grey to pale red, structureless quartzose sand with thin peaty horizons with high organic content material (Rogers, 1980; Roberts, 2001; De Beer, et al., 2008) and reaches a maximum known thickness of 67 m near Atlantis (Rogers (1980). The formation's type area is the Springfontyn Cliffs, located northwest of Koeberg. The formation is frequently exposed at the surface unconformably blanketing weathered Malmesbury Group bedrock and forms undulating vegetated dunes in and around the Koeberg and Duyefontyn sites, as seen along the R27 road (Figure 4-45).

Figure 4-45. Vegetated dune of the Springfontyn Formation exposed along the R27 road leading to the KNPS (S 33°36'37.27"; E 18°25'13.63").

Witzand Formation

The uppermost exposed formation of the Sandveld Group comprises the unconsolidated, unvegetated to partially vegetated, calcareous Holocene coastal dunes that form the youngest deposits of the Sandveld Group (Rogers, 1982; Browning and Roberts, 2015). The holostratotype for the formation is located in the Duynefontyn dune plume at the top of the Springfontyn Cliff just north of Duynefontyn. The formation comprises predominantly moderately-to-well sorted, medium-to-fine grained sand. At Groot Springfontyn, the uppermost Langebaan Formation is overlain by a dark brown palaeosol with a midden containing shells of *Donax, Choromytilus* and *Patella* species. Roberts (2001) notes that the presence of bone and stone implements demonstrate a Holocene age for these deposits.

4.4.3 Structural geology

The structural geology of the Tygerberg Formation in the areas surrounding the Duynefontyn site is largely obscured by Cenozoic cover. Structural characteristics are predominantly obtained from excavations and oriented borehole cores at the Duynefontyn site (Dames and Moore, 1976, 1977), coastal outcrops (e.g., Bloubergstrand, Bokbaai) (Von Veh, 1982; Stowe, 1995; Theron et al., 1992) and inland exposures within a 40 km radius around the KNPS (De Beer et al., 2008).

Figure 4-46 shows stereonet plots depicting poles to bedding, joints and fractures, fold axes, faults, and cleavage at the Duynefontyn site and surrounding area within a 40 km radius around Duynefontyn from various authors (Dames and Moore, 1977; Von Veh, 1982; Theron et al., 1992; Stowe, 1995; De Beer et al., 2008).

- Bedding of the Tygerberg Formation at both the KNPS and Duynefontyn sites strike NNW-SSE (320°-330°) with little variation in strike (Figure 4-46a). A larger variation in strike is encountered in areas within the 40 km radius around the both sites, with bedding striking slightly more NW-SE.
- Bedding mainly dips steeply WSW between 60° and 85° as derived from bedding measurements during excavations at Koeberg, adjacent to the Duynefontyn site.

- The Tygerberg Formation is deformed in a succession of slightly inclined to tight upright folds with axial planes trending NW to NNW.
- A regional deviation fold axes of as much as 60° is observed along coastal exposures north and south of Duynefontyn, a possible consequence of polyphase folding and pitching of folds.
- The wavelengths of folds generally range from a few centimetres to ten of metres. In the Tygerberg area the half-wavelength of adjacent major synclines and anticlines varies from 0.5 to 1.5 km (Theron et al., 1992).
- Folds exbibit both a 'S' and 'Z' symmetry. Folds' plunges vary considerably along axial traces and may be doubly plunging. Folds show considerable variation in symmetry especially on a small-scale within minor folds structures as observed by Von Veh (1982) at Bloubergstrand. Strata at the Duynefontyn site form part of a western limb of an NNW striking regional anticline with an almost horizontal fold axis with second order minor folds.
- Fold structures are transected by several sets of quartz-filled shear veins and open joints.

Dames and Moore (1977) identified both transcurrent and thrust faults at the Duynefontyn site (Figure 4-33). The transcurrent type faults occur as a conjugate system of vertical to subvertical strike-slip faults; a right-lateral strike-slip set with an NNE trend and a left-lateral strike-slip set with a WNW trend. These faults are of a meso-scale and generally occur in a discontinuous *en echelon* pattern with fault widths ranging from hairline to 0.5 m with common fault drag features. The faults are frequently infilled with quartz veining or breccia. Lateral offset along these faults range from a few centimetres to several metres with an unknown amount of vertical displacement. Low angle, NE and NW striking thrust faults dip between 10° and 60° with offset in the order of <10 m. Anastomosing shear zones range from 0.1-3 m in width and are associated with less competent lithologies. De Beer et al. (2008) confirmed these observations within the 40 km radius around the Duynefontyn site, denoting reverse, thrust and strike-slip faults at all scales. Sub-vertical, NNW-SSE striking slaty fracture cleavage is generally weakly developed and is rarely intense enough to obliterate bedding with quartzitic units generally not exhibiting cleavage.

Figure 4-46 show a stereonet plot for all joint measurements in these areas. Joints and fracture discontinuities are generally well developed and exhibit an array of strike orientations and dips. Stowe (1995) conducted a detailed joint analysis of the Tygerberg Formation and identified 5 joint sets: Jp, Jh, J1, J2 and J3. Joint set Jp is ubiquitous and dips steeply towards the WSW at 75-85°. The set is parallel to lithological layers and cleavage. Joint set Jh is extensional, unloading, sub-horizontal joints. J1 joints are described as right-lateral shear joints that generally dip east to ESE at 20-50°. J2 extensional cross joints strike at right angles across bedding and dip NNW at 80-90°. J3 joints strike obliquely NE and dip steeply SE. Regionally the two most prominent main sets are the sub-vertical joints (equivalent to Jp and J2) and the sub-horizontall orientated set. The main strike of joints at the Duynefontyn site is orientated ENE-WSW. Generally, joint and fracture apertures range from tight to slightly open (1 mm) to moderately open (10 – 30 mm) with wide apertures openings (> 30 mm) of 50 mm. Joint and fracture openings are either empty or filled with milky white quartz or occasionally exhibit pyrite mineralisation. Joint sets transect all other structural features. However, no joint set or fracture was found to extend into Cenozoic cover rocks.

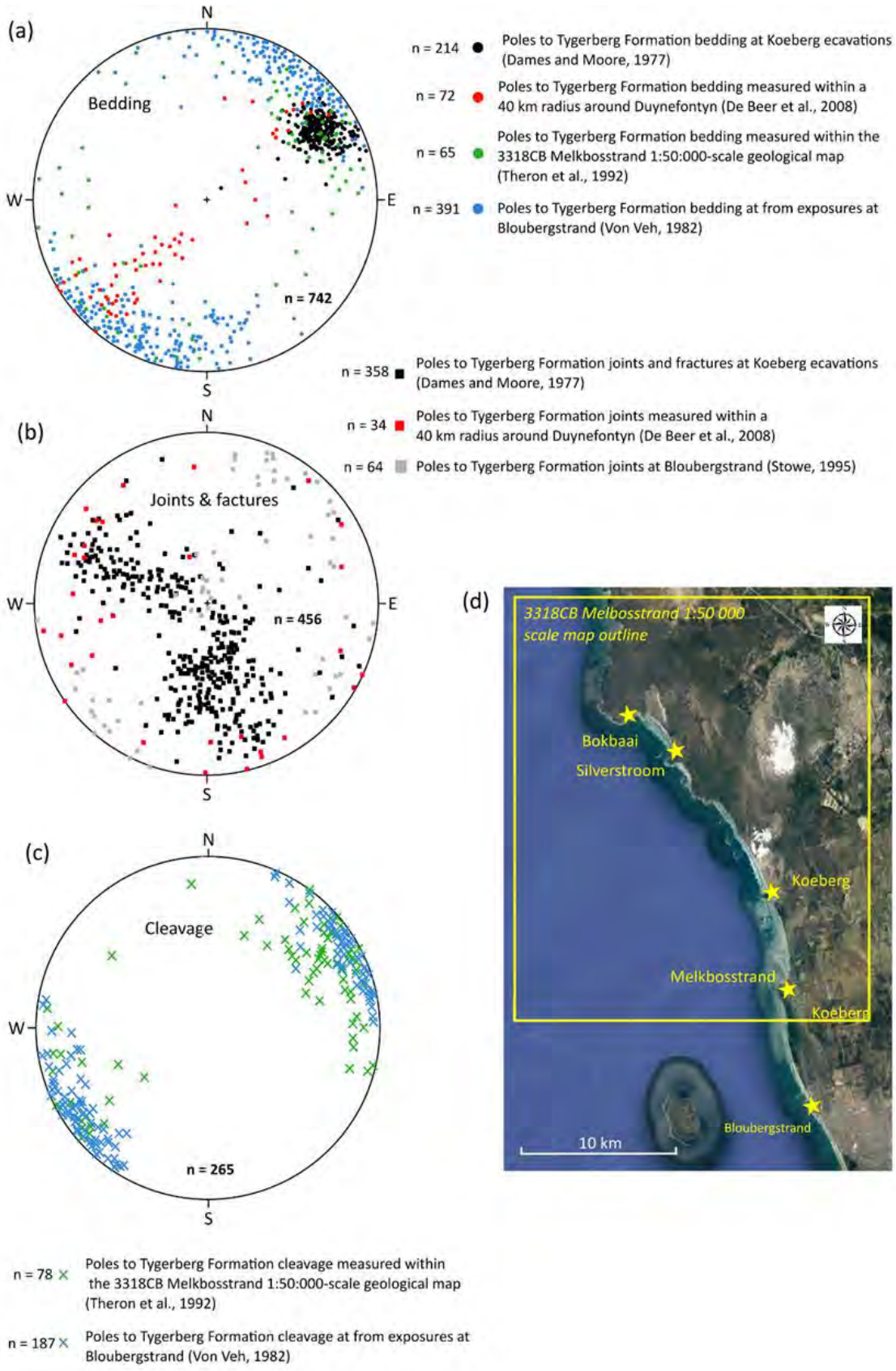

Figure 4-46. Stereonet plots depicting poles to (a) bedding, (b) joints and fractures, and (c) cleavage at the Duynefontyn site and surrounding area within a 40 km radius around the KNPS from various authors (Dames and Moore, 1977; Von Veh, 1982; Theron et al., 1992; Stowe, 1995; De Beer et al., 2008). (d) Index map showing main location from which structural readings are derived.

4.4.4 Regional erosion and Uplift Rates

There are currently two contrasting models for Cenozoic rates of land-level change and geomorphic evolution of southern Africa:

- Episodes of rapid uplift (e.g., King, 1962; Partridge and Maud, 1987).
- Slow to no uplift (e.g., Gurnis et al., 2000; Doucouré and De Wit, 2003).

Partridge and Maud (1987) proposed an episodic uplift model that invoked periods of rapid uplift and long periods of quiescence, resulting in large scale erosion and the development of extensive pediplains. The planar geomorphological features were termed 'African erosion surfaces' (Partridge & Maud, 2000; Partridge et al., 2006). Their model was based largely on field observations and interpretation since analytical tools were limited at that time. Criticism of their model is driven by lack of reliable age-constraints on erosional surfaces and uncertainty in correlating these surfaces over broad regions of the sub-continent. Doubts were also raised as to whether discrete uplift events would result in regional erosion surfaces (Brown et al., 2000; Summerfield, 1996).

More recent data-driven studies provide an alternative view of the episodic uplift model presented by Partridge and Maud (1987). Multiple authors presented evidence of slow rates of erosion and thus low rates of isostatic upliftduring the Cenozoic. Results were based on dating landscape surfaces using cosmogenic nuclides and fission track analysis (e.g., Tinker et al., 2008; Brown et al., 2002, Fleming et al., 1999). A reconstruction of the palaeotopography of the African continent also indicated that the interior topography had already been high in the Cretaceous and that modern topography did not require high uplift rates during the Cenozoic (Doucouré & de Wit, 2003). The long-term uplift (Cretaceous to Cenozoic) history of southern African was however marked by phases of uplift and inactivity (e.g., Baby et al., 2020; Marker and Holmes, 2010; Dauteuil et al., 2015; Walford and White, 2005). Along the southern coast of South Africa (or southern Cape), Tinker et al. (2008) calculated denudation of <1000 m during the Cenozoic. Throughout the Pliocene and Pleistocene, the coastal margin of the southern African Plate has been relatively tectonically stable (Roberts, 2006; Chen et al., 2014; Kounov et al., 2015).

Very slow land erosion rates of 5.4 m/My (4.4 m/My rock uplift rate) were calculated based on the ^{10}Be content of sand samples collected from six different river systems along southern South Africa (Bierman, 2012). Erlanger et al. (2012) inferred incision rates of less than <20 m/Ma with rock uplift rates of 9 m/My near Durban and 16 m/My within the Sundays River Valley. Linear inverse modelling of drainage networks in the Northern and Western Cape yielded average uplift rates of 11 ± 20 m for the past 15 Ma (Rudge et al., 2015). For South Africa, glacial isostatic adjustment models show only minor departures from eustacy (Raymo et al., 2011; Rovere et al., 2014) and are characterised by relatively small uncertainties under various mantle viscosity profiles used to predict glacial isostatic adjustment for Pleistocene and Pliocene time scales (Rovere et al., 2014). Uplift or subsidence during the Pleistocene and Pliocene along passive margins (Austermann et al., 2017; Moucha et al., 2008), appears to have a slight, although still uncertain effect along the western and southwest coasts of South Africa.

The Plio-Pleistocene relative sea level estimates by Hearty et al. (2020) were used to determine long term vertical tectonic uplift. Their results suggest an average, relatively low

uplift rate of 3.5-4.8 m/My during this time period for the broader west coast. This rate would have a minimal uplift effect on MIS 5e (125 ka) and MIS 11 (400 ka) (on average, <2 m). Their rate is lower than those reported by Rudge et al. (2015) for the last 13 ± 5 My from Hondeklip Bay (8 ± 3 m/My) and the 20±10 m/My for Saldanha Bay. Founded on comparison of stratigraphic, palaeontological and proxy sea level data for the Late Tertiary, Roberts (2006) suggests a 0-2 m/My tectonic uplift rate along the West Coast since the basal Pliocene (5.33 Ma). Using palaeontology and regional lithostratigraphy to link marine terraces along the west and southern coasts to the same transgressive episodes and chronologies, Roberts et al. (2006) also suggests that the slightly higher elevation (120 m) of the Alexandria and De Hoopvlei Formations (South Cape Coast) when compared to their lower West Coast counterparts (90-100 m) could indicate relative post basal Pliocene tectonism of ~20-30 m (3.75-5.62 m per My).

A regional study on marine terraces supported by geochronology investigations (Hanson et al., 2012, Bierman, 2012, Erlanger, 2012) provides evidence for relative stability along the southern Cape coast. At Thyspunt, in the Eastern Cape, burial ages derived from six paired CN samples of marine terrace bedrock and overlying beach gravels estimated an uplift rate of 5.0 ± 0.7 m/My. This is relatively similar, although slightly lower than the long-term incision rate of 6.6 ± 1.1 m/My for the Sundays River (near Gqeberha) terraces, some 120 km east of Thyspunt. These low rates compare to similar ^{10}Be denudation rates of between 2.3 ± 0.4 m/My and 8.8 ± 0.2 m/My for river sediment, bedrock outcrops, and fluvial gravels collected from the Cape Fold Belt in the Western Cape (Scharf, 2012).

Twenty-one (21) CN samples collected between Oyster Bay and Cape Recife yielded Middle Pleistocene ages between 250 and 450 ka, coinciding with MIS 9 and MIS 11 (Bierman, 2012). Total history ages for bedrock samples from 13 ± 1 m terraces at Oyster Bay and St. Francis Bay as well as a 12.8 m wave-cut platform at Cape Recife (southeast of Gqeberha) are correlated with MIS 11 (~400 ka) and can also be correlated with MIS 11 terraces at Mossel Bay situated at an elevation of 14 m. This would infer that uplift has been relatively uniform along most of the southern coast of South Africa during the past 400 ka (Hanson et al., 2012). The unexpectedly younger (MIS 5) ages of shorelines at ~10 m amsl at the Brazil nuclear site (West Coast) and Blind River (east coast) remain an unresolved issue but could be due to extreme wave energy or uplift of ~4 m between ~400-130 ka.

Roberts (2006) and Hanson et al. (2012) calculated uplift rates since MIS 5e (~130-117 ka) for the western and southern Cape coast. Late and possible Middle Pleistocene age data correlate with known sea levels above or near present levels, bolstering the notion of a tectonically stable coastal belt. If the maximum uplift rate of ~11.23 m/My inferred from Late Tertiary terraces (Roberts, 2006) is maintained since the inception of the Late Pleistocene (130 ka) to the present, this yields a total uplift of 1.46 m over the past ~130 ka. Ultimately this demonstrates low rates of uplift from the Middle Miocene to the Late Pleistocene, consistent with a stable intraplate setting (Roberts, 2006). Mantle convection (Burke, 1996; Simmons et al., 2007), igneous activity (Conrad & Gurnis, 2003), and flexural isostatic response (Gilchrist & Summerfield, 1990) are regarded as some of the mechanisms responsible for the above-mentioned slow uplift (de Wit, 2007).

The SSM TI Team evaluated results presented in the onshore fault report (Coppersmith et al., 2024) to better understand regional erosion rates and implications for tectonics. In order to evaluate erosion rates in the Western Cape, the authors collected eight bulk sediment samples

from different drainages in the region (Coppersmith et al., 2024). The selection of sample locations was based the position of the drainage relative to the watershed it was eroding. The watersheds eroded both the mountain ranges composed of Table Mountain Group quartzites and the rocks of the Malmesbury Group underlying the flat landscape along the western seaboard.

River sand ^{10}Be data showed that on average the field area is slowly eroding at rates of 5.9±0.5 m/My. These average and range of basin-scale erosion rates are fully consistent with those previously reported for similar South African landscapes. For example, Bierman et al., (2014) reported basin-scale erosion rates in the Eastern Cape region of 3.4 to 6.0 m/My for 8 basins ranging in size from 106 to 21,415 km^2. The mean rate (5.4 m/My) was similar to that reported by Scharf et al., (2012) for 10 smaller catchments underlain by quartzite (5.2 m/My).

Erosion rates of only a few metres per million years mandate that surface features are likely to persist on the landscape for many tens of thousands to hundreds of thousands of years. Such persistence suggests that vertical or horizontal surface offsets from large earthquakes (> 1m slip) should be visible if they were present on the landscape. Even fault scarps produced from more recent smaller earthquakes may remain visible in the landscape for thousands of years. The SSM TI Team thus concludes that the area-wide absence of such scarps is likely not due to erosion removing their surface expression but rather due to a lack of offset over a period of at least several hundred thousand years.

4.5 SITE GEOTECHNICAL STUDIES

The site-specific V_S characteristics are a fundamental input to the site response analysis. Estimates of V_S can come from a variety of sources, each with advantages and limitations. Several phases of geotechnical and geophysical tests were performed across the proposed Duynefontyn site (i.e., northwest of the existing KNPS). Only two V_S profiles from cross-hole testing at the KNPS were available, as documented in the Baseline report (Stamatakos et al.,2022), and these V_S profiles are compared with the more extensive Duynefontyn V_S profiles in Section 4.5.2.

Site investigations at the Duynefontyn site were performed by SRK Consulting (as reported in Du Plessis, 2021) using downhole (DH) seismic testing in 8 boreholes and multi-channel analysis of surface waves (MASW). The MASW tests performed by SRK did not develop V_S profiles deep enough into the rock, and thus are not considered in this analysis. Additional site investigations for this project included combined MASW and microtremor array measurements (MAM) performed at two locations (centred over boreholes DA and SA2) by CGS and interpreted by Prof. Brady Cox. Wireline Workshop performed PS-suspension logging in 6 CGS boreholes (DA, SA2, and ST1-ST4) that were ultimately re-interpreted by Prof. Cox and CGS personnel. The locations of the SRK boreholes, the MASW/MAM surface arrays, and the CGS boreholes are shown in Figure 4-47, and metadata is provided in Table 4-15, Table 4-16 and Table 4-17.

The two MASW/MAM testing locations were each centred on one of the two borehole array sites (i.e., the location of proposed surface and borehole ground-motion instruments at the time and completed during the timeframe of the Duynefontyn SSHAC project). These locations are called DA and SA2, which are in the southern and northern regions of the Duynefontyn site, respectively (Figure 4-47), and are northwest of the existing KNPS. Field testing took place 21-25 April 2022. Cox et al. (2024) interpreted the data from these MASW/MAM tests and produced V_S profiles down to depths of approximately 1500 m below the ground surface. Additional details of the MASW/MAM measurements and analyses are described in Section 4.6.1.

SRK performed DH testing in eight boreholes (labelled BH46-BH53) across the proposed Duynefontyn site and northwest of the existing KNPS. SRK (Du Plessis, 2021). The DH boreholes generally extended 80 m below the ground surface and up to 50 m below the base of the existing sand layer (i.e., top of rock). Drilling took place 26 May through 3 August 2021. Additional details of the DH measurements and analyses are described in Section 4.6.2.

Wireline Workshop performed PS logging to a depth of ~90-100 m (below the ground surface) at the DA and SA2 locations and shallower PS logging (~50 m below the ground surface) at four other locations (ST1-ST4) across the Duynefontyn site and northwest of the KNPS. Matamela and Cox (2024) interpreted the raw data from these measurements to obtain estimates of V_S at discrete points within the depths tested. Field testing took place in November and December 2022. Additional details of the PS logging measurements and analyses are described in Section 4.6.3.

Three different seismic techniques were used to measure V_S due to their complementary nature in terms of depth of profiling, ability to resolve thin layers and wavelength of seismic waves. Additionally, the different techniques provide confirmation of the general velocity

structure and quantification of epistemic uncertainty across different test methods. The MASW/MAM method provides the deepest profiling of V_S and represents wavelengths more similar to earthquake waves but has problems resolving thin layers at depth. Additionally, the presence of the sand above the rock at the site introduces uncertainty in the inverted V_S profiles. The DH method utilizes the same type of waves associated with the site response analyses (i.e., SH waves) and can resolve relatively thin layers, but it is difficult to measure V_S in deep layers because of attenuation of the waves from the impact source at the ground surface. The PS logging method can profile very deep and potentially can resolve very thin layers, but the wavelengths of the seismic waves are so small that the measurements show significant variability over small distances. Both the DH and PS logging methods require the selection of the wave arrival on a time record, which is subjective. The clarity of the arrivals is influenced by many factors; hence, it is important for the picks of the wave arrivals to be evaluated by experienced analysts.

The proposed plan at the Duynefontyn site prior to construction includes removal of the surficial cover strata down to the top of the shallowest rock layer (similar to the excavation performed at the KNPS before its construction). The MASW/MAM, DH, and PS logging tests were performed with the cover strata in place; thus, the resulting V_S profiles inherently include the surficial strata. Therefore, to accurately portray the V_S profile of the sites after excavation of the cover strata, the GMM TI Team modified the measured V_S profiles to exclude the influence of the cover strata, prior to using the V_S profiles in site response analyses. The appropriate method to exclude the cover strata depends on the data collection method and is discussed subsequently in each method-specific section.

Figure 4-47. Locations of SRK boreholes (BH46 through BH53), MASW/MAM surface arrays (DA, SA2), and CGS boreholes (DA, SA2, ST1 through ST4).

Table 4-15. Metadata for MASW testing (Cox et al., 2024).

Site Name	Array Centre Latitude	Array Centre Longitude	Surface Elevation (m above msl)	Array Diameters (m)
DA	-33.664585	18.430594	17.25	50
				300
				1000
SA	-33.657416	18.426505	17.0	50
				300
				1000

Table 4-16. Metadata for the boreholes used for downhole testing by SRK.

Test Name	Latitude	Longitude	Total Borehole Depth (m)	Depth to top of rock (m)	Surface Elevation (m above msl)	Drilling Date
DH_BH46	-33.66506	18.440776	80	29.45	24.75	26 May 2021
DH_BH47	-33.66354	18.43753	81.6	31.6	27.25	7 June 2021
DH_BH48	-33.66116	18.432165	80	30.8	19.5	17 July 2021
DH_BH49	-33.65964	18.429318	80	31.05	16.75	10 July 2021
DH_BH50	-33.65484	18.430676	82.89	33.12	26	17 July 2021
DH_BH51	-33.65654	18.426492	83	32.45	20.75	3 August 2021
DH_BH52	-33.65698	18.423557	72.5	22.55	15	27 July 2021
DH_BH53	-33.65808	18.426838	80	39.0	17.25	20 July 2021

Table 4-17. Metadata for the boreholes used for PS logging.

Test Name	Latitude	Longitude	Surface Elevation (m above msl)	Maximum Depth below surface (m)
DA	-33.664586	18.430594	17.25	100 m
SA2	-33.657417	18.426506	17.0	90 m
ST1	-33.669075	18.430928	13	120 m
ST2	-33.666486	18.436633	21.25	80 m
ST3	-33.663147	18.428228	16.5	80 m
ST4	-33.659836	18.436336	26.75	80 m

4.5.1 Shear-wave velocity profiles from MASW/MAM testing

V_S profiles from MASW/MAM testing are established based on interpretation of dispersion data through inversion. The inversion process involves finding layered earth models whose theoretical dispersion curves best match the experimentally measured dispersion data. This process yields non-unique solutions, each with a "misfit" value (i.e., quality of fit between theoretical and experimental dispersion data). The range of V_S profiles that could reasonably match the dispersion data can vary widely depending on the analyst's approach and assumptions (e.g., mode interpretation, layer thicknesses). The following discussion highlights some of these assumptions, as documented by Cox et al. (2024).

It is typical to initially assume that the dispersion data from MASW/MAM can be fit using a fundamental mode (FM) interpretation. However, in cases where it is expected that there could be a mode jump (e.g., due to a strong interface between low and high V_S material) or when the dispersion data is not fit well with a FM interpretation, other higher modes may also be considered using a multi-mode (MM) interpretation. The decision to adopt a FM or MM interpretation can be guided by additional information (e.g., identifying site-specific characteristics that could explain the presence of mode jumps).

While inverting the MASW/MAM dispersion data into V_S profiles, Cox et al. (2024) assumed different mode interpretations to develop two sets of inversions. The first set of inversions assumed a FM fit to the data and the second set of inversions assumed a MM fit to the data. The FM inversions generated V_S values at depth that were greater than 4,000 m/s (capped at 4,500 m/s), particularly at the DA site. Cox et al. (2024) indicated that these velocities are unlikely for relatively shallow depths (i.e., as shallow as 100 to 500 m). The MM interpretations used the fundamental mode and first higher mode and resulted in maximum values of V_S in the profiles less than about 3,300 m/s (i.e., the maximum V_S of the Al Atik and Abrahamson (2021) V_S profile that the TI Team chose to use for the host V_S profile). However, Cox et al. (2024) indicated that the MM inversions would have likely exceeded this maximum if allowed to do so.

Cox et al. (2024) considered the MM inversions as likely better interpretations of the measured dispersion data. Strong impedance contrasts (e.g., the sand-rock interface at the Duynefontyn site) often yield mode jumps and/or superimposed modes that can be difficult to discern. However, Cox et al. (2024) provided both FM and MM results to the GMM TI Team to enable the consideration of both sets of V_S profiles and assign appropriate weights.

To capture additional epistemic uncertainty in the inversion process, Cox et al. (2024) considered a range of layering ratios (LRs) during the inversions. The LR parameter tunes the average layer thickness in a V_S profile to be thinner or thicker. For example, a higher LR will typically lead to fewer, thicker layers compared to smaller LRs. Cox et al. (2024) considered several LRs during the inversion process, but ultimately selected five LRs that yielded acceptable results: 1.5, 2.0, 3.0, 5.0, and 7.0.

Finally, Cox et al. (2024) also computed horizontal-to-vertical spectral ratios (HVSRs) to guide the inversions. HVSRs were computed for all stations used in MAM testing at the DA and SA2 sites. If he identified a well-defined peak in the HVSR, the frequency of the lowest frequency peak was used to estimate the fundamental resonant frequency of the site. This fundamental frequency is a general characteristic of the site that can be used to further refine the selection of V_S profiles in the inversion process. However, due to the strong impedance contrast between the surficial sand and the underlying rock, these HVSR peaks mainly represent only the sand-rock interface (i.e., peaks observed between 2-5 Hz in Cox et al., 2024). Because the sand will ultimately be removed from the site, the GMM TI Team did not use the HVSR data to judge the inverted V_S profiles in the rock. No lower frequency peaks in the HVSR were observed that may could have been used in the inversions to help constrain the V_S profile in rock.

The GMM TI Team received a total of 20 median V_S interpretations (each median represents 100 individual V_S profiles). The 20 median profiles were developed from combinations of 2 mode interpretations (MM and FM) and five LRs (1.5, 2.0, 3.0, 5.0, and 7.0) for each of the two MASW/MAM sites (DA and SA2). These V_S profiles from the MASW/MAM testing extend to a depth of ~1500 m below ground surface. Figure 4-48, Figure 4-49, Figure 4-50 and Figure 4-51 show the top 100 V_S profiles for the DA-FM, DA-MM, SA2-FM, and SA2-MM interpretations, respectively, as provided by Cox et al. (2024). Also shown are the theoretical dispersion curves for each V_S profile, as well as the experimental dispersion data with uncertainty bounds. When fitting the experimental dispersion data with multiple modes (e.g., Figures 4-49, 4-51), the higher frequencies are fit with the fundamental mode)i.e., lower set of curves) and the lower frequencies with the first higher mode (upper set of curves). The resolution depth (d_{res}), defined as half of the resolution wavelength ($d_{res} = \lambda_{res}/2$ = 1282 m), is highlighted in each figure. At depths greater than the resolution depth, the V_S profiles are constrained by less reliable dispersion data and should be used with caution. Although V_S values below this depth are less certain, they provide guidance that is better than blind assumptions or guesses. Figure 4-52 summarizes the standard deviation of ln V_S (σ_{lnVs}) for each set of 100 profiles for the 5 LR for the DA-FM, DA-MM, SA2-FM, and SA2-MM interpretations. The V_S datasets generally show the most variability in the top 200 m (σ_{lnVs} ~ 0.1 to 0.4), with significant less variability (σ_{lnVs} < 0.05) at depth. The small variability at depth is a result of the large phase velocity (> 3000 m/s) at low frequencies in the dispersion data and the flattening of the dispersion curve at low frequencies (e.g., below 2-3 Hz in Figure 4-48). There are instances of larger variability at depth, but only at a location of a variable

impedance contrast (e.g., between 700-1000 m depth in the MM interpretations). Additionally, the LR7.0 profiles display the smallest variability among all the LR due to the fewer layers used in the inversions. The sigma (σ_{lnVs}) reported here only represent σ_{lnVs} for the individual test locations. Thus, it is not appropriate to compare different test locations to explain the smaller σ_{lnVs} at depth. Additionally, there are some differences in the phase velocities at low frequencies at the two test locations, such that the resulting Vs at depth for the two test locations are somewhat different, particularly for the FM interpretation (Figure 4-53).

The MASW/MAM V_S profiles inherently included the surficial sand, and thus required removal of V_S values that represent the sand layers before they could be used in site response analyses. For each V_S profile, the TI Team established that any shallow layer with V_S less than 500 m/s was associated with sand and was removed. This threshold of 500 m/s was determined from the DH V_S profiles (discussed in the next section) and the associated geologic descriptions from the associated boreholes. Using this approach, the top of the rock was assigned at the top of the shallowest V_S layer with V_S greater than or equal to 500 m/s. These depths were typically about 30 m below the existing ground surface. There is uncertainty in the approach used to remove the sand from the measured V_S profiles, as well as in the V_S threshold used to identify the sand/rock interface, but alternative approaches to define the top of rock (e.g., identifying a V_S contrast) would have introduced their own uncertainties. The GMM TI Team considers the uncertainty associated with the removal of the sand from the V_S profiles relatively modest, and in a general sense the GMM TI Team assumes that it is taken into account via other components of the logic tree (i.e., alternative V_S branches, model error).

The original median V_S profiles are shown in Figure 4-53 and the modified median V_S profiles after removing the sand are shown in Figure 4-54. The V_S profiles before removing the sand (Figure 4-53) indicate that the V_S values in the top 30 m representing the sand are generally below 300 m/s, and then a significant increase in V_S occurs. However, some profiles increase to a value only slightly larger than 500 m/s (e.g., SA2-FM LR1.5) while others increase to values as large as 2500 m/s (e.g., SA2-MM LR7.0). This variability in the velocity that first exceeds 500 m/s leads to significant variability in the V_S at the top of the profiles when the sand is removed (Figure 4-54). This variability is a consequence of the approach used to define the top of rock and is discussed further in the next section.

There are several differences across the 20 median V_S profiles shown in Figure 4-54. As mentioned above, there is significant variability in the V_S at the top of the rock. Also, the V_S values at depth are smaller for the MM interpretations. Finally, the V_S profiles associated with smaller LR have more layers, which result in a more gradual increase in V_S over the top ~400 m. These differences will all contribute to the epistemic uncertainty in the SAF computed from site response analyses.

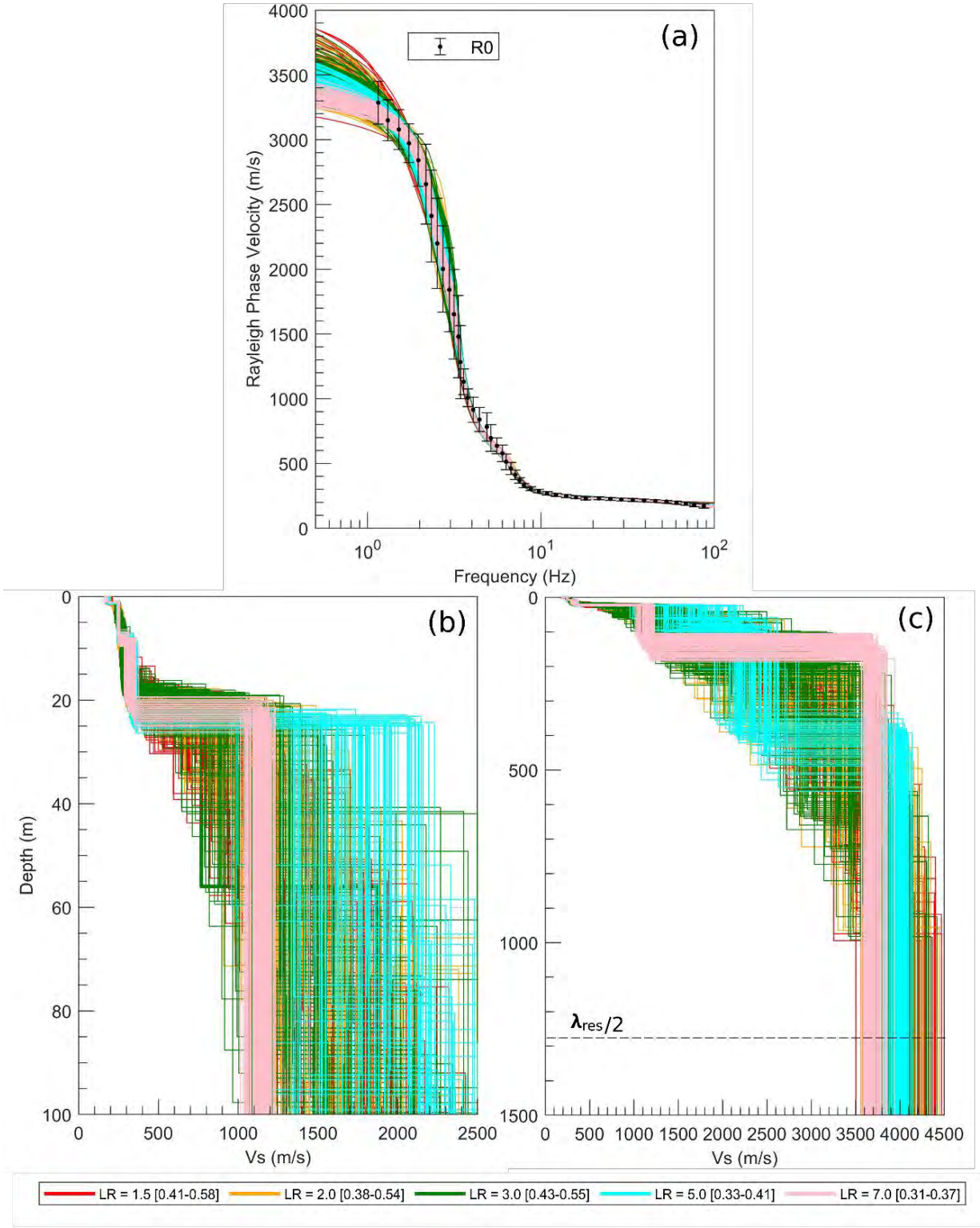

Figure 4-48. Summary of inversion results for the DA-FM inversions: a) theoretical Rayleigh dispersion curves and error bars representing experimental dispersion uncertainty bounds, b) V_S profiles in the upper 100 m, and c) V_S profiles for the entire 1500 m depth associated with the best 100 V_S profiles (based on misfit). Dispersion misfit values indicated inside square brackets.

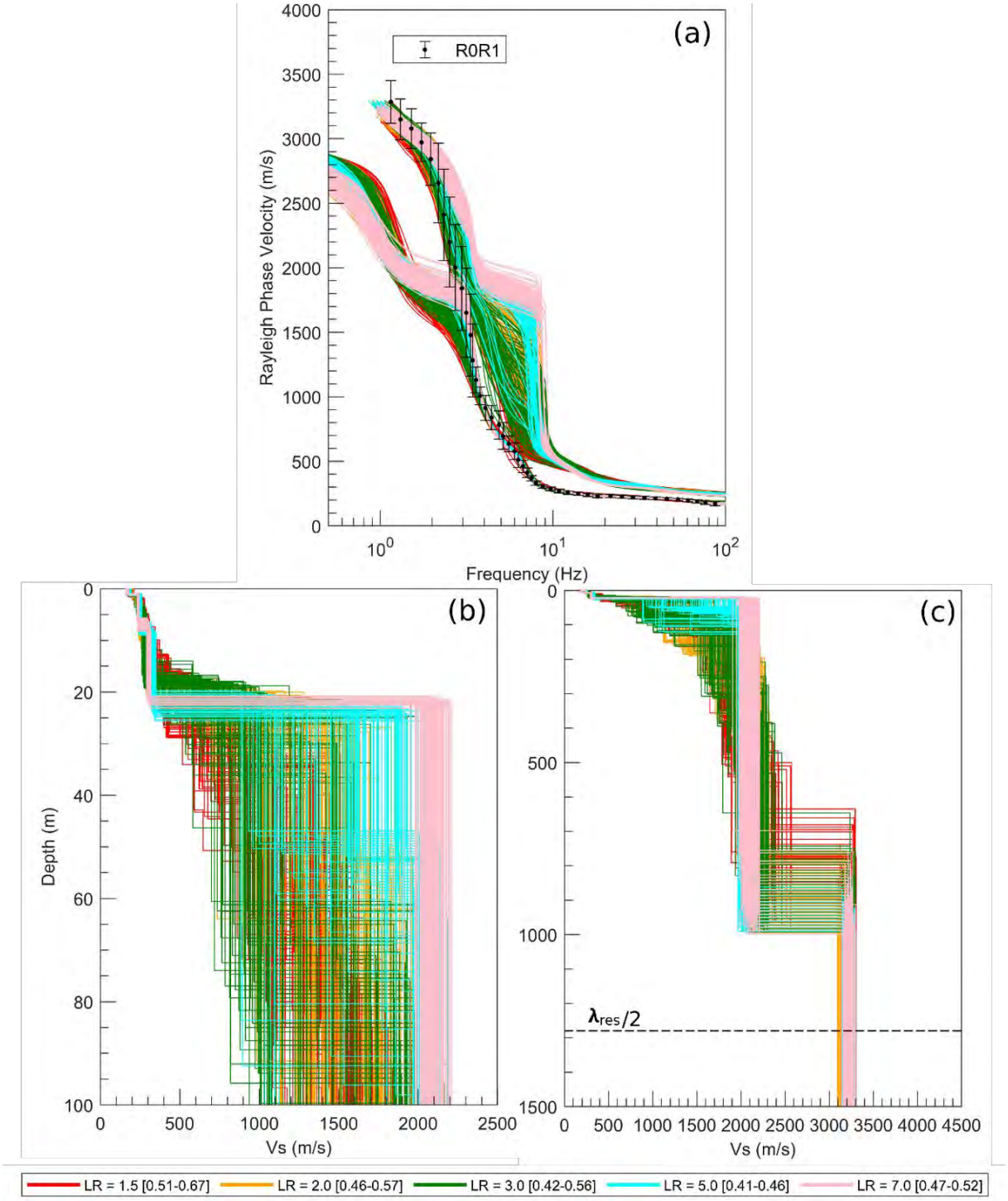

Figure 4-49. Summary of inversion results for the DA-MM inversions: a) theoretical Rayleigh dispersion curves (fundamental mode are lower set of curves, 1st higher mode is higher set of curves) and error bars representing experimental dispersion uncertainty bounds, b) Vs profiles in the upper 100 m, and c) Vs profiles for the entire 1500 m depth associated with the best 100 Vs profiles (based on misfit). Dispersion misfit values indicated inside square brackets.

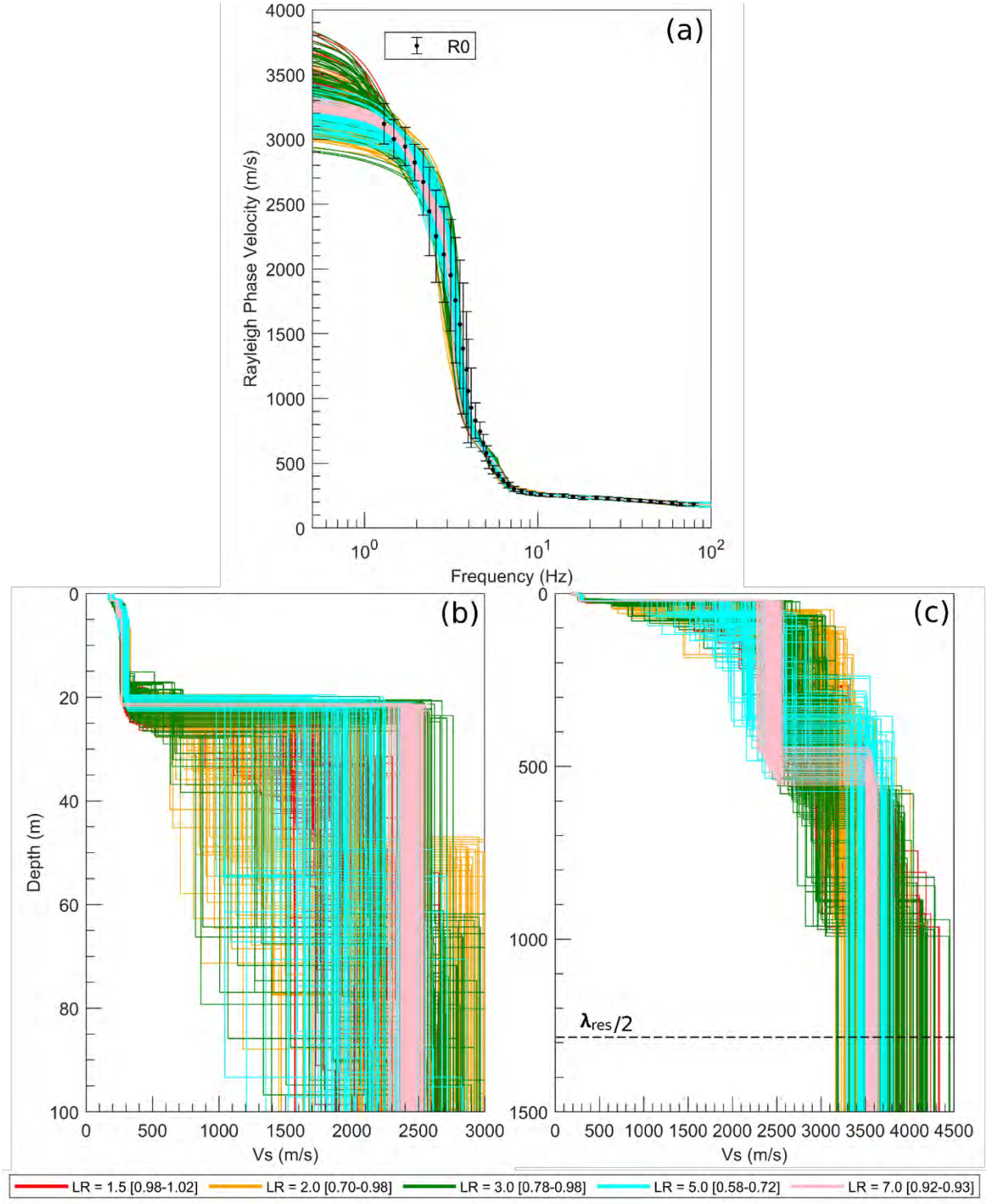

Figure 4-50. Summary of inversion results for the SA2-FM inversions: a) theoretical Rayleigh dispersion curves and error bars representing experimental dispersion uncertainty bounds, b) V_S profiles in the upper 100 m, and c) V_S profiles for the entire 1500 m depth associated with the best 100 V_S profiles (based on misfit). Dispersion misfit values indicated inside square brackets.

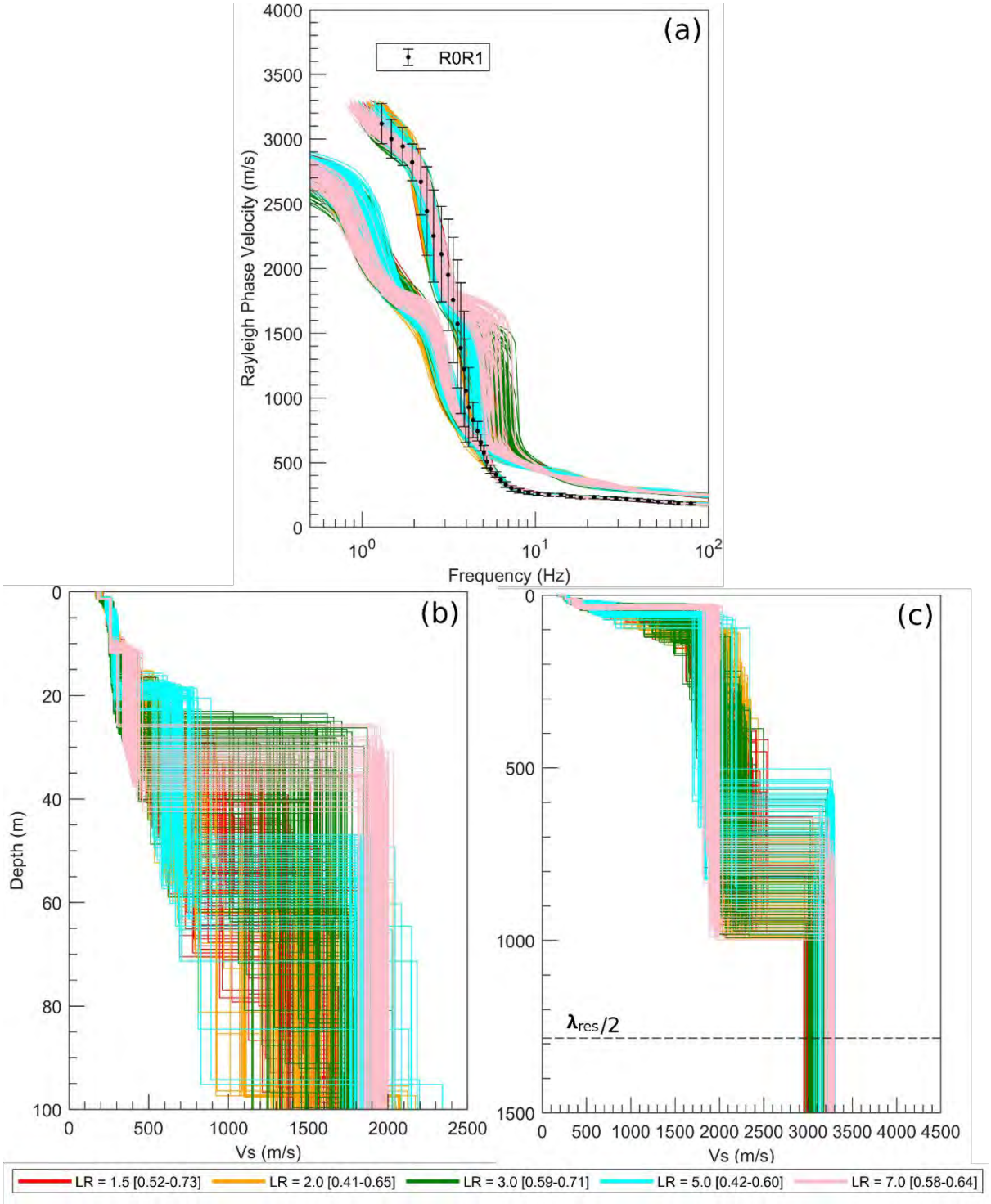

Figure 4-51. Summary of inversion results for the SA2-MM inversions: a) theoretical Rayleigh dispersion curves (fundamental mode are lower set of curves, 1st higher mode is higher set of curves) and error bars representing experimental dispersion uncertainty bounds, b) V_S profiles in the upper 100 m, and c) V_S profiles for the entire 1500 m depth associated with the best 100 V_S profiles (based on misfit). Dispersion misfit values indicated inside square brackets.

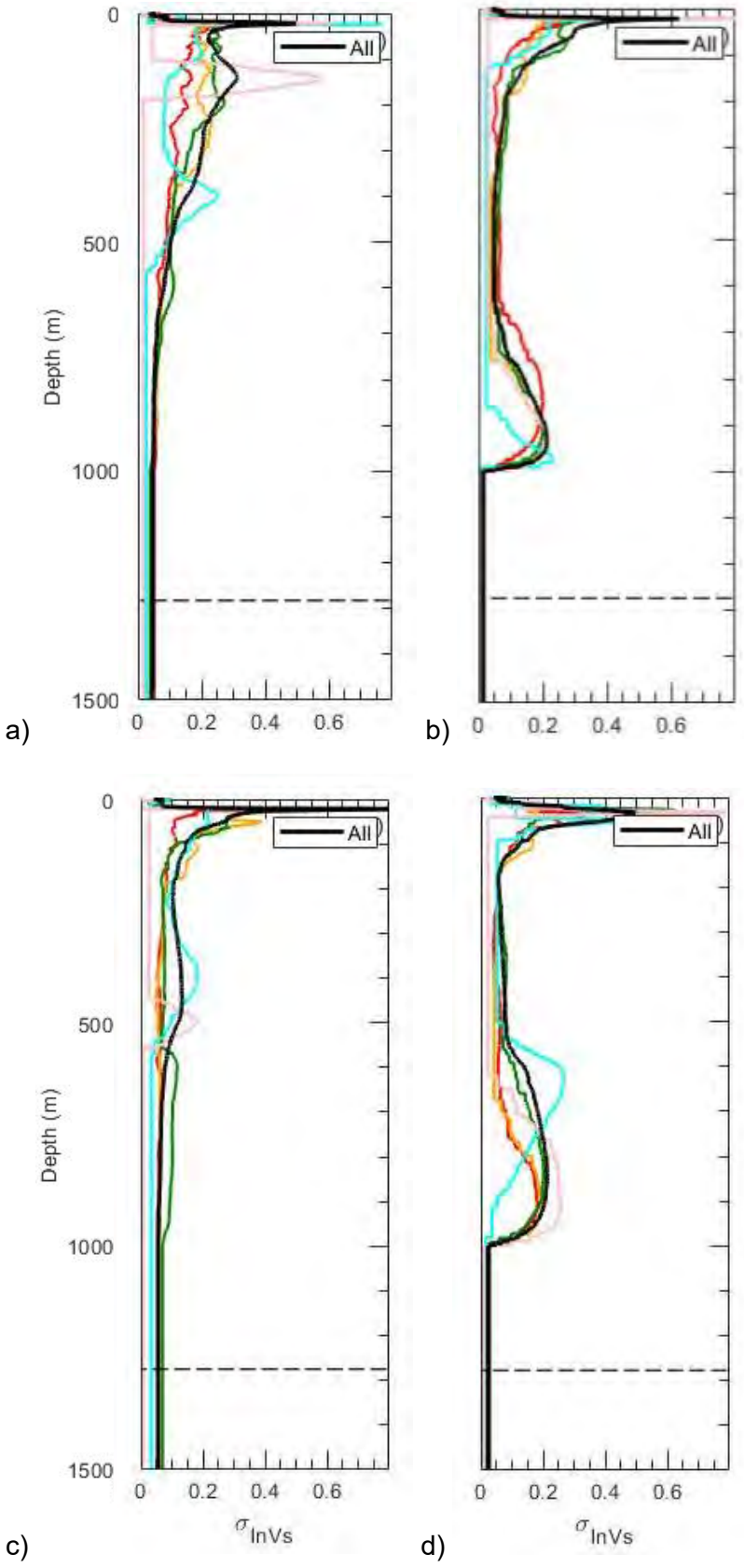

Figure 4-52. Variability in V_S for the top 100 profiles from a) DA-FM, b) DA-MM, c) SA2-FM, and d) SA2-MM interpretations. LR1.5 = red, LR2.0 = yellow, LR3.0 = green, LR5.0 = cyan, LR7.0 = pink, black = average for all LRs.

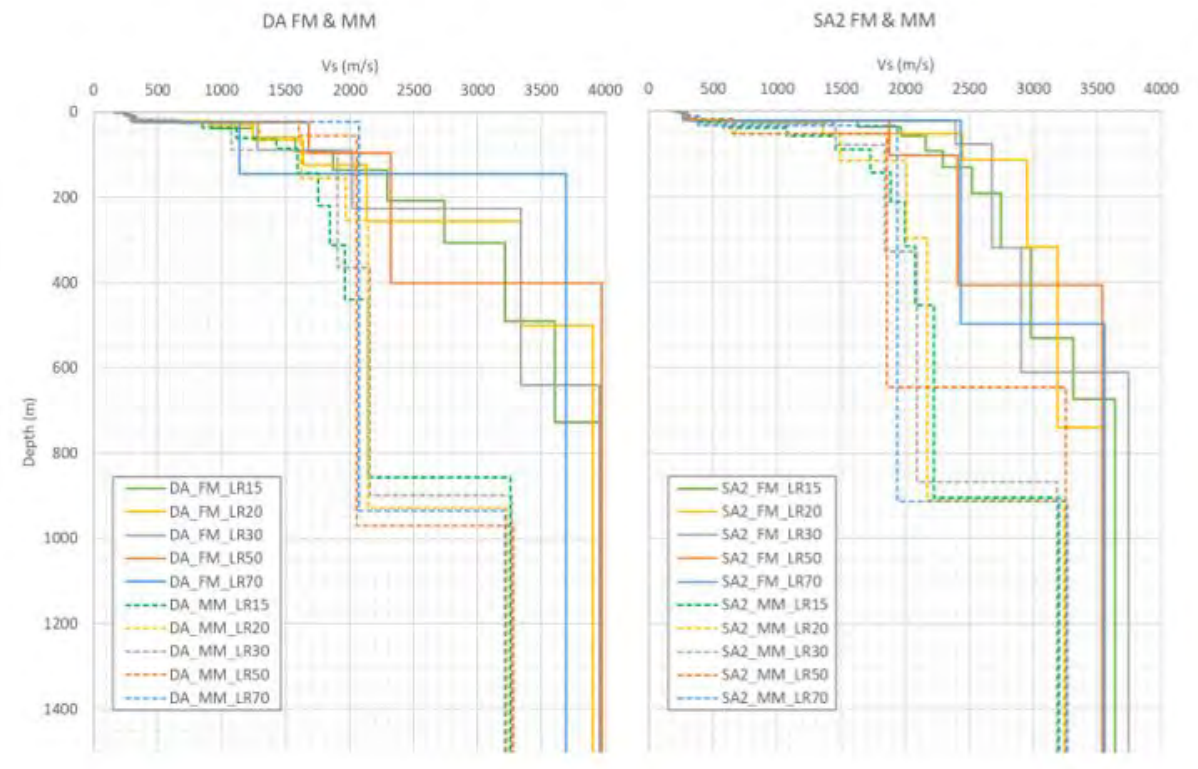

Figure 4-53. Summary of median V_S profiles before surficial sand layers removed for a) DA site and b) SA2 site.

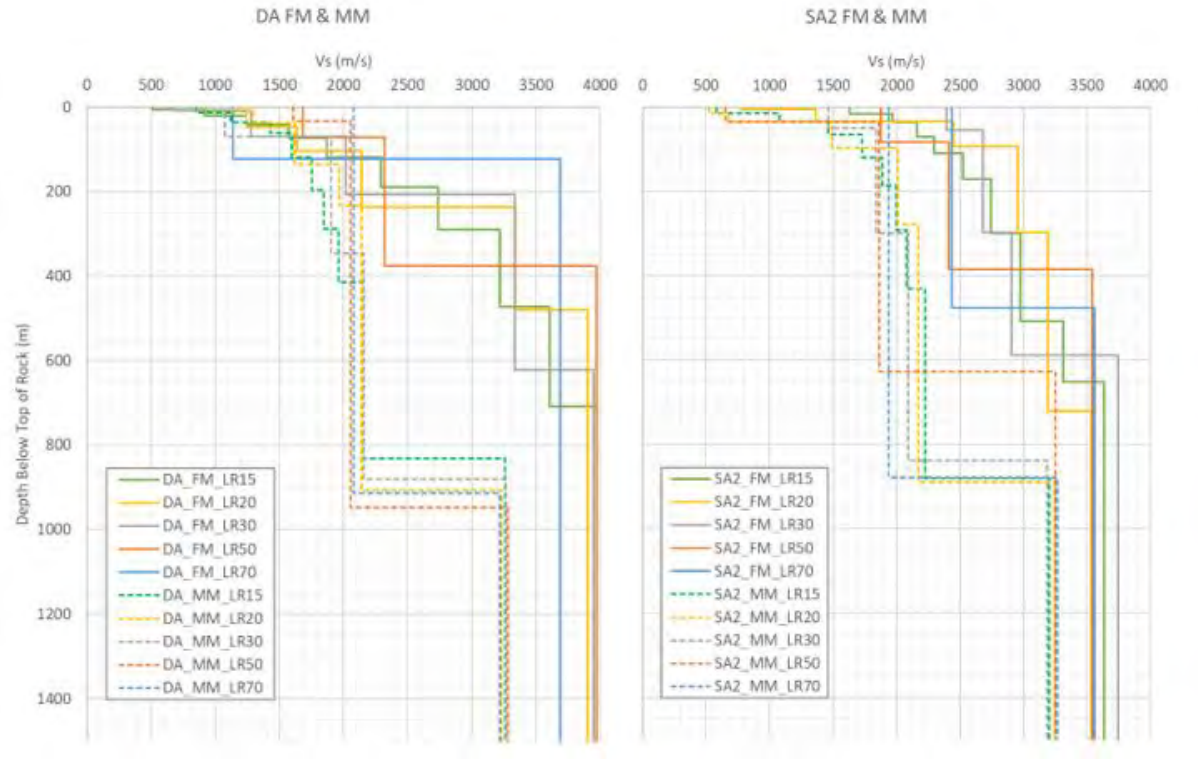

Figure 4-54. Summary of median V_S profiles after surficial sand layers removed for a) DA site and b) SA2 site.

4.5.2 Shear-wave velocity profiles from downhole testing

V_S profiles from DH testing were established based on interpretation of travel times of shear waves (Figure 4-55). There are different approaches that can be used to interpret the travel times to derive a velocity profile. Figure 4-56 shows an example plot of travel time versus depth from the SRK information in Du Plessis (2021). Du Plessis (2021) interpreted the V_S profile from these data in two ways: an interval interpretation where the difference in travel time between adjacent measurements is used to compute velocity and a layered interpretation where layers are identified in the travel time versus depth plot with constant slope (i.e., velocity). As shown in Figure 4-55, the interval interpretation generates thin layers while the layered interpretation generates thicker layers. However, the layered interpretation requires more judgment in terms of identifying the layers where the slope of the travel time curve is constant.

The GMM TI Team considered three sets of interpretations for the eight DH boreholes: (1) the SRK interval interpretation, (2) the SRK layered interpretation, and (3) a revised layered interpretation by Cox (2023, personal communication).

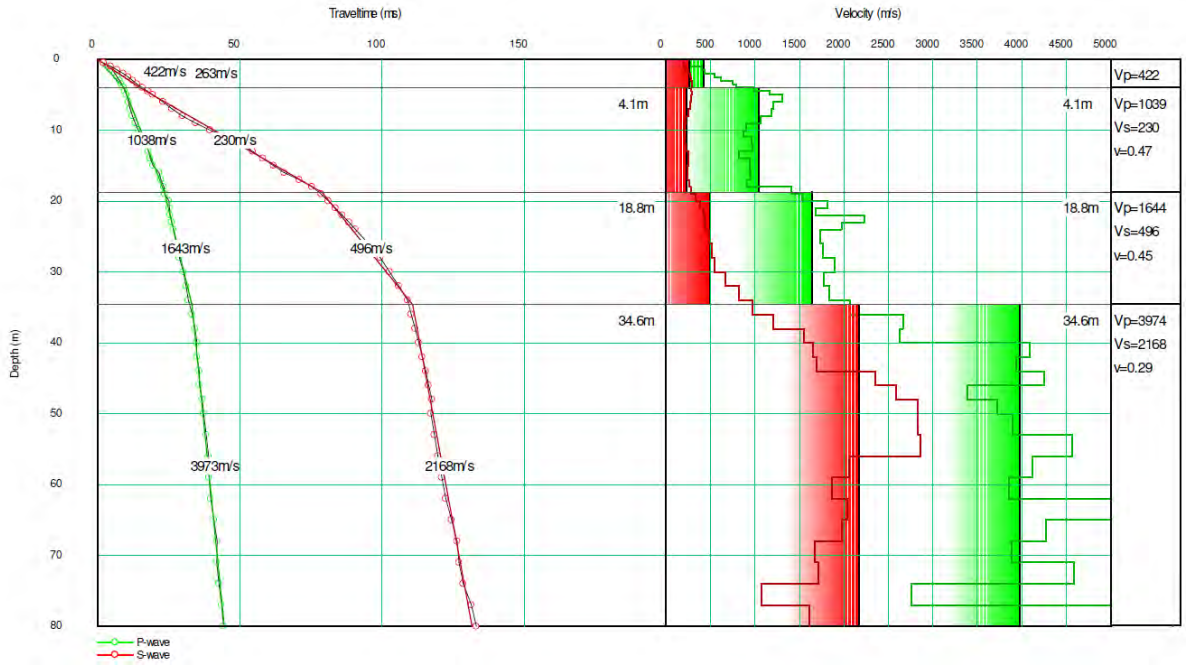

Figure 4-55. Example DH travel time data with SRK's interval (red shading) and layered (red line) V_S interpretations from SRK's BH47. SRK's P-wave interpretations shown in green.

Figure 4-56 shows the V_S profiles for each of these three interpretations. The SRK interval interpretation yields the thinnest layers, the SRK layered interpretation yields the thickest layers, and the Cox (2023) layered interpretations yield layers with thicknesses that are typically in between the two SRK interpretations. Also shown in Figure 4-56 are two cross-hole V_S profiles from the Pebble Bed Modular Reactor (PBMR) in the KNPS area as reported by Heymann and Rust (2002). The PBMR profiles were used in the Baseline report (Stamatakos et al., 2022) and are within the range of the V_S profiles from Duynefontyn. Based on this limited comparison, it can be reasonably assumed that the site amplification analyses performed for Duynefontyn approximately represent KNPS as well.

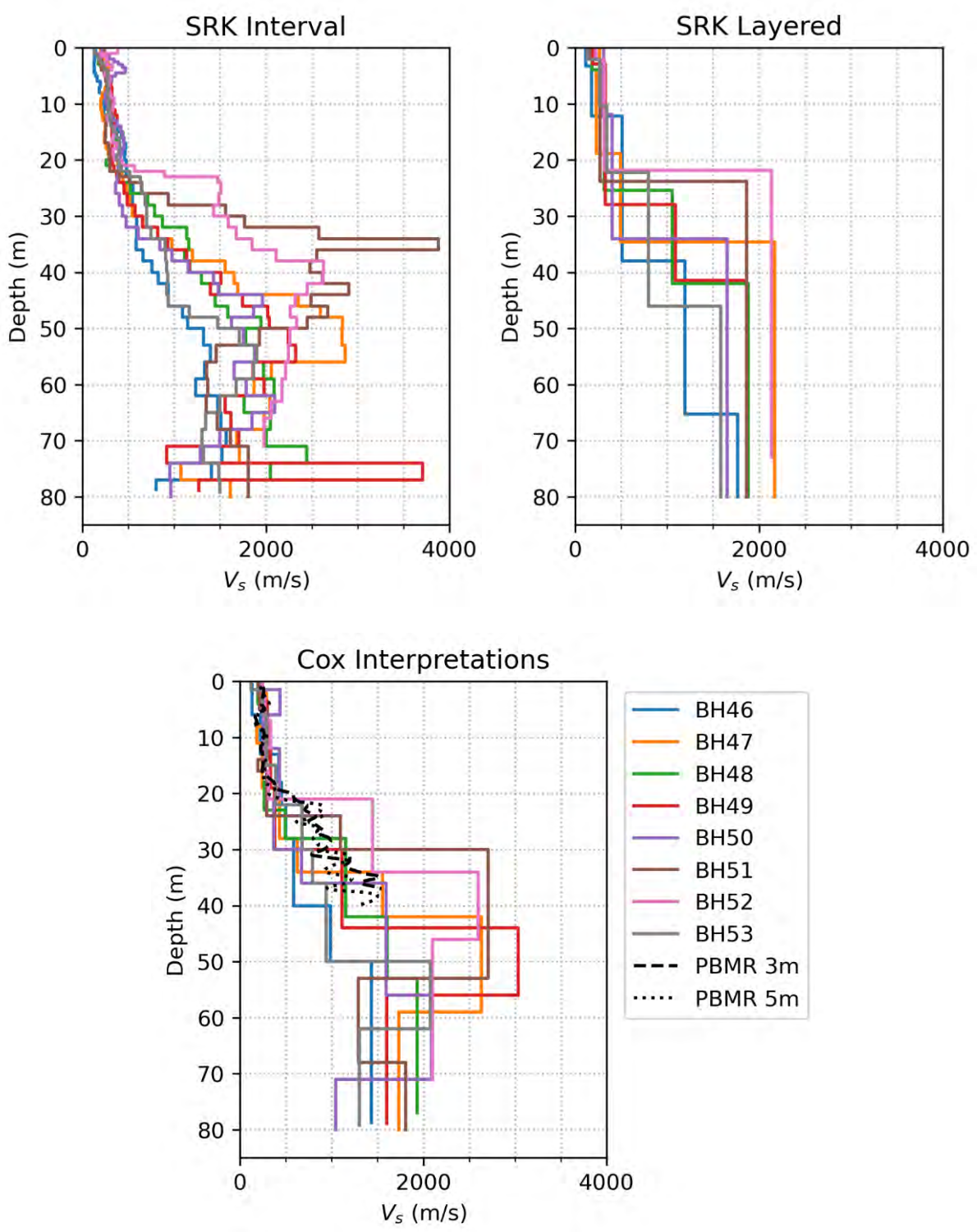

Figure 4-56. Summary of SRK interval interpretations, SRK layered interpretations, and Cox (2023) layered interpretations of V_S profiles from downhole data. Two cross-hole V_S profiles from the PBMR site in the KNPS area are also shown for comparison.

The V_S profiles based on DH measurements include the surficial sand, and thus require removal of V_S values that represent the sand layers before they are used in site response analyses. For each borehole, the TI Team used the descriptions in the boring logs to identify the top of the rock and removed V_S values from the DH profiles above that depth. These

depths were typically about 30 m (see Table 4-16). V_S profiles from the DH testing extend to a depth of ~ 80 m below ground surface or ~50 m below top of rock. The modified V_S profiles (based on the Cox [2023] interpretations) after removing the sand are shown in Figure 4-57. Most of the DH V_S profiles (except BH51) show a similar trend of increasing V_S in the top 20 m followed by a reversal in the V_S (i.e., an increase in V_S followed by a decrease) between depths of about 20 and 40 m.

The depth to the top of rock for the DH measurements is explicitly known from the boring logs, yet the V_S at the top of rock in varies significantly - from a little over 500 m/s to more than 2500 m/s (Figure 4-57). This range is similar to the range obtained for the MAM/MASW profiles after removal of the sand (Figure 4-54), indicating that the approach used to remove the sand from the MASW/MAM profiles did not introduce additional variability in the V_S at the top of rock.

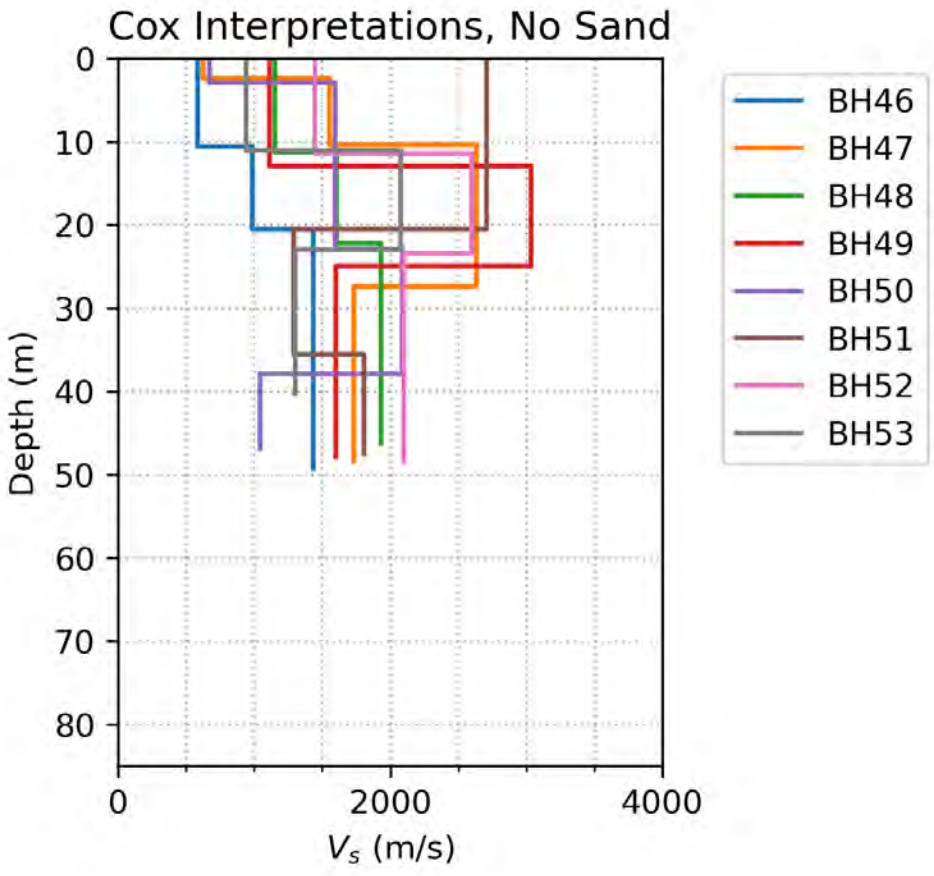

Figure 4-57. DH V_S profiles after sand removal.

4.5.3 Shear-wave velocity profiles from PS logging testing

Similar to the V_S profiles from DH data, V_S profiles from PS logging were established based on interpretation of travel times of shear waves (Matamela and Cox, 2024). As noted earlier, the selection of wave arrivals for the travel times was subjective and, thus, it was important for an experienced analyst to perform this analysis. According to Matamela and Cox (2024), the shear-wave arrival was often unclear on the PS logging time records, making the data difficult to interpret. Thus, Matamela and Cox (2024) assigned a flag to each V_S value with a code to represent data quality based on the level of difficulty in identifying the wave arrival from the time records. The code varied from 1 to 5, with Code 1 corresponding to the high quality or

confidence in the V_S data, Code 2 representing medium confidence, and Code 3 representing low confidence and ambiguous picks. Code 3 data considered two different wave arrivals for the travel-time selection because the analysts could not confidently identify a single wave arrival, and thus two V_S values are reported at each depth for Code 3. Codes 4 and 5 indicated poor waveforms that could not be interpreted with any confidence, and these were excluded from further evaluation. All V_S values were computed using interval travel times.

Figure 4-58 and Figure 4-60 show the V_S values obtained from PS logging based on the Matamela and Cox (2024) interpretations, with the data in Figure 4-58 separated by code and the same data separated by borehole in Figure 4-60. Surficial sand was removed from the V_S profiles by examining the depth to rock noted in each boring log (typically about 30 m below the ground surface), such that the data in these figures only represent the V_S in the rock. Figure 4-58 shows the Code 1 V_S data gradually increasing from about 1000 m/s to 2500 m/s in the top 50 m, with more variability in the data at depths below 50 m. The Code 2 and 3 V_S data are variable at all depths, with values varying between 1500 m/s and 3500 m/s at the same depth. The data separated based on borehole in Figure 4-60 show that the variability is distributed similarly across all the boreholes.

The V_S values identified with high confidence (Code 1) are quite reliable, but these data are relatively few in each borehole. Most of the V_S values are flagged as either medium confidence or low confidence/ambiguous (Code 2 and 3). For this reason, the PS logging data, overall, was deemed to be of low quality. Further discussion of the TI Team's evaluation of the reliability of the PS logging data and its use in developing the V_S profiles for the site response analysis is provided in Section 9.4.2.

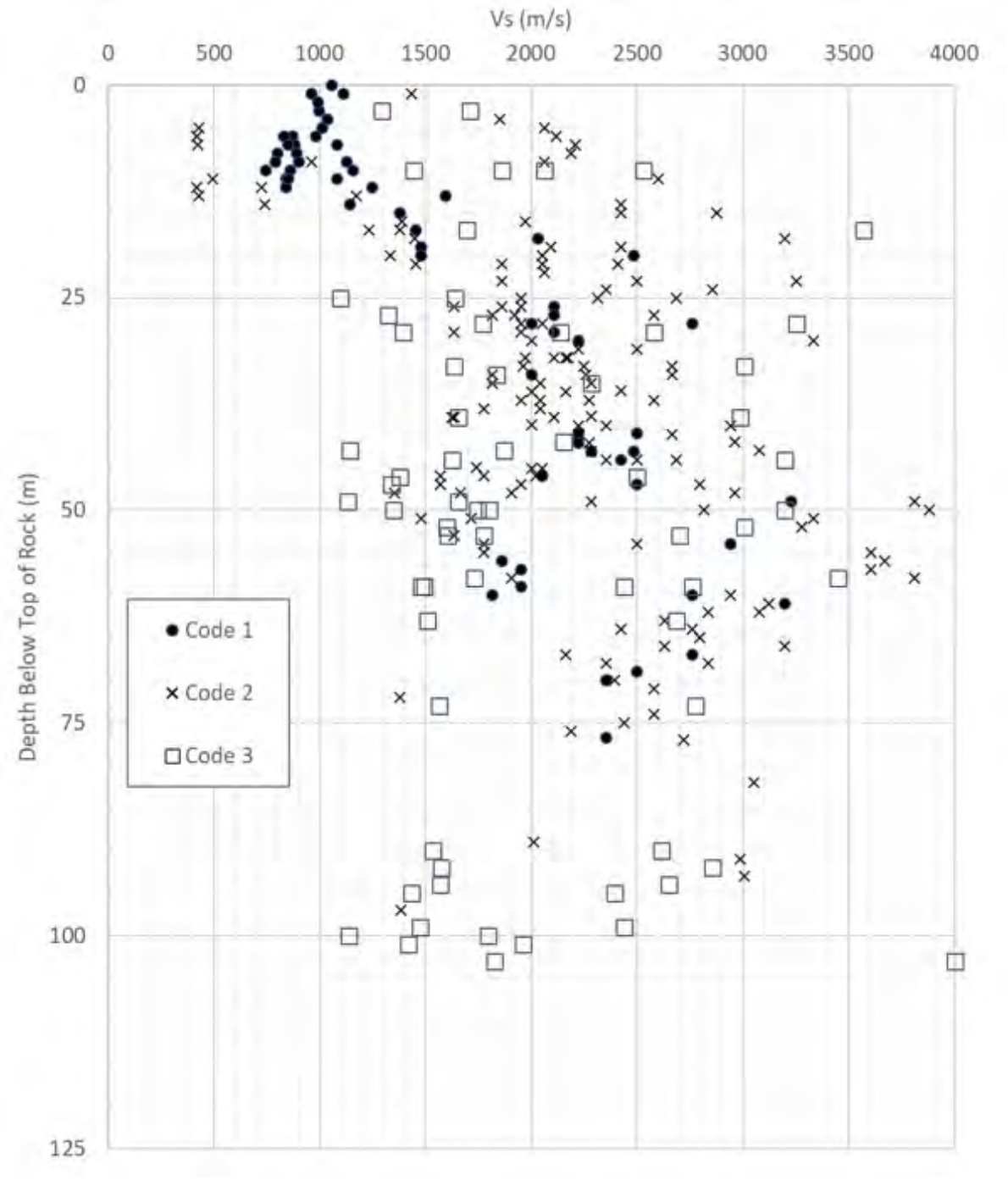

Figure 4-58. V_S estimates obtained from PS logging after removing V_S values in surficial sand, showing only data with highest data quality (codes 1, 2, and 3)

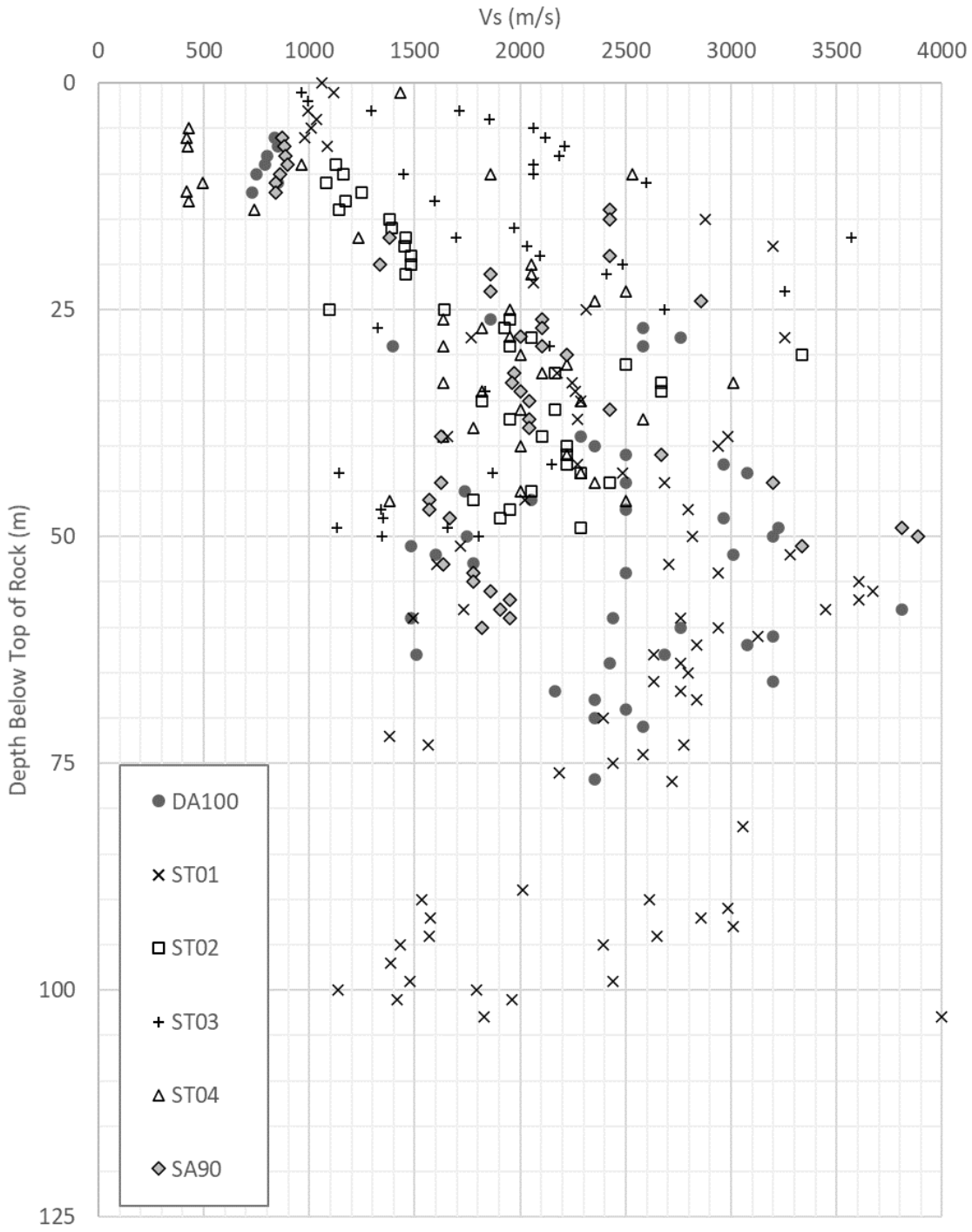

Figure 4-59. V_S estimates (codes 1, 2, and 3) obtained from PS logging after removing V_S values in surficial sand, with values shown separately for each borehole.

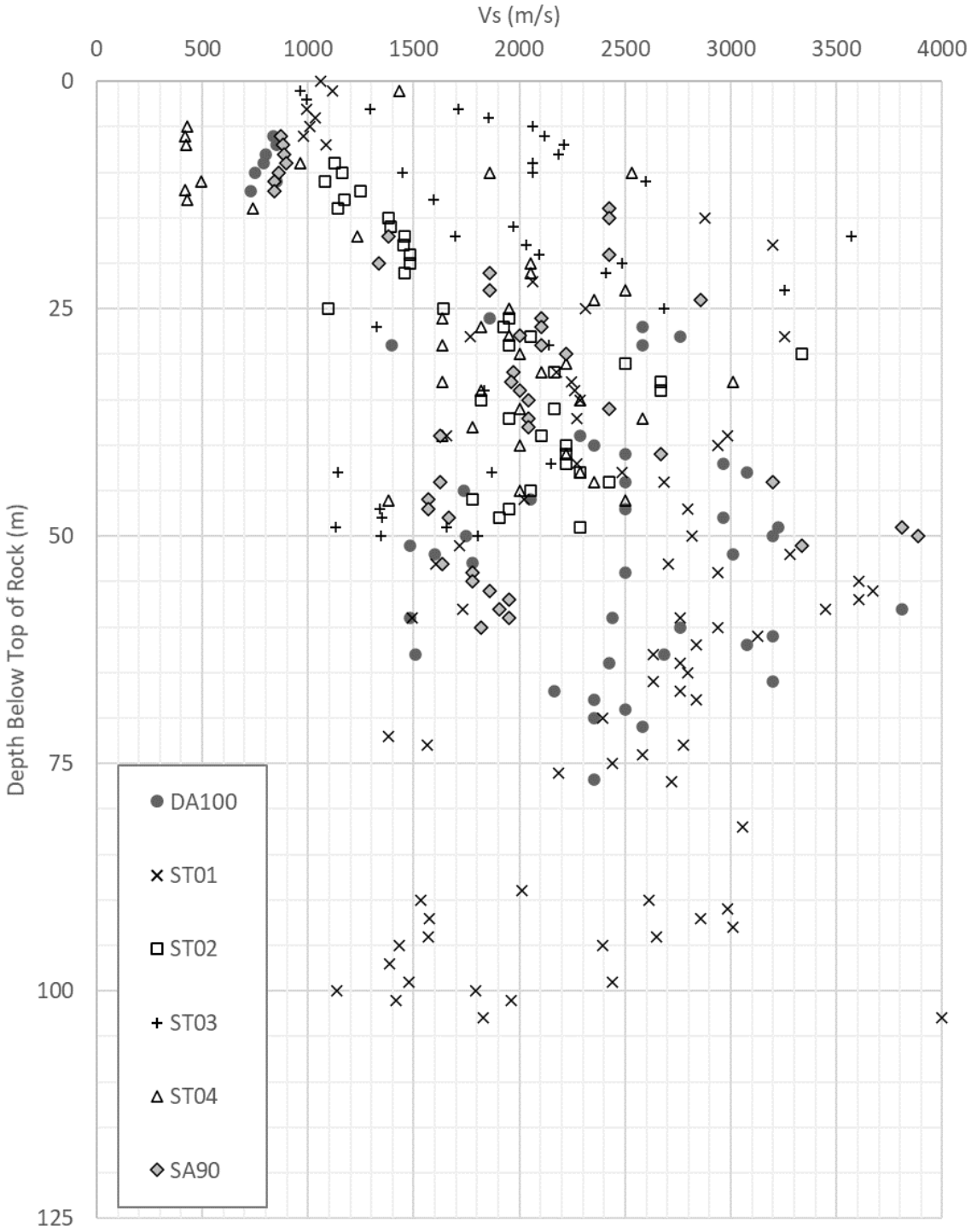

Figure 4-60. V_S estimates (codes 1, 2, and 3) obtained from PS logging after removing V_S values in surficial sand, with values shown separately for each borehole.

4.7 REFERENCES

Agricultural Journal (1909). Agricultural Journal, Department of Agriculture, Cape of Good Hope. Townshend, Taylor & Snashall Printers, Cape Town, South Africa XXIII.

Albini, P.; Strasser, F.O. and Flint, N.S. (2014). Earthquakes from 1820 to 1936 in Grahamstown and Surroundings (Eastern Cape Province, South Africa). Bulletin of Earthquake Engineering 12(1). 45-78.

Albini, P. and Flint, N. (2023). Investigating the Earthquake Records from 1620 to 1969 of Interest for the Duynefontyn Area, South Africa. CGS Report 2022-0127 (Rev.0). Council for Geoscience, Pretoria, South Africa, 400 pp.

Andreoli, M.; Doucoure, M.; van Bever Donker, J.; Brandt, D., and Andersen, N.J.B. (1996). Neotectonics of southern Africa - A review. Africa Geoscience Review. 3. 1-16.

Austermann, J., Mitrovica, J. X., Huybers, P., and Rovere, A. (2017). Detection of a dynamic topography signal in last interglacial sea-level records. Science Advances, 3(7).

Baby, G., Guillocheau, F., Braun, J., Robin, C., and Dall'Asta, M. (2020). Solid sedimentation rates history of the Southern African continental margins: Implications for the uplift history of the South African Plateau. Terra Nova, 32(1), 53–65.

Bakun, W.U. and Wentworth, C.M. (1997). Estimating Earthquake Location and Magnitude from Seismic Intensity Data. Bulletin of the Seismological Society of America 87(6). 1,502-1,521.

Barker, O. (2023). Koeberg - 1976 to 1978 - Memories Observations and Ideas. Prepared for the Council for Geoscience Enhanced SSHAC Level 2 PSHA, Koeberg Nuclear Power Station.

BC Hydro (2012). Probabilistic Seismic Hazard Analysis (PSHA) Model 1-4. BC Hydro Engineering Report E658. Vancouver, Canada.

Beeson, R. (1973). 3318DA Philadelphia Geological Field Map (Unpublished). 1:50,000 Scale. Council for Geoscience, Pretoria, South Africa.

Belcher R.W. and Kisters A.F.M. (2003). Lithostratigraphic correlations in the western branch of the Pan-African Saldania Belt, South Africa: The Malmesbury Group revisited. South African Journal of Geology 106. 327-342.

Bierman, P.R., (2012). Report #1 Cosmogenic Geochronology, Southern Africa Fault Corridor Investigation, Appendix B.3 in Hanson, K., Slack, C. and Coppersmith, R., Thyspunt Geological Investigations—Kango Fault Study, Council of Geoscience Report Number 2012-0035 Rev. 0, 126 pp.

Bird, P.; Ben-Avraham, Z.; Schubert, G.; Andreoli, M. and Viola, G. (2006), Patterns of stress and strain rate in southern Africa, Journal of Geophysical Research 111, B08402.

Brandt, D.; Andreoli, M.A.G. and McCarthy, T.S. (2005). The Late Mesozoic Palaeosoils and Cenozoic Fluvial Deposits at Vaalputs, Namaqualand, South Africa: Possible Depositional Mechanisms and Their Bearing on the Evolution of the Continental Margin. South Africa Journal of Geology 108. 271-284.

Broad, D.S.; Jungslager, E.H.A.; McLachlan, I.R. and Roux, J. (2006). Offshore Mesozoic Basins. In: Johnson, M.R.; Annhaeusser, C.R. and Thomas, R.J. (Eds.). The Geology of South Africa. Geological Society of South Africa, Johannesburg/Council for Geoscience, Pretoria, South Africa. 553-572.

Broad, D.S.; Jungslager, E.H.A.; McLachlan, I.R.; Roux, J. and Van der Spuy, D. (2012). South Africa's Offshore Mesozoic Basins. In: Roberts, D.G. and Bally, A.W. (Eds.). Phanerozoic Passive Margins, Cratonic Basins and Global Tectonic Maps. Elsevier, Rotterdam, Netherlands. 535-564.

Brown, R.W., Gallagher, K., Gleadow, A.J.W. and Summerfield, M.A. (2000). Morphotectonic evolution of the South Atlantic margins of Africa and South America, in M.A. Summerfield (ed.), Geomorphology and Global Tectonics, pp. 255-280, John Wiley, New York.

Brown, R.W., Summerfield, M.A. and Gleadow, A.J.W. (2002). Denudational history along a transect across the Drakensberg Escarpment of Southern Africa derived from apatite fission track thermochronology, Journal of Geophysical Research, 107, 2350

Browning, C. and Roberts, D. L. (2015). Lithostragraphy of the Witzand Formation (Sandveld Group), South Africa. South African Journal of Geology 118(3). 317-322.

Buggisch W.; Kleinschmidt G.; Krumm S. (2010). Sedimentology, geochemistry and tectonic setting of the Neoproterozoic Malmesbury Group (Tygerberg Terrane) and its relation to neighbouring terranes, Saldania Fold Belt, South Africa. Neues Jahrbuch fur Geologie und Palaontologie 257. 85-114.

Chen, F., Friedman, S., Gertler, C. G., Looney, J., O'Connell, N., Sierks, K., and Mitrovica, J. X. (2014). Refining estimates of polar ice volumes during the MIS11 interglacial using sea level records from South Africa. Journal of Climate, 27, 8740–8746.

Chisenga, C.; Van der Meijde, M.; Yan, J.; Fadel, I.; Atekwana, E.A.; Steffen, R. and Ramotoroko, C. (2020). Gravity Derived Crustal Thickness Model of Botswana: Its Implication for the Mw 6.5 April 3, 2017, Botswana Earthquake. Tectonophysics 787. 228479.

Claassen, D.; Black, D.E. and Mthembi, P. (2024). Marine Terraces Studies (DDC5 Activity). CGS Report 2022-0140. Council for Geoscience, Pretoria, South Africa.

Conrad, C.P. and Gurnis, M. (2003). Seismic Tomography, Surface Uplift, and the Breakup of Gondwanaland: Integrating Mantle Convection Backwards in Time. Geochemistry, Geophysics, Geosystems 4(3).

Coppersmith, R.; Slack, C.; Moabi, N.; Dhansay, T.; Cawthra, H.; Claassen, D. and Sethobya, M. (2024). Duynefontyn Onshore Fault Mapping Investigation, DDC6. CGS Report 2023-0001. Council for Geoscience, Pretoria, South Africa.

Cox, B.R.; Abbas, A.; Mulabisana, T.; Jele, V.; Mantsha, R.; Sethobya, M.; Sobothonma, S. and Nxantsiya, Z. (2024). Deep Shear-Wave Velocity Profiling Using MASW and MAM Surface Wave Methods: Duynefontyn Project, South Africa. CGS Report 2023-0203 (Rev.0). Council for Geoscience, Pretoria, South Africa.

Dames and Moore (1975). Foundation Report for the Koeberg Power Station, Cape Province R.S.A.. For the Electricity Supply Commission. NSIP-KBG-007669#P1-6.

Dames and Moore (1976). Geologic Report. Koeberg Power Station, Cape Province, South Africa. For the Electricity Supply Commission. Job 9629-014-45.

Dames and Moore (1977). Supplementary Geologic Report for the Koeberg Power Station, Cape Province R.S.A.. For the Electricity Supply Commission. Job 9629-026-45.

Dauteuil, O., Bessin, P., and Guillocheau, F. (2015). Topographic growth around the Orange River valley, southern Africa: A Cenozoic record of crustal deformation and climatic change. Geomorphology, 233, 5–19.

Day, P.W. and Ridgway, M. (2000). Geotechnical borehole logs at the Koeberg Site.

Day, P.W. and Ridgway, M. (2006). Geotechnical investigation for Pebble bed modular reactor, Koeberg. Jones & Wagner Consulting Civil Engineers, Report JW161/05/9978 (Rev.0), 63 pp.

Day, R.W. (1986). Magnetometric Mapping of the False Bay Dolerites. Joint Geological Survey/University of Cape Town Marine Geoscience Technical Report 16, 217-227.

De Beer, C.H. (1990). Some Aspects of the Tectonics of the Western Branch of the Cape Fold Belt. Abstract Volume. Geocongress 1990. Geological Society of South Africa, Cape Town, South Africa. 666-669.

De Beer, C.H.; Roberts, D.L.; Cole, J.; Engelbrecht, J. and Dondo, C. (2008). The Geology of the Site and Site Vicinity Areas of Koeberg, and an Update on Onland Geological Hazards. CGS Report 2008-0239. Council for Geoscience, Pretoria, South Africa.

De la Torre, C.A. and Bradley, B.A. (2023). 2D Site Response at the Proposed Duynefontyn Nuclear Power Plant Site: The Influence of Steeply Inclined Interbedded Rock Layers. Bradley Seismics. Final Report 2023/09/18.

De Wit, M. (2007). The Kalahari epeirogeny and climate change: Differentiating cause and effect from core to space, *South African Journal of Geology* 110, 367-392.

Dhansay, T.; Musekiwa, C.; Ntholi, T.; Chevallier, L.; Cole, D. and de Wit, M.J. (2017). South Africa's Geothermal Energy Hotspots Inferred from Subsurface Temperature and Geology. South African Journal of Science 113.

Doucouré, C.M. and de Wit, M.J. (2003). Old inherited origin for the present near bimodal topography of Africa. Journal of African Earth Sciences 36. 371-388.

Du Plessis, A. (2021). Multichannel Analysis of Surface Waves (MASW) and Downhole Seismic Investigation at Duynefontyn, Western Cape. Open Ground Resources Report 2758/2021.

Engelsman, B.M. (2022). Geotechnical Characterisation. In: Site Safety Report for Duynefontyn (Rev.1), Section 5.15. Eskom.

Erlanger, E.D., Granger, D.E., and Gibbon, R.J. (2012). Rock uplift rates in South Africa from isochron burial dating of fluvial and marine terraces, Geology 40, 1019-1022.

Fadel, I.; van der Meijde, M. and Paulssen, H. (2018). Crustal Structure and Dynamics of Botswana. Journal of Geophysical Research, Solid Earth 123. 10,659-10,671.

Fitzsimmons, I.C.E. (2000). A Review of Tectonic Events in the East Antarctic Shield and Their Implications for Gondwana and Earlier Supercontinents. Journal of African Earth Sciences 31. 3-23.

Fleming, A., Summerfield, M.A., Stone, J.O., Fifield, L.K. and Cresswell, R.G. (1999). Denudation rates for the southern Drakensberg Escarpment, SE Africa, derived from in-situ–produced cosmogenic (super 36) Cl: Initial results, Journal of the Geological Society of London 156, 209-212.

Flanagan, L.E. and Rosewarne, R. (2008). The Provision of Groundwater Monitoring Boreholes, Progress Report #1 (Completion of Drilling Programme). Report 378412/01F.

Frimmel H.E. (2009) Configuration of Pan-African orogenic belts in southwestern Africa. In: Gaucher C; Sial A.N; Halverson G.P.; Frimmel H.E. (eds). Neoproterozoic-Cambrian tectonics, global change and evolution: a focus on southwestern Gondwana, Vol. 16. Developments in Precambrian geology, Elsevier, 145-151.

Frimmel, H.E.; Basei, M.A.S.; Correa, V.X. and Mbangula, N. (2013). A New Lithostratigraphic Subdivision and Geodynamic Model for the Pan-African Western Saldania Belt, South Africa. Precambrian Research 231. 218-235.

Frimmel HE, Basei MAS, Gaucher C (2011). Neoproterozoic geodynamic evolution of SW Gondwana: a southern African perspective. International Journal of Earth Science 100. 323-354.

Frimmel, H.E. and Frank, W. (1998). Neoproterozoic Tectono-Thermal Evolution of the Gariep Belt and Its Basement, Namibia/South Africa. Precambrian Research 90. 1-28.

Frimmel, H.E.; Klötzli, U.S. and Siegfried, P.R. (1996). New Pb-Pb Single Zircon Age Constraints on the Timing of Neoproterozoic Glaciation and Continental Break-up in Namibia. Journal of Geology 104. 459-469.

Fynn, M. (2018). Micro-Seismic Observations in Leeu Gamka, Karoo, South Africa. MSc Thesis, University of Cape Town, South Africa.

Gardonio, B.; Jolivet, R.; Calais, E. and Leclère, H. (2018). The April 2017 Mw6.5 Botswana Earthquake: An Intraplate Event Triggered by Deep Fluids. Geophysical Research Letters 45(17). 8886–8896. 851-859.

Gasperini P.; Bernardini, F.; Valensise, G. and Boschi, E. (1999). Defining Seismogenic Sources from Historical Earthquake Felt Reports. Bulletin of the Seismological Society of America 89. 94-110.

Gaucher, C.; Frimmel, H.E. and Germs, G.J. (2009). Tectonic Events and Palaeogeographic Evolution of Southwestern Gondwana in the Neoproterozoic and Cambrian. Developments in Precambrian Geology 16. 295-316.

Gilchrist, A.R., and Summerfield, M.A. (1990). Differential denudation and flexural isostasy in formation of rifted-margin upwards, Nature 346, 739-742.

Green, R.W.E. and Bloch, S. (1971). The Ceres, South Africa, Earthquake of September 29, 1969: I. Report on Some Aftershocks. Bulletin of the Seismological Society of America 61(4). 851-859.

Gresse, P.G. (1980). Geologie van die Gebied Oos van die Soutrivier op Vel 3318AB,– Hopefield. Veld verslag van doe Geologiese Opname van Suid Afrika, 6 pp. [English translation: *Geology of the area east of the Sout River on Sheet 3318AR – Hopefield, Field Report of the Geological Survey of South Africa (Unpublished), 6 pp*.].

Gresse, P.G. and Scheepers, R. (1993). Neoproterozoic to Cambrian (Namibian) Rocks of South Africa: A Geochronological and Geotectonic Review. Journal of African Earth Sciences 16. 375-393.

Gresse P.G.; von Veh, M.W. and Frimmel, H.E. (2006). Namibian (Neoproterozoic) to Early Cambrian Successions. In: Johnson, M.R.; Anhaeusser, C.R. and Thomas, R.J. (Eds.). The Geology of South Africa. Geological Society of South Africa, Johannesburg/Council for Geoscience, Pretoria, South Africa. 395-421.

Groshong, R.H. (1989). Half-Graben Structures: Balanced Models of Extensional Fault-Bend Folds. Geological Society of America Bulletin 101(1). 96-105.

Giulio V.; Andreoli; M., Ben-Avraham; Stengel, I., Reshef, M. 2005. Offshore mud volcanoes and onland faulting in southwestern Africa: neotectonic implications and constraints on the regional stress field, Earth and Planetary Science Letters 231, 147-160.

Gurnis, M., Mitrovica, J.X., Ritsema, J. and van Heijst, H.J. (2000). Constraining mantle density structure using geological evidence of surface uplift rates: The case of the African Superplume, Geochemistry, Geophysics, Geosystems 1, Paper No. 1999GC000035.

Hälbich, I.W. (1983). A Tectonogenesis of the Cape Fold Belt (CFB). In: Sönghe, A.P.G. and Hälbich, I.W. (Eds.). Geodynamics of the Cape Fold Belt. Special Publication 12(14). Geological Society of South Africa, Johannesburg, South Africa. 165-175.

Hansma, J.; Tohver, E.; Schrank, C.; Jourdan, F. and Adams, D. (2015). The Timing of the Cape Orogeny: New 40Ar/39Ar Age Constraints on Deformation and Cooling of the Cape Fold Belt, South Africa. Gondwana Research 32.

Hanson, K.L., Coppersmith R., Glaser, L., Roberts, D.L., Claassen, D., and Black, D. (2012). Thyspunt Geological Investigations-Marine terrace studies. *Rev. 0.*, Council for Geoscience, Pretoria, Report number: 2012-0034.

Hartnady, C.J.H.; Newton, A.R. and Theron, J.N. (1974). The Stratigraphy and Structure of the Malmesbury Group in the South-Western Cape. Bulletin of the Chamber of Mines Precambrian Research Unit, University of Cape Town 15. 193-213.

Hartnady, C.J.H.; Joubert, P. and Stowe, C.W. (1985). Proterozoic Crustal Evolution of Southwestern Africa. Episodes 8. 236-244.

Hearty, P.J.; Rovere, A.; Sandstrom, M.R.; O'Leary, M.J.; Roberts, D. and Raymo, M.E. (2020). Pliocene-Pleistocene Stratigraphy and Sea-Level Estimates, Republic of South Africa with Implications for a 400 ppmv CO2 World. Paleoceanography and Paleoclimatology 35(7).

Heidbach, O.; Rajabi, M.; Cui, X.; Fuchs, B.; Müller, J.; Reinecker, K.; Reiter, M.; Tingay, F.; Wenzel, F.; Xie, M. O.; Ziegler, M.-L.; Zoback, M. D. and the WSM Team (2018). The World Stress Map, Database Release 2016: Crustal Stress Pattern Across Scales. Tectonophysics 744. 484-498.

Heidbach, O.; Rajabi, M.; Reiter, K.; Ziegler, M.O. and the WSM Team. (2016). World Stress Map Database Release 2016. GFZ Data Services.

Hendey, Q.B. (1976). The Pliocene Fossil Occurrence in ‘E’ Quarry, Langebaanweg, South Africa. Annals of the South African Museum 69. 215-247.

Hendey, Q.B. (1981). Palaeoecology of the Late Tertiary Fossil Occurrences in “E” Quarry, Langebaanweg, South Africa, and a Reinterpretation of Their Geological Context. Annals of the South African Museum 84. 1-104.

Hendey, Q.B. and Dingle, R.V. (1983). Onshore Sedimentary Phosphate Deposits in Southwestern Africa. Technical Report of the Joint Geological/Survey/University of Cape Town Marine Geoscience Unit 14. 27-40.

Hendey, Q. B. and Gentry, A. W. (1970). A Review of the Geology and Palaeontology of the Plio-Pleistocene Deposits at Langebaanweg, Cape Province. Annals of the South African Museum 56. 75-117.

Heymann, G. and Rust, E., (2002). Geotechnical Parameters from Seismic Cross-Hole Measurements at the PBMR Koeberg Site (Final). G. Heymann CC, ck 9868421/23 / PBMR/2933, 26 June 2002, 43 pp.

Hodge, M.S. (2013). Neotectonic Deformation Features in Plio-Pleistocene Coastal Aeolianites: Palaeoseismology and Earthquake Hazard Implications for the Southern Cape, South Africa. MSc Thesis, University of Cape Town, South Africa.

Johnson, M.R.; Anhaeusser, C.R. and Thomas, R.J. (Eds.) (2006). The Geology of South Africa. Geological Society of South Africa, Johannesburg/Council for Geoscience, Pretoria, South Africa.

Johnston, S.T. (2000). The Cape Belt and Syntaxis and the rotated Falkland Islands: dextral transpressional tectonics along the southwest margin of Gondwana. Journal of African Earth Science 31, 51-63.

Kensley, B.F. (1972). Pliocene Marine Invertebrates from Langebaanweg, Cape Province. Annals of the South African Museum 60. 173-190.

Kent, L.E. (1980). Stratigraphy of South Africa, Part 1. Lithostratigraphy of the Republic of Africa, South West Africa/Namibia, and the Republics of Bophuthatswana, Transkei and Venda. South African Committee for Stratigraphy, Geological Survey South Africa, Handbook 8.

King, L.C. (1962). The Morphology of the Earth: A Study and Synthesis of World Scenery, Oliver and Boyd, Edinburgh, 699 pp.

Kisters, A.F.M. (2022). Geology and Structure of Pan African Basement Rocks in the Western Cape. PowerPoint Presentation (DNSP-PST-117) presented at PSHA Duynefontyn Workshop 2, June 21, Stellenbosch, South Africa.

Kisters, A. and Belcher, R. (2018). The Stratigraphy and Structure of the Western Saldania Belt, South Africa and Geodynamic Implications. In: Siegesmund, S.; Basei, M.; Oyhantçabal, P.; Oriolo, S. (Eds.). Geology of Southwest Gondwana. Regional Geology Reviews. Springer, Cham, Switzerland. 387-410.

Kisters, A.F.M.; Belcher, R.W.; Armstrong, R.A.; Scheepers, R.; Rozendaal, A. and Jordaan, L.S. (2002). Timing and Kinematics of the Colenso Fault, The Early-Palaeozoic Shift from Collisional to Extensional Tectonics in the Pan-African Saldania Belt, South Africa. South African Journal of Geology 105. 257-270.

Kolawole, F.; Atekwana, E.A.; Malloy, S.; Stamps, D.S.; Grandin, R.; Abdelsalam, M.G.; Leseane, K. and Shemang, E.M. (2017). Aeromagnetic, Gravity, and Differential Interferometric Synthetic Aperture Radar Analyses Reveal the Causative Fault of the 3 April 2017 Mw 6.5 Moiyabana, Botswana, Earthquake. Geophysical Research Letters 44(17). 8,837-8,846.

Kounov, A., Niedermann, S., De Wit, M. J., Codilean, A. T., Viola, G., Andreoli, M., and Christl, M. (2015). Cosmogenic 21Ne and 10Be reveal a more than 2 Ma alluvial fan flanking the Cape Mountains, South Africa. South African Journal of Geology, 118(2), 129–144.

Kövesligethy R.D. (1906). Processing of Macroseismic Tremors. Mathematical and Natural Science Bulletin 24. 349-368.

Kuester J.A. (1809). Letter to the Church of the United Brethren, London. Periodical Accounts, 1809, Relating to the Missions of the Church of the United Brethren, Brethren's Society for the Furtherance of the Gospel, London 4. 475-476.

Kuester J.A. and I.C. Kuehnel (1809). Account of the Journey from Genadendal to Gruenekloof, Cape Town, and Back to Genadendal. Periodical Accounts, 1811, Relating to the Missions of the Church of the United Brethren, Brethren's Society for the Furtherance of the Gospel, London 5. 91-95.

Kwadiba, M.T.O.G.; Wright, C.; Kgaswane, E.M.; Simon, R.E. and Nguuri, T.K. (2003). Pn Arrivals and Lateral Variations of Moho Geometry beneath the Kaapvaal Craton. Lithos 71(2-4). 393-411.

Malservisi, R.; Hugentobler, U.; Wonnacott, R. and Hackl, M. (2013). How Rigid Is a Rigid Plate? Geodetic Constraint from the TrigNet CGPS Network, South Africa. Geophysical Journal International 192. 918-928.

Mandl, G. (1988). Mechanics of Tectonic Faulting. Elsevier, Amsterdam, Netherlands. 407.

Manzunzu, B.; Midzi, V.; Durrheim, R.; Pule, T. and Flint, N. (2023). Quantitative Evaluation of Source Parameters of Historical Earthquakes in Southern Africa. Journal of African Earth Sciences 199. 104833.

Marimira, K.; Manzunzu, B.; Shumba, B.T.; Midzi, V. and Saunders, I. (2021). Aftershock Sequence of 22 September 2016, Manica–Zinave Earthquake (Mw5.6), Mozambique. Journal of African Earth Sciences 177.

Marker, M. E., and Holmes, P. J. (2010). The geomorphology of the Coastal Platform in the southern Cape. South African Geographical Journal, 92(2), 105–116.

Markwick, P.J.; Paton, D.A. and Mortimer, E.J. (2021). Reclus, a New Database for Investigating the Tectonics of the Earth: An Example from the East African Margin and Hinterland. Geochemistry, Geophysics, Geosystems 22(11).

Matamela, J. and Cox, B.R. 2024. PS Logging in support of Probabilistic Seismic Hazard Analyses for Duynefontyn. CGS Report 2023-0185, Council for Geoscience, Pretoria, South Africa.

McClay, K.R. (1992). Glossary of Thrust Tectonic Terms, Thrust Tectonics. Springer. 419-433.

McClay, K. and Bonora, M. (2001). Analog Models of Restraining Stepovers in Strike-Slip Fault Systems. AAPG Bulletin 85(2). 233-260.

McFarland, J., Morris, A.P. and Ferrill, D.A. (2012). Stress Inversion Using Slip Tendency. Computers and Geosciences 41. 40-46.

McMillan, I.K.; Brink, G.I.; Broad, D.S. and Maier, J.J. (1997). Late Mesozoic Sedimentary Basins off the South Coast of South Africa. In: Selley, R.C. (Ed.). African Basins 3 in Sedimentary Basins of the World series. Elsevier, Amsterdam. 319-376.

Meert, J. and Lieberman, B. (2008). The Neoproterozoic Assembly of Gondwana and Its Relationship to the Ediacaran-Cambrian Radiation. Gondwana Research 14 (1/2), 5-21.

Meert, J. and Van der Voo, R. (1997). The Assembly of Gondwana 800-550 Ma. Journal of Geodynamics 23. 223-235.

Midzi, V.; Saunders, I.; Manzunzu, B.; Kwadiba, M.T.; Jele, V.; Mantsha, R.; Marimira, K.T.; Mulabisana, T.F.; Ntibinyane, O.; Pule, T.; Rathod, G.W.; Sitali, M.; Tabane, L.; van Aswegen, G. and Zulu, B.S. (2018). The 03 April 2017 Botswana M6.5 Earthquake: Preliminary Results. Journal of African Earth Sciences 143. 187-194.

Miller, R. McG. (1983). The Pan-African Damara Orogen of South West Africa/Namibia. Special Publication Geological Society of South Africa 11. 431-515.

Mitchell, C.; Taylor, G.K.; Cox, K.G. and Shaw, J. (1986). Are the Falkland Islands a rotated microplate? Nature 319, 131-134.

Moorkamp, M.; Fishwick, S.; Walker, R.J. and Jones, A.G. (2019). Geophysical Evidence for Crustal and Mantle Weak Zones Controlling Intra-Plate Seismicity - The 2017 Botswana Earthquake Sequence. Earth and Planetary Science Letters 506. 175-183.

Morris, A.P.; Ferrill, D.A. and Henderson, D.B. (1996). Slip Tendency Analysis and Fault Reactivation. Geology 24. 275-278.

Morris, A.P.; Ferrill, D.A. and McFarland, J.M. (2013). Geological Stress Inversion Using Fault Displacement and Slip Tendency. United States Patent # US 8,589,080 B2. November 19.

Morris, A.P.; Ferrill, D.A. and McGinnis, R.N. (2016). Using Fault Displacement and Slip Tendency to Estimate Stress States. Journal of Structural Geology 83. 60-72.

Moucha, R., Forte, A. M., Mitrovica, J. X., Rowley, D. B., and Quéré, S. (2008). Dynamic topography and long-term sea-level variations: There is no such thing as a stable continental platform. Earth and Planetary Science Letters, 271(1-4), 101–108.

Mulabisana, T.; Meghraoui, M.; Midzi, V.; Saleh, M.; Ntibinyane, O.; Kwadiba, T.; Manzunzu, B.; Seiphemo, O.; Pule, T. and Saunders. I. (2021). Seismotectonic Analysis of the 2017 Moiyabana Earthquake (MW 6.5, Botswana), Insights from Field Investigations, Aftershock and InSAR Studies. Journal of African Earth Sciences 182. 104297.

Murray, E.C. and Saayman, I. (2000). Geohydrological Investigation for Pebble Bed Modular Reactor Project, Koeberg Nuclear Power Station. CSIR Report ENV/S-C 2000-084.

Musson, R.M.W. (2009). MEEP 2.0 User Guide. Earth Hazards and Systems Programme Open Report OR/09/045, British Geological Survey.

Musson, R.M.W. and Jiménez, M.J. (2008). Macroseismic Estimation of Earthquake Parameters. NERIES Technical Report NA4-D3.

Pacific Northwest National Laboratory (PNNL) (2014). Hanford Sitewide Probabilistic Seismic Hazard Analysis. PNNL-23361. Pacific Northwest National Laboratory. Richland, Washington, USA.

Partridge, T.C., Botha, G.A., and Haddon, I.G. (2006). Cenozoic deposits of the interior. In: Johnson, M.R., Anhaeusser, C.R. and Thomas, R.J. (eds.), Geology of South Africa,

Geological Society of South Africa, Johannesburg/Council for Geoscience, Pretoria, pp. 585-604.

Partridge, T.C. and Maud, R.R. (1987). Geomorphic evolution of southern Africa since the Mesozoic, South African Journal of Geology 90 (2), 179 208.

Partridge, T.C., and Maud, R.R. (2000). Macroscale geomorphic evolution of southern Africa, in The Cenozoic of Southern Africa, Eds., T. C. Partridge and R. R. Maud, Oxford Univ. Press, New York, pp. 3-18.

Paton, D.A. (2022). Can (Should?) Thick/Thin Skinned Tectonics Concepts Be Applied to Understanding the Western Cape. PowerPoint Presentation (DNSP-PST-130) presented at PSHA Duynefontyn Workshop 2, 21 June 2022, Stellenbosch, South Africa.

Paton, D.A.; Macdonald, D. and Underhill, J.R. (2006). Applicability of Thin- or Thick-Skinned Structural Models in a Region of Multiple Inversion Episodes: Southern South Africa. Journal of Structural Geology 28. 1933-1947.

Paton, D.A.; Mortimer, E.J.; Markwick, P.J.; Khan, J.; Davids; A.; Tshikovhi, R. and Van der Spuy, D. (2022). Coeval development of extensional and contractional features along transform margins: insights from the Diaz Marginal Ridge Geological Society, London, Special Publications 524, 307-325.

Peruzza, L. (1992). Procedure of Macroseismic Epicentre Evaluation for Seismic Hazard Purposes. Proceedings of XXIII General Assembly of the ESC. 434-437.

Raymo, M. E., Mitrovica, J. X., O'Leary, M. J., DeConto, R. M., and Hearty, P. J. (2011). Departures from eustasy in Pliocene Sea-level records. Nature Geoscience, 4(5), 328–332.

Reid, D.L.; Erlank, A.J. and Rex, D.C. (1991). Age and Correlation of the False Bay Dolerite Dike Swarm, South-Western Cape, Cape Province. South African Journal of Geology 94(2/3). 155-158.

Richter, C.F. (1958). Modified Mercalli Scale Restated. In: Elementary Seismology. W.H. Freeman and Company, San Francisco and London. 136-139.

Roberts, D.L. (2001). The Geology of Melkbosstrand and Environs. Explanation Sheet 3318CB Melkbosstrand. 1:50,000 scale. Council for Geoscience, Pretoria, South Africa.

Roberts, D.L. (2002). Sheet 3318CB Melkbosstrand. 1:50,000 scale geological map series, Council for Geoscience, Pretoria.

Roberts, D.L. (2006). Dating and Preliminary Correlation of Raised Marine and Estuarine Terraces on the Western and Southern Coasts of South Africa, Final Report. CGS Report 2006-0186 (Rev. 0). Eskom NSIP-SHA-018230#P1-206. Council for Geoscience, Pretoria, South Africa.

Roberts, D.L. and Berger, L. (1997). Last Interglacial c.117 kyr Human Footprints, South Africa. South Africa Journal of Science 93. 349-350.

Roberts, D.L. and Siegfried, H.P. (2014). The Geology of the Saldanha, Vredenberg and Velddrif Environs. Geological Map Explanation. Council for Geoscience, Pretoria, South Africa.

Roberts, D.L.; Botha, G.S.; Maud, R.R. and Pether, J. (2006). Coastal Cenozoic Deposits. In: Johnson, M.R.; Anhaeusser, C.R. and Thomas, R.J. (Eds.). The Geology of South Africa. Geological Society of South Africa, Johannesburg/Council for Geoscience, Pretoria, South Africa. 605-628.

Roberts, D.L.; Matthews, T.; Herries, A.I.R.; Boulter, C.; Scott, L.; Dondo, C.; Mthembi, P.; Browning, C.; Smith, R.M.H.; Haarhoff, P. and Bateman, M.D. (2011). Regional and Global Context of the Late Cenozoic Langebaanweg (LBW) Paleontological Site, West Coast of South Africa. Earth-Science Reviews 106. 191-214.

Roberts, D.L.; Cawthra, H.C. and Musekiwa, C. (2013). Dynamics of Late Cenozoic Aeolian Deposition along the South African Coast: A Record of Evolving Climate and Ecosystems. Geological Society, London, Special Publications 388. 353-387.

Rogers, J. (1979). The Sedimentary Succession at the Koeberg Nuclear Power Station, Melkbosstrand. Extended Abstracts. Geocongress 1979, Geological Society of South Africa, Part 1. 310-322.

Rogers, J. (1980). First Report on the Cenozoic Sediments between Cape Town and Eland's Bay. Geological Survey of South Africa Report 1980-136.

Rogers, J. (1982). Lithostratigraphy of Cenozoic Sediments between Cape Town and Eland's Bay. Palaeoecology of Africa 15. 121-137.

Rogers, J. (1983). Lithostratigraphy of Cenozoic Sediments on the Coastal Plain between Cape Town and Saldanha. Technical Report of the Joint Geological Survey/University of Cape Town Marine Geoscience Unit 14. 87-103.

Rogers, J.; Pether, J.; Molyneux, G.; Genis, J.L.V.; Kilham, J.L.C.; Cooper, G. and Corbeti, I.B. (1990). Guidebook. Geocongress 1990, Geological Society of South Africa.

Rovere, A., Raymo, M. E., Mitrovica, J. X., Hearty, P. J., O'Leary, M. J., and Inglis, J. D. (2014). The mid-Pliocene Sea-level conundrum: Glacial isostasy, eustasy and dynamic topography. Earth and Planetary Science Letters, 387, 27–33.

Rowe, C.D.; Backeberg, N.R.; Van Rensburg, T.; Maclennan, S.A.; Faber, C.; Curtis, C. and Viglietti, P.A. (2010). Structural geology of Robben Island: implications for the tectonic environment of Saldanian deformation. South African Journal of Geology 113(1). 57-72.

Rozendaal, A.; Gresse, P.G.; Scheepers, R. and Le Roux, J.P. (1999). Neoproterozoic to Early Cambrian Crustal Evolution of the Pan-African Saldania Belt, South Africa. Precambrian Research 97. 303-323.

Rudge, J.F., Roberts G.G., and White, N.J. (2015). Uplift histories of Africa and Australia from linear inverse modeling of drainage inventories. Journal of Geophysical Research: Earth Surface, Vol. 120, (5), 894-914.

Scharf, T. (2012). Denudation rates and geomorphic evolution of the Cape Mountains, determined by the analysis of in situ-produced cosmogenic 10Be. Unpublished MSc., Nelson Mandela Metropolitan University, pp. 254.

Scheepers, R. (1995). Geology and Petrogenesis of the Late-Precambrian S-, I-, and A-type Granitoids in the Saldania Belt, Western Cape Province, South Africa. Journal of African Earth Science 21. 35-58.

Scheepers, R.; Schoch, A.E.; Johnson, M.R.; Anhaeusser, C.R.; Thomas, R.J. (2006). The Cape Granite Suite. The Geology of South Africa. Geological Society of South Africa, Johannesburg, South Africa. 421-432.

Shumba, B.T.; Midzi, V.; Manzunzu, B.; Ottemöller, L.; Marimira, K.T. (2020). Source Parameters of the Moderate Mozambique–Zimbabwe Border Earthquake on 22 December 2018. Journal of African Earth Sciences 166. 103829.

Siegfried, H.P. (2008a). 3318AC Yzerfontein and 3318AD Darling Geological Field Maps (Unpublished). 1:50,000 Scale. Council for Geoscience, Pretoria, South Africa.

Siegfried, H.P. (2008b). 3318DB Riebeek-kasteel Geological Field Map (Unpublished). 1:50,000 scale. Council for Geoscience, Pretoria, South Africa.

Söhnge, A.P.G. and Hälbich, I.W. (1983). Geodynamics of the Cape Fold Belt. Special Publication of the Geological Society of South Africa 12.

SRK (2008a). Eskom, Duynefontyn Geotechnical Characterization, Borehole Logs.

SRK (2008b). Eskom, Duynefontyn Site Geohydrology, Exploration Borehole Data and Logs.

SRK (2021). Eskom, Geotechnical Investigation, Borehole Data and Logs.

Stacey, T.R. and Wesseloo, J. (1998). Evaluation and Upgrading of Records of Stress Measurement Data in the Mining Industry. SRK Consulting Report GAP 511b. Safety in Mines Research Advisory Committee.

Stamatakos, J.; Watson-Lamprey, J.; Cawthra, H.C.; Claassen, D.; Coppersmith, R.; Johnson, C.; Largent, M.; Manzunzu, B.; Midzi, V.; Mulabisana, T.; Murphy, D.; Rathje, E.; Wooddell, K. (2022). Baseline PSHA for the Duynefontyn Site and the Koeberg Nuclear Power Station. CGS Report 2022-0009 (Rev. 1). Council for Geoscience, Pretoria, South Africa.

Stowe, C.W. (1995). Characteristics of Jointing in the Malmesbury Group, Harbour Area, Cape Town. South African Journal of Geology 98(2). 224-231.

Strasser, F.O.; Albini, P.; Flint, N.S.; Beauval, C. (2015). Twentieth Century Seismicity of the Koffiefontein Region (Free State, South Africa): Consistent Determination of Earthquake Catalogue Parameters from Mixed Data Types. Journal of Seismology 19(4). 915-934.

Summerfield, M.A. (1996). Tectonics, geology, and long-term landscape development. In Adams, W.M., Goudie, A.S. and Orne, A.R. (eds.): The Physical Geography of Africa, Oxford University Press, New York, 17 pp.

Tack, L.; Wingate, M.T.D.; De Waele, B.; Meert, J.; Belousova, E.; Griffin, B.; Tahon, A. and Fernandez-Alonso, M. (2010). The 1375 Ma “Kibaran Event” in Central Africa: prominent emplacement of bimodal magmatism under extensional regime, Precambrian Research.

Tankard, A.J. (1974). Varswater Formation of the Langebaanweg–Saldanha Area, Cape Province. Transactions of the Geological Society SA 77. 263-283.

Tankard, A.J. (1976a). Pleistocene History and Coastal Morphology of the Ysterfontein–Eland's Bay Area, Cape Province. Annals of the South African Museum 69. 73-119.

Tankard, A.J. (1976b). Cenozoic Sea Level Changes: A Discussion. Annals of the South African Museum 71. 1-17.

Tankard, A.J. (2022). Western Cape Crustal Thickness/Composition. PowerPoint presentation (DNSP-PST-128) presented at SSHAC Enhanced Level 2 Workshop 2, June 21, Cape Town, South Africa. 29.

Tankard, A.J.; Jackson, M.P.A.; Erikson, K.A.; Hobday, D.K.; Hunter, D.R.; Minter, W.E.L. (1982). Crustal Evolution of Southern Africa: 3.8 Billion Years of Earth History. Springer-Verlag, New York. 333-363.

Tankard, A.; Welsink, H.; Aukes, P.; Newton, R.; Stettler, E. (2012). Geodynamic Interpretation of the Cape and the Karoo Basins, South Africa. Phanerozoic Passive Margins, Cratonic Basins and Global Tectonic Maps. Elsevier, USA and UK.

Taylor, G.K. and Shaw, J. (1989). The Falkland Islands: new palaeomagnetic data for their origin as a displaced terrane from South America: in Hillhouse J.W. (Ed.), Deep Structure and Past Accreted Terranes, Geophysical Monograph 50.

Thamm, A.G.; Johnson M.R. (2006). The Cape Supergroup. In: Johnson, M.R.; Anhaeusser, C.R.; Thomas, R.J. (Eds.). The Geology of South Africa. Geological Society of South Africa, Johannesburg/Council for Geoscience, Pretoria, South Africa. 443-460.

Theron, J.N. (Compiler) (1975). 3318B Malmesbury – 3319A Ceres Geological Map Series. 1:125,000 Scale. Council for Geoscience, Pretoria, South Africa.

Theron, J.N. (1984). 3318 DC Bellville Geological Map. 1:50,000 Scale. Geological Survey of South Africa, Pretoria.

Theron, J.N. (Compiler). (1990). 3318 Cape Town Geological Map. 1:250,000 Scale. Council for Geoscience, Pretoria, South Africa.

Theron, J.N. (1992). Geological Map Sheet Explanation 3318 Cape Town Geological Map. 1:250,000 Scale. Geological Survey of South Africa, Pretoria. 140.

Theron, J.N.; Gresse, P.G.; Siegfried, H.P. and Rogers, J. (1992). The Geology of the Cape Town Area. Explanation of Sheet 3318. 1:250,000 Scale. Geological Survey of South Africa, Pretoria.

Tinker, J., de Wit, M. and Brown, R. (2008). Mesozoic exhumation of the southern Cape, South Africa, quantified using apatite fission-track thermochronology, Tectonophysics 455 (1-4), 77-93.

Van der Merwe, C. R. (1963). Soil Groups and Subgroups of South Africa. Department of Agricultural Technical Services, Pretoria, South Africa. Science Bulletin 356. 1-355.

Van Hinsbergen, D.J.J.; Buiter, S.J.H.; Torsvik, T.H.; Gaina, C.; and Webb, S.J. (2011). The Formation and Evolution of Africa: A Synopsis of 3.8 Ga of Earth History. Geological Society of London. ISBN 9781862393356.

Viljoen, J.H.A. (2008). 3318DD Stellenbosch Geological Field Map (Unpublished). 1:50,000 Scale. Council for Geoscience, Pretoria, South Africa.

Viola, G.; Kounov, A.; Andreoli, M.A.G. and Mattila, J. 2012. Brittle tectonic evolution along the western margin of South Africa: More than 500Myr of continued reactivation, Tectonophysics 514-517, 93-114.

Visser, H.H. (1988). Geological Report on the Koeberg Nuclear Power Station Site at Duynefontyn 34. ESKOM.

Visser, H.N. and Schoch, A.E. (1973). The Geology and Mineral Resources of the Saldanha Bay Area, Memoir. Geological Survey of South Africa 63.

Von Buchenröder, W.L. (1830). The Cape Town Earthquake of 1809. South African Quarterly Journal, Cape Town.

Von Veh, M.W. (1982). Aspects of Sedimentation, Structure, and Tectonic Evolution in the Tygerberg Terrane, Southwestern Cape Province. Bulletin of the Precambrian Research Unit, University of Cape Town, South Africa 32. 1-88.

Walford, H. L., and White, N. J. (2005). Constraining uplift and denudation of West African continental margin by inversion of stacking velocity data. Journal of Geophysical Research, 110, B04403.

Watkeys, M.K. (2006). Gondwana Break-up: A South African Perspective. In: Johnson, M.R.; Anhaeusser, C.R. and Thomas, R.J. (Eds.). The Geology of South Africa. Geological Society of South Africa, Johannesburg/Council for Geoscience, Pretoria, South Africa. 531-540.

White-Gaynor, A.L.; Nyblade, A.A.; Durrheim, R.; Raveloson, R.; Van der Meijde, M.; Fadel, I.; Paulssen, H.; Kwadiba, M.; Ntibinyane, O.; Titus, N. and Sitali, M. (2020). Lithospheric Boundaries and Upper Mantle Structure Beneath Southern Africa Imaged by P and S Wave Velocity Models. Geochemistry, Geophysics, Geosystems 21(10).

White-Gaynor, A.L.; Nyblade, A.A.; Durrheim, R.J.; Raveloson, R.; Van der Meijde, M.; Fadel, I.; Paulssen, H.; Kwadiba, M.; Ntibinyane, O.; Titus, N. and Sitali, M. (2021). Shear-Wave Velocity Structure of the Southern African Upper Mantle: Implications for Craton Structure and Plateau Uplift. Geophysical Research Letters 48(7).

Yang, Z.; and Chen, W.P. (2008). Mozambique Earthquake Sequence of 2006: High-Angle Normal Faulting in Southern Africa. Journal of Geophysical Research, Solid Earth 113(B12).

CHAPTER 5: SSM DATABASE

5. SSM DATABASE

5.1 DESCRIPTION OF THE SSM DATABASE

Between 2017 and 2023, various investigations were undertaken in support of the PSHA for the Duynefontyn site. The objective of these investigations, termed Duynefontyn data collection (DDC) activities, was to collect additional geological, geophysical and seismological data that would significantly reduce the epistemic uncertainties associated with the identification and characterisation of seismic sources, particularly seismogenic faults within the SSM (Stamatakos and Watson-Lamprey, 2022; Neveling and Chirenje, 2023). This chapter provides a summarised description of the main DDC investigations (Table 5-1). Section 5.2.6 also provides a brief overview of additional studies, the commission of which occurred either through collaboration between the DDC teams and SSM TI Team or the DDC teams themselves to ensure every effort was made to collect data that would assist in the reduction of epistemic uncertainty in the SSM. All the data collected from these activities form part of the SSM database evaluated by the SSM TI Team in the development of the SSM for the Duynefontyn site.

5.2 OVERVIEW OF DUYNEFONTYN DATA COLLECTION ACTIVITIES

Table 5-1 provides a summary of all DDC activities. The synopsis of each DDC activity includes a brief description of their objectives, methodology, results, and findings. The way in which the data was ultimately evaluated and used as inputs in the development of the various portions of the SSM by the SSM TI Team is discussed in detail in Chapters 4 (Geological and Seismotectonic Setting), 6 (Earthquake Catalogue) and 8 (Seismic Source Model).

Table 5-1. Summary of the DDC activities and other supporting studies undertaken and utilised to aid the SSM. The DDC1 (Start-up) activity was not relevant to the development of the SSM, while the DDC3 (Palaeoliquefaction Studies) activity, although initially planned, was not undertaken.

Activity Name	Report Generated	SSM Support Type
DCC2 Syntaxis Studies	Saunders, I. (2024). Review and homogenization of an Earthquake Catalogue for the Ceres area. CGS Report 2023-0162	DNSP Catalogue
DDC4 Historical Seismicity Study	Albini, P. and Flint, N. (2023). Investigating the Earthquake Records from 1620 to 1969 of interest for the Duynefontyn area, South Africa. CGS Report 2022-0127 Rev.0.	DNSP Catalogue
DDC5 Marine Terrace Studies	Claassen, D., Mthembi, P. and Black, D.E. (2024). Marine Terrace Studies. CGS Report 2022-0140, 136 pp.	Neotectonics
Additional Studies Supporting DDC5		
Chirenje, E., Nxantsiya, Z., Sebothoma, S., Sekiba, M., Netsianda, A., Sethobya, M. and Claassen, D. (2018). Report on the seismic refraction and resistivity surveys for marine terrace and bedrock mapping at Duynefontyn, Western Cape, South Africa. CGS Report 2018-0264.		
Chirenje, E., Nxantsiya, Z., Sebothoma, S., Sekiba, Sethobya, M. and Netsianda, A. (2018b). Report on the reconnaissance ground geophysical surveys at Duynefontyn, Western Cape, South Africa. CGS Report 2018-0114.		
DDC6 and 7 Local fault studies	Coppersmith, R. Slack, C., Moabi, N., Dhansay, T., Cawthra, H., Claassen, D., Sethobya, M. (2024). Duynefontyn onshore fault mapping investigation. CGS Report No. 2023-0001.	Neotectonics
Additional Studies Supporting DDC6 and 7		
Mulabisana, T. (2023). Temporary network along the Colenso fault. CGS Report No. 2023-0082.		
Cawthra, H.C. and Van Zyl, F.W. (2023). Duynefontyn Data Collection for Offshore Faults. CGS Report No. 2023-0116 (Rev.0), 126 pp.		
DDC8 Stress Data Analysis	Smart, K.J., Cawood, A.J. and Ferrill, D.A. (2023). Geological Stress Analyses to Support a Probabilistic Seismic Hazard Analysis (PSHA) for a Critical Site in South Africa. SwRI® Project No. 15.27360.	Tectonic Stress Regime
SSM supporting studies not affiliated with a specific DDC activity		
Cole, J. (2023). 3D Magnetic Modelling of dykes in the area around Duynefontyn. CGS Report No. 2023-0002.		Neotectonics
Maré, L. (2022). Magnetic remnance study of the False Bay dolerite suite in support of geophysical modelling of existing Duynefontyn high-resolution aeromagnetic data. CGS Report No. 2022-0152 Rev.0, 24 pp.		
Barker, O. (2023). Koeberg – 1976 To 1978 – Memories, observations and ideas. Banzi Geotechnics, CC, Job No: 214-01-2023-Koeberg Consultations. CGS, 26 pp.		

5.2.1 DDC2: Syntaxis Studies

Seismicity in the syntaxis of the Western Cape Province is inhomogeneous regarding its magnitude, magnitude threshold, and location accuracy due to a less than ideal network geometry, instrument sensitivity, vault conditions (signal-to-noise ratio) and potential contamination from mining activities (e.g. Saunders et al., 2016). Consequently, Saunders (2024) undertook a study aimed at revisiting seismicity for the period between 1971 to 2020 in an area delineated by the corner co-ordinates of 31°S 17°E and 36°S 21°E in support of the development of the Duynefontyn PSHA seismic catalogue (Figure 5-1). Saunders (2024) compiled a task-specific seismic catalogue, referred to as the CERES catalogue, using data primarily from the South African National Seismological Database (SANSD) for the period 1980–2020, augmented with seismic catalogues compiled from previous seismic studies undertaken at the Berg River Reservoir Network between 2000 and 2009, the Nuclear Siting Investigation Programme in the Elim region between 1997 and 2004 (Council for Geoscience, 2004) and a microseismic study undertaken by the University of Cape Town in the Ceres/Tulbagh area by Smit et al. (2015) over the period February–May 2012.

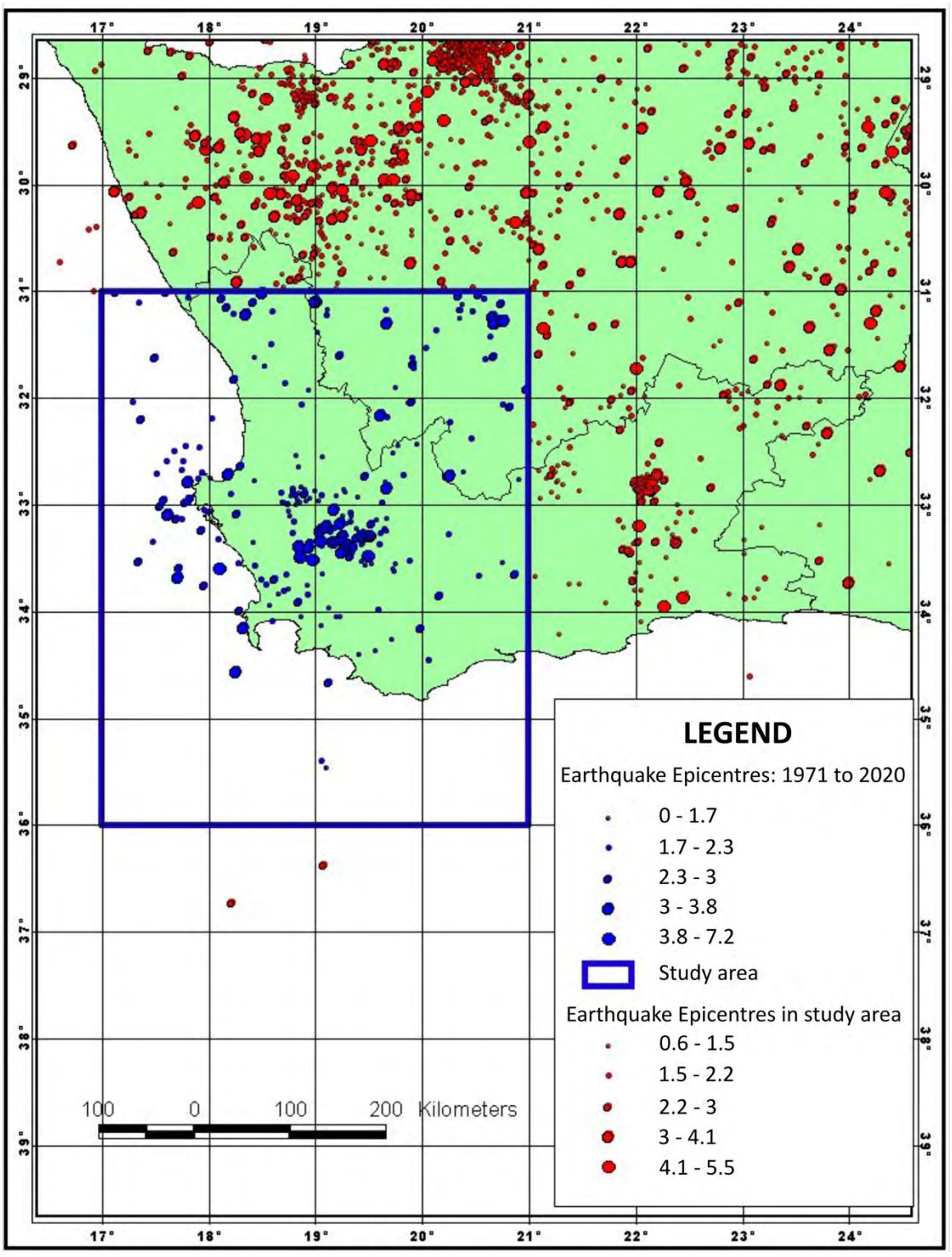

Figure 5-1. Initial events selected for the study area for the 1971 to 2020 period and transferred into the CERES primary database of Saunders (2024).

The syntaxis study had several main objectives and methodologies, which are listed below with some primary results, where applicable:

1) *Recovering phase reading information of earthquakes located in the study area.*

Published seismological bulletins were scanned and optical character recognition was applied prior to conversion with in-house developed software called PyGMI (Cole, 2020).

2) *Homogenising the location methodology.*

The iterative least-squares location methodology of Lienert and Havskov (1995) was used, considering the1D Velocity model of Midzi et al. (2010). The relocated events are shown in Figure 5-2.

3) *Homogenising magnitude determination.*

The local magnitude (M_L) relation of Saunders et al. (2012) was utilised.

4) *Recovering digital waveforms from archive media.*

In total, 165 triggered waveforms were recovered from the 188 listed in the study catalogue, translating to an 87% recovery rate.

5) *Identifying additional earthquake epicentres*.

A total of 78 additional seismic events were identified during this study. Of the 78 events, 46 were identified as raw data from scanned bulletins or located by the addition of phase reading information from International Monitoring stations, events contained in the Nuclear Siting Investigation Programme (Council for Geoscience, 2004), Skuifraam Bergriver Reservoir seismic investigation databases, as well as events from the Smit et al. (2015) database. The remaining 32 events were included through the Saunders and Fourie (2015) publication (reviewing single-station locations). The acceptance criteria for inclusion of new events into the CERES catalogue was a root-mean-square error equal to or below 1 second.

6) *Quantifying location uncertainty*.

Saunders (2024) was able to decrease the root-mean-square of travel-time-residuals from 1.1 seconds to 0.33 seconds after relocation. Average latitude and longitude uncertainties were reduced from 12.5 km to 5.01 km and from 12.4 km to 7.09 km, respectively.

7) Identifying events related to anthropogenic activity.

Saunders (2024) considered the spatial distribution of events in relation to the location of mines/quarries in the Western Cape and the time-of-day distribution of seismic events during periods when surface blasting is allowed in South Africa (Mine Health and Safety Act, 1996). Two methods, viz. the EXFILTER code of Ottemőller (1995) as implemented in the SEISAN earthquake analysis software (Stemler et al., 2018) and the daytime/night-time ratio method of Wiemer and Baer (2000), were used to identify likely anthropogenic events. A total of 252 events were flagged as potential explosions (See Section 6.4).

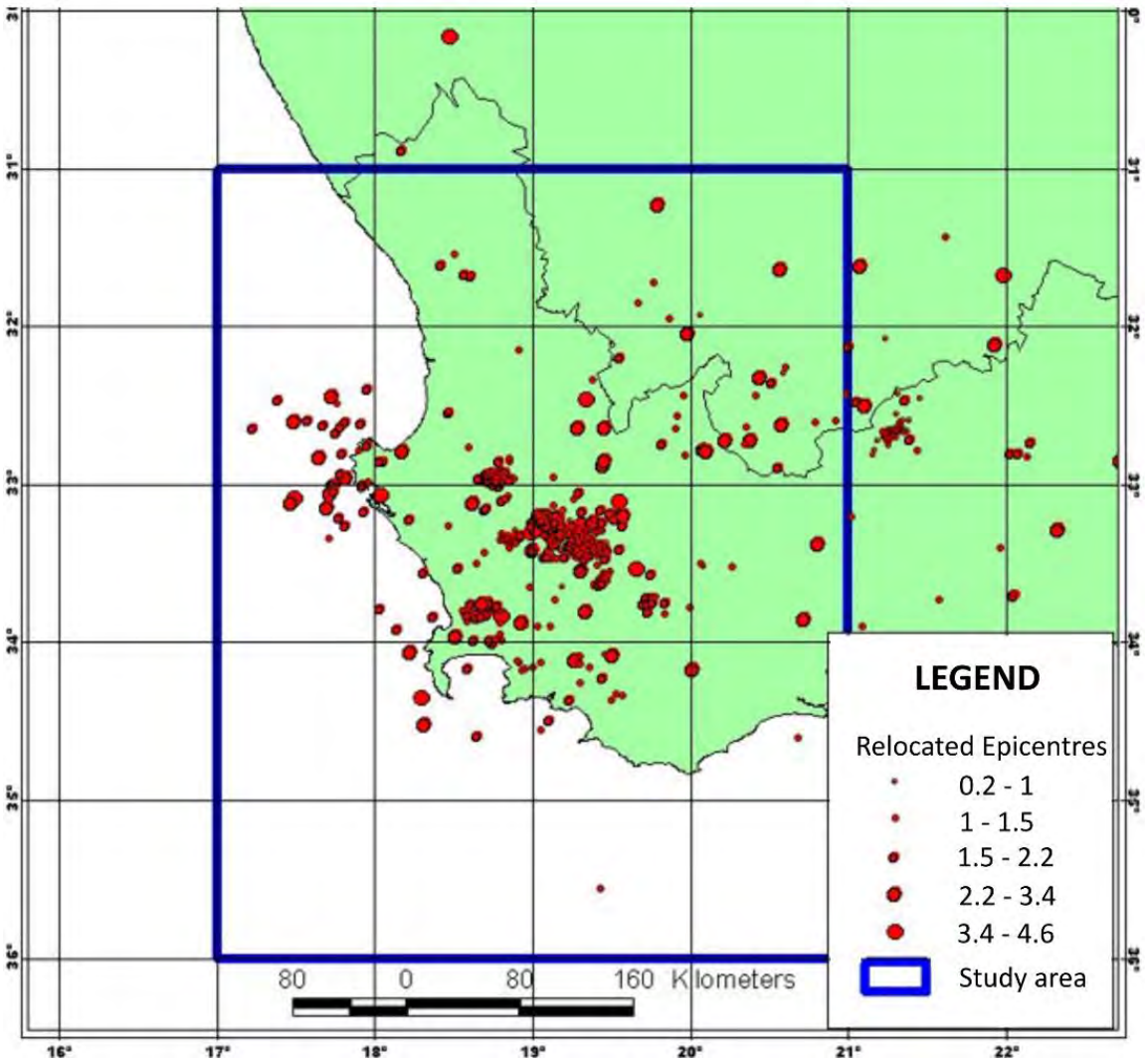

Figure 5-2. The location of epicentre locations of the relocated events with anthropogenic events removed (Saunders, 2024).

8) Determining hypocentral information.

After a review of various methodologies to determine reliability of hypocentral depths (e.g. Guzmán, 1978; Saunders et al., 2008; Brandt, 2014; Mangongolo et al., 2017), Saunders (2024) elected to use the methodology of Li and Thurber (1991), which constrains hypocentral depth calculation using the time difference between the P_n and P_g phase arrivals. Modelling of phase arrivals was determined with the WKBJ method (Chapman, 1978; Chapman and Orcutt, 1985; Chapman et al., 1988; Bender and Orszag, 1999). The focal distribution of 189 seismic events was resolved during this study, ranging from the surface to 12 km depth. Most earthquakes occur at depths of between 5 km and 6 km (Figure 5-3 a–d).

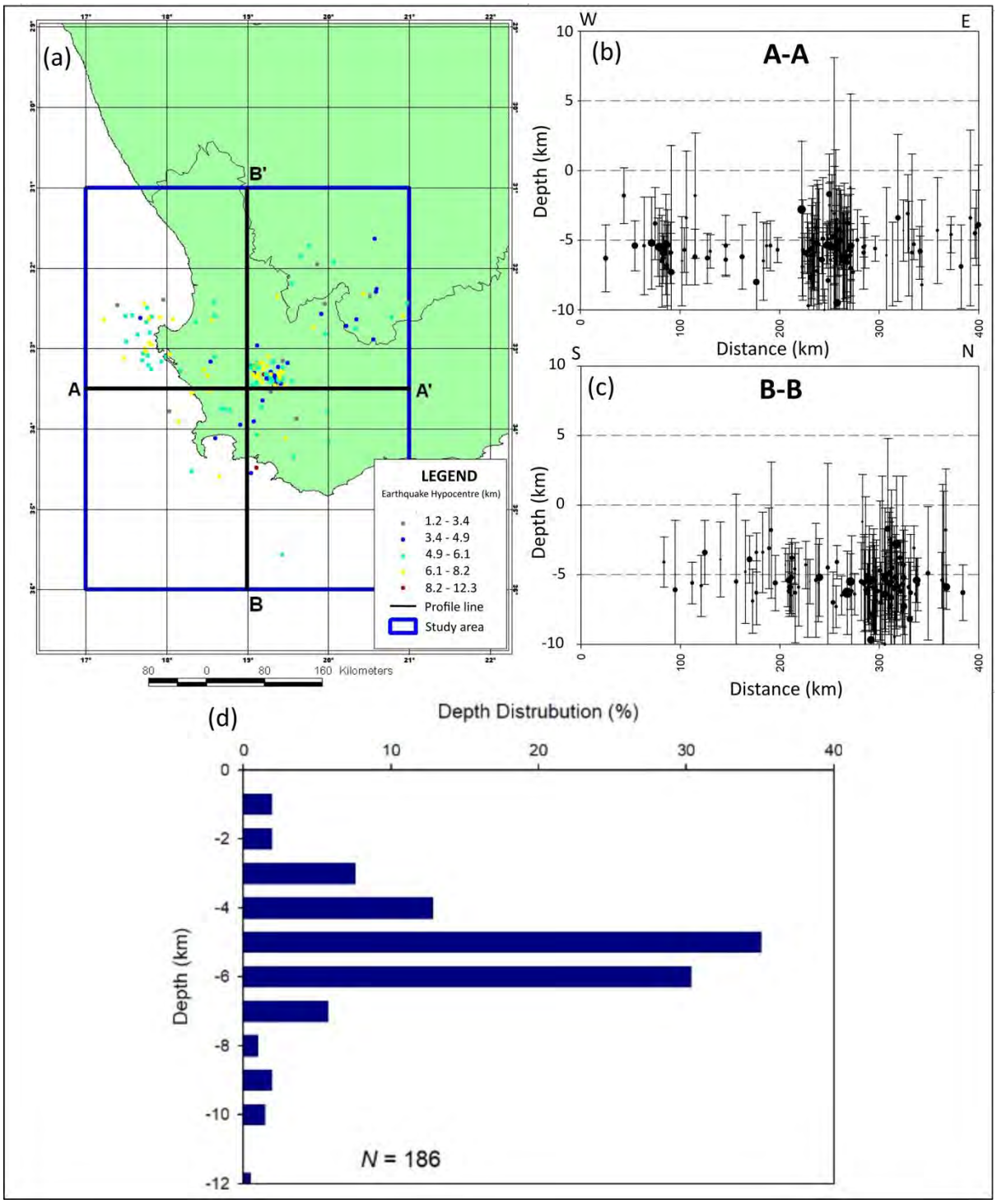

Figure 5-3. (a) The depth distribution of hypocentres determined by Saunders (2024) for the syntaxis study area and the location of depth distribution cross-section profiles A-A and B-B. The figure excludes events with fixed locations. (b) Depth distribution of cross-section A-A and (c) cross-section B-B. (d) Depth distribution presented in 1 km bins considering differentiation between direct phase arrivals and head waves within the syntaxis study area (Saunders, 2024). The event at a depth of 12km (shown on the histogram) is excluded from the cross-sections as it has a high uncertainty in depth.

9) Focal mechanism determination where reliable information is available.

The FOCMEC (Snoke, 2003) and FPFIT codes (Reasenberg and Oppenheimer, 1985), using the SEISAN software (Ottemöller et al., 2018), were used to calculate the nodal planes using a 5° grid search, where six or more P-wave polarity readings and/or amplitude ratios were available. In addition, a composite nodal plane using the FOCMEC code (Snoke, 2003) was determined from 28 events in the Saldanha area, using events with 2 to 5 polarities and a grid search of 5°. The different azimuths and angle of incidence of observations were well represented on the focal sphere. This method assumes that the prevailing stress field generates similar fault plane solutions, representing an average of similar solutions.

Five focal mechanism solutions were determined. An additional focal mechanism was obtained through a composite fault-plane solution. Both N-S and W-E cross-sections indicate steeply dipping faults with Four focal mechanisms indicated strike-slip movement and two indicating normal faulting, as shown in Figure 5-4.

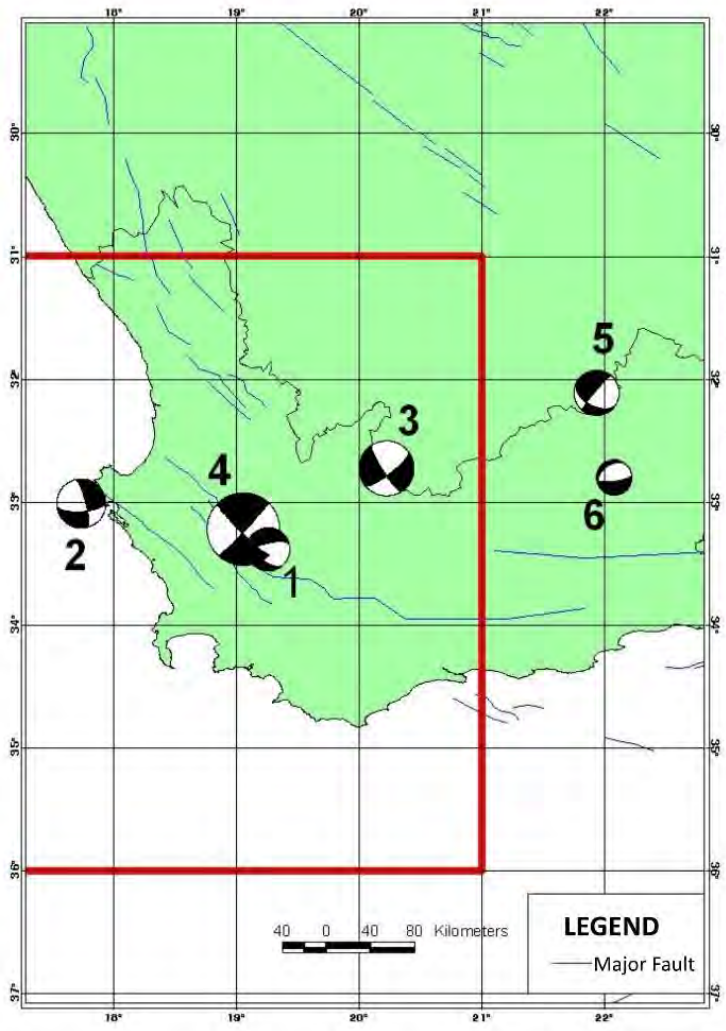

Number	Date (yr/m/d)	Coordinates		Depth (km)	M_L
		Latitude	Longitude		
1	1998/06/30	-33.869	19.262	5 (fixed)	2.2
2	2004/10/22*	-33.013	17.739	5 (fixed)	2.5
3	2009/03/08	-32.727	20.226	5 (fixed)	2.8
4	2015/12/02	-33.222	19.060	9.7	3.7
5	2017/07/22	-32.112	21.937	3.6	2.3
6	2017/10/01	-32.801	22.080	1.8	3.9

Number	FOCMEC Code			FPFIT Code		
	Strike	Dip	Rake	Strike	Dip	Rake
1	133.8	42.0	-42.0	130.0	49.0	-22
2	345.8	73.33	-31.24	ND	ND	ND
3	52.31	69.75	-16.97	149.0	73.0	-162.0
4	134.23	81.35	5.04.0	128.0	69.0	16.0
5	118.67	36.22	-13.93	110.0	28.0	-42.0
6	82.21	70.32	-74.0	96.0	71.0	-74.0

* – Composite fault plane solution

ND – Not determined

Figure 5-4. Focal solutions (lower-hemisphere projections) obtained by Saunders (2024).

10) Statistical evaluation of the compiled catalogue.

Statistical analysis of the CERES catalogue was undertaken to verify its consistency in terms of its temporal and magnitude distribution, magnitude and travel-time residuals, phase residuals, magnitude-frequency distribution and epicentral uncertainty. These were analysed with the PyGMI code (Cole, 2020), highlighting the following:

- The difference in location from the epicentres reported in the SANSD for most events has a horizontal difference in location of less than 50 km.
- The spatial distribution of events and magnitude distribution indicate that the catalogue is incomplete.
- The estimation of the completeness magnitude (M_C) for the catalogue was determined using the frequency-magnitude density function of Gutenberg and Richter (1944).
- The frequency-magnitude relation for the CERES earthquake database was calculated by binning magnitudes at intervals ΔM = 0.1, while the activity rate "*a*" and *b*-value was calculated through a least-squares method. A bimodal distribution is observed with M_C values of M_L~2.6 and M_L~1.4, respectively. Two possible *b*-values were determined: 0.89 and 0.52 (Figure 5-5).
- The root mean square of travel-time residuals, indicating the time difference between phase arrival times predicted by the 1D velocity model and observed phase arrival times, reveal that most root mean square values (81%) are in the 0 to 0.5 second time range with outlier values up to two seconds.
- Arrivals of P-phases and S-phases were estimated to be at 0.08 and -0.04 seconds, respectively. The average latitude uncertainty was reduced from 12.5 km to 5.01 km, and the longitude uncertainty from 12.4 km to 7.09 km.

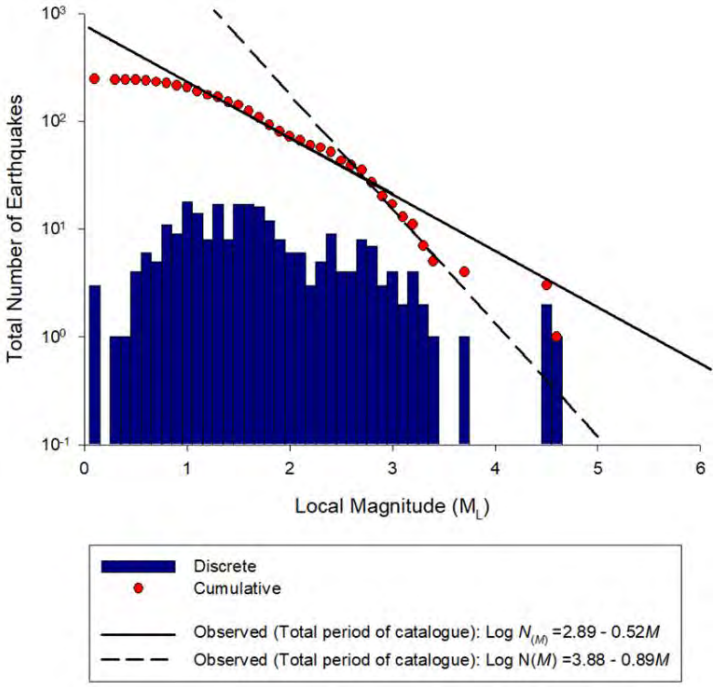

Figure 5-5. Gutenberg-Richter relation determined from the CERES earthquake database. A clear bimodal distribution is demonstrated.

5.2.2 DDC4: Historical seismicity study

Albini and Flint (2023) investigated the historical seismicity within a 350 km radius of the Duynefontyn site. The Western Cape region has hosted moderately large earthquakes and the analysis of historical records can provide extremely valuable information regarding the location, magnitude, and characteristics of earthquakes in the pre-instrumental record. Such information can greatly assist the SSM TI Team when conducting assessments of the completeness of the earthquake catalogue and development of the SSM (See § 4.3).

Albini and Flint (2023) described the pre-instrumental macroseismicity and its intensity distribution in both time and space for a ~350-year period between the year 1620 and 29 September 1969 from a list of historical earthquakes derived from the TNSP Thyspunt catalogue (Strasser and Mangongolo, 2013). The extensive and detailed research into the characterisation of identified historical earthquakes and their documented effects were obtained from various historical documents that included, but were not limited to, published and unpublished archival sources (e.g. documents pertaining to the Dutch and British colonial administration) and contemporaneous narrative sources by residents, travelers and missionaries (e.g. personal journals, letters) in the region. Periodical sources, such as newspapers records and reports from meteorological stations, were also consulted.

To maintain consistency with other PSHA studies in South Africa and the database developed by Midzi et al. (2013), their investigation adopted the MMI-56 macroseismic scale (Musson et al., 2010) to uniformly express the estimates in one single-intensity scale. The methodology followed to interpret and assess earthquake records reported by independent and contemporary sources into intensity data points (IDPs) was that of Musson and Cecić (2002).

Albini and Flint (2023) supplied 74 individual studied events, which were distinguished as follows:

Multiple: 23 earthquakes were complemented with a set of multiple observations and related IDPs in MMI-56; these 23 sets range from 2 to 69 observations.

Solitary: 32 earthquakes had a single observation. 25 newly retrieved earthquakes were not included in any previous catalogue, 6 between 1810 and 1909, and 19 between 1910 and 1952.

False: 10 events in the period 1620 to 1902 were supported by records that turned out to incorrectly report the occurrence of an earthquake and were classified as false events.

Unverified: 3 events listed in the catalogues between 1810 and 1826 were not confirmed by contemporary sources.

The 74 individual events are summarised in Table 4-2. Those events which have multiple IDPs identified by DDC4, were studied by the SSM TI Team in more detail to assess updates to event locations based on the updated locations. The details of the analyses, and additional details on the historical earthquakes, are provided in Section 4.3 (Historical seismicity).

Altogether, the pre-instrumental seismicity of the study area was described by means of:

- 321 newly assigned IDPs in MMI-56 at 155 different localities
- 23 timelines of earthquake effects with more than 1 IDP proposed.

The largest (with ≥ 6 IDPs) nine timelines were further analysed to determine the distribution of earthquake effects in time and space.

Albini and Flint (2023) did not determine the location of the epicentre or estimate the moment magnitude of the events but provided a comprehensive list of 321 intensities in MMI-56, in relation to 55 reappraised earthquakes between 1620 and the main shock of the 29 September 1969 earthquake (Figure 5-6).

The DDC4 authors also provided considerations regarding the completeness of the historical catalogue. Albini and Flint (2023) highlight that completeness depends on the availability of sources of information for the period investigated and on the relative comprehensiveness of the consultation carried out. The identified and consulted sources of earthquake records for the area of investigation in the period 1652–1969 depicted in Figure 5-7 show the availability and variety of the serial sources covering the whole time-window of 350 years of this study. This completely updated dataset provided confidence that for the time window 1620 to 1969, all earthquakes that may have caused macroseismic effects equal to intensity V-VI MMI-56 have been documented.

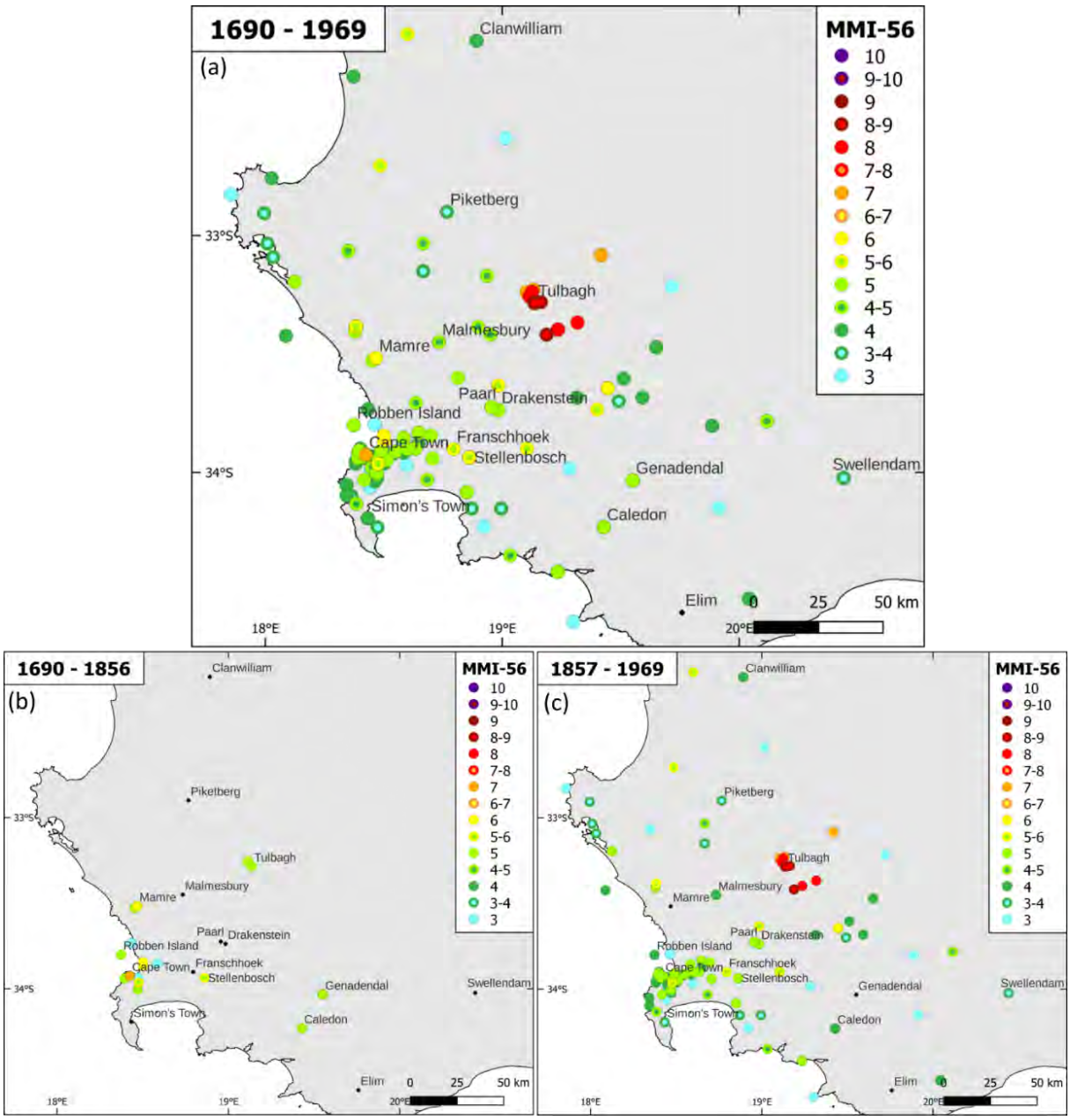

Figure 5-6. (a) The distribution of Maximum Intensity assigned at 121 different places from a total of 155, where at least one intensity value was assessed, for the period 1690–1969. (b) Distribution of maximum observed intensity at 17 different places for the 165 years from 1690–1856, predating the 14 August 1857 earthquake. (c) Distribution of maximum intensity at almost all the mapped places between 1857–1969 (Albini and Flint, 2023).

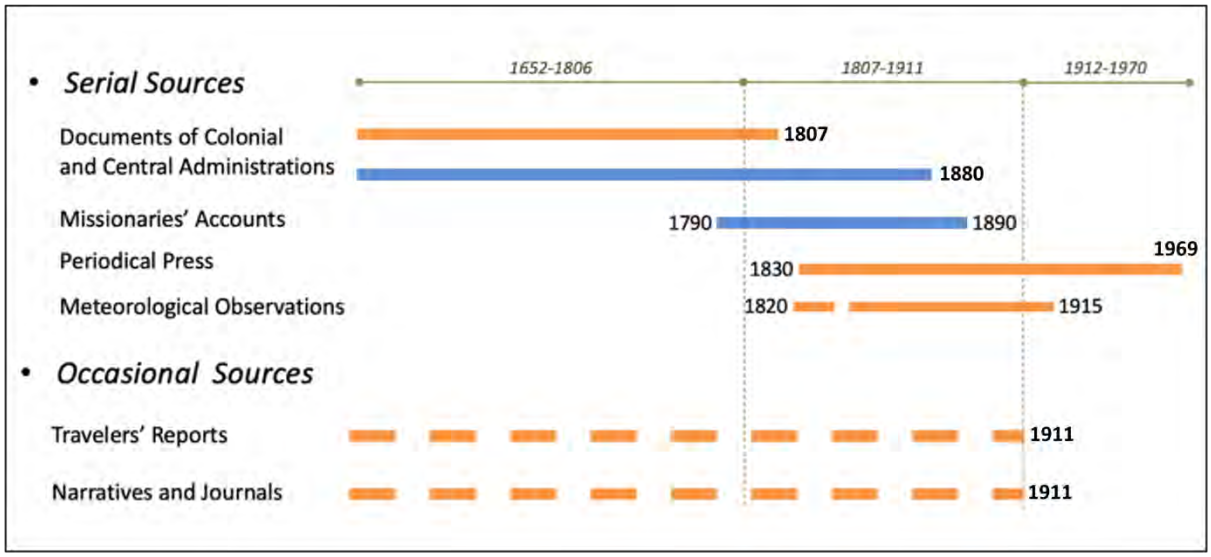

Figure 5-7. Serial and occasional sources identified and consulted for the study period. The solid lines show the availability of serial sources throughout the indicated time window, while orange solid lines show the sources systematically consulted. The blue solid lines indicate that these sources were extensively sampled. The dotted lines depict the occasional sources, the time coverage of which is erratic (After Albini and Flint (2023)). Not to scale.

5.2.3 DDC5: Marine terrace studies

Emergent marine terraces of various ages and elevations occur along the entire southern African coastal belt (e.g. Davies, 1971; 1972; 1973; Roberts, 2006; Hanson et al., 2012; Cooper and Green, 2021). Their development is the combined consequence of global sea-level fluctuations and/or local or regional tectonic uplift/vertical crustal movements at specific times in the geological record (e.g. Choi et al., 2008; Gurrola et al., 2013; Karymbalis et al., 2022). Consequently, a regional marine terrace investigation was conducted along the southwest Cape Coast of South Africa by Claassen et al. (2024) in support of the Duynefontyn PSHA, with the main objectives being:

- To document the altimetry (m amsl) and chronology of marine terraces in the region for the purposes of correlation. Correlation aids the evaluation of potential of surface faulting and deformation and/or tectonic warping along the coastal margin. This includes the assessment of the seismogenic potential of onshore faults, such as the proposed Milnerton-Cape Hangklip and Colenso Faults.
- To evaluate the regional and local rates of tectonic uplift that can be used to identify and characterise the regional tectonic setting.
- To recognise patterns of uplift to evaluate potential capable tectonic sources.

To achieve these objectives, the study undertook various data compilation and collection activities to identify and correlate shoreline indicators across four focus areas: 1) Elands/Lamberts Bay, 2) Saldanha Bay/Velddrif, 3) Koeberg/Duynefontyn, and 4) False Bay along the southwest coast of South Africa (Figure 5-8).

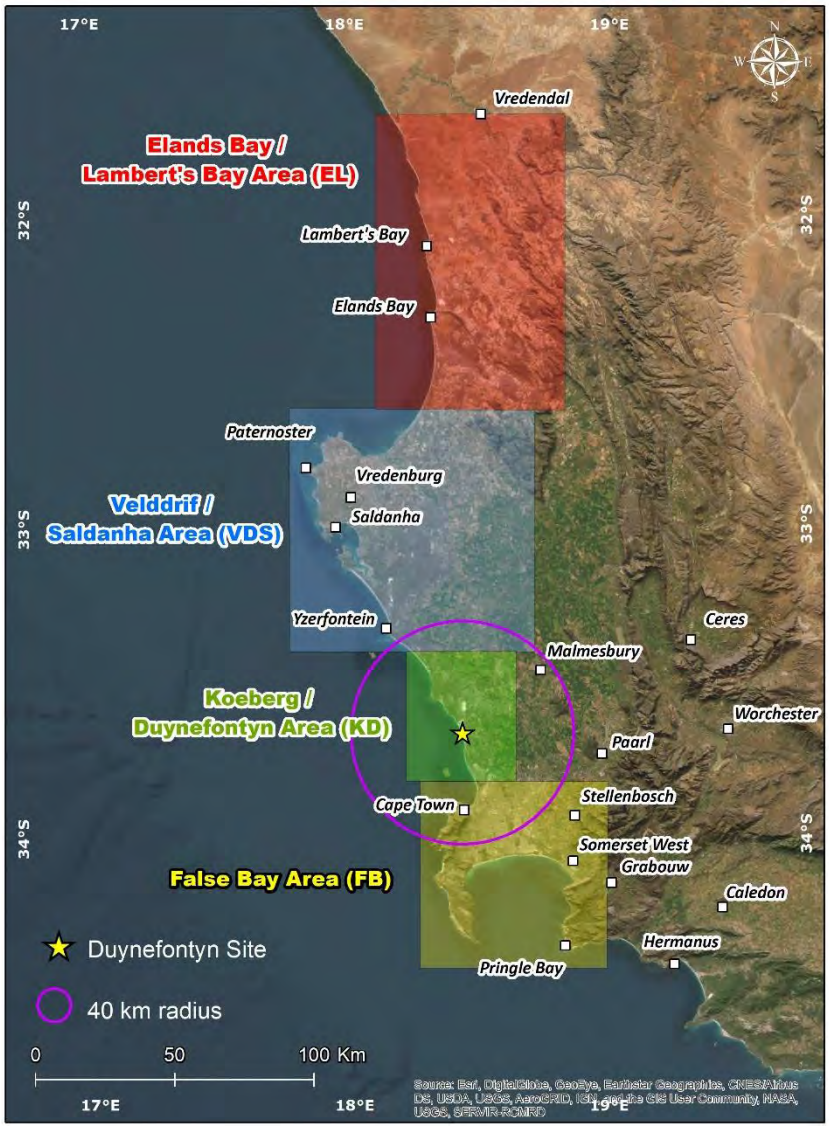

Figure 5-8. Data compilation and collection focus areas for the Duynefontyn marine terrace study. Four focussed areas of investigation are highlighted (Elands/Lamberts Bay, Saldanha Bay/Velddrif, Koeberg/Duynefontyn and False Bay).

Activities associated with the study included the development of the following databases (Figures 5-9 and 5-10):

1. *Desktop shoreline database*

A desktop investigation collated >1,300 published shoreline indicators along the western and eastern cape coasts of South Africa. (Figure 5-9a).

2. *Fieldwork database*

Three field campaigns collected >350 field observations related to wave-cut platforms, shoreline angles, sea-cliffs, and marine related deposits along the southwest coast (Figure 5-9 b).

3. *Ground geophysical surveys (Chirenje et al., 2018 and b)*

A total of 16 groundborne geophysical profiles which included magnetics, multi-electrode resistivity, time domain electromagnetics and seismic refraction, were conducted at the

Duynefontyn and Koeberg sites. Surveys aided in determining the bedrock elevation beneath overburden, buried wave-cut platforms and any possible buried/concealed faults.

4. Topographic LiDAR-derived shoreline angle database

Topographic profiles were utilised to interpret the position and elevation of wave-cut platforms, palaeosea cliffs, and shoreline angles. A total of 46 profiles were created between Bokbaai in the north and Camps Bay in the south, where LiDAR data was available (Figure 5-9 b). A set ranking criterion was used to assess the quality/reliability of the shoreline angle assessments, with only high quality, reliable measurements used in correlation diagrams in the area.

5. Borehole database

A comprehensive collation effort was undertaken to source borehole data that would aid in the identification of buried palaeoshoreline indicators and characterise the subsurface lithostratigraphy. The data from more than 1350 boreholes were incorporated into the database (Figure 5-10 a).

6. *Drilling programme*

Eleven new boreholes were drilled at the Duynefontyn site to identify and correlate the elevation of marine wave-cut platforms and, where possible, identify individual facies beneath the extensive Cenozoic cover that could be used in conjunction with existing borehole data to evaluate any Quaternary deformation (Figure 5-10 b).

7. *Palaeotopography maps*

Interpolated palaeotopography maps were created along the southwest Cape coast in the following five areas with varying resolutions:

- Lamberts Bay to Elands Bay (10 m contour interval)
- Velddrif to just south of Yzerfontein (10 m contour interval)
- Silwerstroom to Koeberg (10 m contour interval)
- Koeberg to Duynefontyn (1 m contour interval)
- False Bay (5 m contour interval)

Interpolated maps were used to create palaeotopographic profiles from which to interpret the occurrence of buried marine terraces and possible tectonic offset in bedrock strata. (Figure 5-10 b).

8. Palaeotopography profiles

A total of 35 palaeotopography profiles were created from interpolated palaeobedrock maps. Profiles were used to interpret the position and elevation of buried wave-cut platforms, palaeosea cliffs, and shoreline angles. A set ranking criterion was used to assess the quality/reliability of the shoreline angle assessments, with only high quality, reliable measurements used in correlation diagrams in the area.

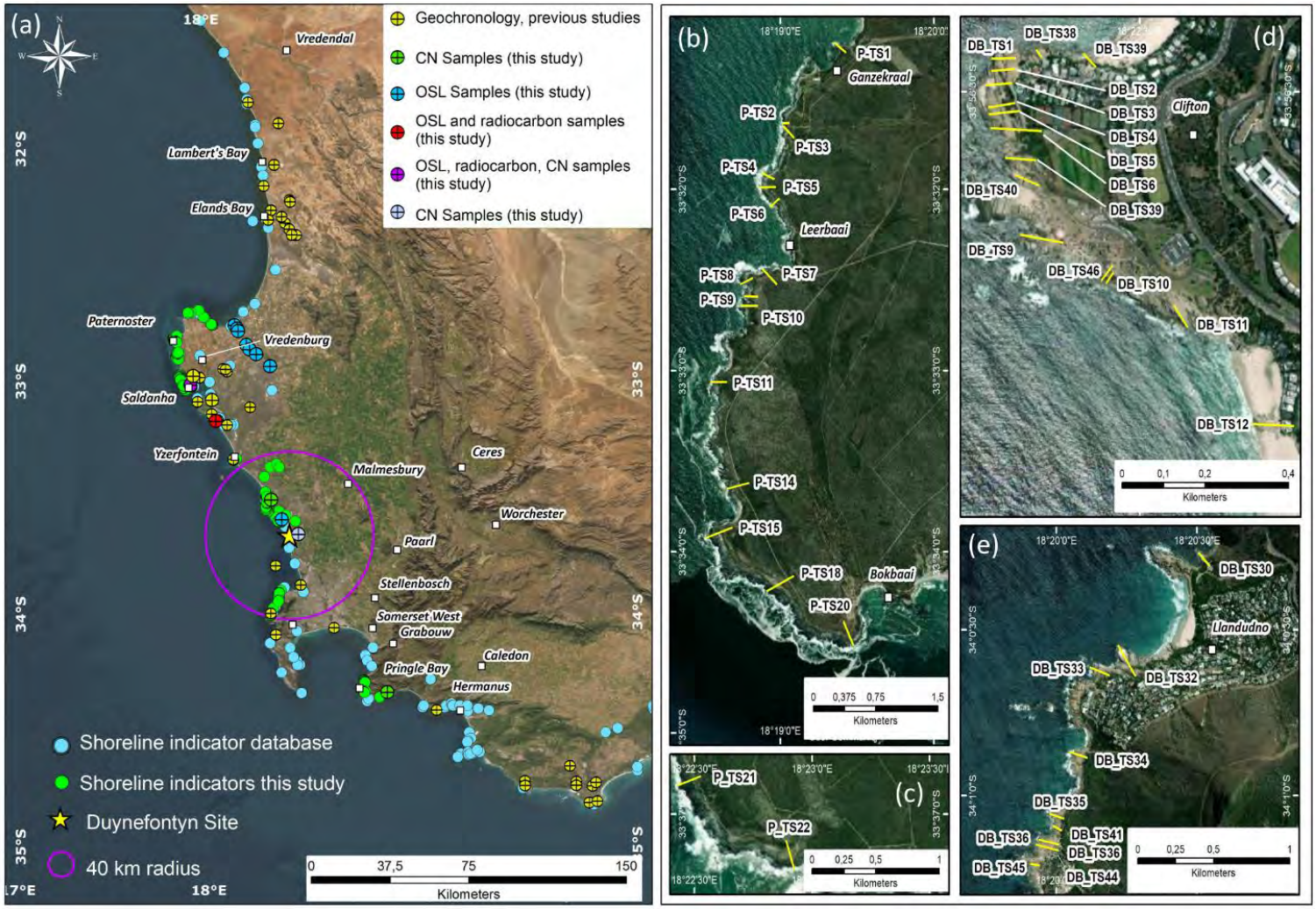

Figure 5-9. (a) Map of the southwest coast of South Africa showing shoreline indicators collated as part of a desktop study, new indicators collected during fieldwork, and relevant Neogene-Quaternary geochronologic data obtained from scientific literature and new samples collected for DDC5 (after Claassen et al., 2024). (b-e) Locations of topographic profiles derived from LiDAR data along the southwest coast of South Africa.

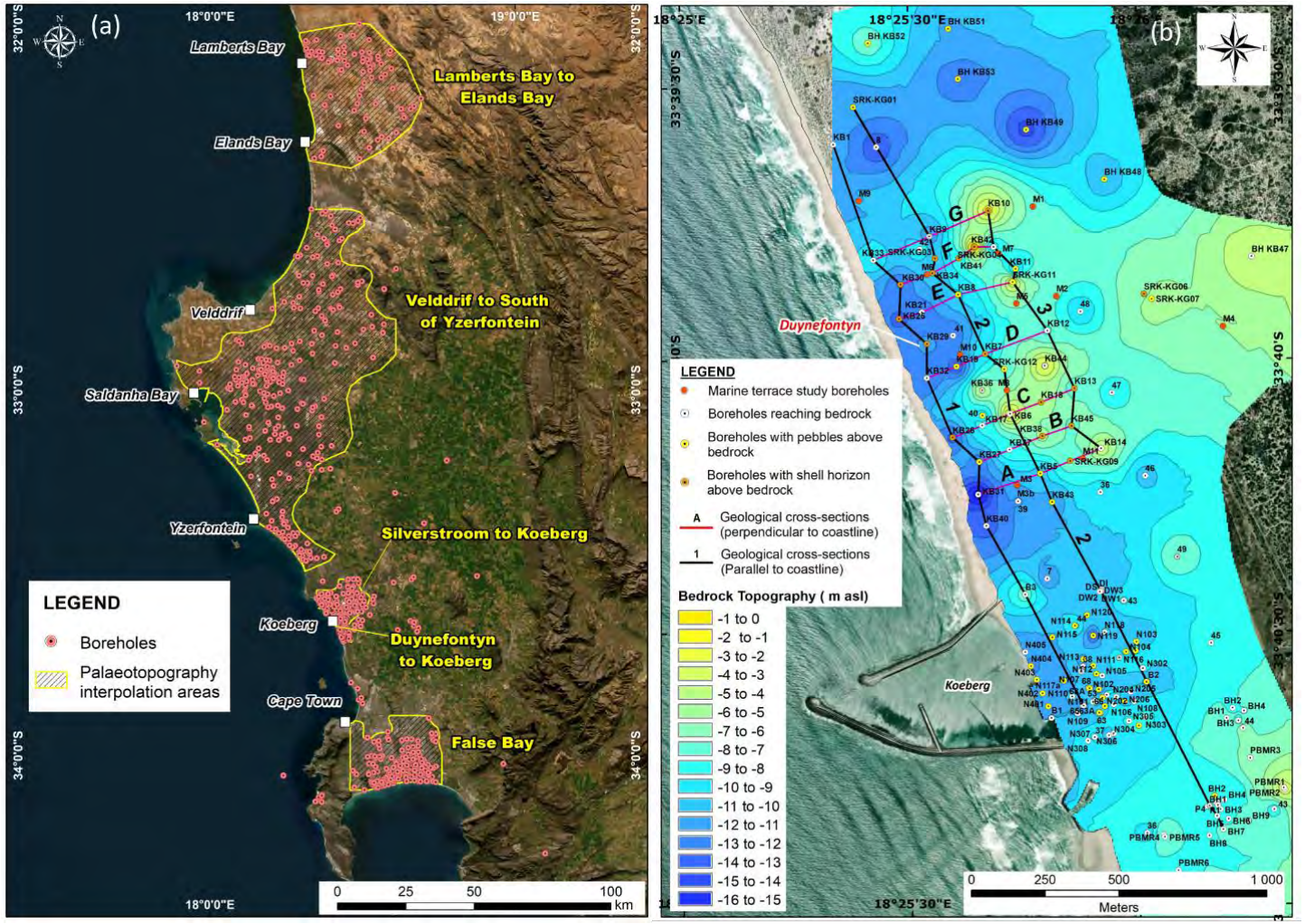

Figure 5-10. (a) Locations of near-coastal boreholes collated as part of the marine terrace study, showing the location of the five areas for which a palaeotopographic bedrock surface was interpolated (after Claassen et al., 2024). (b) Interpolated palaeotopographic bedrock surface at Koeberg and Duynefontyn. The locations of onsite geological cross-sections drawn from existing boreholes and the newly drilled marine terrace boreholes are indicated by solid lines (after Claassen et al., 2024). The interpretation of the palaeotopography is discussed in Section 4-4 (Duynefontyn Site Geology and Figure 4-36).

9. Geological cross-sections

Borehole data collected for the Duynefontyn and Koeberg areas were used to develop the geological cross-sections, seven SW–NE coast-perpendicular profiles, and three NW–SE coast-parallel -trending profiles (Figure 5-10 b). Ten geological cross-sections, seven E–W coast-parallel cross-sections, and three coast-perpendicular cross-sections across the Cape Flats were also drawn from the interpretation of downhole lithologies identified by Henzen (1973) and Wessels and Greeff (1980). Sections aided in defining the subsurface lithostratigraphy and evaluation of possible Cenozoic offset.

10. Cenozoic geochronology database

A Cenozoic geochronology database was compiled from existing literature. It captured the location and age marine and aeolian sediments along the Western and Eastern Cape coastlines. An effort to collect new geochronology data in high priority areas (e.g. coastal regions where faults are mapped to occur), and areas with no available age constraints (geochronological data gaps) were also undertaken. Unfortunately, geochronology results were not obtained in time to be included in the results and discussions of the marine terrace study.

Claassen et al. (2024) outlined that any interpretations and findings from these datasets have inherent uncertainties, limitations, and scientific assumptions that were carefully considered by the SSM TI Team in their evaluation of the data provided by this study (see Section 8.5.2, Colenso Fault).

5.2.3.1 Regional marine terrace evaluation

Across the four focus areas, Claassen et al. (2024) made the following summarised observations regarding palaeoshoreline indicators along the southwest Cape coast:

- Correlation of mapped and radiocarbon-dated shorelines of Middle Holocene age, situated at elevations of ~3.5 ±1 m amsl, are consistent in their altimetry and chronology. No obvious evidence of neotectonic deformation of this terrace was found but can also not be excluded in areas lacking data.

- The Late Pleistocene, Marine Isotope Stage (MIS) 5e (~130-118 ky) is situated at an elevation of ~6 ±1 m amsl, in agreement with known local manifestations of this sea-level highstand. Correlation of fieldwork and topographic profiling using LiDAR data confirmed their occurrence at these elevations across all four data collection areas with no obvious signs of displacement or continental warping of the margin across the area. Due to its consistency across the region, this served as a marker for possible neotectonic offset across the Colenso Fault near Paternoster (See chapter 8.5.2, Colenso Fault). The consistency in terrace elevations across the fault provides evidence for lack of vertical offset within the last ~125 ky. In addition, no obvious large scale horizontal or strike-slip displacement of terraces were encountered.

- The marine terrace situated at elevations of ~9/10±1 m amsl are of an inferred Middle Pleistocene (~400 ky) age and associated with MIS 11. The field occurrence and identification of this terrace proved difficult due to extensive Cenozoic cover.

Regional correlation of this terrace using fieldwork investigations and topographic and palaeotopographic profiles shows it to be consistent in its altimetry and apparent/assumed chronology (See chapter 8.5.2, Colenso Fault), without any vertical offset or any detectable large-scale horizontal offset.

- A ~15 and ~18-21 m amsl terrace is consistently documented across the four areas of investigation. Very little geochronology is available to constrain these terraces, ages but an age range of between 0.88-1.2 Ma is suggested by Roberts (2006). Despite this, their consistency in elevation across the region inspires greater confidence in tectonic stability around the coast (Figure 5-11).

- The collation of various existing data sources made it possible to compare the ~30± 3 m amsl terrace within the region. Geochronology ages for this palaeosea level vary between the Pliocene and perhaps earlier (Miocene); a possible consequence of re-occupation, dating techniques, sampled material, and dating range uncertainties. Despite this, the regional similarity in the elevation of correlated terraces correlated suggests uniformity and lack of any large-scale vertical warping of the coastal margin (Figure 5-11).

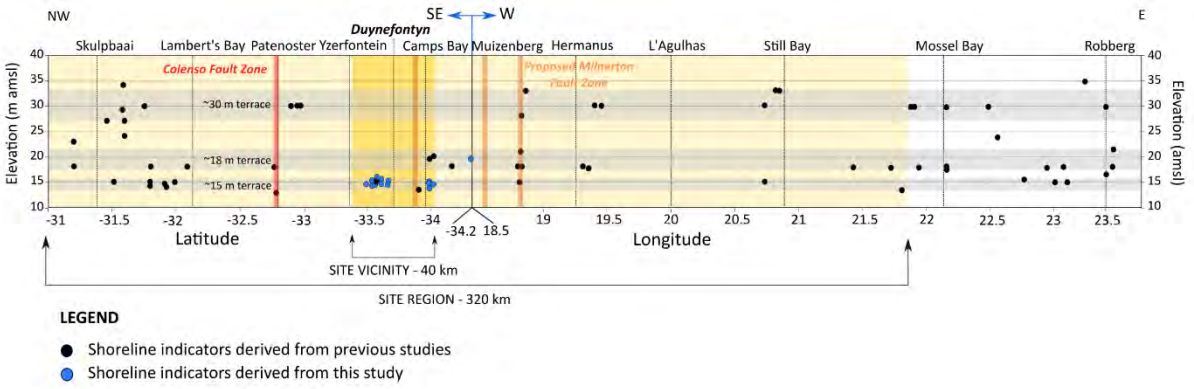

Figure 5-11. Regional shoreline correlation diagram depicting reliable elevation data points against latitude for the ~15, 18 and 30 m terraces along the coastal margin between Skulpbaai and Robberg (Claassen et al., 2024).

5.2.3.2 Evaluation of seismic sources

Investigations undertaken by the marine terrace studies included an assessment of the seismogenic potential of the onshore proposed Milnerton-Cape Hangklip and Colenso fault zones. The SSM TI Team evaluated and incorporated the data derived from this study into the SSM, as detailed in sections 8.5.2 (Colenso Fault) and 8.5.7 (Milnerton Fault).

Colenso Fault

Both headlands (Cape Columbine and Rooisteen) near Paternoster, where the NW-SE trending Colenso Fault is interpreted to extend offshore, exhibit a coast-parallel wave-cut notch, into palaeodune material and capped by a calcrete layer. The base of the cliff is not well defined, but isolated areas with limited cover measured a shoreline angle of 9.0–11.5 m amsl, tentatively correlated with the sea-level highstand associated with the Mid-Pleistocene interglacial MIS 11. There appears to be no vertical offset or visible/obvious fault scarp

observed at any location along the length of the calcrete cap. This evidence extends the notion of lack of offset along the Colenso Fault to ~400 ky.

Proposed Milnerton–Cape Hangklip Fault

Investigations as part of this study to assess the presence of the proposed Milnerton Fault were inconclusive. Its presence in the False Bay area and towards Hangklip/Pringle Bay could not be confirmed. However, if present in the proposed location indicated by previous authors, this study could not find any data to support neotectonic activity associated with such a feature. Subsurface data across the False Bay area does not show offset of any marker beds and fieldwork investigations around Rooi Els and Pringle Bay show terrace elevations assumed to be associated with MIS 11 remaining consistent with areas to the northwest.

5.2.3.3 Evaluation of deformation at the Duynefontyn and Koeberg sites

A 1 m contour interval interpolated bedrock palaeotopography map derived from borehole data for Duynefontyn and Koeberg (Figure 5-10 b) reveals that bedrock occurs exclusively below sea level, reaching values up to -16.8 m amsl. Overburden thickness at both sites ranges between 12.3 m to 35.2 m, with an average thickness of 20.8 m. Thickness increases with increasing distance from the coastline.

Excavations at Koeberg during the construction of the nuclear power plant revealed a weathered, uneven, gently seaward-sloping wave-cut platform. A consistent, lower, well-developed 10 to 12 m below mean sea level and a probable upper 5 to 7 m below mean sea level platform were identified, overlain by marine gravel. The bedrock surface exhibits *Pholad* trace fossils with no offset noted across mapped fractured/faulted zones. The age of this platform is unknown, however, the overlaying ‘Shark Tooth Bed’ (Varswater Formation) located directly above the pebble horizon contains rich fossil content from the Pliocene (~5 Ma). The ages of these fossils would imply a similar or older age for the gravel marker beds above bedrock, in which no obvious signs of large-scale displacements are noted.

5.2.3.4 Uplift rates

The marine terrace study provides a comprehensive desktop review of the regional uplift rates (Claassen et al., 2024). Collectively, authors provide evidence in support of relatively low and uniform rock uplift rates (Table 5-2) from the Middle Miocene to the Late Pleistocene, consistent with a stable continental region, devoid of marked Quaternary neotectonism or Quaternary differential crustal warping along its margin. The collated estimates of regional isostatic rock uplift rates for the southwest Cape coast of South Africa all revealed slow uplift rates in the order of only a few metres per million years (generally between <1 to 6.6 m/My) and is consistent with a stable continental margin.

Table 5-2. Summary of uplift rates determined from various studies along the west and south coasts of South Africa (after Claassen et al., 2024). Dating methods used include optically stimulated luminescence (OSL), radiocarbon (RC) and cosmogenic nuclides (CN).

Uplift Rate	Time Period	Region	Method	Author
3.5–4.8 m/My <2 m/My	Plio-Pleistocene Last 400 ka	Broader west coast	Relative sea-level estimates (Sr Isotopes)	Hearty et al., 2020
0-1.88 m/My ~11.23m/My	Since Pliocene (5.33 My) Since Late Tertiary	West Coast West and South Coast	Relative sea-level estimates /terraces (OSL/RC) Inferred Late Tertiary terraces	Roberts, 2006
3.75-5.62 m/My	Since Pliocene (5.33 Ma)	Tectonism of ~20-30 between south and west coasts	Lithostratigraphy	Roberts, 2006
~4.4 m/My		Wilderness and Cape St. Francis	Catchment-wide erosion rates - Cosmogenic	Hanson et al., 2012 Bierman, 2012 Erlanger, 2011
5.0 ± 0.7 m/My		Thyspunt	Marine terrace bedrock /overlying beach gravel - CN	Hanson et al., 2012 Bierman, 2012 Erlanger, 2011
6.6 ± 1.1 m/My		Sundays River Fluvial Terraces	Sediments overlying terraces - CN	Erlanger, 2011
2.3 ± 0.4 m/My - 8.8 ± 0.2 m/My	Cenozoic	Cape Fold Belt in the Western Cape	Bedrock outcrops, and fluvial gravels - CN	Scharf et al., 2012

5.2.4 DDC6 and 7: Local fault studies

The investigation of onshore faults in the Western Cape was undertaken by Coppersmith et al. (2024) to reduce the uncertainties with regard to important fault parameters such as geometry, recency of slip and slip rate, for input to the fault source characterisation portion of the PSHA study (Figure 5-12). Their efforts were supported by two additional supporting studies, which included an offshore hydroacoustic study (Cawthra and Van Zyl, 2023) and a short-term micro-seismicity monitoring effort along the Colenso Fault (Mulabisana, 2023). In addition, a structural analysis of bedrock faulting in the Western Cape by Moabi and Dhansay (2022) was presented at Workshop 2 and performed in parallel to the onshore mapping effort.

5.2.4.1 Duynefontyn onshore fault mapping investigation

Coppersmith et al. (2024) used information from past studies coupled with new field work to evaluate the recent tectonic history of on-shore faults that may contribute to ground motion at the Duynefontyn site. Several candidate faults identified in previous studies (e.g. De Beer, 2005) were investigated with the aim of identifying their exposure locations, accessing recency of movement and if possible, identify information regarding slip rate, geometry, and other factors relevant to fault source characterisation in the PSHA.

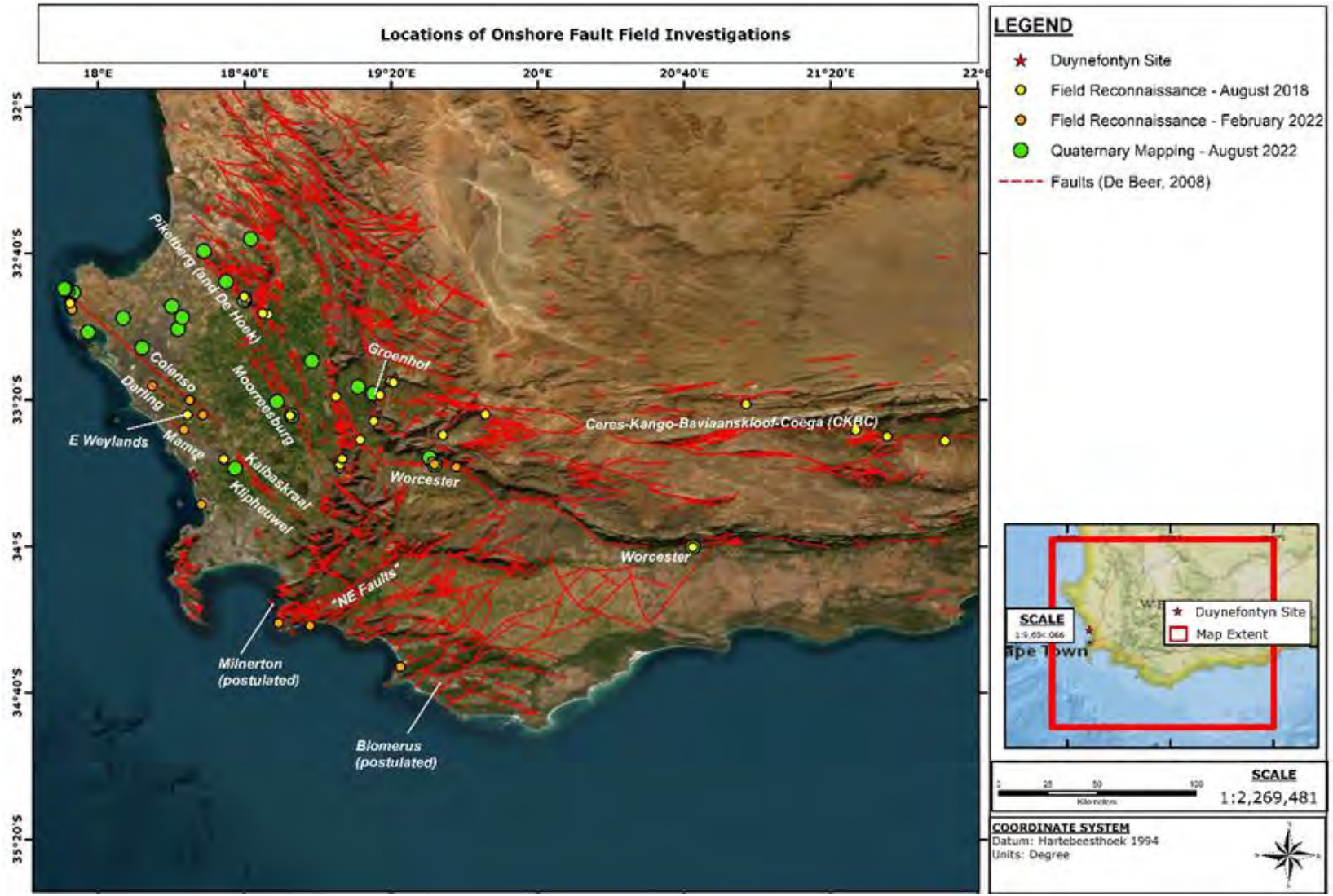

Figure 5-12. Regional map of studied faults in the Western Cape. Orange and yellow dots show locations of field reconnaissance, green dots indicate locations of detailed investigations for sites that showed potential for further neotectonic study.

The objectives of the onshore fault mapping investigation are summarised below:

- Compile existing publications and CGS reports detailing past fault investigations in the Western Cape.
- Work directly with CGS personnel to discuss findings of a structural analysis that provides insight to the location of bedrock faults, the structural complexity, sense of slip, and other features associated with faulting in the syntaxis (Moabi and Dhansay, 2022).
- Perform field reconnaissance along regional bedrock faults where past studies have indicated evidence of bedrock faulting or, in some cases, interpretation of neotectonic activity (Figure 5-12).
- Screen sites “in” or “out” for additional detailed Quaternary mapping based on likelihood of finding evidence to contribute to fault source characterisation.
- For sites that were not screened out, detailed Quaternary mapping appropriate for determining recency or limiting age of faulting, slip rate, and geometry were undertaken. The appropriate method was determined depending on site conditions (e.g. geomorphic mapping, scarp profiling, trenching or drilling, as needed).

Results of the onshore mapping effort provided a revised understanding of the exposures of the major regional faults as well as the lack of Quaternary sedimentation to evaluate the recency thereof (refer to DDC 6-7 report). The major results are summarised below.

- Six regional localities were investigated for Quaternary faulting. Localities were selected based on previous field reconnaissance, GIS-based office mapping, and/or previous studies in the literature.
- The sites for each locality focussed on determining recency of movement along a known bedrock fault. Therefore, locations such as drainages, alluvial deposits, or other young landforms near or onlapping the faults were targeted and mapped where possible. No evidence of Quaternary surface faulting and no outcrop related to obtaining slip rates were observed during detailed analysis and mapping.
- Regionally speaking, the age of faulting is uncertain due to lack of Cenozoic cover in the Western Cape. Drainages eroding through major quartzite ridges currently carry little to no sediment and exhibit low discharge rates when compared to the valleys in which they reside.
- Erosion rates were estimated based on several bulk sediment samples from strategic locations around major watersheds in the Western Cape. Preliminary results indicate very low erosion rates on the order of 3.4 to 6 metres per million years (Coppersmith et al., 2024) that are consistent with earlier published results (Erlanger, 2011; Scharf, 2012; Bierman et al., 2012a and b; Bierman, 2014).
- Evidence for lack of surface faulting since the deposition of a large alluvial fan was found along the Worcester Fault. (1.3 Ma, see Section 8.5.4)
- The sites at Riebeek and Piketberg provided evidence of faulting in the bedrock, but due to little or no Quaternary cover the recency of movement, and therefore the slip rate, could not be determined for these bedrock faults. However, based on no faulting of Holocene sands, the probability of these faults being seismogenic was interpreted to be low.
- The sites along the northern Colenso Fault Zone provided a Plio-Pleistocene aeolianite cover that appears unfaulted, based on the local 2 m resolution Digital Surface Model. In addition, the wave-cut platforms and backedges in the same area show no

detectable vertical or horizontal displacement. The granites along the coastline do however indicate an ancient shear zone with mylonites that must have formed at great depth, suggesting the Colenso Fault Zone system is exhumed. It should also be noted that the subsurface depth and dip direction of the Colenso Fault zone remains unmeasured and thus unknown.

The SSM TI Team evaluated and integrated the data derived from this study into the SSM. See sections 8.5.2.2 (Colenso Fault), 8.5.2.3 (Kalbaskraal and Klipheuwel Faults), 8.5.2.4 (Worcester Fault), 8.5.2.5 (Piketberg–Wellington Fault) and 8.5.2.6 (Groenhof Fault).

5.2.4.2 Duynefontyn offshore hydroacoustic fault supporting study

Cawthra and Van Zyl (2023) conducted an offshore hydroacoustic study along the southwest Cape Coast of South Africa, at selected localities within a 200 km radius of Duynefontyn, as part of the Geological Investigations Programme in support of the Duynefontyn PSHA. The main objective of the study was to investigate the possibility of neotectonic activity along faults, with special emphasis on the Table Bay Fault and the proposed Milnerton Fault that could be exposed at the seafloor or be shallowly buried with sediment. To achieve this objective, the study aims included:

- A review of existing geophysical offshore datasets (De Villiers, 1944; Horwood and Smith, 2007; Cole et al., 2007; de Wet, 2013; Anadarko Petroleum Corporation data, as published in Palan, 2017; MacHutchon et al., 2020; de Wet and Compton, 2021) and associated geological information relating to offshore faults along the continental margin of the southwest Cape coast (Dames and Moore, 1976; Hartnady, 2003; De Beer, 2007; Horwood, 2009).
- The collection and interpretation of new hydroacoustic data included high-resolution multibeam bathymetry, 19 regional boomer sub-bottom profiles, and a grid of pinger sub-bottom profiles in the multibeam blocks, with a particular focus on the Table Bay and False Bay areas where the Table Bay and proposed Milnerton–Cape Hangklip Fault is projected to occur offshore (Figure 5-13).
- Identification of any new prospective offshore fault sources that may be relevant to the PSHA study for the proposed Duynefontyn site in a geological context that includes sea-level change and sediment deposition on the continental shelf that need consideration in the analysis of neotectonic movement. The assessment of fault activity was undertaken by evaluating the offset of:
  - Early Cretaceous (132 ± 6 Ma, Reid et al., 1991) roughly NW–SE-trending dykes associated with the False Bay Dolerite Suite.
  - Cemented Quaternary deposits draping the bedrock strata.
  - Sediment-filled palaeochannels. The last active incision likely occurred from 125–20 ka (e.g. Cawthra et al., 2020). On this overall sea-level regression, terrestrial sediments were likely scoured out and the post-glacial marine transgression from 20 ka to the present deposited marine sands in these channels.

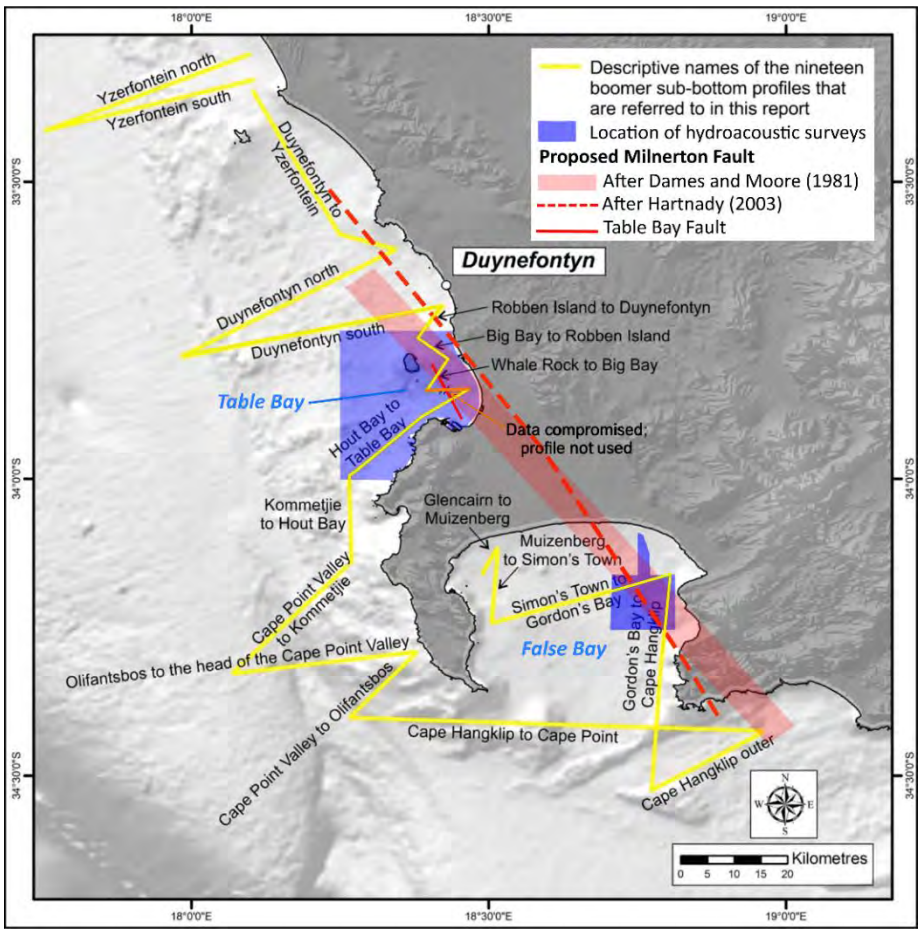

Figure 5-13. Map showing the location of newly collected hydroacoustic data that included high-resolution multibeam bathymetry around Table Bay and False Bay, as well as 20 Pinger and boomer sub-bottom profiles.

Survey results led Cawthra and Van Zyl (2023) to make the following general observations about the offshore environment:

- Multibeam echosounder mapping in the large marine embayments of Table Bay and False Bay has illuminated structural features (bedding, faults, folds) of rock outcrops (Table Mountain Group, Malmesbury Group, False Bay Dolerite Suite Dykes) and superficial sediment cover characteristics. Both bays are relatively sediment-starved and bedrock is well exposed on the seafloor.
- The exposed bedrock on the southwestern Cape seafloor is perhaps less helpful when sub-bottom profiling is considered. Both the boomer and pinger instruments struggled to penetrate seafloor units. Where pockets of marine sediment are preserved draping the Palaeozoic and Neoproterozoic bedrock exposures, these were imaged in detail. However, for the purposes of this investigation, the only place this proved useful was where the sediments indicate topographic lows in bedrock sequences, pointing toward the location of incised palaeochannels.
- Palaeochannels in this area do not have layered sequences preserved to assist with interpretations across Pleistocene glacial-interglacial cycles. Unfortunately, the acoustic characteristics of the sediment packages on this shelf seemingly represent deposition associated with the postglacial marine transgression since the termination of the (Last Glacial Maximum) LGM at ~20 ka. If associated with the LGM, these

channel-fill sediments can be identified as the Witzand Formation of the Sandveld Group which, where it has been sampled offshore in the vicinity of Table Bay and False Bay, represents modern marine shelf sands that shift in accordance with swell and current activities and tend to be preserved in bathymetric lows.

- Parts of bays protected from erosional forces have fringe sandy beaches. These sediments are acoustically transparent in their seismic character due to their tendency to be massive units of homogenous material. As such, are also not particularly helpful in investigating evidence of neotectonic activity on seafloor faults. In both bays, some reflectors were noted in the unconsolidated sediment, and these may represent the ravinement surface of the postglacial marine transgression. However, this was not helpful in the determination of recency of activity. In one boomer profile from Glencairn to Muizenberg, an apparent offset in this reflector surface was likely an incised palaeochannel of the Zandvlei River.

In assessing the offshore data collected in term of the aims of this supporting study, Cawthra and Van Zyl (2023) made the following relevant conclusions in support of the SSM:

- The proposed Milnerton Fault is not evident in the sea-floor stratigraphy of False Bay.
- High-resolution hydroacoustic mapping methods, with sufficient coverage to provide context, have shown that features previously mapped as faults in Table Bay may likely represent large-scale shear zones between folds. These folds are interpreted as structural features related to intense folding.
- There is no evidence from marine sediments of neotectonic movement. However, Pleistocene sediments are mostly scoured away, and almost only Holocene deposits are preserved on this part of the shelf which drape shallow or surficial bedrock.
- The nature of geological contacts between plutons of the Cape Granite Suite and Neoproterozoic Malmesbury Group rocks could not be determined but may be fault controlled as is often the case in the onshore geological record and linked to cooling after emplacement (e.g., Kisters and Belcher, 2018). If so, these are ancient structures.

The SSM TI Team evaluated and incorporated the data derived from this study into the SSM, as detailed in sections 8.5.1 (Table Bay Fault) and 8.5.7 (Proposed Milnerton Fault Zone).

5.2.4.3 Microseismic monitoring along the Colenso Fault

Mulabisana (2023) conducted a microseismic study along the full length of the Colenso Fault aimed at assessing its activity (Figure 5-13 a and b). A network of temporary seismic stations was installed along the fault to monitor earthquakes that might occur along it or be associated with the structural feature. Seven mobile Centaur Digitisers and Nanometrics Seismometer stations were deployed over a 6-month period from September 2023 to February 2023. The data was transmitted to the Council for Geoscience in real-time, where it was analysed. Only 16 events with clear waveform readings were recorded. Only 5 events were recorded near the Colenso Fault and were concentrated along a weak alignment parallel to the fault but offset 5–10 km to the northeast (Figure 5-14 a). Ultimately, if these hypocentres are associated with the Colenso Fault, data implies a dip of ~60° to the northeast. The average error ellipse on three hypocentre locations were between 0.8 km and 9.2 km. Unfortunately, depth and focal mechanism solutions of all recorded events could not be determined, as waveform data from the study was of poor quality (noisy) given the proximity of the stations to the coast. Unfortunately, with these limitations in the data, the findings from the Mulabisana (2023) study

could not be used as a reliable indicator of activity along the fault. The SSM TI Team evaluated and incorporated the data derived from this study into the SSM, as detailed in Section 8.5.2 (Colenso Fault).

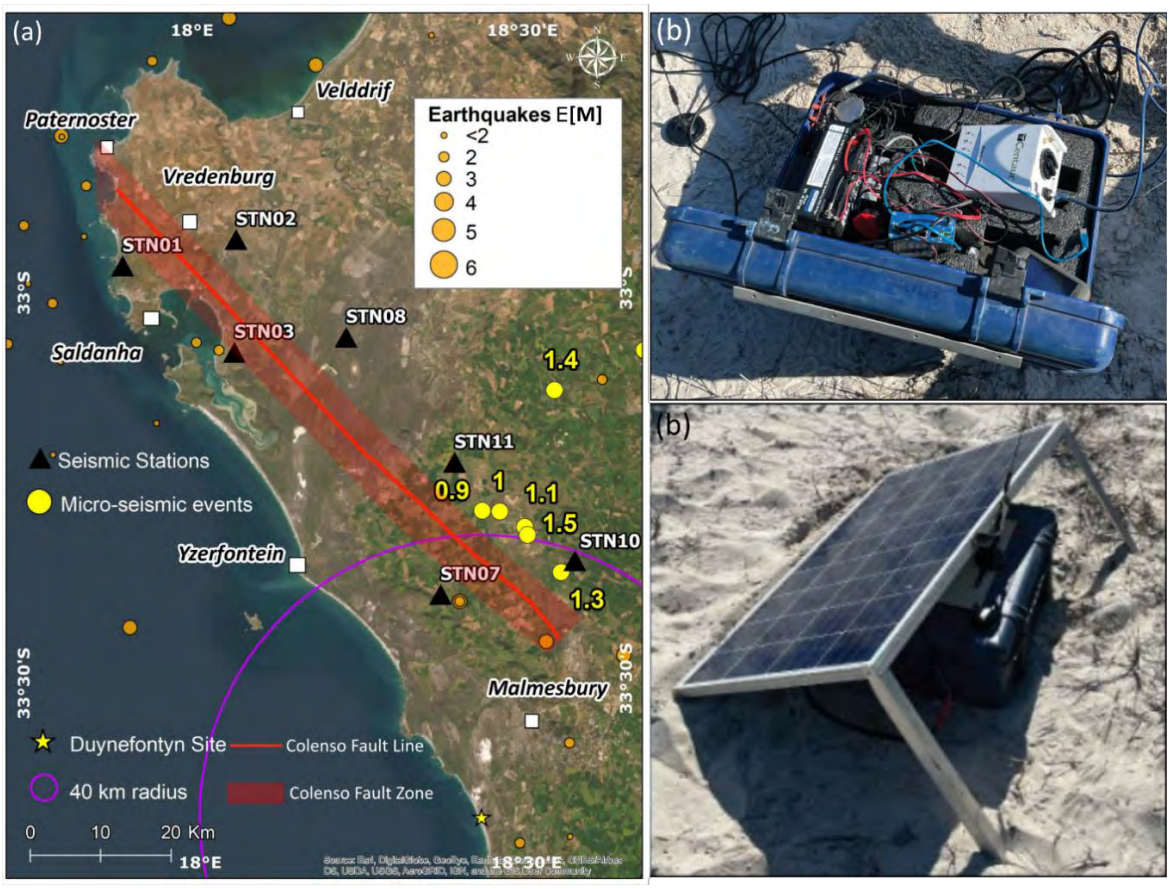

Figure 5-14. (a) Map showing the location of seismic stations and microseismic events recorded by Mulabisana (2023) along the Colenso Fault. (b and c) Mobile Centaur Digitisers and Nanometrics Seismometer stations were deployed.

5.2.5 DDC8: Stress data analysis

Smart et al. (2023) undertook geological stress analyses along the southwest region of the Western Cape Province of South Africa in support of the Duynefontyn PSHA. Stress data assist neotectonic studies by characterising in the present-day stress field, the expected fault movements during future earthquakes and the expected slip direction on fault planes. The study by Smart et al. (2023) involved two tasks that were undertaken using Southwest Research Institute's 3DStress® software:

- Present-day stress state assessment; and
- Analysis of slip tendency of mapped faults as a function of fault orientation and stress state.

To assess the present-day stress state, Smart et al. (2023) used the stress inversion technique (McFarland et al., 2012; Morris et al., 2013) fault orientations, displacement magnitudes and slip tendency analysis (Morris et al., 1996). The 3DStress based stress inversion analysis employed six earthquake focal mechanism solutions between 1969 and 2016, with magnitudes ranging from 1.8 to 6.2 that were within approximately 200 km of the Duynefontyn

site (Figure 5-15). Additionally, to provide qualitative verification, horizontal stress azimuth data from the World Stress Map database was used (Heidbach et al., 2016, 2018). This World Stress Map data includes both onshore earthquake-based orientations that indicate approximately east–west maximum horizontal stress directions, and offshore borehole-breakout-based orientations that indicate approximately NW–SE maximum horizontal stress directions (Figure 5-15). The borehole-breakout-based S_{Hmax} orientations from the World Stress Map database were not used directly by Smart et al. (2023) in their stress state determination. Rather, the borehole-breakout-based S_{Hmax} orientations were qualitatively compared to the 3DStress-inversion-based maximum principal stress orientation (NW-SE trend) and shown to be generally compatible.

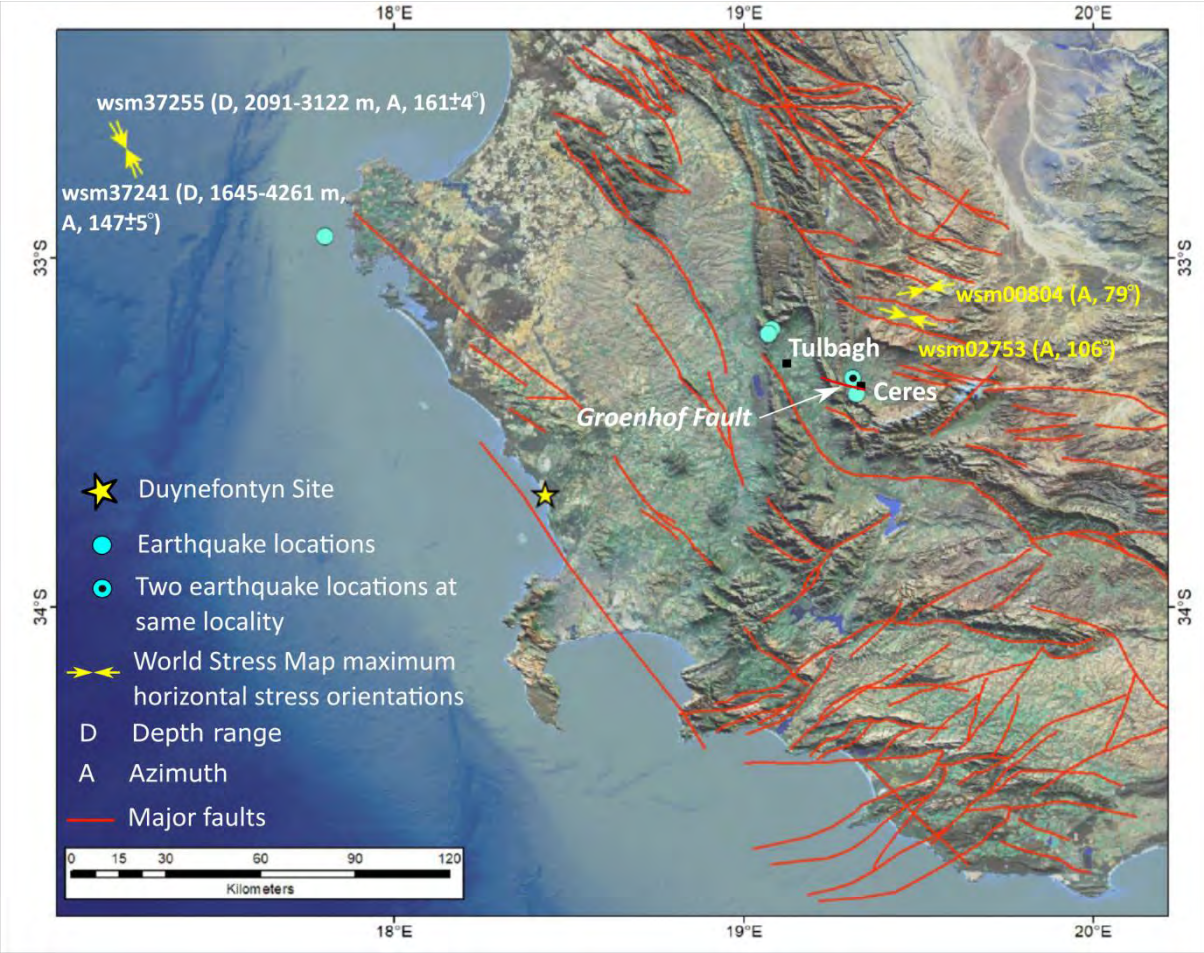

Figure 5-15. Map showing earthquake locations, fault traces and World Stress Map maximum horizontal stress orientations after Heidbach et al. (2016, 2018). The interval depth range (D) and azimuth (A) of borehole breakouts as derived from the World Stress Map is also included (after Smart et al., 2023).

Slip tendency analysis was undertaken to evaluate the potential for fault activity and likely slip directions on mapped faults in the interpreted most likely and alternative stress states. Slip tendency relies on the active stress state and orientation of the fault surface. The analysis focused on faults with a length of >15 km for which strike, and dip values were provided. Faults were separated into two groups based on fault dip then analysed for each stress-state solution.

Their investigations revealed the following summarised results and conclusions from stress analysis (Figure 5-16 a-f):

- Stress solutions show that intermediate principal stress (σ_2) is moderately to steeply plunging, suggesting a predominantly strike-slip stress regime.
- The most likely stress state is characterised by:

- a maximum principal stress (σ_1) orientation of 106°/05° (E-SE, shallowly plunging) (Figure 5-16a)
- an intermediate principal stress (σ_2) orientation of 002°/69° (Figure 5-16b)
- minimum principal stress (σ_3) orientation of 198°/20° (Figure 5-16c); and
- a stress ratio (Φ) of 0.54 (Figure 5-16d). Smart et al. (2023) also considered the variability in relative stress magnitudes and considered two additional stress ratios: (1) Φ = 0.29 (i.e. σ_2 closer in magnitude to σ_3) (Figure 5-16e); and (2) Φ = 0.79 (i.e. σ_2 closer in magnitude to σ_1) (Figure 5-16f).

Stress inversion results and analysis also led Smart et al. (2023) to consider an alternative stress state characterised by:

- A maximum principal stress (σ_1) orientation of 152°/29° (SE, shallowly plunging);
- An intermediate principal stress (σ_2) orientation of 344°/60°;
- A minimum principal stress (σ_3) orientation of 245°/05°; and
- A stress ratio (Φ[1]) of 0.54.

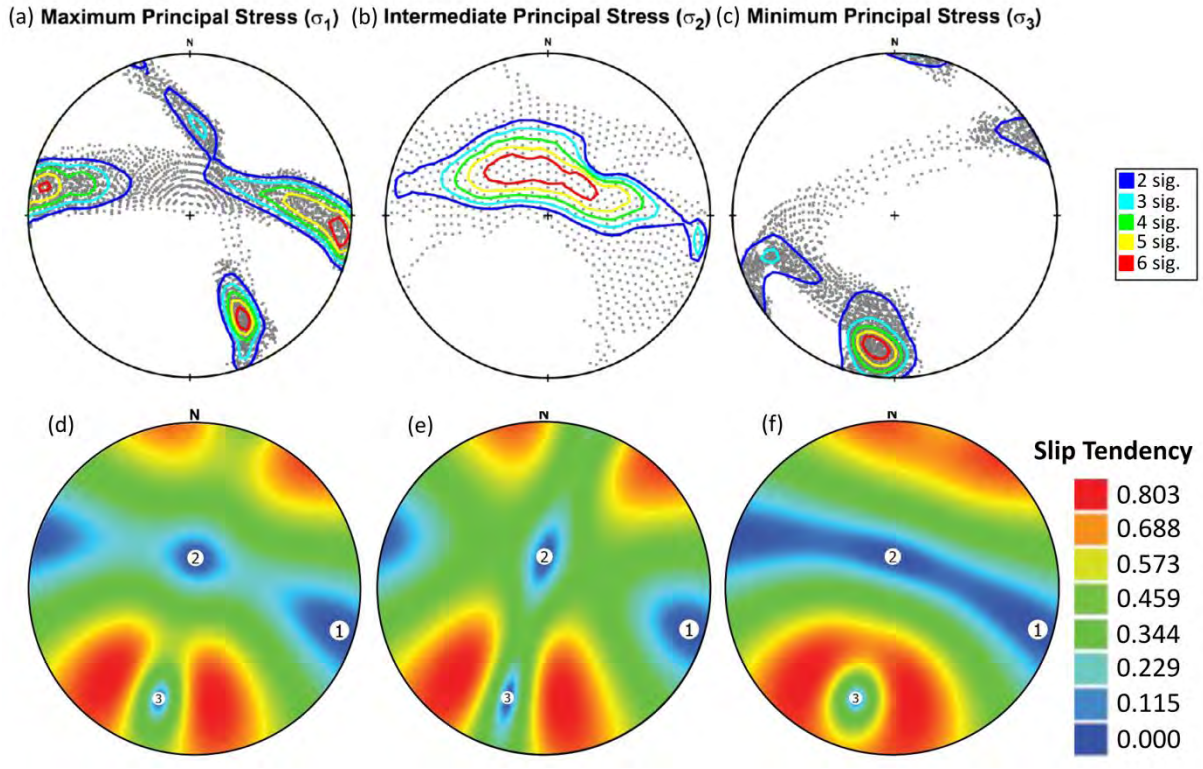

Figure 5-16. (a-c) Stress inversion results. (a) σ_1 orientations dominantly trend either east southeast or southeast (gentle plunge). (b) σ_2 orientations span a girdle from northeast to northwest (steep plunge). (c) $\sigma_3$3 orientations dominantly trend south-southwest (gentle plunge). (d-f) Stress state solutions. (d) Slip tendency stereoplot showing most likely stress state solution with Φ = 0.54, © Φ = 0.29, and (f) Φ = 0.79 (Smart et al., 2023).

[1] *Smart et al., (2023) defines the stress ratio (Φ) as: Φ =σ2−σ3/σ1−σ3 (after (Bishop, 1966; Lisle et al., 2006).*

The effect of the various stress-state solutions on the slip tendency and slip direction were assessed for 16 faults sources, eight vertical (90° dipping) faults and eight 60° south-dipping faults (Figure 5-17 a-c). Results reveal that regardless of stress state solution, the highest slip tendencies (>0.7) are associated with the 90° dipping faults, characterised by shallow to moderate rake angles (i.e. strike-slip to oblique-slip motion sense). However, the 60° south-dipping faults rarely show slip tendencies > 0.5 with more moderate rake angles (i.e. oblique- to dip-slip motion sense). For the three variants of the most likely stress state (i.e. E-SE σ_1), some faults display their largest slip tendencies when $\Phi = 0.29$, whereas others have higher slip tendency when $\Phi = 0.79$. With regard to the rake angle, the stress state with $\Phi = 0.29$ has shallower rake angles compared to $\Phi = 0.54$ or $\Phi = 0.79$. The alternative stress-state solution (SE σ1) results in overall lower slip tendency values for the fault dataset, with only three faults exceeding a slip tendency of 0.7 and six faults with slip tendencies < 0.4. Although the slip tendencies are lower, seven of the faults show rake angles of ≥ 10°.

As part of the overall stress analysis, 27 offshore seismic PASA profiles were examined, from which three were chosen (D2C, W2002-15, BGR03-11) for interpretation (Figure 5-17 a–d) based on data quality, orientation, position, and depth of penetration (in two-way travel time) to:

- provide regional tectonic context for the present-day stress state assessment, and
- identify, if present, faults in seismic profiles that show evidence for having been active in relatively recent geologic history.

The review and interpretations of offshore seismic reflection profiles provide approximate constraints on potential crustal domains along the southwest coast of South Africa including likely oceanic crust, rifted continental crust, syn-rift and post-rift sedimentary packages above basement, and possible volcanic rocks. Interpreted structures include faults in continental basement rock that likely developed during Mesozoic rifting and opening of the South Atlantic Ocean. Normal faults and thrust faults were interpreted to be present within shallower post-rift strata, but were interpreted to be related to slumping, flexure, and compaction rather than crustal scale faulting (Figure 5-17 b-d).

The SSM TI Team evaluated and incorporated the data derived from this study into the SSM, as detailed in Sections 8.2.5 (Point sources and virtual ruptures) and 8.4.2 (Style of faulting).